EP-025

소아 PBSCT 후 침윤성 아스페르길루스 감염으로 발생한 광범위 협부-중안면 괴사 결손의 지연 ALT 유리피판 재건 : 7년 장기추적

(Delayed ALT Free Flap Reconstruction for Extensive Buccal–Midfacial Necrosis Caused by Invasive Aspergillosis after Pediatric PBSCT: A 7-Year Follow-up)

부산대학교

임 현, 김민욱, 서정렬,이재우★

Purpose: 면역저하 소아에서 말초 조혈모세포이식(PBSCT) 후 발생한 침습성 Aspergillus 감염이 부비동을 넘어 협부 및 구강까지 진행하여 광범위한 구강–중안면 복합 결손을 유발한 증례에서, 단계적 감염원 제거 후 지연성 전외측대퇴(Anterolateral thigh, ALT) 유리피판으로 재건하고 7년 장기 기능적 결과를 보고하고자 한다.

Methods: 11세 여아(AML1/ETO 양성)는 2019년 1월 haploidentical PBSCT 시행 후 Tacrolimus 면역억제 하에 심한 백혈구/호중구 감소(WBC 660/μL, ANC 570/μL)를 보였고, 간정맥폐쇄성질환(veno-occlusive disease) 등 전신 상태 불안정이 동반되었다. 이후 우측 협부의 피부 변색과 함께 급속 진행성 괴사가 발생하며 부비동 침범 소견을 보였고, 내시경 생검에서 침습성 Aspergillus 감염이 확진되었다.

Meropenem, vancomycin 및 amphotericin B, voriconazole 등 항균, 항진균 치료에도 불구하고 병변이 진행하여, 다학제적 감염원 제거 수술을 단계적으로 시행하였다(내시경 부비동 수술, 비갑개 절제술, 상악 절제술, 이하선 절제술, 기관 절개술, 광범위 협부 변연절제술).

수술 과정에서 괴사 범위가 시기별로 변화하고 조직 경계의 명확한 demarcation이 지연되었으며, 활동성 감염 및 전신 상태 불안정이 지속되어 즉시 재건은 지양하고 감염 조절 및 전신 안정화 이후 최종 재건을 계획하였다.

2019년 3월 12일, 최종 변연절제 후 10×6 cm의 복합 결손에 대해 전외측대퇴(ALT) 유리피판을 시행하였다. 도플러로 천공지(perforator)를 확인한 뒤 14×6 cm 크기로 피판을 설계하여 Lateral circumflex femoral artery의 descending branch를 혈관경으로 확보하여 피판을 거상하였고(혈관경 약 12 cm), 수혜혈관으로는 안면동맥 및 동반정맥(venae comitantes)을 선택하여 end-to-end로 미세문합(9-0 nylon)을 시행하였다. 피판의 일부는 구강 내 피복(lining) 재건에 사용하고, 나머지는 외부 협부 연부조직 결손의 피복에 이용하였다. 공여부는 일차 봉합하였으며, 폐쇄흡인 배액관을 유지하였다.

Results: 피판은 혈관 합병증 없이 생존하여 외부 연부조직 결손과 구강 내 결손을 동시에 재건할 수 있었다. 수술 후 초기에는 안와저 침범 가능성 및 타액 누출이 의심되는 소견이 있었으나, 추가적인 침습적 처치 없이 보존적 치료와 면밀한 경과 관찰로 안정적으로 조절되었다.

2020년 3월에는 우측 협부 농양이 지연성으로 발생하여 CT에서 병변이 확인되었고, Klebsiella pneumoniae가 동정되어 정주 항생제 치료 후 임상적으로 호전되었다. 이후 초음파 유도 흡인에서 혈성 액체가 배액 되었으나 배양검사는 음성이었으며, 2020년 5월에는 기존 금속판 주변의 염증성 육아조직에 대해 국소 소파술과 부분 금속판 제거를 시행하고 국소피판으로 봉합하였다. 이 과정에서도 유리피판의 생존은 유지되었고 피판 소실은 발생하지 않았다.

2026년 1월(이식 후 7년) 추적 관찰에서 환아는 완전 관해 상태였으며, 또래 수준의 일반식 섭취가 가능했다. Drooling이나 임상적으로 확인되는 타액누공은 없었고, 위관/튜브 의존 없이 영양 상태를 유지하였다. 발화는 미세한 조음 오류만 남은 기능적 수준의 명료한 언어가 가능했으며, 개구는 약 2.5 finger breadths로 유지되었다.

Conclusion: 면역저하 소아에서 침습성 진균성 부비동염이 구강-중안면까지 확장되어 복합 결손을 유발한 경우, 적극적이고 단계적인 감염원 제거로 감염을 안정화한 뒤 시행하는 지연성 ALT 유리피판 재건은 장기간 안정적인 피복과 구강 기능(섭식 및 발화)을 제공할 수 있다.

또한 지연성 감염 합병증이 발생하더라도 항생제 치료 및 제한적 재수술로 피판 생존과 기능을 유지할 수 있음을 시사한다.

Fig 1.
PBSCT후 심한 면역저하 상태에서 우측 협부의 피부 변색이 급격히 악화되며 괴사가 진행하는 초기 임상 소견

Fig 2.
ALT free flap (전외측대퇴 유리피판)의 설계 및 채취(거상) 과정을 보여주는 수술 중 사진

Fig 3.
감염 조절 후 지연성 전외측대퇴(ALT) 유리피판 재건술 직후 소견으로, 피판 관류가 안정적이며 외부 및 구강 내 피복(lining)의 insetting이 양호함을 보여줌

Fig 4.
수술 후 7년 추적 관찰에서 재건 상태는 안정적으로 유지 되었으며, 구강 섭취 및 기능이 보존되었음

EP-026

치료 불응성 탈모성 모낭염에 대한 Orticochea 피판을 이용한 수술적 경험: 증례 보고

(Surgical Management of Refractory Folliculitis Decalvans Using an Orticochea Flap: A Case Report)

더 프라우병원

오상호*

INTRODUCTION: Folliculitis decalvans (FD) is a rare, chronic inflammatory scalp disorder characterized by recurrent pustules and progressive scarring alopecia. Current literature primarily focuses on its etiology and disease progression, with treatment modalities mostly limited to conservative approaches such as topical agents or photodynamic therapy (PDT).

To date, cases involving surgical excision and flap reconstruction have rarely been reported. In this study, we present a case of FD successfully treated with en-bloc excision and flap coverage.

CASE PRESENTATION

Figure 1. Preoperative images.

A 46-year-old male with thick and multiple pus drainage nodule from vertex to temporal area for 6 years visited our clinic. Until now, paitient received repetitive triamcinolone injection.

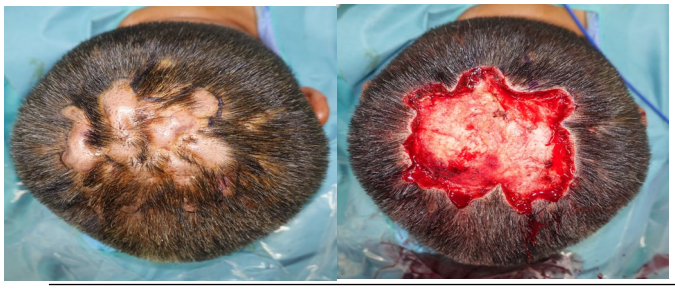

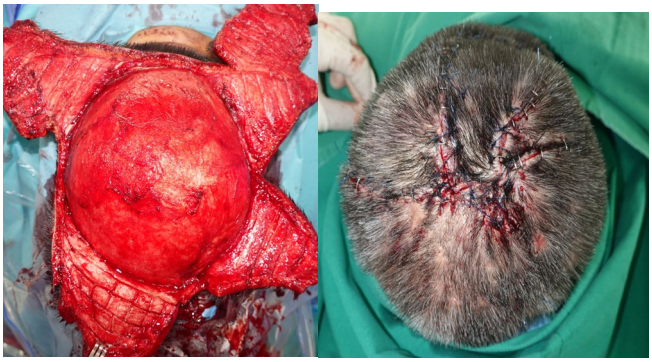

Figure 2. Intraoperative images

Enbloc resection and Orticochea flap with multiple galeatomy was performed for soft tissue coverage

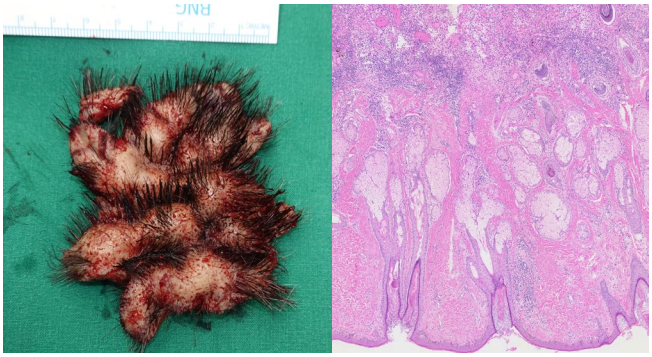

Figure 3. Gross and histological images

Perifollicular neutrophilic infiltration associated with follicular rupture and surrounding fibroplasia.

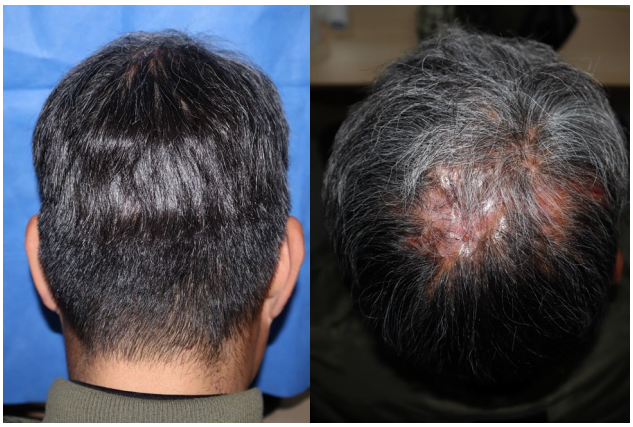

Figure 4. Postoperative follow up images

CONCLUSION: While the management of folliculitis decalvans has traditionally been restricted to medical therapy, this case demonstrates that surgical excision and flap reconstruction can be an effective treatment option for refractory cases.

EP-027

관절낭내 하악과두골절의 관혈적 정복 및 내고정술에서 이전 경이하선 접근법의 타당성

(Feasibility of the preauricular transparotid approach in open reduction and internal fixation of intracapsular mandibular condyle fracture

고려대학교 안암병원

이수빈, 박호진★

Background: Mandibular condyle fractures pose surgical challenges owing to their proximity to the facial nerve and the complex temporomandibular joint anatomy. Traditional approaches limit exposure and hinder effective fracture management. The preauricular transparotid approach is a potential alternative. We aimed to assess the feasibility of this approach and the postoperative complications.

Methods: This retrospective study analyzed 45 patients with intracapsular condylar fractures treated using open reduction and internal fixation via a preauricular transparotid approach.(Fig.1) The surgical incision begins at the root of the helix, follows the preauricular crease, and extends around the earlobe. A skin flap is elevated above the SMAS layer, followed by blunt dissection of the parotid gland. The temporal and zygomatic branches of the facial nerve are carefully identified and preserved during dissection. A vertical incision is made in the masseter muscle to expose the condylar head. Fractures are reduced and fixed using positional screws or mini-plates depending on fragmentation. Preoperative CT scans evaluate displacement, segment distance, cortical height difference, fracture angle, and ramus height, as well as nerve distance based on Pitanguy's line. (Fig. 2.) Postoperative outcomes include radiologic assessment of reduction, screw angle, ramus height, mouth opening, and chin deviation. (Fig. 3.)

Results: This study included 45 patients who underwent OR/IF for intracapsular condylar head fractures, with an average age of 35.2 years, a mean time to surgery of 9.5 days, hospital stay of 5.5 days, and operation time of 193.5 minutes.(Table 1.) Preoperative CT showed multidirectional displacement, with fracture segments located 17–24 mm from the condylar stump despite smaller displacement distances. (Table 2.) The fracture line averaged 44.2° in inclination, and anatomical considerations indicated screw placement within 9.6 mm, close to the facial nerve. Postoperatively, ramus height and symmetry significantly improved, with anatomical or near-anatomical reduction achieved in most patients. (Table 3.) Temporary facial nerve weakness occurred in some cases but resolved within weeks without permanent damage. Overall, functional outcomes were favorable, with good mouth opening and minimal complications such as mild joint symptoms or slight deviation.

Conclusion: The approach enhances visualization, facilitates precise fixation, and results in inconspicuous scarring during OR/IF of intracapsular condylar fractures. It requires careful surgical techniques and increases the risk of transient facial nerve weakness. Further research should compare its outcomes with those of traditional approaches and optimize surgical outcomes.

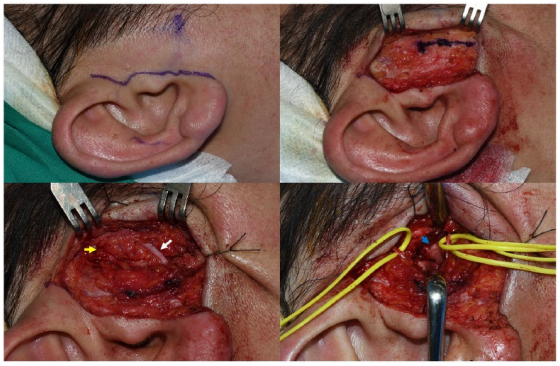

Fig. 1. Surgical procedure of the preauricular transparotid approach with ear lobular extension. (Above, left) An incision line is designed starting from the root of the helix and following the natural crease of the preauricular skin down to the earlobe. This incision then extends further, encircling the earlobe. (Above, right) The skin flap is elevated above the superficial musculoaponeurotic system (SMAS) layer. The SMAS incision site is drawn by palpating the condyle head. (Below, left) After SMAS incision, the parotid gland is bluntly dissected, and the facial nerve temporal (yellow arrow) and zygomatic (white arrow) branches of the facial nerve are dissected from the surrounding tissues. (Below, right) A vertical incision is made in the masseter muscle, and the condyle head (blue arrow) is exposed.

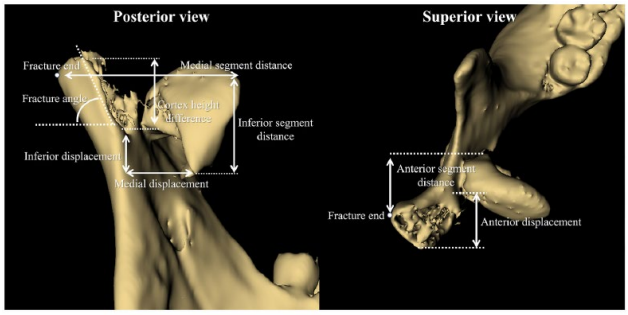

Fig. 2. Methods for measuring displacement distance and segment distance.

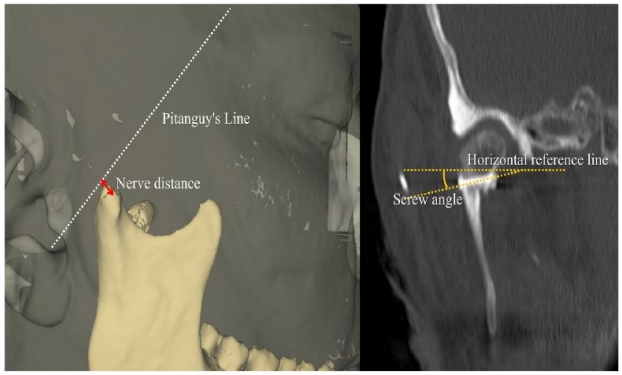

Fig. 3. Methods for measuring nerve distance and screw angle. Nerve distance is determined as the shortest distance from the Pitanguy's line, a line extending from 0.5 cm below the tragus to 1.5 cm above the lateral eyebrow, to the end of the condylar stump (red arrow). Screw angle refers to the angle between the horizontal reference line and the screw on the coronal view of postoperative CT images.

Table 1
Summary of patient demographics, duration of surgery, and hospital stay (n = 45).

Demographics		
Sex (n)	Male	28
	Female	17
Age (years)		35.2 ± 10.1
Sides (n)	Right	19
	Left	26
Etiology	MVA	6
	Fall	35
	Assault	4
Duration of surgery (minutes)		193.5 ± 20.1
Hospital stays (days)		5.5 ± 0.8

MVA: motor vehicle accident.

Table 2
Displacement distance, segment distance, cortex height difference, fracture angle, and nerve distance measured from the preoperative CT images.

		Average	Range
Displacement distance (mm)	Anterior	7.2 ± 2.9	(2.3–14.7)
	Medial	9.3 ± 3.4	(3.3–18.7)
	Inferior	9.9 ± 2.8	(5.3–17.9)
Segment distance (mm)	Anterior	17.0 ± 2.6	(10.1–21.9)
	Medial	24.0 ± 3.9	(11.9–30.6)
	Inferior	17.8 ± 3.7	(8.8–25.2)
Cortex height difference (mm)		9.6 ± 2.7	(6.7–14.4)
Fracture angle (degrees)		44.2 ± 10.6	(10.7–44.2)
Nerve distance (mm)		5.5 ± 2.8	(1.2–12.3)

EP-028

자가 늑연골을 이용한 소이증 재건술 후 발생한 수술부위 감염의 음압창상치료와 보존적 변연절제를 통한 구제 치료

(Salvage of Surgical Site Infection After Autologous Microtia Reconstruction Using Negative-Pressure Wound Therapy and Conservative Debridement)

성균관대학교 의과대학
강북삼성병원

조원석, 김규남★

Purpose: Surgical site infection (SSI) following autologous rib cartilage microtia reconstruction is an uncommon but potentially devastating complication because infection of the avascular cartilage framework can rapidly lead to framework loss. Traditional management has often favored aggressive debridement or framework removal. This study evaluates salvage-oriented treatment strategies and proposes a structured management approach for SSI after microtia reconstruction.

Methods: A retrospective case series was conducted of patients who developed SSI following autologous rib cartilage microtia reconstruction between March 2021 and November 2025. SSI was defined based on clinical findings requiring intervention beyond routine postoperative care. Nine patients were identified. Treatment strategies were analyzed with respect to infection control, framework preservation, and wound healing outcomes.

Results: SSI occurred at variable time points, ranging from early postoperative infection to delayed presentations. Identified pathogens included Gram-positive cocci and multidrug-resistant Gram-negative organisms. Negative-pressure wound therapy (NPWT) was applied in cases with wound dehiscence, persistent drainage, or cartilage exposure. Conservative staged debridement was performed only after clear demarcation of nonviable tissue. Overall auricular framework preservation was achieved in all patients, with no cases requiring complete framework removal, although limited cartilage loss occurred in some cases.

Conclusion: SSI after autologous microtia reconstruction can be successfully managed using a structured salvage-oriented approach that emphasizes early culture-guided antimicrobial therapy, NPWT, and conservative staged intervention. This strategy enables preservation of the auricular framework and maintains overall auricular contour even in complex infection scenarios

Fig 1. Application of negative-pressure wound therapy (NPWT) for surgical site infection following microtia reconstruction.

Fig 2. Early postoperative coagulase-negative Staphylococcus infection. (A) Postoperative day 10 showing purulent discharge and partial cartilage necrosis at the postauricular incision. (B) Early postoperative appearance after staged debridement and wound edge approximation. (C) Follow-up photograph demonstrating stable soft-tissue coverage and preservation of overall auricular contour despite limited tail cartilage loss.

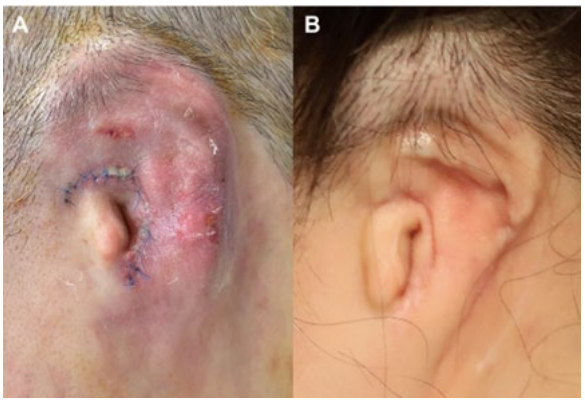

Fig 3. Early postoperative Serratia marcescens infection. (A) Postoperative day 7 demonstrating erythema and purulent discharge at the postauricular incision following rib cartilage framework implantation. (B) Post-treatment appearance showing resolution of infection and preservation of auricular contour after limited excision of nonviable helix-tail cartilage.

EP-029

악성 변화를 동반한 외상성 창상으로 발생한 광범위 안면부 결손의 이마 중앙부 피판술을 이용한 후 재건 : 증례 보고

Paramedian Forehead Flap Reconstruction for Extensive Central Facial Defect Following Malignant Transformation of a Chronic Traumatic Wound : A Case Report

성균관대학교 의과대학
강북삼성병원

조원석, 김규남★

Purpose: Chronic non-healing facial wounds may undergo malignant transformation and result in extensive composite defects that challenge reconstruction. The paramedian forehead flap (PMFF) remains the gold standard for large nasal and central facial defects because of its robust vascularity and versatility. We present reconstruction of a massive central facial defect after basal cell carcinoma arising in a chronic traumatic wound.

Methods: A 59-year-old man presented with a chronic glabellar–nasal ulcer following nasal avulsion injury from a traffic accident. The lesion measured 9×7 cm with exposed bone and persistent infection. During planned reconstruction, intraoperative frozen biopsy revealed basal cell carcinoma consistent with malignant transformation in a chronic wound. Multidisciplinary staged wide excisions involving the glabella, nasal dorsum, medial cheek, medial canthus, lacrimal system, and ethmoid sinus resulted in an 11×9 cm composite defect without distant metastasis. Reconstruction was performed using a two-stage supratrochlear-based PMFF with skin grafting.

Results: The flap survived completely and provided stable soft-tissue coverage. Postoperative radiotherapy (60 Gy) was delivered without flap compromise. The patient maintained nasal airway patency and demonstrated acceptable aesthetic contour. Radiation-induced epiphora occurred but required conservative management. At 9-month follow-up, there was no evidence of recurrence.

Conclusion: Even in massive defects and suboptimal wound bed conditions caused by chronic infection, the PMFF provides reliable structural stability and superior aesthetic integration due to its excellent color, thickness, and texture match with nasal and midfacial skin. Therefore, the PMFF remains a reliable reconstructive option for extensive central facial defects following oncologic resection.

Fig 1. Preoperative clinical photographs at initial presentation (A, B). Large chronic ulcer involving the glabella and nasal dorsum following traumatic nasal avulsion injury. The wound demonstrates exposed bone, unhealthy granulation tissue, and extensive soft-tissue loss across the central facial aesthetic units.

Fig.2 First-stage surgical management and wound stabilization. (A) Immediate postoperative appearance following wide excision and split-thickness skin graft for temporary coverage and wound bed preparation. (B) One-month postoperative appearance demonstrating stable graft take and preparation for definitive reconstruction.

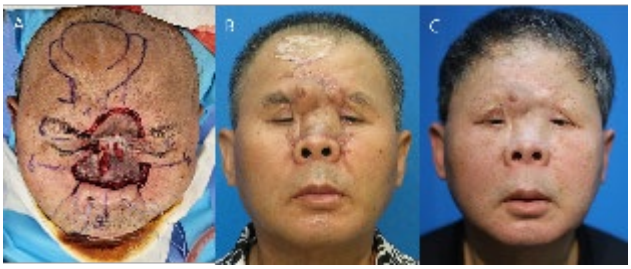

Fig 3. Definitive reconstruction using a paramedian forehead flap. (A) Intraoperative design of wide oncologic resection and supratrochlear-based paramedian forehead flap. (B) Early postoperative appearance following flap inset. (C) Seven-month postoperative appearance demonstrating stable coverage, restoration of central facial contour, and acceptable aesthetic outcome.

EP-030

요골 전완 유리피판에서 정맥 유출 개선을 위한 단일 대정맥의 전략적 준비

(Strategic Preparation of a Large Single Vein for improving Venous Outflow in the Radial Forearm Free Flap)

한림대학교

김기현, 안정훈, 김경민, 우상석, 이준원, 김성환, 최재구, 서인석★

Purpose: The radial forearm free flap (RFFF) is a widely used workhorse flap in head and neck reconstruction. Despite its reliability, flap compromise most commonly results from venous outflow insufficiency. In the cervical region, recipient veins are typically large and lack venae comitantes, often leading to caliber mismatch and unfavorable venous drainage when standard distal pedicle dissection is performed.
We present a pedicle preparation strategy aimed at securing a single large-caliber donor vein to improve venous return and flap reliability.

Methods: At our institution, a modified pedicle dissection technique was applied in 125 RFFF cases. During flap elevation, the venous pedicle was dissected proximally toward the cubital region to preserve the venous confluence and obtain the largest possible venous caliber, enabling direct end-to-end anastomosis to large cervical veins.(Figure 1)
Clinical outcomes and flap survival were evaluated following application of this technique.

Results: The donor veins consistently converged near the cubital fossa, allowing preparation of a single large-caliber vein suitable for direct anastomosis to recipient cervical veins such as the external jugular vein. Size mismatch and the need for additional venous manipulation were minimized.
Proximal pedicle dissection also improved pedicle positioning and reduced redundancy during inset. With this technique, overall flap survival approached 98–99%, and venous congestion was rarely encountered.

Conclusion: Proximal pedicle dissection to secure a large single donor vein improves venous outflow and simplifies microvascular anastomosis in RFFF. This practical and reproducible strategy enhances flap reliability in head and neck reconstruction and may reduce venous complications associated with conventional distal pedicle preparation.

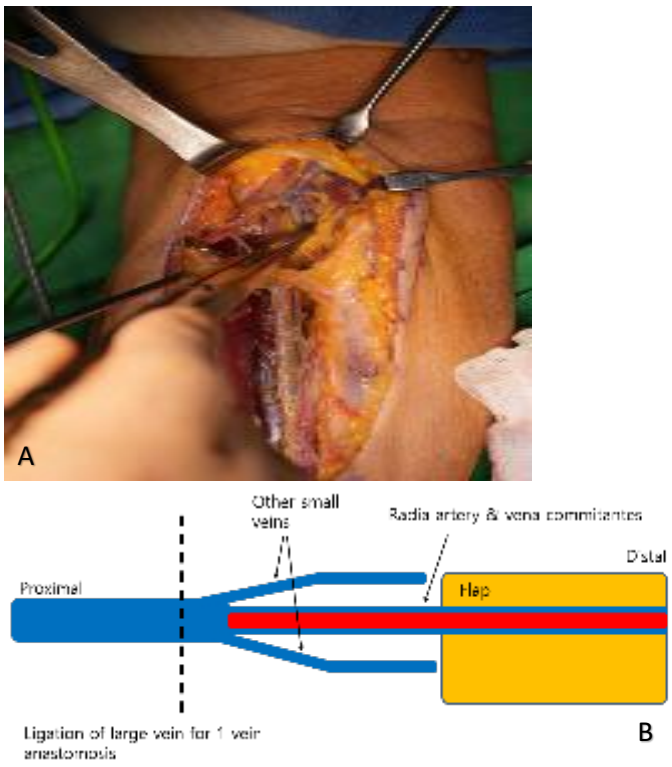

Figure 1. Modified venous pedicle dissection technique in radial forearm free flap (RFFF).
(A) Intraoperative photograph showing proximal dissection of the venous pedicle toward the cubital region.
(B) Schematic illustration of the modified technique

EP-031

귀 켈로이드에 대한 Core Extirpation : 조직 보존적 수술 기법 및 치료 결과

Core Extirpation for Ear Keloids :
A Tissue-Preserving Surgical Technique
and Its Outcomes

고려대학교 안암병원
박시현 , 박호진★

Purpose: Core extirpation (CE) is a tissue-preserving surgical technique that removes the central bulk of a keloid while retaining a thin peripheral shell of pathologic tissue as a skin flap. By avoiding injury to surrounding uninvolved skin, this approach may minimize postoperative auricular shape distortion, which is particularly important in the auricle with its complex three-dimensional structure. However, clinical outcomes and recurrence rates following CE for ear keloids have not been sufficiently reported. This study aimed to evaluate the clinical efficacy, aesthetic outcomes, and recurrence following CE for auricular keloids.

Methods: Patients who underwent CE for auricular keloids between July 2022 and December 2025 were retrospectively reviewed. Keloid location and size were documented preoperatively. Postoperative outcomes were assessed based on recurrence-related symptoms (redness, pruritus, and pain) and standardized photographic evaluations focusing on helical rim notching, auricular structural changes, or volume loss. Patients who developed postoperative keloid-related symptoms received intralesional steroid injections, and the number of patients requiring injections and the total number of injections were recorded.

Results: A total of 32 patients with 42 lesions were included in the study. Postoperative keloid-related symptoms, particularly pruritus, developed in 7 patients (21.8%) and resolved within 3 weeks after surgery. Two patients (6.2%) required postoperative intralesional steroid injections due to redness and pruritus, and the symptoms resolved after a mean of two injections. Among the 42 lesions, 37 (88.1%) demonstrated excellent auricular shape without ear notching or loss of normal auricular volume. Three lesions (7.1%) showed good auricular shape but had mild skin irregularity caused by residual scar tissue. Two lesions were graded as moderate because the patients had previously undergone multiple wedge resections, resulting in pre-existing auricular deformity compared with the contralateral ear. During the mean follow-up period of 5.7 months, no clinical recurrences were observed.

Conclusion: Core extirpation is an effective surgical option for auricular keloids, demonstrating excellent aesthetic outcomes and a low recurrence rate. Preservation of the peripheral skin flap may prevent postoperative ear distortion and reduce wound tension, contributing to durable results. CE represents a reliable, tissue-conserving approach for the management of ear keloids.

Fig. 1.

Fig. 2.

EP-032

3차원 CT를 이용한 한국인 하악골의 생물학적 성별에 따른 형태학적 특성 분석

(An analysis of mandibular characteristics according to biological sex using 3D CT scans in Koreans)

한림동탄성심병원
성형외과

이중현, 김병준, 윤인모, 정소연★

Purpose: With the increasing demand for facial feminization surgery (FFS), precise knowledge of sex-based andibular morphology has become clinically relevant. In this study, "male" and "female" refer to biological sex as recorded in medical records; gender identity was not assessed. We aimed to analyze sex differences in mandibular morphology using three-dimensional (3D) computed tomography (CT) in a Korean population and to provide anatomic data applicable to mandibular contouring in FFS.

Methods: A retrospective analysis was conducted on 275 Korean patients who underwent facial CT between 2017 and 2019. Three- dimensional cephalometric analysis was performed to evaluate angular, linear, and transverse mandibular parameters, as well as non-metric features including chin shape and inferior mandibular border contour. Statistical comparisons were performed between sexes.

Results: Significant gender differences were observed in mandibular angle, mandible length, antegonial notch distance, intercondylar width, and intergonial width (all $p < 0.001$). Ramus length and chin width did not demonstrate statistically significant differences. Non-metric analysis revealed significant gender differences in chin morphology and inferior mandibular border contour ($p < 0.001$). Males predominantly exhibited a round or square chin (79.5%) and a rocker-shaped inferior border, whereas females commonly demonstrated a pointed chin (82.3%) and a straight inferior mandibular border (94.4%).

Conclusion: The gender-specific mandible features are characterized by differences in angularity, transverse width, antegonial morphology, and inferior border contour. These findings provide population-specific morphological reference ranges that may support individualized preoperative assessment for mandibular contouring in facial feminization surgery.

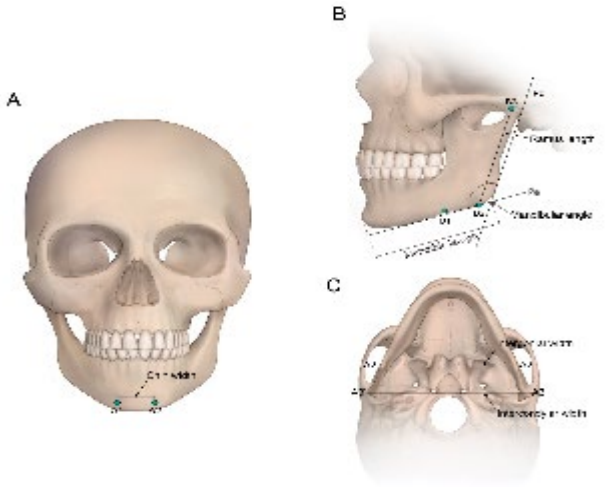

Figure 1. Linear and angular measurements of the mandible. (**A**) A frontal view illustrating chin width, defined as the distance between the right and left mental tubercles (A1-A1′). (**B**) A lateral view demonstrating the mandibular angle, formed by the intersection of the bottom plane of the mandibular corpus (Pa) and the posterior plane of the mandibular ramus (Pb). Mandible length was defined as the distance from the most anterior point of the chin to a line placed along the posterior border of the ramus, and ramus length was defined as the distance between B2 and B3. (**C**) An inferior view showing transverse measurements, including intergonial width (A2-A2′) and intercondylar width (A3-A3′).

Figure 2. Non-metric mandibular morphology classification.
Representative three-dimensional CT images demonstrating the categorical classification of non-metric mandibular features.
(A) Pointed chin morphology.
(B) Square chin morphology.
(C) Round chin morphology.
(D) Rocker-shaped (notched) inferior mandibular border contour.
(E) Straight inferior mandibular border contour.

Measurement	Definition
Ramus length	The distance from the highest point on the condyle (B3) to the gonion (B2)
Mandible length	The distance from the most anterior point of the chin to a line placed along the posterior border of the ramus
Mandibular angle	The angle formed by the inferior border of the mandibular body (Pa) and the posterior border of the ramus (Pb)
Intercondylar width	The distance between the most lateral points of the right and left condyle heads (A3-A3′)
Intergonial width	The distance between the right and left gonions (A2-A2′)
Chin width	The distance between the right and left mental tubercles (A1-A1′)
Antegonial notch distance	The distance between the most concave part of the lower border of the mandible (B1) and the mandibular plane line (Pa)

Table 1. Definitions of CT-based mandibular measurements.

Measurements Number		Male 151	Female 124	*p*-Value [a], [b]
Intercondylar width		126.9 ± 7.6	122.6 ± 6.1	<0.001
Intergonial width		101.3 ± 4.5	98.4 ± 2.2	<0.001
Mandibular angle		120.7 ± 3.7	123.3 ± 4.0	<0.001
Mandible length		73.5 ± 2.3	68.6 ± 4.2	<0.001
Ramus length		58.3 ± 4.8	56.1 ± 2.6	0.073
Chin width		22.7 ± 4.3	22.1 ± 3.7	0.703
Antegonial notch distance		2.6 ± 0.7	1.2 ± 0.3	<0.001
Chin shape	Pointed	31	102	<0.001
	Round/Square	120	22	
Lower border	Notch	102	7	<0.001
	Straight	49	117	

Table 2. Statistical analysis of CT-based mandibular measurements between male and female.

EP-033

척추 종양 절제 후 발생한 후경부 결손의 방사선 조사 구역 기반 재건 전략: 국소 피판술보다 방사선 비조사 원위부 피판술의 우선순위 설정

(Radiation Field–Based Reconstructive Strategy for Posterior Neck Defects Following Spinal Tumor Resection: Prioritizing Non-irradiated Distant Flaps Over Local Options)

중앙대학교 의과대학 성형외과학교실 [1]

최주헌, 우수현★

Purpose: Traditional reconstructive algorithms for posterior neck defects often prioritize local flaps, such as the trapezius flap, as the first-line option. However, in spinal tumor cases requiring postoperative radiotherapy (RT), the RT field frequently encompasses the upper and middle trapezius portions, compromising their vascular integrity. [Figure 1] We propose that in the irradiated wound defects, distant non-irradiated flaps should be considered the primary option rather than local irradiated tissue.

Methods: We reviewed three patients with chronic posterior neck wound dehiscence following tumor resection and RT. [Table 1] In the first case, an initial attempt with a bilateral keystone flap (local irradiated tissue) failed, resulting in recurrent dehiscence. [Figure 2] Subsequently, all cases, including the revision of the first, were successfully reconstructed using latissimus dorsi (LD) pedicled flaps. [Figure 3] These healthy, non-irradiated musculocutaneous flaps provided robust vascularity and sufficient volume to obliterate dead space and ensure stable coverage of exposed hardware.

Results: All LD flaps survived without recurrence of dehiscence or hardware-related infections. By avoiding the "not-truly-non-irradiated" local options and opting for a distant flap, we achieved rapid wound healing. This early aggressive reconstruction prevented oncologic treatment delays, significantly improving the quality of life for these metastatic cancer patients.

Conclusion: For posterior neck defects within the RT field, the conventional preference for local flaps should be re-evaluated. Prioritizing non-irradiated distant flaps (e.g., LD flap) as the primary reconstructive option, rather than a salvage procedure, ensures long-term wound stability, minimizes surgical failures, and facilitates uninterrupted oncological care.

Category	Patient 1	Patient 2	Patient 3
Sex / Age	F / 76	M / 66	M / 73
Diagnosis	Cervical Plasmacytoma (metastatic Multiple Myeloma)	Metastatic Pancreatic Ca.	Metastatic HCC
Radiotherapy (RT)	(1) Pre-op: 300cGy/1fx (2) Post-op: 6/9 fx	Post-op RT (10 fx)	Palliative RT (10 fx) - between repeated OPs
Local Treatment (Prior to LD flap)	Resuture, N.P.W.T., Bilateral Keystone flap	Aspirations, N.P.W.T., Closure	Multiple Debriclosures
Outcome of flap	Stable / No recurrence (POD#850)	Stable / No recurrence (POD#127)	Stable / No recurrence (POD#41)

Table 1. Summary of clinical data for three patients who underwent latissimus dorsi (LD) pedicled flap reconstruction for posterior neck defects, which shows the stability of LD flap up to the present.

Fig. 1. Representative 3D radiation dose maps for Patient 1, 2, and 3. Across all cases, the isodose curves demonstrate that the radiation field was not limited to the target tumor but extensively encompassed adjacent soft tissue structures including upper thorax and trapezius.

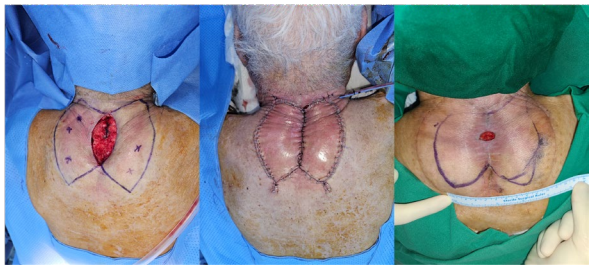

Fig. 2. Failure of initial attempt of reconstruction with Bilateral keystone advancement flap in patient 1. Tissues surrounding the posterior neck defect are also compromised by adjuvant radiation therapy, leading to recurrent wound dehiscence and failure of reconstruction.

Fig. 3. Definitive reconstruction was successfully achieved in all patients using a non-irradiated distant flap (LD pedicled flap); (A) Patient 1, (B) Patient 3. By transposing healthy, vascularized tissue from outside the radiation field, stable wound closure was maintained without further complications, which enhanced the quality of life and life expectancy by scheduled adjuvant oncologic treatments without further delay.

EP-034

Bowen병 절제 후 mid-cheek lift를 이용한 하안검 재건: 증례 보고

가톨릭대학교 은평성모병원

장지형, 나은영, 신종원, 김지윤★

Purpose : The lower eyelid is essential for maintaining the tear-corneal film, protecting the globe, and preserving facial aesthetics. Reconstruction of lower eyelid defects after tumor excision should aim not only to restore coverage but also to achieve aesthetic balance by improving orbital bulging. We report a case of a lower eyelid defect following excision of Bowen's disease that was successfully reconstructed using a mid-cheek lift.

Methods : A 67-year-old man presented with Bowen's disease located 0.5 cm inferior to the left lower eyelid margin and lateral to the mid-pupil line. The lesion measured 1 × 1 cm and was removed with Mohs surgery, leaving a 1.5 × 1.3 cm defect with the orbicularis oculi muscle (OOM) preserved. Reconstruction was performed through a subciliary incision. Dissection was carried out in the plane between the suborbicularis oculi fat (SOOF) and periosteal fat. The orbicularis retaining ligament was released, whereas the premaxillary space and zygomaticocutaneous ligament (ZCL) were preserved. The SOOF was then suspended to the arcus marginalis using 4-0 Vicryl sutures to create a mid-cheek lift. After additional suspension of the OOM, redundant skin was trimmed to complete the reconstruction.

Results : The defect was fully covered. At 6 months after surgery, the patient showed favorable functional and aesthetic outcomes without complications such as ectropion.

Conclusions : Mid-cheek lift is an effective option for reconstruction of anterior lamellar defects lateral to the mid-pupil line while preserving the premaxillary space and ZCL.

Fig. 1. Preoperative clinical photo showing a 1x1cm lesion of Bowen's disease located lateral to

Fig. 2. Lower eyelid defect measuring 1.5×1.3 cm after Mohs surgery.

Fig. 3. The mid-cheek was elevated through the prezygomatic space, followed by mid-cheek lift. Preservation of the premaxillary space and the zygomaticocutaneous ligament was achieved.

Fig. 4. Clinical photo at 6 months postoperatively, showing no ectropion and aesthetically acceptable results.

EP-035

식도암 수술로 인한 기관식도루 발생 후 후방 늑간동맥 천공지 피판을 이용한 기관 결손 재건: 증례 보고

(Tracheal Defect Coverage with Posterior Intercostal Artery Perforator Flap Following Esophageal Cancer Surgery-Induced Tracheoesophageal Fistula: A Case Report)

가톨릭대학교 은평성모병원
서해진, 김지윤★

Purpose: Esophageal cancer surgery complications, particularly anastomotic leakage, can lead to catastrophic outcomes. A subsequent tracheoesophageal fistula may rapidly progress to respiratory failure, making prompt and effective coverage crucial. We report a case of tracheal defect coverage using a pedicled posterior intercostal artery perforator (PICAP) flap.

Methods: An 80-year-old male underwent esophageal cancer surgery by general surgery and showed no complications until postoperative day (POD) 14. However, he suddenly developed respiratory failure with decreased oxygen saturation, requiring intubation. Bronchoscopy revealed a 3x1 cm tracheal defect. Initial coverage with acellular dermal matrix (ADM) failed, prompting cooperation with plastic surgery to utilize a pedicled PICAP flap. Under general anesthesia, with the patient in the lateral position, an 8x3 cm PICAP flap was designed at the 5th intercostal space. Flap elevation began distally, carefully preserving the cranial pedicle and sparing the serratus muscle until reaching the latissimus dorsi muscle area. After flap elevation, the surgical team switched to one-lung ventilation, performed rib resection, and entered through the parietal pleura to access the tracheal defect. The flap was inset, and the procedure concluded.

Results: The patient was extubated seven days postoperatively but subsequently developed respiratory failure again, ultimately resulting in death.

Conclusion: Tracheal defect coverage remains highly challenging; however, the pedicled intercostal muscle flap may serve as a valuable additional option.

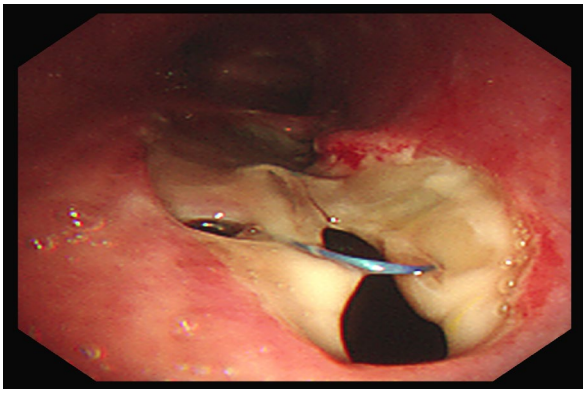

Fig. 1. A 3x1cm tracheal defect observed preoperatively via bronchoscopy

Figure 2. Pedicled posterior intercostal artery perforator flap after elevation.

Fig. 3. Insetting of the pedicled posterior intercostal artery perforator flap into the thoracic cavity toward the tracheal defect.

EP-036

승모근 중앙부의 잔존 섬유화 밴드로 인한 재발성 사경의 치료: 증례 보고

(Management of Recurrent Torticollis Caused by a Residual Fibrotic Band of the Central Trapezius Muscle: A Case Report)

세종충남대학교병원[1]
충남대학교의과대학[2]

김주학[1], 양호직[1], 경현우★ [2*]

Purpose: This study reports a rare case of recurrent congenital muscular torticollis (CMT) caused by a residual fibrotic band in the central portion of the trapezius muscle and emphasizes the importance of evaluating extra-SCM structures in recalcitrant cases.

Methods: A 6-year-old boy presented with persistent head tilt after a primary bipolar release of the sternocleidomastoid (SCM) and partial release of the lower trapezius. While the SCM was soft and pliable on palpation, a distinct tight band was identified in the central belly of the trapezius. A secondary operation was performed to release this specific central band directly, followed by Z-plasty for skin lengthening and contour improvement.

Results: Intraoperatively, a thickened, cord-like fibrotic band was identified within the central trapezius, distinct from the previously operated lower site. Complete transection of the band immediately restored full passive range of motion. At the 6-month follow-up, the head tilt was fully corrected, and the patient achieved a symmetrical neck contour without scar contracture.

Fig. 1. Preoperative Clinical Photograph. A 6-year-old boy presenting with recurrent right-sided torticollis. Despite previous bipolar release of the sternocleidomastoid (SCM) and partial lower trapezius release, persistent right head tilt and restricted left lateral bending are evident. The previously operated SCM area is soft, but a tight band is palpable along the central trapezius.

Fig. 2. Before release: Through a direct incision over the central trapezius (superior to the previous surgical site), a distinct, thick, cord-like fibrotic band (indicated by the arrow) is identified within the muscle belly, causing severe contracture. The SCM was confirmed to be completely released.

Fig. 3. After release: Complete transection of the fibrotic band was performed. The release of the central band immediately resolved the tethering effect, allowing for full passive range of motion of the neck. A Z-plasty design is marked on the overlying skin to lengthen the scar line.

Fig. 4. Postoperative Clinical Photograph. At the 6-month follow-up, the patient demonstrates full, unrestricted range of motion. The persistent head tilt has been fully corrected. The neck contour is symmetrical, and the Z-plasty has successfully prevented scar contracture, resulting in a favorable aesthetic outcome.

Conclusion: In recurrent CMT where the SCM is fully released, the trapezius muscle should be suspected. Surgeons must explore the entire muscle belly, as fibrotic bands can be located centrally rather than at the insertions. Targeted release combined with Z-plasty is effective for achieving both functional and aesthetic success.

EP-037

개두술후 발생된 만성 전두동염과 경막외 농양을 동반한 만성 골수염의 단회 재건술

One stage reconstruction of chronic post-craniotomy osteomyelitis with frontal sinusitis and epidural abscess using dermofat graft obliteration, and immediate titanium mesh cranioplasty

경희대학교병원

김영진, 박준, 강상윤, 범진식★

Purpose : Chronic post-craniotomy osteomyelitis with frontal sinusitis and epidural abscess presents a complex reconstructive challenge. Conventional staged treatment of delayed cranioplasty leaves a skull defect, risks brain injury, and is technically demanding due to scalp-dura adhesions and skin contraction, with additional cost and time burden. To address these limitations, we performed one-stage reconstruction using dermofat graft and titanium mesh cranioplasty.

Methods : Two patients with clinical and radiologic evidence of post-craniotomy osteomyelitis, chronic frontal sinusitis, and epidural abscess, underwent one-stage reconstruction.

Step 1 – Radical debridement : All potential sources of chronic infection were completely removed: fixatives, foreign body granuloma, artificial dura, frontal sinus mucosal lining, and all previously implanted foreign body materials.

Step 2 – Immediate reconstruction : Following debridement, immediate coverage was performed using a dermofat graft combined with titanium mesh cranioplasty.

Dermofat graft: harvested thin and wide to maximize graft survival via the dermal and subdermal plexus; placed dermis-side toward the dura. Serves to reinforce the dura, obliterate epidural dead space, provide frontal sinus obliteration, and restore soft tissue volume.

Titanium mesh: its porous structure allows sufficient vascularization to the underlying dermofat graft while providing structural protection and cranial contour restoration.

Results: Both patients showed well-maintained dermofat grafts and titanium mesh throughout follow-up, with no recurrence of infection or inflammation. . In case 1, facial CT at 1 year postoperatively confirmed stable dermofat. In case 2, follow-up MRI at 2 years confirmed a well-maintained dermofat graft with mild scar contracture at the skin-island portion.

Conclusion: One-stage reconstruction using dermofat graft and immediate titanium mesh cranioplasty proved effective in managing chronic post-craniotomy frontal osteomyelitis with frontal sinusitis and epidural abscess.

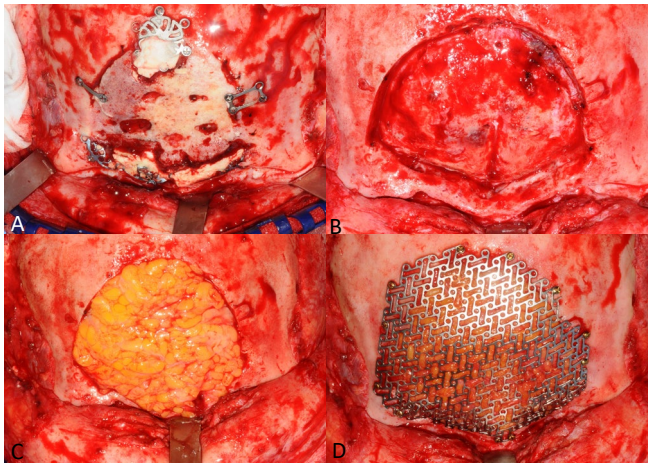

Fig. 1. Intraoperative pictures (A) Infected bone with previously placed fixative materials before debridement (B) Wound bed after total debridement of all infected materials (C) Dermofat graft placement (D) Titanium mesh over the dermofat graft

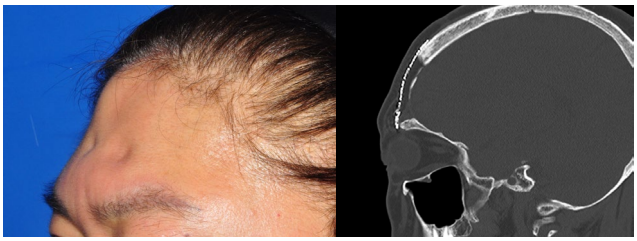

Fig. 2. a 58-year-old woman who developed forehead depression and pain after aneurysmal neck clipping via bifrontal approach. Left: preclinical photograph. Right : postoperative 1 year CT, showing well stable titanium mesh and dermofat graft

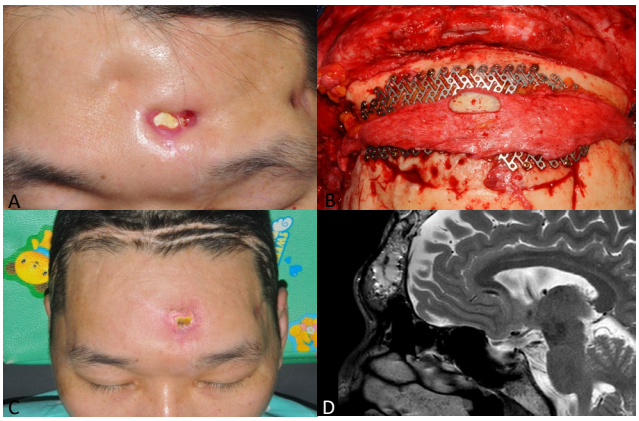

Fig. 3. a 41-year-old man with a history of multiple cranial procedures with forehead fistula. Due to severe skin thinning from repeated surgeries and chronic inflammation, a skin island attached to the dermofat was used for defect closure without an additional flap. (A) Preoperative photo with craniocutaneous fistula. (B) Dermofat graft with skin island (C) Postoperative 2 weeks photo. (D) Postoperative 5 years MRI T2 image, showing showing stable dermofat graft

EP-038

얕은 엉덩 휘돌이 동맥 천공지 피판을 이용하여 재건한 파리-롬베르그 증후군 1례: 11년 추적 관찰

A case of Parry-Romberg syndrome reconstructed with superficial circumflex iliac artery perforator flap: 11 year follow up

고려대학교

이준형, 김덕우★, 유희진, 이태열

Purpose: Parry-Romberg syndrome causes progressive unilateral facial atrophy requiring durable volume restoration. We share our experience of treating Parry-Romberg syndrome using a deepithelialized superficial cicumflex iliac artery perforator flap with 11 year follow up

Methods: A 24 year old female underwent reconstruction at age 13 for severe unilateral facial soft tissue deficiency, resulting in a 25cc volume difference between the right and left cheeks. A 18 x 7 cm SCIP flap was harvested from the right inguinal area and completely deepithelialized (50g). Through a preauricular incision, a supra-SMAS pocket was created for insetting. Microvascular anastomosis was performed to the facial artery and vein. An additional 10g of remnant tissue was used as a composite graft for philtral correction

Results: Flap survival was complete without vascular compromise or donor-site morbidity. Immediate postoperative symmetry was achieved, with a significant reduction in the volume difference. At 11-year follow-up, the reconstructed side maintained stable volume without significant atrophy or need for major revision

Conclusion: Deepithelialized superficial cicumflex iliac artery perforator flap provides reliable and durable long term volume restoration in adolescent patients with Parry-Romberg syndrome, demonstrating stable outcomes even with significant preoperative volume discrepancies

Fig 1. Preoprative photo

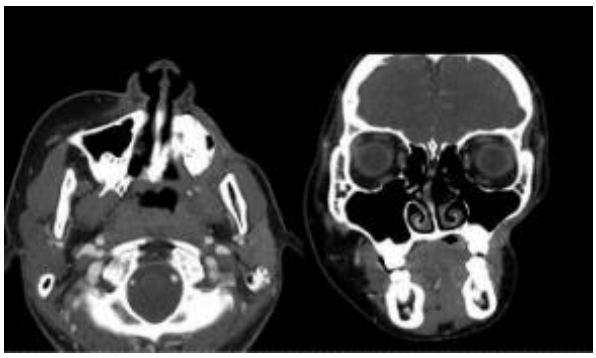

Fig 2. Preoperative CT

Fig 3. Intraoperative photo showing deepithelialized SCIP flap

Fig 4. Postoperatvie photo

EP-039

양측성 구순비변형에서 비중격확장이식편의 효과 : 비형태 변화에 대한 분석

(Effect of Septal Extension Graft in Bilateral Cleft Lip Nose Deformity Correction : Analysis of Nasal Morphologic Changes)

부산대학교병원 성형외과학교실

안주헌, 배용찬★

Purpose: Tip refinement in bilateral cleft lip nasal deformity remains surgically challenging, particularly in achieving stable projection and rotation. This study aimed to quantitatively evaluate morphologic changes following septal extension graft (SEG) in patients undergoing secondary cleft rhinoplasty using standardized two-dimensional photogrammetric analysis.

Methods: Seventeen patients with bilateral cleft lip nasal deformity who underwent secondary rhinoplasty with septal extension graft (SEG) and had a minimum follow-up of 6 months were retrospectively analyzed. Standardized frontal, lateral, and basal photographs were obtained under consistent positioning.
Objective morphometric parameters were measured using two-dimensional image-based analysis (ImageJ software), based on predefined anatomical landmarks.

- **Tip Deviation (TD, frontal view):**
  The angle between (1) a perpendicular line to the horizontal line connecting the bilateral endocanthia (En–En) and (2) a line connecting the midpoint of En–En to the pronasale (Prn). Smaller angles indicate less deviation from the facial midline.

- **Goode Ratio (lateral view):**
  Defined as the ratio of nasal tip projection to nasal length. Nasal length was measured as the distance from nasion (N) to pronasale (Prn). Tip projection was defined as the horizontal distance from pronasale (Prn) to a vertical line drawn through the alar crease (Ac).

- **Columellar–Labial Angle (CLA, lateral view):**
  The angle formed between the columella line (connecting subnasale [Sn] to columella point [C]) and the upper lip line (Sn to labrale superius [Ls]). Larger angles indicate increased tip rotation.

- **Columella Proportion Index (CPI, basal view):**
  Defined as the ratio of columellar length (Sn–C) to total nasal tip height (Sn–Prn) in the basal view.

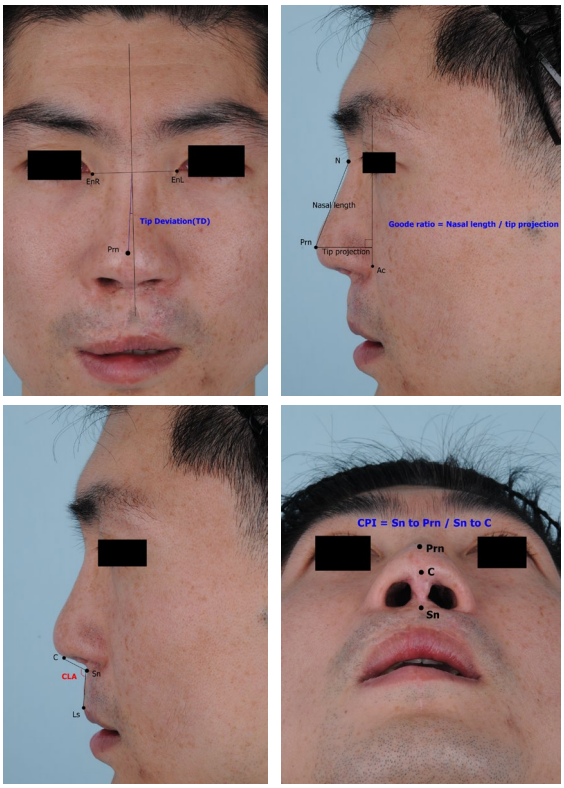

Fig1. Clinical example images with measurement markings: tip deviation (TD, upper left), Goode ratio (upper right), columellar–labial angle (CLA, lower left), and columella proportion index (CPI, lower right).

Results:

Parameter	Preop	Postop	p-value
TD (°)	2.96 ± 1.69	2.00 ± 2.06	0.138
Goode ratio	0.49 ± 0.08	0.58 ± 0.08	< 0.001
CLA (°)	88.64 ± 13.17	99.17 ± 9.95	0.006
CPI	0.49 ± 0.09	0.54 ± 0.08	0.073

Table 1. Preoperative and postoperative changes in morphometric parameters following septal extension graft.

Conclusion: Secondary cleft rhinoplasty with septal extension graft significantly corrected underprojection and insufficient rotation of the nasal tip in bilateral cleft lip deformity.
Postoperative morphometric parameters moved toward normal aesthetic proportions, highlighting the role of SEG in achieving predictable structural control of the cleft nasal tip.

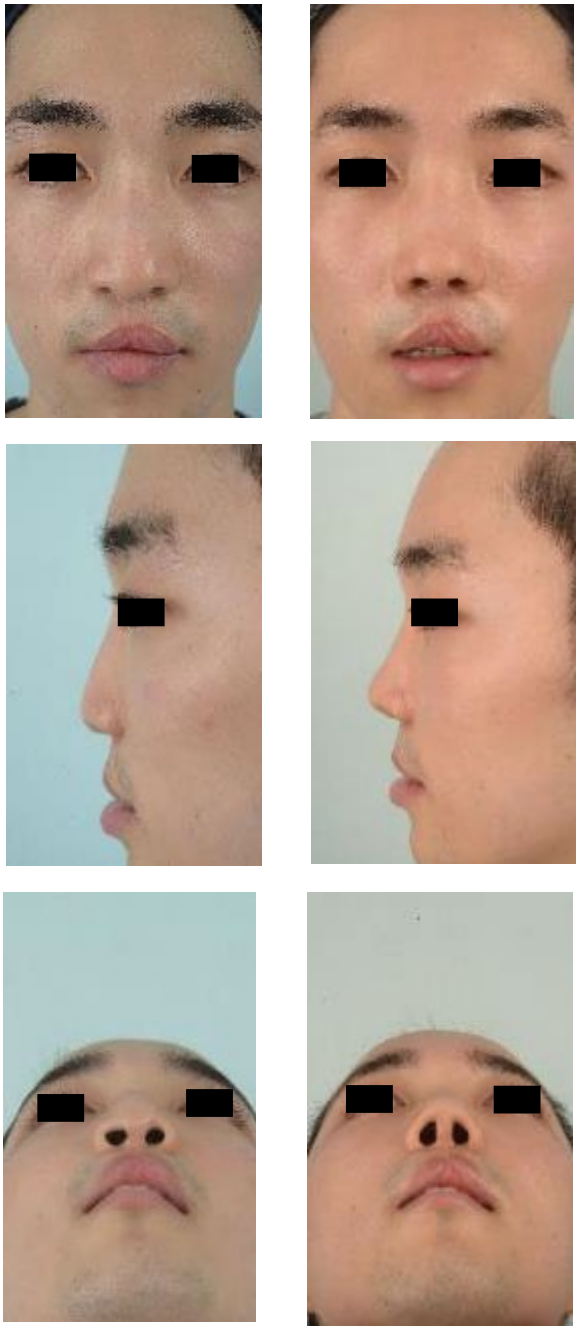

Fig2. (**Case 1)** preoperative (left) and postoperative (right, 6 months) photographs of a patient with bilateral cleft lip nasal deformity. Frontal, lateral, and basal views (top to bottom) demonstrate improved nasal tip projection and rotation following septal extension graft.

Fig3. (**Case 2)** preoperative (left) and postoperative (right, 6 months) photographs of a patient with bilateral cleft lip nasal deformity. Frontal, lateral, and basal views (top to bottom) demonstrate improved nasal tip projection and rotation following septal extension graft.

EP-040

Orbicularis oculi myocutaneous flap과 결합된 다중 재건 기법의 임상적 유용성과 기능적 결과

(Clinical Utility and Functional Outcomes of Multimodal Reconstructive Techniques Integrated with Orbicularis Oculi Myocutaneous Flaps)

부산대학교

정희태, 배용찬★

Purpose: The orbicularis oculi myocutaneous (OOMC) flap is a well-established option for periocular reconstruction due to its reliable vascularity, thin profile, and excellent tissue match.

- However, its application is often limited by restricted flap size and mobility.
- This study aimed to evaluate the clinical utility and functional outcomes of OOMC flaps in combination with adjunctive reconstructive techniques for complex periocular defects.

Methods: A retrospective review was conducted of 65 patients with 79 periocular defects who underwent reconstruction using a total of 90 OOMC flaps over a 20-year period.

- The primary outcomes included the frequency and types of adjunctive procedures, postoperative complications, and functional outcomes.

Results: A total of 90 OOMC flaps were used for 79 defects

- Multimodal reconstruction was required in **35 defects (44.3%)** to achieve complete closure.
- Adjunctive techniques included skin grafts (n=16), secondary OOMC flaps (n=13), composite grafts (n=6), nasolabial flaps (n=5), forehead flaps (n=5), and cheek rotation flaps (n=1).
- Eyelid function and structural integrity were preserved in all cases. Complications were rare and included one case of tumor recurrence, one entropion, and one partial flap necrosis.

Fig. 1. (A) Preoperative photograph after MMS showing the post-excisional defect on medial canthal region and upper and lower eyelid, Rt. (B) Immediate postoperative photography following reconstruction with an OOMC flap and paramedian forehead flap. (C) Postoperative photograph at 18 months showing a satisfactory result.

Fig. 2. (A) Preoperative photograph after MMS showing the post-excisional defect on lateral side of lower eyelid, Lt. (B) Immediate postoperative photograph following reconstruction with an OOMC flap and a cheek rotation flap. (C) Postoperative photograph at 12 months showing a satisfactory result.

Conclusion: OOMC flaps provide reliable outcomes in periocular reconstruction.

- However, complex defects frequently necessitate a **multimodal reconstructive strategy**.
- The combination of OOMC flaps with adjunctive reconstructive techniques allows for effective defect coverage while maintaining functional integrity and a low complication profile.
- These findings support the use of a tailored, multimodal strategy in managing complex periocular defects.

EP-041

골화성 모기질종 증례보고 및 발병기전에 대한 새로운 가설

(Ossifying Pilomatricoma and a Novel Hypothesis for Its Pathogenesis)

강원대학교 성형외과

편효준, 이상열★

Purpose: Pilomatricoma is a benign skin appendageal tumor derived from hair follicle matrix cells that commonly affects the head, neck, and upper extremities in the pediatric population. Since the original tumor description, diverse variants have been reported in the literature. Among its variants, ossifying pilomatricoma, characterized by florid osseous metaplasia, is recognized as a distinct entity. However, its pathogenesis remains unclear. This study presents a rare case of ossifying pilomatricoma and proposes a novel hypothesis regarding its pathogenesis based on a comprehensive literature review.

Methods: A 14-year-old boy presented with a 5-year history of an asymptomatic protruding mass in the right preauricular region. Physical examination revealed a firm, dome-shaped mass measuring 1.5 cm in diameter, adherent to the overlying skin without skin changes. The lesion was completely excised under local anesthesia, and the specimen was submitted for histopathological examination.

Results: Gross examination revealed a reddish-brown, well-circumscribed mass with a stony hard consistency. Histopathological examination demonstrated a nodular tumor with extensive osseous metaplasia, composed predominantly of shadow cell clusters and laminated trabecular bone without basaloid components. The stroma exhibited marked ossification with osteoclast-like multinucleated giant cells. Bone marrow–like structures containing mononuclear cells and fibrofatty tissue were observed within the bony trabeculae. Immunohistochemical staining showed positivity for anti-myeloperoxidase antibodies in these cells. Based on these findings, the lesion was diagnosed as ossifying pilomatricoma. No recurrence or complications were observed during the 6-month follow-up period.

Conclusion: We propose that metaplastic ossification in ossifying pilomatricoma represents a form of foreign body reaction to keratinous materials containing shadow cells in long-standing lesions, serving as a walling-off mechanism to protect surrounding tissues. Further studies are required to elucidate the exact pathogenesis of this process.

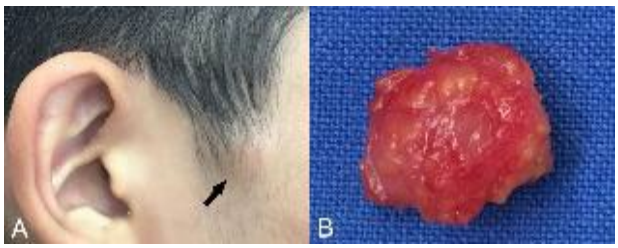

Figure 1.
(A) A dome-shaped mass in the preauricular region (arrow).
(B) A gross specimen shows a reddish-brown colored globular mass covered with fibroadipose tissue.

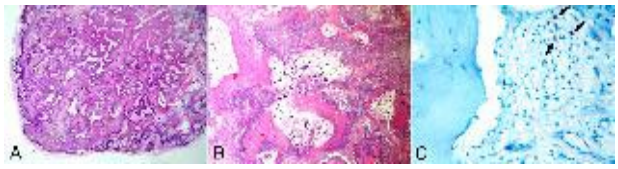

Figure 2.
(A) Histopathological study shows a well-circumscribed nodular tumor with extensive ossification (H&E, ×15).

(B) Histopathological study shows shadow cell clusters, laminated trabecular bones, osteoclast-like multinucleated giant cells, and bone marrow structures enclosed by bony trabeculae (H&E, ×100).

(C) Immunohistochemical study shows a few cells (arrows) positive for antimyeloperoxidase antibodies within the bone marrow structure (400 ×).

EP-042

소아에서 Wharton관 타석증에 의해 발생한 피부 누공: 증례 보고

(Cutaneous Fistula Secondary to Wharton's Duct Sialolithiasis in an Adolescent: A Case Report)

건양대학교병원

석상일, 고인창★, 임수연

Purpose: Submandibular sialolithiasis is rare in the pediatric population, accounting for approximately 2–3% of all reported cases. While glandular inflammation is common, extension to the overlying skin is rarely reported. We report a rare pediatric case of Wharton's duct sialolithiasis accompanied by submandibular gland inflammation with cutaneous involvement requiring surgical management.

Methods: A 15-year-old boy presented with a chronic oval, reddish, elevated lesion (2.0 × 1.5 cm) with a central opening and overgranulation tissue in the right submandibular area that had persisted for four months. The patient had previously undergone incision and drainage at another hospital. Computed tomography (CT) revealed a 10-mm sialolith located in the distal Wharton's duct with associated submandibular gland atrophy and surrounding inflammatory changes. A cutaneous inflammatory lesion measuring approximately 34 mm was also identified. Excision of submandibular gland and fistulectomy were performed.

Results: The fistulous tract and affected submandibular gland were successfully removed. Histopathologic examination demonstrated chronic inflammatory changes consistent with sialolithiasis. At four-month follow-up, the patient showed complete resolution of symptoms with satisfactory wound healing and no evidence of recurrence.

Conclusion: Pediatric sialolithiasis is uncommon and typically presents with localized glandular symptoms. Cutaneous fistula may occur as a rare complication of chronic sialolithiasis. Accurate identification of the underlying cause using imaging studies such as CT is essential, and definitive treatment requires elimination of the source of infection.

Fig 1. Preoperative photograph showing an oval, reddish, elevated mass like lesion in the right submandibular region. Open wound and peri-lesional overgranulation tissue is noted

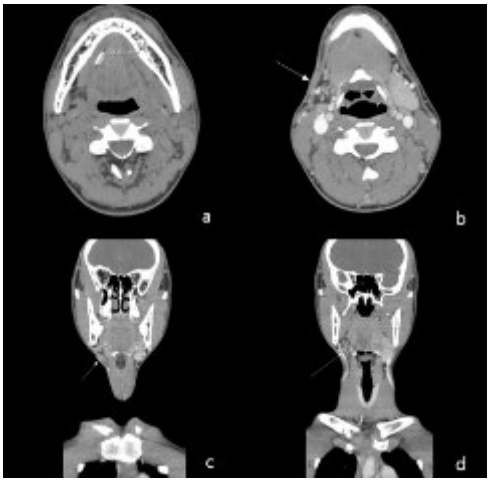

Fig 2. (a) Hyperdense sialolithiasis measuring approximately 10.8 mm located in the distal Wharton's duct. (b) Inflammatory changes and soft tissue swelling are observed around the right submandibular gland, consistent with chronic sialadenitis. (c) Inflammatory lesion measuring approximately 34 mm in the right submandibular region, extending toward the overlying skin. (d) Atrophy of the right submandibular gland associated with obstructive sialolithiasis.

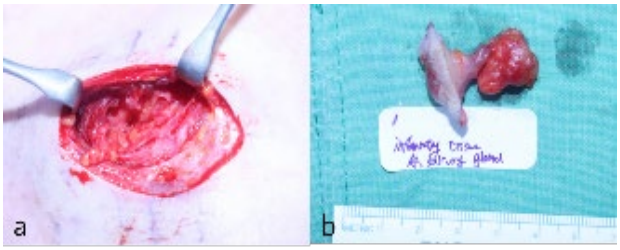

Fig 3. Submandibular gland with perilesional inflammation excision was done. (a) Intraoperative clinical photo. (b) A fistulous tract connecting the submandibular gland to the overlying skin was identified.

Fig 4. The patient shows a well-healed surgical site in the right submandibular area following submandibular gland excision and fistulectomy. The previous cutaneous inflammatory lesion and fistulous opening have completely resolved, leaving a linear postoperative scar without signs of recurrent inflammation.

EP-043

악성 종양으로 의심되었던 경부 거대 평활근종 케이스 보고

(Giant Leiomyoma of the Cervical Paravertebral Space Mimicking a Malignant Soft Tissue Tumor: A Case Report)

가톨릭대학교 여의도성모병원

이윤재★

Purpose: Leiomyoma is a benign smooth muscle tumor most commonly arising in the uterus and extremities. Occurrence in the deep cervical space is extremely rare and may mimic malignant soft tissue tumors on imaging studies.

Methods: A 44-year-old woman presented with a three-month history of a right-sided neck mass accompanied by mild discomfort. MRI demonstrated an approximately 11-cm mass with T1 iso-signal intensity relative to muscle, heterogeneously high signal intensity on T2-weighted images, and strong homogeneous enhancement, displacing the right brachial plexus anteriorly. Radiologic differential diagnoses included leiomyoma and low-grade leiomyosarcoma.

Figure.1 Preoperative clinical photograph showing a prominent swelling in the right posterior cervical region (red circle), corresponding to a large paravertebral mass.

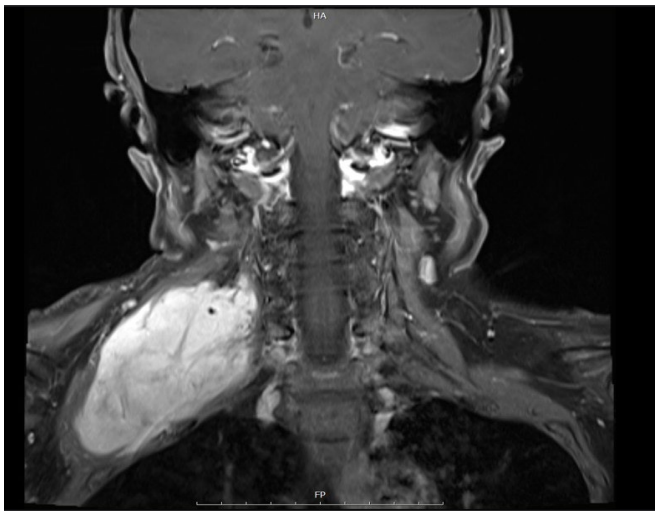

Figure 2. Coronal contrast-enhanced MRI showing a large enhancing mass in the right cervical paravertebral space, displacing adjacent structures and extending along the posterior neck.

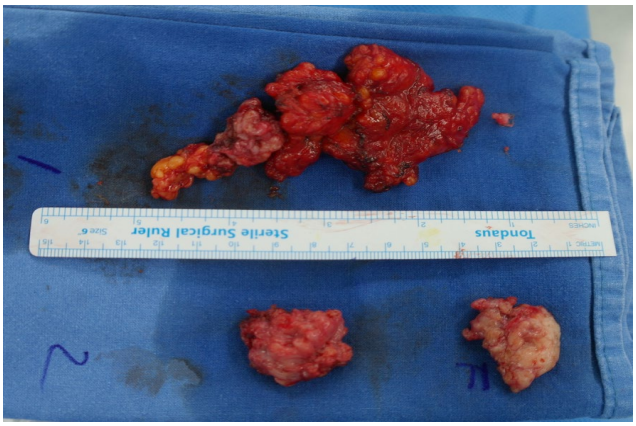

Figure 3. Gross photograph of the excised soft tissue mass.

Results: Ultrasound-guided core needle biopsy was performed preoperatively, suggesting leiomyoma. Intraoperatively, the tumor was adherent to surrounding soft tissues within the paravertebral space, making dissection challenging. Histopathologic examination confirmed leiomyoma. Immunohistochemical staining demonstrated positivity for smooth muscle actin, while S-100, CD117, CD34, and desmin were negative. The Ki-67 proliferation index was low (1%), supporting the benign nature of the lesion.

Conclusion: Deep cervical Leiomyoma is a rare benign tumor that may closely mimic malignant soft tissue tumors on radiologic evaluation. Complete surgical excision is generally considered the treatment of choice and is usually curative. However, in deep neck locations such as the paravertebral space, complete resection may be technically challenging due to the proximity of critical neurovascular structures including the brachial plexus and major vessels. In such cases, subtotal resection may be considered to preserve neurological function and prevent surgical morbidity. Therefore, careful postoperative surveillance with periodic imaging can be an acceptable management strategy when complete resection is not feasible.

EP-044

MRI에서 지방육종이 의심된 측두근 내 재발성 거대 지방종: 증례 보고

(Recurrent Large Intramuscular Lipoma of the Temporalis Muscle Mimicking Liposarcoma on MRI: A Case Report)

연세대학교 원주의과대학
원주세브란스기독병원
성형외과학 교실

오창훈, 전우상, 김지예, 김석원★

Purpose: Intramuscular lipoma has been reported to be rare, may infiltrate skeletal muscle, and can recur after incomplete excision. MRI findings may overlap with those of atypical lipomatous tumor(ALT) or well-differentiated liposarcoma (WDL). We present a recurrent temporalis intramuscular lipoma radiologically mimicking a malignant lipomatous tumor.

Methods: A 76-year-old woman presented with a progressively enlarging right temporal mass. She had undergone prior lipoma excision in 2017. Contrast-enhanced MRI revealed multilobulated T1-hyperintense fatty masses with heterogeneous enhancement within the anterior temporalis muscle. The largest lesion measured 9 × 9 cm, raising suspicion for malignancy.

Results: Through a preauricular incision extended along the previous scar, nerve-sparing complete excision was performed. The tumor was located beneath the deep temporal fascia and interdigitated with temporalis muscle fibers. Intraoperative frozen section suggested a benign lipomatous lesion. Final histopathology demonstrated mature adipose tissue infiltrating skeletal muscle without lipoblasts or nuclear atypia, excluding ALT or WDL. At 3-month follow-up, there was no limitation of mastication, contour deformity, or temporal branch dysfunction.

Conclusion: Recurrent deep temporal intramuscular lipoma may mimic malignant lipomatous tumors on MRI. When imaging is equivocal, definitive histopathologic evaluation with selective frozen section is critical. Adequate exposure and a nerve-sparing approach allow safe complete resection. Long-term surveillance may be warranted, given the potential for recurrence or multifocal disease after incomplete excision.

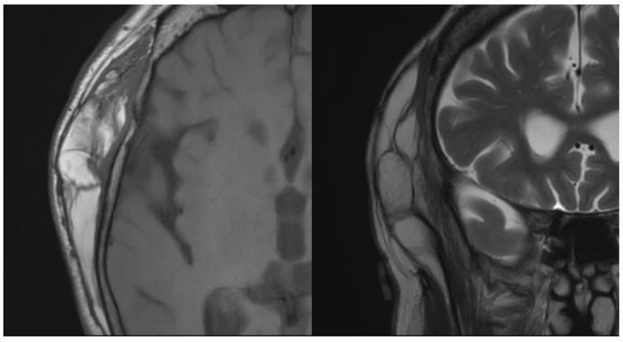

(A) (B)

Fig. 1. Preoperative MRI demonstrating a deep temporal lipomatous mass. (A) T1-weighted image. (B) T2-weighted image

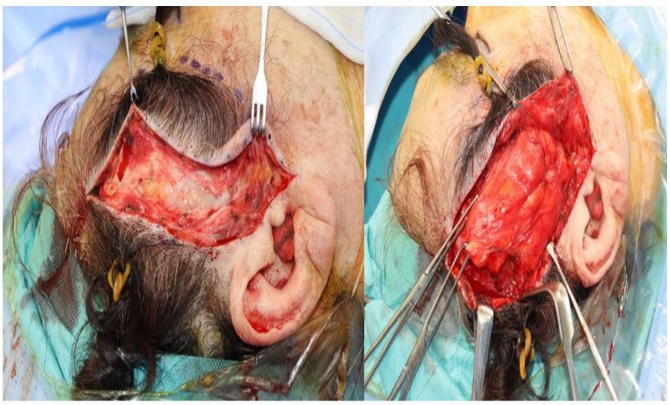

(A) (B)

Fig. 2. Operative steps for excision of a deep temporal intramuscular lipoma: (A) incision design, (B) tumor dissection

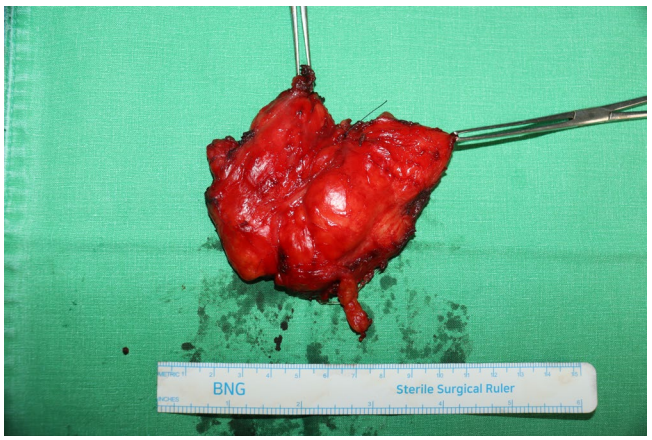

Fig. 3. Gross specimen of the excised temporalis intramuscular lipoma (multilobulated mass).

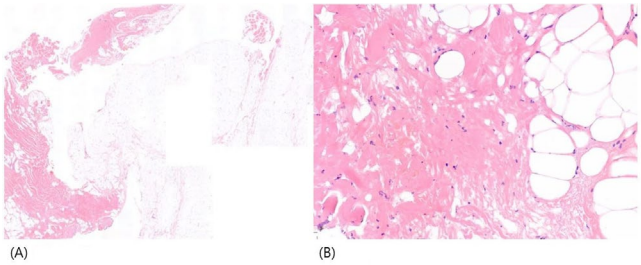

Fig. 4. Histopathology of intramuscular lipoma. (A) Low-power (H&E, ×40). (B) High-power showing mature adipocytes without atypia (H&E, ×200).

EP-045

다발성 기저세포암 진단의 경각심: 귀 뒤 및 목 부위의 광범위한 침범 사례 보고

(Diagnostic Vigilance in Multi-focal Basal Cell Carcinoma: A Case Report of Extensive Postauricular and Neck Involvement)

순천향대 구미병원
배진오, 위서영★

Purpose: Basal cell carcinoma (BCC) typically presents as a solitary, slow-growing lesion. However, atypical multi-focal presentations can lead to diagnostic delays or inadequate management. We report a case of multi-focal BCC involving the postauricular regions, emphasizing the necessity of thorough evaluation even when lesions appear clinically discrete.

Methods: A 77-year-old female presented with multiple masses on the postauricular regions persisting for 30 years. Due to their hyperkeratotic surface and clustered distribution, a provisional diagnosis of verruca vulgaris was initially made. (Fig. 1) Diagnostic evaluation began with an initial 0.6 x 0.5 cm excisional biopsy. Following the histopathologic confirmation of BCC, additional specimens (2.5 x 0.5 cm) were obtained from the postauricular area 3 weeks later to assess the multi-centric distribution (Fig. 2). Under local anesthesia, the lesions were surgically excised for pathologic analysis.

Results: Histopathological analysis confirmed BCC in postauricular regions. Microscopic evaluation revealed characteristic nests of basaloid cells with peripheral palisading and peritumoral clefting (Fig. 3). The tumor exhibited a fragmented distribution with significant skip lesions. Complete wide excision was achieved with clear margins. No recurrence was observed during the 24-month follow-up period (Fig. 4).

Conclusions: Long-standing BCC can manifest as multiple separated nodules, mimicking benign multicentric conditions. When managing multiple skin adnexal masses, clinicians must maintain a high index of suspicion for malignancy. Meticulous preoperative mapping and comprehensive biopsy are essential to ensure oncological safety and prevent recurrence.

Fig. 1 Multiple, discrete, and erythematous nodules, each approximately 0.5 x 0.5 cm

Fig 2. The excised specimen from the postauricular area measures approximately 2.5 x 0.5 cm

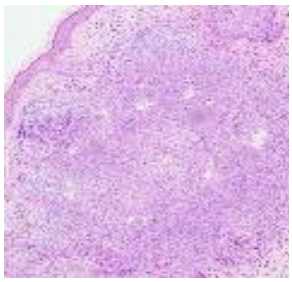

Fig 3. Histopathologic findings of BCC. H&E staining reveals basaloid cell nests with characteristic peripheral palisading and peritumoral clefting.

Fig 4. Postoperative clinical appearance at 24-month follow-up.

EP-046

조절되지 않는 당뇨병 환자에서 비강형 NK/T세포 림프종이 안면 봉와직염으로 오진된 사례

Extranodal NK/T-Cell Lymphoma, Nasal Type, Misdiagnosed as Facial Cellulitis in a Patient with Uncontrolled Diabetes Mellitus: A Case Report

순천향대학교부속
천안병원 성형외과

김민욱, 김준혁, 최환준, 이다운, 변제연★

Purpose: Extranodal NK/T-cell lymphoma (ENKTL), nasal type, is a rare and aggressive lymphoma that may initially mimic common inflammatory conditions. We report a case of ENKTL misdiagnosed as facial cellulitis in a patient with uncontrolled diabetes and highlight the importance of early biopsy and multidisciplinary treatment.

Methods: A 56-year-old man with uncontrolled diabetes presented with painful edema, heat sensation, and necrotic change involving the right cheek and nasal ala, initially diagnosed as facial cellulitis (Figure 1). Despite intensive intravenous antibiotic therapy, the lesion progressed. Subsequent nasal cavity biopsy confirmed ENKTL, nasal type. The patient then underwent concurrent chemoradiotherapy, followed by radical resection of the right midface including the zygoma, cheek soft tissue, and nasal ala. The postablative defect before reconstruction is shown in (Figure 2), and intraoperative defect coverage with flap reconstruction is shown in (Figure 3).

Results: The lesion did not respond to standard treatment for cellulitis, and biopsy established the correct diagnosis of ENKTL. After chemoradiotherapy and multidisciplinary surgical salvage, immediate reconstruction was successfully performed by the plastic surgery team. The patient showed stable postoperative recovery with satisfactory flap survival and facial contour restoration (Figure 4). At 6-month follow-up, there was no evidence of local recurrence or distant metastasis.

Conclusion: ENKTL may be masked by secondary infection and may closely resemble facial cellulitis, particularly in immunocompromised patients such as those with uncontrolled diabetes. When facial inflammatory lesions are refractory to antibiotics or accompanied by progressive necrosis, prompt deep biopsy should be considered. Early diagnosis and coordinated multidisciplinary treatment are essential for oncologic control and successful reconstruction.

Figure 1. Preoperative frontal and oblique photographs showing diffuse swelling, erythema, and necrotic change involving the right cheek, nasal ala, and perinasal region, initially suspected to represent facial cellulitis..

Figure 2. Pre-reconstructive lateral photograph showing the right alar and perinasal defect after disease progression and ablative treatment.

EP-046

Figure 3. Intraoperative photographs showing the postablative right midfacial defect and immediate flap inset for defect coverage.

Figure 4. Immediate postoperative frontal and oblique photographs showing external appearance after reconstruction with satisfactory contour restoration of the right midface and nasal region..

EP-047

악하선에서 기원한 거대 경부 메르켈세포암종 증례 보고

(A rare case of Huge size Merkel cell Carcinoma on neck originated from submandibular gland)

원광대학교

이량우, **나영천**★

Purpose: Merkel cell carcinoma(MCC) is a highly aggressive cutaneous neuroendocrine carcinoma, with a three-year mortality rate of approximately 33%, more than twice that of melanoma. Classically, MCC presents as a rapidly enlarging, firm, violaceous nodule on sun-exposed skin and extends into deeper tissues. However, MCC originating within the submandibular region without cutaneous involvement is extremely uncommon. This report describes the clinical presentation of an unusual case of presumed primary submandibular gland MCC.

Methods: An 86-year-old man presented with a rapidly enlarging, tender mass on the right anterior neck that had developed over three months. A core needle biopsy confirmed MCC. Magnetic resonance imaging(MRI) showed a 7.2×4.0×5.5cm homogeneous enhancing mass with one indeterminate right level II lymph node, warranting further assessment.

Results: The patient underwent wide local excision with right cervical lymph node biopsy under general anesthesia. Frozen section analysis revealed clear margins and no nodal metastasis. Finally, sentinel lymph node biopsy and neck lymph node levels I–IV showed no metastatic disease.

Conclusion: Clinicians should consider MCC in the differential diagnosis of rapidly enlarging cervical masses, even when no skin lesion is present. Prompt biopsy, appropriate surgical management, and adjuvant radiotherapy are essential components of treatment and may improve outcomes in this highly aggressive tumor.

Fig. 1. Preoperative clinical photograph without any skin lesion.

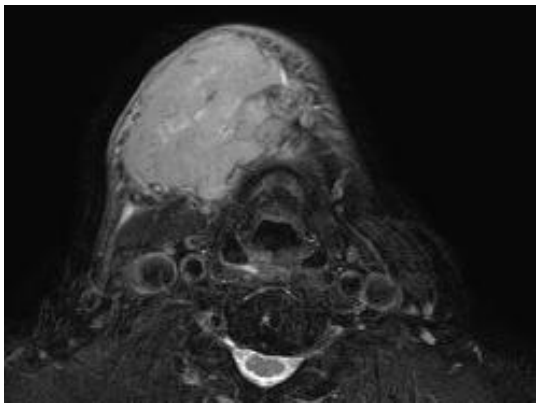

Fig. 2. Axial image of MRI.

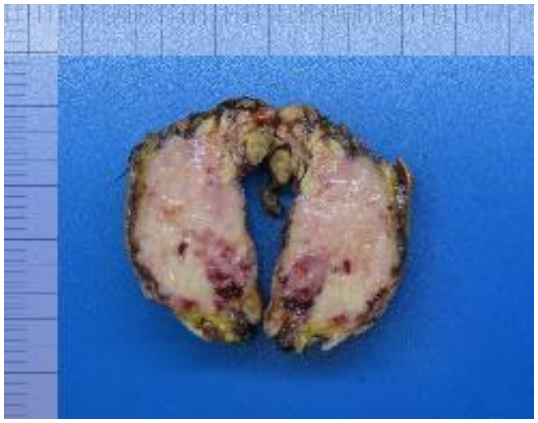

Fig. 3. Gross photo of the mass.

EP-048

누점 플러그 삽입술 후발생한 누낭염과 연관된 재발성 내안각 농양 증례 보고

Recurrent Medial Canthal Abscess Associated with Dacryocystitis Following Punctal Plug Insertions: A Case Report

가톨릭대학교 의과대학
성형외과학교실

김초롱, 전대원, 이중호★

Purpose: Prior ophthalmologic procedures are often radiologically occult and may not be recalled by patients; thus, without thorough history taking, they can be easily missed during evaluation. However, as such interventions can cause recurrent periorbital abscesses, evaluating this history is essential for plastic surgeons commonly encountering facial abscesses. We report a case of recurrent abscesses caused by migrated punctal plugs.

Methods: A 53-year-old female presented with a left medial canthal abscess (Figure 1). Five months prior, the abscess was treated with incision and drainage (I&D) and oral amoxicillin/clavulanate for seven days. However, she returned with excruciating pain and palpable fluctuation. Facial CT and MRI revealed an approximately 2x2 cm abscess pocket in the medial canthal area and a 1.5 cm dacryocele, with no other abnormal findings, including foreign bodies (Figure 2). Further history taking revealed that she had undergone repeated punctal plug insertions for the treatment of dry eye syndrome one and three years prior to her visit.

Results: An I&D was performed, and a wound culture isolated Escherichia coli. The infectious lesion resolved with intravenous antibiotics (Figure 3). After resolution of the infection, she underwent dacryocystorhinostomy by an ophthalmologist.

Conclusion: Migrated punctal plugs can trigger recurrent infections in the medial canthal area. In this case, plug-induced nasolacrimal obstruction and stasis likely predisposed the patient to dacryocystitis. Furthermore, the resulting epiphora and subsequent frequent eye-rubbing are thought to have triggered recurrent infection by enteric bacteria. To prevent recurrent eyelid infection, plastic surgeons must investigate prior ophthalmologic history, especially when imaging is negative.

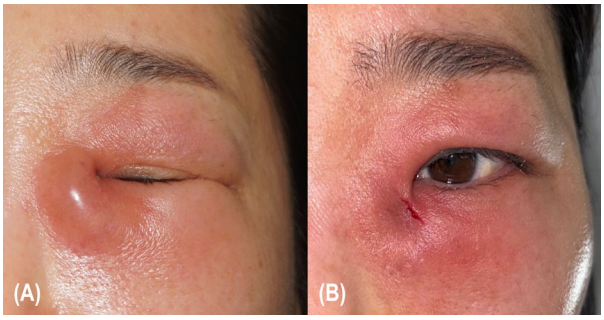

Fig. 1. Clinical presentation of the recurrent medial canthal abscess. (A) At the time of re-presentation, the patient exhibited aggravated pain and palpable fluctuation at the left medial canthal area. (B) Immediate appearance after surgical incision and drainage (I&D).

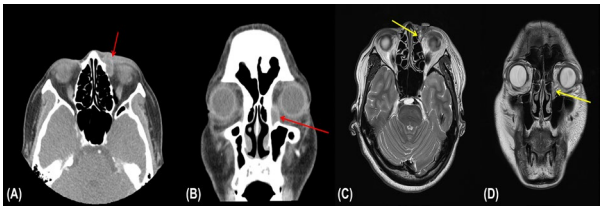

Fig. 2. Radiological findings of the left medial canthal area. (A, B) Contrast-enhanced facial CT (axial and coronal scans) reveals a 1.5 cm dacryocele with peripheral thin enhancement (red arrows), suggesting dacryocystitis. (C, D) T2-weighted face MRI (axial and coronal scans) shows a residual small abscess and persistent nasolacrimal duct obstruction (yellow arrows). Diffuse high-signal intensity in the periorbital and orbitomaxillary areas indicates extensive combined cellulitis.

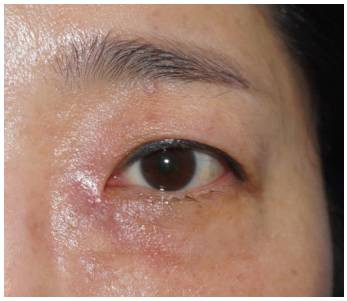

Fig. 3. Postoperative clinical progress. Complete resolution of the lesion at the final follow-up, showing successful healing without residual inflammatory symptoms.

EP-049

표피낭종으로 오인된 이개전부의 염증성 근섬유아세포종: 드문 증례 보고

(Preauricular Inflammatory Myofibroblastic Tumor(IMT) Mimicking an Epidermal Cyst: A Rare Case Report)

가천대학교

손희준, 차진한★

Purpose: Inflammatory myofibroblastic tumor (IMT) is a rare intermediate-grade mesenchymal tumor that most commonly arises in the lung or abdominopelvic cavity. Occurrence in the facial soft tissue is extremely uncommon and may mimic benign lesions such as epidermal cysts. We report a rare case of preauricular IMT initially misdiagnosed as an epidermal cyst and discuss its clinicopathologic features and prognosis.

Methods: A 37-year-old man presented with a slowly growing subcutaneous mass in the right preauricular area. Preoperative computed tomography and ultrasonography performed at another hospital suggested an epidermal cyst. Surgical mass excision was performed for diagnostic and therapeutic purposes, and the wound was closed with bilateral advancement flap.

Results: The excised mass measured 2.3 × 1.6 × 1.3 cm. Histopathologic examination confirmed inflammatory myofibroblastic tumor composed of spindle-shaped myofibroblastic cells with inflammatory cell infiltration. Immunohistochemistry demonstrated ALK positivity, supporting the diagnosis of IMT, while S-100 and desmin were negative. CD34 positivity was observed in vascular structures, consistent with reactive vascular proliferation. Follow-up CT performed 1 month after surgery demonstrated complete removal of the lesion, and no recurrence has been observed.

Conclusion: In this study, we introduce a rare case of inflammatory myofibroblastic tumor of the preauricular region, an uncommon location for this tumor. Although IMT generally shows low metastatic potential, local recurrence has been reported; therefore, long-term follow-up is recommended. After consultation with the oncology department, no additional treatment or imaging was required. The patient remains under surveillance without evidence of recurrence.

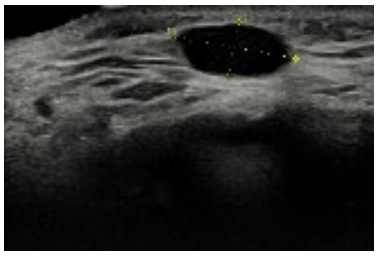

(A)

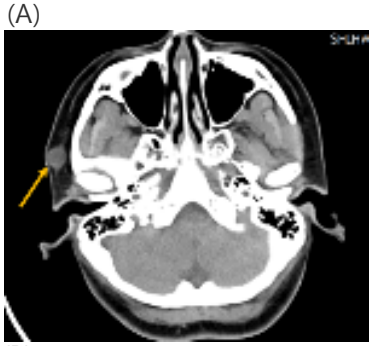

(B)

Fig. 1. Preoperative imaging of the right retroauricular mass. (A) Ultrasonography showing a well-defined subcutaneous lesion initially suspected as an epidermal cyst. (B) Computed tomography demonstrating a localized soft tissue mass in the right retroauricular region.

(A)

(B)

Fig. 2. (A) Preoperative. A 1.0cm-sized bulging nodule on right preauricular area. (B) Postoperative. a round shape defect was closed by bilateral advancement flap.

EP-050

뺨에 발생한 피부염증 병변으로 오인된 치아유래 피부 누공 증례보고

(Odontogenic cutaneous fistula on cheek mimicking dermatologic inflammatory lesion: A case report)

중앙대학교 광명병원

배태희★, 김우주

Purpose: Odontogenic cutaneous fistulas (OCF) are frequently misdiagnosed due to their clinical resemblance to common dermatological lesions. These lesions originate from chronic dental infections that track through the bone and soft tissue to the skin surface. Early identification and elimination of the dental source are critical for successful treatment.

Methods: A 54-year-old female patient presented with a persistent, discharging erythematous nodule on her cheek.Despite previous dermatological treatments, the lesion recurred. Radiographic evaluation revealed a periapical abscess associated with a mandibular 2nd molar teeth, confirming a diagnosis of odontogenic cutaneous fistula.
The causative tooth was surgically extracted to remove the primary source of infection. Following the resolution of the inflammatory phase, the remaining cutaneous defect and tethered scar tissue were excised. To achieve an aesthetically pleasing result and restore the facial contour, reconstruction was performed using a local transposition flap.

Results: The wound healed well and no recurrence was observed.

Conclusion: A high index of suspicion for dental etiology is essential when evaluating chronic facial lesions. This case demonstrates that the combination of definitive dental treatment (extraction) and plastic reconstructive surgery (local flap coverage) provides an excellent functional and cosmetic outcome for patients with long-standing odontogenic fistula.

Fig.1. Preoperative photograph

Fig.2. CBCT image shows radiolucent lesion on right 2nd molar teeth of mandible

Fig.3. Intraoperative photograph

Fig.4. Immediate postoperative photograph

EP-051

안와 주변 혈종의 초기 평가 및 관리의 중요성: 전두분지 신경 압박 사례 보고

(Critical Importance of Initial Evaluation and Management of Periorbital Hematoma: A Case of Frontal Branch Nerve Compression)

순천향대 구미병원
배진오, 위서영★

Purpose: Hematomas are common findings in facial trauma. If not appropriately managed, they may lead to complications such as soft tissue infection or necrosis and therefore often require prompt evacuation. In regions where critical neural structures are present, persistent hematomas may also cause nerve compression resulting in functional palsy. We report this case to emphasize the importance of early hematoma evacuation to minimize the risk of nerve injury.

Methods: A 61-year-old female presented with frontal branch palsy and a 3.0 x 3.0 cm supraorbital hematoma, 10 days after a slip-down injury. Despite an initial local clinic visit, the hematoma remained unevacuated. CT imaging confirmed an 18.32 x 22.38 mm subcutaneous hematoma (Fig. 1). Under local anesthesia, incision and drainage were performed; intraoperative findings confirmed direct compression of the frontal branch by the organized hematoma (Fig. 2).

Results: Approximately 4cc of organized hematoma was evacuated, and the extensive soft tissue swelling gradually subsided during a 5-day hospitalization. However, at the one-month follow-up evaluation, the patient exhibited persistent ptosis and a loss of brow elevation on the left side (Fig. 3). The 10-day delay in initial treatment likely resulted in prolonged compressive neuropraxia or ischemic injury to the frontal branch. No other complications, such as infection or skin necrosis, were observed.

Conclusion: A persistent hematoma can continuously compress adjacent nerves and potentially result in neural injury. Therefore, early recognition and prompt evacuation are essential to minimize nerve damage, and clinicians should maintain careful vigilance to avoid overlooking hematomas in the supraorbital region.

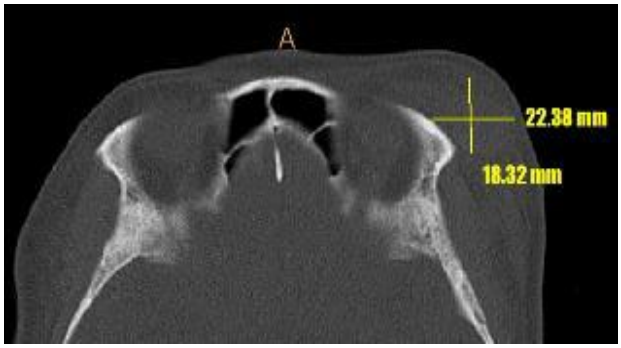

Fig. 1 CT scan demonstrates an 18.32 x 22.38 mm subcutaneous hematoma in the left supraorbital region.

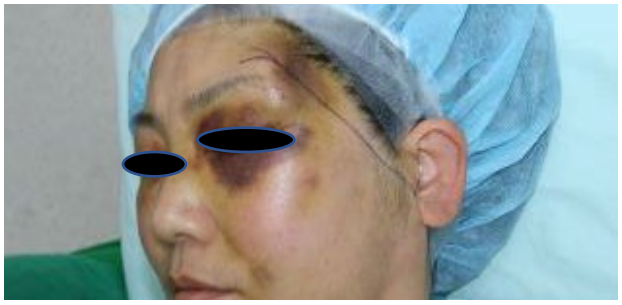

Fig. 2 The clinical photograph shows significant periorbital ecchymosis and swelling masking the underlying nerve status.

Fig. 3 Follow-up photograph reveals frontal branch nerve palsy, characterized by inability to elevate the left eyebrow.

EP-052

외측흉부 기반 전거근 피판과 흉배동맥 천공지 피판을 이용한 자가면역질환 환자의 안면 연부조직 증강술

Facial Soft Tissue Augmentation in Patients with Autoimmune Disease Using Lateral Thoracic–Based Serratus Anterior Muscle and Thoracodorsal Artery Perforator Flaps

한양대학교 의과대학
성형외과학교실
한양대학교 서울병원
성형외과

안중권, 장란숙, 김효성, 김지영, 김연환★

Purpose: Autoimmune disease–related facial lipoatrophy is characterized by chronic inflammation, progressive volume loss, and unpredictable graft survival. Conventional treatments such as fat grafting or alloplastic materials often show high resorption and complication rates. This study evaluated the outcomes of lateral thoracic–based serratus anterior fascia and muscle flaps and thoracodorsal artery perforator (TDAP) flaps for facial soft tissue augmentation in this population.

Methods: A retrospective review was performed of seven patients who underwent reconstruction between 2012 and 2025 for autoimmune-related facial soft tissue depression. Traumatic, oncologic, and congenital cases were excluded. Data collected included defect location, flap type, operative time, complications, secondary procedures, and follow-up duration. Serratus anterior flaps were used for smaller defects without skin loss, while TDAP flaps were selected when longer pedicles, larger volume, or skin resurfacing were required.

Results: All patients were female, with a mean age of 53.4 years. Diagnoses included lupus-associated panniculitis (n=3) and rheumatoid arthritis–associated panniculitis (n=4). Defects involved the cheek (n=5) and chin (n=2). Serratus anterior flaps were used in four cases and TDAP flaps in three. Mean operative time was 150 minutes. No flap loss or vascular complications occurred. Over a mean follow-up of 18.9 months, stable volume retention and satisfactory symmetry were achieved.

Conclusion: Lateral thoracic–based serratus anterior and TDAP flaps provide reliable, durable augmentation with minimal donor morbidity and short operative time in autoimmune-related facial lipoatrophy.

Age	Diagnosis	Defect location	Flap	Recipient vessels	Flap size (cm)	Op time (min)	Complications	Secondary procedure
43	Lupus panniculitis	Lt. cheek	SAm	STV	12 × 6	120	None	None
47	Lupus panniculitis	Rt. cheek	SAm	STV	3 × 5	120	None	None
40	Rheumatoid panniculitis	Rt. lower chin	SAm	FV	3 × 4	120	None	None
60	Lupus panniculitis	Lt. lower chin	SAm	FV	3 × 4	120	None	Fat injection
60	Rheumatoid panniculitis Calcinosis cutis	Lt. cheek	TDAP	STV	10 × 6	150	Brow ptosis	Fat injection
59	Rheumatoid panniculitis Calcinosis cutis	Rt. cheek	TDAP	FV	11 × 8	210	None	None
65	Rheumatoid panniculitis	Lt. cheek	TDAP	FV	11 × 7	210	Brow ptosis	Debulking Midface lift

SAm, serratus anterior muscle; TDAP, thoracodorsal artery perforator (deepithelized); STV, superficial temporal vessels; FV, facial vessels

Table 1. Clinical characteristics, operative details, and postoperative outcomes of patients undergoing facial soft tissue augmentation with lateral thoracic-based SAm and TDAP free flaps for autoimmune disease–related facial lipoatrophy.

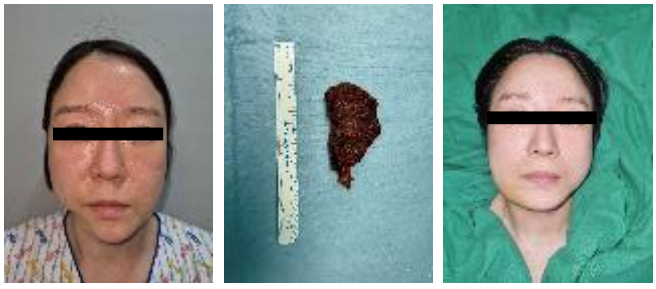

Figure 1. Clinical photographs of a 40-year-old female patient with rheumatoid panniculitis presenting with a depression deformity of the right lower chin. (Left) Preoperative view demonstrating the contour depression. (Middle) Harvested 3 × 4 cm SAm free flap for soft tissue volume augmentation, subsequently anastomosed to the facial vessels. (Right) Postoperative view showing improved contour of the right lower chin.

Figure 2. Clinical photographs of a 60-year-old female patient with rheumatoid panniculitis and calcinosis cutis presenting with a depression deformity of the left cheek. (Left) Preoperative view of left cheek depression. (Middle) Harvested TDAP free flap measuring 10 × 6 cm prior to partial deepithelialization for soft tissue augmentation and defect coverage. (Right) Defect of the left cheek following excision of calcinosis cutis.

Cont'd. (Left) Immediate postoperative lateral view demonstrating coverage of the left cheek defect. (Right) Postoperative frontal view demonstrating restoration of soft tissue volume and contour.

EP-053

안각동맥 천공지 기반 비 구순피판을 이용한 하안검 화상 결손의 재건

(Reconstruction of Lower Eyelid Burn Defects Using an Angular Artery Perforator Based Nasolabial Flap)

한강수병원 성형외과[1]
한강수병원 화상외과[2]

김지헌[1], **고장휴**★[1], **신진수**[1], **황용재**[1], **이주형**[2], **노지현**[2]

Purpose: Lower eyelid reconstruction is a formidable challenge due to intricate anatomy and its role in ocular protection. Defects exceeding 25% of the eyelid length typically require flaps or skin grafts. Reconstruction aims to restore globe coverage, eyelid closure, and aesthetics while preserving vision. In burn injuries, the superficial orbicularis oculi and tarsal plate are highly vulnerable, leading to retraction and functional impairment. Therefore, appropriate techniques are essential to maintain ocular function and prevent vision loss in these complex cases.

Methods: We report the clinical case of a 51-year-old female patient who presented with a persistent 2.5 × 1.0 cm defect on her left lower eyelid. This defect, which involved the middle lamella and the arcus marginalis, occurred three months following a drill-assisted dacryocystorhinostomy. To restore both function and form, reconstruction was performed using a 2.5 × 1.2 cm pedicled nasolabial flap based on a single angular artery perforator. The flap was meticulously harvested and rotated approximately 90 degrees to fill the defect, while the donor site was closed using a full-thickness skin graft after 10days after initial operation, to ensure minimal tension.

Results: The postoperative recovery was uneventful, with no signs of flap necrosis or eyelid retraction. During the follow-up period, the patient demonstrated excellent eyelid margin stability and a superior tissue match in terms of color and texture.

Conclusion: The angular artery perforator-based nasolabial flap provides dependable structural support and satisfactory cosmetic outcomes, representing a highly versatile and valuable option for the reconstruction of extensive and complex lower eyelid defects.

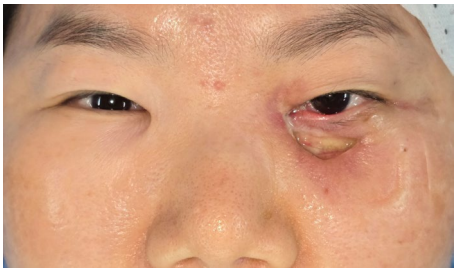

Fig.1. Initial wound presentation at the first hospital visit. A third-degree burn caused full-thickness skin defect of left lower eyelid.

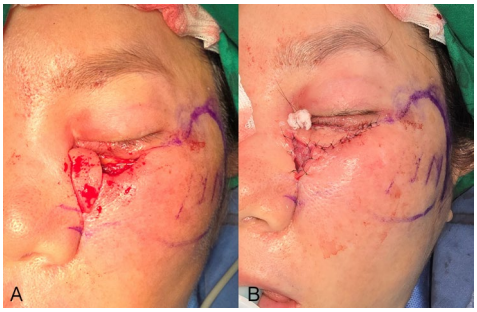

Fig.2. (A) An angular artery perforator based nasolabial flap has been elevated.
(B) The flap has been transposed 90 degrees anticlockwise, and medial canthal area was compressed with pillow. Donor site defect was covered with artificial dermis initially and full thickness skin graft was done after 10 days of first operation.

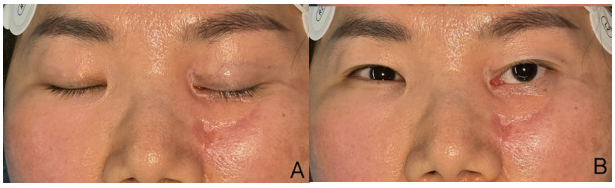

Fig.3. One-year postoperative result.
(A) Closed status of eyes: note the symmetry, skin texture, and the intact status of eyelid margins.
(B) Open status of eyes: although there is mild scar contracture of lower eyelid tissues, the height of both lower eyelid is almost even. No excessive bulkiness of the nasolabial flap was observed.

EP-054

두개안면부 골종의 진단 및 치료 지침

(Diagnostic and treatment protocols for peripheral craniofacial osteomas)

경북대학교 의과대학
성형외과학교실

강현수, 류정엽, 서만수, 최강영, 양정덕, 정호윤, 이준석★

Purpose: Osteomas are benign, slow-growing bony tumors that commonly develop in the craniofacial region. However, standardized diagnostic and treatment protocols remain limited. This study aimed to establish a systematic approach for diagnosis, genetic evaluation, and surgical management of craniofacial osteomas, with emphasis on lesion distribution and gender prevalence.

Methods: A retrospective review was conducted on 141 patients with craniofacial osteomas at Kyungpook National University Hospital between October 2011 and September 2025. All patients underwent clinical examinations and three-dimensional computed tomography for diagnostic confirmation. Surgical excision was performed using direct, endoscopic, or bicoronal approaches based on lesion characteristics. Whole exome sequencing was per-formed in patients with multiple large osteomas to evaluate mutations in EXT1, EXT2, APC, MSH2, and MLH1 genes associated with Gardner's syndrome.

Results: A total of 148 osteomas were identified. The frontal bone was the most common site (60.1%), followed by the parietal, mandibular, and occipital bones. Females accounted for 79.1% of cases (Fig. 1). At the six-month postoperative follow-up, a 3D head CT was performed, and no cases requiring reoperation for recurrence in the same area were recorded in our institution (Fig. 2). One case involved a patient with dozens of severe multiple osteomas, for which genetic testing revealed no mutations (Fig. 3).

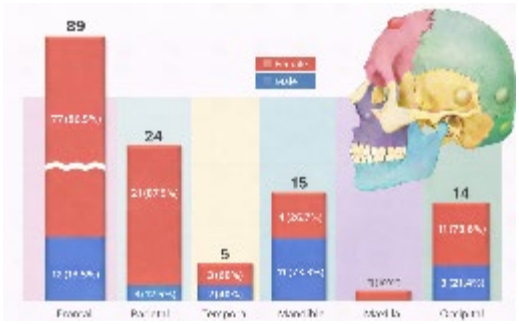

Fig. 1. Incidence and gender distribution of peripheral craniofacial osteomas.

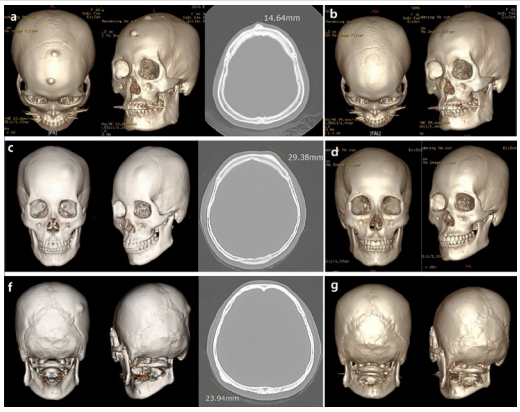

Fig. 2. Three-dimensional and axial head computed tomography of peripheral craniofacial osteomas.

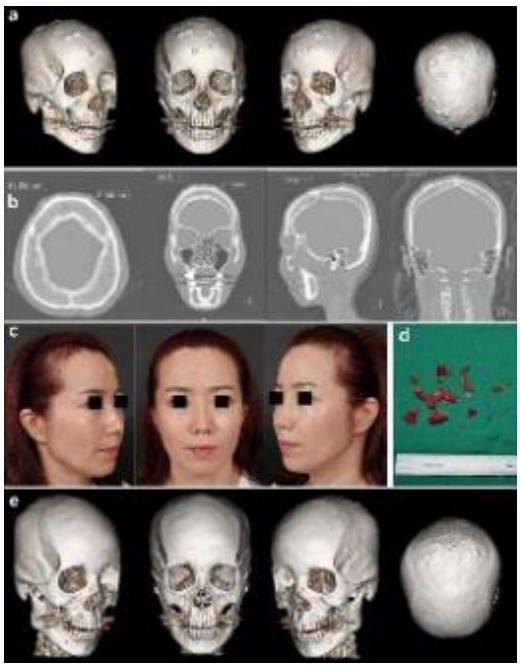

Fig. 3. Non-syndromic multiple osteomas.

Conclusion: Craniofacial osteomas are benign, slow-growing lesions most frequently found in the frontal bone and more prevalent among females. The integration of imaging-based diagnosis, tailored surgical techniques, and selective genetic testing allows for accurate evaluation, effective treatment, and favorable postoperative outcomes.

EP-055

안와 주변부 박리 손상과 상안검 흉터 구축의 재건: 증례 보고

(The Management of Periocular Avulsive Injury Followed by Upper Eyelid Scar Contracture: A Case Report)

대구가톨릭대학교
의과대학 성형외과학교실

김민석, 한동길★

Purpose: Periocular avulsive injuries can occur from various sources, including vehicle accidents, falls, and occupational trauma. Among these, injuries caused by a grinder tend to be more severe, involving orbital fractures, periocular deep tissue injury, and eyeball rupture. We present a case managed with immediate reconstruction of traumatic ptosis and secondary correction of lagophthalmos.

Methods: A 74-year-old man presented with right periocular trauma after a broken fragment struck on his face during a grinder task. Physical evaluation demonstrated full-thickness avulsive injuries of the right upper eyelid measuring 4.0 cm length and lower eyelid-to-cheek, measuring 7.0 cm length, fortunately only with corneal epithelial defect and commotio retinae. The patient underwent thorough irrigation and layer-by-layer reconstruction: Palpebral conjunctiva, tarsal plate, Müller's muscle, levator aponeurosis, orbicularis oculi muscle with absorbable sutures, and skin with nylon. The right lower eyelid-to-cheek was reconstructed in the same way.

Results: Traumatic ptosis was still noted in the immediate postoperative period and fully recovered after 1-month. During subsequent close observation, progressive contracture of the right upper eyelid with resultant lagophthalmos was noted. After 3-months and 2-weeks from initial injury, multiple Z-plasties were performed to improve eyelid mobility and lagophthalmos. No complications were noted at 1-year after initial trauma.

Conclusion: Periocular injuries caused by a grinder involving high-velocity projectiles result in extensive soft-tissue damage. Despite optimal primary reconstruction, traumatic ptosis, secondary contracture and lagophthalmos can occur due to severe initial tissue morbidity. So, immediate intervention through the meticulous layer-by-layer reconstruction of severed tissues with subsequent revision yields superior results.

Fig. 1. (A) Initial photograph taken at the emergency department. Full-thickness avulsive injury of the right upper and lower eyelid to cheek is noted. (B) Immediate postoperative photograph of the first operation: Meticulous layer-by-layer reconstruction was done and a silastic drain was placed. Initially traumatic ptosis in right upper eyelid was observed.

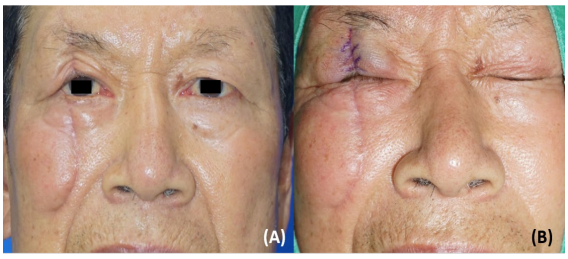

Fig. 2. (A) Preoperative photography of second operation. Traumatic ptosis was fully recovered at 1 month after initial reconstruction. (B) Design photography of the second operation. Lagophthalmos and scar contracture of the right upper eyelid were observed. To correct these problems, multiple Z-plasties were performed.

Fig. 3. (A) Immediate postoperative photograph of surgical correction of lagophthalmos and scar contracture. (B) Photograph taken 1 year after initial trauma. Successful restoration of appearance with natural eyelid and functional recovery from traumatic ptosis without further contracture or lagophthalmos were observed.

EP-056

동일 병변 내에서 관찰된 피부섬유육종과 광선각화증: 희귀 사례 보고

(Collision Tumor of Dermatofibrosarcoma Protuberans and Actinic Keratosis: A Rare Coexistence)

동국대학교 경주병원
성형외과학 교실

안유진, 이준호★

Purpose: Dermatofibrosarcoma protuberans (DFSP) is a rare, locally aggressive cutaneous sarcoma, whereas actinic keratosis (AK) is a common premalignant epidermal lesion. The simultaneous occurrence of these two distinct pathologies within a single lesion—known as a collision tumor—is extremely rare and poses significant diagnostic challenges. We report a case of a collision lesion comprising DFSP and AK to highlight the importance of accurate clinicopathological correlation and deep tissue sampling.

Methods: An 80-year-old man presented with a solitary, 0.6 × 0.8 cm erythematous ulcerative lesion on the right temple. Initial punch biopsy suggested only AK. Due to persistent ulceration, a repeat deep biopsy was performed. Immunohistochemical staining with CD34 and smooth muscle actin (SMA) was utilized to characterize the dermal component.

Results: The initial superficial biopsy indicated only actinic keratosis. However, the subsequent deep biopsy revealed a complex histology: the epidermis showed atypical keratinocytes consistent with AK, while the underlying dermis contained a storiform proliferation of spindle cells. Immunohistochemistry demonstrated diffuse CD34 positivity and SMA negativity, confirming the diagnosis of DFSP and excluding smooth muscle tumors. The patient underwent Mohs micrographic surgery to ensure clear margins, followed by bilobed flap reconstruction. At the 2-month follow-up, complete healing was observed without recurrence

Conclusion: Clinicians should suspect collision tumors when AK presents with atypical features like ulceration or induration. Deep biopsy is essential to reveal underlying neoplasms such as DFSP. Mohs micrographic surgery offers precise margin control and optimal outcomes for these complex lesions.

Fig. 1. Preoperative photograph of an 80-year-old man with a soli- tary erythematous ulcerative lesion measuring 0.6×0.8 cm on the right temple.

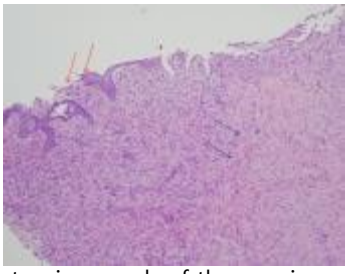

Fig. 2. Photomicrograph of the specimen stained with hematoxylin and eosin (×100). Atypical keratinocytes confined to the epidermis consistent with actinic keratosis (red arrows), along with storiform spindle cell proliferation in the dermis characteristic of dermatofi- brosarcoma protuberans (blue arrows).

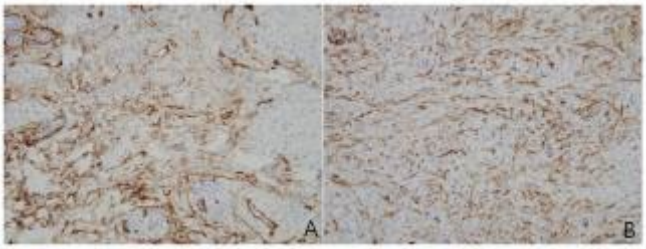

Fig. 3. Photomicrographs of the specimen immunohistochemically stained for CD34 (A, ×200) and smooth muscle actin (SMA) (B, ×200). Diffuse and strong positivity for CD34 is observed in dermal spindle cells, supporting the diagnosis of dermatofibrosarcoma protuberans, while SMA staining is negative, consistent with the typical immunophenotype and aiding in the exclusion of smooth muscle tumors..

Fig. 4. Postoperative photograph taken 2 months after Mohs micro- graphic surgery and bilobed flap reconstruction. Complete healing without recurrence or complications is observed.

EP-057

안면 외상 후 발생한 천측두동맥 가성동맥류의 현미경하 절제 : 증례 보고

(Excision of Traumatic Pseudoaneurysm of the Superficial Temporal Artery Under Microscopic Guidance: A Case Report)

분당서울대학교병원

강명진, 김종호★

Purpose: Traumatic pseudoaneurysms of the facial region are rare vascular lesions following blunt or penetrating facial trauma. The superficial temporal artery (STA), due to its superficial course, is one of the major arteries susceptible to facial pseudoaneurysm formation. We report a case of traumatic pseudoaneurysm of the STA frontal branch, managed with microscope-assisted en bloc excision.

Methods: A 74-year-old male developed a pulsatile mass on the left forehead with intermittent pain during follow-up after fall-related facial trauma. Craniofacial computed tomography revealed an aneurysmal dilatation in the cutaneous layer suggestive of a traumatic pseudoaneurysm of the frontal branch of the superficial temporal artery. Feeding vessels were identified and ligated under microscopic guidance, and the pseudoaneurysm was excised en bloc.

Results: Histopathological examination confirmed a vascular wall with myxoid degeneration and dystrophic calcification, consistent with pseudoaneurysm. The patient was discharged on the day of surgery without complications, with no recurrence at follow-up.

Conclusion: Traumatic pseudoaneurysm of the STA should be considered in the differential diagnosis of pulsatile masses after facial trauma. Microscope-assisted excision enables precise feeding vessel identification and complete en bloc removal with favorable outcomes.

Fig. 1. Preoperative photographs of a 74-year-old male showing a pulsatile mass on the left forehead (red circle). (A) Frontal view. (B) Left oblique view demonstrating the mass along the expected course of the frontal branch of the superficial temporal artery. (C) Left lateral view.

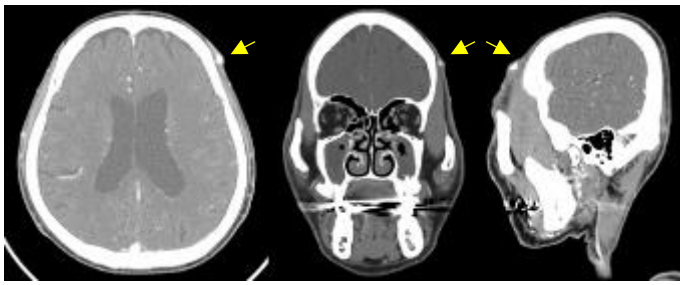

Fig. 2. Craniofacial computed tomography (CFCT) performed on December 12, 2025. Axial, coronal, and sagittal views showing an approximately 4-mm aneurysmal dilatation in the left forehead cutaneous layer (arrow), suggestive of traumatic pseudoaneurysm.

Fig. 3. Intraoperative photographs under operating microscope. After linear incision and subcutaneous dissection, the pseudoaneurysm is identified with its feeding vessels.

Fig. 4. Excised pseudoaneurysm specimen measuring 0.6 x 0.5 cm and histopathological examination (H&E staining) showing vascular wall with myxoid degeneration and dystrophic calcification, consistent with chronic degenerative changes of a pseudoaneurysm.

EP-058

접힌 비순섬 피판을 이용한 전층 비익 결손의 단일 단계 재건 : 증례 보고

(Folded nasolabial island flap for single-stage reconstruction of full-thickness alar defects: a case series)

순천향대학교

황용선, 김준혁★

Purpose: Reconstruction of full-thickness nasal alar defects remains challenging because restoration of the mucosal lining, structural support, and external skin. Conventional techniques, including forehead flaps and nasolabial flaps, often require multi-stage procedures, resulting in increased patient burden, surgical risk, and medical cost. We report three cases of full-thickness alar defects reconstructed using a folded nasolabial island flap (FNIF) in a single stage.

Methods: Three patients with full-thickness nasal alar defects underwent reconstruction using the FNIF technique between October 2010 and October 2025. The defects were caused by basal cell carcinoma and squamous cell carcinoma. The FNIF involves elevation of a nasolabial island flap with a pedicle, followed by folding and transposition of the flap to reconstruct both the internal nasal lining and the external alar contour simultaneously. Postoperative outcomes were assessed based on physician evaluation and patient satisfaction, focusing on aesthetic outcomes and nasal airway function.

Results: The patients were aged 72, 49, and 90 years. All flaps survived completely without complications such as necrosis, infection, or venous congestion. Nasal airway patency was well maintained in all cases, and no collapse of the reconstructed nostril lining was observed. Both physician evaluation and patient satisfaction demonstrated excellent functional and aesthetic outcomes. Mild alar thickness or asymmetry occurred in some cases but was successfully corrected with secondary debulking procedures.

Conclusion: The folded nasolabial island flap is a reliable and straightforward technique for single-stage reconstruction of large full-thickness alar defects, providing stable structural support and satisfactory aesthetic outcomes without the need for cartilage grafting or multi-stage procedures.

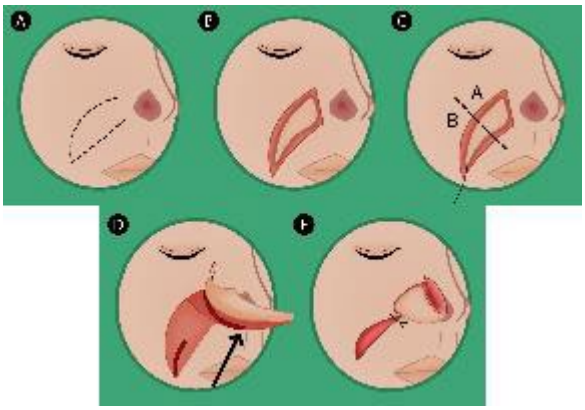

Figure1. Schematic illustration of the folded nasolabial island flap technique. (A) Flap design. (B) Incision. (C) The A portion forms the external skin and the B portion forms the mucosal lining; folding of the flap provides strong structural support. (D) Pedicle dissection and flap elevation. (E) Flap inset.

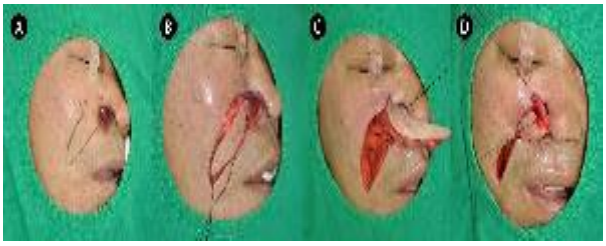

Figure2. Operative procedure of the folded nasolabial island flap reconstruction. (A) Flap design. (B) Dissection and island flap elevation. (C) Flap transposition. (D) Flap inset and coverage of the alar defect.

Figure3. Operative procedure in another case of folded nasolabial island flap reconstruction. (A) Flap design. (B) Dissection and island flap elevation. (C) Flap transposition. (D) Flap inset and coverage of the alar defect.

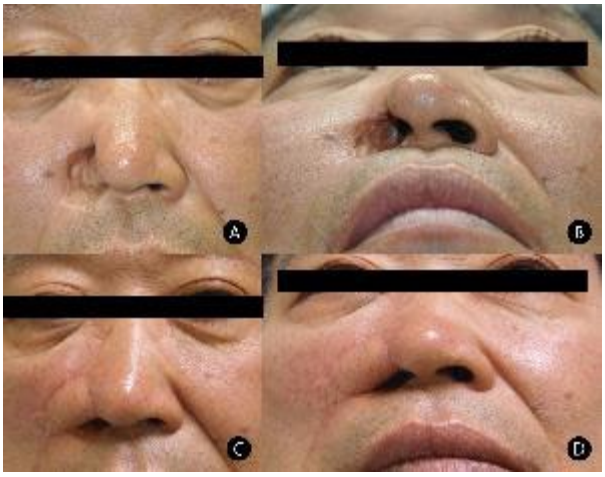

Figure4. Clinical photographs of another case. (A, B) Preoperative images. (C, D) Postoperative images at 3 months.

EP-059

양측성 구순열의 단계적 수술법: 수술 프로토콜 및 초기 임상 결과

(Staged side by side Bilateral Cleft Lip Repair in complete bilateral cleft lip patients: Surgical Protocol and Early Outcomes)

서울아산병원 성형외과[1]
이스트만 치과[2]

오지혜[1], 김영철[1], 권순만[2], 오태석★[1]

Purpose: The one-stage repair in bilateral complete cleft patients is the standard for bilateral cleft lip repair. However, prolabial tissue sacrifice and lateral muscle recruitment often causes excessive upper lip tightness. This study introduces a novel two-stage side by side repair overcoming these limitations and presents early outcomes

Methods: A retrospective review analyzed 17 infants who underwent the two-stage bilateral cleft lip repair between December 2023 and February 2026. Clinical data, including the duration of presurgical nasoalveolar molding (NAM), timing of staged surgeries were investigated. Postoperative aesthetics at 1 year of age were evaluated using the Asher-McDade system by two blinded raters.

Results: The mean presurgical NAM duration was 101.4±9.7 days. The first and second cheiloplasty stages were performed at mean ages of 3.1±0.4 and 8.8±0.5 months, respectively, followed by palatoplasty at 11.7±0.7 months. An postsurgical NAM, lip taping, and a nasal retainer were used between stages. Asher-McDade evaluation yielded mean scores of 1.65 for nasal form, 1.35 for symmetry, 1.95 for vermilion border, and 2.00 for profile, quantitatively demonstrating favorable aesthetics.

Fig. 1. Two-staged Surgical Protocol of Bilateral Cleft Lip

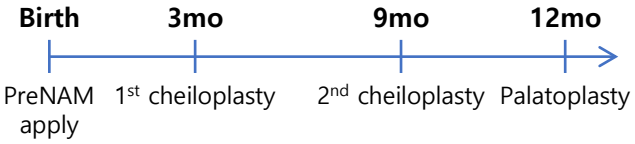

Table 1. Comparison of Asher-McDade Scores

Category	1st Evaluation (Mean ± SD)	2nd Evaluation (Mean ± SD)	p-value
Nasal Form	1.65 ± 0.88	1.65 ± 0.67	1
Nasal Symmetry	1.40 ± 0.68	1.35 ± 0.59	0.716
Vermilion Border	2.20 ± 0.89	1.95 ± 0.83	0.021
Nasal Profile (including upper lip)	2.55 ± 1.15	2.00 ± 0.97	0.004

Fig. 2. Preoperative, Post-first Repair and Post-second Repair Photography

Conclusion: This two-stage side by side repair effectively mitigates the upper lip tightness inherent in conventional one-stage repair. Implementing this staged surgical protocol achieves reliable, aesthetically pleasing early outcomes, offering a viable alternative to the traditional paradigm.

EP-060

한국인 환자에서 안면부 Keystone 피판 재건술 후 흉터에 대한 환자 및 관찰자 평가

(Patient and Observer Scar Assessment of Facial Keystone Flap Reconstruction in Korean Patients)

성균관대학교 의과대학
강북삼성병원 성형외과학교실

김우섭, 김규남★

Purpose: Facial reconstruction using keystone flaps (KFs) provides reliable outcomes; however, few studies have evaluated postoperative scarring using patient reported outcomes. We assessed scar outcomes after facial KF reconstruction using the Patient and Observer Scar Assessment Scale (POSAS) and explored associations with clinical and sociodemographic factors.

Methods: In this retrospective observational cohort study, 43 Korean patients (27 males, 16 females; mean age: 49.95 ± 20.66 [range, 10–88] years) who underwent facial KF reconstruction between January 2020 and November 2022 were stratified by age (≤30, 40s–50s, ≥60 years), KF type (hemi-KF vs. other types), and sex.

Results: Patients aged ≤30 years showed significantly higher total Patient Scar Assessment Scale (PSAS) scores (18.53 ± 5.69) than those aged 40s–50s (13.33 ± 3.27) and ≥60 years (11.82 ± 3.28) ($p < 0.001$). Observer Scar Assessment Scale and patient satisfaction scores did not significantly differ across flap types or sex; however, the hemi-KF group showed a trend toward better outcomes, and female patients reported higher PSAS scores.

Conclusion: Facial KF reconstruction yields generally satisfactory scar outcomes. Younger patients are more critical of scars, and female patients exhibit greater aesthetic sensitivity. Patient reported scar assessments are essential for individualized counseling, planning, and scar care in facial reconstruction.

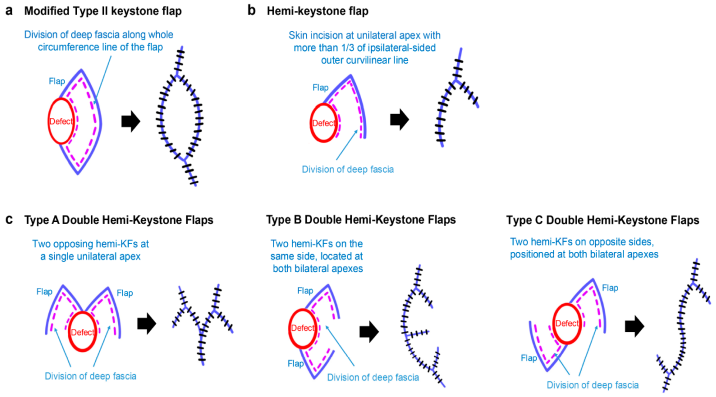

Figure 1. Schematic illustrations of the modifications of keystone flap (KF) techniques used in this study. (a) Modified Type II KF technique. (b) Hemi-KF technique. (c) Double hemi-KFs techniques: Type A, Type B, and Type C.

Table 1. Comparison of Patient Scar Assessment Scale and Observer Scar Assessment Scale scores among age-stratified groups.

PSAS	Group A (Mean ± SD)	Group B (Mean ± SD)	Group C (Mean ± SD)	*p*-Value	Post Hoc Analysis
Pain	2.35 ± 1.169	1.40 ± 0.507	1.27 ± 0.467	0.001	A > B, C
Itching	2.71 ± 1.312	1.47 ± 0.640	1.64 ± 0.674	0.004	A > B
Color	3.53 ± 1.663	2.67 ± 0.724	1.73 ± 0.786	0.001	A, B > C
Stiffness	3.29 ± 1.047	2.53 ± 0.743	2.18 ± 0.603	0.003	A > B, C
Thickness	3.12 ± 0.993	2.60 ± 0.828	2.55 ± 0.934	0.129	A > C
Irregularity	3.53 ± 1.068	2.67 ± 0.976	2.45 ± 0.934	0.020	A > C
Total score	18.53 ± 5.691	13.33 ± 3.266	11.82 ± 3.281	0.001	A > B, C
Overall patient satisfaction score	3.76 ± 1.480	2.80 ± 0.862	2.82 ± 0.874	0.074	NA
OSAS	**Group A (Mean ± SD)**	**Group B (Mean ± SD)**	**Group C (Mean ± SD)**	***p*-Value**	**Post Hoc Analysis**
Vascularity	2.50 ± 0.829	2.70 ± 1.014	2.14 ± 0.234	0.339	NA
Pigmentation	2.53 ± 0.819	2.87 ± 1.288	2.18 ± 0.337	0.253	NA
Thickness	3.18 ± 0.749	3.37 ± 0.812	3.18 ± 1.079	0.403	NA
Pliability	2.82 ± 0.749	2.93 ± 0.799	2.55 ± 0.820	0.311	NA
Relief	2.76 ± 0.752	2.73 ± 0.799	2.55 ± 0.820	0.572	NA
Surface area	3.50 ± 0.729	3.37 ± 0.855	2.82 ± 1.007	0.034	A > C
Total score	17.29 ± 3.759	17.97 ± 4.011	15.41 ± 4.061	0.111	NA
Objective scar rating	3.56 ± 0.846	3.77 ± 0.904	3.09 ± 1.221	0.063	NA

Table 2. Comparison of Patient Scar Assessment Scale and Observer Scar Assessment Scale scores between groups stratified by flap type.

PSAS	Group D (Mean ± SD)	Group E (Mean ± SD)	*p*-Value
Pain	1.92 ± 1.129	1.47 ± 0.514	0.186
Itching	2.00 ± 1.233	2.00 ± 0.935	0.693
Color	2.65 ± 1.198	2.94 ± 1.638	0.655
Stiffness	2.62 ± 1.061	2.94 ± 0.748	0.132
Thickness	2.65 ± 1.018	3.00 ± 0.791	0.088
Irregularity	2.88 ± 1.107	3.06 ± 1.088	0.517
Total score	14.73 ± 6.004	15.41 ± 3.825	0.337
Overall patient satisfaction score	3.08 ± 1.197	3.35 ± 1.272	0.466
OSAS	**Group D (Mean ± SD)**	**Group E (Mean ± SD)**	***p*-Value**
Vascularity	2.48 ± 0.922	2.47 ± 0.649	0.364
Pigmentation	2.58 ± 1.046	2.53 ± 0.819	0.611
Thickness	3.08 ± 0.717	3.50 ± 0.984	0.176
Pliability	2.67 ± 0.706	2.97 ± 0.874	0.308
Relief	2.60 ± 0.788	2.85 ± 0.745	0.291
Surface area	3.13 ± 0.672	3.50 ± 1.104	0.233
Total score	16.54 ± 3.658	17.82 ± 4.387	0.304
Objective scar rating	3.42 ± 0.913	3.65 ± 1.101	0.587

Table 3. Comparison of Patient Scar Assessment Scale and Observer Scar Assessment Scale scores between groups stratified by sex.

PSAS	Group F (Mean ± SD)	Group G (Mean ± SD)	*p*-Value
Pain	1.48 ± 0.580	2.19 ± 1.276	0.472
Itching	1.81 ± 0.962	2.31 ± 1.302	0.796
Color	2.70 ± 1.463	2.88 ± 1.258	0.288
Stiffness	2.67 ± 0.832	2.88 ± 1.147	0.065
Thickness	2.59 ± 0.694	3.13 ± 1.204	0.052
Irregularity	2.70 ± 0.993	3.38 ± 1.147	0.245
Total score	13.96 ± 4.109	16.75 ± 6.445	0.110
Overall patient satisfaction score	2.93 ± 1.207	3.63 ± 1.147	0.124
OSAS	**Group F (Mean ± SD)**	**Group G (Mean ± SD)**	***p*-Value**
Vascularity	2.59 ± 0.832	2.28 ± 0.774	0.473
Pigmentation	2.76 ± 1.050	2.22 ± 0.657	0.501
Thickness	3.26 ± 0.685	3.22 ± 1.095	0.179
Pliability	2.81 ± 0.709	2.75 ± 0.913	0.079
Relief	2.76 ± 0.698	2.59 ± 0.898	0.027
Surface area	3.03 ± 0.800	3.25 ± 1.017	0.045
Total score	17.48 ± 3.531	16.31 ± 4.629	0.356
Objective scar rating	3.52 ± 0.882	3.50 ± 1.169	0.072

EP-061

중증 치매를 동반한 초고령 환자의 비익 기저세포암에서 방사선치료 단독 치료: 조기 완전 임상 반응

Radiotherapy Alone for Nasal Ala Basal Cell Carcinoma in a Very Elderly Patient with Severe Dementia: Early Complete Clinical Response

연세대학교 원주의과대학
원주세브란스기독병원
성형외과학 교실

전우상, 이훈범, 김석원, 김지예★

Purpose: Basal cell carcinoma (BCC) of the nasal ala is typically managed surgically; however, operative treatment may be impractical in very elderly patients with severe cognitive impairment due to poor compliance and high risk of postoperative wound-care failure. We describe the early clinical response and feasibility of radiotherapy alone for nasal ala BCC in an 81-year-old woman with severe dementia.

Methods: An 81-year-old woman with hypertension, diabetes mellitus, and severe dementia presented with a right nasal alar lesion present for 1 year (Fig. 1). Punch biopsy confirmed BCC (approximately 1.0 × 1.0 cm). Given markedly poor compliance (e.g., immediate removal of dressings after biopsy) and high risk of postoperative wound-care failure, surgery was deferred. Definitive intensity-modulated radiotherapy (IMRT) was delivered to the primary lesion only, using a hypofractionated regimen of 40 Gy in 10 fractions (Sep 29–Oct 15, 2025). Acute toxicity and clinical response were assessed during and after treatment.

Results: The planned radiotherapy course was completed without interruption. Immediate post-treatment findings showed expected acute erythema/erosion (Fig. 2), without significant documented toxicity requiring intervention beyond brief topical care. At 1 month post-radiotherapy, the nasal alar lesion demonstrated complete clinical resolution with minimal residual dyspigmentation/scarring (Fig. 3), and follow-up was concluded.

Conclusion: Radiotherapy alone may be a practical option for selected very elderly patients with nasal ala BCC when severe cognitive impairment and poor compliance make surgical treatment and postoperative wound care unreliable.

Fig. 1. Pre-radiotherapy clinical photograph showing an ulcerated lesion on the right nasal ala, confirmed as basal cell carcinoma by punch biopsy

Fig. 2. Immediate post-radiotherapy appearance after completing hypofractionated RT (40 Gy in 10 fractions), demonstrating expected acute erythema/erosion.

Figure 3. One-month post-radiotherapy photograph showing complete clinical resolution with minimal residual dyspigmentation/scarring.

EP-062

하안검 섬모하 절개 후 고령 환자에서 발생한 중간층 섬유화 유발 하안검 외반증

(Middle Lamellar Fibrosis-Induced Lower Eyelid Ectropion in an Elderly Patient After Subciliary Approach)

가톨릭대학교 의과대학
성형외과학교실
김예린, 신종원★

Purpose: Lower eyelid ectropion is typically associated with skin deficiency (anterior lamellar shortening). However, severe ectropion can occur in elderly patients even without skin loss. This report analyzes the mechanism of ectropion induced by middle lamellar fibrosis following orbital surgery and shares a successful surgical management case.

Methods: A 78-year-old female presented with severe ectropion after undergoing orbital floor fracture repair via a subciliary approach. Revision surgery was performed to restore eyelid function. Intraoperatively, dense fibrotic adhesions were identified in the middle lamella. Treatment involved meticulous adhesiolysis at the arcus marginalis level combined with lateral tarsal strip fixation to provide horizontal support.

Results: The revision surgery successfully restored vertical eyelid mobility and corrected the ectropion without the need for a skin graft. The patient maintained a stable eyelid position without recurrence during a 1-year follow-up period. Postoperative MRI analysis confirmed that an early hematoma had progressed into fibrosis in the septal area, causing the mechanical restriction.

Conclusion: In elderly patients, postoperative hematoma can lead to significant middle lamellar fibrosis, resulting in severe ectropion even if skin resection was minimal. Meticulous hemostasis is crucial to prevent this complication. For treatment, direct release of middle lamellar adhesions is essential along with horizontal tightening of the eyelid.

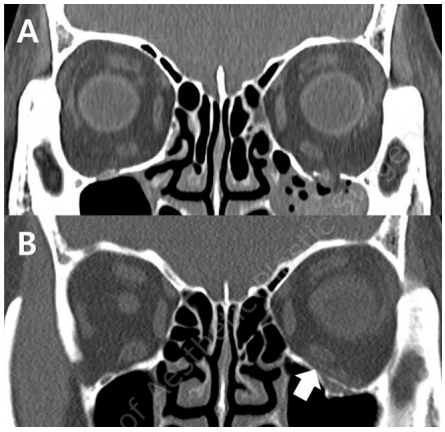

Fig. 1. (A) Preoperative computed tomography scan showing a blowout fracture of the left orbital floor. (B) Postoperative scan obtained 6 months after the initial repair, demonstrating stable reconstruction of the orbital floor with an implant.

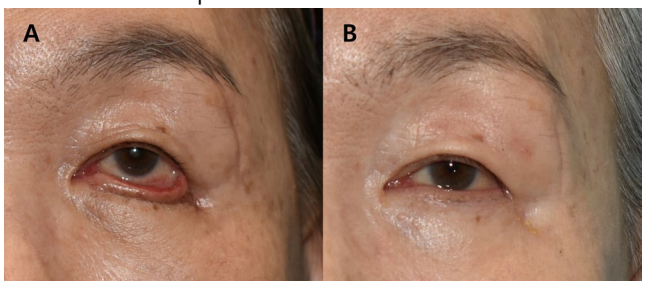

Figure 2. Severe ectropion before revision surgery (A) and restored symmetry and eyelid position 1 year after revision (B).

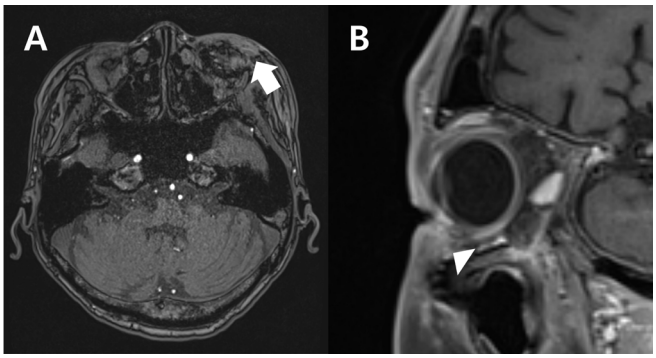

Fig. 3. Post-initial surgery showing a preseptal hematoma at 1 week (A) and subsequent fibrotic changes at 2 months (B).

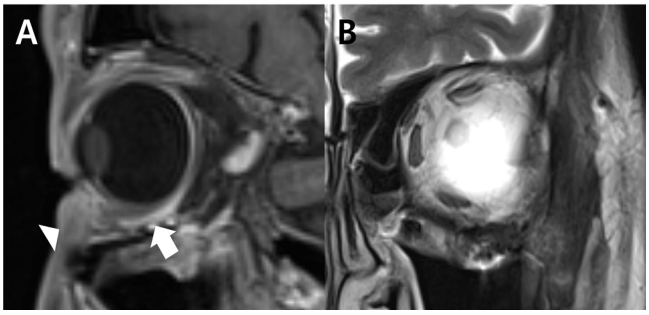

Fig. 4. Sagittal view showing inflammatory changes in the anterior lamella (A) and coronal view showing intact extraocular muscles and internal orbital structures (B).

EP-063

기저세포모반증후군(고를린 증후군): 희귀 증례 보고

Nevoid Basal Cell Carcinoma Syndrome (Gorlin Syndrome): A Rare Case Report

노원을지대학교병원 성형외과
홍주현, 이동락, 민경희★

Purpose: Nevoid basal cell carcinoma syndrome (NBCCS), or Gorlin syndrome, is a hereditary disorder characterized by multiple basal cell carcinomas (BCCs) and systemic abnormalities. This case highlights that NBCCS can present late with incomplete phenotypic features, necessitating systematic application of diagnostic criteria and long-term multidisciplinary surveillance.

Methods: We report a 63-year-old male with a history of multifocal BCCs beginning approximately 20 years ago, who underwent staged wide excisions and reconstructions. Contrast-enhanced neck CT was performed to evaluate for potential regional metastasis or deep soft tissue invasion, and a detailed physical examination was performed to identify additional syndromic features.

Results: The patient underwent wide excision of 18 lesions, and histopathological examination confirmed that all excised specimens were BCCs. Computed tomography revealed lamellar calcification of the falx cerebri and tentorium cerebelli, fulfilling a major diagnostic criterion. Despite the absence of palmar pits and skeletal anomalies, a clinical diagnosis of NBCCS was made based on the presence of two major criteria: multiple BCCs and falx calcification.

Conclusion: This case underscores that NBCCS can remain undiagnosed until late adulthood, particularly when the phenotypic expression is incomplete. Establishing a formal diagnosis of NBCCS is essential for directing appropriate management, most notably the avoidance of radiotherapy, and for initiating long-term, multidisciplinary surveillance to monitor for systemic complications and new cutaneous malignancies.

Fig. 1. Schematic diagrams illustrating the distribution of the eight histologically confirmed basal cell carcinomas identified during the first surgical stage. Lesions were localized on the forehead, both cheeks, left nasolabial fold, and the right parietal scalp.

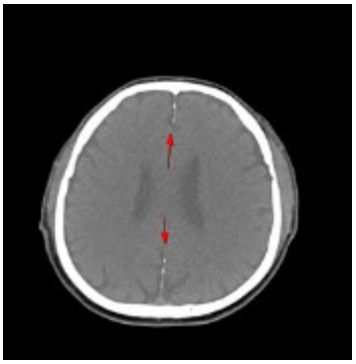

Fig. 2. An axial contrast-enhanced CT scan at the level of the skull base, revealing prominent, high-density lamellar calcification along the posterior falx cerebri and tentorium cerebelli.

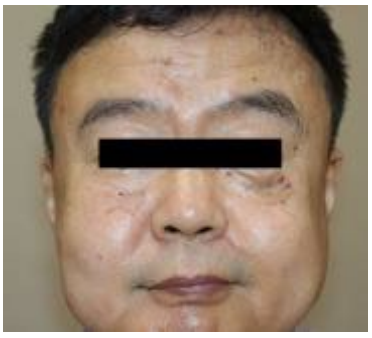

Fig. 3. Postoperative state after the first surgery: A clinical photograph showing the stable integration of full-thickness skin grafts (FTSG) on both cheeks and well-healed surgical scars from the first stage.

Fig. 4. Preoperative presentation of the second stage: Clinical photographs taken two years after the initial surgery demonstrate a new lesion in the left postauricular region along with multiple lesions on the face and scalp.

EP-064

코 기저세포암 절제 후 발생한 결손의 비배부 피판을 이용한 재건술: 한국인 4례 분석

Reconstruction with Dorsal Nasal Flap after Excision of Basal Cell Carcinoma of the Nose: A Study of 4 Korean Patients

노원을지대학교병원 성형외과
정재환, 이동락★

Purpose: Non-melanoma skin cancers frequently arise on the nose, where reconstruction demands precise contour restoration. Korean patients present added complexity due to thicker, more sebaceous skin prone to alar distortion. This study evaluates outcomes of the dorsal nasal flap for nasal skin cancer defects in a Korean cohort.

Methods: A retrospective review of four Korean patients (3 female, 1 male; ages 66–86) who underwent wide excision followed by dorsal nasal flap reconstruction. Cancer locations included supratip (n=2), nasal tip (n=1), and alae (n=1), with post-excisional defects ranging from 1.4 to 2.6cm.

Results: All flaps were successfully transposed in a single stage with no revision required. No flap necrosis, infection, or alar distortion occurred. Patient satisfaction was high across color match, contour, and scarring.

Conclusion: The dorsal nasal flap is a reliable, single-stage reconstructive option for Korean patients, whose thick and sebaceous nasal skin often makes other techniques like skin grafting aesthetically inferior. Our findings suggest that for medium-sized distal nasal defects in this demographic, the dorsal nasal flap offers a predictable, complication-free, and highly aesthetic outcome.

Table 1. Summary of Patient Demographics, Clinical Characteristics, and Surgical Outcomes.

Case No.	Age/Sex	Diagnosis	Defect size (cm)	Location	Follow-up	Complications
1	71/F	BCC	1.4*1.3	Nasal ala	6 months	Minor pin-cushioning
2	66/F	BCC	2.6*1.5	Supratip	4 months	None
3	67/M	BCC	1.8*1.3	Supratip	4 months	None
4	86/F	BCC	1.7*1.7	Nasal tip	1 month	None

Note. *M, male; F, female; BCC, basal cell carcinoma*

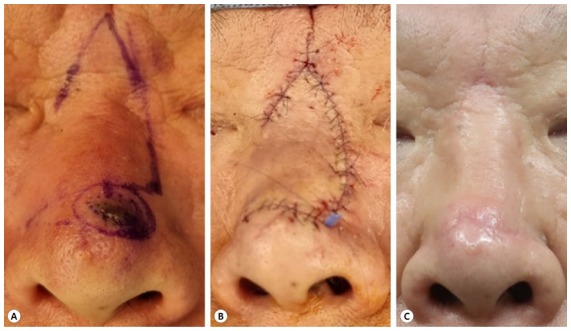

Fig. 1. Representative case of dorsal nasal flap reconstruction. (A) Preoperative view of a basal cell carcinoma on the nasal supratip with planned 5mm excision margins. (B) Immediate postoperative result following rotation and advancement of the dorsal nasal flap. (C) Clinical follow-up at 6 months showing favorable color match and minimal scarring without distortion.

EP-065

후두신경통의 최신 수술적 치료: 증례군 및 문헌고찰

(Case Series and Literature Review of Up-to-Date Surgical Management of Occipital Neuralgia)

서울아산병원[1]
아문성형외과의원[2]

장서연[1] , 이석준[1] , 박주석[2] , 정우식★[1]

Purpose: Nerve decompression is an emerging surgical treatment option for patients with occipital neuralgia. However, limited research is available on the efficacy of this treatment in South Korea. This retrospective study evaluates the efficacy of nerve decompression surgery in patients with chronic migraines, specifically focusing on occipital neuralgia, in South Korea.

Methods: Between January 2019 and December 2022, six patients diagnosed with occipital neuralgia, who had not responded to conservative treatments, underwent nerve decompression surgery. This procedure, performed under local anesthesia, involved decompression of the greater and/or lesser occipital nerves. Patient data were analyzed for headache frequency and intensity (using the Numeric Rating Scale [NRS]) and the decrease in oralmedications needed postsurgery.

Results: Results showed significant improvement in headache symptoms postsurgery, with the average preoperative NRS score of 7.9 dropping to 3.7 postoperatively. Additionally, the average number of medications used decreased from 3.2 to 1.3. No significant surgical complications were reported..

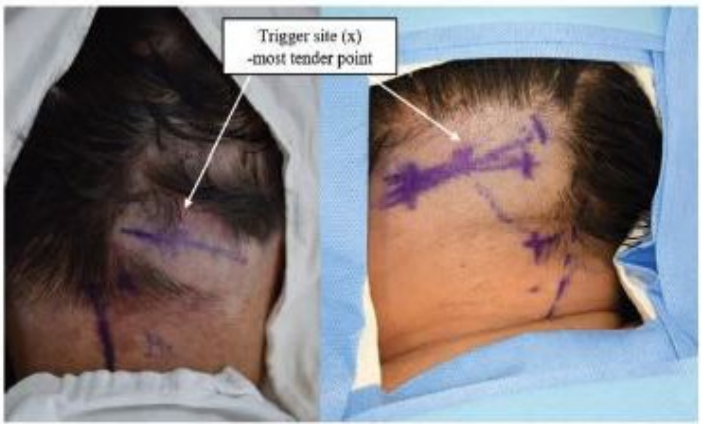

Fig. 1
A 5-cm horizontal incision is outlined in the hair-bearing lower occipital region, and the most tender points identified by the patient are marked with "x".

Fig. 2
Intraoperative photo of nerve decompression-dissected and released greater occipital nerve.

n	Age	Sex	Smoking	Alcohol	Headache	Decompressed nerve
1	38	F	-	-	Left occiput	Left GON
2	45	M	-	-	Left occiput	Left GON, LON
3	28	M	-	Once per week	Left occiput, forehead	Left LON
4	53	M	Past (6 years)	Once per week	Left occiput	Left GON
5	81	M	Past (20 years)	-	Right occiput, forehead	Right GON, LON
6	40	M	-	Once per week	Both occiput	Left GON

Abbreviations: F, female; GON, greater occipital nerve; LON, lesser occipital nerve; M, male.

Table. 1
Demograp;hic details and operation method (n=6)

Conclusions: The study highlights the potential of nerve decompression as an effective treatment for occipital neuralgia, particularly in cases resistant to traditional medical management.

#	Frequency (per week)		NRS score		Number of oral pills		Follow-up
	PreOP	PostOP	PreOP	PostOP	PreOP	PostOP	
1	3-5	1-5	9	6	4	2	7 months
2	3-5	1-7	7	3	3	2	6 months
3	1-2	0.5	7-8	2-5	3	1	4 months
4	1-5	1	8	4	3	2	4 months
5	5	2-3	8	3-5	2	0	6 months
6	3-5	1-2	8	1-2	4	1	2 years

Abbreviation: NRS, Numeric Rating Scale; PreOP: preoperative state; PostOP: postoperative state

Table. 2
Differences before and after decompression surgery (PreOP > PostOP)

EP-066

성인 환자에서 점액낭종으로 추정되어 절제한 병변에서 예기치 않게 점액표피암이 진단된 증례 보고

(Unexpected Diagnosis of Mucoepidermoid Carcinoma Following Excision of a Presumed Mucocele in an Adult Patient: A Case Report)

순천향대학교 구미병원

김은찬, 위서영★

Background: Mucoceles are common benign lesions of the minor salivary glands. They typically present as painless, fluctuant swellings and are often treated with simple surgical excision. In contrast, mucoepidermoid carcinoma (MEC) is the most common malignant salivary gland tumor. Although MEC most commonly arises in the parotid gland, involvement of intraoral minor salivary glands is uncommon and may clinically resemble benign lesions such as mucoceles. This report presents a case in which a lesion clinically suspected to be a mucocele was unexpectedly diagnosed as MEC after excision.

Methods: A 72-year-old male presented with a 6-month history of a painless, slowly enlarging swelling on the right lower lip (Fig 1). The lesion intermittently changed in size and was associated with a history of minor lip-biting trauma. Clinical examination revealed a 1.5 × 1.2 cm soft, dome-shaped submucosal nodule with intact mucosa and no ulceration or cervical lymphadenopathy. A provisional diagnosis of mucocele was made. The lesion was surgically excised under local anesthesia and submitted for histopathologic examination (Fig 2).

Results: Microscopic evaluation revealed a neoplasm composed of mucous-producing, intermediate, and epidermoid cells arranged in cystic and solid patterns. Intracytoplasmic mucin was identified without significant atypia or high mitotic activity (Fig 3). Findings were consistent with low-grade MEC. Surgical margins were clear, and imaging showed no regional or distant metastasis. No recurrence was observed at 12-month follow-up.

Conclusions: Malignant salivary gland tumors may clinically mimic benign lesions such as mucoceles. Routine histopathologic examination of excised oral lesions is essential to ensure accurate diagnosis and appropriate management.

Figure 1. Preoperative clinical photograph showing a small, dome-shaped submucosal swelling on the right lower lip with intact overlying mucosa. The lesion appeared soft and fluctuant without ulceration, clinically suggestive of a mucocele..

Figure 2. Excised specimen measuring approximately 1.5 cm in greatest dimension, appearing as a well-circumscribed, tan-pink soft tissue nodule..

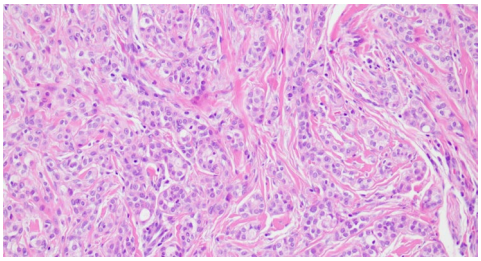

Figure 3. Hematoxylin and eosin–stained section demonstrating a neoplasm composed of mucous-producing cells, intermediate cells, and epidermoid cells arranged in cystic and solid patterns within fibrous stroma.

EP-067

재발성 MRSA 양성 두피 결손에서 두개골 재건 없이 노출된 경막을 국소 회전 피판으로 덮은 증례 보고

(Local Rotation Flap Coverage Over Exposed Dura Without Calvarial Reconstruction in a Recurrent MRSA-Positive Scalp Defect: A Case Report)

순천향대학교 구미병원

김은찬, 김세영★

Background: Reconstruction of scalp defects with exposed dura after multiple prior operations is challenging, particularly in patients with diabetes and a history of MRSA infection. Coverage without calvarial reconstruction is generally considered high risk for infection and flap failure. This report describes successful reconstruction of a temporoparietal scalp defect with exposed dura using a local rotation flap without calvarial reconstruction in a patient with multiple prior infections.

Methods: A 42-year-old man with Moyamoya disease developed a temporoparietal 7x5 cm scalp defect with calvarial bone loss and dural exposure following STA–MCA bypass and prior rotational flap surgery (Fig 1). Preoperative images revealed bony defect with soft tissue changes (Fig 2,3). After radical debridement of nonviable tissue and irrigation, a local rotation flap was designed in the parieto-occipital scalp. A 10 × 8 cm curvilinear flap was elevated as a full-thickness scalp flap, including skin, subcutaneous tissue, and galea, in the subgaleal plane. The flap was rotated anteriorly and temporally to cover the exposed dura directly without bony reconstruction or synthetic material.

Results: Despite previous MRSA-positive wound cultures and elevated inflammatory markers, the flap survived completely without necrosis, dehiscence, or cerebrospinal fluid leakage. Serial laboratory monitoring showed no progression of infection. The wound remained stable with durable soft tissue coverage over the dura after 1 month follow-up (Fig 4).

Conclusions: A large posteriorly based local rotation flap can provide reliable coverage directly over exposed dura without calvarial reconstruction, especially in patients with prior MRSA infection, when meticulous debridement and infection control are ensured.

Figure 1. Preoperative clinical view. Preoperative lateral view of the fight temporoparietal scalp demonstrating postoperative skin and soft tissue defect with wound breakdown following neurosurgical intervention.

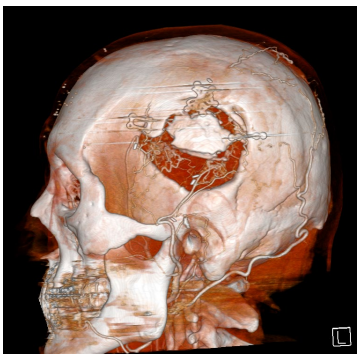

Figure 2. Preoperative imaging findings. Three-dimensional reconstructed computed tomography demonstrating the right 7 x 5 cm temporoparietal craniotomy defect with fixation hardware in situ.

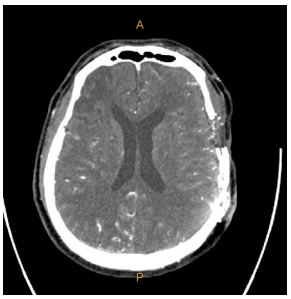

Figure 3. Preoperative axial CT image. Axial computed tomography scan showing the temporoparietal cranial defect and surrounding postoperative changes.

Figure 4. Postoperative clinical photo. Postoperative lateral view showing stable soft-tissue coverage of the right temporoparietal scalp following reconstruction with a local rotation flap after 1 month follow-up without any complications

EP-068

흉배동맥 천공지 유리피판을 이용한 두피 재건: 증례군 연구

Scalp Resurfacing with a Versatile Thoracodorsal Artery Perforator Free Flap: A Case Series

한양대학교 의과대학
성형외과학교실
한양대학교 서울병원
성형외과

안중권, 장란숙, 김효성, 김지영, 김연환★

Purpose: Scalp defects following wide excision of malignant skin tumors present significant reconstructive challenges due to limited tissue elasticity, frequent calvarial exposure, and prior radiation. This study evaluates the clinical outcomes and reliability of the thoracodorsal artery perforator (TDAP) free flap for oncologic scalp reconstruction.

Methods: A retrospective review was conducted of 14 patients who underwent scalp reconstruction with a TDAP free flap between February 2016 and January 2026. Patients reconstructed with local, regional, or alternative free flaps were excluded. Demographic data, diagnosis, body mass index (BMI), defect location, flap size, pedicle length, operative time, recipient vessels, postoperative complications, secondary procedures, follow-up duration, and tumor recurrence were analyzed. All reconstructions were performed by a single senior surgeon. The superficial temporal vessels were used as recipient vessels in all cases.

Results: The cohort included 8 females and 6 males with a mean age of 62.4 years. Diagnoses included basal cell carcinoma, squamous cell carcinoma, basosquamous carcinoma, angiosarcoma, malignant melanoma, and other malignant tumors. The mean BMI was 23.6 kg/m². The average flap size was 97 cm², with a mean pedicle length of 9.7 cm. The mean operative time was 134.3 minutes. One patient developed venous thrombosis requiring re-exploration; no total flap loss occurred. Secondary procedures were performed selectively for contour refinement or scar revision. No local tumor recurrence was observed during follow-up.

Conclusion: The TDAP free flap provides reliable vascularity, adequate pedicle length, and stable coverage for oncologic scalp defects, with low complication rates and satisfactory oncologic outcomes.

Sex	Age	Diagnosis	BMI	Flap	Location	Flap dimension (cm²)	Op time (min)
F	52	BCC	26.6	TDAP	Lt. temple	56	120
F	25	SCC	24.2	TDAP	Rt. temple and vertex	80	210
F	32	BCC	18.6	TDAP	Lt. temple	42	90
F	85	SCC	12.8	TDAP	Lt. temple	48	150
M	84	BCC	23.6	TDAP	Lt. temple	72	120
M	56	BSCC	34.6	TDAP	Lt. temple and vertex	165	150
F	38	Procarcinoma	29.9	TDAP	Rt. Temple	63	120
M	74	SCC	16.7	TDAP	Rt. temple	70	120
M	65	angiosarcoma	25.4	TDAP	Rt. temple	120	120
F	76	Malignant melanoma	28.8	TDAP	Lt.temple and vertex	154	120
M	78	SCC	21.4	TDAP	Rt. temple	168	140
M	72	SCC	23.6	TDAP	Rt. temple and vertex	210	150
F	84	BSCC	21.6	TDAP	Lt. temple	56	120
F	52	SCC	22.1	TDAP	Lt. temple	54	150

BCC, basal cell carcinoma; SCC, squamous cell carcinoma; BSCC, basosquamous cell carcinoma; TDAP, thoracodorsal artery perforator free flap

Table 1. Patient demographics, tumor diagnoses, defect locations, and operative characteristics in patients who underwent scalp reconstruction with a thoracodorsal artery perforator free flap.

Figure 1. Clinical photographs of a 56-year-old male patient (BMI 34 kg/m²) diagnosed with basosquamous cell carcinoma, with underlying diabetes mellitus and hypertension. (Left) Preoperative view showing the scalp malignancy involving the temple and vertex regions. (Right) Intraoperative view after wide oncologic excision demonstrating the resultant scalp defect prior to reconstruction.

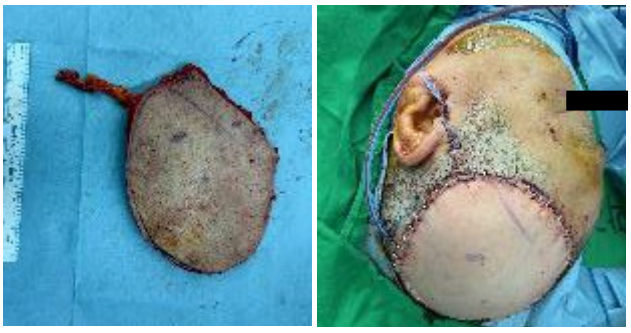

Figure 2. Intraoperative images demonstrating thoracodorsal artery perforator free flap reconstruction for the scalp defect in the same patient. (Left) Harvested TDAP flap measuring 15 × 11 cm (total area 165 cm²) with a pedicle length of 14 cm. (Right) The flap was anastomosed end-to-end to the superficial temporal vessels. Despite the patient's high BMI, defattening of the flap allowed it to match the surrounding contour.

EP-069

기저세포암의 광범위 절제술 후 볼 점막 전층 피부 이식을 이용한 상순 재건술: 증례 보고

Upper Lip Reconstruction Using Buccal Mucosal Full-Thickness Skin Graft After Wide Excision of Basal Cell Carcinoma: A Case Report

노원을지대병원[1]

장재혁[1], 민경희[1]★

Purpose: The upper lip plays a critical role in facial aesthetics, speech, and oral competence. Reconstruction of upper lip defects following oncologic resection requires careful consideration of both functional and cosmetic outcomes. We report a case of upper lip reconstruction using a buccal mucosal full-thickness skin graft (FTSG) after wide excision of basal cell carcinoma.

Methods: An 83-year-old male patient presented with a 2 × 1.2 cm black pigmented lesion on the upper lip that had been present for three years (Fig.1). A punch biopsy confirmed basal cell carcinoma. Wide excision was performed, resulting in a 3 × 1.5 cm defect of the upper lip. Reconstruction was achieved using a full-thickness graft harvested from the left buccal mucosa (Fig.2).

Fig.1 Clinical photograph showing a 2 x 1.2 cm basal cell carcinoma on the upper lip and the surgical defect after wide excision.

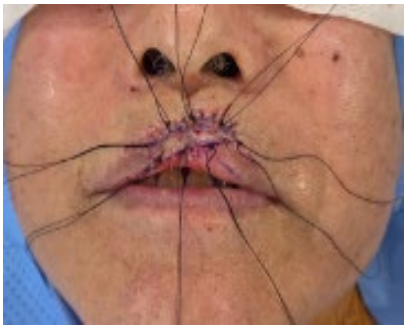

Fig.2 Coverage of the defect using a left buccal mucosal graft.

Results: The graft survived completely without postoperative complications, including infection, hematoma, or partial necrosis. The donor site healed uneventfully. Functional outcomes, including oral competence and speech, were preserved, and satisfactory aesthetic results were achieved (Fig.3).

Conclusion: Buccal mucosal grafting is a reliable and effective option for reconstruction of partial-thickness upper lip defects following tumor excision. Given its similar texture and color to lip mucosa, concealed donor site, and minimal morbidity, it represents a valuable reconstructive option, particularly in elderly patients.

Fig.3 Excellent esthetic outcome observed at the 10-day postoperative follow-up.

EP-070

이마에 발생한 고를린 증후군의 드문 증례 보고

한림대학교성심병원

김준일, 김재현, 정찬민★

Purpose: Gorlin syndrome, also known as Nevoid basal cell carcinoma syndrome(NBCCS), is a genetic disorder associated with basal cell carcinomas (BCCs) and skeletal anomalies. Typically patients show up with early-onset or multiple BCCs. This paper presents a patient with NBCCS on forehead with a rib abnormality and palmar pits

Methods: A 28-year-old female presented at our clinic with a BCC on forehead which was treated with wide excision (Fig. 1). The lesion was diagnosed by biopsy (Fig. 2). Subsequently, a second BCC emerged in a distinct region on the patient's forehead within a year (Fig. 3). The patient had palmar pits and further radiologic examination revealed a rib anomaly, specifically the absence of the 12th rib (Fig. 4). The correlation between these findings prompted a diagnosis of Gorlin syndrome. A second wide excision was performed to manage the recurrent BCC.

Results: The patient was discharged from the hospital three days post-surgery. The wound was stable, and a follow-up after three months with consultation to oncology confirmed the patient's complete recovery without any complications.

Conclusion: NBCCS, or Gorlin-Goltz syndrome, is a systemic condition along with multiple or early onset BCCs. While noticing BCC through biopsy may be straightforward, it is essential to make a multidisciplinary approach to a patient with possible NBCCS. The presence of recurrent BCCs, coupled with palmar pits and the absence of the 12th rib emphasizes that diagnosing should not be limited to cutaneous lesions but should encompass various systemic conditions.

Fig 1. Preoperative gross photography of BCC (1st BCC: upper forehead)

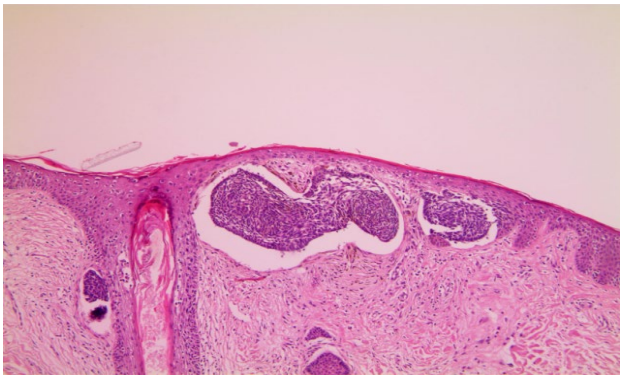

Fig 2. Basaloid cells with palisading seen in H&E staining (x100)

Fig 3. Preoperative gross photography of BCC (2nd BCC: left forehead)

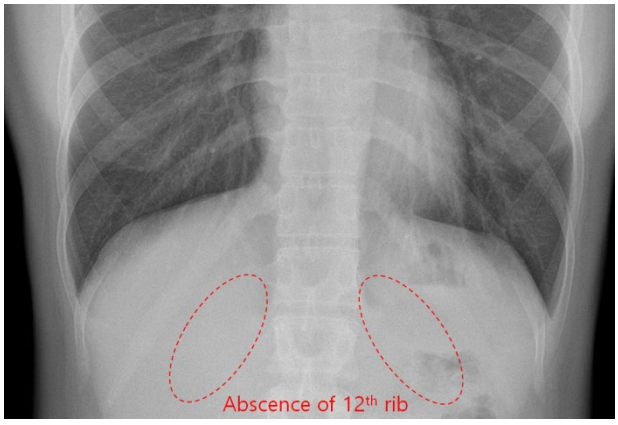

Fig 4. Radiologic findings: absence of the 12th rib

EP-071

두피에 발생한 미세낭성 부속기암의 드문 증례

한림대학교성심병원

이명섭, 김재현, 정찬민★

Purpose: Microcystic adnexal carcinoma (MAC) is a malignant tumor originating from sweat glands, predominantly occurring in the head and neck region. It grows slowly and, although metastasis is rare, it exhibits locally aggressive behavior. It is known to occur very rarely. We report a case of a patient who presented to our hospital with a gradually enlarging mass on the scalp that had been developing over the past year, leading to a diagnosis of MAC.

Methods: A 51-year-old patient presented to our hospital with a 4 × 3 × 2cm sized mass with protrusion in the left frontal scalp (Fig. 1). A punch biopsy raised concerns for a malignant tumor, prompting us to proceed with an excisional biopsy (Fig. 2). Histopathological analysis revealed strands of basaloid epitheloid cells with ductal lumina, consistent with a diagnosis of MAC (Fig. 3). Imaging studies showed no evidence of lymph node involvement or metastasis to other areas. Subsequently, we performed wide excision with negative resection margins, followed by reconstruction with a full-thickness skin graft for the defect.

Results: The wound healed without complications (Fig. 4). The patient underwent follow-up for 11 months after the surgery, and regular imaging studies revealed no recurrence or metastasis

Conclusion: This case underscores the necessity of considering microcystic adnexal carcinoma in the differential diagnosis of scalp lesions due to its potential for local aggressiveness and perineural invasion. Prompt detection and surgical management are crucial, and diligent follow-up is imperative for early identification of potential recurrences.

Fig 1. Preoperative gross photography

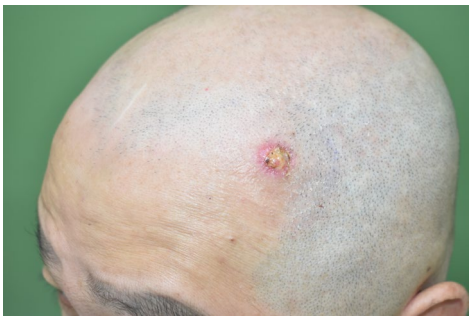

Fig 2. Postoperative gross photography of the excision site

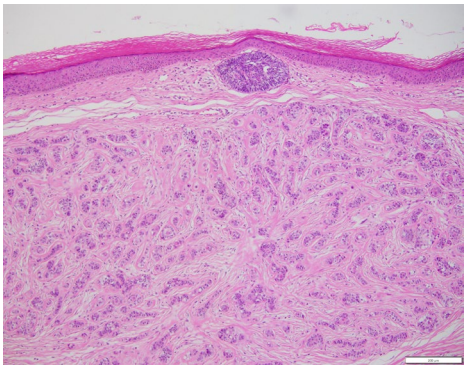

Fig 3. Pathological tumor staining with hematoxylin-eosin (HE). A separation zone is seen between the epidermis and the tumor, with cords of basaloid epithelial cells exhibiting ductal structures (HE, × 100).

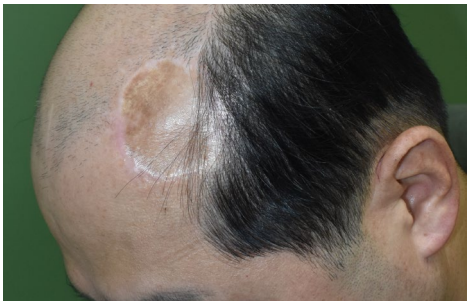

Fig 4. Postoperative gross photography after 11 months of surgery

EP-072

안면부 비흑색종 피부암 재건 시 무세포 진피 기질(ADM)의 유용성: 피판 크기 최소화 및 미용적 결과 향상을 위한 전략

(Utility of Acellular Dermal Matrix (ADM) in Reconstruction of Facial Non-Melanocytic Skin Cancer: Strategies for Minimizing Flap Dimensions and Enhancing Aesthetic Outcomes)

동국대학교 의과대학 성형외과학교실[1]

윤우혁[1], **이준호**★[1]

Purpose: Reconstructing facial defects after non-melanocytic skin cancer (NMSC) excision requires balancing aesthetics with function. This study evaluates the utility of Acellular Dermal Matrix (ADM) in reducing required flap dimensions and minimizing donor site morbidity.

Methods: Patients with NMSC facial defects underwent reconstruction using a hybrid approach. ADM was implanted into the wound bed to restore dermal thickness and provide a vascular scaffold. This allowed for the use of smaller local flaps or thin skin grafts that would otherwise be insufficient for deep defects. Outcomes were assessed based on flap size, tension-related distortion, and contour symmetry.

Results: The integration of ADM allowed for a significant reduction in the surface area and rotation arc of the required flaps. By providing essential vertical thickness, ADM prevented the "sunken" appearance often associated with traditional skin grafting. Key findings indicated minimal tension on adjacent structures, leading to a lower incidence of secondary deformities. Furthermore, the use of ADM facilitated the closure of defects in "tight" anatomical regions, such as the nasal and temporal areas, where skin laxity is insufficient for large flap mobilization.

Conclusion: ADM serves as a highly effective adjunct in facial NMSC reconstruction by acting as a biological volume filler and structural foundation. Its use successfully minimizes the necessity for extensive flap harvesting, reduces scar burden, and preserves the natural architecture of the face. For complex facial defects, the ADM-hybrid approach represents a tissue-conservative alternative that optimizes both functional and cosmetic surgical goals.

Fig. 1. Pre and postoperative photograph: A) Preoperative: Bowen's disease is noted on nasal dorsum, B) Postoperative: after ADM graft, integration with surrounding tissue is noted on 1 month post-op

Fig. 2. Intra and postoperative photograph : A) Intraoperative: Integration of ADM allowed for smaller flap elevation and inset, B) Postoperative: 1 year after surgery, both functional and cosmetic surgical goals were met.

EP-073

표피낭종을 모사한 인중의 기저세포암: 중심점 소견을 동반한 증례 보고

(Philtrum basal cell carcinoma with a central spot : A mimic of epidermal cyst)

순천향대 구미병원
배진오, 위서영★

Purpose: Basal cell carcinoma (BCC) presents with diverse clinical features, occasionally leading to misdiagnosis as benign lesions. While epidermal cysts are common on the face, BCC can simulate their appearance, including the presence of a central punctum-like spot. We report a case of BCC on the philtrum that was clinically indistinguishable from an epidermal cyst upon initial presentation. Such clinical mimicry may obscure the possibility of an underlying malignancy during initial evaluation.

Methods: A 62-year-old female presented with a persistent 0.2 x 0.2 cm nodule on the philtrum (Fig. 1). The mass exhibited a distinct central black spot, remarkably mimicking the classic punctum of an epidermal cyst. Under local anesthesia, an excisional biopsy was performed to ensure definitive diagnosis (Fig. 2).

Results: Histopathological analysis of the philtrum lesion revealed BCC. Microscopic evaluation with H&E staining demonstrated characteristic nests of basaloid cells exhibiting peripheral palisading and prominent peritumoral clefting (Fig. 3). The postoperative course was uneventful, with no immediate functional or surgical complications observed.

Conclusions: The presence of a central spot should not be considered pathognomonic for an epidermal cyst, as BCC can present with remarkably similar features. Clinicians should not rely solely on clinical appearance; instead, they must perform an excisional biopsy for persistent nodules to confirm the diagnosis and provide early management. Even when a lesion strongly resembles a benign epidermal cyst, the possibility of malignancy such as BCC should always be considered during clinical evaluation.

Fig. 1 The mass on the philtrum exhibited a distinct central black spot measuring 0.2 x 0.2 cm, mimicking the classic punctum of an epidermal cyst.

Fig. 2 The specimen measures approximately 0.4 x 0.4 cm. The central black spot, which clinically mimicked a punctum, is clearly visible on the surface of the excised nodule.

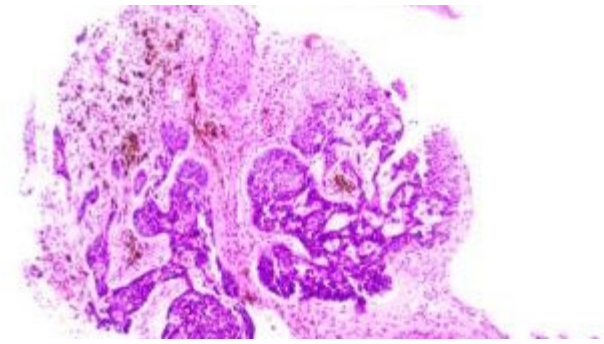

Fig. 3 H&E staining reveals nests of basaloid cells with characteristic peripheral palisading and peritumoral clefting, confirming the diagnosis of basal cell carcinoma.

EP-074

양측성 구순구개열 환자에서 발생한 대형 구개누공 재건을 위한 안면동맥 근점막 피판에 대한 임상경험

(Anterior Palatal Fistula Repair Using Superiorly Based Facial Artery Myomucosal Flap in Bilateral Complete Cleft Palate Patients)

서울아산병원[1]
이스트만치과[2]

장서연[1], 김영철[1], 권순만★[2], 오태석[1]

Purpose: Large palatal fistulas are difficult to treat due to poor vascularity and scarring. The facial artery myomucosal (FAMM) flap is a robust, well-vascularized option for these challenging cases. We describe our surgical technique and clinical experience using the FAMM flap for palatal fistula repair in bilateral cleft patients.

Methods: A retrospective review was conducted of pediatric cleft patients who underwent palatal fistula repair using a FAMM flap between 2018 and 2025. Patient demographics, operative details, and fistula characteristics, staged by the Pittsburgh classification, were analyzed. Clinical outcomes were evaluated based on fistula closure rates, postoperative complications, and speech outcomes.

Results: Eight patients (5 males; median age 9 years, range 4–16) with bilateral complete cleft lip and palate were included. Pittsburgh type IV was the most frequent fistula (50%). All repairs were performed using superiorly based FAMM flaps. Initial closure was achieved in all cases, though two (25%) recurred during follow-up. Minor complications included dehiscence (25%) and partial necrosis (12.5%), with no total flap loss. Postoperative speech evaluation demonstrated no hypernasality in 75% of patients, while mild and mild-to-moderate hypernasality were observed in one patient each.

Conclusions: The superiorly based FAMM flap is a reliable, single-stage reconstructive strategy for challenging palatal fistulas in bilateral cleft patients. It provides robust vascularity to scarred tissues, ensuring high initial closure rates with manageable complications and preserved speech function.

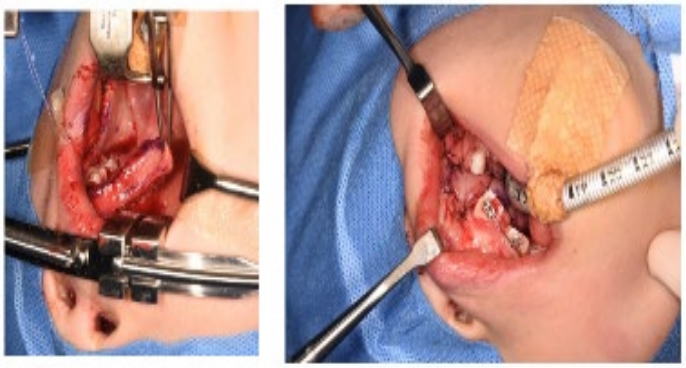

Fig. 1. Superiorly based FAMM flap in palatal fistula repair

Variable	Value
Sex	
Male	5 (62.5%)
Female	3 (37.5%)
Age, years	Median 9 (range, 4–16)
Cleft type	
Bilateral complete CLP	8 (100%)
Primary palatoplasty technique	
Three-flap	4 (50%)
Two-flap	2 (25%)
Staged repair	2 (25%)
Pittsburgh classification	
Type IV	4 (50%)
Type V	2 (25%)
Type VI	2 (25%)

Table. 1. Demographics and fistula profile (n=8)

Variable	Value
Pedicle type	
Superiorly based	8 (100%)
Side	
Left	7 (87.5%)
Right	1 (12.5%)
Adjunct procedure	
None	4 (50%)
Alveolar bone graft (ABG)	3 (37.5%)
IVV with buccal fat pad transfer	1 (12.5%)
Operative time, minutes	Median 196 (range, 130–237)

Table. 2. Operative details

Variable	n (%)
Initial successful closure	8 (100%)
Overall recurrence	2 (25%)
Speech outcome	
Hypernasality - none	6 (75%)
Hypernasality - mild	1 (12.5%)
Hypernasality - mild to moderate	1 (12.5%)
Complications	
Distal dehiscence	2 (25%)
Partial dehiscence	1 (12.5%)
Flap tip necrosis	1 (12.5%)
Total flap loss	0

Table. 3. Outcomes

EP-075

지역응급의료센터에 내원한 전동킥보드 및 자전거 탑승자의 두개안면 손상 양상 비교 분석: 단일 기관 후향적 연구

(Comparative Analysis of Craniofacial Injury Patterns in Electric Scooter and Bicycle Riders Presenting to a Local Emergency Medical Center: A Retrospective Single-Center Study)

노원을지대학교병원 성형외과

김승현, 홍주현, 이동락, 민경희★

Purpose: The proliferation of electric scooters (e-scooters) has increased e-scooter-related craniofacial trauma. This study compared demographic characteristics, injury circumstances, craniofacial injury patterns, and clinical outcomes between e-scooter and bicycle riders at a local emergency medical center.

Methods: This single-center retrospective study reviewed 365 patients (e-scooter n=57, bicycle n=308) presenting with craniofacial injuries to Nowon Eulji Medical Center between January 2023 and November 2025. Fracture sites, soft tissue injury locations and surgical procedures were coded independently per anatomical site. Welch's t-test and chi-square or Fisher's exact test were applied ($p < 0.05$).

Results: E-scooter riders were significantly younger (32.2 ± 15.8 vs. 49.0 ± 21.9 years, $p < 0.001$), more frequently injured at nighttime (45.6% vs. 18.2%, $p < 0.001$), more often transported by EMS (68.4% vs. 52.6%, $p = 0.027$), and more alcohol-involved (28.1% vs. 9.1%, $p < 0.001$). Fracture rates were comparable (15.8% vs. 16.6%, $p = 0.886$), with orbital fractures most common in both groups. Cheek and chin injuries were more prevalent in e-scooter riders (22.8%; 17.7% vs. 10.0%), while forehead injuries predominated in bicycle riders (20.3%). Concurrent intracranial hemorrhage occurred exclusively in bicycle riders (0% vs. 5.2%, $p = 0.078$). Surgical rates trended higher in e-scooter riders (52.6% vs. 40.6%, $p = 0.091$).

Conclusion: E-scooter craniofacial injuries predominantly affect younger adults, occurring more frequently at night with greater alcohol involvement. Despite comparable fracture rates, distinct soft tissue distributions and absence of intracranial hemorrhage in e-scooter riders suggest different injury biomechanics. Mandatory helmet legislation, alcohol enforcement, and nighttime speed restrictions are warranted.

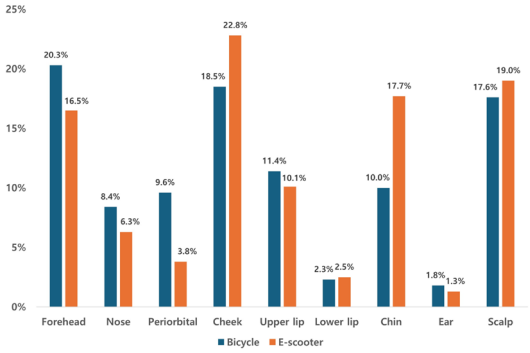

Fig. 1. Anatomical distribution of soft tissue craniofacial injuries in bicycle and e-scooter riders

Table 1. Baseline Characteristics and Circumstances of E-scooter vs Bicycle Injuries

Variables	Total (N=365)	Bicycle (n=308)	E-scooter (n=57)	p-value
Age (years), mean ± SD	46.3 ± 21.5	49.0 ± 21.9	32.2 ± 15.8	<0.001[a]
Age group, n (%)				<0.001[b]
16-19 years	53 (14.5)	43 (14.0)	10 (17.5)	
20-29 years	68 (18.6)	43 (14.0)	25 (43.9)	
30-39 years	37 (10.1)	29 (9.4)	8 (14.0)	
40-49 years	34 (9.3)	29 (9.4)	5 (8.8)	
50-59 years	47 (12.9)	42 (13.6)	5 (8.8)	
60-69 years	53 (14.5)	52 (16.9)	1 (1.8)	
70-79 years	55 (15.1)	53 (17.2)	2 (3.5)	
≥80 years	18 (4.9)	17 (5.5)	1 (1.8)	
Sex, n (%)				0.141[b]
Male	266 (72.9)	229 (74.4)	37 (64.9)	
Female	99 (27.1)	79 (25.6)	20 (35.1)	
Time of day, n (%)				<0.001[b,c]
Day (07:00-14:00)	120 (33.0)	105 (34.2)	15 (26.3)	
Evening (14:00-22:00)	162 (44.5)	146 (47.6)	16 (28.1)	
Night (22:00-07:00)	82 (22.5)	56 (18.2)	26 (45.6)	
Season, n (%)				0.549[b,c]
Spring (Mar-May)	105 (28.8)	90 (29.2)	15 (26.3)	
Summer (Jun-Aug)	114 (31.2)	92 (29.9)	22 (38.6)	
Autumn (Sep-Nov)	108 (29.6)	92 (29.9)	16 (28.1)	
Winter (Dec-Feb)	38 (10.4)	34 (11.0)	4 (7.0)	
Route of arrival, n (%)				0.027[b]
EMS (119)	201 (55.1)	162 (52.6)	39 (68.4)	
Self-transport	164 (44.9)	146 (47.4)	18 (31.6)	
Helmet use, n (%)				0.218[b]
Yes	51 (14.0)	46 (14.9)	5 (8.8)	
No	314 (86.0)	262 (85.1)	52 (91.2)	
Alcohol involvement, n (%)				<0.001[b]
Yes	44 (12.1)	28 (9.1)	16 (28.1)	
No	321 (87.9)	280 (90.9)	41 (71.9)	
Loss of consciousness, n (%)				0.283[b]
Yes	65 (17.8)	52 (16.9)	13 (22.8)	
No	300 (82.2)	256 (83.1)	44 (77.2)	

[a] *Student's t-test (Welch's t-test due to unequal variances, Levene's test p<0.05)*
[b] *Pearson's chi-square test*
[c] *Fisher's exact test*

Table 1. Baseline Characteristics and Circumstances of E-scooter vs Bicycle Injuries

Table 2. Clinical Outcomes and Treatment of E-scooter vs Bicycle Injuries

Variable	Total (N=365)	Bicycle (n=308)	E-scooter (n=57)	p-value
Injury type, n (%)				0.886[a]
without fractures	305 (83.6)	257 (83.4)	48 (84.2)	
with fractures	60 (16.4)	51 (16.6)	9 (15.8)	
Fracture site, n (%)	N=93	N=77	N=16	0.228[a]
Frontal	5 (5.4)	5 (6.5)	0 (0.0)	
Orbital	27 (29.0)	23 (29.9)	4 (25.0)	
Nose	23 (24.7)	20 (26.0)	3 (18.8)	
Maxilla	18 (19.4)	14 (18.2)	4 (25.0)	
Zygoma	17 (18.3)	14 (18.2)	3 (18.8)	
Mandible	3 (3.2)	1 (1.3)	2 (12.5)	
Surgery performed, n (%)				0.091[a]
Yes	155 (42.5)	125 (40.6)	30 (52.6)	
No	210 (57.5)	183 (59.4)	27 (47.4)	
Type of surgery, n (%)	N=228	N=193	N=35	0.919[a,c]
Primary closure	199 (87.3)	169 (87.6)	30 (85.7)	
CR	12 (5.3)	10 (5.2)	2 (5.7)	
OR/IF	9 (3.9)	7 (3.6)	2 (5.7)	
FTSG	3 (1.3)	3 (1.6)	0 (0.0)	
Gillies'	3 (1.3)	2 (1.0)	1 (2.9)	
Burrhole trephination	1 (0.4)	1 (0.5)	0 (0.0)	
Tertiary closure	1 (0.4)	1 (0.5)	0 (0.0)	
Hospitalization, n (%)				0.490[a]
Yes	30 (8.2)	24 (7.8)	6 (10.5)	
No	335 (91.8)	284 (92.2)	51 (89.5)	

[a] *Pearson's chi-square test*
[c] *Fisher's exact test*
(CR, closed reduction; OR/IF, open reduction and internal fixation; FTSG, full-thickness skin graft)

Table 2. Clinical Outcomes and Treatment of E-scooter vs Bicycle Injuries

EP-076

이마에 발생한 다발성 골종: 내시경적 치료 및 가드너 증후군 평가

(Multiple Osteomas of the Forehead: Endoscopic Management and Evaluation for Gardner Syndrome)

조선대학교 의과대학
성형외과학교실

<u>이현정</u>, 최우영★, 천지선, 양정열

Purpose: Osteoma is a benign osteogenic tumor that commonly arises in the craniofacial skeleton, particularly the frontal bone. While solitary osteomas are relatively common, multiple craniofacial osteomas are uncommon and may raise suspicion for syndromic conditions such as Gardner syndrome. We report a case of multiple osteomas involving the forehead that were successfully treated using an endoscopic approach and highlight the clinical importance of evaluating potential syndromic associations.

Methods: A 48-year-old woman was referred from a local hospital with multiple palpable nodules on the forehead and scalp that had gradually increased in number over the previous year. The patient initially noticed a single lesion, followed by the development of additional nodules. Physical examination revealed multiple firm, non-tender bony nodules on the forehead (Fig. 1). Three-dimensional computed tomography demonstrated multiple well-defined bony protrusions arising from the frontal bone, consistent with osteomas (Fig. 2). Surgical excision was performed via a hairline incision using an endoscopic approach, allowing identification and removal of multiple bony lesions arising from the frontal bone.

Results: Multiple well-circumscribed bony nodules were successfully excised (Fig. 3). Histopathologic examination demonstrated mature lamellated bone with Haversian-like canals of variable sizes and shapes, consistent with osteoma (Fig. 4). Because multiple craniofacial osteomas can be associated with Gardner syndrome, further evaluation was performed. The patient had no family history of colorectal cancer, and colonoscopic examination revealed no evidence of colonic polyps. The postoperative course was uneventful.

Conclusion: Multiple osteomas of the forehead are uncommon and may be associated with syndromic conditions such as Gardner syndrome. Therefore, when multiple craniofacial osteomas are identified, appropriate clinical evaluation and systemic screening should be considered. Endoscopic excision through a hairline incision represents a safe and effective surgical option, offering favorable cosmetic outcomes.

Fig. 1. Preoperative frontal photograph demonstrating multiple palpable bony nodules on the forehead (circles).

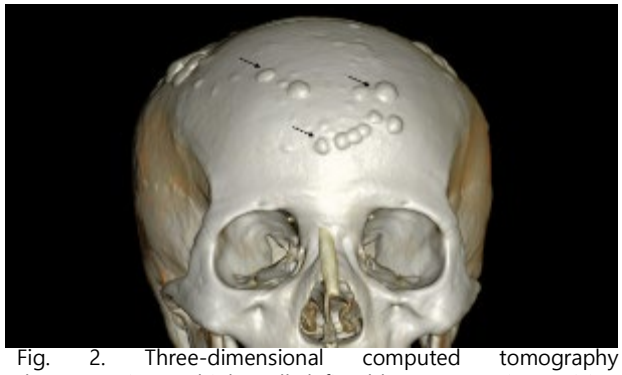

Fig. 2. Three-dimensional computed tomography demonstrating multiple well-defined bony protrusions arising from the frontal bone (arrows), consistent with osteomas.

Fig. 3. Gross specimens of multiple excised osteomas demonstrating multiple well-circumscribed bony nodules of varying sizes (surgical ruler shown for scale).

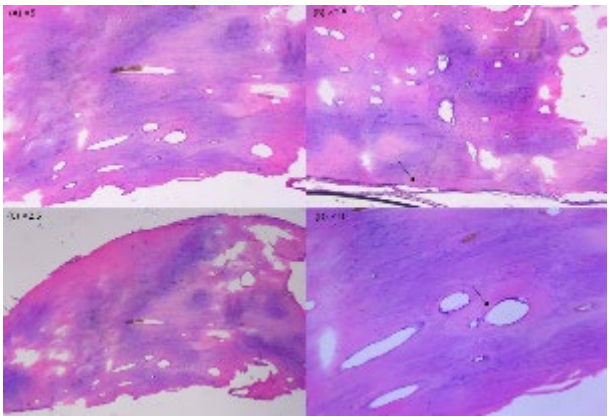

Fig. 4. Histopathologic findings of the excised lesions demonstrating mature lamellated bone with Haversian systems (arrows), consistent with osteoma (H&E stain; original magnification ×2.5–×10).

EP-077

안면바비에서 안륜근 구축 교정을 위한 외안각성형술 및 수직 안검열 확대술

(Lateral Canthoplasty and Vertical Palpebral Fissure Enlargement for the Correction of Orbicularis Oculi Muscle Contracture in Facial Palsy)

가톨릭대학교 의과대학 성형외과학교실

장지형, 신종원★

Purpose : This study presents a case of periocular asymmetry caused by Orbicularis Oculi Muscle (OOM) contracture after facial palsy and describes its surgical correction using combined lateral canthoplasty and vertical palpebral fissure enlargement.

Methods : An 81-year-old woman with a 10-year history of unilateral facial palsy presented with lower eyelid elevation and reduced horizontal and vertical palpebral fissure dimensions on the affected side. Under local anesthesia, complete lateral canthotomy, lateral canthoplasty, and posterior lamellar shortening through a transconjunctival approach were performed. Surgical outcome was assessed by comparing preoperative and postoperative photographic measurements, including horizontal palpebral fissure length, Margin Reflex Distance 2 (MRD2), and medial and lateral scleral triangle areas..

Results : At 1-year follow-up, objective analysis demonstrated improvement in both horizontal and vertical palpebral fissure dimensions with better ocular symmetry (Fig. 1). Horizontal palpebral fissure length increased from 19.7 mm to 23.2 mm, and MRD2 improved from 2.6 mm to 4.3 mm. The medial scleral triangle area increased from 3.1 mm^2 to 11.1 mm^2, and the lateral scleral triangle area increased from 3.5 mm^2 to 11.6 mm^2. Mild chemosis resolved with conservative management, and no major complications, including epiphora, lagophthalmos, or ectropion, were observed.

The defect was fully covered. At 6 months after surgery, the patient showed favorable functional and aesthetic outcomes without complications such as ectropion.

Conclusions : This case suggests that combined lateral canthoplasty and vertical palpebral fissure enlargement can be considered for selected patients with periocular asymmetry caused by OOM contracture after facial palsy.

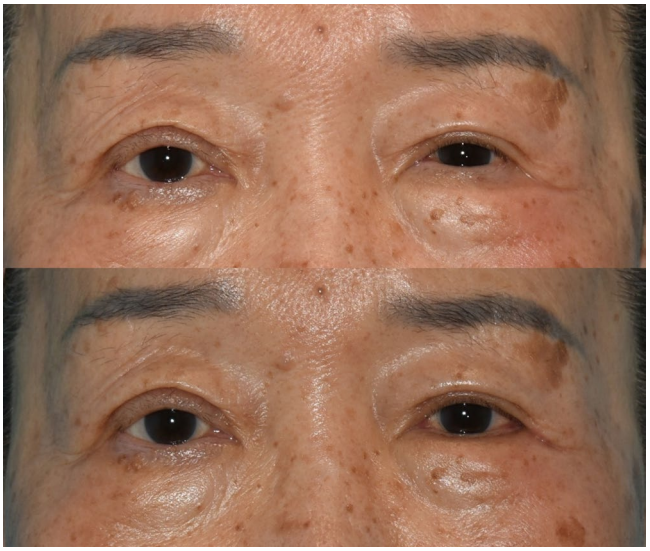

Fig. 1. Preoperative (upper) and postoperative photograph obtained at the 1-year follow-up (lower). Compared with the preoperative state, ocular asymmetry is notably improved, with favorable changes in the horizontal palpebral fissure width, margin reflex distance 2, and both the medial and lateral scleral triangle areas.

EP-078

두피의 증식성 외모근초 종양

(Proliferating Trichilemmal Tumor of the Scalp)

강원대학교병원

김익준 ,이상열★

Purpose: Proliferating trichilemmal tumor (PTT) is an uncommon adnexal neoplasm derived from the outer root sheath, typically presenting as a slow-growing scalp nodule with a predilection for elderly women. However, long-standing lesions may enlarge to a giant size and exhibit locally aggressive behavior. We report a case of a long-standing giant PTT and review its clinicopathologic features and clinical implications.

Methods: An 88-year-old woman presented with a slow-growing scalp mass that had persisted for over 40 years. Physical examination revealed a flesh-colored, dome-shaped tumor with ulceration and hemorrhagic crusting in the occipital region, measuring 8 × 5 × 3.5 cm. The lesion was surgically excised with a 10 mm margin of normal scalp tissue, followed by reconstruction with a meshed full-thickness skin graft.

Results: Histopathological examination demonstrated well-demarcated lobules composed of stratified squamous epithelium with abrupt trichilemmal keratinization, without evidence of malignancy or local invasion. Based on these findings, the lesion was diagnosed as a benign PTT. The large size and long clinical history were consistent with a giant variant. Complete excision with adequate margins was successfully achieved.

Conclusion: Although PTT is generally benign, long-standing lesions with large size and ulceration may demonstrate aggressive behavior and potential for malignant transformation. Complete surgical excision with adequate margins is essential, and careful histopathologic evaluation along with long-term follow-up is recommended due to the risk of recurrence and, rarely, metastasis.

Fig 1. A flesh-colored, dome-shaped mass (8 × 5 × 3.5 cm) with ulceration and hemorrhagic crusting a necrotic portion in the occipital region

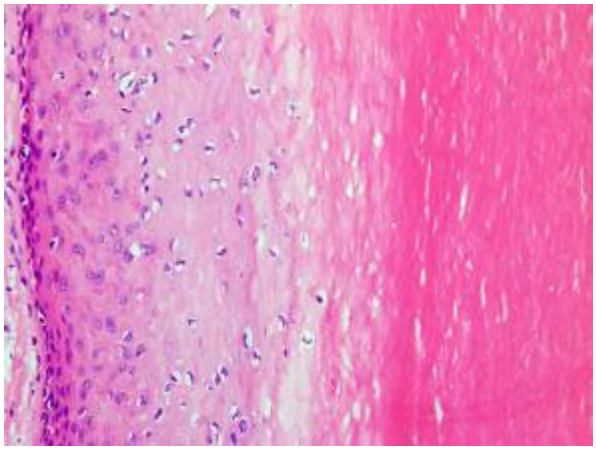

Fig 2. Histopathology reveals an abrupt transition of nucleated epithelial cells to anucleated keratinized cells without the formation of granular layers (H and E, 200×)

EP-079

후궁성형술 후 발생한 관상 염증성 누공 1예

한림대학교성심병원

이명섭, 김재현, 정찬민⋆

Purpose: Patients with surgical site infections can develop abscesses along with inflammation, often requiring antibiotics or drainage procedures. This inflammation resolves as healing progresses, with the formation of granulation tissue in the surrounding area. However, to the best of our knowledge, cases of tubular inflammatory granulation tissue tracts extending from the surgical site to the skin are uncommon. We present a case of a patient with a history of surgical site infection following laminoplasty, who presented with a mass on the posterior neck two years after surgery.

Methods: A 42-year-old patient presented to our hospital with a mass on the posterior neck (Fig. 1). The patient underwent laminoplasty 2 years ago, with a history of surgical site infection leading to abscess formation. Symptoms improved following antibiotic treatment at that time. Ultrasonography revealed that the mass was connected to the C-spine area (Fig. 2). Magnetic resonance imaging confirmed multiple tubular inflammatory tracts extending from the C-spine to the mass (Fig. 3). We excised the mass and a portion of the tracts, and histological examination confirmed inflamed granulation tissue.

Results: The wound healed without complications and the patient was satisfied with the outcome (Fig. 4).

Conclusion: This case emphasizes the rare occurrence of tubular tract formation after surgery, highlighting the need to identify uncommon post-surgical inflammatory responses. This suggests that lesions appearing as simple masses may require imaging to assess the internal characteristics if there is a history of surgical site infection.

Fig 1. Preoperative gross photography before excision

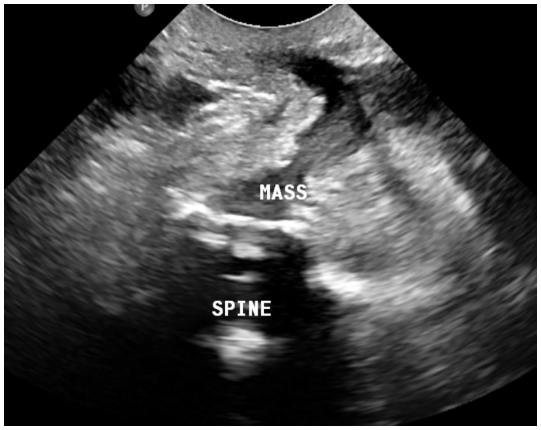

Fig 2. Ultrasonograhpy showing the lesion is connected to the C-spine.

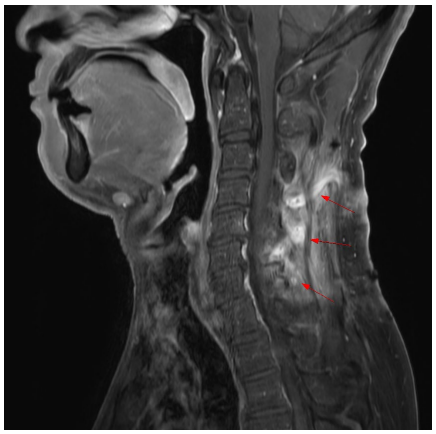

Fig 3. Preoperative magnetic resonance imaging (MRI). T1 sagittal view of contrast enhanced neck MRI showing multiple tubular inflammatory tracts and granulomas.

Fig 4. Postoperative gross photography after 3 months of surgery

EP-080

뺨에 발생한 원발성 점액성 선암의 드문 증례

한림대학교성심병원

이명섭, 김재현, 정찬민★

Purpose: Mucinous adenocarcinoma (MAC) is a malignant tumor originating from epithelial tissue, characterized by the secretion of large amounts of mucin. It commonly occurs in glandular organs such as the colon, breast, and lung. MAC can also manifest in the eccrine glands of the skin, though it is extremely rare, with an incidence rate of 0.07 per million person-years. This report presents a case of a patient who was admitted to our hospital with a nodule on the cheek, which was diagnosed as primary MAC of the skin.

Methods: A 66-year-old patient presented to our hospital with a nodule in the left cheek. The excisional biopsy results confirmed the presence of MAC with abundant mucin and predominant malignant epithelial cells (Fig. 1). Subsequent magnetic resonance imaging confirmed the absence of lymph node metastasis (Fig. 2). The patient refused all other examinations, preventing any further investigation of different areas. We performed wide excision with a resection margin of 1cm, and the defect was reconstructed using a local flap (Fig. 3). Negative resection margins were confirmed.

Results: The wound healed without complications and the patient was satisfied with the outcome (Fig. 4).

Conclusion: The exceptional occurrence of MAC on the skin underscores the critical need for clinical vigilance. Early detection and comprehensive diagnostic approaches, including histopathological examination and imaging, are crucial for accurate diagnosis and timely management, potentially improving patient outcomes.

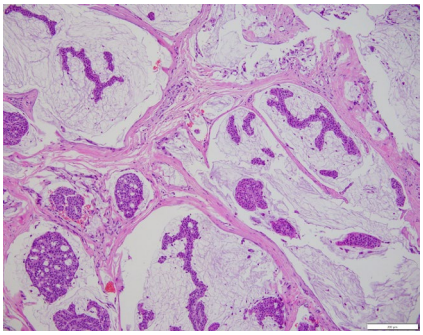

Fig 1. Pathological tumor staining with hematoxylin-eosin (HE). Abundance of mucin, predominance of malignant epithelial cells over mucin are observable (HE, 100).

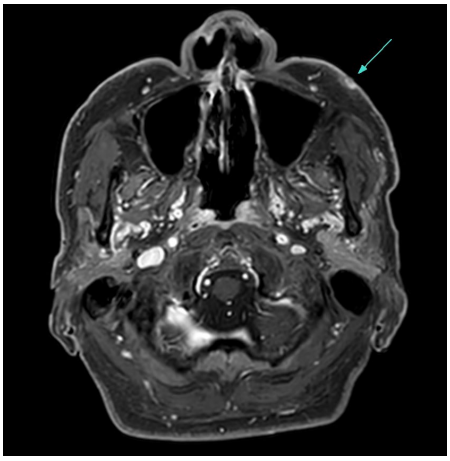

Fig 2. T1 axial view of contrast-enhanced neck magnetic resonance imaging showing a 6 × 7 × 3 mm size lesion in the left anterior cheek. No enlarged lymph nodes were found.

Fig 3. Preoperative gross photography before wide excision

Fig 4. Postoperative gross photography following wide excision

EP-081

귓불에 발생한 거대 켈로이드의 치료: 증례 보고

(Treatment of Huge Keloid on Earlobe: A Case Report)

한양대학교 의과대학
성형외과학교실
한양대학교 구리병원
성형외과

이보현, 이장현★

Purpose: Keloids are benign fibroproliferative scars caused by abnormal wound healing and frequently occur on the ear following ear piercing. Management remains challenging because of their tendency to progressively enlarge and recur after treatment. Here, we report a case of a large earlobe keloid that developed after previous excision and describe its surgical management.

Methods: A 56-year-old female patient with underlying conditions of anxiety disorder and panic disorder had undergone excision of a keloid on her left earlobe at a local clinic approximately 20 years ago. Although the mass had gradually increased in size over time without further treatment, she presented to the outpatient clinic due to increasing discomfort caused by the weight of the lesion.

Results: The surgery was performed under general anesthesia. An incision was made along the keloid margin, extending across the anterior aspect of the earlobe, part of the earlobe itself, and the posterior aspect of the earlobe. Dissection was carried out along the SMAS layer, and the keloid was completely excised. There was no exposure of the auricular cartilage at the defect site. The remaining defect was reconstructed using a split-thickness skin graft harvested from the thigh.

Conclusion: The skin graft at the recipient site was well taken, with no evidence of recurrence during the 6-month follow-up period. Early surgical intervention before the lesion becomes excessively large may facilitate reconstruction and improve patient comfort. Because recurrence is unpredictable, long-term follow-up is necessary after surgical treatment of keloids.

Fig. 1. Preoperative photographs of a 56-year-old woman with a large keloid involving the left earlobe at presentation. Lateral (left), frontal (center), and posterior (right) views demonstrate the size and extent of the lesion.

Fig. 2. Intraoperative photographs. Defect after complete excision of the earlobe keloid (left). Reconstruction with a split-thickness skin graft harvested from the thigh (right).

Fig. 3. Gross photographs of the excised keloid specimen. The anterior surface is shown (left), and the posterior surface with the stalk attached to the earlobe is shown (right).

Fig. 4. Postoperative photographs at 6 months after surgery. Lateral (left) and frontal (right) views demonstrate a well-healed reconstruction without evidence of keloid recurrence.

EP-082

혀 결손 재건에서 VRAM 피판의 유용성

(Revisiting the VRAM Flap: a Reliable Option for Total Tongue Reconstruction)

순천향대학교 부속 서울병원

윤현민, 탁민성★

Purpose: Tongue reconstruction requires a sufficiently bulky flap to facilitate optimal postoperative functional recovery, particularly for swallowing and articulation. Although the anterolateral thigh (ALT) free flap is widely preferred, the vertical rectus abdominis myocutaneous (VRAM) free flap may serve as a reliable alternative. This study evaluates our clinical experience with VRAM free flaps for tongue reconstruction and assesses their functional and surgical outcomes.

Methods:A retrospective review was conducted of eight patients who underwent tongue reconstruction using a VRAM free flap between 2022 and 2025. Seven patients underwent total glossectomy, and one underwent hemiglossectomy. The mean follow-up duration was 12 months. Postoperative outcomes, including flap survival, complications, maintenance of muscle bulk, and tolerance of oral intake, were assessed.

Results: Complete flap survival was achieved in all patients. Partial necrosis occurred in three cases; however, the underlying muscle bulk remained intact, and all patients improved following minor revision procedures. At the final follow-up, seven patients were able to tolerate a soft diet, whereas one patient required L-tube feeding despite preserved swallowing ability. No donor-site complications were observed, and flap bulk was satisfactorily maintained throughout the follow-up period.

Conclusion: Although the ALT free flap remains the preferred option for tongue reconstruction, the VRAM free flap provides stable long-term bulk maintenance and satisfactory functional outcomes. It may be particularly advantageous in cases requiring substantial volume preservation and should be considered a valuable option in the reconstructive surgeon's armamentarium.

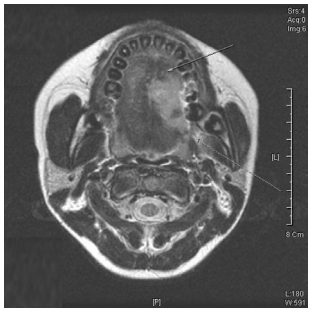

Fig. 1. Preoperative MRI of a 21-year-old woman with biopsy-proven squamous cell carcinoma shows an approximately 4cm ulcerating mass on the left side of the tongue (arrow).

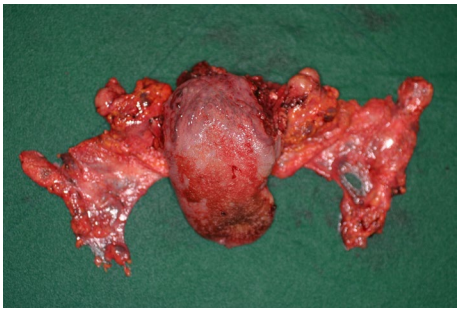

Fig. 2. Resected specimen following total glossectomy and bilateral supraomohyoid neck dissection (SOND) performed via a pull-through approach by the ENT department.

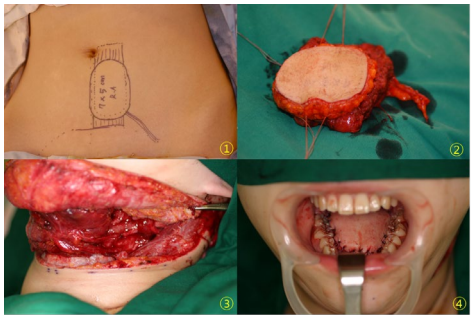

Fig. 3. Harvest of a vertical rectus abdominis myocutaneous (VRAM) free flap with a 7 × 5 cm skin paddle (1,2). Microvascular anastomosis to the superior thyroid artery and vein is shown (3), followed by immediate postoperative appearance (4).

Fig. 4. Postoperative finding at 7 months, showing satisfactory healing without complications.

EP-083

흉터 유사 병변에서 발생한 경부 융기성 피부섬유육종의 대흉근근피판을 이용한 재건

(Pectoralis Major Myocutaneous Flap Reconstruction for Cervical Dermatofibrosarcoma Protuberans Arising in a Scar-like Lesion)

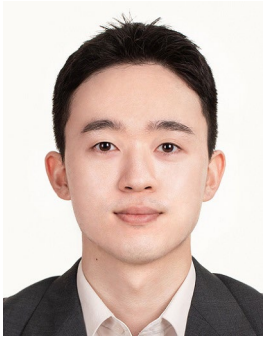

경상국립대학교병원
성형외과

김태호, 이경석★

Purpose : Dermatofibrosarcoma protuberans of the neck is rare and may present as a long-standing keloid-like or scar-like lesion. This report describes a case initially suspected as keloid or dermatofibroma, later diagnosed as dermatofibrosarcoma protuberans, and reconstructed with a pectoralis major myocutaneous (PMMC) flap.

Methods : A 62-year-old man had a 10-year history of an enlarging pruritic nodular neck lesion originating from multiple erythematous nodules, repeatedly traumatized with crusting and scarring, initially suspected as keloid or dermatofibroma. Under this impression, wide excision was performed, but frozen biopsy suggested possible sarcoma, so the cervical defect was left uncovered and the operation was temporarily completed without reconstruction.

Results : Final pathology confirmed dermatofibrosarcoma protuberans, and he subsequently underwent combined surgery with neck mass resection, bilateral neck dissection, and creation of a large cervical defect, followed by reconstruction using a PMMC flap with an 8×15 cm skin paddle based on the distal third of thoracoacromial artery. The flap was elevated in the avascular plane between pectoralis major and minor, tunneled over the clavicle, rotated to the neck with adequate pedicle length and minimal tension, survived completely without major complications, and tolerated adjuvant radiotherapy (5000 cGy/25 fx).

Conclusion : Dermatofibrosarcoma protuberans can clinically mimic scar-like or keloid-like lesions, particularly in previously traumatized or operated areas, and suspicious lesions require thorough evaluation to prevent misdiagnosis and insufficient excision. In addition, the pectoralis major myocutaneous flap provided a reliable reconstructive option after wide cervical resection in this setting.

Fig. 1. Pre-operative photograph of neck lesion

Fig. 2. Photograph of neck lesion following initial wide excision

Fig. 3. Intra-operative photograph of cervical lesion

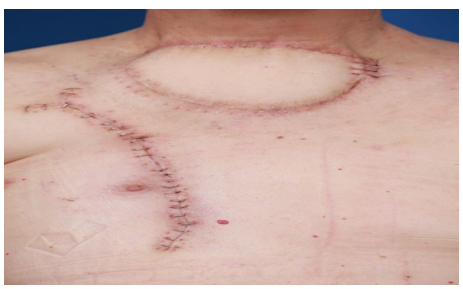

Fig. 4. Post-operative photograph following PMMC flap reconstruction

EP-084

하안검 제자리 악성흑색종 절제 후 발생한 결막유착의 설하점막이식 및 실리콘 시트 삽입을 이용한 재건

(Reconstruction of Lower Eyelid Symblepharon with Lingual Mucosal Graft and Silicone Sheet Following Excision of Malignant Melanoma In Situ: A Case Report)

동국대학교 의과대학 성형외과학교실[1]

한승민[1], **이준호**★[1]

Purpose: To report a case of successful reconstruction of lower eyelid symblepharon after wide excision of malignant melanoma in situ using a lingual mucosal graft and silicone sheet placement, with restoration of ocular motility and resolution of diplopia.

Methods: A 78-year-old woman with hypertension and diabetes underwent wide excision and mustarde cheek rotational flap of a right lower eyelid melanoma in situ on February 25, 2025. She subsequently developed horizontal and vertical diplopia, mild limitation of adduction and abduction, and symblepharon at the inferior temporal conjunctiva of the right eye. On September 11, 2025, the patient underwent adhesiolysis followed by reconstruction with a 2.0 × 1.5 cm lingual mucosal graft and interposition of a 1 mm silicone sheet with temporary tarsorrhaphy. Tarsorrhaphy stitches were removed on postoperative day 5 and the silicone sheet on postoperative day 12.

Results: At postoperative week 5, binocular diplopia and motility limitation were improved, and the mucosal graft remained well-engrafted with no recurrence of adhesion. Functional and cosmetic outcomes were satisfactory

Conclusion: Lingual mucosal graft with silicone sheet interposition effectively restored eyelid and conjunctival function in lower eyelid symblepharon following oncologic resection. This technique achieved stable anatomical results and significant functional improvement even in an elderly patient with systemic comorbidities.

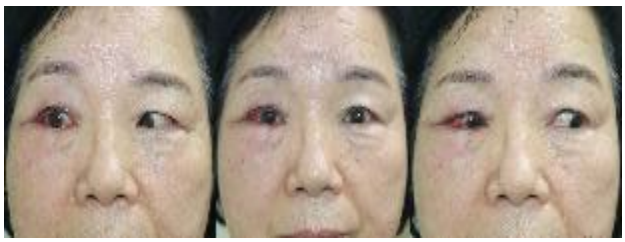

Fig. 1. Preoperative photographs of the right eye showing symblepharon at the inferior temporal conjunctiva with horizontal and vertical diplopia and mild limitation of adduction and abduction.

Fig. 2. Intraoperative views: (A) Lingual mucosal graft inset after adhesiolysis. (B) Silicone sheet interposition with temporary tarsorrhaphy.

Fig. 3. Five weeks postoperatively, the right lower eyelid shows a well-engrafted lingual mucosal graft without recurrent symblepharon and improved ocular motility, including adduction and abduction.

EP-085

드물게 발생하는 지연성 외상성 점액낭종과 연관된 만성 안와 하벽 골절의 재건술: 증례 보고

(Reconstruction of a Chronic Orbital Floor Fracture Associated with a Rare Delayed Traumatic Mucocele: A Case Report)

중앙대학교 의과대학 성형외과학교실 [1]
중앙대학교 광명병원 성형외과 [2]

정인호[1], 김우섭[2], 김한구[1], 배태희[2], 우수현[1], 김우주[2], 강신혁★ [1]

Purpose: Traumatic orbital mucoceles are rare, delayed complications that can manifest decades after initial injury, which often exacerbate enophthalmos and obscure critical structural landmarks, making surgical reconstruction challenging. We report a rare case of a massive mucocele associated with a chronic orbital floor fracture and emphasize the importance of clinical suspicion and precise anatomical restoration in managing such late-onset complications.

Methods: A 68-year-old male who injured right orbital floor fracture 30 years ago presented to the clinic with an associated mucocele. Due to severe anatomical distortion, a surgical navigation system was used to precisely identify the remaining orbital rims. After meticulous excision of the mucocele, the patency of the sinus drainage pathway was intraoperatively confirmed by assessing the sinus mucosa to ensure adequate ventilation and minimize potential recurrence risk.

Results: Using navigation-guided landmarks, a titanium plate was intraoperatively contoured to accurately restore the orbital floor and anterior maxillary wall, and prevent descent of orbital contents. Computed tomography (CT)-based measurements of proptosis remained stable and symmetric at 15/15 mm. Forced duction tests confirmed full ocular motility. During a 9-month follow-up, the patient showed no signs of recurrence, demonstrating successful short-to-midterm stability before being lost to follow-up.

Conclusion: Mucocele formation in chronic orbital fractures is rare and requires high clinical suspicion in patients with old trauma. Successful management depends on accurate anatomical restoration and ensuring sinus patency. This strategy provides predictable functional recovery even in complex cases where traditional landmarks are obscured by chronic pathological changes, ensuring both anatomical restoration and long-term functional stability.

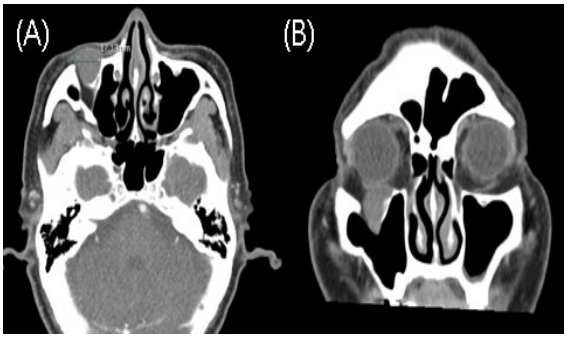

Fig. 1. Preoperative radiologic evaluation. (A, B) Computer-tomography images of the mucocele at the right inferior orbital wall in (A) axial and (B) coronal view, demonstrating a well-defined, expansive mass in the right infraorbital region. While the lesion presented clinically as a conventional protruding mass upon gross inspection, the CT image reveals a mucocele originating from a chronic orbital floor fracture.

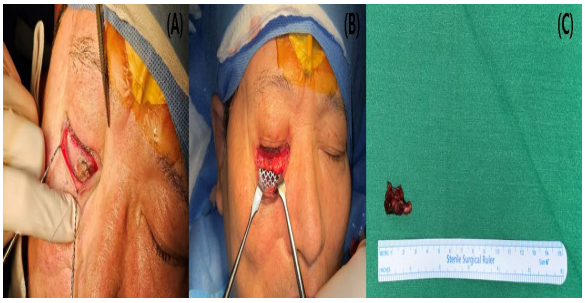

Fig. 2. (A) Intra-operative images of the mucocele, involving right inferior orbital wall and anterior maxillary wall, and (B) orbital wall reconstruction with titanium plate was designed after the successful resection of mucocele. (C) Clinical photo of a resected mucocele.

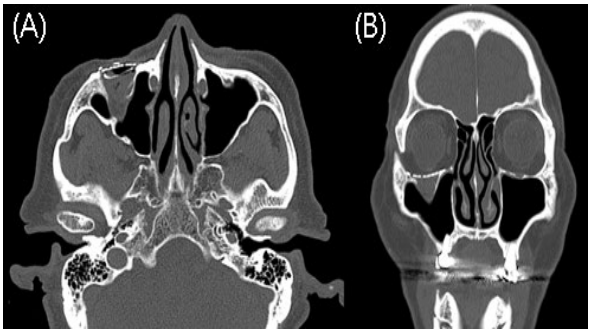

Fig. 3. (A) Postoperative radiologic evaluation. (A, B) Computer-tomography images of the lesion after reconstruction on right inferior orbital wall were achieved in (A) axial and (B) coronal view, with preserved level of proptosis as 15/15mm.

EP-086

연소성 황색육아종에서 피부 로사이-도프만병으로의 이행

(Cutaneous Rosai-Dorfman Disease Following Juvenile Xanthogranuloma)

전남대학교

김승현, 김민, 김동완, 최준호, 황재하, 김광석★

Purpose: Rosai-Dorfman disease (RDD) is a rare histiocytic disorder. While the skin is the most common extranodal site, purely cutaneous RDD (CRDD) is exceptionally rare, accounting for only 3% of cases. Both xanthogranuloma and RDD are non-Langerhans cell histiocytoses, often posing diagnostic challenges. We report a rare case where an initial Juvenile xanthogranuloma(JXG) transitioned into CRDD, suggesting a potential phenotype change

Methods: A 12-year-old girl presented with a 7 x 6 mm skin mass on her left cheek. To minimize scarring, a staged excision was planned. Partial excision was initially performed, with histopathology suggesting JXG. Fifteen months later, a complete excision was performed. The specimen underwent comprehensive immunohistochemical staining. Systemic involvement was assessed via contrast-enhanced CT and laboratory evaluations.

Results: The first-stage histopathology suggested xanthogranuloma with S100-negativity. However, the second-stage specimen revealed pathognomonic features of RDD, such as emperipolesis, and showed positivity for CD68, S100, and Cyclin D1, while testing negative for CD1a, Langerin, and OCT2. Systemic evaluation confirmed the absence of lymphadenopathy or extranodal involvement, diagnosing purely CRDD. Genetic analysis for the MAPK-ERK pathway mutations showed no known mutations, including BRAF. Postoperatively, the wound healed well, and the patient is undergoing scar management with no recurrence or systemic symptoms

Conclusion: This case illustrates a rare histological evolution from JXG to CRDD over 15 months within the histiocytic lineage. Clinicians should be alert to such potential transformations; longitudinal monitoring and repeat biopsies in evolving lesions are essential for accurate diagnosis and appropriate systemic management.

Fig. 1A. Preoperative photograph for the first-stage excision. To minimize the final scar length, a partial excision was strategically planned as the initial step.

Fig. 1B. Preoperative photograph for the second-stage excision performed 15 months later.

Fig. 1C. Clinical follow-up at one month postoperatively, demonstrating stable wound healing without any complications and a minimized scar following the staged-excision approach.

EP-087

만성 염증을 동반한 표피낭종으로 인한 광범위 두개골 골수염에서 자유 피판을 이용한 재건 : 증례 보고

(Extensive Calvarial Osteomyelitis Induced by Chronic Inflammation of an Epidermal Inclusion Cyst: Reconstruction with a Free Anterolateral Thigh Flap : A Case Report)

가톨릭대학교 의과대학
의정부성모병원 성형외과

김사라, 서보미, 정성노, 권호, 이준호★

Purpose: Epidermal inclusion cysts (EICs) are common benign cutaneous lesions. However, long-standing lesions with recurrent inflammation and inadequate treatment may progress to deep secondary infection.
We report a case of extensive calvarial osteomyelitis arising from a scalp EIC that had been present for two years, with persistent purulent discharge beginning six months prior to presentation.

Methods: A 76-year-old male presented with a chronic scalp lesion initially presumed to be an EIC. Over two years, repeated cycles of inflammation and partial healing occurred, followed by progressive purulent discharge during the six months preceding admission. Magnetic Resonance Imaging demonstrated biparietal calvarial osteomyelitis involving both the outer and inner tables with minimal epidural extension.
Following multidisciplinary evaluation, radical debridement was performed, resulting in a 6.0 × 12.0 cm cranial defect with exposed dura mater. A free anterolateral thigh (ALT) fasciocutaneous flap measuring 14 × 9 cm with a 14-cm vascular pedicle was harvested. End-to-end microvascular anastomosis to the superficial temporal vessels was performed under operative microscopy.

Results: The flap remained viable without vascular compromise. The postoperative course was uneventful, and stable wound coverage was achieved without evidence of recurrent infection.

Conclusion: Recurrent cycles of inflammation and incomplete healing in an inadequately treated EIC can ultimately progress to extensive calvarial osteomyelitis with dural exposure.
Radical debridement followed by vascularized free ALT flap reconstruction provides reliable coverage and effective infection control in advanced cranial defects.

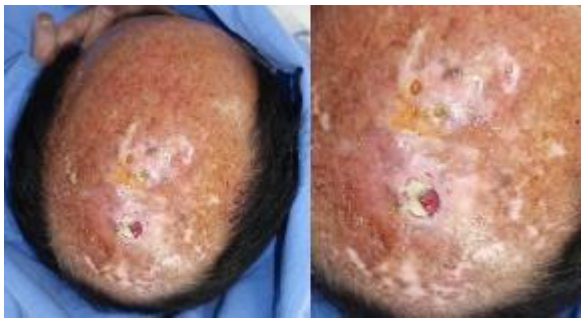

Fig. 1. Preoperative scalp wound

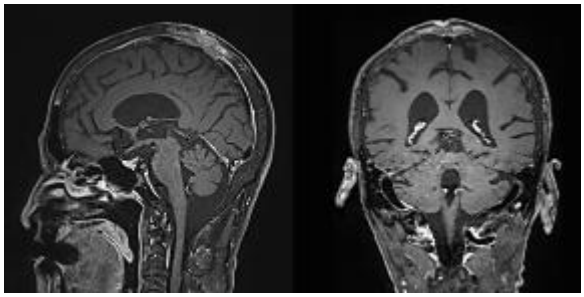

Fig. 2. Preoperative Magnetic Resonance Imaging

Fig. 3. Intraoperative defect after debridement (dura mater exposure)

Fig. 4. Immediate postoperative photo

EP-088

연속적인 지방 이식을 이용한 수술 후 반안면 위축증의 재건 – 5년 MRI 연구

(Post-surgical hemifacial atrophy reconstructed with serial fat grafts - 5 year MRI study)

고려대학교

송한상, 유희진, 이태열, 김덕우★

Purpose: To evaluate longitudinal changes and the stabilization timeline of hemifacial fat volume following serial autologous fat grafting in a patient with post-surgical hemifacial atrophy using MRI volumetric analysis.

Methods: A patient with hemifacial atrophy after a maxillary swing operation for nasopharyngeal cancer in June 2018 underwent two autologous fat grafting procedures in May 2021 and January 2022. Serial MRI scans were obtained, and three-dimensional volumetric analysis was performed to measure fat volume of both the affected and contralateral hemiface to assess graft stability and physiological volume changes.

Results: Preoperative fat volume of the affected hemiface was 30.71 cm^3, increasing to 129.80 cm^3 immediately after the first graft. A marked reduction to 71.86 cm^3 was observed at 7 months postoperatively. Thereafter, volume remained relatively stable, measuring 72.15, 77.90, 64.85, 84.43, and 85.88 cm^3. No distinct increase was observed after the second graft, likely because MRI was not obtained immediately postoperatively. Volume fluctuations after stabilization showed patterns similar to the contralateral side. These parallel changes suggest physiological fat variation, likely associated with body weight changes, rather than graft resorption.

Conclusion:
Autologous fat grafting demonstrated significant early volume reduction followed by long-term stabilization. MRI volumetric analysis confirmed that fat graft volume stabilizes approximately 6 months after the procedure and remains durable for several years. Serial fat grafting is an effective and reliable method for reconstructing post-surgical hemifacial atrophy.

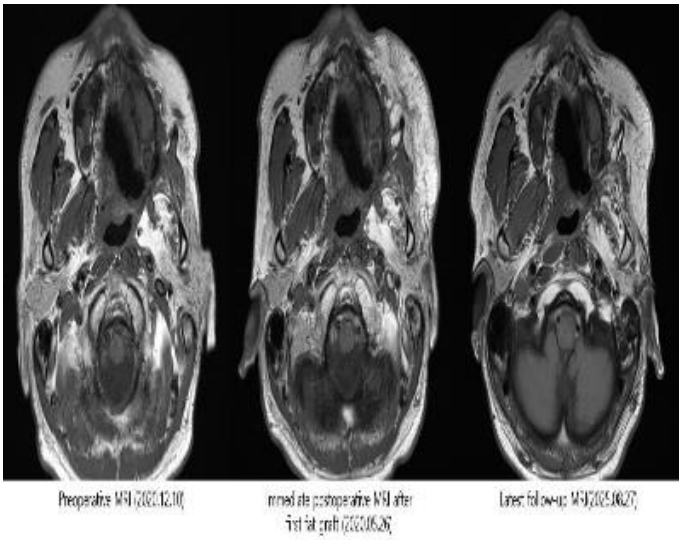

Fig. 1. Serial axial MRI demonstrating volumetric change

Fig. 2. Hemifacial Fat Volume Changes After Serial Fat Grafting

EP-089

소아 비골 골절의 정복술 및 비강 내 패킹 후 발생한 마취 후 후두경련: 증례 보고

(Post-Anesthetic Laryngospasm After Reduction with Intranasal Packing in Pediatric Nasal Bone Fracture: A Case Report)

대구가톨릭대학교
의과대학 성형외과학교실

김준우, 한동길★

Purpose: Laryngospasm is one of the major causes of post-extubation airway obstruction in pediatric patients. We report a pediatric case of laryngospasm after closed reduction with intranasal packing in nasal bone fracture. We considered intranasal packing to be a contributing factor in this patient and conducted this case study.

Methods: A 24 kg, 9-year-old boy without a history of asthma, allergy, or recent upper respiratory inflammation underwent closed reduction of nasal bone fracture under general anesthesia with orotracheal intubation. The operation procedure, including intranasal packing, was completed successfully. Immediately after extubation in the operation room, the patient showed respiratory distress with acute desaturation to a lowest oxygen saturation of 88.7%. Laryngospasm was clinically suspected by the attending anesthesiologist. Immediate management consisted of 100% oxygen with manual positive-pressure ventilation via oropharyngeal airway and oropharyngeal suctioning, resulting in prompt improvement. The patient was transferred to post-anesthesia care unit where short-acting bronchodilators(salbutamol) inhalation was additionally administered.

Results: The patient became alert and vital signs were stabilized within 30 minutes. No recurrent desaturation occurred during hospitalization, and the patient was discharged without any complications. Subsequent outpatient follow-up showed no further adverse events.

Conclusion: Pediatric patients are more vulnerable to laryngospasm than adults, particularly during emergence. Especially, nasal surgery with intranasal packing is known to increase the risk of laryngospasm due to bilateral obstruction forcing oral breathing. Thus, we should maintain heightened awareness of laryngospasm risk when pediatric patients undergo nasal surgery with intranasal packing. Prompt recognition and intervention can prevent severe complications.

EP-090

신생아 비강 튜브 감염 후 발생한 전비극 결손 동반 비변형의 구조적 재건술

(Structural Reconstruction of Nasal Deformity with Anterior Nasal Spine Defect Following Neonatal Nasal Tube–Related Infection)

강동성심병원 성형외과

정지원, 김결희*, 정철훈, 장용준, 황나현

Purpose: Infectious injury from nasal tube placement at birth may result in combined soft tissue contracture and structural bone loss of the anterior nasal spine. Reconstruction is challenging because both nasal contour and skeletal support must be restored simultaneously. We present a case managed with combined soft tissue advancement, implant augmentation, and autologous bone reconstruction.

Methods: A patient presented with right alar rim and base depression, septal deviation with partial defect, and anterior nasal spine deficiency secondary to neonatal nasal tube–associated infection (Figure 1). Scar release, V-Y advancement flap, augmentation rhinoplasty, and maxilloplasty were performed. After contracture release and exposure of the piriform aperture, a V-Y advancement flap was used to improve soft tissue deficiency. Dorsal augmentation was performed with a 3-mm silicone implant, and a shield graft harvested from the left conchal cavum was applied for tip support. A 5 × 3 cm bicortical iliac bone graft was harvested using a subcrestal window technique and fixed to both alar bases and the anterior nasal spine region with titanium screws to restore skeletal support(Figure 2).

Results: Postoperative recovery was uneventful. Alar base depression improved, nasal projection was restored, and stable structural support was achieved. At the 6-month follow-up, the patient maintained stable nasal contour and structural support without any complications (Figure 3).

Conclusion: In nasal deformities associated with anterior nasal spine defects, isolated rhinoplasty is insufficient. Simultaneous restoration of skeletal support with autologous bone grafting is essential for durable correction and long-term structural stability.

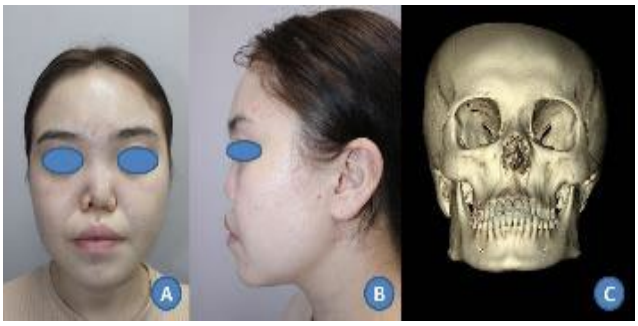

Fig 1. Preoperative photographs and computed tomography demonstrating nasal deformity with anterior nasal spine defect secondary to neonatal nasal tube–related infection

Fig 2. Intraoperative views showing V-Y advancement flap and fixation of autologous iliac bone graft to the anterior nasal spine and alar base

Fig 3. Six-month follow-up photographs demonstrating improved nasal contour, alar base, and restored structural support

EP-091

전두측두부 다발성 호산구성 혈관림프구증식증의 단계적 절제: 증례보고

(Staged Excision of Multifocal Angiolymphoid Hyperplasia with Eosinophilia in the Frontotemporal Region: A Case Report)

가톨릭대학교 의과대학
성형외과학교실

이창준, 백상운, 이준용, 유결, 김라윤★

Purpose: Angiolymphoid hyperplasia with eosinophilia (AHLE) is a rare benign vascular proliferative disorder characterized by abnormal blood vessel growth accompanied by lymphoid and eosinophilic inflammatory infiltration. Despite its benign nature, AHLE is associated with a high risk of recurrence, particularly in multifocal lesions where complete excision may result in significant aesthetic deformity. We present a case of recurrent multifocal AHLE involving the frontotemporal region successfully treated with staged excision, achieving near-complete resolution with favorable aesthetic outcome.

Methods: 54-year-old man presented with multiple erythematous nodules involving the left forehead and temporal region that had progressively enlarged over 10 years (Fig. 1A). The patient had previously undergone punch biopsy–confirmed AHLE and two sessions of cryotherapy at another institution, followed by recurrence and repeated ulceration. Computed tomography demonstrated multiple soft tissue masses abutting underlying musculature (Fig. 1B). Laboratory evaluation revealed elevated serum IgE levels without eosinophilia. Considering the anticipated extensive defect following single-stage excision, staged surgical removal was planned. Two sequential excisions targeting scattered satellite lesions were performed with primary closure (Fig. 2A, 2B). During the third stage, the remaining clustered nodules were completely excised, and the resultant defect was reconstructed using a local flap combined with full-thickness skin grafting (Fig. 2C, 2D).

Results: Histopathologic examination confirmed AHLE (Fig. 3). The wound healed completely without lateral canthal distortion, and no recurrence was observed at 3-month follow-up with satisfactory contour (Fig. 4).

Conclusion: Staged excision may provide an effective approach for complete removal of extensive multifocal AHLE in cosmetically sensitive facial regions while minimizing aesthetic deformity.

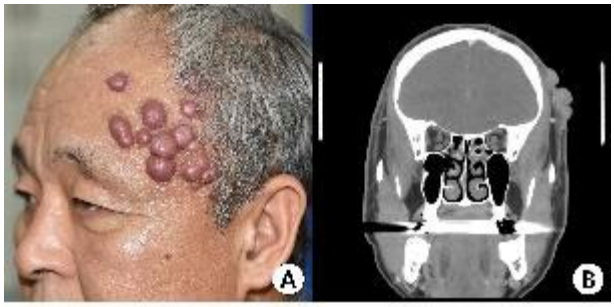

Fig. 1. Initial presentation. (A) Clinical photograph of multifocal nodular lesions in the left frontotemporal region. (B) Computed tomography image showing multiple soft tissue masses.

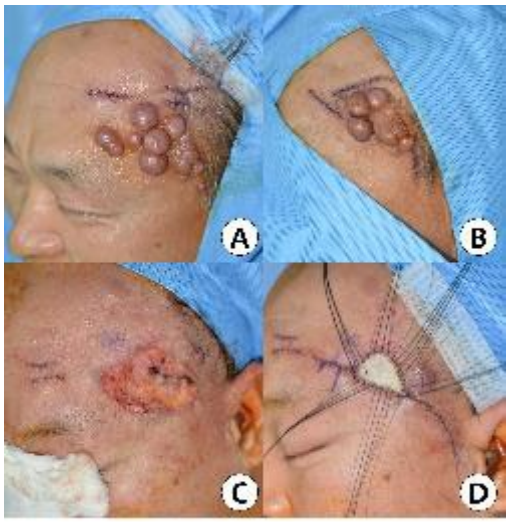

Fig. 2. Intraoperative photographs during staged excision. (A) After the first excision. (B) After the second excision. (C) After complete lesion excision. (D) Reconstruction with local flap and full-thickness skin graft.

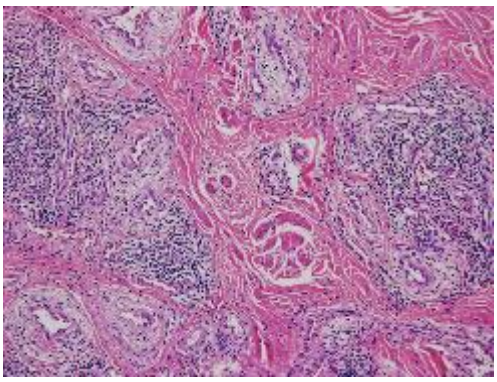

Fig. 3. Histopathologic findings showing vascular proliferation with lymphoid and eosinophilic infiltration, consistent with AHLE (H&E stain, x100).

Fig. 4. Postoperative photographs at 3-month follow-up demonstrating complete wound healing without lateral canthal distortion. (A) Frontal view. (B) Lateral view.

EP-092

판코니 빈혈 환자의 재발성 구강 편평세포암에 대한 순차적 유리피판 재건술

(Sequential Free Flap Reconstruction for Recurrent Oral Cavity Squamous Cell Carcinoma in a Patient with Fanconi Anemia)

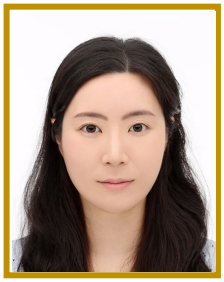

경상국립대학교

김지승, 김태호, 김민형, 신재봉, 김남균, 이경석, 김준식★

Purpose: Patients with Fanconi anemia (FA) face a significantly high risk of aggressive, early-onset head and neck squamous cell carcinoma (HNSCC) and frequent locoregional recurrence. This study evaluates the challenges and clinical outcomes of performing sequential microsurgical reconstructions in an FA patient requiring repeated oncologic resections.

Methods: A 27-year-old male with FA presented with recurrent buccal mucosal SCC. We performed a sequential reconstruction following oncologic ablation. The initial soft tissue defect was addressed using a superficial circumflex iliac artery perforator (SCIP) free flap(Fig. 1). Following a local recurrence eighteen months later involving the mandible(Fig. 2A), an extensive salvage surgery was performed, consisting of a segmental mandibulectomy reconstructed with a double-barrel fibular osteocutaneous free flap using microvascular anastomosis(Fig. 2B–D).

Results: Both the SCIP and fibular flaps achieved successful uptake without vascular complications or donor-site morbidity(Fig. 3). However, despite successful structural restoration and negative resection margins, the patient developed progressive functional impairment, including severe trismus (interincisal distance < 1 cm) and masticatory dysfunction(Fig. 4). This was attributed to the cumulative effects of repeated surgeries, radiotherapy, and extensive scarring inherent to the aggressive disease course of FA.

Conclusion: Sequential free flap reconstruction is a viable and necessary approach for managing recurrent HNSCC in FA patients. Surgeons must adopt a flexible, long-term reconstructive strategy that preserves potential donor sites and recipient vessels. While microsurgical success is achievable, clinicians should anticipate persistent functional limitations due to the necessity of multiple salvage procedures and the impact of adjuvant therapies.

Fig. 1. (Lt.) Recurrent ulcer-like lesion on the left buccal mucosa in a 27-year-old male patient with FA.
(Rt.) Postoperative intraoral photograph demonstrating reconstruction with a SCIP free flap following wide excision.

Fig. 2. (A) Recurrent whitish ulcerofungating lesion arising around the previous operative site 18 months after the initial reconstruction. (B) Design of a 10-cm fibular free flap on the patient's left lower leg. (C) Fibular flap with a 4 × 7.5 cm skin paddle after osteotomy for the double-barrel technique. (D) Restoration of bony continuity using a double-barrel fibular free flap following segmental mandibulectomy.

Fig. 3. Postoperative panoramic radiograph demonstrating mandibular reconstruction with a double-barrel fibular free flap.

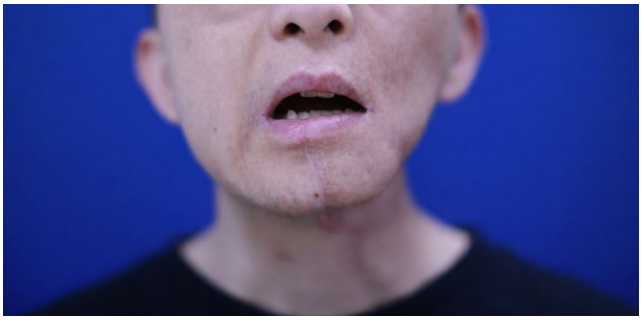

Fig. 4. Clinical photograph showing progressive trismus with an interincisal distance of less than 1 cm after reconstruction.

EP-093

전두골에 발생한 골수염과 이에 대한 재건 전략

(Osteomyelitis developed on the frontal bone and subsequent reconstruction strategies)

한림동탄성심병원
성형외과

이중현, 김병준, 윤인모, 정소연★

Purpose: Osteomyelitis developed on the frontal bone accompanying the soft tissue infection is rare but may lead to fatal consequences. The origin of infection is commonly associated with sinusitis; however, it is hard to be localized. Once it develops, treatment strategies need to include eradication of infected tissue, radically wide debridement, and reconstruction planning. In addition, use of antimicrobial agents is another crucial part of the treatment.

Methods: Two patients suffered from recurrent infections on the frontal area. Skin and soft tissue were cicatricial with repeated inflammation and infection. Computed tomography scanning was taken to see the bony structure and bone infection was identified. Subsequently, magnetic resonance scans were also examined to reveal osteomyelitis. All the hard and soft tissues were under wide spreading infections. Surgical approach with coronal incision included wide debridement and frontal bone reconstruction. Microbiologic cultures were performed during the eradication procedure. One received autologous bone grafting of single-stage procedure with the eradication and reconstruction. The other had early eradication and delayed reconstruction with titanium mesh.

Results: No recurrence of infection was observed during the follow-up of six months. Patients were satisfied with the forehead contour subjectively. Only minor numbness and paresthesia were reported over the scalp.

Conclusion: Frontal bone osteomyelitis is uncommon but potentially severe conditions. Early surgical intervention including eradication is important to minimize the infection expanding. The reconstruction planning is also critical to restore the forehead contour. This report presents different two types of treatments for frontal bone osteomyelitis.

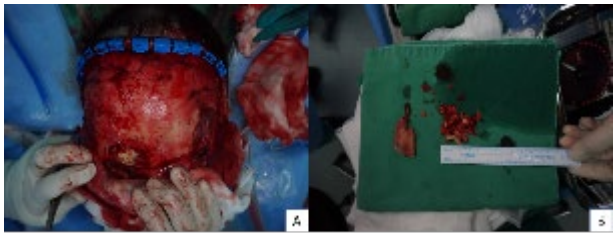

Figure 1. (A) Intraoperative photograph of the first patient demonstrating infected frontal bone with osteolytic destruction and exposed necrotic bone. (B) Debrided specimens of osteolytic frontal bone removed during surgical management of osteomyelitis.

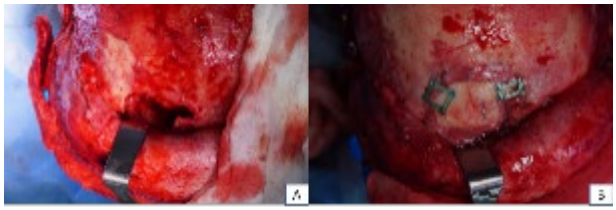

Figure 2. (A) Intraoperative photograph during the secondary operation of the first patient, demonstrating a residual frontal bone defect following prior debridement for osteomyelitis. (B) Intraoperative view of the first patient demonstrating autologous bone graft reconstruction of the frontal bone defect after complete debridement of osteomyelitic tissue

Figure 3. (A) Three-dimensional CT reconstruction of the second patient showing osteolytic defects of the frontal bone caused by osteomyelitis, demonstrating cortical destruction of the anterior frontal table. (B) Intraoperative photograph demonstrating multiple areas of cortical destruction of the frontal bone caused by osteomyelitis after wide exposure through a coronal approach. (C) Postoperative follow-up photograph after resection of the infected frontal bone, demonstrating a healed surgical incision with visible contour depression at the resected site.

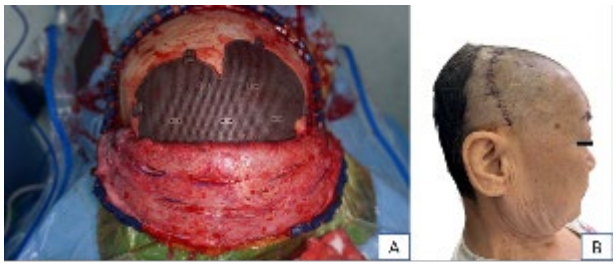

Figure 4. (A) Intraoperative photograph showing frontal bone reconstruction using a titanium mesh following radical debridement for osteomyelitis. (B) Follow-up clinical photograph of the second patient after reconstruction with a titanium mesh, demonstrating restoration of the previous frontal contour depression and stable wound healing without evidence of recurrent infection.

EP-094

상안와부에서 양성 연부조직 종양으로 오인된 가성낭종 유사 병변: 진단적 함정

(A Pseudocyst-like Lesion of the Upper Orbital Area Mimicking a Benign Soft Tissue Tumor: A Diagnostic Pitfall)

조선대학교 의과대학
성형외과학교실

이현정, 천지선⋆, 최우영, 양정열

Purpose: Palpable masses in the upper orbital area are commonly presumed to be benign soft tissue lesions such as lipomas, dermoid cysts, or epidermal inclusion cysts based on clinical examination. However, certain non-epithelial degenerative cystic lesions may present with similar clinical features, leading to diagnostic confusion. We report a case of a pseudocyst-like lesion containing gelatinous material in the upper orbital area that clinically mimicked a benign soft tissue tumor, highlighting the limitations of clinical diagnosis.

Methods:A 74-year-old woman presented with a palpable mass in the left upper orbital area that had gradually increased in size over one year. On physical examination, the lesion measured approximately 1×1 cm and was relatively well-circumscribed, soft and elastic in consistency, non-tender, and without overlying skin discoloration or inflammatory changes (Fig. 1). The lesion was clinically considered a superficial, mobile soft tissue mass. Based on these findings, a benign soft tissue tumor was suspected, including lipoma in the differential diagnosis. Given the small size and clinically superficial nature of the lesion, and considering the patient's preference, surgical excision was performed without prior imaging for definitive diagnosis and treatment.

Results: Intraoperatively, a well-circumscribed cystic lesion was identified and completely excised. Gross examination revealed a cystic lesion containing transparent, jelly-like gelatinous material (Fig. 2). Histopathologic examination demonstrated a fibrous-walled cystic lesion measuring 0.7×0.3 cm, containing acellular, homogeneous eosinophilic gelatinous material. No identifiable epithelial lining was observed (Fig. 3). There was no evidence of lipomatous tissue, keratinous debris, or malignancy. Based on these findings, the lesion was interpreted as a non-epithelial cystic lesion with pseudocyst-like features rather than a definable epithelial cyst or neoplasm. The postoperative course was uneventful, with no recurrence during follow-up.

Conclusion: Non-epithelial cystic lesions in the upper orbital area may clinically mimic benign soft tissue tumors, posing a potential diagnostic challenge. Clinical examination alone may be insufficient for accurate differentiation, and histopathologic evaluation remains essential for definitive diagnosis. Recognition of such lesions may help reduce misdiagnosis and supports the role of surgical excision in both diagnosis and management of orbital masses.

Fig. 1. Preoperative photograph demonstrating a palpable subcutaneous mass in the left upper orbital area (arrow).

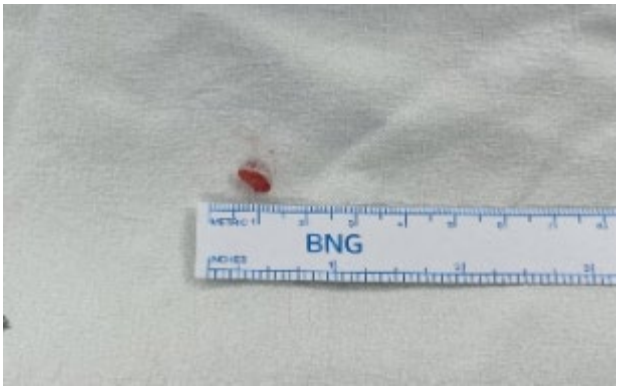

Fig. 2. Gross specimen obtained after surgical excision showing a small cystic lesion measuring approximately 0.7cm in greatest dimension.

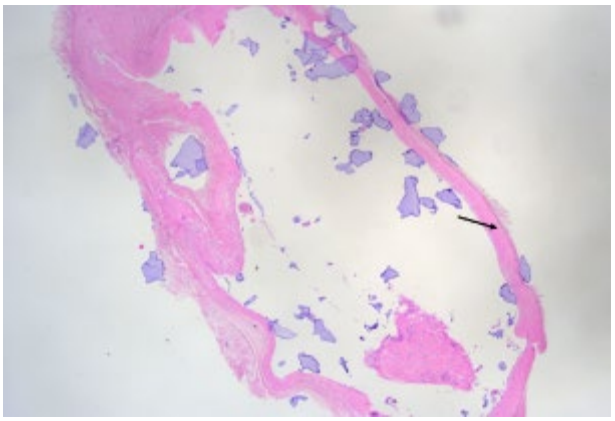

Fig. 3. Histopathologic findings (H&E stain, low magnification) showing a fibrous capsule (arrow) surrounding acellular, homogeneous eosinophilic gelatinous material without identifiable epithelial lining.

EP-095

점액낭종으로 임상적으로 오인된 하순의 혈관평활근종: 증례 보고

(Angioleiomyoma of the Lower Lip Clinically Mimicking a Mucocele: A Case Report)

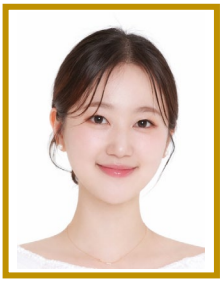

가톨릭대학교 의과대학
성형외과교실

김정현, 이준호, 서보미, 권호, **정성노**★

Purpose: Angioleiomyoma is a benign smooth muscle tumor of vascular origin that is rarely encountered in the oral cavity. Because of its nonspecific clinical appearance, it is frequently misdiagnosed as common benign lesions such as mucocele. We report a case of angioleiomyoma of the lower lip that was initially suspected to be a mucocele and was confirmed by histopathological examination following surgical excision.

Methods: A 58-year-old female patient presented with an incidentally noted painless submucosal mass on the lower lip. The lesion was soft, well circumscribed, and covered by intact mucosa without ulceration or erythema, leading to a provisional diagnosis of mucocele (Figure 1). Excisional biopsy was performed under local anesthesia using 2% lidocaine with 1:100,000 epinephrine. An elliptical incision was designed around the lesion, and the mass was excised en bloc. Following excision, bilateral subcutaneous flap elevation was performed to achieve tension-free layered closure and preserve the contour of the lower lip.

Results: Gross examination revealed a pale gray soft tissue mass measuring less than 1 cm in diameter (Figure 2). Histopathological analysis demonstrated a benign vascular smooth muscle tumor composed of proliferating smooth muscle bundles surrounding vascular channels. These findings were consistent with angioleiomyoma (Figure 3). The postoperative course was uneventful, with satisfactory wound healing and preservation of lip symmetry. No functional impairment or recurrence was observed during follow-up.

Conclusion: Although uncommon, angioleiomyoma should be considered in the differential diagnosis of benign lower lip masses. Complete surgical excision provides both definitive diagnosis and excellent functional and cosmetic outcomes with a low risk of recurrence.

Fig. 1. Preoperative clinical photograph showing a localized submucosal mass on the lower lip.

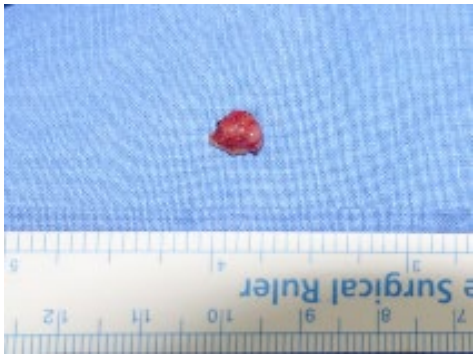

Fig. 2. Gross photograph of the excised specimen demonstrating a small, pale gray soft tissue mass measuring less than 1 cm in diameter.

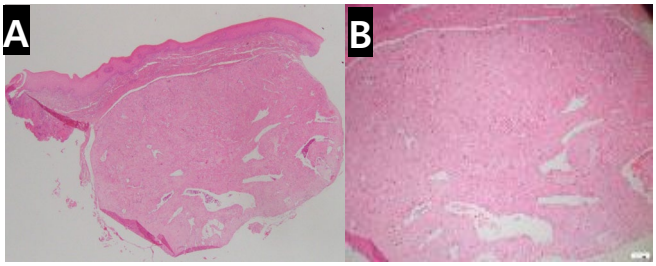

Fig. 3. Histopathological findings of the lesion.
(A) H&E stain, (×10) a well-circumscribed smooth muscle nodule with numerous thick-walled vascular channels.
(B) H&E stain, (×40) showing smooth muscle bundles surrounding vascular structures, consistent with angioleiomyoma.

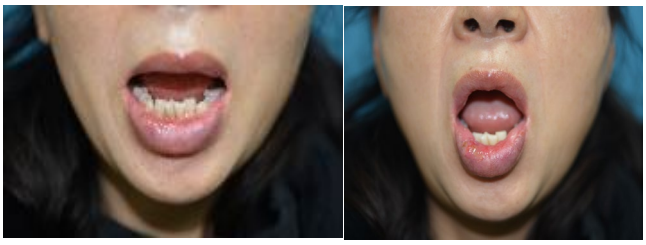

Fig. 4. Postoperative clinical photograph obtained at 6 months after surgery demonstrating satisfactory wound healing and preserved contour and symmetry of the lower lip without evidence of recurrence.

EP-096

안와벽 재건술 후 발생한 지연성 안와 출혈로 인한 복시

(Delayed postoperative orbital hemorrhage with diplopia after uneventful orbital wall reconstruction)

인제대학교

김성준, 이수향*

Purpose: To present a case of delayed postoperative retrobulbar hemorrhage causing diplopia after orbital wall reconstruction and to emphasize the need for early recognition of this rare but vision-threatening complication.

Methods: We describe a case of a 19-year-old male who sustained a right inferomedial orbital wall fracture following blunt facial trauma. The patient underwent orbital wall reconstruction on post-trauma day 11. Clinical findings, imaging studies, surgical intervention, and postoperative outcomes were reviewed.

Results: Immediate postoperative evaluation, including facial bone computed tomography and physical examination, revealed no complications. However, five days after surgery, the patient developed delayed-onset diplopia, strabismus, and proptosis. Imaging confirmed retrobulbar hematoma with globe displacement. Emergent surgical exploration and hematoma evacuation were performed, resulting in improvement of proptosis and diplopia, although mild residual diplopia persisted at follow-up.

Conclusion: Delayed postoperative retrobulbar hemorrhage, although rare, can occur even after an initially uneventful orbital wall reconstruction and may lead to significant visual morbidity. Prompt recognition and timely intervention are essential, and clinicians should maintain a high index of suspicion when new ocular symptoms develop postoperatively.

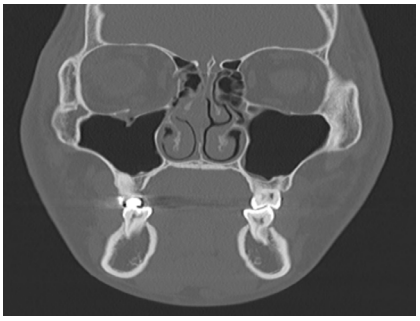

Figure 1. Preoperative Computed Tomography

Preoperative orbital computed tomography demonstrating a right inferomedial orbital wall fracture. Coronal views show a bony defect involving the orbital floor and medial wall.

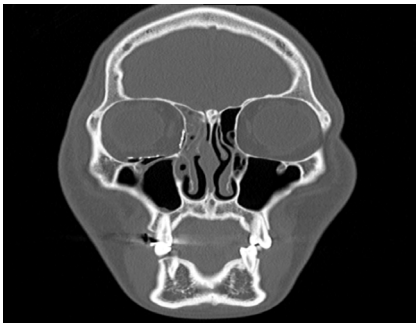

Figure 2. Immediate Postoperative Computed Tomography

Immediate postoperative computed tomography showing appropriate implant positioning along the inferomedial orbital wall without evidence of retrobulbar hematoma or globe displacement.

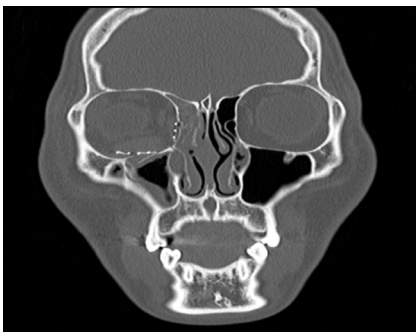

Figure 3. Delayed Postoperative Orbital Hemorrhage

Computed tomography obtained five days after surgery demonstrating a retrobulbar hematoma in the right orbit with associated globe displacement and proptosis.

EP-097

견갑골 피판의 안전한 거상을 위한 흉배-각동맥 혈관경의 3차원 해부학적 주행 분석

(Three-Dimensional Trajectory Analysis of the Thoracodorsal-Angular Pedicle for Safe Elevation of Scapular Flaps)

울산대학교

박상천, 정우식, 최종우, 김영철★

Background: The thoracodorsal-angular pedicle provides a reliable and long blood supply for scapular flaps. To enhance surgical precision during flap harvest, this study quantitatively analyzes its 3D trajectory and distance to the scapula, establishing objective guidelines for safe bone flap design.

Method: Three-dimensional models of the scapula and thoracodorsal-angular pedicles were reconstructed using 3-matic software (n=44). The spatial trajectory from the pedicle origin to the distal angular branch was extracted as a continuous curve, and the shortest distance to the bone was measured. To account for individual length variations, the cumulative arc length of each pedicle was normalized to a 0–100% scale using linear interpolation. Subsequently, K-means clustering (K=2) was applied to the normalized distance data to classify the morphological course of the pedicle.

Result: The quantitative analysis revealed two distinct morphological patterns among the pedicle trajectories (n=44). Type A (Gradual descent, n=19) started further from the bone at the origin (mean distance 28.8 mm) and maintained a spacious distance at the mid-course (11.4 mm), gradually approaching the inferior angle (6.0 mm). Type B (Steep and close course, n=25), the predominant variant, originated closer to the bone (17.2 mm), exhibited a steep drop to 5.7 mm by the mid-course, and remained tightly attached distally (4.3 mm).

Conclusion: The thoracodorsal-angular pedicle exhibits two distinct 3D trajectories. The frequent steep drop observed in Type B necessitates meticulous dissection near the mid-course. This objective classification establishes a reliable anatomical basis for preserving the tissue cuff and ensuring safe flap elevation.

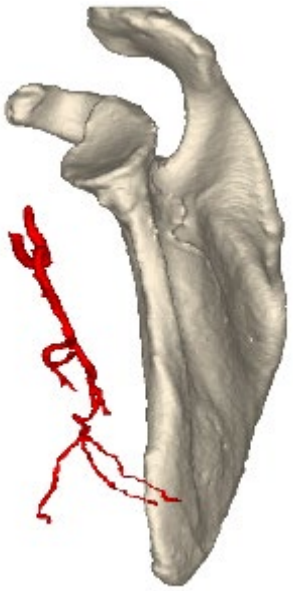

Figure 1. Three-dimensional models of the scapula and thoracodorsal-angular pedicles were reconstructed using 3-matic software. The spatial trajectory from the pedicle origin to the distal angular branch was extracted as a continuous curve.

Figure 2. The shortest distance from the pedicle to the bone was measured.

Figure 3. K-means clustering analysis (K=2) of the three-dimensional trajectory of the thoracodorsal-angular pedicle. The x-axis represents the normalized pedicle length from the proximal origin (0%) to the distal end near the inferior angle of the scapula (100%). The y-axis shows the shortest 3D distance between the vascular pedicle and the bone surface in millimeters. Solid lines indicate the mean distance for each morphological pattern: Type A (blue, n=19) demonstrates a gradual descent with a safer dissection margin, whereas Type B (red, n=25) exhibits a steep drop toward the bone by the mid-course. The shaded areas surrounding the solid lines represent the standard deviation for each group.

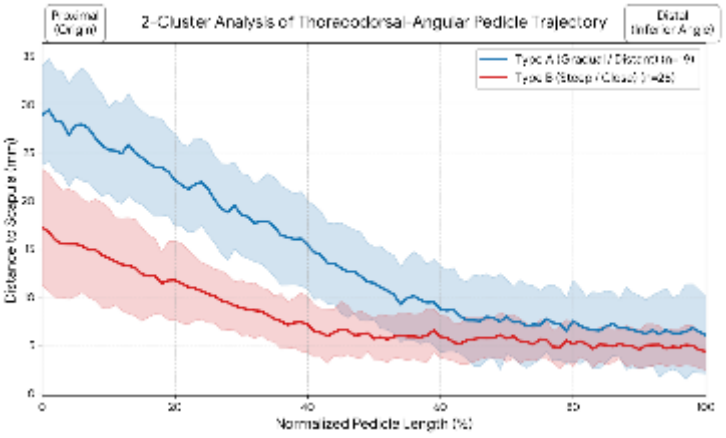

EP-098

하안검 및 외안각에 발생한 피지샘암에 대한 복합 이식과 회전 피판술을 이용한 재건 : 증례 보고

(Sebaceous Gland Carcinoma of the Lower Eyelid and Lateral Canthus Reconstructed with a Composite Graft and Rotation Flap : A Case Report)

경희대학교 의과대학
성형외과학 교실

차은총, 김영진, 범진식, 박준, 강상윤★

Purpose: Sebaceous carcinoma (SC) a rare and aggressive malignancy, usually arising in the periocular region. The primary goal of reconstruction is to restore both function and aesthetics. While vascularized flaps combined with mucosal grafts are commonly used, these procedures can be technically demanding and time-consuming. Here, we introduce a case of successful reconstruction of lower eyelid and lateral canthus with composite graft and rotation flap.

Methods: An 85-year-old female presented with a persistent, firm, solitary nodule on the right lower eyelid visited our clinic. The size of tumor was 7x8mm with extension into the lateral canthus and the palpebral conjunctiva. A wide excision resulted in full-thickness defect involving the lateral canthus, upper and lower eyelid margins. A composite graft was harvested from the lateral aspect of contralateral lower eyelid. The posterior lamella of the graft was positioned in line with the conjunctiva margin, while the anterior lamella was rotated 90 degrees counterclockwise to provide more extensive skin coverage. Finally, the lateral canthal defect was reconstructed using a rotation flap.

Results: Permanent pathology revealed sebaceous carcinoma with tumor-free margins. There were no wound complications following the surgery. The horizontal palpebral fissure lengths for both eyelids were 25mm, indicating symmetry. This method successfully restored structural integrity and the lateral canthal contour.

Conclusion: Composite grafting is a valuable technique to avoid asymmetry compared to direct closure. It is also more convenient in reconstructing anterior and posterior lamella simultaneously. By combining it with a rotation flap, it can be effectively used in the reconstruction of lateral canthus and upper eyelid defects.

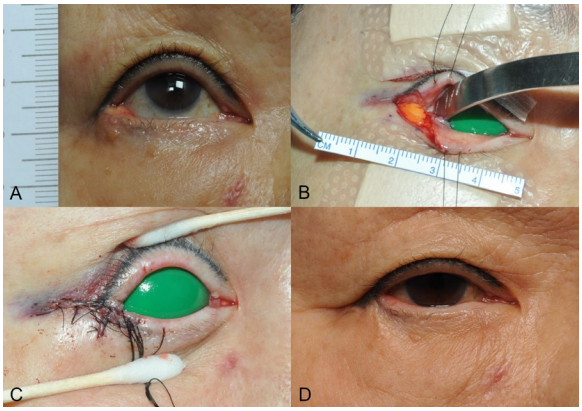

Fig. 1. Intraoperative and postoperative clinical photos (A) showing a solitary nodule in the right lower lid involving lateral canthus, (B) a full-thickness defect of upper and lower eyelid and lateral canthus, (C) the defect was reconstructed with composite graft combined with a rotation flap, (D) postoperative view at 6-month follow-up.

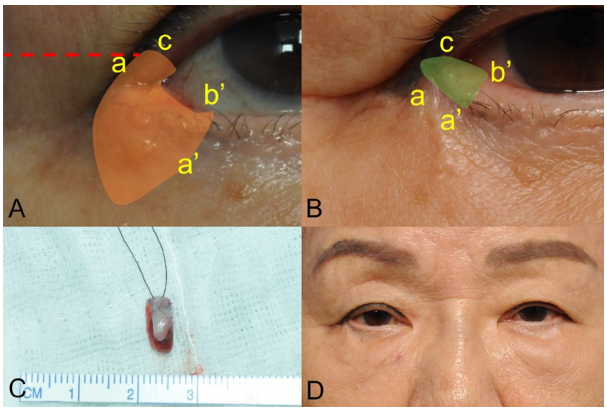

Fig. 2. Schematic illustration of a combined rotation flap and composite graft for lateral canthal reconstruction. The orange-shaded area indicates the primary defect, and the green-shaded area represents the composite graft. The red dotted line indicates the additional incision line for the rotation flap (A, B). A harvested composite graft with a horizontal length of 5 mm (C). Postoperative view at 6 months, demonstrating favorable symmetry of both eyelids and palpebral fissure length (D).

EP-099

재발성 편평세포암 절제 후 수직 복직근 근피판(VRAM sandwich flap)을 이용한 재건술에 대한 증례 보고

(Recurred squamous cell carcinoma ablation and subsequent reconstruction with vertical rectus abdominis myocutaneous sandwich flap: A case report)

한림동탄성심병원
성형외과

이중현, 김병준, 윤인모, 정소연★

Purpose: Squamous cell carcinoma (SCC) of the oral mucosa has a higher recurrence rate than other SCC types. Recurrence is often associated with local invasion of surrounding tissues and regional lymph nodes. Therefore, salvage surgery usually requires more extensive resection of potentially involved structures. In addition, adjuvant radiotherapy is commonly administered after surgery, which should be considered in reconstructive planning.

Methods: A female patient had undergone wide lip-cheek resection and lip-switch flap on her left cheek for oral squamous cell carcinoma (OSCC). A recurrent lesion was identified on the primary cancer site during cancer surveillance period. Several lymph nodes on her neck were also invaded. Extensive resection including all the layers of affected tissues were conducted and the lymph nodes were dissected. A vertical rectus abdominis myocutaneous flap (VRAM) was elevated and folded in half to reconstruct the mucosa and skin area together.

Results: Venous crisis developed and the anastomosis needed to be revised at early time of flap transfer. Eventually, the transferred flap was well survived in both sides of mucosa and skin even after postsurgical radiotherapy. No additional revision surgery was required, and donor site complication was not observed.

Conclusion: Recurred SCC shows poor prognosis in many cases. Salvage surgery at early stage should be the primary choice of treatment. Wide resection with secured margins and nearby lymph nodes is a vital role in the treatment. Following flap reconstruction is also critical to facilitate postsurgical adjuvant radiotherapy.

Figure 1. (A) Postoperative view after reconstruction of lip squamous cell carcinoma using a superior labial artery–based Abbe–Estlander flap, demonstrating restoration of lip contour and oral competence.

(B) Intraoral photograph demonstrating recurrence of squamous cell carcinoma in the buccal mucosa at the prior operative site.

Figure 2. (A) Intraoperative view of an extensive composite defect of the skin and buccal mucosa following wide resection for recurrent squamous cell carcinoma (SCC) and neck lymph node dissection, performed in collaboration with the head and neck surgery team.

(B) Elevation of a vertical rectus abdominis myocutaneous (VRAM) flap based on the deep inferior epigastric vessels for reconstruction.

(C) Harvested free vertical rectus abdominis myocutaneous (VRAM) flap demonstrating the deep inferior epigastric artery and accompanying veins forming the vascular pedicle.

Figure 3. Immediate postoperative photograph in the recovery room following secondary debulking of the free vertical rectus abdominis myocutaneous (VRAM) flap.

Figure 4. (A) Clinical photograph obtained 3 months postoperatively, showing maintained flap viability and contour following free VRAM flap reconstruction.

(B) Intraoral view obtained 3 months after surgery, showing well-healed mucosa with no clinical evidence of tumor recurrence.

EP-100

두피 결손 재건 후 요골 전완 유리피판 부분 괴사에 대한 단계적 봉합 치료

(Serial Progressive Approximation Suturing for Definitive Closure after Partial Loss of a Radial Forearm Free Flap in a Post-craniotomy Scalp Defect)

성균관대학교

윤병우, 김규남★

Purpose: Extensive post-craniotomy scalp necrosis is frequently reconstructed with free tissue transfer; however, partial flap loss remains a challenging complication with limited salvage options. We report NPWT-assisted progressive direct closure after partial loss of a radial forearm free flap (RFFF), highlighting the role of a residual viable flap layer as a biologic dressing.

Methods: A 51-year-old man underwent aneurysm clipping followed by craniectomy for subarachnoid hemorrhage and developed a right temporoparietal scalp necrosis (15 × 5 cm). After aggressive debridement, RFFF was inset and anastomosed end-to-end to the superficial temporal artery and vein. Postoperatively, partial flap loss occurred; although the superficial component became necrotic, viability was preserved in a portion of the deep fat layer. Nonviable tissue was excised in a staged manner. Salvage consisted of NPWT-assisted progressive direct closure using serial, traction-assisted approximation sutures with deep anchoring to incrementally advance wound edges. Approximation and NPWT changes were performed at weekly intervals over 3 months until tension-balanced direct closure was achieved**.**

Results: Progressive direct closure was successfully completed without repeat microsurgery, tissue expansion, or additional donor-site morbidity. During the closure period, the remaining viable RFFF layer provided effective temporary coverage consistent with a biologic dressing, facilitating wound bed protection and gradual approximation. Follow-up demonstrated complete epithelialization, durable healing, and acceptable scalp contour.

Conclusion: In partial flap loss after scalp free flap reconstruction, NPWT-assisted progressive direct closure is a pragmatic salvage strategy. Residual viable flap tissue may function as a biologic dressing during staged closure, reducing the need for secondary free tissue transfer.

Fig. 1.
Pre-reconstruction presentation. Right temporoparietal post-craniotomy scalp necrosis after aneurysm clipping and decompressive craniectomy, demonstrating a full-thickness soft-tissue defect (~15 × 5 cm) prior to definitive coverage.

Fig. 2.
Index reconstruction with free tissue transfer. Immediate postoperative appearance after RFFF inset with end-to-end microvascular anastomosis to the superficial temporal artery and vein.

Fig. 3.
Partial flap loss with residual viability. Postoperative partial loss of the RFFF: superficial necrosis with preservation of viability in a portion of the deep fat layer, followed by staged excision of nonviable tissue and initiation of NPWT-assisted salvage.

Fig. 4.
Final outcome after NPWT-assisted progressive direct closure. Healed scalp at follow-up after ~3 months of progressive direct closure using serial approximation suturing with weekly NPWT dressing changes; the remaining viable deep flap layer served as temporary biologic coverage during staged closure, culminating in complete epithelialization and durable wound healing.

EP-101

무증상 안와하벽 골절의 지연성 함몰 진행: 추적 CT의 중요성

(Importance of Follow-up CT in Asymptomatic Orbital Floor Fractures with Delayed Progression)

연세대학교 원주의과대학
원주세브란스기독병원
성형외과학 교실

오창훈, 전우상, 김석원, 김지예★

Purpose: Orbital floor fractures with minimal initial displacement may appear stable on early CT and remain asymptomatic, however delayed progressive orbital floor depression can occur, increasing orbital volume and risking late enophthalmos. We report a case in which follow-up CT after initial observation revealed interval progression and prompted reconstruction despite persistent absence of diplopia, emphasizing the need for structured follow-up.

Methods: A 27-year-old man sustained a left orbital floor fracture in a rear-seat motor vehicle collision. Outside-hospital CT on post-trauma day (PTD) 0 showed mild displacement, and observation was selected. Follow-up was performed to reassess functional sequelae (diplopia and extraocular movement limitation) and to evaluate interval anatomical changes. At PTD 17, follow-up CT demonstrated interval worsening with increased orbital floor depression compared with the initial study. Given radiologic progression and concern for delayed enophthalmos, orbital floor reconstruction was planned.

Results: Orbital floor reconstruction with a porous polyethylene implant with titanium mesh (Medpor Titan) was performed without complications. Postoperative CT confirmed restoration of the orbital floor contour with satisfactory reduction. The patient remained free of diplopia and extraocular movement limitation.

Conclusion: Even in the absence of diplopia or extraocular movement limitation and with minimal initial displacement, orbital floor fractures can progress on interval imaging. Clinical follow-up with repeat CT, when indicated, is essential to detect delayed depression early. Radiologic progression on follow-up CT may support considering reconstruction in selected patients to help prevent delayed enophthalmos.

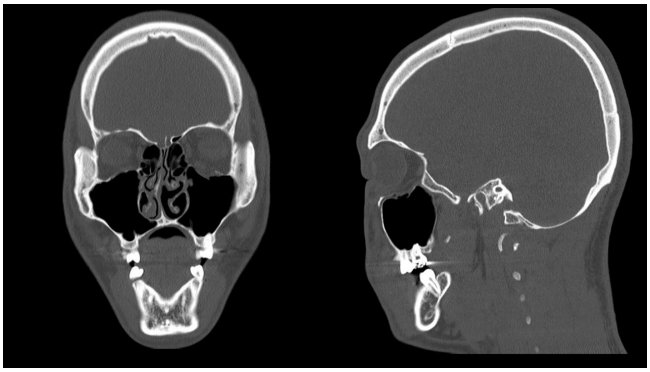

Fig. 1. Initial CT (PTD 0) showing a mild displaced orbital floor fracture.

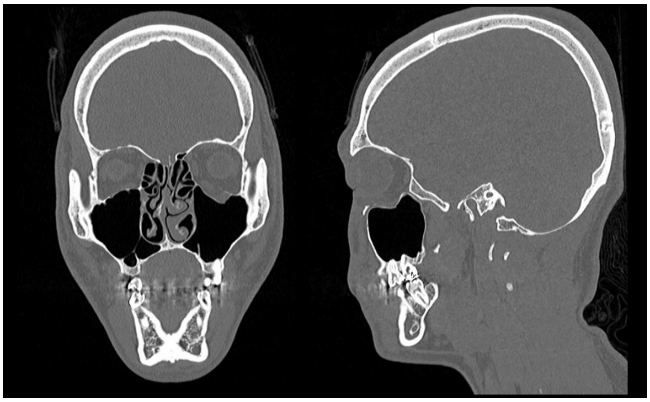

Fig. 2. Follow-up CT (PTD 17) showing interval worsening with increased orbital floor depression.

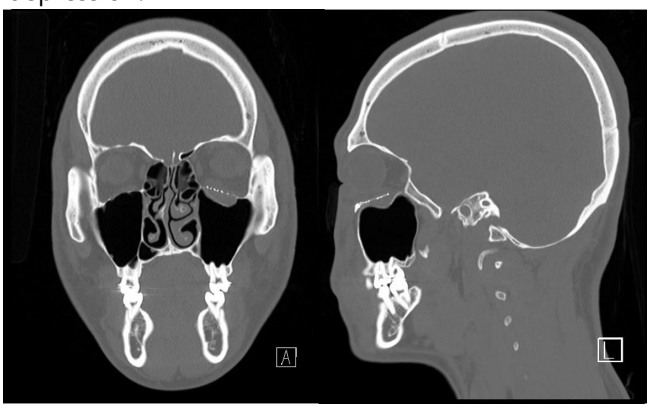

Fig. 3. Postoperative CT showing restoration of the orbital floor contour after reconstruction with Medpor Titan.

EP-102

개 교상 후 발생한 복합 상순 결손에 대한 점막 V-Y 전진 피판과 비순구 회전 피판을 이용한 재건

Subunit-Based Reconstruction of a Composite Upper Lip Defect Using a Mucosal V-Y Advancement Flap and Nasolabial Fold Rotational Flap Following Dog Bite Injury

가톨릭대학교 의과대학 성형외과교실

권다윤, 이준호, 서보미, 권호, **정성노★**

Purpose: Reconstruction of complex upper lip defects requires restoration of oral competence, anatomical continuity, and aesthetic harmony while respecting distinct lip subunits. Traumatic defects involving both the vermilion and adjacent cutaneous upper lip present significant reconstructive challenges. This case reports the functional and aesthetic outcomes of subunit-based reconstruction using a mucosal V-Y advancement flap combined with a nasolabial fold rotational flap following a dog bite injury.

Methods: A 64-year-old man presented with a 3 × 4 cm composite defect involving the left upper lip vermilion and adjacent cutaneous philtral column. Following initial wound care and infection control, definitive reconstruction was performed. The vermilion was reconstructed using a mucosal V-Y advancement flap to restore lip height and continuity, while the cutaneous upper lip and philtral column were reconstructed using a nasolabial fold rotational flap. Each aesthetic subunit was reconstructed individually according to its tissue characteristics. Flap inset was performed with meticulous alignment to the contralateral white roll and philtral landmarks to restore anatomical symmetry and continuity.

Results: Postoperative healing was uneventful, with no complications such as infection, wound dehiscence, or flap necrosis. At postoperative 1-month and 6-month follow-up, stable wound healing and satisfactory symmetry were observed

Oral competence was fully preserved, with no drooling or functional limitation. The reconstructed vermilion demonstrated good color and contour match, and the overall aesthetic outcome was favorable.

Conclusion: Subunit-based reconstruction using a mucosal V-Y advancement flap combined with a nasolabial fold rotational flap enables precise anatomical restoration and reliable functional preservation.

Fig. 1. Initial presentation.

Fig. 2. Immediate postoperative view.

Fig. 3. Postoperative 1-month follow-up.

Fig. 4. Postoperative 6-month follow-up demonstrating preserved oral competence.

EP-103

수술 계획의 변경을 초래한 안와 확장을 동반한 급속 진행성 안면부 보웬병: 증례 보고

Rapid Progression of High-Risk Facial Bowen's Disease Resulting in Loss of Surgical Feasibility and Orbital Preservation through Palliative Radiotherapy

인제대학교 부산백병원

이동훈, 윤지영★

Purpose: Bowen's disease is generally regarded as a slowly progressive carcinoma in situ; however, facial lesions in elderly patients may demonstrate aggressive clinical behavior. We report a case in which rapid progression during surgical preparation resulted in loss of surgical feasibility.

Methods: An 89-year-old man with multiple comorbidities presented with a 2 × 2 cm exophytic mass on the nasal dorsum. A punch biopsy performed at an outside hospital suggested squamous cell carcinoma in situ with blurring of the basement membrane. Histopathologic slides reviewed at our institution showed positivity for p53, Ki-67, and p63, indicating a high-risk lesion. Limited palliative excision with skin grafting was initially considered feasible. However, extensive preoperative medical evaluation was required due to advanced age and comorbidities, resulting in an unavoidable delay before surgery.

Results: During the preoperative period, the tumor progressed rapidly. Imaging revealed enlargement to a 5.7 × 4 cm enhancing mass with nasal bone erosion and invasion of the medial extraconal orbital space. Complete resection would have required orbital exenteration. Given the anticipated morbidity, surgery was deemed infeasible. Conventional fractionated radiotherapy (66 Gy in 33 fractions) achieved marked tumor regression with preservation of the globe.

Conclusion: High-risk facial Bowen's disease may progress rapidly and compromise surgical options. When treatment delay is unavoidable, timely reassessment and consideration of non-surgical modalities may help preserve function and avoid mutilating surgery.

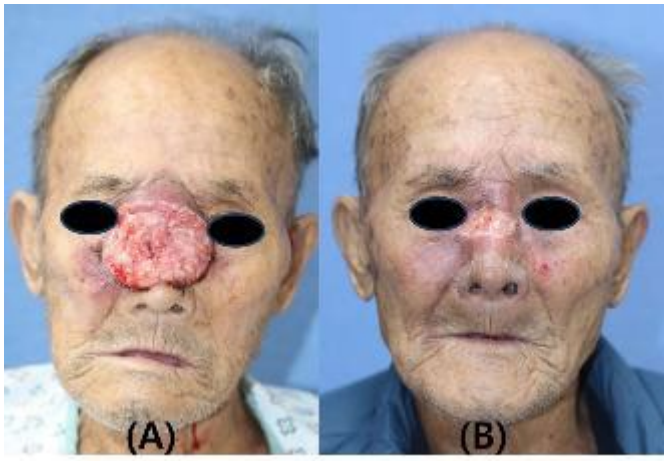

Figure 1. Clinical findings before and after radiotherapy.
(A) Pre-treatment photograph demonstrating a large exophytic mass involving the nasal dorsum and periorbital region.
(B) Post-radiotherapy photograph showing marked tumor regression with preservation of the globe.

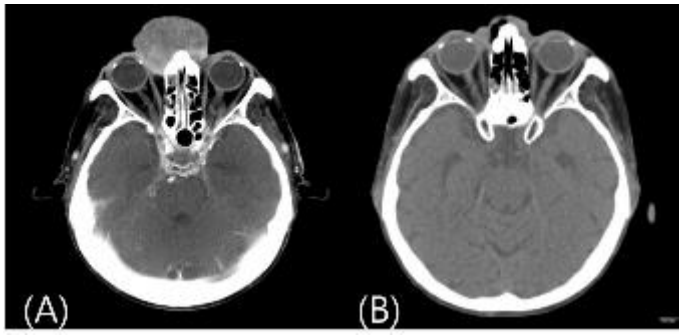

Figure 2. Radiologic findings before and after radiotherapy.
(A) Pre-treatment contrast-enhanced CT showing a 5.7 × 4 cm enhancing mass with invasion of the medial extraconal orbital space.
(B) Post-radiotherapy CT demonstrating significant tumor reduction and resolution of orbital invasion.

EP-104

모피지선 병변을 동반한 이마의 다발성 피지낭종: 증례 보고

(Steatocystoma Multiplex of the Forehead with Multiple Distinct Pilosebaceous Lesions: A Case Report)

단국대학교병원

이석우, 김현석★

Purpose: Steatocystoma multiplex (SM) is a rare disorder of the pilosebaceous unit, predominantly involving the trunk and proximal limbs. Facial lesions without initial scalp or systemic distribution are uncommon and present unique diagnostic and aesthetic challenges. This case represents a rare manifestation of SM localized to the forehead, accompanied by various heterogeneous pilosebaceous lesions.

Methods: A 55-year-old man without relevant family history presented with multiple small, yellowish, firm round papulocystic lesions on the forehead that had progressed over eight years. (Fig 1.) The lesions were asymptomatic but requested removal for cosmetic reasons. Over several sessions, 12 lesions were removed via surgical excision, with histopathologic examination performed in eight lesions for detailed histopathologic evaluation (Fig 2.)

Results: Histopathologic examination revealed a heterogeneous group of diagnoses. Three lesions were confirmed as steatocystoma, characterized by flattened sebaceous lobules within the cyst wall. The remaining lesions corresponded to pilar cysts, sebaceous hyperplasia, epidermal cysts, acne vulgaris, and foreign body granulomas. One year later, the patient returned with an additional lesion on scalp (Fig 3.)

Conclusion: This case describes a rare presentation of SM localized to the forehead without scalp involvement. Accurate histopathologic evaluation is essential for distinguishing SM from other clinically cystic lesions and guides appropriate management.

Fig.1 Clinacal photo showing multiple yellowish-colored papule and nodule on forehead

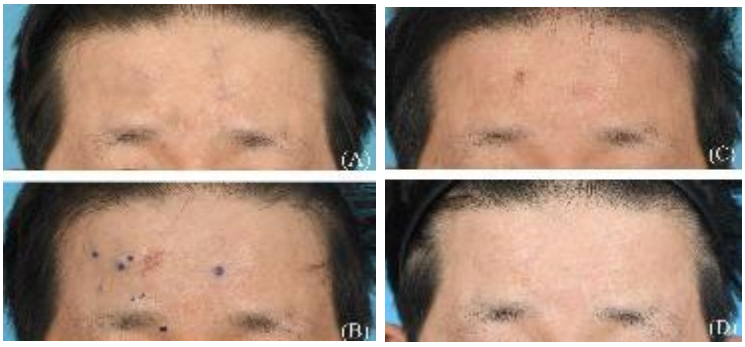

Fig.2 Histopathologic findings of excised lesions, H&E staining. (A) Biopsy-confirmed steatocystoma (original magnification x100). (B) Pilar cyst (original magnification x100). (C) Sebaceous hyperplasia (original magnification x200). (D) Epidermal cyst (original magnification x100). (E) Acne vulgaris, showing nodular mixed dermal infiltrates. (original magnification x40). (F) Foreign body granulomas, showing many multinucleated giant cells. (original magnification x40

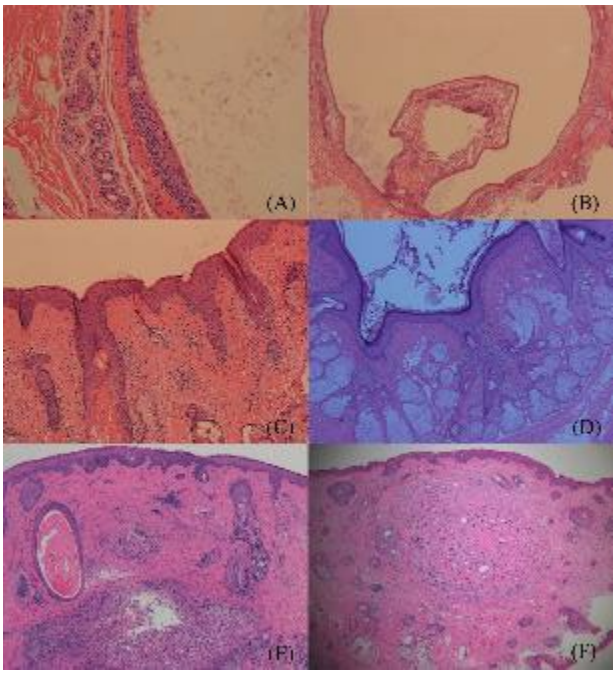

Fig 3. Clinical photo. Late-onset multiple lesions on scalp.

EP-105

뒷머리선 악성 증식성 모낭상피종양에 대한 천공지 기반 섬피판술을 이용한 수술적 치험례

(Surgical treatment of malignant proliferating trichilemmal tumor on posterior hairline using a perforator-based island flap : A case misdiagnosed as eccrine poroma)

한양대학교 의과대학
성형외과학교실
한양대학교구리병원
성형외과

이보현, 정재아, 장정우⋆

Purpose: Proliferating trichilemmal tumor (PTT) is a rare skin tumor derived from external root sheath of hair follicle. Although only small number of its malignant conversion is reported, it has been noted to have a potential for metastasis and recurrence. For this reason, accurate diagnosis and complete excision with appropriate reconstruction are essential. We present a case of malignant PTT lesion reconstructed using a perforator-based island flap (PBIF).

Methods: A 64-year-old female patient with a recurrent mass on posterior hairline was referred to our hospital. The 1 x 1cm sized exophytic mass emerged 2 years ago, and the patient underwent 3 times of excision in previous clinics as it always recurred. The results of biopsy that the patient brought was eccrine poroma which made us to perform simple excision for surgical treatment. However, the result of biopsy revealed the mass as malignant PTT.

Results: There remained remnant cells on the base of lesion microscopically, but no distant metastasis was observed through additional work-up. Wide excision with 1cm margin of free tissue and full thickness including fascia was performed. The defect was reconstructed with a PBIF. After Doppler tracing for a perforator, the island flap was elevated from neck under meticulous dissection not to injure great auricular nerve. The flap was rotated to the defect, and its donor site could be hidden on neck wrinkles.

Conclusion: The reconstruction was successful without any complication, and no recurrence was observed during the follow-up period. Correct diagnosis and appropriate surgical approach enable successful outcome and favorable prognosis.

Fig. 1. A 64-year-old female patient with a recurrent mass on posterior hairline. (Left) A 1 x 1 x 1.5cm size mass removed from the lesion. (Right) The lesion with incomplete excision of remnanat malignant proliferating trichilemmal tumor.

Fig. 2. Intraoperative photographs. (Left) A defect after complete excision and flap design. (Right) Flap coverage using a perforator-based island flap.

Fig. 3. Postoperative photographs. (Left) Picture on postoperative 2 weeks. (Right) Picture on postoperative 3 months.

EP-106

활발한 골 리모델링을 동반한 재발성 관골 골종의 완전 절제를 위한 수술적 고찰: 증례 보고

(Recurrent Zygomatic Osteoma with Active Osteogenic Remodeling and Considerations for Complete Eradication: A Case Report)

가톨릭대학교
성형외과학교실

심진솔, 김동연★

Purpose: Osteomas are rare, slow-growing benign tumors, but their manifestation within the zygomatic bone represents an even more exceptional clinical entity. Although surgical excision is typically curative with recurrence rates below 5%, we report a rare case of zygomatic osteoma exhibiting a unique "broccoli-like" morphological evolution and discuss the surgical challenges in achieving complete eradication.

Methods: A 48-year-old female presented with a recurring mass on the left zygoma. Her medical history included an initial excision in 2013 and a navigation-assisted intraoral re-excision in 2024. Despite subtle postoperative findings in early 2025, the lesion evolved into a third recurrence by late 2025. A longitudinal analysis using serial CT scans and intraoperative findings was conducted to investigate the regrowth mechanisms and the limitations of restrictive surgical access.

Results: Follow-up CT revealed an 8x4 mm focal bony protrusion with an adjacent 13x7 mm calcified fatty lesion. Intraoperatively, the recurrent tissue was notably brittle and interspersed within the soft tissue. Histopathology confirmed a benign compact osteoma with associated cartilage caps and callus formation, indicating active osteogenic remodeling. The recurrence was attributed to microscopic foci remaining anterior to the zygomaticofacial nerve, which were difficult to eradicate via a purely intraoral approach due to efforts to preserve neural function.

Conclusion: Complete eradication of all osteogenic foci, including brittle and fragmented segments, is paramount to preventing recurrence in zygomatic osteomas. In complex or recurrent cases, a combined approach—incorporating an infraorbital incision—is recommended to ensure direct visualization, nerve preservation, and definitive resection.

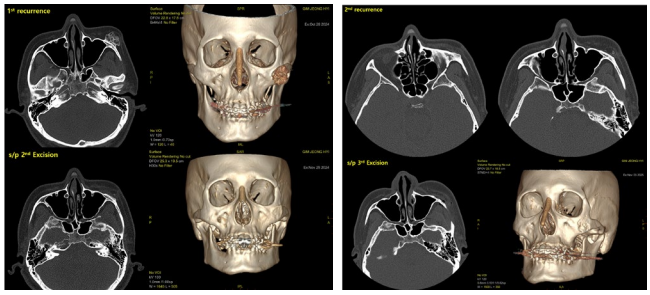

Fig 1. & 2. Serial computed tomography (CT) images illustrating the longitudinal progression of the zygomatic osteoma. Images demonstrate the initial recurrence, postoperative status following the second operation, subsequent second recurrence, and postoperative findings after the third operation, presented in both axial and three-dimensional reconstructions. A progressive, irregular ("broccoli-like") morphological evolution is noted over time.

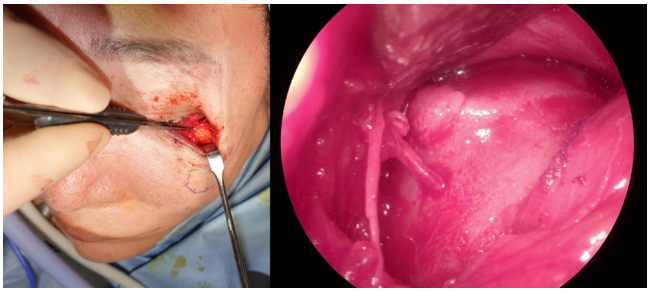

Fig 3. Endoscopic intraoperative view obtained during the third operation, demonstrating the recurrent osteoma at the time of second recurrence. The lesion appears fragmented, brittle, and interspersed within surrounding soft tissue, reflecting active remodeling and incomplete prior eradication.

Fig 4. Gross photograph of the excised osteoma specimen from the third operation, showing irregular, fragmented bony components consistent with the intraoperative findings.

EP-107

만성 광선 손상에 기인한 극심한 피부 취약성을 동반한 진행성 협부 편평세포암의 미세혈관 재건술

Reconstruction of a Advanced-Stage Giant Cutaneous Squamous Cell Carcinoma Using an Anterolateral Thigh Free Flap and Early Secondary Ectropion Correction : A Case Report

중앙대학교 의과대학 성형외과학교실 [1]
중앙대학교 광명병원 성형외과 [2]

정인호[1], 김우섭[2], 김한구[1], 배태희[2], 강신혁[1], 김우주[2], 우수현[1]*

Purpose: Surgical management of giant squamous cell carcinoma (SCC) in patients with severe comorbidities requires a balance between radical resection and functional restoration. We present a case of T4a cheek SCC in a high-risk patient successfully reconstructed with an anterolateral thigh (ALT) free flap, followed by aggressive management of secondary ectropion.

Methods: A 70-year-old male Tungsten Inert Gas (TIG) welder with idiopathic pulmonary fibrosis and extreme skin fragility, secondary to occupational actinic damage from long-term TIG welding, underwent wide excision with a 1-cm safety margin guided by navigation and NIM neuro-monitoring. The procedure involved resection of the superficial parotid gland, masseter muscle, and intraoperatively confirmed eroded zygoma, followed by Stensen's duct ligation. A 15x7cm2 ALT free flap was utilized for reconstruction, with viability assessed via indocyanine green (ICG) angiography.

Results: Histopathology revealed a moderately differentiated SCC (3.8x3.0cm2) with a 15-mm invasion depth and perineural invasion. Despite achieving clear margins, paralytic and mechanical ectropion developed immediately due to facial nerve branch sacrifice and flap weight. A lateral tarsal strip procedure was performed on postoperative day (POD) 11, which successfully restored the lower eyelid position and tension.

Conclusion: The ALT free flap is a robust option for extensive facial defects in medically compromised patients. Early functional intervention, such as the lateral tarsal strip, is crucial for managing secondary complications like ectropion to achieve optimal clinical results in complex head and neck reconstructions.

Fig. 1. (A, B) Preoperative photographs of squamous cell carcinoma on the left cheek, showing an ulcerative lesion and extreme skin fragility secondary to occupational exposure. (C) Intraoperative markings illustrating the planned resection extent.

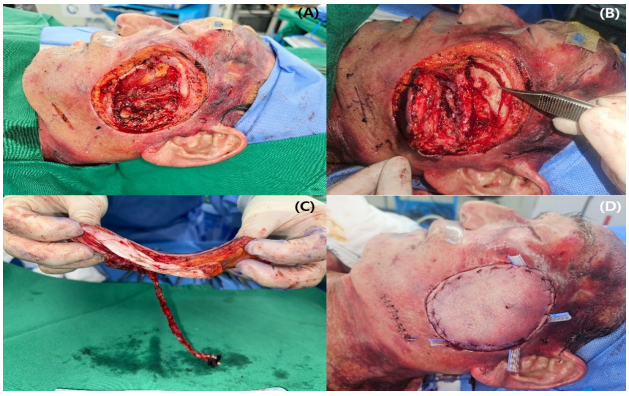

Fig. 2. Intraoperative photographs illustrating the surgical procedure. (A) Final defect after wide excision. (B) Deep resection involving superficial masseter muscle and part of zygoma. (C) Harvested anterolateral thigh (ALT) free flap with its vascular pedicle. (D) Immediate postoperative view after flap insetting.

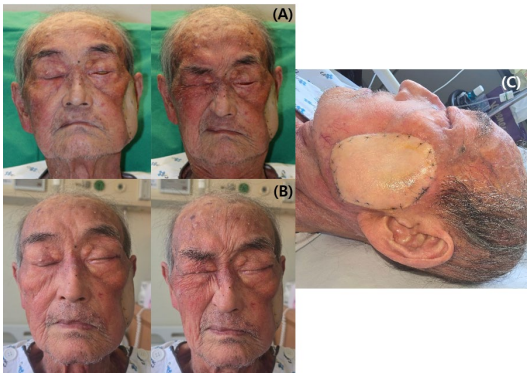

Fig. 3. (A) Pre-operative view before lateral tarsal strip (LTS) procedure, each image shows symptomatic ectropion of the left lower eyelid. (B) Two weeks after LTS operation, the photo demonstrates improved ectropion and less conjunctival exposure. (C) 45 days after flap surgery.

EP-108

안면부에 발생한 다발성 한공암종: 증례 보고

(Multiple Synchronous Eccrine Porocarcinoma of the Face : A Case Report)

경희대학교 의과대학
성형외과학 교실

차은총, 김영진, 강상윤*

Purpose: Eccrine porocarcinoma is a rare malignant tumor originating from the sweat gland. It mostly develops on the lower extremities or head and neck region as papules, nodules, or plaques. Here, we report a rare case of two synchronous porocarcinoma on the lateral periocular and cheek area, which were initially diagnosed as Bowen's disease.

Methods: An 81-year-old male presented with two crateriform lesions, each measuring 10x5mm^2 and 5x5mm^2 on right lateral periocular and cheek areas, located 4cm apart. Four years prior, the patient was diagnosed with Bowen's disease and treated with CO_2 ablation at the dermatology department. Two years later, he experienced recurrence and received methyl aminolevulinate photodynamic therapy (MAL-PDT). Upon a second recurrence, punch biopsies on both lesions confirmed porocarcinoma and the patient was referred to our department. CT and PET scans showed no evidence of systemic metastasis.

Results: Two serial wide local excisions with frozen biopsy were performed for both periocular lesion and the cheek lesion. The periocular defect was reconstructed with a radial forearm free flap while cheek area was managed with direct closure under local anesthesia. Both pathology results revealed eccrine porocarcinoma with no involvement of resection margins. No recurrence or metastasis was found during 1 year follow-up period.

Conclusion: A porocarcinoma is rare malignancy with high morbidity that warrants early intervention and evaluation. In our case, the location and distance of tumors made a single immediate reconstruction challenging. Consequently, two separate reconstructions of each defect allowed adequate safety margins and allowed functional and aesthetic outcomes.

Fig. 1. An 81-year-old male with two distinct, crateriform, porocarcinoma on right lateral periocular (red arrow) and cheek area (yellow arrow), each located 4cm apart.

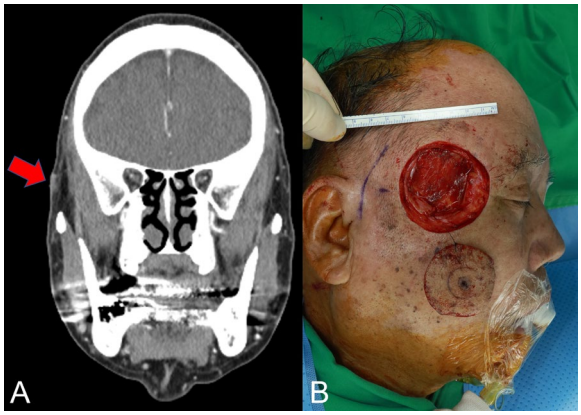

Fig. 2. Preoperative CT shows tumor infiltration deep to the SMAS layer and extensive subcutaneous involvement (A). Based on these findings, the excision was extended beyond the clinical tumor boundaries to deep temporal fascia, resulting in a 6x6cm^2 size defect following wide excision (B).

Fig. 3. Post operative photography at 6 months shows brow ptosis due to the frontal branch injury. Despite the ptosis, the overall aesthetic and functional results of the reconstruction are satisfactory.

EP-109

혈관육종 절제 후 두개골 노출을 동반한 광범위 두피 결손의 부분층 피부이식을 이용한 단계적 재건

(Staged Reconstruction Using Split-Thickness Skin Graft for an Extensive Scalp Defect with Bare Calvarium Following Angiosarcoma Resection)

가톨릭대학교 의과대학
성형외과학교실

이창준, 김라윤, 이준용, 유결, 백상운*

Purpose: Scalp angiosarcoma is an aggressive malignancy with a high risk of local recurrence and frequently presents with ulcerative and hemorrhagic lesions requiring surgical resection. Wide excision often necessitates periosteal removal depending on tumor invasion, and exposure of bare calvarial bone results in an ungraftable wound bed, making reconstruction particularly challenging. We report a case of an extensive scalp defect with periosteal loss following angiosarcoma resection that was successfully managed through staged reconstruction using split-thickness skin graft (STSG).

Methods: A 78-year-old male presented with extensive hemorrhagic scalp lesions and was diagnosed with angiosarcoma on biopsy (Fig. 1). Wide excision with a 2-cm safety margin was performed, including periosteal resection in suspected areas, resulting in multiple regions of exposed bare calvarium (Fig. 2A). Cortical burring of the outer table was performed to induce pinpoint diploic bleeding, thereby improving vascularity of the wound bed (Fig. 2B). Serial negative pressure wound therapy (NPWT) was applied over a one-month period to promote granulation tissue formation (Fig. 2C). Delayed reconstruction was subsequently completed using acellular dermal matrix placement followed by STSG, given the extensive size of the defect (Fig. 3).

Results: At 2-month follow-up, the skin graft demonstrated good take with stable coverage of the reconstructed scalp defect (Fig. 4).

Conclusion: A staged reconstructive approach using calvarial burring and serial NPWT can effectively convert exposed bare calvarium into a graftable wound bed, enabling reliable reconstruction of extensive scalp defects following angiosarcoma resection.

Fig. 1. Preoperative clinical photographs showing extensive ulcerative, hemorrhagic scalp lesions. (A) Frontal view. (B) Vertex view. (C) Left lateral view. (D) Right lateral view.

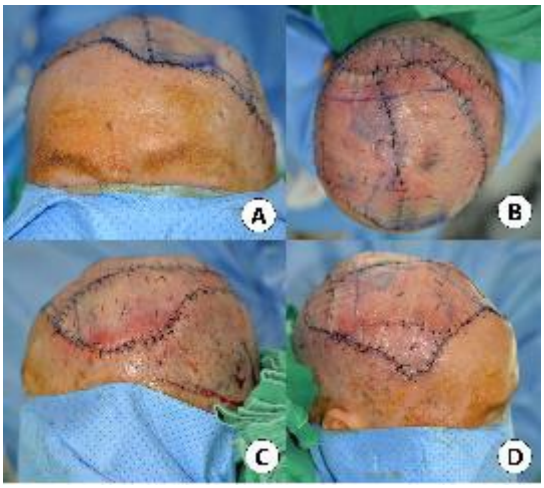

Fig. 2. Intraoperative vertex views demonstrating staged wound bed preparation. (A) Extensive defect immediately after wide excision. (B) (B) Cortical burring of the outer table performed over areas of exposed bare calvarium. (C) Well-prepared wound bed following serial NPWT.

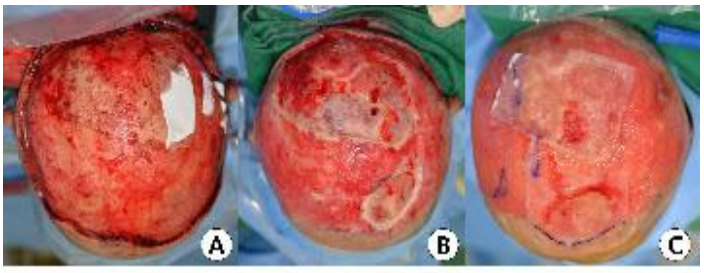

Fig. 3. Intraoperative photographs showing split-thickness skin grafting of the scalp defect. (A) Frontal view. (B) Vertex view. (C) Left lateral view. (D) Right lateral view.

Fig. 4. Postoperative clinical photographs at 2-month follow-up showing well-maintained skin graft coverage. (A) Vertex view. (B) Left lateral view.

EP-110

재발성 지방종으로 오인된 볼의 다형선종 유래 암종

(Carcinoma ex-Pleomorphic Adenoma of the Cheek Masquerading as Recurrent Lipoma)

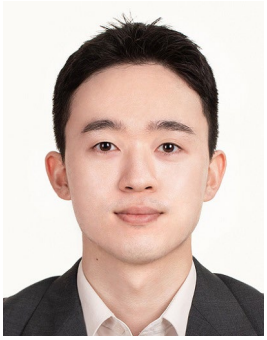

경상국립대학교병원
성형외과

김태호, 이경석*

Purpose : Large longstanding facial masses may clinically mimic lipoma but require consideration of sarcoma or salivary malignancy. The author presents an 88-year-old woman with a 20-year cheek mass initially excised as lipoma 15 years prior, later diagnosed as carcinoma ex-pleomorphic adenoma requiring wide excision and partial parotidectomy.

Methods : An 88-year-old woman presented with a recurrent 7.8 cm left cheek mass that had slowly enlarged over 10 years following previous lipoma excision 15 years prior. Contrast-enhanced MRI revealed a 7.7 cm enhancing mass in the left buccal space with an additional 2 cm deep lesion and indeterminate parotid lymph nodes, concerning for malignancy including sarcoma. Wide excision and partial parotidectomy were performed under general anesthesia with facial nerve monitoring.

Results: Wide excision of superficial and deep masses was performed through elliptical incision. Intraoperative frozen biopsy confirmed pleomorphic adenoma in the deep mass. Facial nerve integrity was preserved during dissection, Stensen's duct was ligated after confirming obstruction, and parotid superficial lobe with lymph nodes was resected with negative margins. Final pathology confirmed carcinoma ex-pleomorphic adenoma (myoepithelial carcinoma, minimally invasive, negative margins). Postoperative transient left facial nerve palsy improved significantly by 3-month follow-up with excellent wound healing and no recurrence.

Conclusion : Large facial masses require thorough preoperative imaging including MRI to assess salivary gland infiltration even without rapid growth, ensuring appropriate safety margins during wide excision. This case highlights the need for sarcoma/malignancy suspicion in atypical longstanding masses and careful multidisciplinary workup to guide oncologic resection and facial nerve preservation.

Fig. 1. Preoperative photograph of large facial mass

Fig. 2. Intraoperative photograph showing the cheek mass

Fig. 3. Sequential postoperative photographs of left facial nerve palsy recovery at 3 weeks and 3 months

Fig. 4. Three-month postoperative photograph of healed surgical wound

EP-111

눈 주위 색소침착 치료를 위한 Poly-p-dioxanone 주입 후 발생한 촉지성 결절: 증례 보고

(Palpable Nodule Formation Following Poly-p-Dioxanone Filler Injection for Periorbital Hyperpigmentation: A Case Report)

인제대학교

김성준, 이수향*

Purpose: To highlight the occurrence of palpable nodule formation following poly-p-dioxanone–based biostimulatory filler injection in the periorbital region.

Methods: A 40-year-old female underwent Ultracol injection for the treatment of periorbital hyperpigmentation. Clinical findings, management, and follow-up outcomes were evaluated.

Results: Several days after the procedure, a palpable nodule developed in the left lower eyelid. The lesion was not visible on inspection but was clearly detectable on palpation. The patient reported no pain, tenderness, or inflammatory signs. Conservative management, including saline injection and manual massage, led to partial improvement; however, the nodule persisted on follow-up.

Conclusion: Palpable but non-visible nodules may develop after poly-p-dioxanone filler injection, particularly in thin and anatomically sensitive areas such as the lower eyelid. Careful physical examination, appropriate injection technique, and close postoperative follow-up are essential when using biostimulatory fillers in the periorbital region.

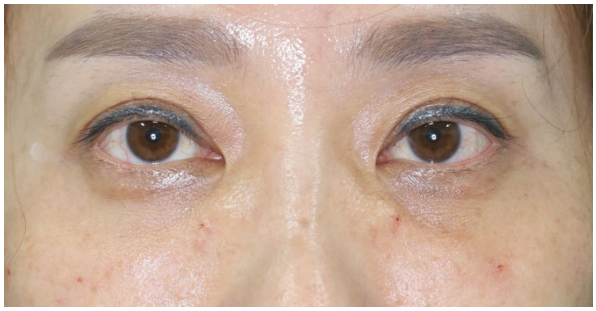

Figure 1. Immediate Post-procedural Appearance

Clinical photograph obtained immediately after Ultracol injection for periorbital hyperpigmentation. No visible contour deformity or skin irregularity is observed in the infraorbital region.

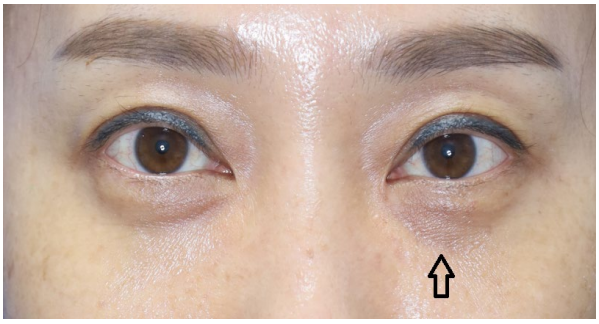

Figure 2. Delayed Palpable Nodule Formation

Clinical photograph obtained several days after the procedure. No visible external deformity is noted; however, a firm subcutaneous nodule was palpable in the right infraorbital area (arrow).

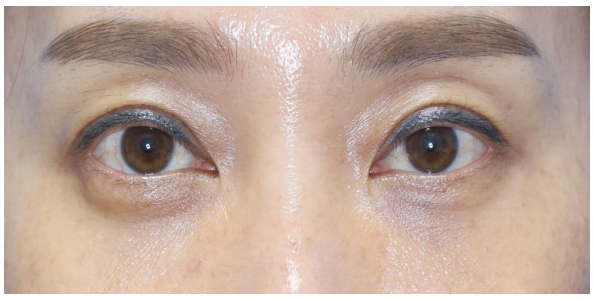

Figure 3. Follow-up Examination

Follow-up clinical photograph demonstrating persistent but non-visible infraorbital nodule without erythema, swelling, or tenderness.

EP-112

인간 교상에 의해 발생한 부분적 하구순 결손의 양측 근점막 전진 피판을 이용한 재건: 증례 보고

(Reconstruction of a Partial Lower Lip Defect Caused by a Human Bite Using Bilateral Myomucosal Advancement Flaps: A Case Report)

가톨릭대학교 의과대학
의정부성모병원 성형외과

김사라, 서보미, 정성노, 권호, 이준호*

Purpose : Human bite injuries of the lower lip carry a high risk of polymicrobial infection and frequently disrupt the vermilion line, necessitating precise reconstruction for optimal functional and aesthetic outcomes.
We report the clinical outcome of bilateral myomucosal advancement flap reconstruction for a near–half-width lower lip defect caused by a human bite.

Methods : A 49-year-old male presented 1–2 days after sustaining a human bite injury. Examination revealed a contaminated lower lip defect involving nearly half of the lip width, with disruption of the vermilion line and underlying orbicularis oris muscle.
Under general anesthesia, meticulous irrigation and debridement were performed. Bilateral myomucosal advancement flaps were elevated, including orbicularis oris muscle, and advanced medially to restore muscular continuity and achieve precise vermilion alignment.
Intravenous amoxicillin-clavulanate and metronidazole were administered during hospitalization, followed by oral antibiotics after discharge. Postoperative wound status and signs of infection were closely monitored.

Results: : No postoperative infection or wound dehiscence occurred. Sutures were removed on postoperative day 7. At 3-week follow-up, the continuity and symmetry of the vermilion line were well maintained, without microstomia or functional limitation in oral opening.

Conclusion : For human bite–induced lower lip defects involving nearly half of the lip width, bilateral myomucosal advancement flap reconstruction following thorough debridement provides reliable infection control and satisfactory functional and aesthetic outcomes.

Fig. 1. Preoperative lower lip defect

Fig. 2. Intraoperative photo

Fig. 3. Immediate postoperative vermilion reconstruction

Fig. 4. Postoperative outcome

EP-113

지방종 절제 후 재발성 이마 종괴로 나타난 연속적인 반응성 신경 병변

(Sequential Reactive Neural Changes Presenting as a Recurrent Forehead Mass after Lipoma Excision)

순천향대학교 부속 서울병원

박찬경, 강상규*

Purpose: Recurrent masses in prior surgical sites are often suspected to represent recurrence of the original mass. However, reactive neural changes can present as palpable masses that mimic a recurred lesion. We report a case of a recurrent forehead mass years after lipoma excision, demonstrating sequential histopathologic findings of traumatic neuroma followed by scar-associated neural fibrosis.

Methods: A 65-year-old woman underwent surgical excision of a forehead lipoma at our institution 11 years prior. She had noticed gradual enlargement of a palpable mass at the previous surgical site for approximately three years before presenting to our clinic. Examination revealed a firm, localized mass at the excision site without sensory deficit. The mass was excised under local anesthesia. Histopathology revealed small nerve fascicles enveloped in collagen, consistent with traumatic neuroma. One year later, she returned with enlargement at the same site (Fig. 1). The mass was re-excised, and histopathology showed dermal nerve bundles with collagenous fibrosis and no evidence of recurrent neuroma or neoplastic change (Fig. 2).

Results: Both lesions were completely excised. The postoperative course was uneventful, without neurologic deficits or wound complications. At follow-up, the patient remains stable without recurrence and continues under surveillance.

Conclusion: Reactive neural changes may present as recurrent masses at prior surgical sites. Histopathologic findings from the first re-excision were consistent with traumatic neuroma, whereas the subsequent specimen demonstrated organized dermal nerve bundles with fibrosis, suggesting scar-associated neural remodeling rather than true tumor recurrence. Recognition of this post-excisional neural alteration may help avoid misdiagnosis and guide appropriate management

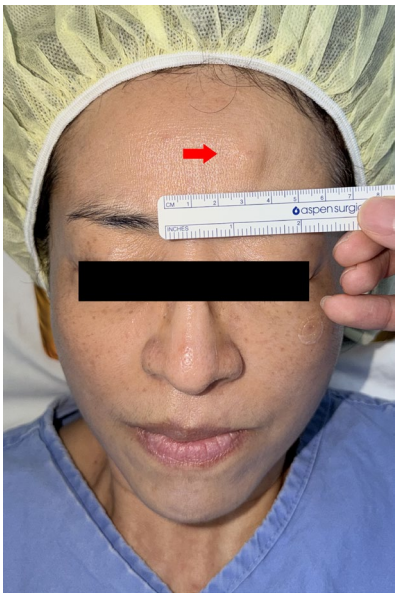

Figure 1. Preoperative photograph demonstrating a well-defined, round mass on the left forehead.

Figure 2. Gross specimen obtained after excision, showing a nodular soft tissue mass with an irregular surface.

EP-114

하부 이마 골종의 안전한 절제 및 완벽한 신경 보존을 위한 피하 박리 동반 모낭 보존 전방 모발선 접근법: 증례보고

(The Trichophytic Anterior Hairline Approach with Subcutaneous Dissection for Safe Resection and Complete Nerve Preservation in Lower Forehead Osteomas: a case report)

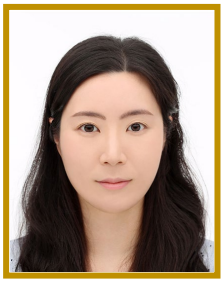

경상국립대학교

김지승, 김태호, 김민형, 신재봉, 김남균, 이경석, 김준식*

Purpose: Surgical resection of lower forehead osteomas presents significant challenges due to their anatomical proximity to the supraorbital nerve (SON) and supratrochlear nerve (STN) (Fig. 1). Conventional approaches, such as bicoronal or endoscopic techniques, frequently carry risks of permanent forehead hypoesthesia, conspicuous scarring, and localized alopecia. This study introduces an advanced, single-stage surgical strategy designed to ensure complete nerve preservation through a remote-access approach, while simultaneously achieving rigid, permanent contour reconstruction and minimizing aesthetic morbidity.

Methods: A 55-year-old female presented with an enlarging lower forehead mass. A zigzag trichophytic incision was designed 0.5cm superior to the anterior hairline, extending between the bilateral temporal crests (Fig. 1). Dissection proceeded through the subcutaneous layer to avoid follicular damage. To protect the STN, a vertical incision was made in the frontalis muscle medial to the nerve's course, exposing the tumor (Fig. 2). Following subperiosteal enucleation of the osteoma using a pneumatic burr and osteotome, the defect was reconstructed with a Medpor® implant, which was rigidly fixed with an 8-hole microplate.

Results: The osteoma was completely resected without neurosensory deficits in the SON or STN distributions. The hairline scar was virtually imperceptible, and no localized alopecia was observed. Rigid fixation ensured a smooth, natural forehead contour with no hardware migration or infection during follow-up (Fig .3).

Conclusion: The anterior hairline approach using a trichophytic incision and subcutaneous dissection provides an anatomically safe corridor for treating lower forehead osteomas. This technique effectively prevents nerve injury while achieving superior aesthetic and structural outcomes through rigid microplate fixation.

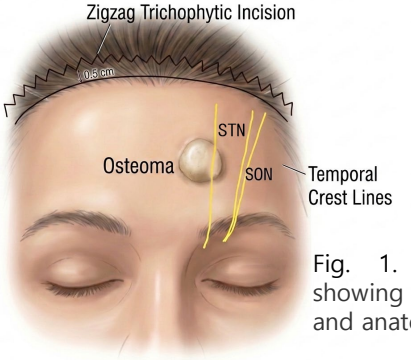

Fig. 1. Schematic illustration showing preoperative planning and anatomical landmarks

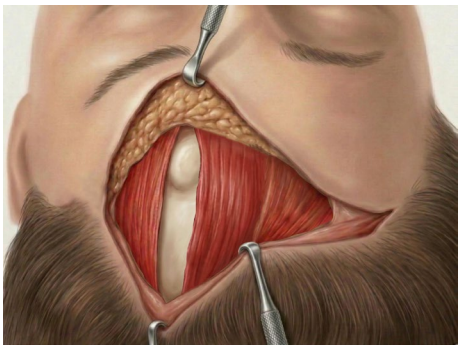

Fig. 2. Schematic illustration showing the vertical incision of the frontalis muscle to safely expose the osteoma while ensuring protection and preservation of the supratrochlear nerve (STN)

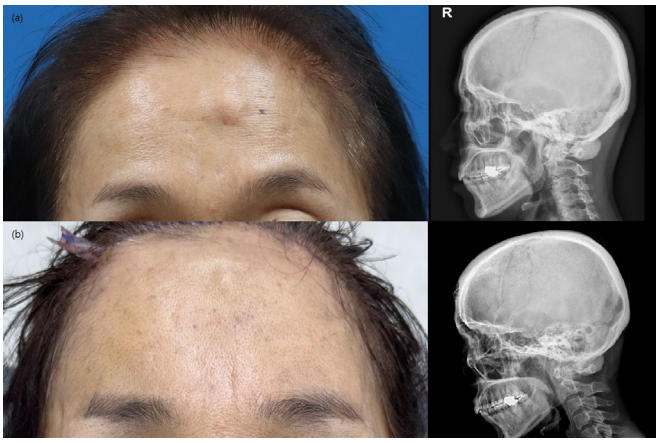

Fig. 3. (a) Pre-surgical photograph and lateral skull radiograph of a 55-year-old female patient presenting with an osteoma on the left forehead within the STN region. (b) Post-surgical images and a lateral skull X-ray taken at three days demonstrate favorable wound healing concealed within the hairline, alongside a refined forehead profile.

EP-115

수막종 수술 후 두피 절개 부위에 대형 복합이식편을 적용하여 교정한 증례 보고

한림대학교성심병원

심승용*, 김재현, 정찬민

Purpose: : This case report aims to document and analyze the successful application of a composite graft to resolve an incorrect incision following meningioma surgery in a 43-year-old female patient. The purpose is to illustrate the effectiveness of composite grafts of broader area in immediate reconstruction of a substantial scalp soft tissue defect resulting from an erroneous incision design.

Methods : Initialy incision design was incorrect causing almost all of the skin soft tissue flap of the parietal scalp to be separated except for 0.5cm wide galea aponeurotica attached. Immediate reconstruction of 6 x 10 cm scalp defect were employed with the corresponding flap (Figure 1).

Results : Immediate application of a composite graft successfully reconstructed the extensive soft tissue defect caused by the incorrect incision. Graft exhibited optimal viability and the patient demonstrated both aesthetic and functional improvement during postoperative period (Figure 2). 2 month follow-up revealed no major complications with the graft integrating seamlessly into the surrounding tissues (Figure 3).

Conclusion: : It is well-established that composite grafts face challenges in survival beyond the diameters of 1.5cm. However in cases similar to the one presented herein, where a small connection remains intact with the recipient site and immediate reconstruction is feasible, a broader composite graft can emerge as an effective solution. This case underscores the efficacy of composite grafts in resolving substantial scalp defects resulting from incorrect incisions during meningioma surgery. Positive outcome supports the consideration of composite grafts as a valuable tool in the armamentarium for reconstructive procedures following surgical errors.

Fig 1. Intraoperative photography of immediate reconstruction with 6 x10 cm size composite graft on parietal scalp

Fig 2. Gross photography of composite graft on 3 days after the surgery

Fig 3. Gross photography of composite graft on 2 months after the surgery

EP-116

방사선 유발 피부손상에서 체외충격파 치료의 보호 효과

(Protective Effects of Extracorporeal Shock Wave Therapy on Radiation-Induced Cutaneous Injury)

경상국립대학교병원
성형외과

신재봉, 이경석*

Purpose : Radiation therapy frequently causes skin injury and progressive fibrosis, which remain difficult to prevent or treat. This study evaluated the protective effects of extracorporeal shock wave therapy (ESWT) on radiation-induced cutaneous injury and investigated its underlying mechanisms.

Methods : Human dermal fibroblasts were exposed to irradiation (20 Gy) followed by ESWT treatment. Cell viability, migration, and fibrosis-related signaling pathways were analyzed. For in vivo evaluation, a murine dorsal skin irradiation model (45 Gy) was established, and ESWT was applied after irradiation. Skin injury severity, histologic changes, and molecular markers related to fibrosis were assessed.

Results : ESWT significantly improved viability and migration of irradiated dermal fibroblasts compared with irradiated controls. Treatment with ESWT also reduced TGF-β1 expression in irradiated fibroblasts. In the murine model, ESWT significantly decreased the severity of radiation-induced skin injury. Histologic analysis demonstrated reduced collagen deposition and decreased numbers of α-SMA–positive myofibroblasts in ESWT-treated skin. Furthermore, ESWT suppressed TGF-β1 and phosphorylated Smad3 expression while increasing mature vessel density in irradiated tissue.

Conclusion : ESWT attenuates radiation-induced skin injury by modulating TGF-β–associated fibrotic signaling and promoting tissue repair. These findings suggest that ESWT may serve as a potential therapeutic strategy for preventing or mitigating radiation-induced skin fibrosis.

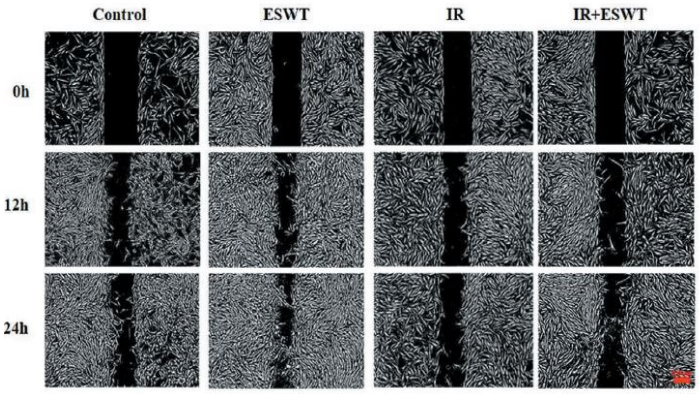

Fig. 1. Effects of ESWT on irradiated human skin fibroblast migration.

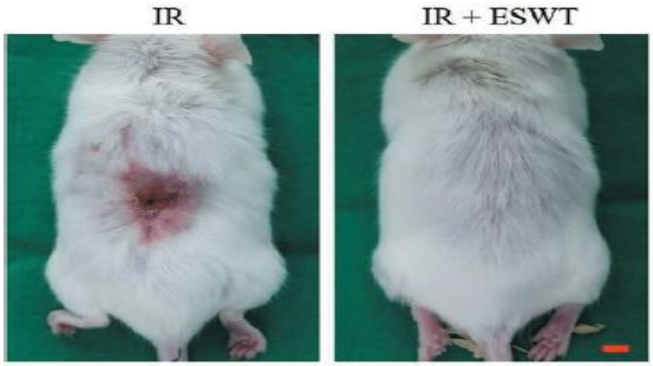

Fig. 2. Clinical evaluation of skin injury 8 weeks after irradiation of mice.

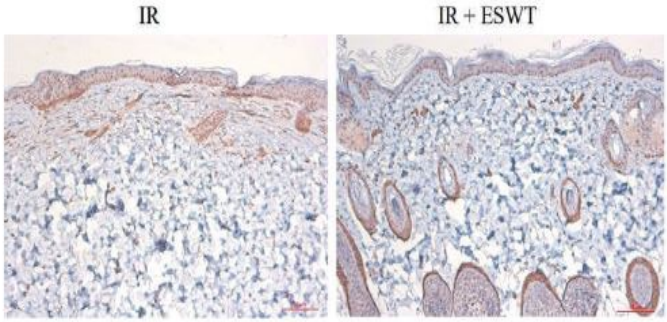

Fig. 3. Immunohistochemical staining of α-SMA in the skin of irradiated mice.

EP-117

성형외과에서 Propofol–Ketamine 기반 감시하 마취의 장기적 안전성과 임상 적용: 15년간의 후향적 분석

(Long-Term Safety and Clinical Application of Propofol–Ketamine–Based Monitored Anesthesia Care in Plastic Surgery: A 15-Year Retrospective Analysis)

한림대학교

김경민, 안정훈, 김기현, 우상석, 이준원, 김성환, 최재구, 서인석*

Purpose: Modified monitored anesthetic care (MAC) using a single bolus of propofol combined with ketamine has been applied in outpatient plastic surgery to achieve rapid, short-duration sedation without endotracheal intubation. Propofol was selected for its rapid onset, short duration, minimal cumulative effect, and antiemetic properties, making it suitable for ambulatory procedures. Ketamine was added as an analgesic adjunct to preserve spontaneous respiration and maintain hemodynamic stability while reducing procedural pain.

Methods: From January 2012 to February 2026, 11,475 operations were performed at our institution, of which 1,743 cases (15.2%) were conducted under MAC. Representative procedures included skin tumor excision/biopsy (n=640), closed reduction of nasal bone fracture (n=232), and debridement with local flap reconstruction (n=180). Sedation (propofol 1 mg/kg and ketamine 1 mg/kg) was administered immediately prior to painful steps without continuous infusion.

Results: Sedation was rapidly achieved and maintained for a procedure-appropriate duration with prompt recovery. No clinically significant hypotension or hypertension compared to baseline was observed. Adverse events were infrequent: decreased oxygen saturation in 56 cases (3.2%), nausea in 38(2.2%), dizziness in 68 (4.0%), and hallucination in 14 (0.8%). All desaturation episodes were successfully corrected with jaw-thrust maneuver, supplemental oxygen via mask, and oral suction; no patient required endotracheal intubation. Symptoms resolved within 30–60 minutes without sequelae.

Conclusion: Low dose bolus propofol combined with ketamine provides effective, safe, and reliable short-duration sedation. Compared with general anesthesia, it avoids intubation-related complications such as postoperative sore throat while providing sufficient anesthetic and analgesic effects, making it a valuable alternative in selected outpatient plastic surgical procedures.

Table 1. Distribution of surgical procedures performed from 2012 to 2026 and the proportion conducted under monitored anesthetic care (MAC).

	수술 개수	(%)
Excision and biopsy	640	36.7
Closed reduction (Nasal bone Fx.)	232	13.3
Debridement and local flap	180	10.3
Irrigation and debridement	150	8.61
Fat injection / Graft	100	5.74
Scar revision	88	5.05
Blepharoplasty	63	3.61
Subdermal excision (Bromhidrosis)	51	2.93
Open / Corrective rhinoplasty	45	2.58
그 외	194	11.1
Total	1743	100

Table 2. Incidence of adverse events during monitored anesthetic care (MAC), presented as number and percentage relative to MAC cases and total procedures.

Symptom	
Decreased Oxygen saturation (<80)	56 (3.2%)
Postoperative nausea	38 (2.2%)
Postoperative dizziness	68 (4.0%)
Postoperative hallucination	14 (0.8%)

EP-118

켈로이드 치료의 새로운 임상적 접근: 병변 내 항생제-스테로이드 병합 요법의 효과에 대한 다기관 후향적 연구

(A New Clinical Approach to Keloid Management: A Multicenter Retrospective Study on the Efficacy of Intralesional Antibiotic–Steroid Combination Therapy)

서울대학교 [1]
에버성형외과 [2]

최낙원 [1], 박영오 [2], 김백규* [1]

Purpose: 켈로이드의 정확한 병리학적 기전은 아직 명확히 밝혀지지 않았으며, 높은 재발률과 불만족스러운 치료 결과로 인해 대표적인 난치성 질환으로 여겨져 왔다. 기존의 치료는 주로 섬유조직의 증식 억제에 집중해 왔으나, 본 연구는 켈로이드의 발생 및 진행이 혈류 감소 부위에서의 미세 감염과 이로 인한 국소 면역 반응 저하에 의해 매개될 가능성에 초점을 맞추고 있다. 이러한 병리학적 가설에 기반하여 항생제와 스테로이드를 병합하여 병변 내 주사함으로써 미세 감염을 조절하는 새로운 치료 요법을 고안하였으며, 그 임상적 효능을 탐색하고자 한다.

Methods: 분당서울대학교병원 성형외과와 에버성형외과에서 총 48명의 환자를 대상으로 다기관 후향적 연구를 수행하였다. 환자군은 스테로이드 단독 주사 군(24명)과 항생제(gentamicin)-스테로이드 병합 주사 군(24명)으로 분류되었다. 두 군 모두 1개월 간격으로 총 3회의 주사 치료를 받았으며, 치료 직후 3개월간의 휴지 기간을 가졌다. 최종적인 임상 평가는 마지막 주사 시행 6개월 후 추적 관찰 시점에 밴쿠버 흉터 척도(Vancouver Scar Scale)를 측정하여 두 군 간의 개선 정도를 비교 분석하였다.

Results: 분석 결과, 스테로이드 단독 주사 요법 군은 VSS 점수가 치료 전 평균 8.83점에서 치료 후 7.79점으로 1.04점의 개선을 나타냈다. 반면, 항생제-스테로이드 병합 주사 군은 치료 전 평균 8.71점에서 치료 후 5.71점으로 3.00점의 개선을 보였다. 두 군 모두에서 임상적 개선이 관찰되었으나, 병합 주사 군에서 VSS 점수의 감소 폭이 통계적으로 유의하게 더 뚜렷한 양상을 확인하였다.

Conclusion: 본 연구는 켈로이드의 병리학적 기전에 있어 미세 감염 조절의 중요성을 시사하며, 항생제 병합 요법이 기존 단독 요법보다 우수한 임상적 유효성을 보유하고 있음을 입증한다. 이러한 결과는 향후 난치성 켈로이드의 표준 치료 지침을 보완하고, 환자 개별 특성에 맞춘 정밀한 맞춤형 치료 전략을 수립하는 데 있어 중요한 학술적 및 임상적 근거를 제공할 것으로 기대된다.

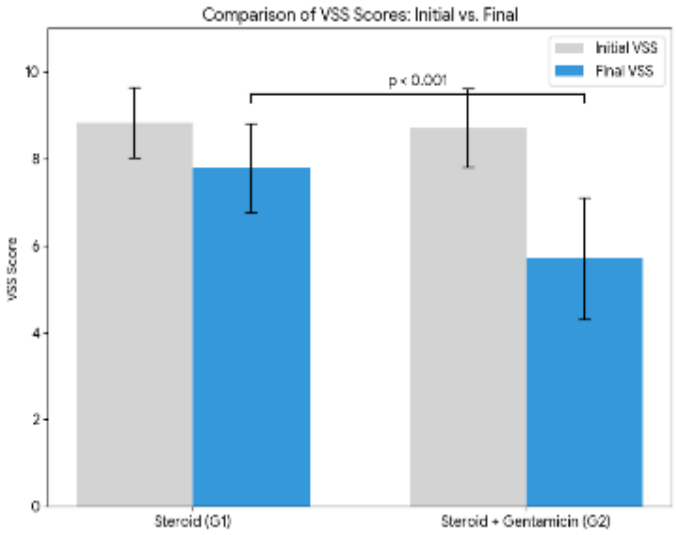

Fig. 1 Vancouver Scar Scale (VSS) Score Improvements by Treatment Group.

Fig. 2 44-year-old male patient with keloid on the right shoulder.

Fig. 3 30-year-old male patient with keloid on the chest.

EP-119

백서 좌골신경 결손 모델에서 탈세포화 동종 신경이식의 신경 재생 촉진에 대한 FK-506의 효과

(Effect of FK-506 on Nerve Regeneration in Acellular Allogeneic Nerve Grafts in a Rat Sciatic Nerve Defect Model)

서울대학교

최진일, 이세연, Celige Li, 김승환, 정용욱, 김병준*

Purpose: Allogeneic nerve grafts are an alternative to autografts to avoid donor-site morbidity. FK-506 has been reported to enhance nerve regeneration through neurotrophic and immunomodulatory effects. This study evaluated the effect of FK-506 on nerve regeneration in a rat sciatic nerve defect model reconstructed with autografts or acellular allografts.

Methods: A 15-mm sciatic nerve defect was created in Lewis rats and reconstructed with a 20-mm isograft (ISO) or supercritical extraction–processed acellular allograft (SC). Animals were assigned to FK-506–treated (5 mg/kg, subcutaneous injection for 3 weeks) or untreated groups, resulting in four groups. Nerve regeneration was assessed at 2, 4, 6, 8, and 10 weeks using the sciatic functional index (SFI) and the tibialis anterior (TA) muscle cross-sectional area ratio measured by ultrasound. Histological analysis and TA wet muscle mass ratio were evaluated at 10 weeks.

Results: At 10 weeks, SFI values were highest in the order of ISO, ISO+FK-506, SC+FK-506, and SC (Figure 1). TA muscle ratio and wet muscle mass ratio were highest in ISO+FK-506, followed by ISO, SC+FK-506, and SC (Figure 2). Axon counts at the graft midpoint and distal nerve showed the same trend (Figures 3, 4). ISO and ISO+FK-506 demonstrated significantly greater regeneration than SC and SC+FK-506, whereas FK-506 treatment did not produce statistically significant differences within the ISO or SC groups.

Conclusion: FK-506 treatment was associated with improved overall nerve regeneration parameters in both autografts and acellular allografts. Combined use of FK-506 with nerve grafts may enhance graft efficacy and represent a potential adjunctive strategy for peripheral nerve reconstruction.

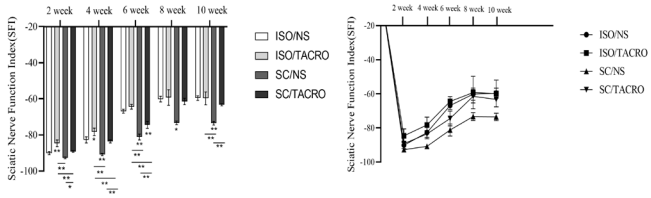

Fig. 1. Sciatic nerve function index measurement. At 10 weeks, SFI values were highest in the order of ISO, ISO+FK-506, SC+FK-506, and SC (−59.1, −59.7, −64.0, and −74.1, respectively, *p<0.05, **p<0.01)

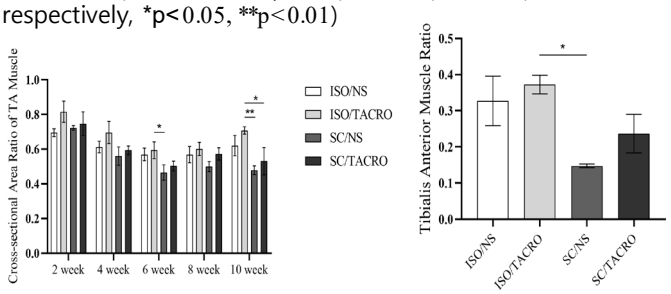

Fig. 2. Results of the TA muscle cross-sectional area ratio (ultrasound) and wet muscle mass ratio. The TA muscle cross-sectional area ratio measured by ultrasound was highest in the ISO+FK-506 group, followed by ISO, SC+FK-506, and SC (0.708, 0.638, 0.549, and 0.478, respectively, *p<0.05, **p<0.01). Similarly, the TA wet muscle mass ratio was highest in ISO+FK-506, followed by ISO, SC+FK-506, and SC (0.37, 0.34, 0.29, and 0.18, respectively, *p<0.05, **p<0.01).

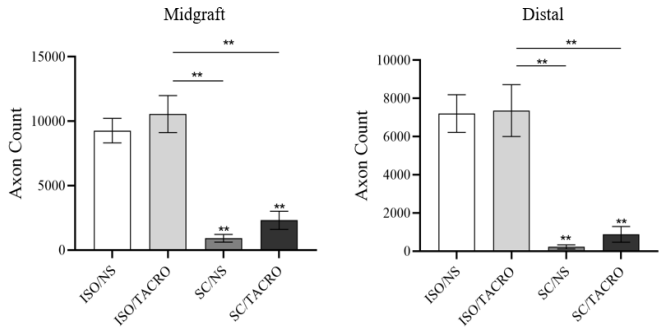

Fig. 3. Axon counts at the graft midpoint (left) and distal nerve (right). Axon counts at the graft midpoint were highest in ISO+FK-506, followed by ISO, SC+FK-506, and SC (10556, 8593, 1945, 772, respectively). Axon counts at the distal nerve were also highest in ISO+FK-506, followed by ISO, SC+FK-506, and SC. (7363, 6665, 738, 188, respectively). ISO and ISO+FK-506 showed significantly greater regeneration than SC and SC+FK-506, whereas FK-506 treatment did not result in statistically significant differences within the ISO or SC groups.

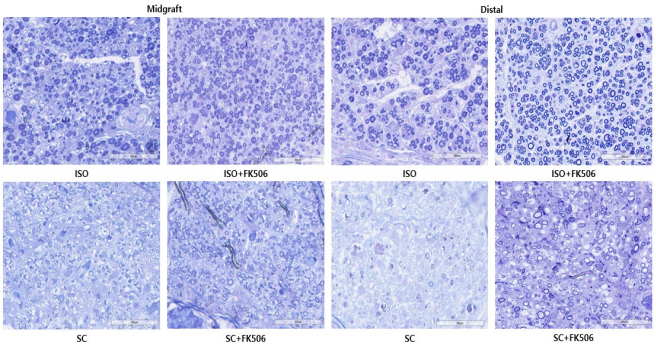

Fig. 4. Toluidine blue staining of the graft midpoint (left) and distal nerve (right) (x40).

EP-120

PRESS: 욕창 재건 수술 대상자 선정을 위한 새로운 위험도 계층화 알고리즘

(PRESS: A Novel Risk Stratification Algorithm for Surgical Candidate Selection in Pressure Sore Reconstruction)

가천대학교

손희준, 김유진*

Purpose: Pressure sore reconstruction is frequently performed in patients with multiple systemic comorbidities and limited functional support. Previous studies have mainly focused on ulcer characteristics or recurrence risk factors, while evaluation of patient-related risk factors remains limited. This study aimed to develop a clinical algorithm incorporating systemic comorbidities, anesthetic risk, cardiopulmonary function, neurologic status, and social support factors to guide surgical candidate selection.

Methods: A retrospective review of 87 patients who underwent surgical treatment for pressure sores over a five-year period was performed. Clinical variables including systemic comorbidities, anesthetic risk, functional status, caregiver support, and ulcer characteristics were analyzed. Based on the distribution of these variables and their association with postoperative outcomes, a scoring system the PRESS (Pressure Reconstruction Eligibility Stratification Score) was developed. Each variable was assigned a weighted score reflecting overall surgical risk. Using the cumulative PRESS scores derived from the patient cohort, a surgical candidate selection algorithm was subsequently constructed in a reverse manner.

Results: Reconstruction was primarily performed using V-Y advancement flaps (n=66) and perforator-based fasciocutaneous pedicled flaps (n=21). Unfavorable outcomes occurred in approximately 18% of patients, including recurrence, new pressure sores, reoperation, prolonged ICU care, and mortality. Higher PRESS scores were associated with increased postoperative complications.

Conclusion: Unlike previous approaches focusing mainly on wound-related factors, the PRESS score integrates systemic comorbidities, anesthetic risk, functional status, and social support factors to provide a more comprehensive framework for determining surgical eligibility. Further studies with larger cohorts are needed to validate the algorithm and refine the weighting of individual risk factors.

Outcome	n
favorable healing	71
Recurrence	7
New pressure sore	4
Reoperation	2
Prolonged ICU care	1
Mortality	2

Table 1. Postoperative outcomes

Domain	Variable	Criteria	Score
Systemic comorbidities	Major systemic disease	Diabetes mellitus, chronic kidney disease, severe malnutrition, active infection	1
	Multiple comorbidities	≥2 significant systemic diseases	2
Anesthetic, cardiopulmonary risk	ASA class	ASA I–II	0
		ASA III	1
		ASA IV or severe cardiopulmonary dysfunction	2
Neurologic, functional status	Mobility status	Ambulatory or partial mobility	0
		Paraplegia	1
		Quadriplegia or complete immobility	2
Social support	Caregiver support	Adequate caregiver support for repositioning and wound care	0
		Limited caregiver support	1
		No caregiver support	2
Ulcer severity	PUSH score	0–5	0
		6–10	1
		11–13	2
		>14	3

Table 2. Components of the PRESS (Pressure Reconstruction Eligibility Stratification Score), (Total PRESS score: 0–11)

Outcome	Mean PRESS score	Range
Favorable outcome	4.2	1 – 9
Unfavorable outcome	8.8	7 - 11

Table 3. Mean PRESS score according to outcome ; The mean PRESS score was significantly higher in patients with unfavorable outcomes compared with those with favorable outcomes.

PRESS score	Risk group	Surgical recommendation
0 – 5	Low risk	Reconstruction recommended
6 – 8	Moderate risk	Careful patient selection
≥ 9	High risk	Consider conservative management

Table 4. Risk stratification and recommended management according to the PRESS score.

EP-121

분말형 및 액상형 히알루로니다제의 알레르기 유발 가능성 비교 분석: 1,056명의 임상 사례를 통한 안전 투여 가이드라인 제시

(Comparative Analysis of Allergic Potential Between Powder-form and Liquid-form Hyaluronidase : A Clinical Study of 1,056 Patients and Implications for Safe Administration)

가톨릭대학교
성형외과학교실

심진솔, 최종윤, 김동연*, 최익균

Purpose: Hyaluronidase is essential for managing hyaluronic acid filler complications. This study evaluates the allergic potential of powder-form hyaluronidase (BM hyrunidase & H-lase) compared to liquid-form hyaluronidase (Hirax). Based on clinical data from three institutions, this research aims to provide a verified safety profiles and standardized screening protocols.

Methods: A retrospective analysis was conducted on clinical records and intradermal allergy skin test (AST) results from a total cohort of 1,056 patients. This study compared the powder-form group (n=958; BM hyaluronidase n=843, H-lase n=115) and the liquid-form group (n=98; Hirax). AST positivity rates were analyzed to evaluate formulation-dependent immunogenicity.

Results: The powder-form formulations demonstrated a significantly higher AST positivity rate (BM hyaluronidase 14.35%, H-lase 7.8%) compared to the liquid-form, which maintained a near-zero positivity rate in primary screening. However, cross-reactivity was observed where powder-positive patients occasionally reacted to conventional liquid forms.

Notably, recombinant human hyaluronidase (Tergase) showed high purity and minimal reactivity even in sensitized individuals. These disparities are attributed to protein denaturation and immunogenic stabilizers (e.g., lactose) inherent in the lyophilization of powder forms.

Conclusion: Liquid-form hyaluronidase provides a superior safety profile with a significantly lower immunogenic potential than powder-form alternatives. However, since hypersensitivity reactions remain a significant clinical risk even with improved formulations, relying solely on formulation choice is insufficient. Therefore, establishing a routine AST protocol is essential for early detection of hypersensitivity. Furthermore, implementing a standardized prophylaxis strategy, including pre-medication for high-risk cases, is a critical clinical mandate to prevent severe complications such as airway edema and ensure patient safety.

Variable		BM Hyrunidase (N=843)	H-lase (N=115)	Hirax (N=98)
Gender, n (%)	Female	783 (92.9%)	53 (46.1%)	43 (43.9%)
	Male	59 (7.0%)	62 (53.9%)	55 (56.1%)
Age (years)	Mean ± SD	34.4 ± 8.0	50.3 ± 18.5	45.4 ± 21.4
AST results, n (%)	Positive	121 (14.35%)	9 (7.8%)	0 (0.0%)
	Negative	722 (85.65%)	106 (92.2%)	98 (100.0%)

Table 1. Baseline characteristics and allergy skin test (AST) results across hyaluronidase formulations. Powder-form groups show higher AST positivity rates compared to the liquid-form group, which demonstrates no positive reactions.

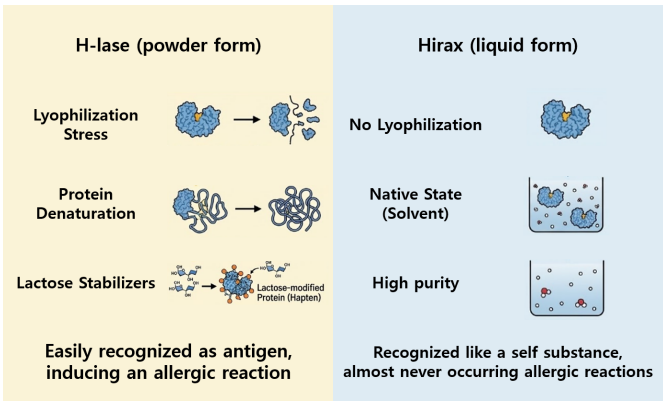

Fig 1. & 2. Baseline characteristics and allergy skin test (AST) results across hyaluronidase formulations. Powder-form groups show higher AST positivity rates compared to the liquid-form group, which demonstrates no positive reactions.

EP-122

젠타마이신 탑재 3D 프린팅 돼지 유래 ECM 지지체의 개발 및 체외 생체적합성 평가

(Development of a Gentamicin-Loaded 3D-Printed Porcine ECM Scaffold and Its In Vitro Biocompatibility)

아주대학교 의과대학 성형외과학교실

김민지, **김형기**, 홍승희, 한은희, 임수진, 이일재*

PURPOSE

- **Infected soft tissue defects** are a major challenge in reconstructive surgery.
- The ideal implantable material should support **both tissue regeneration and local infection control**.
- We developed a **gentamicin-loaded 3D-printed porcine ECM scaffold** and evaluated its in vitro biocompatibility.

METHODS

- Porcine type I collagen scaffolds fabricated by extrusion-based 3D bioprinting with chemical (EDC/NHS) or physical (dehydrothermal) crosslinking.
- Gentamicin sulfate loaded via controlled immersion in 2.0% solution.
- L929 mouse fibroblasts seeded; cell adhesion, activity, proliferation, and infiltration evaluated.
- Six experimental groups (Fig. 1):

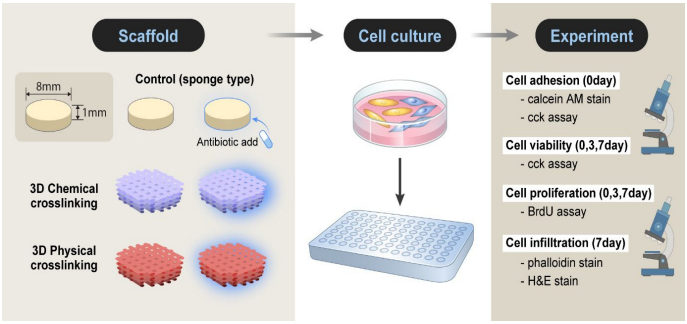

Fig. 1. Schematic of study design and six experimental groups.

RESULTS

Cell Adhesion

- Cell adhesion was **significantly enhanced in all 3D-printed groups** vs. control (C+G: 1.12×, 3D-Chem: 1.29×, 3D-Chem+G: 1.07×, 3D-Phys: 1.35×, 3D-Phys+G: **1.46×**).
- In physically crosslinked scaffolds, adhesion **remained stable** despite antibiotic presence.

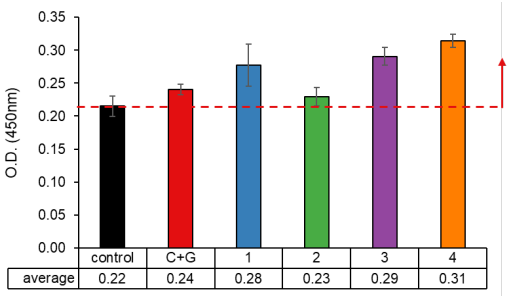

	control	C+G	1	2	3	4
average	0.22	0.24	0.28	0.23	0.29	0.31

Fig. 2. Cell adhesion (CCK-8 assay, OD 450 nm).

Cell Activity

- Cell viability was **higher in chemically crosslinked groups** than physically crosslinked ones (vs. C+G: 3D-Chem **1.02×**, 3D-Chem+G **1.07×**; 3D-Phys 0.89×, 3D-Phys+G 0.76×).
- Chemical crosslinking maintained **higher viability even with antibiotics**.

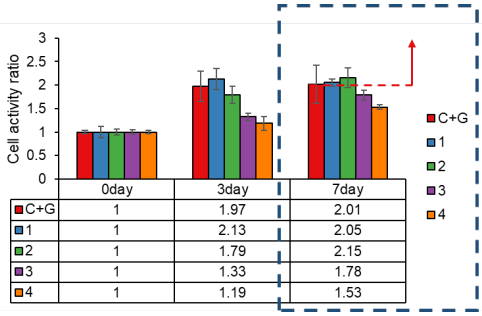

	0day	3day	7day
C+G	1	1.97	2.01
1	1	2.13	2.05
2	1	1.79	2.15
3	1	1.33	1.78
4	1	1.19	1.53

Fig. 3. Cell activity at days 0, 3, 7 (CCK-8 assay).

Cell Proliferation

- Both crosslinking methods showed **significantly enhanced proliferation** vs. C+G (3D-Chem: 1.38×, 3D-Chem+G: 1.51×, 3D-Phys: 1.29×, 3D-Phys+G: **1.84×**).
- Regardless of crosslinking method, **antibiotic-containing groups showed higher proliferation**.

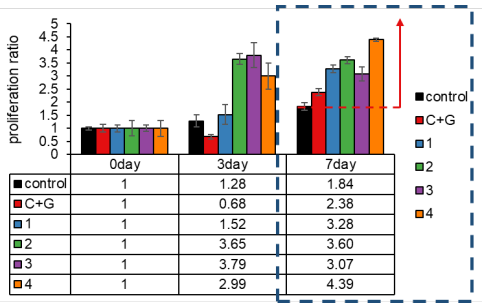

	0day	3day	7day
control	1	1.28	1.84
C+G	1	0.68	2.38
1	1	1.52	3.28
2	1	3.65	3.60
3	1	3.79	3.07
4	1	2.99	4.39

Fig. 4. Cell proliferation at days 0, 3, 7 (BrdU assay).

Cell Infiltration

- 3D-printed groups showed **more effective cell infiltration** than sponge control (Phalloidin up to **3.37×**; H&E up to **1.52×**).
- Cell distribution **varied with pore architecture** of the scaffold.

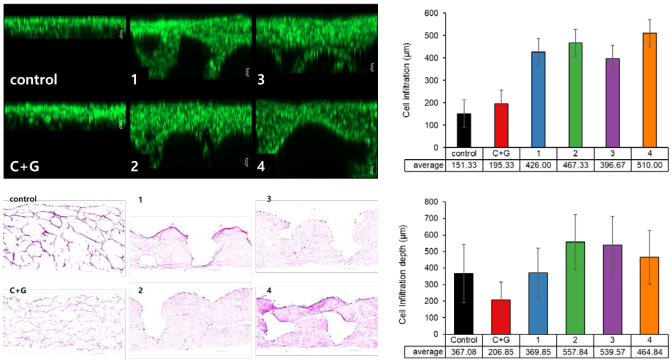

	control	C+G	1	2	3	4
average	151.33	195.33	426.00	467.33	396.67	510.00

	Control	C+G	1	2	3	4
average	367.08	206.85	369.85	557.84	539.57	464.84

Fig. 5. Cell infiltration at day 7: (A) phalloidin z-stack images, (B) infiltration depth by z-stack, (C) H&E histology, (D) infiltration depth by H&E (μm).

CONCLUSION

- The **gentamicin-loaded 3D-printed porcine ECM scaffold** exhibited excellent in vitro biocompatibility and maintained antibacterial activity.
- **Chemical crosslinking** was identified as the **optimal manufacturing method**.
- Findings support clinical potential as an **implantable biomaterial** for infected soft tissue defects.

EP-123

다발성 Pilomatricoma 환자에서의 임상적 특성 및 추가 병변 발생 분석

(Clinical Characteristics and Subsequent Lesion Development in Patients with Multiple Pilomatricomas)

부산대학교

이승훈, 이재우*

Purpose: Pilomatricoma is a benign tumor with a low reported recurrence rate following excision. However, some patients present with synchronous multiple lesions, and the clinical significance of this presentation remains unclear. This study aimed to evaluate whether synchronous pilomatricomas are associated with subsequent lesion development at different anatomical sites.

Methods: A retrospective review was conducted of **290 patients** who underwent surgical excision of **pilomatricoma** at a single institution. Clinical variables including age, sex, lesion multiplicity, and follow-up duration were collected. The primary outcome was the development of a subsequent pilomatricoma at a different anatomical site during follow-up. True local recurrence at the initial surgical site was separately assessed.

Results: Among 290 patients, 20 (6.9%) presented with synchronous multiple lesions, while 270 (93.1%) had solitary lesions. During follow-up, 8 patients (2.8%) developed additional pilomatricomas at new anatomical sites. **No true local recurrence was observed at the original excision sites. The rate of subsequent lesion development was higher in patients with synchronous lesions compared to those with solitary lesions (10% [2/20] vs. 2.2% [6/270]).** Although the overall number of events was low, synchronous presentation demonstrated a higher relative risk of subsequent lesion development.

Conclusion: Pilomatricoma demonstrates an excellent local control rate after complete excision, with no observed true local recurrences in this cohort. However, patients presenting with synchronous lesions may have an increased likelihood of developing additional pilomatricomas at different sites. **These findings suggest that synchronous presentation could represent a clinical marker of multifocal susceptibility.** Larger studies are warranted to further clarify this association.

Table 1. Baseline Characteristics of Patients with Pilomatricoma

Variable	Solitary (n=270)	Synchronous (n=20)
Age, years (mean ± SD)	7.6 ± 9.4	7.5 ± 6.5
Male, n (%)	120 (44.4%)	12 (60%)
Female, n (%)	150 (55.6%)	8 (40%)
Follow-up duration, months (mean ± SD)	8.8 ± 7.8	13.6 ± 11.8
Metachronous lesion, n (%)	**6 (2.2%)**	**2 (10%)**

Table 2. Clinical Characteristics of Patients with Subsequent Lesions (n=8)

Case	Age at presentation	Sex	Initial presentation	First lesion site	Time to new lesion (mo)	Additional lesion site	Total lesions
1	7	M	Solitary	HN	7	UE	2
2	6	F	Solitary	TR	10	HN	2
3	16	F	Solitary	HN	36	HN	2
4	5	F	Synchronous	HN; LE	55	HN	3
5	16	M	Solitary	HN	24	HN; HN	3
6	9	M	Synchronous	HN; UE	7	HN	3
7	6	F	Solitary	UE	14	HN	2
8	9	F	Solitary	UE	8	UE	2

Abbreviations: HN, head and neck; UE, upper extremity; LE, lower extremity; TR, trunk; mo, months.

EP-124

쥐의 만성 공동 상처 모델에서 항바이오필름 화학 작용제의 예비 평가

Preliminary Assessment of
Anti-Biofilm Chemical Agents
in a Rat Model of Chronic Cavity Wounds

가톨릭대학교
성형외과학교실

심진솔, 심형섭*

Purpose: Biofilm formation is a major factor contributing to delayed healing in complex chronic wounds, particularly in cavity-type lesions where conventional topical therapies have limited penetration. This study aimed to establish a bead-induced chronic cavity wound model in rats and to perform a pilot evaluation of several candidate chemical agents with potential anti-biofilm and antimicrobial activity.

Methods: A chronic cavity wound model was created by subcutaneous implantation of small beads in the dorsal region of rats to generate persistent cavities prone to biofilm formation. The wounds were inoculated with common wound pathogens and allowed to develop biofilm structures. Candidate agents including high-concentration ethanol, a poloxamer-based surfactant, synthetic antimicrobial peptides, and selected antimicrobial agents were applied individually to the cavity wounds. Antimicrobial efficacy was assessed using bacterial viability assays, colony-forming unit (CFU) quantification, and preliminary histological evaluation.

Results: All tested agents demonstrated varying levels of antimicrobial activity against biofilm-associated bacteria. High-concentration ethanol showed the most pronounced reduction in bacterial viability, suggesting strong biofilm dissolution capability.
Surfactant treatment demonstrated moderate reductions in bacterial viability, indicating potential biofilm destabilization effects.
Antimicrobial peptides and conventional antimicrobial agents showed variable bactericidal activity within the biofilm environment.

Conclusion: This pilot study demonstrates the feasibility of a bead-induced rat chronic cavity wound model for evaluating anti-biofilm therapies. The results suggest that several candidate chemical agents possess measurable antimicrobial or biofilm-disrupting effects and may serve as potential components of a chemical debridement strategy for complex chronic wounds.

Pilot Evaluation of Candidate Chemical Agents in a Rat Bead-Induced Chronic Cavity Wound Model

Agent category	Candidate material	Proposed mechanism	Anti-biofilm effect	Bacterial viability reduction	Remarks
Alcohol	High-concentration ethanol (70–100%)	Rapid protein denaturation and biofilm dissolution	Strong	Marked reduction	Rapid action but potential tissue toxicity
Surfactant	Poloxamer / propylbetaine-based surfactant	Disruption of biofilm matrix and improved penetration	Moderate	Moderate reduction	May facilitate penetration of other agents
Antimicrobial peptide	Synthetic AMP	Direct bactericidal activity and biofilm membrane disruption	Moderate	Variable reduction	Potential synergistic effect with antibiotics
Antibiotic	Rifampin / doxycycline / triclosan	Antibacterial activity against biofilm-associated bacteria	Variable	Variable reduction	Possible role in preventing biofilm reformation

Table 1. Summary of candidate chemical agents evaluated for anti-biofilm activity, including their proposed mechanisms, relative anti-biofilm effects, and impact on bacterial viability. High-concentration ethanol demonstrates strong biofilm disruption and marked bacterial reduction, whereas other agents show moderate to variable efficacy.

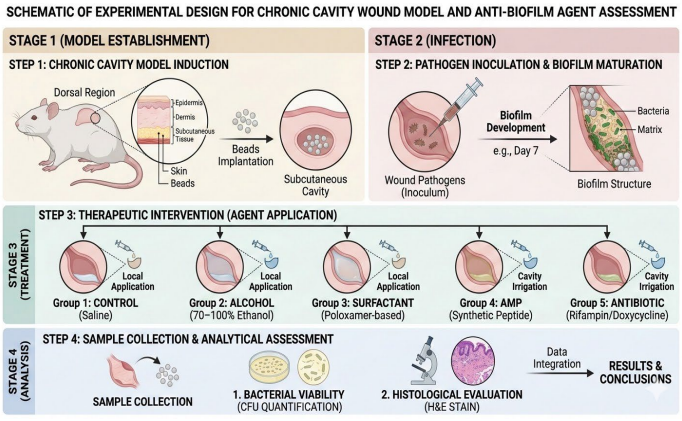

Fig 1. Schematic illustration of the experimental design for the bead-induced chronic cavity wound model and anti-biofilm agent assessment. The model establishment includes subcutaneous bead implantation to create a chronic cavity, followed by pathogen inoculation and biofilm maturation. Therapeutic interventions with candidate chemical agents are applied, and outcomes are evaluated through bacterial viability assays and histological analysis.

EP-125

근막절제술을 시행받은 구획증후군-유발 랫드에서 고압산소치료의 효용성

(Efficacy of Hyperbaric Oxygen Therapy Post-Fasciotomy for Acute Compartment Syndrome in a Rat Model)

계명대학교 동산병원 성형외과[1]
더프라우 병원 성형외과[2]

이원준[1], 조태희[1], 정운혁[1], 김준형[1], 손대구[1], 오상호[2], 최재훈[1*]

Purpose: Acute compartment syndrome (ACS) is a medical emergency where delayed fasciotomy often leads to permanent muscle damage. While hyperbaric oxygen therapy (HBOT) is an approved adjunctive treatment, its molecular mechanisms and efficacy when applied specifically during the reperfusion period post-fasciotomy are not fully elucidated.

Methods: Twelve Sprague-Dawley rats were divided into HBO and control groups. ACS was induced via hind limb cuff compression (120–140 mmHg) for 3 hours. Fasciotomy was performed 24 hours post-injury. The HBO group received 100% oxygen at 2.5 ATA for 2 hours daily for 5 consecutive days starting immediately post-fasciotomy. Muscle tissues were harvested 7 days after therapy for histological (Masson's trichrome) and molecular (qPCR, Western blot, IHC) analysis.

Results: The HBO group showed markedly reduced collagen deposition compared to the control group. Furthermore, the HBO group exhibited significantly lower numbers of Pax7-positive cells (p value = 0.026), reduced VEGF-A protein expression (p value = 0.01), and fewer CD31-positive capillaries (p value = 0.04). No significant differences were observed in muscle weight or CD68-positive macrophage counts.

Conclusion: HBOT applied during the reperfusion phase post-fasciotomy appears to accelerate the muscle regeneration process. The reduction in early-phase regeneration markers (Pax7, VEGF-A) and fibrosis suggests that HBOT facilitates a faster transition toward tissue maturation, potentially improving clinical outcomes in cases of delayed fasciotomy.

Fig. 1. Gross picture of Rat Model with Induced Acute Compartment Syndrome

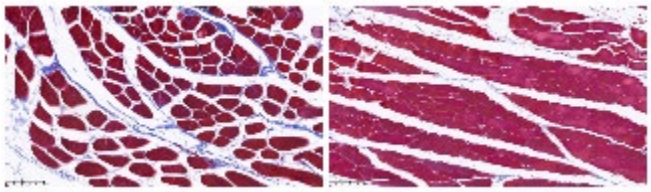

Fig. 2. Histopathological Analysis of Muscle Fibrosis. Masson's trichrome staining of the tibialis anterior (TA) muscle. (Left) The control group shows increased collagen deposition (blue staining).

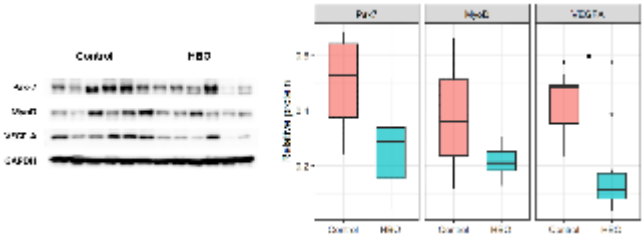

Fig. 3. Protein Expression of Myogenic and Angiogenic Markers : Western blot and quantitative analysis of Pax7, MyoD, and VEGF-A.

EP-126

만성 창상에서 MolecuLight 형광영상신호를 이용한 Pseudomonas aeruginosa 검출: 창상 배양검사와의 비교

(Cyan Fluorescence on MolecuLight Imaging for Detecting Pseudomonas aeruginosa in Chronic Wounds: Comparison with Wound-bed Culture)

순천향대학교

현동윤, 박은수, 신호성, 남승민*

Purpose: Pseudomonas aeruginosa (PA) is associated with delayed healing and infection progression in complex wounds, yet bedside localization of bacterial burden remains challenging. MolecuLight fluorescence imaging provides real-time visualization of bacteria-associated fluorescence, and cyan signals have been linked to *Pseudomonas* spp (Figure 1). We evaluated the clinical correlation and agreement between cyan fluorescence on MolecuLight imaging and wound-bed culture for PA.

Methods: We analyzed 19 patients who underwent MolecuLight fluorescence imaging and wound-bed culture at a single institution between February 2025 and January 2026. Cyan fluorescence was classified as positive ("clearly observed") or negative ("not clearly observed"). Culture identification of PA served as the reference standard. Sensitivity, specificity, positive predictive value (PPV), negative predictive value (NPV), accuracy, and Cohen's kappa (κ) were calculated. Representative wound-bed and cyan fluorescence images are provided (Figure 2)

Results: PA was isolated in 9/19 patients (47.4%). Cyan fluorescence was positive in 14/19 (73.7%); among these, 7 were culture-positive for PA. Cyan fluorescence was negative in 5/19 (26.3%), including 2 culture-positive cases. Diagnostic performance of cyan fluorescence for culture-confirmed PA was sensitivity 77.8% (7/9), specificity 30.0% (3/10), PPV 50.0% (7/14), NPV 60.0% (3/5), and accuracy 52.6% (10/19). Agreement between cyan fluorescence and culture was low (κ≈0.08) (Table 1).

Conclusion: In this small cohort, cyan fluorescence demonstrated relatively high sensitivity but low specificity and low agreement with wound-bed culture for PA. Cyan fluorescence may support targeted sampling and bedside decision-making (cleansing/debridement planning), but it should not replace culture, and negative cyan findings should not be used to rule out PA.

Figure 1. MolecuLight fluorescence imaging device. Representative photograph of the MolecuLight system used for point-of-care fluorescence imaging to visualize bacteria-associated signals in wounds.

Figure 2. Representative wound-bed photograph and corresponding MolecuLight fluorescence imaging. (A) White-light wound-bed photograph at the time of culture sampling. (B) Corresponding MolecuLight fluorescence image demonstrating cyan fluorescence signal within the wound field, suggesting possible *Pseudomonas* spp.–associated fluorescence.

	Culture PA (+)	Culture PA (-)	Total
Cyan fluorescence (+)	7	7	14
Cyan fluorescence (-)	2	3	5
Total	9	10	19

Table 1. Correlation between cyan fluorescence and wound-bed culture for Pseudomonas aeruginosa (n=19)

EP-127

초고령 환자에서 성형 및 재건 수술이 삶의 질에 미치는 영향에 대한 장기 연구

(Evaluating the Influence of Plastic and Reconstructive Surgery on Quality of Life in Super-Seniors, long term study)

한림대학교

안정훈, 김경민, 김기현, 우상석, 이준원, 김성환, 최재구, 서인석*

Purpose: Korea has already entered a super-aged society. Although advances in diagnostic and therapeutic medicine have extended life expectancy, it remains unclear whether these improvements have enhanced quality of life among the elderly. As interest in improving well-being among the super-elderly grows, the demand for aesthetic and reconstructive surgery has also increased. This study evaluated whether such surgical interventions improve quality of life in super-senior patients and compared with those reported approximately three decades ago.

Methods: We retrospectively reviewed the medical records of 133 super-senior patients (aged ≥85 years) who underwent surgery between January 2018 and January 2026. Demographic characteristics, disease distribution, types of plastic and reconstructive procedures, anesthetic methods, postoperative complications, and functional and aesthetic outcomes were analyzed. Findings were compared with those of a similar study conducted about 30 years earlier.

Results: The mean age was 87.47 ± 2.45 years, including 56 men and 77 women. Pressure sores were the most common diagnosis (34.58%), followed by skin and soft tissue defects (18.79%) and skin cancer (17.29%). Flap reconstruction was the most frequent procedure (35.38%), followed by debridement (27.81%) and skin graft (13.53%). Postoperative complications included partial flap necrosis, partial skin graft failure, and hematoma. Quality of life improved in 42.86% and remained unchanged in 26.37%, while deterioration decreased from 24% in the previous study to 10.99%.

Conclusion: Compared with three decades ago, super-senior surgical care4 shows broader patient inclusion, increased use of flap reconstruction, and reduced quality-of-life deterioration, likely reflecting advances in surgical techniques and perioperative management.

Table 1. Distribution of diagnosis patients, undergoing surgery

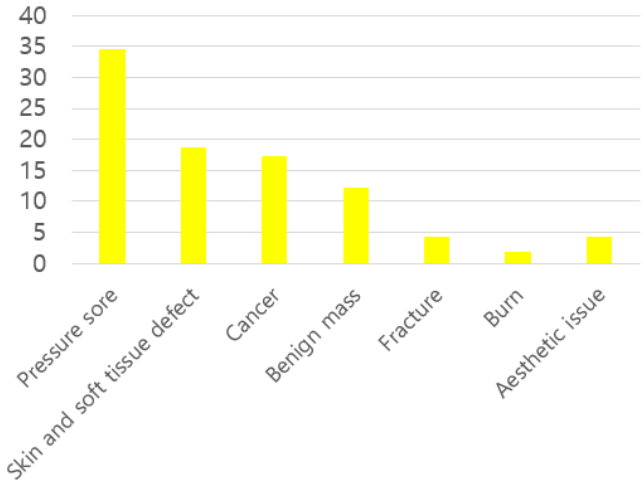

Table 2. Types and proportions of surgery patients underwent

Flap surgery	35.4%
Debridement	27.8%
Skin graft	13.5%
Benign mass excision	10.8%
ORIF and/or CR	7.5%
Aesthetic surgery	5%

EP-128

외과적 매듭 유형에 따른 매듭 안정성 비교: 평평한 매듭 형성의 영향

(Comparison of knot security in various surgical knots: Impact of flat tying)

동국대학교 일산병원
성형외과
추교빈, 김경현, 임수아, 조상헌, 어수락*

Purpose: Surgeon's knot which is based on the flat knot is a standard in surgical suture. However, unequal tension on both hands during flat knot formation may convert it into a sliding form, which we termed"sliding surgeon's knot". This study compares security of sliding surgeon's knot with other surgical knots.

Methods: Six knot configurations were tested using 4-0, 5-0, 6-0, and 7-0 nylons: sliding surgeon's knot (SU[S]), flat surgeon's knot (SU[F]), four-throw sliding knot (S[4]), four-throw flat knot (F[4]), three-throw sliding knot (S[3]) and three-throw flat knot (F[3]). Knots were tied under standardized conditions and tested with a universal testing machine (H5KT; Tinius Olsen Co). Primary outcomes were maximal force to failure (N) and elongation at yield (mm).

Results: SU[F] showed greater strength and elongation than SU[S] in 4-0, 5-0, and 7-0 nylons, particularly in 4-0 Nylon (20.60 N and 7.64 mm, $p<0.0001$). In 6-0 nylon, F[4] showed highest breaking strength of 4.92 N and SU[F] showed maximal elongation of 10.91 mm. Flat knots revealed better knot security than sliding knots in equal throw counts. In all suture materials, F[3] and F[4] showed no difference, whereas F[3] was superior to S[4]. Although F[4] performed better than SU[S] in 4-0 and 5-0 nylons, differences were not significant in 6-0 and 7-0 nylons.

Conclusion: Flat surgeon's knot surpassed other surgical knots in most suture materials. Maintaining flat configuration was more important than throw count for knot security. Therefore, proper formation of flat surgeon's knot with balanced tension on both hands is important to prevent unintended sliding and maintain knot security.

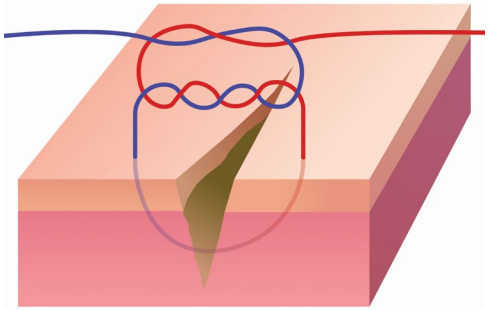

Fig. 1. The flat surgeon's knot with a double loop in the first throw followed by square knot.

Fig. 2. The sliding surgeon's knot in which imbalance of tension between the two hands converts both the first double loop and the second square knot into a sliding form.

Fig. 3. Clinical photograph of three-throw flat surgeon's knot.

Fig. 4. Clinical photograph of three-throw sliding surgeon's knot.

EP-129

SGLT2 억제제 중단 시점이 수술 후 당뇨병성 케토산증 및 상처 감염에 미치는 영향: 수술 전 3일 중단 지침 준수 여부에 따른 비교 연구

(Impact of SGLT2 Inhibitor Discontinuation Timing on Postoperative Diabetic Ketoacidosis and Wound Infection: A Comparative Study of the Three-Day Washout Protocol)

동국대학교 의과대학 성형외과학교실[1]

윤우혁[1], **이준호**[1*]

Purpose: Current guidelines recommend discontinuing SGLT2 inhibitors (SGLT2i) three days before general anesthesia to prevent euglycemic diabetic ketoacidosis (DKA). However, compliance is often hindered by emergency surgeries, fixed-dose combinations, or patient unawareness. This study evaluates whether failing to meet this 3-day discontinuation window impacts postoperative DKA and wound infection rates.

Methods: A retrospective review was conducted on diabetic patients treated with SGLT2i undergoing surgery. Patients were categorized into the Discontinued Group (stopped ≥3 days prior) and the Continued Group (stopped <3 days or continued). Postoperative DKA incidence, glucose levels, and wound infection (SSI) rates were compared between the two groups.

Results: Among the study population, there were no statistically significant differences in the incidence of postoperative DKA between the Discontinued and Continued groups ($P > 0.05$). Similarly, the rate of wound infections showed no significant correlation with the timing of SGLT2i cessation. Even in cases of unintentional continuation or emergency surgery, clinical outcomes remained stable without an increase in major metabolic complications.

Conclusion: Failing to discontinue SGLT2i three days before surgery did not significantly increase the risk of postoperative DKA or wound infection. While preoperative washout is ideal, these findings suggest that unintentional continuation may not necessitate surgery cancellation, provided vigilant perioperative monitoring is maintained.

Table. 1. A total of 357 diabetic patients (55.5% male; mean age 63.8 ± 11.2 years) were included, with 21.3% undergoing emergency surgery.

Variable	Total (n = 357)
Sex, n (%)	
Male	**198 (55.5%)**
Female	**159 (44.5%)**
Age, years	
Mean ± SD	**63.8 ± 11.2**
< 50 years, n (%)	**62 (17.4%)**
50–64 years, n (%)	**134 (37.5%)**
≥ 65 years, n (%)	**161 (45.1%)**
Type of diabetes	
Type 2 diabetes, n (%)	**349 (97.8%)**
Duration of diabetes, years	**9.6 ± 6.4**
Surgery type	
Elective surgery, n (%)	**281 (78.7%)**
Emergency surgery, n (%)	**76 (21.3%)**

Table. 2. No increase in postoperative DKA or SSI despite failure to meet the 3-day washout period

Outcome	Discontinued ≥3 days	Continued <3 days	P value
Postoperative DKA, %	0.8	1.0	>0.05
Surgical site infection, %	4	4.3	>0.05
Mean postoperative glucose (mg/dL)	162	165	NS

EP-130

혈관주위 Hyaluronidase의 혈관투과를 통한 혈관 내 Hyaluronic Acid의 분해기전

(Transvascular Transport of Perivascualr Hyaluronidase Enables Intraluminal Hyaluronic Acid Degradation)

연세대학교
홍동현, 최영호, 강은혜,
홍종원, 현영민, 양은정*

Purpose: Perivascular hyaluronidase injection is widely used to treat hyaluronic acid (HA) filler–associated vascular occlusion, yet the mechanism by which the enzyme reaches intravascular HA remains unclear. This study aims to provide direct *in vivo* evidence of transvascular delivery and intraluminal degradation of hyaluronic acid (HA) following perivascular hyaluronidase injection.

Methods: A murine hind limb arterial occlusion model was developed using fluorescein-labeled HA. Two-photon intravital microscopy was employed to visualize intravascular HA and Alexa Fluor 594-conjugated hyaluronidase. Hyaluronidase was administered perivascularly at low (1mg/mL) and high (50mg/mL) concentrations. Mean fluorescence intensity (MFI) within the lumen was quantified to evaluate penetration kinetics and the cumulative effects of repeated dosing.

Results: Control observations confirmed stable intravascular HA fluorescence, validating the model. Upon perivascular injection, labeled hyaluronidase accumulated at the vessel wall before traversing into the lumen. High-dose hyaluronidase induced a significant, time-dependent reduction in intraluminal HA fluorescence, whereas low-dose administration showed negligible effects. Repeated injections resulted in a progressive, cumulative decrease in the HA signal, confirming dose-dependent degradation.

Conclusion: This study provide direct intravital imaging evidence that perivascularly administered hyaluronidase can across the arterial wall to degrade intraluminal HA *in vivo*. These findings provide mechanical support for high-dose and repeated administration in the management of HA filler-associated vascular complications and highlight the potential for transvascular delivery of therapeutic macromolecules in vascular pathology.

Figure 1.

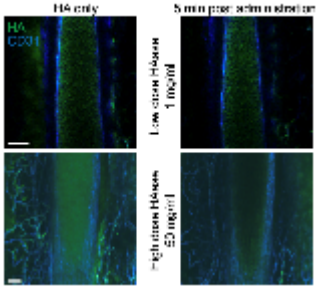

Figure 2.

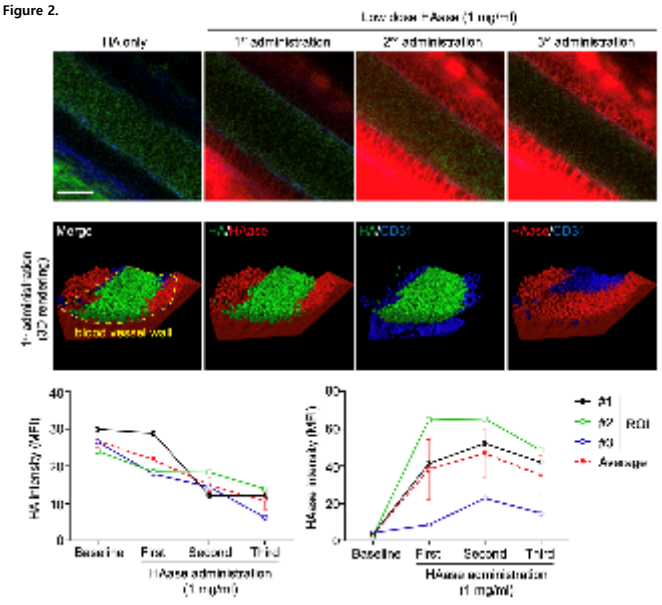

Fig 1. Representative intravital images showing intravascular HA signal in the HA-only group, low-dose HYAL group (1 mg/mL), and high-dose HYAL group (50 mg/mL) at 5 minutes post injection. Quantification of relative HA expression demonstrates significant reduction only in the high-dose group. Data are normalized to HA-only control.

Fig2. Effect of repeated perivascular HYAL injections on intravascular HA degradation. Sequential injections (first, second, and third) resulted in progressive reduction of HA MFI. Quantification demonstrates cumulative decrease in HA signal with repeated dosing. Corresponding HYAL MFI within the vascular lumen increased following each injection, supporting enhanced intraluminal enzyme presence.

Data are presented as mean ± SD. Statistical comparisons were performed using repeated-measures ANOVA with appropriate post hoc testing. Scale bar, 50 μm.
Abbreviations: HA, hyaluronic acid; HYAL, hyaluronidase; MFI, mean fluorescence intensity

EP-131

중증 당뇨발 환자에서 HbA1c가 임상 경과 및 사지 예후를 예측하는 지표로서의 유용성

(HbA1c as a Predictor of Clinical Course and Limb Outcomes in Severe Diabetic Foot)

가톨릭대학교
김승윤, 심형섭*

Purpose: Severe diabetic foot infections frequently require prolonged treatment and may ultimately result in major amputation. While poor glycemic control is known to negatively affect wound healing and infection control, the clinical significance of glycated hemoglobin (HbA1c) as a predictor of disease progression remains underrecognized. This study aimed to evaluate the relationship between HbA1c level at presentation and the clinical course of patients with severe diabetic foot.

Methods: A retrospective analysis was performed on patients presenting with severe diabetic foot requiring surgical management at a tertiary referral center. HbA1c levels at presentation were reviewed and patients were stratified into three groups: ≤8.5%, 8.5–10%, and ≥10%. Clinical outcomes including infection control, number of surgical debridements, time to wound stabilization, and amputation rate were analyzed.

Results: Patients with HbA1c ≤8.5% generally demonstrated more favorable clinical courses with relatively faster infection control and fewer surgical interventions. Those with HbA1c between 8.5% and 10% showed intermediate outcomes. In contrast, patients with HbA1c ≥10% experienced significantly prolonged infection control periods, more frequent surgical debridement, and higher rates of progression to major amputation.

Table 1. Clinical outcomes based on HbA1c level

HbA1c level (%)	Outcome 1 (Healed without surgery)	Outcome 2 (Minor amputation)	Outcome 3 (Major amputation)	total
<8.5	11	4	1	16
8.5-10.5	7	6	3	16
>10.5	2	9	4	15
Total	20	19	8	47

Conclusion: HbA1c at presentation may serve as a practical predictor of clinical trajectory in severe diabetic foot. Patients with HbA1c levels above 10% appear particularly vulnerable to prolonged infection and limb loss. Early identification of high-risk patients may facilitate timely multidisciplinary intervention and more aggressive management strategies aimed at limb preservation.

EP-132

성형외과 주도 고압산소치료: 재건 치료에서의 임상 경험과 확장된 적용

(Plastic Surgery–Driven Hyperbaric Oxygen Therapy: Clinical Experience and Expanded Indications in Reconstruction)

한림대학교

김기현, 안정훈, 김경민, 우상석, 이준원*, 김성환, 최재구, 서인석

Purpose: Hyperbaric oxygen therapy (HBOT) increases tissue oxygen tension and is traditionally used for conditions such as sudden sensorineural hearing loss and chronic wounds. However, its role in plastic and reconstructive surgery remains unclear. We evaluated the feasibility and safety of a plastic surgery–directed HBOT service.

Methods: We retrospectively reviewed 41 patients treated with HBOT under plastic surgery supervision. Indications included sudden sensorineural hearing loss (n=14), compromised skin grafts (n=9), local flap compromise (n=8), diabetic foot wounds (n=8), and peripheral tip necrosis (n=2). HBOT was administered with 100% oxygen at 2.0–2.5 atmospheres absolute for 60–90 minutes per session, once or twice daily, until clinical improvement. Patient characteristics, indications, and treatment protocol are summarized in (Table 1).

Results: All skin grafts achieved successful take without complete loss. No total flap necrosis occurred, and early ischemic or congestive changes improved without major revision. Diabetic foot wounds showed enhanced granulation, enabling secondary closure or reconstruction. Peripheral tip necrosis progression was limited. All patients with hearing loss completed treatment. No significant HBOT-related complications were observed.

Conclusion: Plastic surgery–directed HBOT enabled safe and effective application across reconstructive conditions involving tissue hypoxia. Surgeon-led assessment allowed appropriate patient selection and integration of HBOT into reconstructive care.

Category	Variable	Value
Patients (n=41)	Indications	SSNHL (14), Skin graft (9), Flap compromise (8), Diabetic foot (8), Tip necrosis (2)
HBOT Protocol	Settings	100% O_2, 2.0–2.5 ATA, 60–90 min/session, 1–2 sessions/day
Outcomes	Skin graft	100% take, no complete loss
	Flap	No total necrosis; improved ischemia/congestion
	Diabetic foot	Enhanced granulation, enabled closure
	Tip necrosis	Progression limited
	SSNHL	Completed without interruption
Safety	Complications	No HBOT-related complications

Table 1. Summary of Patients, HBOT Protocol, and Outcomes

EP-133

미세수술에서 혈관경 식별 및 모니터링을 위한 휴대용 초음파의 임상적 핵심 요점

(Clinical Pearls of Portable Ultrasound for Pedicle Identification and Monitoring in Microsurgery)

순천향대학교 [1]

김성운,최창용,신호성,정형화*

Purpose: Intraoperative and postoperative vascular assessment is critical in microsurgical reconstruction. High-frequency ultrasound provides real-time image with high portability. This study highlights the clinical utility of portable ultrasound for intraoperative guidance and postoperative monitoring in microsurgery.

Methods: Portable high-frequency ultrasound was utilized during microsurgical breast reconstruction procedures and postoperative follow-up. Intraoperatively, ultrasound was applied during flap elevation and secondary flap debulking to identify and trace the vascular pedicle. Postoperatively, ultrasound was used for monitoring.

Results: Intraoperative ultrasound enabled precise localization and continuous visualization of the vascular pedicle during flap debulking, minimizing the risk of inadvertent pedicle injury. In DIEP flap procedures, ultrasound facilitated rapid identification of the deep inferior epigastric pedicle which is unclear due to scarring. Postoperatively, ultrasound provided reliable bedside evaluation of pedicle patency where direct clinical monitoring can be limited due to preserved skin envelopes and buried flaps.

Conclusion: Extremely portable, handheld ultrasound enables immediate, real-time pedicle visualization across intraoperative and postoperative settings. Its bedside accessibility and dynamic imaging capability enhance surgical precision during flap debulking pedicle identification, while providing reliable monitoring supporting safer decision-making without interrupting workflow.

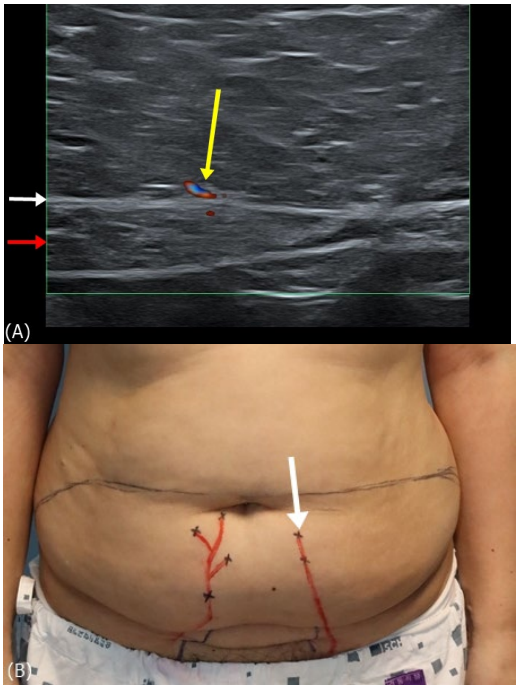

Fig 1. **(A)** Preoperative ultrasound identified the presumed vascular pedicle within the flap. Arrow; *Yellow*: Deep inferior epigastric artery perforator, *Red*: Rectus abdominis muscle, *White*: Rectus sheath
(B) The corresponding surface point was marked preoperatively(white arrow) to guide surgical planning for secondary debulking.

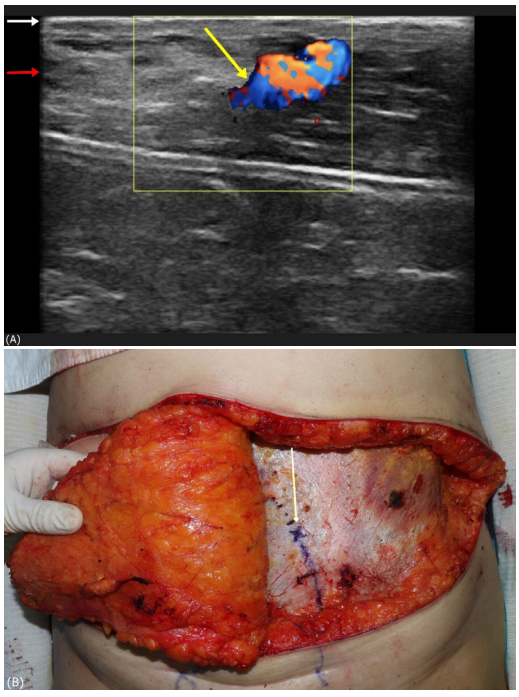

Fig 2. **(A)** Portable color Doppler ultrasound visualized the vascular pedicle beneath the flap tissue. Arrow; *Yellow*: Deep inferior epigastric artery perforator intramuscular course, *Red*: Rectus abdominis muscle, *White*: Rectus sheath
(B) Gross intraoperative view showing the elevated flap and marked presumed pedicle course. Reduced overlying tissue thickness during debulking improved ultrasound visualization, allowing safer tissue reduction and helping prevent pedicle injury.

EP-134

지속적 국소 산소치료(Continuous Topical Oxygen, NATROX® O_2)를 이용한 절단 후 만성 족저 창상 치유 보조 : 증례보고

(Supporting Healing in a Chronic Post-amputation Plantar Wound Using Continuous Topical Oxygen (NATROX® O_2): A Case Report)

순천향대학교

현동윤, 남승민, 차한규, 박은수*

Purpose: Chronic wounds after diabetic foot surgery may persist because of local hypoxia, microvascular dysfunction, infection risk, and pressure-related factors. Continuous topical oxygen therapy (cTOT) provides low-flow oxygen under an occlusive dressing and may support bacterial killing, angiogenesis, fibroblast activity, and collagen synthesis (Figure 1).

Case presentation: A 68-year-old man underwent transmetatarsal amputation for an infected right diabetic foot with necrosis and suspected osteomyelitis, followed by fillet coverage. Despite standard wound care, a chronic plantar stump wound remained. The target lesion measured 2.0 × 1.8 cm (3.6 cm^2) on the plantar aspect (Figure 2A).

Intervention: NATROX® O_2 cTOT was used as an adjunct for approximately 10 weeks together with standard care as clinically indicated (debridement, moisture balance, infection control, and off-loading). The oxygen delivery device was placed directly on the wound bed and sealed with a secondary dressing to maintain continuous oxygen delivery. A small delayed-healing area along the incision line received topical oxygen only as supportive care; outcome assessment focused on the plantar wound.

Results: The wound demonstrated reduced exudate and progressive granulation and epithelialization during treatment. Representative images are shown mid-course and at completion (Figure 1B–C). No clinically significant local adverse events or worsening infection occurred.

Conclusion: Adjunctive NATROX® O_2 cTOT combined with standard care was associated with favorable healing progression in a chronic plantar stump wound after transmetatarsal amputation. Continuous topical oxygenation may be a practical adjunct for hard-to-heal diabetic foot–related surgical wounds.

Figure 1. NATROX® O_2 continuous topical oxygen therapy (cTOT) system.
A portable oxygen generator delivers low-flow oxygen via tubing to a single-use oxygen delivery system (ODS) placed on the wound bed under a sealed dressing, enabling continuous topical oxygenation.

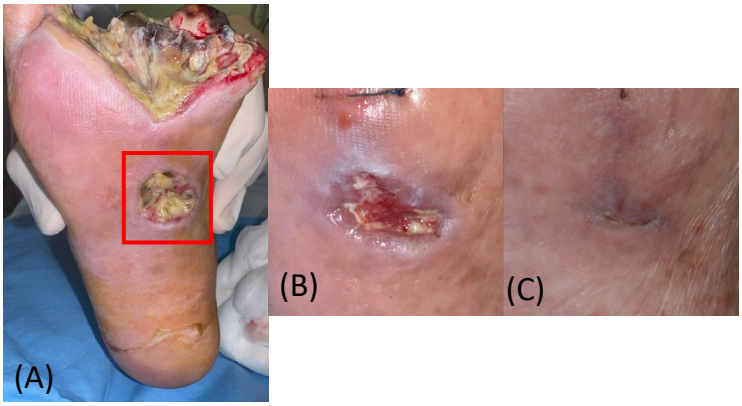

Figure 2. Serial photographs of the chronic plantar stump wound. **(A)** Baseline at initiation of therapy. **(B)** Mid-course (~Week 5): decreased exudate with granulation/epithelialization progression. **(C)** End of treatment (~Week 12): clinically meaningful improvement.

EP-135

적외선 카메라를 활용한 당뇨발의 허혈 모니터링 연구

(Revolutionizing Diabetic Foot Monitoring : A Portable Infrared Camera Study on Blood Circulation)

순천향대학교[1]
울산대학교[2]

강영훈[1], **서현석**[2], **박창식**[2], **홍준표**[2], **Rocio Perez Heredia**[2], **정형화***[1]

Purpose: This study aimed to evaluate whether temperature recovery measured by a portable infrared camera after a cooling stress test correlates with skin perfusion pressure in diabetic foot patients. We also assessed its potential usefulness as a simple screening tool for ischemia.

Methods : A prospective observational study was performed in diabetic foot patients who underwent skin perfusion pressure measurement. Thermographic images were obtained using a smartphone-based infrared camera before cooling, immediately after cooling, and at 30, 60, and 90 seconds after a standardized cooling stress test. Correlation, linear regression, and ROC analyses were performed to assess the relationship between recovery temperature and perfusion status.

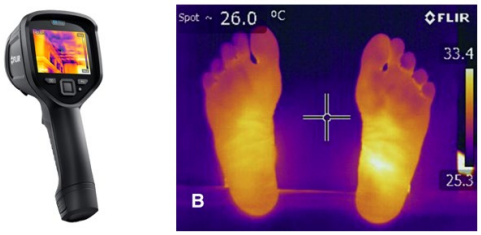

Fig 1. Portable infrared camera and representative thermographic image illustrating color-coded skin

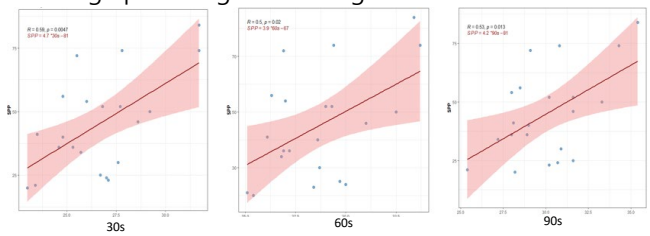

Fig 2. Scatter plots of recovery-phase temperature versus skin perfusion pressure at 30, 60, and 90 seconds after cooling. All three time points showed significant positive correlations, strongest at 30 seconds.

Results: A total of 21 patients were included, with 9 limbs classified as ischemic and 12 as non-ischemic based on skin perfusion pressure. Recovery-phase temperatures at 30, 60, and 90 seconds showed significant positive correlations with skin perfusion pressure ($r = 0.5924$, $p = 0.0047$; $r = 0.5026$, $p = 0.0202$; $r = 0.5311$, $p = 0.0132$, respectively), with the strongest correlation observed at 30 seconds. In univariable linear regression, recovery-phase temperatures at all three time points were significantly associated with skin perfusion pressure. ROC analysis showed modest diagnostic performance, with the highest AUC at 30 seconds (0.713).

Conclusion: Portable infrared thermography after a cooling stress test may provide a simple and accessible adjunctive method for perfusion assessment in diabetic foot patients. Early recovery temperature, particularly at 30 seconds, showed the strongest relationship with skin perfusion pressure and demonstrated the best performance for ischemia discrimination. Although not a replacement for conventional vascular studies, this method may be useful as a rapid screening tool in clinical settings.

	β(95%CI)	p-value
baseline	3.40(-0.509~7.308)	0.0845
imm	2.54(-1.13~6.21)	0.164
30s	4.74(1.646~7.845)	**0.005**
60s	3.9(0.678~7.113)	**0.02**
90s	4.20(0.982~7.415)	**0.013**

Table 1. Univariable linear regression showing significant associations between recovery-phase temperatures (30–90 s) and SPP, while baseline and immediate values were not significant.

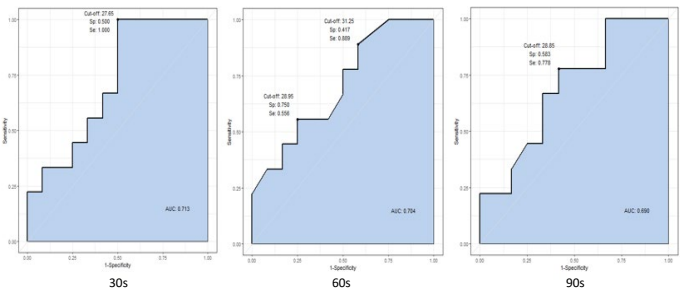

Fig 3. ROC curves for recovery-phase temperatures at 30, 60, and 90 seconds in detecting ischemia. All time points showed modest diagnostic performance (AUC 0.69–0.71), exceeding random classification.

EP-136

인간 창상 치유를 재현하기 위한 3D 프린팅 스플린트 기반 창상 수축 억제 랫 전 층 피부결손 모델의 개발 및 검증

(Development and Validation of a 3D-Printed Splint-Based Full-Thickness Rat Wound Model that Eliminates Contraction and Recapitulates Human Re-epithelialization-Driven Healing)

울산대학교병원 성형외과

전동준, 하원*

Purpose: 설치류를 이용한 소동물 창상 모델(Wound model)은 wound healing연구의 표준 전임상 모델이지만, 치유의 대부분이 수축 (wound contraction)에 의해 이루어져 인간의 재상피화 중심 치유와 차이가 있다. 본 연구는 창상 수축을 완전히 억제하여 인간 피부 치유를 재현할 수 있는 3D 프린팅 스플린트 기반 창상 모델을 개발하고 창상 모델 로서의 유용성을 평가하고자 하였다.

Methods : 2x2cm 크기의 창과, 외측 rim이 피하로 삽입되어 고정되는 구조의 TPU 기반 3D 프린팅 스플린트를 설계, 제작하였다. 각 변에 4개의 고정홀을 배치하여 총 4개의 봉합으로도 고정이 가능하도록 제작하였다. 랫 전 층 피부결손 모델은 기존의 모델과 다르게 skin island를 중심에 두어 재상피화가 방사형으로 퍼지도록 설계하였으며, 기존 스플린트를 이용한 모델과 비교하여 창상 수축 정도, 스플린트 탈락률을 평가하였다.

Results : 기존 스플린트의 경우 wound healing이 90%이상의 wound contraction으로 이루어졌으며 개발된 스플린트는 창상 수축을 완전히 억제하여 wound contraction 0%를 보였으며 100% 재상피화 중심의 치유 양상을 나타냈다. 피하 고정 구조로 인해 스플린트 탈락은 관찰되지 않았다.

Conclusion : 본 모델은 인간 피부 치유와 유사한 재상피화 기반 창상 치유를 안정적으로 재현할 수 있는 재현성 높은 전임상 플랫폼이다. 피부이식, 조직공학 및 재생치료 연구에서 재건 결과 평가의 정확도를 향상시킬 수 있는 기초재건 연구 모델로 활용이 가능할 것으로 사료된다.

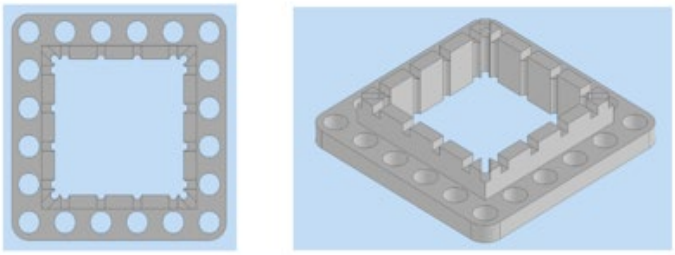

Fig. 1. TPU-based 3D-printed splint design.

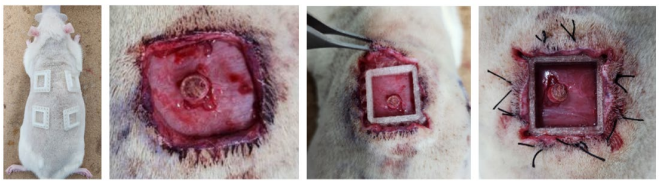

Fig. 2. Surgical procedure of the splinted wound model

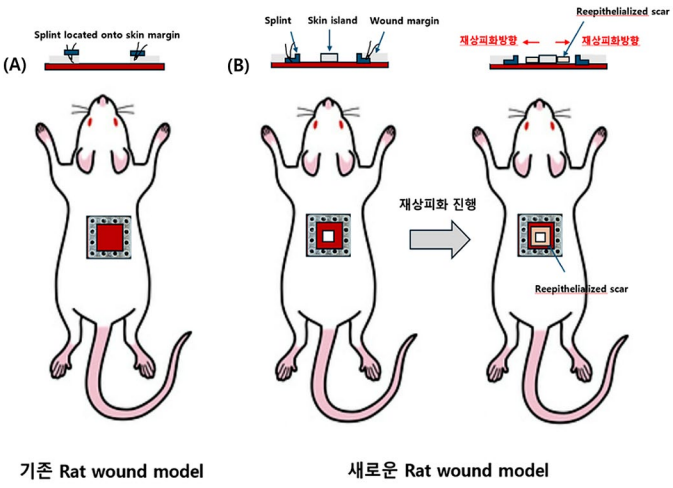

Fig. 3. Comparison of healing mechanisms between models.
(A) Conventional rat wound model : contraction-dominant closure.
(B) TPU-splinted wound model : restrained contraction and re-epithelialization-dominant healing.

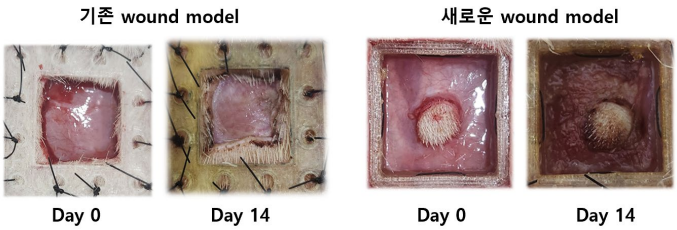

Fig. 4. Representative gross photographs at Day 0, 14.
The conventional model shows marked contraction by Day 14, whereas the splinted model demonstrates complete suppression of wound contraction with re-epithelialization-driven closure.

EP-137

단시간 반복 동결-해동 공정을 이용한 혈소판 추출물(HPL)의 신속 제조 및 성장인자 최적화

(Rapid Preparation and Growth Factor Optimization of Human Platelet Lysate (HPL) Using a Short-Cycle Repeated Freeze–Thaw Protocol)

울산대학교병원 성형외과

<u>전동준</u>, 하원*

Purpose : 혈소판 추출물(Human platelet Lysate, HPL)은 재생치료에 활용가능한 성장인자 풍부 생리활성 물질이지만 기존 동결-해동 공정은 제조시간이 길어 환자로부터 혈소판 농축액 채취 후 적용하기까지 하루 이상 걸리게 되는 단점이 있다. 본 연구는 혈소판 추출물의 빠른 임상적용이 가능하도록 단시간 내 성장인자 방출을 최대화하는 최적의 동결-해동 조건을 규명하고자 하였다.

Methods : 혈소판 농축액을 5 mL씩 소분 후 –80°C에서 1시간, 2시간, 4시간, overnight(12시간) 동결하고 1·3·5·7회 해동을 반복하였다. 이후 PDGF-BB, VEGF, EGF 농도를 ELISA로 측정하여 조건 별 성장인자 방출량을 비교하였다.

Results : 2시간 동결군은 4시간 및 overnight 동결군과 유의한 차이가 없었으며 1시간 동결군보다 높은 성장인자 농도를 보였다. 동결-해동 3회 이후 농도 증가가 포화되어 최적 조건은 2시간 동결-해동 3회였다. 해당 조건은 기존 overnight 방식(36시간) 대비 총 제조시간을 약 6시간으로 단축하면서 동등 이상의 성장인자 농도를 유지하였다.

Conclusion : 단시간 반복 동결-해동 기반 HPL 제조 공정은 당일 제조·적용이 가능한 임상 친화적 생산 전략으로, 재생치료에서 활용도를 높일 수 있을 것으로 기대된다.

Fig. 1. Preparation method of Human platelet lysate.

PDGF-BB

	1시간	2시간	4시간	8시간
1회	11.6 / 10.5 / 10.7	15.3 / 15.7 / 14.9	15.6 / 14.6 / 14.9	15.9 / 15.5 / 15.6
3회	19.5 / 17.3 / 17.5	25.3 / 24.3 / 26.1	25.4 / 24.5 / 25.1	25.4 / 25.1 / 25.2
5회	21.5 / 20.1 / 21.1	25.8 / 25.1 / 26.4	26.1 / 27.1 / 26.9	26.5 / 25.7 / 25.5
7회	23.3 / 22.1 / 22.5	25.9 / 25.5 / 26.5	26.5 / 27.1 / 26.9	26.6 / 26.1 / 26.1

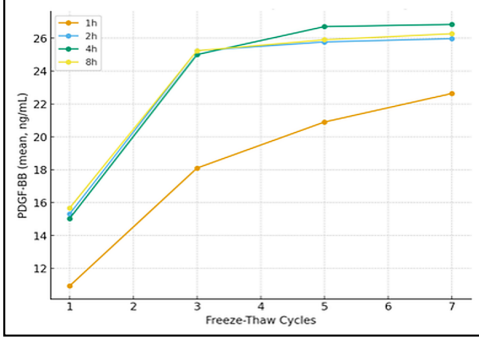

VEGF

	1시간	2시간	4시간	8시간
1회	3.7 / 3.1 / 3.2	5.1 / 5.5 / 5.4	5.3 / 5.4 / 5.1	5.3 / 5.6 / 5.1
3회	6.4 / 5.9 / 6.1	9.4 / 9.1 / 8.6	8.8 / 8.4 / 7.6	9.6 / 9.5 / 9.1
5회	8.5 / 8.1 / 8.2	9.5 / 9.2 / 8.8	9.0 / 9.1 / 9.2	9.6 / 9.5 / 9.2
7회	8.9 / 9.1 / 9.0	9.5 / 9.4 / 9.1	9.1 / 9.5 / 9.3	9.7 / 9.8 / 9.2

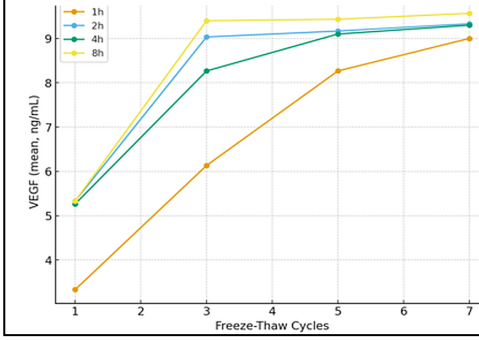

EGF

	1시간	2시간	4시간	8시간
1회	2.3 / 3.1 / 2.4	4.9 / 4.3 / 4.4	5.1 / 4.1 / 4.2	5.2 / 5.6 / 5.5
3회	4.1 / 4.2 / 4.2	8.9 / 9.0 / 9.1	9.1 / 8.8 / 8.1	9.2 / 9.1 / 8.9
5회	6.7 / 6.4 / 6.9	9.1 / 9.0 / 9.1	9.2 / 8.9 / 8.3	9.2 / 9.1 / 9.1
7회	7.1 / 6.7 / 7.0	9.2 / 9.3 / 9.5	9.2 / 8.9 / 8.8	9.3 / 9.3 / 9.1

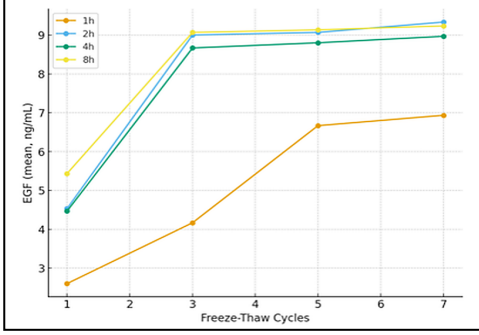

Fig. 2. ELISA-measured PDGF-BB, VEGF, and EGF levels in HPL by freezing duration and freeze-thaw cycle number.

EP-138

폐암 환자에서 피부 전이와 유사한 양상을 보인 동맥류성 피부섬유종 진단의 어려움: 증례 보고

(Diagnostic challenge of aneurysmal dermatofibroma mimicking cutaneous metastasis in a patient with lung cancer: A case report)

가톨릭대학교 성형외과학교실

정소윤, 최장연*

Purpose: To differentiate a suspected cutaneous metastasis from a benign mimic, a wide local excision with 5-mm safety margins was performed. The excised tissue underwent histopathological evaluation using hematoxylin and eosin (H&E) staining. Furthermore, rigorous immunohistochemical staining—specifically for CD34, human herpesvirus-8 (HHV-8), and Ki-67—was conducted to thoroughly rule out other primary malignancies and confirm the exact cellular pathology.

Methods: A 71-year-old male with a history of advanced non-small cell lung cancer (stage IVB squamous cell carcinoma) presented with a two-centimeter blackish nodule on his right chest wall. A positron emission tomography-CT (PET-CT) scan demonstrated hypermetabolic activity in the lesion with a maximum standardized uptake volume of 6.9. This high fluorodeoxyglucose uptake raised a strong clinical suspicion of cutaneous metastasis.

Results: Histopathological examination unexpectedly revealed spindle-like cells arranged in a storiform pattern alongside multiple blood-filled pseudovascular spaces. Immunohistochemistry showed that the spindle cells were negative for both CD34 and HHV-8, while the Ki-67 proliferation index was remarkably low at 5%.
These findings definitively confirmed a diagnosis of aneurysmal dermatofibroma (ADF).
The patient remained stable with no evidence of recurrence during a 1-year follow-up.

Conclusion:
ADF is a rare benign neoplasm that can clinically and radiologically mimic malignant tumors, leading to false-positive PET-CT interpretations. Comprehensive histopathological and immunohistochemical evaluations are critical for ambiguous cutaneous lesions to prevent cancer upstaging and avoid inappropriate alterations to treatment plans.

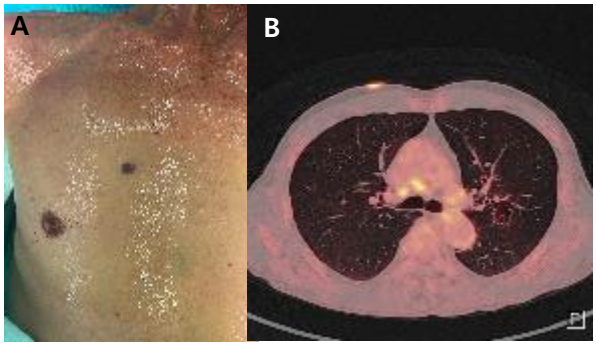

Fig 1. (A) Clinical photograph showing a well-circumscribed, blackish nodule on the right chest wall
(B) Positron emission tomography-CT demonstrating increased fluorodeoxyglucose uptake (maximum standardized uptake volume, 6.9)

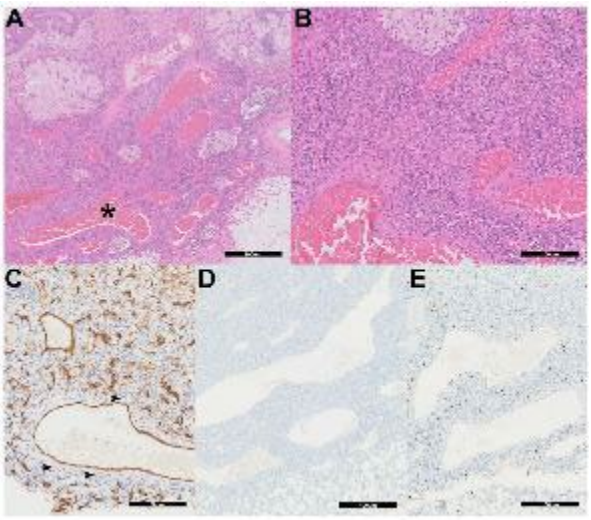

Fig 2. Histopathologic and immunohistochemical features of aneurysmal dermatofibroma. (A) The specimen demonstrates a dermal-based spindle-like cell proliferation with multiple blood-filled pseudovascular spaces (asterisk) characteristic of aneurysmal dermatofibroma (B) Higher magnification shows the storiform arrangement of spindle-like cells surrounding the aneurysmal spaces (C) CD34 immunohistochemistry reveals positive staining limited to endothelial cells lining vascular structures, while the spindle cell component remains negative (D) Human herpesvirus-8 immunohistochemistry is negative throughout the lesion, excluding Kaposi sarcoma. (E) Ki-67 immunohistochemistry demonstrates low proliferative activity with scarce positive nuclei. H&E, hema- toxylin and eosin.

EP-139

좌측 뺨의 피부 섬모 낭종 : 희귀 증례 보고

(Cutaneous ciliated cyst (CCC) on woman's cheek - a rare case report)

노원을지대학교병원 성형외과[1]
노원을지대학교병원 병리과[2]
김승현[1], 김은경[2], 이동락[1], 민경희[1*]

Purpose: Cutaneous ciliated cysts (CCC) are rare benign lesions with fewer than 70 cases reported worldwide, predominantly occurring in the lower extremities of young women during their reproductive years. Prognosis is excellent following complete excision, with no reported malignant transformation. Facial presentation is exceedingly rare, and we report an unusual case of CCC arising on the cheek of a young woman, emphasizing the diagnostic challenges associated with this atypical location.

Methods: A 22-year-old female presented with a painless mass on the left cheek that had been present for 10 years, with progressive enlargement over the past year. Ultrasound examination revealed a 0.72 × 0.76 cm well-defined oval-shaped anechoic cystic lesion in the left lower periorbital soft tissue, initially suggesting a non-neoplastic cystic lesion such as epidermal inclusion or skin appendageal cyst. Complete surgical excision was performed for both treatment and definitive diagnosis.

Results: Histopathological examination revealed a cyst located in the deep dermis (H&E, ×20). High-power field examination confirmed the diagnosis of cutaneous ciliated cyst, demonstrating characteristic ciliated cuboidal epithelium lining the cyst wall (H&E, ×200).

Conclusion: This case represents one of the extremely rare presentations of CCC on the facial region. The preoperative ultrasound findings were nonspecific, mimicking common benign cysts. Histopathological examination remains essential for accurate diagnosis. Complete surgical excision resulted in full resolution without recurrence, and CCC should be considered in the differential diagnosis of cystic lesions even in atypical locations such as the face.

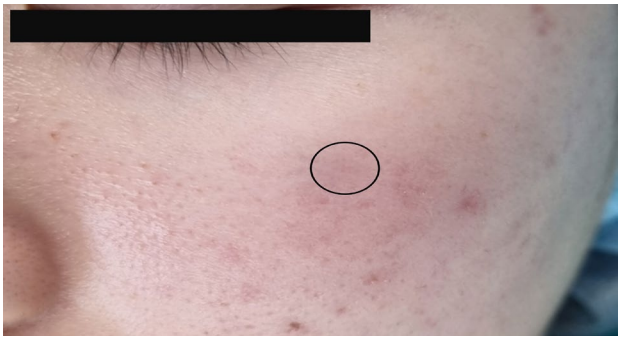

Fig. 1. Preoperative photograph showing a skin-colored, slightly elevated subcutaneous mass on the left cheek (circle). The lesion was non-tender and had been present for 10 years with progressive enlargement over the past year.

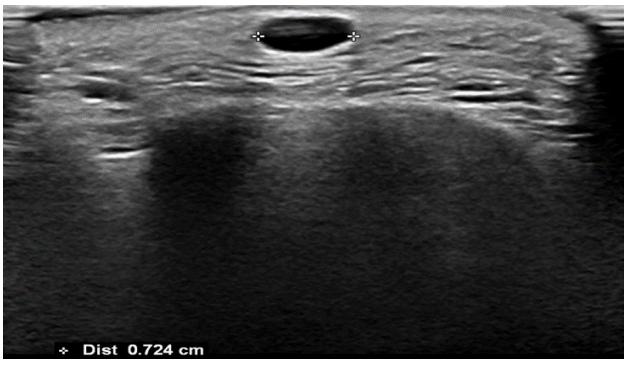

Fig. 2. Ultrasonographic Findings. Ultrasonography demonstrating a 0.72 × 0.76 cm well-defined, oval-shaped anechoic cystic lesion with small echogenic content in the left lower periorbital soft tissue, located beneath the dermal layer. The imaging characteristics suggested a non-neoplastic cystic lesion such as epidermal inclusion cyst or skin appendageal cyst.

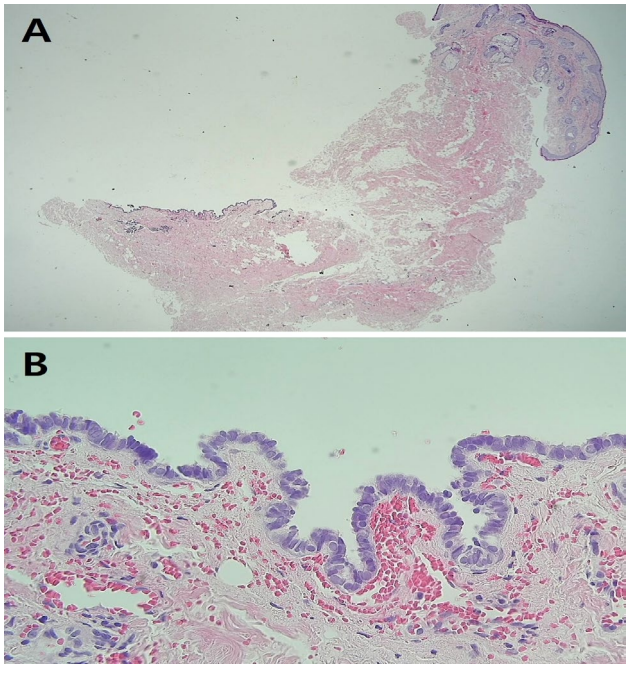

Fig. 3. Histopathological Findings. (A) There was a cyst located in the deep dermis. (H&E, x20); (B) The cyst was lined by a single layer of ciliated cubooidal epithelium. (H&E, x200)

EP-140

임플란트 기반 유방 재건 후 초음파상 액체 저류는 미미하나 임상적으로 뚜렷한 유방 팽창: 피막 구축에 선행할 수 있는 초기 임상 징후

Early Postoperative Breast Distension with Minimal Ultrasonographic Fluid as a Potential Early Clinical Sign Preceding Capsular Contracture After Implant-Based Breast Reconstruction

인제대학교 부산백병원

<u>이동훈</u>, 윤지영*

Purpose: Capsular contracture remains a common complication after implant-based breast reconstruction. We observed early postoperative breast distension without substantial peri-implant fluid on ultrasonography. This study aimed to describe this clinical–imaging discordance and evaluate its association with subsequent capsular contracture.

Methods: We retrospectively reviewed seven patients who developed clinically apparent breast distension 3–5 weeks after implant-based reconstruction. Demographics, reconstructive characteristics, ultrasonographic findings, and outcomes were analyzed. All patients received silicone implants with acellular dermal matrix. Ultrasonography was performed to evaluate peri-implant fluid collection and associated soft-tissue changes. Capsular contracture was diagnosed clinically and graded using the Baker classification when available.

Results: The mean age was 48.9 years (range, 31–63), and most cases were direct-to-implant reconstructions. Ultrasonography consistently demonstrated minimal peri-implant fluid insufficient to explain the degree of distension; some patients showed chest wall thickening or edematous changes. In two patients, ultrasound-guided aspiration yielded small fluid volumes (20–28 mL) disproportionate to the clinical swelling. No patient had clinical or laboratory evidence of infection, seroma, or hematoma. All patients subsequently developed clinically significant capsular contracture during follow-up.

Conclusion: Early postoperative breast distension with minimal ultrasonographic fluid may represent a preliminary clinical sign of capsular contracture. Recognition of this pattern may support closer surveillance, although larger prospective studies are needed to clarify its predictive value.

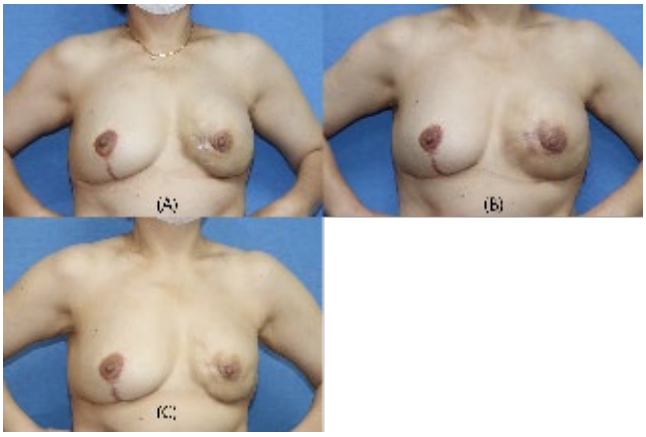

Figure 1. Serial clinical photographs of the left breast after implant-based breast reconstruction.
(A) Postoperative 2 weeks.
(B) Postoperative 5 months demonstrating clinically apparent breast distension.
(C) Postoperative 1 year showing development of capsular contracture.

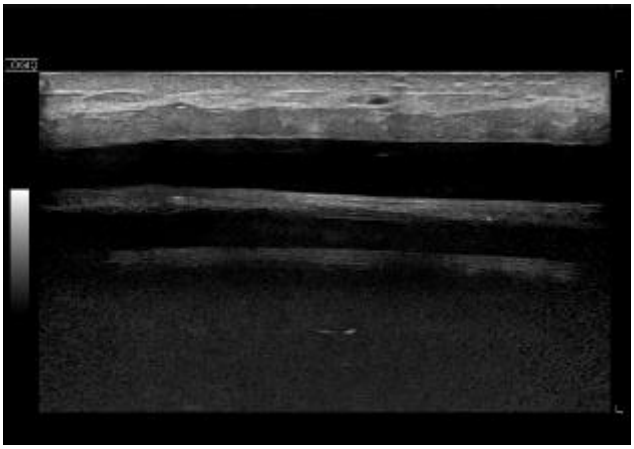

Figure 2. Radiologic findings before and after radiotherapy.
(A) Pre-treatment contrast-enhanced CT showing a 5.7 × 4 cm enhancing mass with invasion of the medial extraconal orbital space.
(B) Post-radiotherapy CT demonstrating significant tumor reduction and resolution of orbital invasion.

Table 1. Clinical characteristics of patients with early postoperative clinically apparent breast distension and minimal ultrasonographic fluid following implant-based breast reconstruction

case	Age	Reconstruction type	ADM use	Onset of distension	Baker grade	Ultrasonographic findings
1	41	DTI	MegaDerm ®	3 weeks	III	Chest wall thickening with edematous change; no drainable hematoma
2	63	DTI	AlloDerm ™	5 weeks	III	Small peri-implant fluid collection, not drainable
3	31	Two-stage	MegaDerm ®	4 weeks	II	Small-volume fluid collection aspirated (28 mL), disproportionate to clinical distension
4	53	DTI	MegaDerm ®	3 weeks	III	Scant peri-implant fluid not amenable to aspiration
5	54	DTI	MegaDerm ®	5 weeks	III	Small peri-implant fluid collection, not amenable to aspiration
6	51	Two-stage	MegaDerm ®	7 weeks	III	Small peri-implant fluid collection, not amenable to aspiration
7	45	DTI	MegaDerm ®	4 weeks	II	Small peri-implant fluid collection, not amenable to aspiration
8	50	DTI	MegaDerm ®	4 weeks	III	Small peri-implant fluid collection, not drainable
9	42	DTI	PZB skin series B	2 weeks	III	Small peri-implant fluid collection, not drainable

DTI, direct-to-implant; ADM, acellular dermal matrix.

Table 1. Clinical characteristics of patients with early postoperative breast distension and minimal ultrasonographic fluid following implant-based breast reconstruction

EP-141

국민건강보험 급여 확대 이후 한국의 유방재건술 전국적 추이(2015–2023): 10년간의 변화

Nationwide Trends in Breast Reconstruction in Korea (2015–2023) A Decade of Change Following Insurance Coverage Expansion

연세대학교 원주의과대학
원주세브란스기독병원
성형외과학 교실

전우상, 이훈범, 김석원, 김지예*

Purpose: To characterize nationwide trends in breast reconstruction (BR) in Korea after National Health Insurance (NHI) coverage expansion in April 2015, focusing on changes in annual volume, reconstructive technique, operationally defined timing, and facility-level concentration.

Methods: Using Korean National Health Insurance Service (NHIS) claims data, BR procedures performed between January 2015 and December 2023 were identified (procedure codes N7140–N7150). Reconstructions were categorized as autologous (N7140–N7147) or implant-based (N7148–N7150). Reconstruction timing was operationally defined by same-day concurrence with total mastectomy claims (N7130, N7135): concurrent cases were classified as immediate BR and non-concurrent cases as delayed BR. Facility type was classified as tertiary hospital, general hospital, or clinic. Temporal trends were assessed using linear regression and categorical comparisons using chi-square tests.

Results: A total of 56,129 BR procedures were identified from 2015 to 2023. Annual BR volume increased from 3,201 in 2015 to 6,317 in 2023 (1.97-fold; $p<0.001$) (Fig. 1). Implant-based reconstruction increased from 1,817 (56.8%) in 2015 to 5,178 (82.0%) in 2023, whereas autologous reconstruction decreased from 1,384 (43.2%) to 1,139 (18.0%) ($p<0.001$) (Fig. 2). Operationally defined immediate BR increased from 2,084 (65.1%) in 2015 to 5,193 (82.2%) in 2023 ($p<0.001$) (Fig. 3). BR remained concentrated in tertiary hospitals, increasing from 74.3% in 2015 to 78.7% in 2023 (Fig. 4).

Conclusion: Following NHI coverage expansion, breast reconstruction volume in Korea nearly doubled, with a marked shift toward implant-based and operationally defined immediate reconstruction and persistent concentration in tertiary hospitals. These findings may inform system-level planning for long-term implant surveillance and equitable access to reconstructive services.

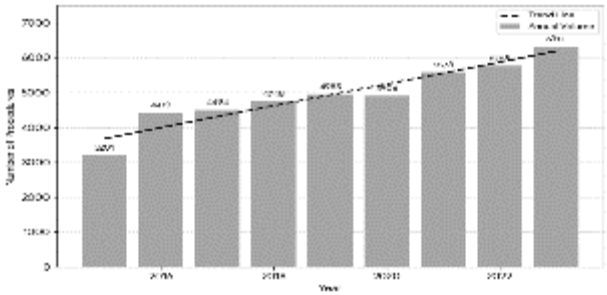

Fig. 1. Trends in annual volume of breast reconstruction (2015–2023).
Annual counts of breast reconstruction procedures identified from NHIS claims data are shown by year. The dashed line represents the fitted linear trend.

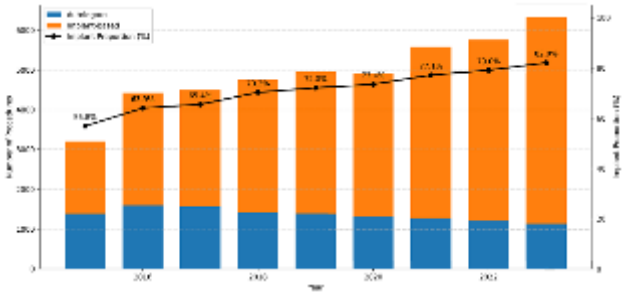

Fig. 2. Trends in reconstruction technique and implant proportion (2015–2023).
Annual numbers of autologous and implant-based breast reconstructions are presented, with the implant-based proportion (%) overlaid as a line.

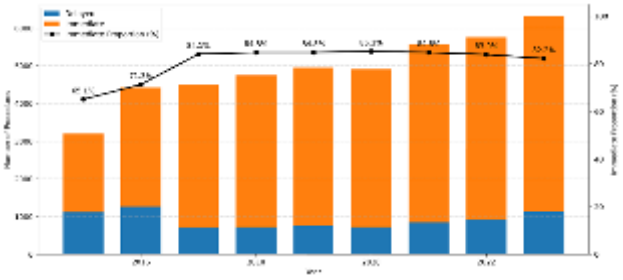

Figure 3. Trends in reconstruction timing and proportion of immediate reconstruction (2015–2023).
Annual numbers of operationally defined immediate and delayed breast reconstructions are shown, with the proportion of immediate reconstruction (%) overlaid as a line. Immediate reconstruction was defined as breast reconstruction claims concurrent with total mastectomy on the same day.

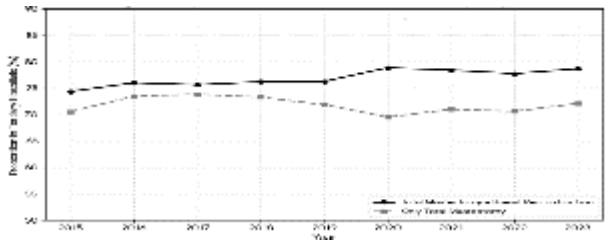

Figure 4. Proportion of procedures performed in tertiary hospitals (2015–2023).
The yearly proportion of total mastectomy cases with breast reconstruction and total mastectomy only cases performed in tertiary hospitals is shown.

EP-142

복부 유리피판 유방재건에서 피판높이-상복부 길이 비율 (FEL ratio)을 이용한 공여부 합병증 예측

(The Flap-to-Epigastric Length Ratio (FEL Ratio) as a Predictor of Donor Site Complications in Abdominal Free Flap Breast Reconstruction)

성균관대학교
류경은, 문구현, 우경제*

INTRODUCTION

- Flap height is often determined subjectively and may increase donor-site tension when excessive. The epigastric length (EL) reflects abdominal anatomy but has not been systematically incorporated into flap design.
- This study evaluates the relationship between EL and flap height and investigates whether a higher flap-to-epigastric length (FEL) ratio is associated with increased donor-site complications.

METHODS

- Patients undergoing DIEP or SIEA flap breast reconstruction (2023–2025) were retrospectively reviewed.
- Epigastric length and flap height were measured, and the flap-to-epigastric length (FEL) ratio was calculated and stratified by quartiles (Low/Intermediate/High)
- Donor-site complications were analyzed in relation to the FEL ratio, with predictive performance assessed using ROC analysis.

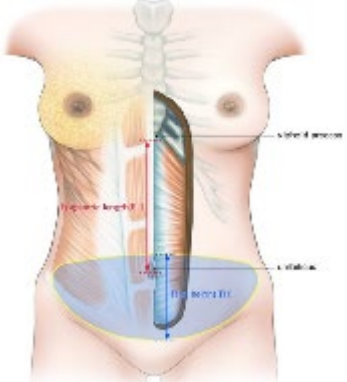

Fig. 1. Definition of epigastric length (EL) and flap height (FH).

RESULTS

- Seventy cases (64 DIEP and 6 SIEA flaps) were included.
- Flap height demonstrated a modest correlation with CT-based epigastric length ($r = 0.263$, $p = 0.030$) and a strong correlation with clinically measured epigastric length ($r = 0.579$, $p < 0.001$)
- Patients in the high FEL ratio group (upper quartile) demonstrated significantly higher overall donor-site complication rates than those in the low FEL ratio group (lower quartile) (58.8% vs. 17.6%, $p = 0.045$), with seroma being the most frequent complication.
- On logistic regression analysis, a high FEL ratio was independently associated with an increased risk of abdominal complications (odds ratio, 6.67; $p = 0.018$).
- Receiver operating characteristic analysis demonstrated significant diagnostic performance of the FEL ratio (area under the curve, 0.673; $p = 0.016$), with an optimal cutoff value of 66.81%.

Table 1. Comparison of rates of donor site complications of the three groups.

Complication profiles	Overall (n = 68)	Low FEL ratio (n = 17)	Intermediate FEL ratio (n = 34)	High FEL ratio (n = 17)	p-value
Donor complication	28 (41.2%)	3 (17.6%)	15 (44.1%)	10 (58.8%)	0.045*
Delayed wound healing	13 (19.1%)	0	9 (26.5%)	4 (23.5%)	0.067
Seroma	11 (16.2%)	1 (5.9%)	3 (8.8%)	7 (41.2%)	0.005*
Hematoma	1 (2.9%)	1 (6.7%)	0	0	
Hypertrophic scar	5 (7.4%)	1 (5.9%)	3 (8.8%)	1 (5.9%)	0.898

Table 2. Univariable and multivariable analysis to identify predictors for development of donor complication.

Variables	UVA OR (95% CI)	Unadjusted P value	MVA OR (95% CI)	Adjusted P value
BMI	1.167 (1.00, 1.36)	0.052	1.144 (0.96, 1.36)	0.131
Flap-Epigastric Length ratio				
Low FEL ratio	Ref		Ref	
Intermediate FEL ratio	3.684 (0.89, 15.22)	0.072	2.84 (0.66, 12.32)	0.162
High FEL ratio	6.667 (1.38, 32.28)	0.018*	4.92 (0.97, 25.03)	0.055

Table 3. Diagnostic Performance of FEL ratio for predicting abdominal complications.

Variable	AUC	95% CI	Cutoff	Sensitivity	Specificity	p-value
FEL ratio	0.673	0.54-0.80	0.6681	0.82	0.50	0.016*

CONCLUSION

- A short epigastric length combined with a disproportionately tall flap height is associated with increased donor-site morbidity.
- Epigastric length may serve as a simple and practical reference for flap height determination to reduce abdominal complications.

EP-143

미세혈관 유방 재건술에서 동맥 Coupler 사용을 위한 알고리즘적 접근: 수기 봉합과의 비교

An Algorithmic Approach to Arterial Coupler Use in Microsurgical Breast Reconstruction: Comparison with Hand-Sewn Sutures

서울아산병원[1]

강현일[1], **김형배**[1*], **한현호**[1], **엄진섭**[1]

Purpose: Microsurgical breast reconstruction offers superior outcomes after mastectomy, but vascular micro-anastomosis remains technically demanding. Venous couplers are widely adopted, whereas the use of arterial couplers remains controversial. This study aimed to establish an algorithmic approach for arterial coupler use and compare outcomes with hand-sewn sutures

Methods: A retrospective review was performed on 105 patients undergoing deep inferior epigastric perforator flap breast reconstruction by a single surgeon. Patients were divided into an arterial coupler group (N=62) and a hand-sewn suture group (N=43). An intraoperative algorithm guided coupler use, requiring the absence of atherosclerosis, intact intima, and adequate vessel laxity. Demographics, operative details, micro-anastomosis time, and postoperative outcomes were analyzed.

Results : Patients in the coupler group were younger (47.6±8.6 vs. 53.0±7.9 years, p=0.001) and underwent more robot assisted procedures (16.1% vs. 2.3%, p=0.025). Micro-anastomosis time was significantly shorter with couplers (19.6±8.9 vs.26.1±6.5 minutes, p<0.01). Flap survival was comparable between groups (96.8% vs. 100%, p=0.512). Complication rates, including arterial/venous insufficiency, hematoma, and infection, showed no significant differences. Two coupler failures occurred: One venous congestion and one late thrombosis, both attributed to multifactorial causes rather than device failure.

Conclusions: Arterial couplers, when used under strict algorithmic selection criteria, provide reliable outcomes comparable to hand-sewn sutures while significantly reducing operative time. This approach enhances efficiency in microsurgical breast reconstruction and may guide future standardized practice.

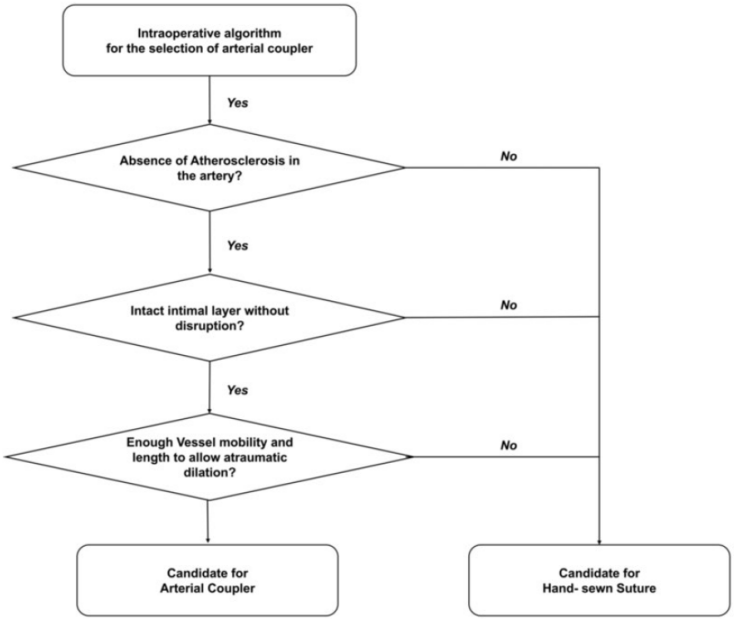

Fig. 1. The intraoperative algorithm for selection of the arterial coupler.

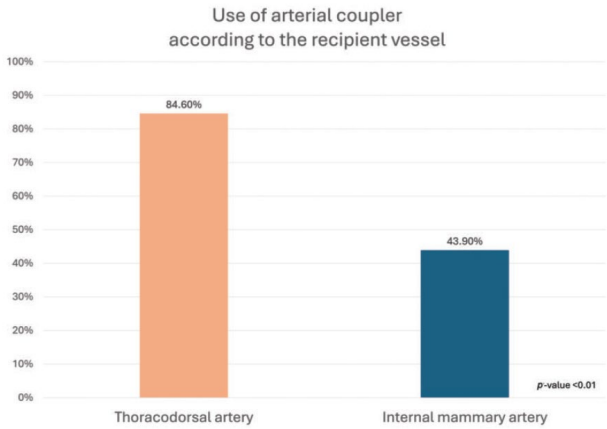

Fig. 2. The use of arterial coupler according to the recipient vessel.

Table 1. Reconstructive outcomes

Variable	Arterial coupler (N = 62)	Arterial hand-sewn (N = 43)	p-value
Revisional surgery	4 (6.5%)	3 (7.0%)	1.0
Arterial insufficiency	2 (3.2%)	0 (0.0%)	
Venous insufficiency	2 (3.2%)	1 (2.3%)	
Others	0 (0.0%)	2 (4.7%)	
Flap survival	60 (96.8%)	43 (100.0%)	0.512
Hematoma (Breast)	1 (1.6%)	4 (9.3%)	0.156
Infection	1 (1.6%)	0 (0.0%)	1.0
Seroma (breast)	1 (1.6%)	1 (2.3%)	1.0

EP-144

유두보존 유방절제술 후 대흉근 전면 즉시 보형물 재건에서 피판 괴사의 예측 인자 분석

(Predictive Factors for Flap Necrosis after Nipple-Sparing Mastectomy with Prepectoral Direct-to-Implant Breast Reconstruction)

부산대학교[1]
서일병원[2]

이치현[1], 이현승[1], 배성환[2*]

Purpose:
- Prepectoral direct-to-implant (DTI) breast reconstruction following nipple-sparing mastectomy (NSM) has gained popularity due to favorable aesthetic and reconstructive outcomes.
- However, mastectomy flap necrosis remains a clinically significant complication that can compromise both surgical outcomes and implant viability.
- This study aimed to identify predictive factors for flap necrosis and establish clinically relevant cut-off values.

Methods:
- A retrospective analysis was conducted on 339 breasts undergoing NSM with prepectoral DTI reconstruction between 2018 and 2024.
- The primary outcome was mastectomy flap necrosis, categorized as major (requiring debridement) or minor (managed conservatively).
- Collected variables included: Patient factors (age, BMI, smoking, comorbidities), oncologic factors (histology, adjuvant therapies), surgical factors (incision type, mastectomy weight, implant size, flap thickness)
- Flap thickness was measured intraoperatively as both minimum (typically near the nipple–areola complex) and maximum thickness.
- Univariate and multivariable logistic regression analyses were performed to identify independent predictors.
- Receiver operating characteristic (ROC) curve analysis in the lateral radial incision cohort was used to determine clinically relevant threshold values.

Surgical Technique:
- All mastectomies were performed through either an inframammary fold or lateral radial incision.
- Prepectoral direct-to-implant reconstruction was performed, with implant size determined based on mastectomy weight and intraoperative sizer assessment.
- The implant was wrapped with acellular dermal matrix using an anterior coverage technique and fixed to the pectoralis major fascia to ensure stability.
- The inframammary fold was reconstructed, and quilting sutures were selectively applied to reduce dead space and prevent implant displacement.
- A closed-suction drain was placed, followed by layered closure and postoperative compressive garment application.

Results:
- Major flap necrosis occurred in **18.0%** of cases, while minor necrosis occurred in **3.2%**.
- Multivariable analysis identified: **Mastectomy weight, Minimum flap thickness** as independent predictors of flap necrosis ($p < 0.01$).
- **Hypertension** was also significant when considering overall necrosis.
- Minimum flap thickness differed significantly by incision type ($p < 0.001$)
  - Lateral radial: **3.68 mm**
  - Inframammary fold: **4.84 mm**
- Although incision type was associated with necrosis in univariate analysis, it was not significant in multivariable models, suggesting that **differences are primarily mediated by flap thickness**.
- ROC analysis in the lateral radial cohort identified:
  - **350 g** as the threshold for mastectomy weight
  - **5 mm** as the threshold for minimum flap thickness

Conclusion:
- **Mastectomy weight** and **minimum flap thickness** are key determinants of flap necrosis in prepectoral DTI breast reconstruction.
- Maintaining a flap thickness of at least **5 m**m and exercising caution in cases with mastectomy weight exceeding **350 g** may help reduce the risk of necrosis and related complications.
- These findings provide practical intraoperative guidance for improving reconstructive outcomes.

EP - 145

유방보존술 후 생분해성 스페이서를 이용한 용적 유지와 영상 추적 안전성에 대한 임상적 분석

(Radiologic Safety and Volume Preservation of a 3D-Printed Bioresorbable Spacer in Breast-Conserving Surgery: A Retrospective Analysis of 53 Patients)

Kyung Jun Heo[1,2], Jee Hyun Ahn[3], Min Jung Kim[4], Eun Jin Park[5], Seho Park[3], Wooyeol Baek[1,2]

[1] Department of Plastic and Reconstructive Surgery, Yonsei University College of Medicine

[2] Institute for Human Tissue Restoration, Department of Plastic and Reconstructive Surgery, Yonsei University College of Medicine

[3] Division of Breast Surgery, Yonsei University College of Medicine,

[4] Department of Radiology, Research Institute of Radiological Science, Yonsei University College of Medicine

[5] PLCOskin, Department of Research, Seoul, Korea

연세대학교 세브란스병원
허경준 , 백우열*

Purpose: Breast-conserving surgery (BCS) is an established oncologic treatment for early-stage breast cancer; however, postoperative volume deficiency and contour deformity remain common concerns. Existing reconstructive options, including local flaps, fat grafting, and acellular dermal matrix (ADM), may increase surgical complexity or interfere with postoperative imaging surveillance. TissueDerm is a novel three-dimensional (3D) printed bioresorbable polycaprolactone spacer designed to preserve lumpectomy cavity volume while allowing host tissue integration. This study aimed to evaluate the clinical safety and radiologic surveillance compatibility of the TissueDerm BCS spacer.

Methods: A retrospective review was conducted of 53 consecutive female patients who underwent BCS with TissueDerm spacer implantation between July 2024 and May 2025.Postoperative complications, adjuvant treatment timelines, and oncologic outcomes were assessed. Radiologic evaluation was performed using routine postoperative breast imaging at approximately 6 months, including MRI, CT, mammography, and ultrasonography. MRI findings were independently reviewed by two breast radiologists with emphasis on Breast Imaging Reporting and Data System categorization and the presence of spacer-related artifacts or abnormal findings.

Results:
The mean age was 48.6 years, and the mean tumor size was 17.3 mm. The mean operative time was 116 min, and drains were used in 6 patients (11.3%). No intraoperative complications were recorded. No major postoperative complications occurred. No seroma, infection, wound dehiscence, hematoma, fat necrosis, or foreign body reaction was documented.

MRI follow-up was available in all 53 patients. No spacer-related artifact limited interpretation. BI-RADS categories were 1-2 in 43 patients (81.1%), 3 in 9 (17.0%), and 4 in 1 patient (1.9%); the higher-category finding was investigated and confirmed benign. During a median clinical follow-up of 12 months, no local recurrence or distant metastasis was observed.

Figure 1. TissueDerm BCS spacer, a bioresorbable collagen-based mesh.

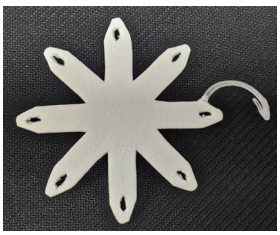

Spacer component before assembly

Assembled spacer

Figure 2. **Representative clinical case demonstrating volume preservation** Preoperative (left) & Postoperative (right) image demonstrating preservation of breast contour (right).

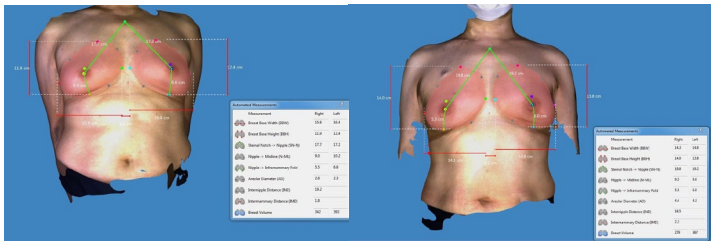

Three-dimensional (3D) surface images

Figure 3. MRI findings after partial mastectomy with spacer

MRI performed at 6 months postoperatively demonstrates stable dome-shaped tissue formation at the surgical site following placement of the TissueDerm BCS spacer. No imaging artifacts interfering with oncologic surveillance were identified.

Figure 4. Postoperative mammographic findings following TissueDerm BCS spacer

Mammography performed after placement of the TissueDerm BCS spacer demonstrates preservation of breast contour without evidence of collapse. Symmetry between both breasts is maintained. No fluid collection or inflammatory changes are observed.

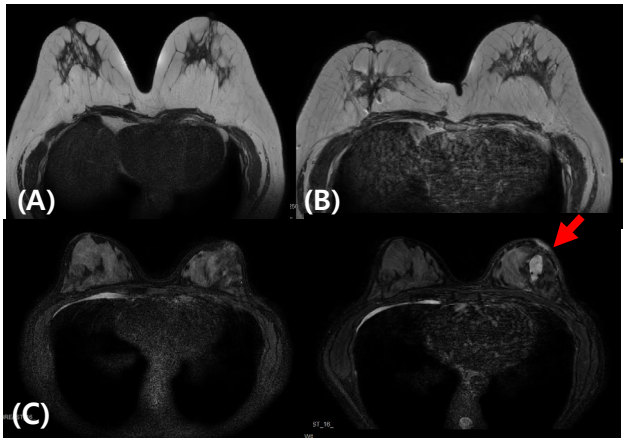

Figure 5. Comparison of postoperative breast contour with and without spacer placement.
(A) Preoperative MRI without spacer placement.
(B) Postoperative MRI showing contour deformity without spacer placement.
(C) Preoperative MRI with TissueDerm spacer placement.
(D) Postoperative MRI showing preserved breast contour with spacer placement.

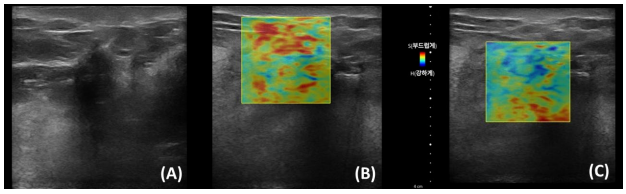

Figure 6. Elastographic evaluation of tissue characteristics following TissueDerm BCS spacer placement

(A) Conventional ultrasonography of the surgical site following spacer placement. (B) Elastography of the spacer-inserted region after radiotherapy, demonstrating relatively soft and compliant tissue characteristics. (C) Elastography of a control site without spacer placement.

Table 1. Radiologic outcomes on postoperative MRI

Variable	Value
Total patients with MRI at 6 months	53
Spacer-related artifact interfering surveillance	0
BI-RADS 1-2	43 (81.1%)
BI-RADS 3	9 (17.0%)
BI-RADS 4	1 (1.9%)
Higher-category finding confirmed benign	1
Local recurrence during follow-up	0

Conclusion:

The TissueDerm BCS spacer demonstrated favorable postoperative safety, with no major complications or delays in adjuvant therapy. In addition, it showed effective space maintenance and supported autologous tissue regeneration, thereby contributing to preservation of breast contour after breast-conserving surgery. Radiologic evaluation across serial MRI, CT, ultrasonography, and mammography confirmed stable imaging characteristics and radiologic transparency without compromising diagnostic quality or oncologic surveillance. Collectively, these findings suggest that the 3D-printed bioresorbable TissueDerm BCS spacer is a safe and imaging-compatible option for volume preservation in breast-conserving surgery.

EP-146

Skin-sparing mastectomy 후 유두재건에서 Long V-Y flap technique의 유두 크기 유지 및 대칭성 향상에 대한 유효성

(Advancing Nipple Reconstruction in Skin-Sparing Mastectomy:
The Efficacy of the Long V-Y Flap Technique for Enhanced Size Retention and Symmetry)

성균관대학교 의과대학
강북삼성병원 성형외과학교실

김우섭, 김준규*

Purpose: Nipple reconstruction is the final stage of breast reconstruction after skin-sparing mastectomy (SSM) and is important for achieving breast symmetry and aesthetic completion. Although several techniques have been described, long-term maintenance of nipple projection and volume remains a common limitation due to postoperative tissue contraction and resorption. This study aimed to evaluate the clinical outcomes of the previously described long V-Y flap technique, with particular focus on postoperative projection and volume changes.

Methods: This study retrospectively reviewed 27 patients who underwent nipple reconstruction using the long V-Y flap after SSM with tissue expander–implant reconstruction. Nipple projection and volume were measured immediately postoperatively and at follow-up beyond 6 months. The rates of projection and volume loss were calculated. Outcomes were descriptively compared with projection loss rates reported for other flap techniques in the literature.

Results: The mean nipple volume loss was 34.23%, and the mean projection loss was 32.79% at follow-up. Nipple width showed minimal change over time. Compared with previously reported data for skate, star, bell, and arrow flaps, the long V-Y flap demonstrated numerically lower projection loss rates.

Conclusion: The long V-Y flap may be a useful option for nipple reconstruction after SSM, particularly in cases requiring larger nipple reconstruction. In our cohort, it showed relatively favorable short- to mid-term maintenance of projection and volume. Further studies with larger sample sizes and longer follow-up are warranted.

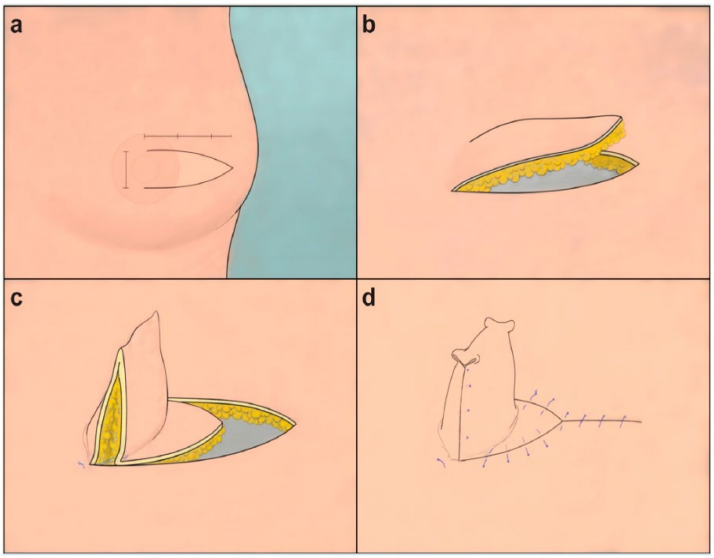

Figure 1. Diagrammatic representation of the long V-Y flap design for nipple reconstruction. (a) The flap base is marked at the planned nipple site, designed with a 1:2.5 width-to-length ratio and a half-fusiform shape, tapering in the middle. (b) The flap is meticulously separated with concurrent elevation of the skin and subcutaneous fat layers. (c) The flap is advanced toward the base and folded to achieve the desired height. (d) Depiction of the flap-folding, highlighting the inward manipulation of sharp rectangular tips at the top using a three-point suture, avoiding cuts that could restrict blood flow.

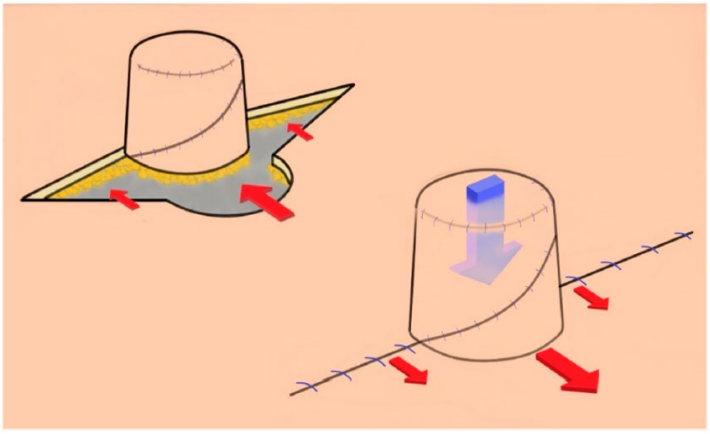

Figure 2. Nipple reconstruction using the CV flap method. Shown is the nipple reconstruction using the CV flap method illustrating various mechanisms that contribute to the reduction in nipple size post-reconstruction. The red arrows indicate the skin retraction forces triggered by the closure of the donor defect, leading to retraction of the adjacent skin. The blue arrow represents two factors: (a) the number of lobules, where multiple lobules increase scar formation and disrupt the blood supply, potentially resulting in necrosis, fat atrophy, and (b) external pressure forces exerted by clothing or posture.

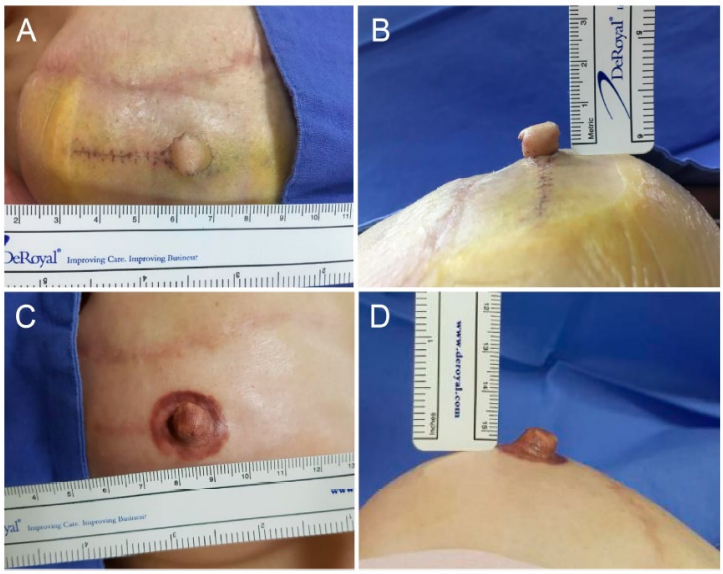

Figure 3. Clinical photographs of a 36-year-old female patient who underwent nipple reconstruction using the Long V-Y Flap Technique. (A,B) Immediate postoperative appearance showing a nipple width of 11 mm and height of 8 mm. (C,D) At 3 months postoperatively, the nipple maintained its width at 11 mm with a slight reduction in height to 7 mm.

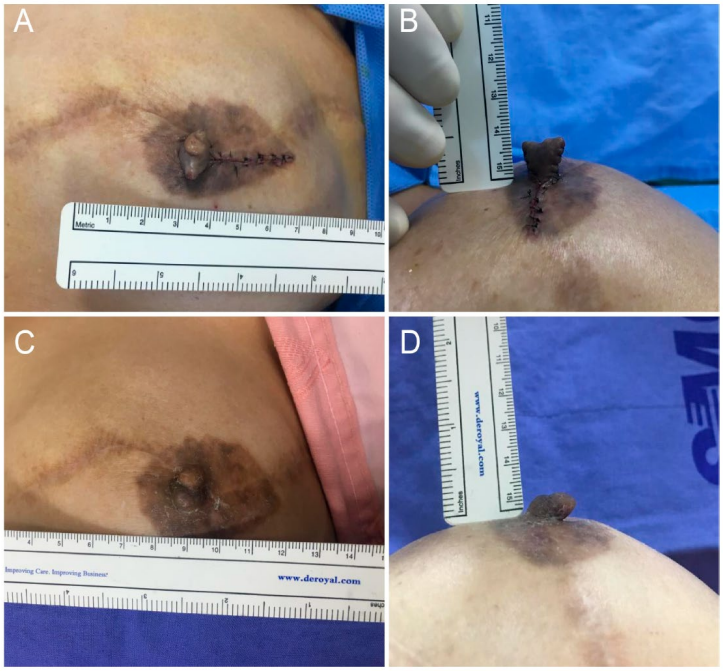

Figure 4. Clinical photographs of a 60-year-old female patient who underwent nipple reconstruction using the Long V-Y Flap Technique. (A,B) Immediate postoperative views showing a nipple width of 10 mm and height of 11 mm. (C,D) At 3 months postoperatively, the nipple width was slightly increased to 11 mm while the height decreased to 7 mm.

EP-147

환자의 재건 선호도가 충족되지 못한 상황에서의 유방 재건: 수술 계획 변경에 따른 환자 만족도 분석

When Reconstructive Preference Is Constrained: Patient-Reported Outcomes After Altered Breast Reconstruction Plans

이화여자대학교 의과대학
조정목, 김수민, 박진우*

[Purpose] : Choice between implant-based and autologous breast reconstruction in breast cancer patients is preference-sensitive. In March 2024, nationwide resignation of residents in South Korea substantially limited access to immediate deep inferior epigastric perforator free flap(DIEP-FF) reconstruction for approximately 18 months. As a result, some patients who initially preferred DIEP-FF at our institution underwent direct-to-implant(DTI) reconstruction instead. We evaluated patient-reported outcomes in this externally constrained setting.

[Methods] : In this initial report, patients undergoing unilateral prepectoral implant-based breast reconstruction between March 2024 and August 2025 were reviewed. Expander-based cases and those without completed BREAST-Q questionnaires were excluded. Patients who initially preferred DIEP-FF were offered temporary expander placement for delayed DIEP-FF or conversion to DTI. Those converting to DTI comprised the study group, while patients who initially chose and underwent DTI served as controls. BREAST-Q scores at 6–12 months were compared.

[Results] : Among 187 reconstructions performed during the study period, follow-up duration was not sufficient for all patients to complete postoperative assessment. 12 patients were included in study group and 40 in control group for analysis. Baseline clinical characteristics were similar between two groups. Between 6 and 12 months postoperatively, psychosocial well-being, sexual well-being, satisfaction with breasts, and physical well-being scores were lower in the study group, though not statistically significant.

[Conclusion] : Although not statistically significant, patients whose reconstructive preference was externally altered demonstrated consistently lower BREAST-Q scores across domains. These preliminary findings suggest potential impact of disrupted preference alignment on patient-reported outcomes and support the value of preserving patient choice in reconstructive decision-making whenever feasible.

Table 1. Clinical and surgical characteristics

	Study group (%)	Control group (%)	P value
No. of patients	12	40	
Mean age ± SD, yr	47.83 ± 9.21	43.73 ± 8.78	0.166
Mean BMI ± SD, kg/m²	23.40 ± 3.47	22.78 ± 3.30	0.572
Smoking history	0	1 (2.5)	>0.999
Diabetes mellitus	1 (8.3)	0	0.231
Hypertension	1 (8.3)	3 (7.5)	>0.999
Dyslipidemia	2 (16.7)	5 (12.5)	0.656
Cancer-related treatment			
Preoperative radiotherapy	0	3 (7.5)	>0.999
Neoadjuvant chemotherapy	1 (8.3)	7 (17.5)	0.663
Adjuvant chemotherapy	2 (16.7)	7 (17.5)	>0.999
Adjuvant radiotherapy	1 (8.3)	1 (2.5)	0.412
Mastectomy type			>0.999
Nipple-sparing	10 (83.3)	32 (80.0)	
Skin-sparing	2 (16.7)	8 (20.0)	
Mastectomy weight ± SD, g	194.33 ± 57.81	189.73 ± 89.97	0.868
Axillary surgery			0.553
Sentinel lymph node biopsy	11 (91.7)	38 (95.0)	
Axillary lymph node dissection	1 (8.3)	2 (5.0)	
Balancing procedure	1 (6.7)	14 (35.0)	0.143

Table 2. Pre- and post-operative BREAST-Q scores

	Study group	Control group	P value
Psychosocial well-being ± SD			
Pre-operative	59.17 ± 4.23	62.55 ± 2.18	0.465
Post-operative	60.67 ± 2.80	66.73 ± 2.79	0.262
Sexual well-being ± SD			
Pre-operative	57.11 ± 4.26	52.82 ± 2.15	0.388
Post-operative	46.73 ± 3.38	53.18 ± 3.18	0.310
Physical well-being: Chest ± SD			
Pre-operative	81.75 ± 5.34	78.98 ± 2.50	0.610
Post-operative	72.75 ± 4.07	73.98 ± 2.43	0.806
Satisfaction with breasts ± SD			
Pre-operative	52.75 ± 3.40	54.45 ± 2.33	0.717
Post-operative	60.33 ± 1.80	61.68 ± 2.78	0.797

Figure 1. Pre- and post-operative BREAST-Q scores

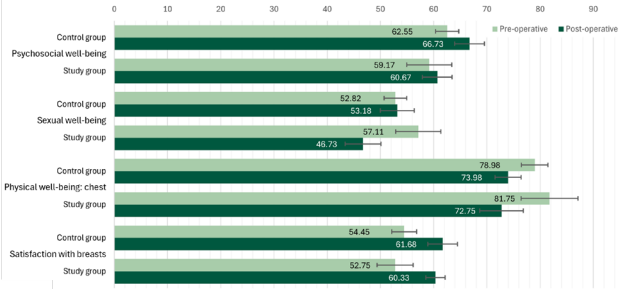

EP-148

다면체 매트릭스 구성(PMC) 기법: 무세포 동종진피(ADM) 외피의 기하학적 표준화와 유방 전층 재건술 시 수술 효율성에 관한 후향적 코호트 연구

(The Polyhedral Matrix Configuration (PMC) Technique: A Retrospective Cohort Study of Geometric Standardization of Acellular Dermal Matrix Wrapping and Operative Efficiency in Prepectoral Breast Reconstruction)

고신대학교 의과대학
성형외과학교실

박정진, 이형석, 박진형, 김윤수*

Purpose: Prepectoral breast reconstruction with acellular dermal matrix (ADM) typically requires intraoperative manual tailoring, introducing structural variability and workflow delays. We developed the Polyhedral Matrix Configuration (PMC) technique—a geometric method for standardizing ADM shell creation—and compared it to our traditional "tear-drop" wrap to determine whether standardization improves structural integrity and operative efficiency.

Methods: We reviewed 227 consecutive patients undergoing immediate prepectoral reconstruction from January 2021 to December 2024 (tear-drop group: n=155; PMC group: n=72). PMC transforms planar ADM into a 3D dome using pre-designed wedge resections and butt-joint sutures, eliminating material overlap (Figure 1 and 2). Standardization permits back-table fabrication during mastectomy ("parallel two-team workflow", Figure 3). Bilateral cases were excluded, and subgroup analysis controlled for higher robotic mastectomy rates in the PMC cohort.

Results: PMC reduced plastic surgery time by 44.6 minutes (95% CI: 35.2–54.0, p<0.001), with efficiency gains across both conventional (32.8 min, p<0.001) and robotic mastectomies (60.8 min, p<0.001). Despite zero-overlap design, PMC showed no increase in major complications (p>0.99) and lower visible rippling rates (OR 0.28, 95% CI: 0.08–0.97, p=0.032). BREAST-Q "Satisfaction with Breasts" scores were higher in PMC group (mean difference +7.3 points, 95% CI: 3.1–11.5, p=0.001). Clinical outcomes demonstrated maintained projection and smooth contours (Figure 4).

Conclusion: Geometric standardization enables both design precision and operative efficiency. By separating reconstruction preparation from mastectomy through a reproducible protocol, PMC reduces operative time while improving aesthetics through stable, single-layer construction.

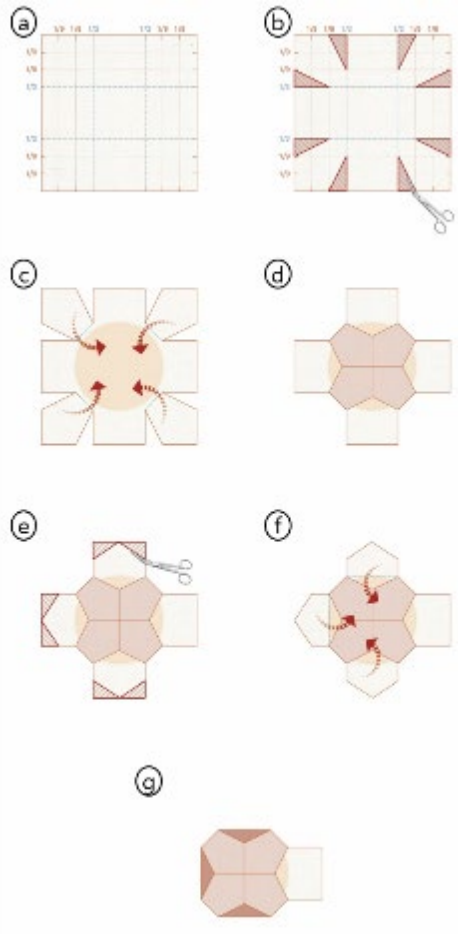

Fig 1. PMC technique assembly protocol. (a) Template marking with 9 × 9 grid. (b) Wedge resection of triangular sections at 1:2 base-to-height ratio. (c) Corner flaps fold to form octagonal base. (d) Butt-joint sutures create zero-overlap alignment. (e) Peripheral trimming shapes sidewall contours. (f) Completed

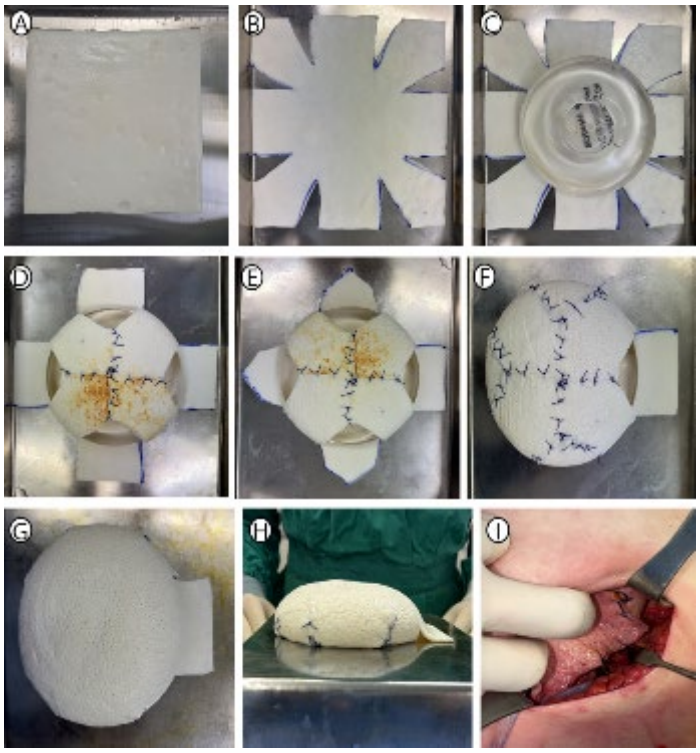

Fig 2. PMC shell assembly during surgery. (A) ADM sheet secured to sterile sizer on back table. (B–E) Sequential wedge resection and butt-joint suturing create 3D volume. (F,G) Completed dome-shaped PMC module ready for insertion. (H) Final view after implant insertion. The zerooverlap construct creates a smooth interface with overlying tissue. (I) The window's edge anchors to pectoralis major fascia.

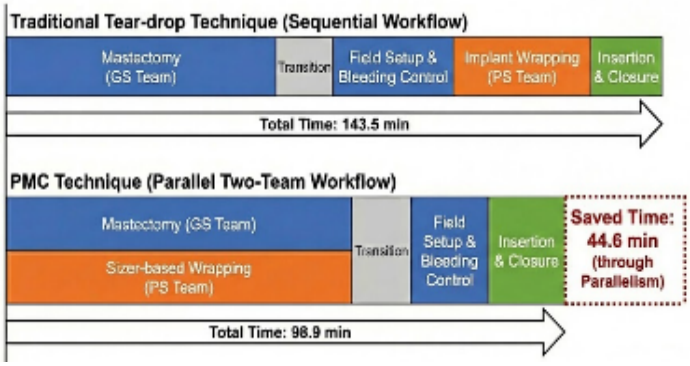

Fig 3. Operative workflow comparison. (Top): Traditional tear-drop technique—reconstruction starts after mastectomy completion. (Bottom): PMC technique—plastic surgery team fabricates ADM shell on back table during mastectomy. Red dashed box indicates mean time saved (44.6 min) through parallel processing.

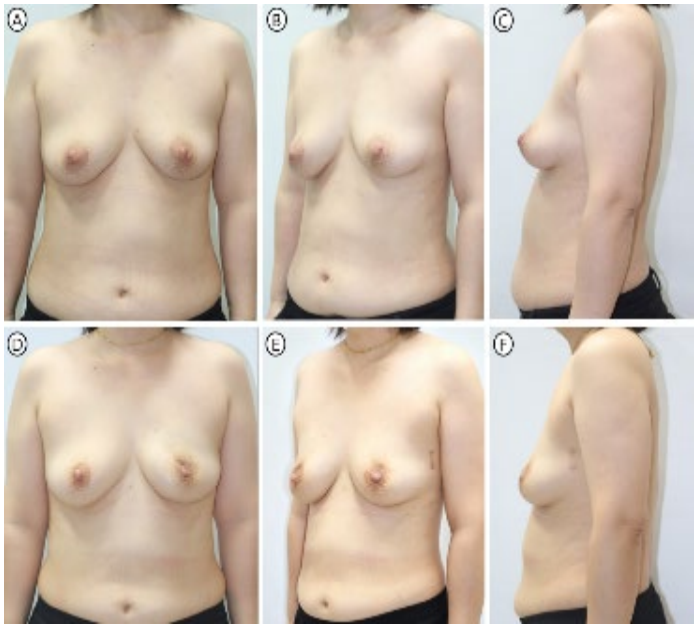

Fig 4. Representative case—preoperative and 6-month postoperative views. A 40-year-old patient (BMI 24.8 kg/m2) underwent immediate prepectoral reconstruction following left robotic nipple-sparing mastectomy. Reconstruction used a 235 cc Mentor smooth round implant wrapped in 18 × 18 cm2 Bellacell ADM via lateral vertical incision. (A–C) Preoperative baseline morphology. (D–F) Six-month postoperative results show maintained projection and symmetry with smooth upper pole transition despite thin skin envelope from robotic dissection.

EP-149

종양성형 유방보존술에서 무세포동종진피의 장기적 형태 및 부피 유지:2년 후향적 연구

(Long-Term Shape and Volume Retention of Acellular Dermal Matrix in Oncoplastic Breast-Conserving Surgery: A 2-Year Retrospective Study)

고신대학교 의과대학 성형외과학교실

김민준, 박진형, 이형석, 김윤수*

Purpose: To quantitatively assess the long-term volume stability of acellular dermal matrix (ADM) in oncoplastic breast-conserving surgery (OBCS) and analyze surgical and aesthetic outcomes.

Methods: This retrospective study examined 172 breast cancer patients who underwent OBCS with immediate ADM-based volume replacement (2020–2022). Patients received either diced ADM with sheet ADM (n = 102) or diced ADM with paste ADM (n = 70) (Figure 1). The ADM volume was evaluated using MRI at 6, 12, and 24 months postoperatively (Figure 2).

Results: Long-term volume stability was achieved in both groups with minimal volume reduction (4.3–4.5%) at 24 months ($p < 0.001$). Early surgical complications included hematoma (4.1%), seroma (2.3%), and wound issues (1.2%), with no infections or ADM non-incorporation. Contour irregularities occurred in 16.3% of cases. Radiotherapy (87% of patients) did not significantly impact ADM volume retention (Figure 3).

Conclusion: ADM provides predictable, durable volume replacement in OBCS, with excellent volume stability even with radiotherapy. This quantitative assessment of ADM volume retention over two years supports ADM as a reliable option for breast-conserving surgery, potentially expanding treatment options for patients with unfavorable tumor-to-breast volume ratios (Figure 4).

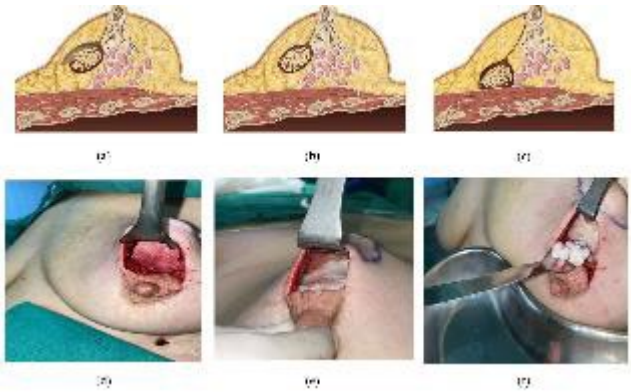

Fig. 1. Conceptual illustration and intraoperative demonstration of three distinct acellular dermal matrix (ADM) application techniques. (a, d) Diced ADM with Sheet technique: Illustrated concept and corresponding intraoperative image showing diced ADM fragments (1-2 mm^3) placed in the lumpectomy defect, followed by positioning of a sheet ADM layer as a superficial cover, secured with absorbable sutures. (b, e) Diced ADM with Paste-type micronized technique: Illustrated concept and corresponding intraoperative image demonstrating diced ADM fragments placed in the defect cavity and supplemented with injectable paste-type micronized ADM, allowing precise contour refinement. (c, f) Diced ADM Only technique: Illustrated concept and corresponding intraoperative image showing diced ADM fragments alone used to fill the defect without additional sheet or paste supplementation.

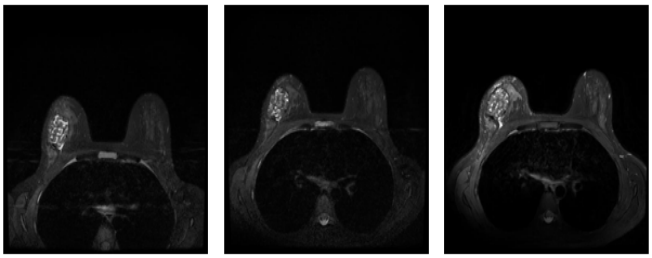

(a) (b) (c)

Fig. 2. Serial magnetic resonance imaging demonstrating long-term volume stability of diced ADM with paste type ADM in a 40-year-old patient who underwent oncoplastic breast-conserving surgery. T2-weighted axial images show consistent low signal intensity (white arrows) of the ADM construct at (a) 6 months postoperatively, (b) 12 months postoperatively, and (c) 24 months postoperatively. Quantitative analysis revealed minimal volume reduction (3.7%) over the 24-month follow-up period, confirming the long-term stability of the ADM reconstruction. Note the well-defined margins and homogeneous signal characteristics of the ADM throughout the follow-up period, indicating successful tissue integration without significant degradation or resorption.

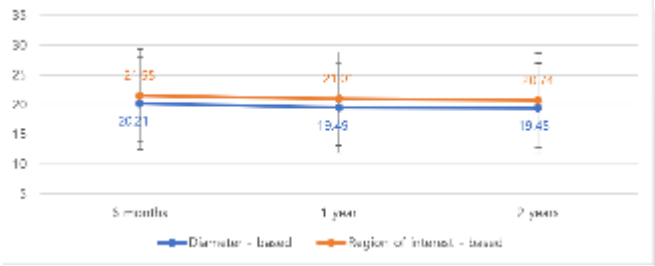

Fig. 3. Volumetric changes in ADM at MRI follow-up at 6 months, 1 year, and 2 years in patients who received radiotherapy (n=149). Radiotherapy did not significantly impact the rate or extent of volume loss.

Fig. 4. Preoperative (a, d), postoperative (b, e) 6-month and postoperative (c, f) 12-month photographs. (a,b,c) 45-year-old patient's tumor is located in the lower inner quadrant of the left breast, and the resected breast tissue was 21 g. Total 24.5 cm^3 of diced ADM and paste ADM was used; (d,e,f) 40-year-old patient's tumor is located in the upper outer quadrant of the left breast, and the resected breast tissue was 29.5 g. Total 33 cm^3 of diced ADM and sheet ADM was used.

EP-150

영상 기반 3차원 재구성을 이용한 유두 부피 측정의 새로운 접근

(Validation of a Video-Based Three-Dimensional Technique for Nipple Volume Measurement: A Comparative Study With Conventional Methods)

충남대학교병원 성형외과[1]
충남대학교 의과학과 [2]
충남대학교 성형외과학 교실[3]
서울대학교 영상의학과[4]

김동현[1,2], **이동헌**[4], **허지혜**[4], **오한슬**[1], **유보람**[1], **권혁재**[1], **오상하***[1,3]

Purpose : With the increasing demand for nipple reconstruction following mastectomy, accurate and objective nipple volume assessment has become essential for both clinical evaluation and research standardization. Conventional techniques including mold based water displacement, geometric approximation, CT, and Antera 3D® are limited by procedural complexity, cost, radiation exposure, or patient discomfort. This study aimed to propose and validate a novel non-contact, video-based three-dimensional nipple volume measurement method using Gaussian splatting and to compare its accuracy with established techniques.

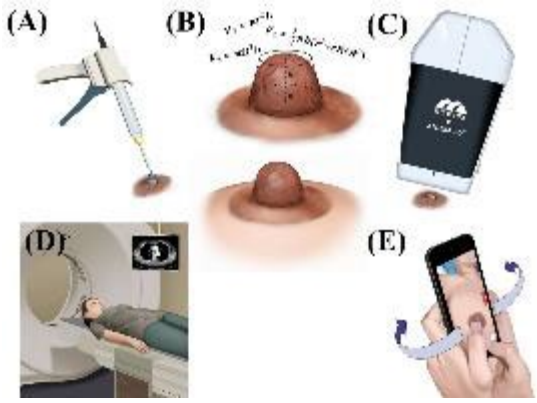

Fig.1 Schematic diagram showing five nipple volume measurement methods. Nipple volume can be measured using silicone molds with water displacement(A), manual geometric estimation(B), or 3D imaging devices(C). It can also be calculated through volumetric reconstruction from CT scans with 3D modeling(D). Recently, smartphone video with Gaussian splatting and surface meshing has emerged as a novel method(E).

Methods : We retrospectively analyzed 37 nipples from 32 women for 2 years. Silicone mold–based water displacement was used as the reference standard. Comparative methods included geometric estimation, CT-based reconstruction, Antera 3D®, and a smartphone-based approach using Gaussian splatting with 3D mesh algorithms. Volumes(cm^3) were compared using one-way ANOVA, mean squared error, and Bland–Altman analysis to assess agreement and accuracy.

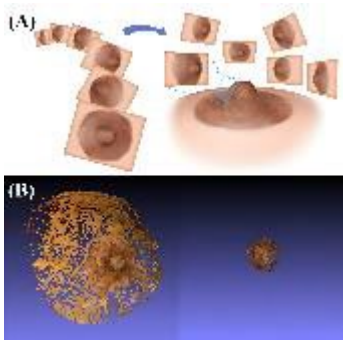

Fig.2 (A) Video-based measurement uses Gaussian splatting of sequential frames, followed by boundary extraction and postprocessing to estimate volume. (B) MeshLab rendering demonstrates boundary delineation before and after processing.

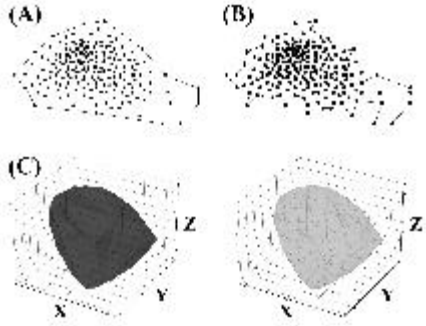

Fig.3 Convex hull creates a smooth outer boundary but ignores concave details. Alpha shape captures surface indentations for more accurate anatomy. Final 3D meshes enable volumetric and morphological analysis.

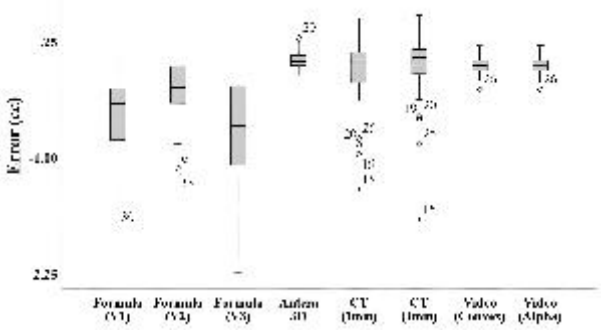

Table1. Box-plot analysis comparing the measurement errors of each of methods against the reference standard.

Results : Significant differences were observed among methods($F=8.788$, $p<0.001$). Antera 3D® demonstrated the lowest MSE(0.011), followed by video-based convex(0.018) and alpha(0.019) reconstructions. CT-based methods showed moderate accuracy (MSE=0.145–0.165), whereas formula-based methods exhibited higher errors (MSE=0.519–0.935). Bland–Altman analysis demonstrated good agreement between the video-based methods and the reference standard without systematic bias.

Conclusions : The proposed video-based Gaussian splatting method provides accuracy comparable to established techniques while offering a low-cost, non-contact, and highly accessible alternative. This approach represents a practical and scalable option for clinical and research applications in nipple reconstruction assessment.

EP-151

조직확장기를 이용한 유방 재건술에서 수술 전·후 근적외선 인도시아닌 녹색 혈관조영술의 임상적 유용성에 관한 후향적 연구

서울대병원

정용욱, 윤세훈, 홍기용*

Purpose: Perfusion-based guidance for timing expander-to-implant exchange in two-stage tissue expander/implant breast reconstruction remains limited. We used serial indocyanine green angiography (ICGA) to quantify longitudinal mastectomy skin flap (MSF) perfusion and scar vascular maturation.

Methods: Consecutive patients underwent immediate tissue expander placement after mastectomy and expander-to-implant exchange (Jan 2022 - Oct 2025) with intraoperative ICGA at stage 1 (ICGA-1; after temporary skin closure) and immediately pre-incision at stage 2 (ICGA-2) by a single plastic surgeon. Perfusion in a standardized central MSF region was normalized to the mirror-matched contralateral breast to compute a normalized relative perfusion unit ratio (NRR) (Figure 1). Perfusion recovery (PR) was the percent change in NRR between stages. Persistent venous-phase enhancement within the incision scar (Figure 2) was assessed. Predictors of PR were evaluated using linear regression; predictors of intra-scar contrast retention using logistic regression.

Results: 40 patients completed staged reconstruction with mean NRR increased from 0.77 ± 0.12 (ICGA-1) to 0.87 ± 0.09 (ICGA-2), with mean PR 10.27 ± 10.51%. In multivariable analysis, lower baseline NRR, higher ratio of rest period after final inflation to total interval between surgical stages were associated with higher PR ($p < 0.01$), whereas absolute inter-stage interval did not. Intra-scar contrast retention was independently predicted only by inter-stage interval, with majority disappearing after 289.6 days (Figure 3).

Conclusion: Serial ICGA identified two parameters: intra-flap perfusion recovery from baseline perfusion and intra-scar contrast retention which can be useful factors to evaluate safety of second stage operation and incision choice.

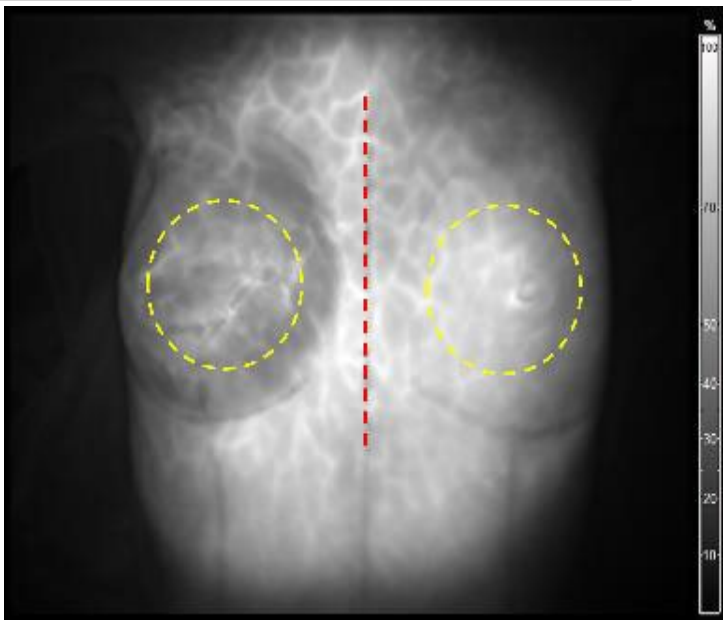

Fig 1. Standardized breast ROI–based quantification of normalized perfusion (NRR). ROIs were placed on a centrally located breast skin region expected to be most nearly perpendicular to the NIR camera axis and mirrored to the contralateral breast for normalization.

Fig 2. The intra-scar contrast enhancement during venous phase of ICGA (30 seconds after initiation of arterial phase). This patient underwent second stage implant exchange 170 days after the initial operation in the right. There was marked contrast enhancement in the previous operative scar, which sustained until the end of the examination.

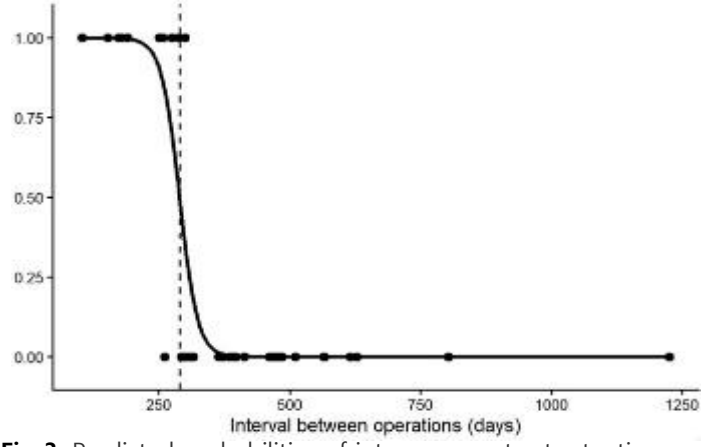

Fig 3. Predicted probabilities of intra-scar contrast retention. Each dot represents an individual patient outcome, plotted at the observed binary value of intra-scar contrast retention presence or absence. The solid line indicates the fitted logistic regression curve, and the dashed vertical line denotes the interval (289.6 days) corresponding to a predicted probability of 0.5

EP-152

방사선 치료 후 발생한 모세혈관 확장증으로 인한 유방 피부 피판 손상 및 보형물 기반 유방 재건 실패: 증례 보고

Post-radiotherapy Telangiectasia Causing Mastectomy Skin Flap Compromise and Failure of Implant-Based Breast Reconstruction

연세대학교

이주엽, 노태석, 김영석, 윤인식, 김지민, 민경현*

Purpose: Postmastectomy radiotherapy significantly increases the risk of complications in implant-based breast reconstruction. Among radiation-related changes, progressive telangiectasia may indicate underlying microvascular injury and impaired perfusion of the mastectomy skin flap. We report a case of implant reconstruction failure associated with radiotherapy-induced telangiectasia in the absence of clear infection or seroma.

Methods: : A case of progressive skin flap compromise following implant-based breast reconstruction after radiotherapy was retrospectively reviewed.

Results: A 42-year-old woman with left breast cancer underwent nipple-sparing mastectomy followed by prepectoral tissue expander insertion. After adjuvant radiotherapy to the chest wall and regional lymphatics (total dose 4005 cGy), implant-based reconstruction with a silicone implant and acellular dermal matrix was performed. Several months later, progressive erythema, skin thinning, and prominent telangiectasia developed over the mastectomy skin flap. Laboratory findings and clinical course did not clearly support overt infection or significant seroma formation. Despite conservative management and surgical intervention including partial capsulectomy and implant exchange, the skin progressively deteriorated with violaceous discoloration and epidermal erosion, suggesting radiation-induced microvascular injury and compromised skin perfusion. Ultimately, the implant was removed and the reconstruction was converted to an autologous deep inferior epigastric artery perforator (DIEP) flap. Following the conversion to autologous reconstruction, the skin condition improved markedly.

Conclusion: Post-radiotherapy telangiectasia may represent clinically significant microvascular injury that compromises mastectomy skin flap viability and jeopardizes implant-based reconstruction. Recognition of these vascular changes is important when determining reconstructive strategies in irradiated patients. Autologous tissue transfer may also help improve radiation-related skin changes and associated telangiectatic symptoms.

Fig. 1. Early postoperative erythematous change of the irradiated mastectomy skin flap.

Fig. 2. Thinning and compromised condition of the mastectomy skin flap overlying the implant during

Fig. 3. Progressive violaceous discoloration reflecting radiation-induced microvascular injury.

Fig. 4. Improved skin condition on postoperative day 15 after conversion to DIEP flap reconstruction.

EP-153

원통형 무세포진피기질을 이용한 방사선 치료 후 상외측 유방 함몰 교정: 증례 보고

(Correction of Post-Radiation Upper Lateral Breast Depression Using Cylindrical Acellular Dermal Matrix: A Case Report)

순천향대학교 부속 서울병원

박찬경, 송우진*

Purpose: Postmastectomy radiation therapy (PMRT) following two-stage breast reconstruction can induce soft tissue fibrosis and volume contraction, resulting in localized contour deformities. We report successful correction of radiation-associated upper lateral breast depression using a cylindrical acellular dermal matrix (ADM) during expander-to-implant exchange.

Methods: : Postmastectomy radiation therapy (PMRT) following two-stage breast reconstruction can induce soft tissue fibrosis and volume contraction, resulting in localized contour deformities. We report successful correction of radiation-associated upper lateral breast depression using a cylindrical acellular dermal matrix (ADM) during expander-to-implant exchange.

Results: : The previously depressed contour demonstrated marked improvement (Fig. 4). The patient was discharged on postoperative day 1 without any perioperative complications. During follow-up, no adverse events related to the ADM, including infection or contour irregularities, were observed, and the restored volume was well maintained.

Conclusion: : Radiation-induced contour depression following two-stage breast reconstruction can be effectively corrected with cylindrical ADM insertion at the time of expander-to-implant exchange. This technique provides localized structural support without additional donor-site morbidity and offers a simple and reliable option for managing PMRT-related contour deformities.

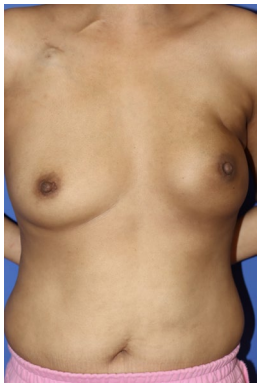

Figure 1. Preoperative photograph showing a visible depression in the upper lateral portion of the left breast.

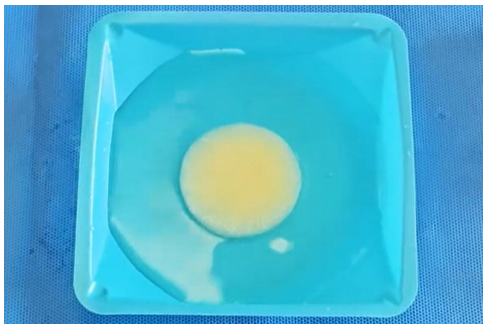

Figure 2. Cylindrical acellular dermal matrix (Surederm®; HansBiomed Co., Ltd., Seoul, Korea) used in this case, measuring 5 cm in diameter and 1 cm in thickness.

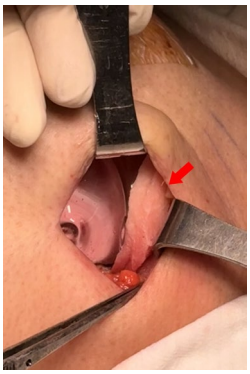

Figure 3. Intraoperative photograph demonstrating placement and fixation of the cylindrical acellular dermal matrix in the area of contour deformity.

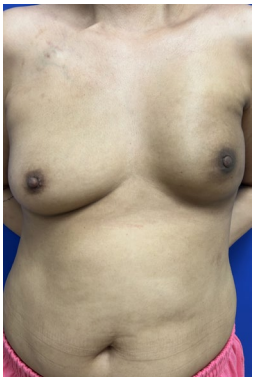

Figure 4. Postoperative photograph obtained 2 weeks after surgery, showing improvement of the upper lateral contour deformity.

EP-154

전흉근 보형물 기반 유방재건술에서 포켓형 무세포진피기질(ADM)의 ADM 사용량 감소 효과 : 유방절제술 용적과 무관

(Pocket-Type ADM Reduces Acellular Dermal Matrix Utilization Independent of Mastectomy Volume in Prepectoral Implant-Based Breast Reconstruction)

이화여자대학교

정가영, 조정목*, 이미경, 박진우

Purpose: As prepectoral implant-based breast reconstruction has become increasingly adopted, the use of acellular dermal matrix (ADM) has correspondingly increased. However, full wrapping with sheet-type ADM requires substantial material, raising concerns regarding cost and patient financial burden. This study compared surgical outcomes, operative time, and ADM utilization between pocket-type and sheet-type ADM in prepectoral implant-based reconstruction.

Methods: A retrospective analysis was performed on patients who underwent prepectoral implant-based breast reconstruction between January and December 2025. Intraoperative variables, including mastectomy volume, ADM amount used, and operative time, were evaluated. Postoperative complications were assessed.

Results: A total of 148 reconstructions were included (sheet-type, n=114; pocket-type, n=33). The mean ADM amount was significantly higher in the sheet-type group compared with the pocket-type group (298.3 ± 6.2 vs. 247.0 ± 9.0; p < 0.001). After adjusting for mastectomy volume, pocket-type ADM remained independently associated with reduced ADM usage, requiring approximately 62 units less ADM for the same mastectomy volume (β = –61.7; p < 0.001). No significant interaction between ADM type and mastectomy volume was observed. Postoperative complication rates did not differ significantly between groups.

Conclusion: Pocket-type ADM significantly reduces ADM utilization in prepectoral implant-based breast reconstruction while maintaining comparable surgical outcomes. This approach may alleviate patient financial burden without compromising safety.

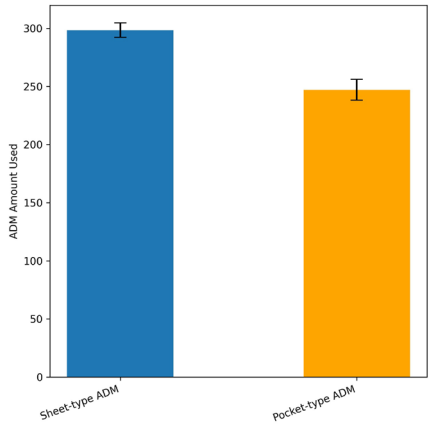

Fig. 1. Comparison of ADM amount used between sheet-type and pocket-type ADM groups.

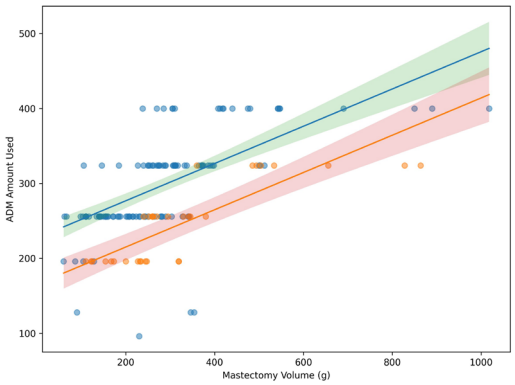

Fig. 2. Association between mastectomy volume and ADM amount used according to ADM type. Linear regression lines represent ANCOVA-adjusted models with parallel slopes. Pocket-type ADM demonstrated significantly lower ADM usage compared to sheet-type ADM after adjustment for mastectomy volume (p < 0.001)

Complications	Overall yes/N (%)	Group 1 yes/N (%)	Group 2 yes/N (%)	p-value
Seroma	3 (2.7)	3 (3.6)	0 (0.0)	1.000
Hematoma	1 (1.1)	1 (1.5)	0 (0.0)	1.000
Infection	6 (5.5)	4 (4.8)	2 (7.7)	0.625
Rupture	1 (0.9)	1 (1.2)	0 (0.0)	1.000
Contracture	10 (11.1)	9 (13.4)	1 (4.3)	0.442
Rippling	20 (19.2)	17 (21.0)	3 (13.0)	0.553
Animation deformity	1 (1.2)	1 (1.6)	0 (0.0)	1.000
Upper pole depression	42 (40.4)	36 (44.4)	6 (26.1)	0.179

Table. 1. Postoperative complication rates were not significantly different between the sheet-type(n=114) and pocket-type(n=33) groups.

EP-155

즉시보형물유방재건술에서 보형물 삽입 위치 결정에서 고려 요소들

(Considering Factors for Deciding Implant Planes in Direct-to-Implant Breast Reconstruction)

경북대학교 의과대학
성형외과학교실

장용준, 박태환, 류정엽, 서만수, 최강영, 양정덕, 정호윤, 이준석*

Purpose: Considering the increasing importance placed on the quality of life among those who survive cancer, breast reconstruction is no longer limited to only compensating for breast loss; achieving the patient's preferences is now considered. However, the optimal surgical approach (subpectoral plane vs. prepectoral plane) in single-stage direct-to-implant breast reconstruction (DTIBR) has not been established. The aim of this study was to summarize the principles for selecting between the subpectoral and prepectoral planes in DTIBR.

Methods: In this retrospective study, we evaluated 543 patients with breast cancer who underwent DTIBR between March 2018 and October 2025. Postmastectomy reconstruction was performed in the subpectoral plane when the defect showed greater breast height than width, whereas the prepectoral plane was used when breast width exceeded height (Figure 1). Complications requiring reoperation were analyzed. Patient satisfaction was evaluated based on overall satisfaction, esthetic outcome, physical symptoms, psychosocial impact, and decision satisfaction using a visual analog scale.

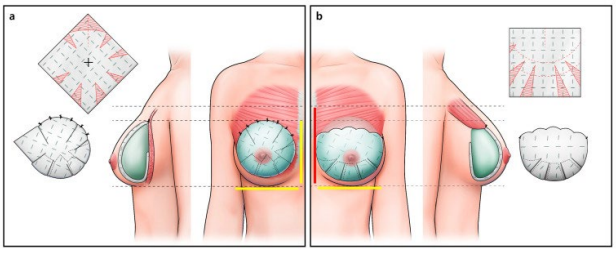

Figure 1. Direct-to-implant breast reconstruction. (a) Prepectoral breast reconstruction. Following nipple-sparing mastectomy, when the breast width was greater than or equal to the breast height, a large diamond-shaped acellular dermal matrix (ADM) was designed and positioned in the prepectoral plane. The ADM was radially trimmed to create a pocket that adequately enveloped the implant, allowing for optimal direct-to-implant (DTI) placement. (b) Subpectoral breast reconstruction. Following nipple-sparing mastectomy, a rectangular ADM was used if the breast width was smaller than the height. The pectoralis major muscle was adequately released over the upper pole to relieve tension, and the ADM was shaped in an octopus-like pattern to provide smooth, supportive coverage of the lower pole. DTI was then performed in the subpectoral plane. Yellow stick length < red stick length.

Results: The subpectoral dual-plane approach was most commonly used between 2018 and 2019, while the prepectoral plane became predominant after 2020. Overall, 83 (14.4%) patients developed major complications. The overall satisfaction score was 4.1 ± 0.80 in the subpectoral group and 4.35 ± 0.70 in the prepectoral group, showing a statistically significant difference (p value = 0.012) (Table 1) (Figure 2).

Category	Questions	Subpectoral Plane (n = 213)	Prepectoral Plane (n = 363)	*p* Value
Overall part	Q1. Overall, are you satisfied with your breast reconstruction?	4.10 ± 0.80	4.35 ± 0.70	0.012 *
Esthetic part (mean = 4.5)	Q2. Are you satisfied with breast symmetry achieved after reconstruction?	4.45 ± 0.75	4.55 ± 0.70	0.28
	Q3. Are you satisfied with the size of your breast after reconstruction?	4.50 ± 0.70	4.60 ± 0.65	0.22
	Q4. Are you satisfied with the shape of your breast after reconstruction?	4.40 ± 0.80	4.55 ± 0.75	0.18
	Q5. Are you satisfied with the scar resulted after breast reconstruction?	4.35 ± 0.85	4.50 ± 0.80	0.21
Physical symptoms (mean = 4.0)	Q6. Are you satisfied with how your breasts feel after reconstruction?	4.10 ± 0.85	3.95 ± 0.90	0.19
	Q7. Are you satisfied with the level of pain you had to endure after reconstruction?	3.85 ± 0.95	4.15 ± 0.90	0.008 *
Psychosocial part (mean = 4.2)	Q8. Have you experienced a loss of confidence or self-esteem after breast reconstruction?	4.35 ± 0.85	4.05 ± 0.90	0.018 *
	Q9. Are you satisfied with your sexual attractiveness after breast reconstruction?	4.25 ± 0.80	4.65 ± 0.65	0.24
Decisional part	Total score	4.40 ± 0.55	4.05 ± 0.85	0.091

Table 1. Patient's satisfaction using modified KNU Breast-Q. * Statistically significant difference between the two groups (p < 0.05).

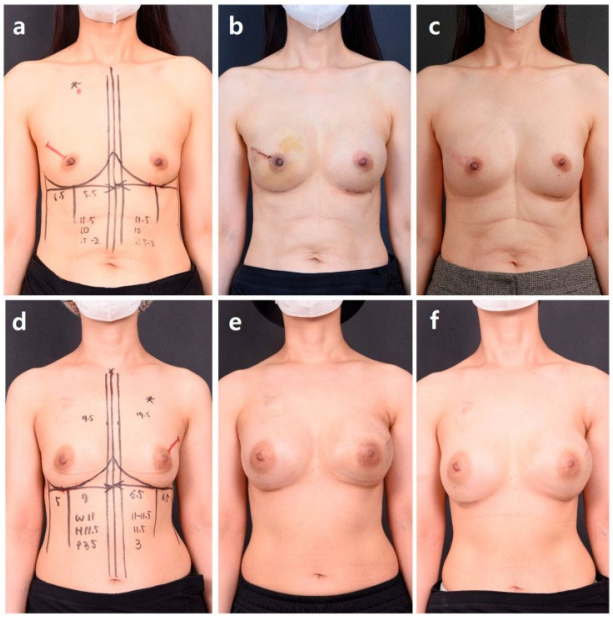

Figure 2. Prepectoral plane selection. Cases in which the preoperative breast width was greater than its height and the postmastectomy defect profile showed the same relationship. A 47-year-old woman with cancer of the right breast who has undergone right nipple-sparing mastectomy and contralateral balancing augmentation. Direct-to-implant breast reconstruction was performed on the right side using a Mentor 275 cc smooth round high-profile implant (diameter, 10.8 cm; projection, 4.4 cm), and a Sebbin LSM 210 cc implant (diameter, 11.0 cm; projection, 3.2 cm) was placed in the left breast for esthetic balancing. (a) Preoperative findings show breast volume of 180 cc. (b) Postoperative findings at 3 weeks. (c) Postoperative findings at 6 months. Cases in which the preoperative breast width smaller than its height exhibited the reversed pattern postmastectomy, showing a defect profile of breast width being greater than the height. A 44-year-old woman with cancer of the left breast who has undergone left nipple-sparing mastectomy and contralateral balancing augmentation. Direct-to-implant breast reconstruction was performed on the left side using a Mentor 330 cc smooth round high-profile implant (diameter, 10.8 cm; projection, 4.4 cm), and a Sebbin Integrity 210 cc implant (diameter, 11.0 cm; projection, 3.2 cm) was placed in the right breast for esthetic balancing. (d) Preoperative findings show breast volume of 180 cc. (e) Postoperative findings at 1 month. (f) Postoperative findings at 6 months.

Conclusion: The subpectoral and prepectoral planes have distinct advantages and limitations. Ultimately, the reconstructive surgeon should determine the most appropriate option in DTIBR. Selecting the surgical plane based on the postmastectomy defect reduces complications while improving patient satisfaction.

EP-156

전기소작 유무가 잔존 피막 리모델링에 미치는 영향: 전임상 래트 모델 비교

(Comparative Analysis of Remnant Capsule Remodeling with and without Electrocauterization in a Preclinical Rat Model)

서울대학교 의과대학
성형외과학교실[1]
보라매병원 성형외과[2]
에톤 성형외과[3]
서울대학교병원 성형외과[4]

김재우[1,2], 양희웅[1,4], 조정목[1,3], 김승빈[4], 장학[1,4], 홍기용*[1,4]

Purpose: The fibrous capsule that forms around breast implants can lead to some complications. Electrocautery is frequently used in capsule manipulation (including popcorn technique) during re-operation; however, its long-term biological effect on the remnant capsule is unknown.

This study aimed to evaluate and compare the long-term changes and remodeling processes of the remnant fibrous capsule with and without electrocauterization after silicone implant removal in a preclinical rat model.

Methods: Six Sprague-Dawley rats received bilateral silicone implants. After 3 months, the implants were removed. The left-side capsule was electrocauterized, and the right served as the non-cauterized control. Specimens were harvested 6 months later for Hematoxylin and Eosin, Masson's Trichrome, and immunohistochemistry (IHC) using turnover markers.

Results: Capsule thickness was not significantly different (p = 0.18). IHC showed significantly higher expression of α-smooth muscle actin (p = 0.01), Type I collagen (p = 0.04), and platelet endothelial cell adhesion molecule-1 (p = 0.03) in the cautery group, indicating altered long-term remodeling activity.

Conclusion: Electrocauterization of the remnant capsule stimulates more active turnover and enhanced angiogenesis. These findings suggest electrocautery induces a distinct, long-term activated biological response in the fibrous capsule, which may inform clinical strategies for capsular revision.

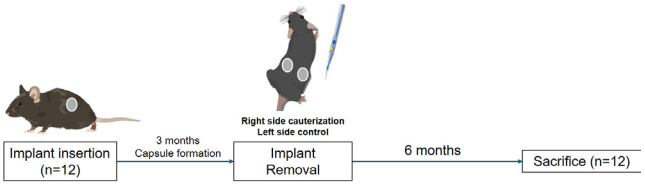

Fig 1. Schematic representation of overall experimentation

Fig 2. Gross photo of harvested capsule specimen and harvested site. The right column are electrocauterized, and the left are non-cauterized control specimens. Cauterization marks are noted in yellow.

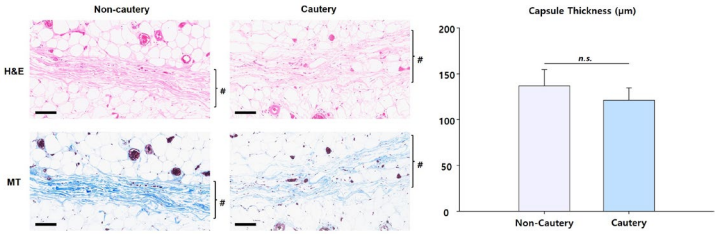

Fig 3. Hematoxylin-Eosin staining and Masson's Trichrome staining. The left is a non-cauterized control, while the right is an electrocauterized specimen. Comparison of capsule thickness between cauterized and non-cauterized groups was insignificant (p = 0.18)

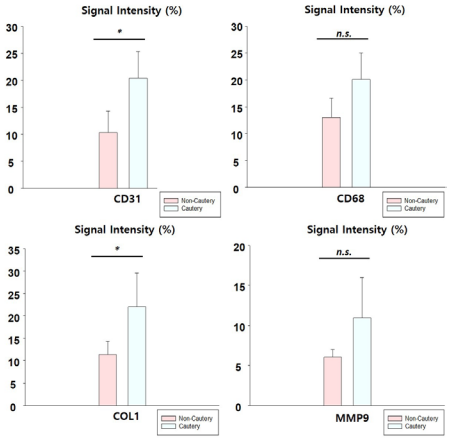

Fig 4. IHC staining of CD31, CD68, type 1 collagen, matrix metalloproteinase-9 and comparison of signal intensity.

EP-157

무세포 진피 기질의 탈세포화 방법이 보형물 기반 유방 재건술의 수술 결과에 영향을 미치는가?

(Is Decellularization Process of Acellular Dermal Matrix Related to Surgical Outcome in Implant-Based Breast Reconstruction?)

아주대학교 의과대학
성형외과학교실

한형민, 이순성, 이일재*

Purpose: Various ADM products employ different decellularization methods in implant-based breast reconstruction, yet the impact on surgical outcomes remains unclear. This study compared supercritical CO_2-decellularized ADM (SCDerm®) with conventional ADMs.

Methods: A retrospective study of 768 implant-based breast reconstructions (Jan 2020–Dec 2024) at a single institution. SC-CO_2 group (SCDerm®; n=181) vs. conventional ADMs (n=587). Primary outcomes: return to OR and implant loss. Analysis: GEE and IPTW.

Table 1. Baseline Patient Characteristics

Variable	Total (N=768)	SCDerm® (n=181)	Others (n=587)	p-value
Demographics				
Age, years (mean±SD)	47.27±7.91	46.77±7.66	47.42±7.99	0.474
BMI, kg/m² (mean±SD)	23.13±6.06	23.41±10.67	23.05±3.61	0.181
Comorbidities, n (%)				
Hypertension	83 (10.8)	15 (8.3)	68 (11.6)	0.212
Diabetes mellitus	32 (4.2)	8 (4.4)	24 (4.1)	0.845
Smoking	39 (5.1)	5 (2.8)	34 (5.8)	0.105
Oncologic treatment, n (%)				
Neoadjuvant chemotherapy	214 (27.9)	46 (25.4)	168 (28.6)	0.400
Adjuvant chemotherapy	498 (64.8)	90 (49.7)	408 (69.5)	<0.001
Preoperative radiotherapy	47 (6.1)	7 (3.9)	40 (6.8)	0.148
Postoperative radiotherapy	139 (18.1)	35 (19.3)	104 (17.7)	0.621
Mastectomy type, n (%)				0.009
SSM	199 (25.9)	39 (21.5)	160 (27.3)	
NSM	528 (68.8)	132 (72.9)	396 (67.5)	
MRM	10 (1.3)	6 (3.3)	4 (0.7)	
Reconstruction method, n (%)				0.043
Direct-to-implant	427 (55.6)	113 (62.4)	314 (53.5)	
Tissue expander	311 (40.5)	65 (35.9)	246 (41.9)	
Delayed reconstruction	30 (3.9)	3 (1.7)	27 (4.6)	
Implant position, n (%)				<0.001
Prepectoral	533 (69.4)	160 (88.4)	373 (63.5)	
Subpectoral	235 (30.6)	21 (11.6)	214 (36.5)	

SCDerm® , supercritical carbon dioxide-processed acellular dermal matrix; BMI, body mass index; SSM, skin-sparing mastectomy; NSM, nipple-sparing mastectomy; MRM, modified radical mastectomy.

Table 2. Complication Rates by ADM Type

ADM Type	n	Return to OR	Major	Minor
SCDerm®	181	8 (4.4)	5 (2.8)	3 (1.7)
Conventional ADMs	587	62 (10.5)	29 (4.9)	33 (5.6)
CryoDerm®	286	32 (11.2)	14 (4.9)	18 (6.3)
OneStep®	123	17 (13.8)	8 (6.5)	9 (7.3)
MyDerm®	113	7 (6.2)	4 (3.5)	3 (2.7)
PZB®	38	4 (10.5)	2 (5.3)	2 (5.3)
CelluDerm®	25	2 (8.0)	1 (4.0)	1 (4.0)
Others	2	0 (0.0)	0 (0.0)	0 (0.0)
Total	768	70 (9.1)	34 (4.4)	36 (4.7)

Values are presented as n (%). SCDerm® , supercritical carbon dioxide-processed acellular dermal matrix; ADM, acellular dermal matrix.

Results: Overall RTOR: 9.1% (70/768). SCDerm® 4.4% vs. conventional 10.5% (Table 2). GEE analysis (ref: OneStep®): SCDerm® OR=0.887, p=0.002 (Table 3). Risk factors: postop RT (OR=1.115, p=0.002), subpectoral position (OR=1.077, p=0.013). After IPTW adjustment (Table 4), SCDerm® showed significant RTOR reduction (OR=0.939, 95% CI 0.903–0.978, p=0.002). Implant loss: NS (OR=0.911, p=0.142) (Table 5).

Table 3. GEE Multivariable Analysis

Variable	OR	95% CI	p-value
ADM Type (ref: OneStep®)			
SCDerm®	0.887	0.824–0.956	0.002
CryoDerm®	0.989	0.919–1.064	0.757
MyDerm®	0.910	0.840–0.986	0.022
PZB®	0.928	0.820–1.051	0.238
CelluDerm®	0.914	0.803–1.039	0.170
Postoperative radiotherapy	1.115	1.040–1.196	0.002
Pathology: ILC (ref: DCIS)	1.173	1.033–1.333	0.014
Implant position: Subpectoral	1.077	1.016–1.142	0.013

OR, odds ratio; CI, confidence interval; ILC, invasive lobular carcinoma; DCIS, ductal carcinoma in situ. Model adjusted for age, BMI, hypertension, diabetes, smoking, chemotherapy, radiotherapy, pathology, mastectomy type, axillary procedure, reconstruction method, and implant position.

Table 4. Covariate Balance (IPTW)

Variable	Before IPTW			After IPTW		
	SCDerm®	Others	p	SCDerm®	Others	SMD
Age, years	46.77±7.66	47.42±7.99	0.326	47.25	47.24	0.001
BMI, kg/m²	23.41±10.67	23.05±3.61	0.657	22.98	23.07	0.015
Hypertension	15 (8.3)	68 (11.6)	0.212	17 (10.1)	63 (10.8)	0.023
Diabetes	8 (4.4)	24 (4.1)	0.845	5 (3.0)	24 (4.1)	0.059
Smoking	5 (2.8)	34 (5.8)	0.105	6 (3.6)	30 (5.1)	0.074
Adjuvant CTx	90 (50.0)	408 (69.5)	<0.001	94 (55.6)	377 (64.3)	0.178
Prepectoral	160 (89.4)	373 (63.5)	<0.001	125 (74.0)	408 (69.6)	0.098

SMD, standardized mean difference; CTx, chemotherapy. SMD < 0.10 indicates excellent balance.

Table 5. IPTW-Weighted Primary Outcomes

Outcome	OR	95% CI	p-value
SCDerm® vs Others (ref)			
Return to OR	0.939	0.903–0.978	0.002
Implant loss	0.911	0.805–1.032	0.142

OR, odds ratio; CI, confidence interval; IPTW, inverse probability of treatment weighting. Weighted N = 762.

Conclusion: SC-CO_2 decellularized ADM (SCDerm®) showed significantly lower RTOR rates compared to conventional ADMs. The detergent-free processing may reduce complications by eliminating residual chemical irritants, supporting consideration of decellularization method in ADM selection.

EP-158

불완전한 파라핀 제거술 후 발생한 중증 양측 유방 구축에서 광범위 절제 및 양측 유경성 복직근 피판 재건을 시행한 증례보고

(Severe Bilateral Breast Contracture after Previous Incomplete Paraffin Excision Managed with Skin-Inclusive Radical Excision and Bilateral Pedicled Transverse Rectus Abdominis Myocutaneous Flap Reconstruction: A Case Report)

인제대학교 해운대백병원

신예지, 윤성호, 선욱, 이경아*

Purpose: Breast paraffin injection frequently induces progressive paraffinoma, a chronic foreign-body reaction. Surgical management becomes particularly formidable in cases with prior incomplete excision, leading to a complex interplay of residual foreign material and extensive scar contracture. While conventional approaches focus on contour correction, severe skin involvement necessitates a radical, skin-inclusive excision.

Methods: A 61-year-old female presented with severe bilateral breast contracture following paraffin injection 30 years prior and a subsequent failed removal surgery. Physical examination and imaging revealed diffuse dystrophic calcifications involving the entire skin envelope and the presternal area (Fig. 1). A radical resection was performed, encompassing the bilateral breast tissue, nipple-areolar complexes (NAC), and involved presternal skin. The resulting extensive soft tissue defect was reconstructed using bilateral pedicled transverse rectus abdominis myocutaneous (TRAM) flaps (Fig. 2).

Results: Histopathological analysis confirmed residual paraffinoma characterized by chronic inflammation, foreign-body giant cell reaction, and dense interstitial fibrosis. The postoperative course was uneventful. At the 1-year follow-up, the patient remained asymptomatic with stable reconstructive outcomes and no evidence of recurrence or skin compromise (Fig. 3).

Conclusion: Extensive paraffinomas with secondary skin contracture from prior surgical failures require an aggressive, radical surgical approach. This case demonstrates that bilateral pedicled TRAM flaps provide a robust and reliable solution for total breast reconstruction following wide-safety-margin, skin-inclusive resection.

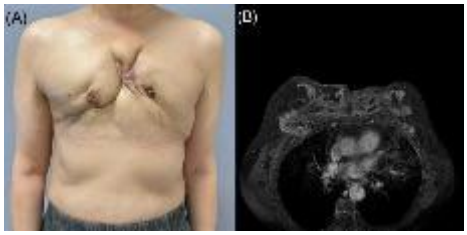

Fig. 1. Preoperative clinical and imaging findings. (A) Clinical Presentation: Severe bilateral breast deformity and skin contracture following paraffin injection and incomplete prior excision. Note the extensive soft tissue distortion and loss of the natural skin envelope. (B) Breast MRI: T2-weighted imaging demonstrates diffuse infiltrative paraffinomas involving both breasts and the presternal area, confirming the necessity for radical, skin-inclusive resection.

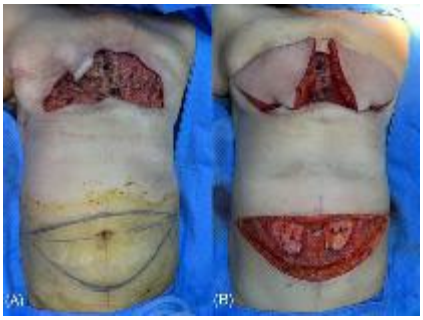

Fig. 2. Intraoperative findings and surgical procedure. (A) Intraoperative view after skin-inclusive excision by the general surgery team, showing the extensive defect. (B) Intraoperative photograph during TRAM flap reconstruction, demonstrating flap inset for defect coverage.

Fig. 3. Postoperative clinical photographs after bilateral TRAM flap reconstruction. (A) Immediate postoperative clinical photograph demonstrating successful bilateral TRAM flap. (B) Long-term follow-up at 12 months postoperatively, showing stable reconstruction without complications.

EP-159

임플란트 기반 재건 후 피부 손상을 동반한 난치성 장액종에서 유경성 복직근피판 전환술: 증례보고 및 실제 적용 적응증

(Conversion to Pedicled Transverse Rectus Abdominis Myocutaneous Flap for Refractory Seroma with Skin Compromise after Implant-Based Reconstruction: A Case Report and Practical Indications)

인제대학교 해운대백병원

<u>신예지</u>, 윤성호, 선욱, 이경아*

Purpose: Refractory seroma accompanied by progressive skin compromise poses a critical threat to implant-based breast reconstruction. When complications persist despite repeated surgical revisions, salvage strategies must be redefined. We report a successful salvage case and propose practical indications for converting to autologous reconstruction.

Methods: A patient underwent two-stage implant-based reconstruction following a mastectomy in April 2021. The clinical course was complicated by cellulitis and refractory seroma, necessitating expander removal and capsulectomy in August 2021. After stabilization, a second tissue expander was placed in December 2022, followed by a permanent implant in December 2023 (Fig. 1). However, a recurrent refractory seroma led to skin compromise and a focal defect (Fig. 2). In February 2024, salvage surgery was performed, involving implant removal, radical capsulectomy, and complete excision of the seroma cavity, followed by reconstruction using a pedicled transverse rectus abdominis myocutaneous (TRAM) flap (Fig. 3).

Results: The postoperative recovery was uneventful, with the skin defect successfully replaced by stable, vascularized tissue. At the one-year follow-up, there was no evidence of recurrent seroma, infection, or other complications (Fig. 4).

Conclusion: Conversion to autologous reconstruction should be considered when: (1) seroma persists despite aggressive management, (2) skin compromise is progressive, or (3) a chronic cavity with pathological capsular tissue is present. In such cases, radical excision combined with a TRAM flap provides a reliable and definitive salvage solution.

Fig. 1. Clinical photographs after replacement with the second tissue expander. (A) Preoperative view with the second tissue expander in situ. (B) Postoperative view following the exchange of the second tissue expander for a permanent implant.

Fig. 2. Refractory seroma after implant-based reconstruction. Persistent fluid collection is observed despite previous interventions.

Figure 3. Intraoperative findings and surgical procedure. (A) Intraoperative view demonstrating a focal skin defect and the underlying refractory seroma cavity during the elevation of the pedicled TRAM flap. (B) Gross specimen of the excised chronic seroma cavity and the inflamed capsule.

Fig. 4. Postoperative clinical photographs after TRAM flap reconstruction. (A) Follow-up at 7 days postoperatively demonstrating stable flap integration. (B) Long-term follow-up at 13 months postoperatively, showing a stable outcome without any evidence of recurrent seroma or complications.

EP-160

유방절제술 후 ADM-wrapping 보형물 기반 유방재건에서 고정(fixation) 여부에 따른 합병증 발생률 비교: 후향적 코호트 연구

(Complication Rates According to Fixation Versus Non-Fixation in ADM-Wrapped Implant-Based Breast Reconstruction : A Retrospective Cohort Study)

부산대학교

정희태, 박종수*

Purpose: To evaluate whether fixation of ADM-wrapped implants reduces postoperative complications compared with non-fixation in immediate breast reconstruction following mastectomy.

Methods: A retrospective cohort study included 65 patients (68 breasts) undergoing immediate ADM-wrapped implant-based reconstruction between June 2024 and December 2025. Thirty-one patients underwent implant fixation to the pectoralis muscle or chest wall, and 34 patients (37 breasts) underwent reconstruction without fixation; all patients used postoperative compressive garments. Complications analyzed were implant malposition, mobile implant, infection, rippling, skin flap necrosis, seroma, hematoma, fat necrosis, capsular contracture, and implant change or loss. Categorical variables were compared using Fisher's exact test.

Results: Mean age was 48.1 ± 8.5 years in the fixation group and 50.1 ± 8.3 years in the non-fixation group (p = 0.341). Mean BMI was higher in the fixation group (23.5 ± 2.9 vs. 22.1 ± 2.5 kg/m², p = 0.036). Total complications were similar (16 vs. 16, p = 0.49). No implant malposition occurred (p = 1.0). Rates of mobile implant (3.2% vs. 2.7%, p = 1.0), rippling (6.5% vs. 5.4%, p = 0.60), major skin flap necrosis (6.5% vs. 2.7%, p = 0.60), minor necrosis (9.7% vs. 2.7%, p = 0.65), hematoma (6.5% vs. 0%, p = 0.45), seroma (12.9% vs. 18.9%, p = 0.23), capsular contracture (0% vs. 2.7%, p = 0.45), and implant change or loss (3.2% vs. 2.7%, p = 1.0) did not differ significantly.

Conclusion: Implant fixation did not significantly reduce postoperative complications. Routine fixation may not be necessary and should be individualized

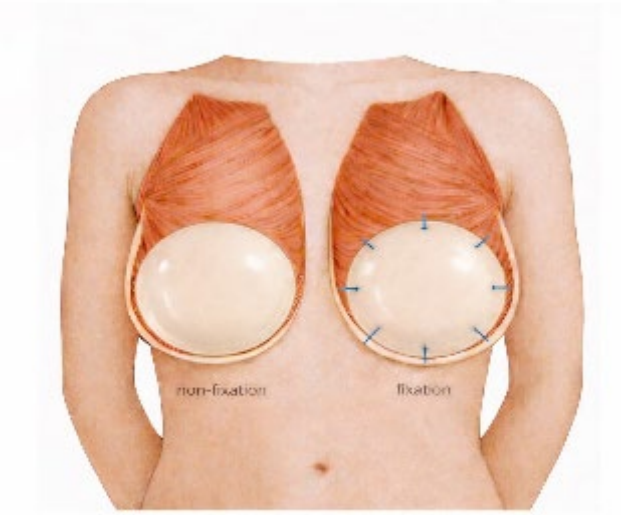

Fig. 1. Schematic Illustration of Fixation versus Non-Fixation Techniques. This illustration shows right-side non-fixation and left-side fixation methods.

Table 1. Comparison of postoperative complication between the fixation and non-fixation groups after direct-to-implant reconstruction.

	Fixation N=31 (%)	Non-Fixation N=37(%)	*P value*
Total Complications	16	16	0.49
Implant malposition	0	0	1.0
Mobile implant	1	1	1.0
Infection	2	2	1.0
Rippling	2	1	0.6
Skin flap necrosis			
Major	2	1	0.6
Minor	3	2	0.65
Hematoma	1	0	0.45
Seroma	4	7	0.23
Fat necrosis	0	0	1.0
Capsular Contracture	0	1	0.45
Implant change or loss	1	1	1.0

Table 2. Definition of Complications

Implant malposition: Implant displacement ≥5 cm from the intended position
Mobile implant: Lateral implant displacement ≥10 cm between sitting and supine positions
Rippling: Grade ≥2 (visible on movement; visible at rest)
Capsular contracture: Baker grade III or IV
Skin flap necrosis:
Major: Full thickness skin necrosis; Surgical intervention required; Lead to implant removal
Minor: Partial thickness skin necrosis; Spontaneously healed after dressing

EP-161

유두보존유방절제술 후 2단계 보형물 기반 유방재건에서 무세포진피기질 피복 방법에 따른 수술 결과의 차이

(Impact of Total Versus Partial Acellular Dermal Matrix Coverage in Two-stage Implant-Based Reconstruction After Nipple-Sparing Mastectomy)

부산대학교

금창렬, 이재우, 서정렬, 남수봉*

Purpose: Acellular dermal matrix (ADM)는 prepectoral 보형물 기반 유방 재건에서 보형물 피복 및 연부조직 지지를 위해 널리 사용되고 있다. 그러나 ADM의 적용 범위에 따른 임상적 효과는 아직 명확하지 않다. 본 연구에서는 보조치료 여부를 고려하여 ADM의 부분 적용과 전체 적용 간 수술 후 합병증을 비교하고자 하였다.

Methods: 2019년부터 2023년까지 유두보존유방절제술 후 2단계 prepectoral 재건을 시행받은 환자를 대상으로 후향적 코호트 연구를 시행하였다. 환자들은 부분 ADM 적용군(n=109)과 전체 ADM 적용군(n=51)으로 나뉘었다.

부분 ADM군은 조직 확장기 삽입 시 ADM을 하부 절반에 적용하고, 2차 보형물 삽입 시 상부에 추가로 피복하였다. 전체 ADM군에서는 조직 확장기 삽입 시점부터 ADM을 이용하여 보형물 전체를 피복하였다.

보조치료 여부에 따라 무치료군, 항암치료 단독군, 방사선치료 단독군, 항암+방사선 병합군의 네 군으로 분류하였고, 2차 보형물 삽입 후 1년 이내 발생한 합병증을 분석하였다. 주요 평가 변수는 장액종과 Baker grade III–IV의 피막 구축이었다.

Results: 피막 구축은 부분 ADM 군에서 14.3%, 전체 ADM 군에서 7.8%에서 발생하였으며, 통계적으로 유의한 차이는 없었다(p=0.28). 장액종은 각각 11.9%, 7.8%에서 발생하였으며, 역시 유의한 차이는 없었다(p=0.44).

보조치료 여부에 따른 하위군에서 전체 ADM군이 부분 ADM군에 비해 일관되게 낮은 피막 구축 발생률을 보였다.

특히 보조치료를 시행하지 않은 군(7.4% vs 0%)과 항암치료 단독군(20.8% vs 0%)에서 상대적으로 큰 차이를 보였다.

Conclusion:

전체 ADM 적용은 모든 보조치료 하위군에서 피막 구축 감소 경향을 보였다. 이는 ADM의 광범위한 적용이 피막 구축을 예방하는데 잠재적인 효과를 가질 수 있음을 시사하며, 향후 더 많은 표본을 포함한 추가 연구가 필요할 것으로 생각된다.

Table 1. Baseline characteristics

Variable	Partial ADM (n=109)	Complete ADM (n=51)	p-value
Chemotherapy, n (%)	45 (41.3%)	26 (51.0%)	0.24
Radiotherapy, n (%)	31 (28.4%)	31 (60.8%)	<0.001

Table 2. Overall complications within 1 year after implant insertion

Outcome	Partial ADM (n=109)	Complete ADM (n=51)	p-value
Capsular contracture	15 (14.3%)	4 (7.8%)	0.28
Seroma	13 (11.9%)	4 (7.8%)	0.44

Table 3. Capsular contracture by adjuvant therapy

Group	Partial ADM	Complete ADM	p-value
No therapy	4/54 (7.4%)	0/12 (0%)	0.331
CTx only	5/24 (20.8%)	0/8 (0%)	0.160
RTx only	2/10 (20.0%)	1/13 (7.7%)	0.385
CTx + RTx	4/21 (19.0%)	3/18 (16.7%)	0.847

Table 4. Seroma by adjuvanat therapy

Group	Partial ADM	Complete ADM	p-value
No therapy	1/54 (1.9%)	1/12 (8.3%)	0.236
CTx only	5/24 (20.8%)	0/8 (0%)	0.160
RTx only	2/10 (20%)	1/13 (7.7%)	0.385
CTx + RTx	5/21 (23.8%)	2/18 (17.9%)	0.303

EP-162

가성혈관종성 기질증식증으로 인한 양측 거대유방증에서 피부 절제 유방절제술 후 보형물을 이용한 즉시 유방재건술

Immediate direct-to-implants breast reconstruction after bilateral gigantomastia caused by pseudoangiomatous stromal hyperplasia

고려대학교

이수빈, 이형철 *, **정승필, 이정현**

Background: Gigantomastia is a rare condition characterized by excessive breast enlargement causing physical and psychological distress, often influenced by hormonal factors. When associated with pseudoangiomatous stromal hyperplasia (PASH), management remains unclear and controversial. Surgical treatment is often required, and this report presents two patients who underwent mastectomy with immediate direct-to-implant reconstruction.

Case report A 43-year-old woman (patient 1, Fig. 1) presented with recurrent gigantomastia after prior reduction mammoplasty, showing rapid breast regrowth within months. Imaging revealed multiple masses with increased vascularity, and histopathology later confirmed PASH. (Fig. 3) She underwent bilateral skin-reducing mastectomy with immediate implant-based reconstruction and free nipple composite grafting. The resected tissue weighed 4,343 g on the right and 4,467 g on the left, with 360 cc implants inserted, and maintained stable results without recurrence at 3 years. (Fig. 5) A 39-year-old woman (patient 2, Fig. 2) presented with progressive breast enlargement of more than two cup sizes over 1–2 years, causing functional impairment, with no evidence of malignancy on evaluation. She underwent bilateral skin-reducing mastectomy followed by immediate implant-based reconstruction. The resected tissue weighed 3,403 g on the right and 3,825 g on the left, and 320 cc implants were inserted using a Wise-pattern skin redraping technique. At 3 months postoperatively, no recurrence was observed and outcomes were stable. (Fig. 4)

Discussion: PASH is a rare benign breast disease with variable presentations, ranging from incidental findings to palpable masses or gigantomastia. Histologically, it shows myofibroblastic proliferation with slit-like spaces resembling low-grade angiosarcoma. Imaging findings often mimic fibroadenoma, making diagnosis challenging. Due to its rarity, standardized treatment has not been established, but surgical excision is recommended for large, rapidly growing, or suspicious lesions. Recurrence rates after excision vary widely, and previous reports show frequent recurrence even after reduction mammoplasty or local excision. Many recurrent cases ultimately require mastectomy, as incomplete removal increases recurrence risk. Although mastectomy is effective, it can cause significant psychological distress, particularly in younger patients. Immediate breast reconstruction and appropriate management of the nipple–areolar complex can improve aesthetic and psychological outcomes.

Conclusion: To the best of our knowledge, this is the first case report of immediate breast reconstruction using the direct-to-implant technique in a patient with recurrent bilateral gigantomastia caused by PASH who underwent therapeutic mastectomy. The direct-to-implant approach offers a convenient one-stage reconstruction option with good aesthetic outcomes. Further research and clinical experience will contribute to refining the selection criteria for this technique in patients with PASH and optimizing overall reconstructive strategies in the future.

Figure 1. Serial clinical photographs of patient 1 demonstrating progressive breast enlargement despite previous surgery. These images illustrate the failure of the initial surgical intervention and the need for additional treatment.
(A) A 43-year-old patient with a rapid, more than two-fold increase in breast size within a year.
(B) Four months after reduction mammoplasty at a local clinic, the breast size began to increase again.
(C) Preoperative photograph obtained at a year after undergoing reduction mammoplasty.

Figure 2. Preoperative clinical photograph of patient 2 presenting with a 2-cup size breast enlargement over the past 1–2 years.

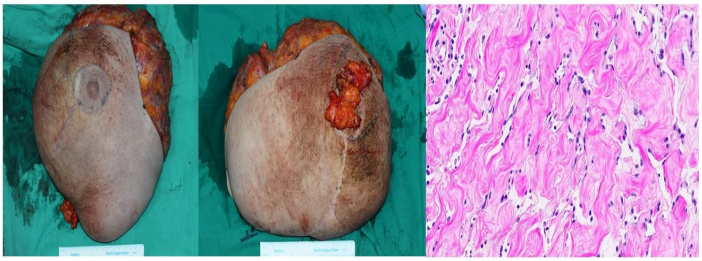

Figure 3. Gross specimen and pathological findings following skin-reducing mastectomy of patient 1. These pathological findings are consistent with a proliferative vascular process and support the diagnosis suggested by the imaging studies.(A) Specimens obtained after skin-reducing mastectomy via a Wise pattern. Post-mastectomy, the left breast tissue weighed 4467 g and right breast tissue weighed 4343 g.(B) Microscopic examination of the excised masses. Histologically, complex interanastomosing channels lined by slender spindle cells were present in the dense collagenous intralobular and interlobular stroma. (Hematoxylin and eosin, 20×).

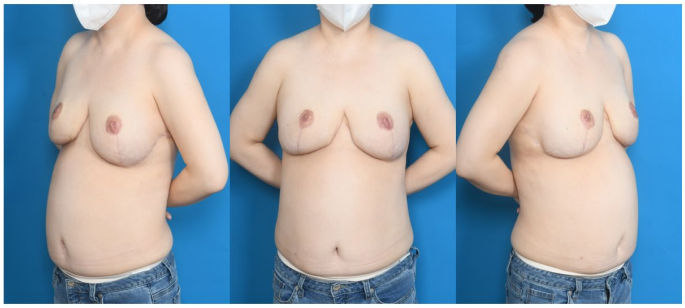

Figure 4. Postoperative appearance 10 months after surgery of patient 1. The photographs demonstrate stable breast contour and complete integration of the free nipple grafts without evidence of graft necrosis or recurrent enlargement. These findings indicate a favorable long-term surgical outcome and support the effectiveness of the procedure.

EP-163

장기 혈액투석 환자에서 ADM을 이용한 Prepectoral 임플란트 기반 즉시 유방재건

(Immediate Prepectoral Implant-based Breast Reconstruction using Acellular Dermal Matrix in a Patient Undergoing Long-term Hemodialysis)

대구가톨릭대학교
의과대학 성형외과학교실

박재용, 심정수*, 오상아

Purpose: Patients with end-stage renal disease (ESRD) undergoing maintenance hemodialysis are considered high-risk candidates for elective reconstructive procedures due to impaired wound healing, immune dysfunction, and increased susceptibility to infection. Evidence regarding implant-based breast reconstruction in this population remains limited. We report a case of immediate implant-based breast reconstruction using acellular dermal matrix (ADM) in a patient receiving long-term hemodialysis.

Methods: A 65-year-old woman with ESRD, HBV carrier status, and hypertension underwent nipple-sparing mastectomy followed by immediate breast reconstruction using a prepectoral implant placement technique with ADM support. A 170-cc smooth-surface, round, moderate classic profile silicone implant (Mentor; REF 350-7170MC, LOT 2033787, SN 2033787-047) was used, along with a 16 × 16 cm ADM (thickness 1.0–2.0 mm; SCDERM RECON, 250192S0002). Perioperative management was coordinated with the nephrology team, including optimization of dialysis timing and fluid balance. Preoperative hemodialysis was performed at a local medical center on the day prior to surgery, followed by surgery. Postoperative hemodialysis was resumed on postoperative day 1 at our institution and continued at 2-day intervals on weekdays until discharge. Hemodialysis was performed using a standard bicarbonate-based dialysate consisting of Hemosol® A solution (5.5 L) and BiBag® powder (650 g). A 1 g bolus of cefazolin was administered as empirical antibiotic prophylaxis preoperatively. No antibiotics were administered postoperatively

Results: Perioperative laboratory findings after hemodialysis demonstrated no clinically significant electrolyte imbalance, with Na/K/Cl levels of 144/4.9/97 mmol/L preoperatively and 153/4.3/107 mmol/L postoperatively. Renal function parameters, including BUN (mg/dL), Cr (mg/dL), and eGFR (mL/min/1.73 m²), were 32.2/4.89/9 preoperatively and 21.5/3.50/13 postoperatively, consistent with ESRD status and showing appropriate post-dialysis changes. The postoperative course was uneventful despite the patient's high-risk condition. Major complications, including hematoma, seroma, surgical site infection, wound dehiscence, or implant loss, did not occur. With a body mass index of 27.7, surgical drain removal was achieved within the expected postoperative period, with the 100-cc Jackson–Pratt drain removed on postoperative day 9 and the 400-cc Hemovac on postoperative day 11. The patient underwent hemodialysis on postoperative day 13 in accordance with her regular schedule and was discharged on postoperative day 14, with a total hospital stay of 16 days. The patient achieved stable reconstruction with satisfactory aesthetic outcomes during follow-up.

Conclusion: This case suggests that immediate implant-based breast reconstruction using ADM may be a feasible option even in patients undergoing long-term hemodialysis when careful multidisciplinary perioperative management is implemented. Larger studies are warranted to further evaluate its safety and clinical applicability.

Fig. 1. Preoperative photograph of a 65-year-old woman with ESRD prior to unilateral nipple-sparing mastectomy and implant-based reconstruction with ADM support. The lesion, measuring 2.7 × 3.1 cm, extends into the superior aspect of the upper outer quadrant.

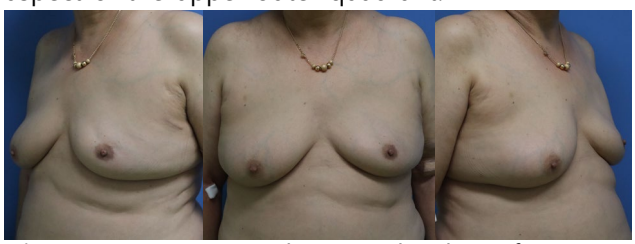

Fig. 2. Postoperative photograph taken after 6months 22 days after implant placement. No major complications occured,.

EP-164

국소 진행성 유방 종양을 모방한 거대 엽상종양 1례

(Angioleiomyoma of the Lower Lip Clinically Mimicking a Mucocele: A Case Report)

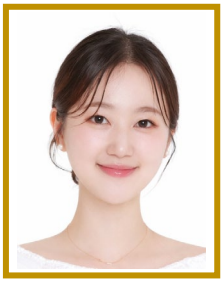

가톨릭대학교 의과대학
성형외과교실 [1]
일반외과교실 [2]
김정현 [1], 이준호 [1], 정성노 [1], 김용석 [2], **서보미** [1] *

Purpose: Phyllodes tumors of the breast are rare fibroepithelial neoplasms that account for 0.3 to 1% of all breast tumors. Their inherent recurrence or metastatic potential necessitates surgical removal and histopathological grading. Giant phyllodes tumors over 10cm in diameter are very uncommon in developed nations due to the breast cancer screening system.

Methods: This 37 year-old female patient presented with a fungating mass with extensive discharge and surface bleeding for which she had recieved bleeding control several times in the past year. She had never undergone a breast cancer screening. Biopsy was performed suspecting malignancy, but pathology reports sugessted neurofibroma. Computed tomography findings revealed an irregular heterogenously enhancing mass of the left breast, 20cm at maximum length, with areas of low attenuation suggesting cystic degeneration or necrosis. Several left axillary lymph nodes were enlarged.

Results: Mastectomy of the lesion resulted in a specimen weighing 2.02kg, and an 22 x 16 cm soft tissue defect with exposed pectoralis major fascia. The patient refused other reconstructive options and coverage was done with a split-thickness skin graft.

Histopathological findings revealed epithelial cells lining clefts and cellular spindle cell stroma, correlating with the diagnosis of phyllodes tumor. Stromal atypia was mild, stromal cellularity mildly increased, and mitotic activity was <5/10 HPF, indicating classification of a benign subtype.

Conclusion: Rapidly growing giant phyllodes tumors clinically resemble malignant lesions, with fungating or necrotic areas and high vascularity. Complete surgical excision is crucial, but lymph node dissection is not necessary. Monitoring for local recurrence is essential.

Fig. 1. Preoperative clinical photograph
A large fungating mass occupying the left breast is noted, with surface ulceration, active bleeding, and serosanguinous discharge. The lesion shows rapid growth and extensive skin involvement.

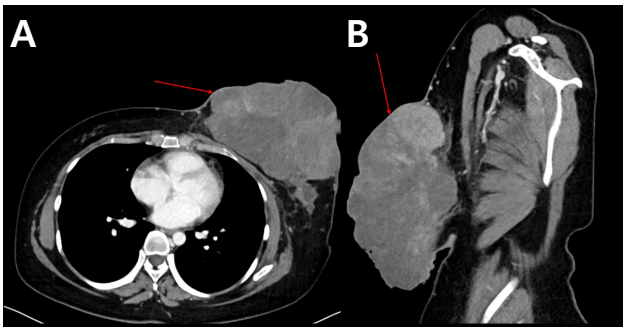

Fig. 2. Preoperative computed tomography (CT) findings.
Axial (A) and sagittal (B) contrast-enhanced CT images demonstrate a large, irregular, heterogeneously enhancing mass in the left breast measuring approximately 16×10×20 cm. Areas of low attenuation suggest cystic degeneration or necrosis. Associated overlying skin thickening and multiple enlarged left axillary lymph nodes are noted.

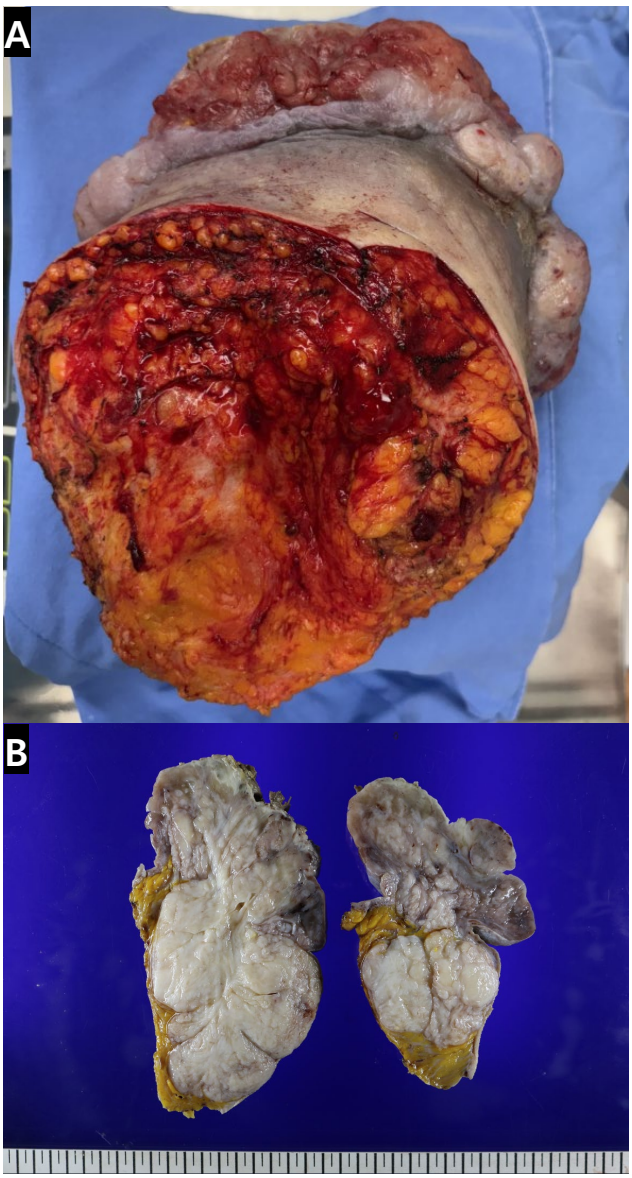

Fig. 3. Gross findings of the resected tumor.
(A) The resected specimen shows a large, well-circumscribed, lobulated mass measuring 19.5 × 9.0 cm.
(B) The cut surface is firm and pale gray with a bulging appearance and heterogeneous internal architecture.

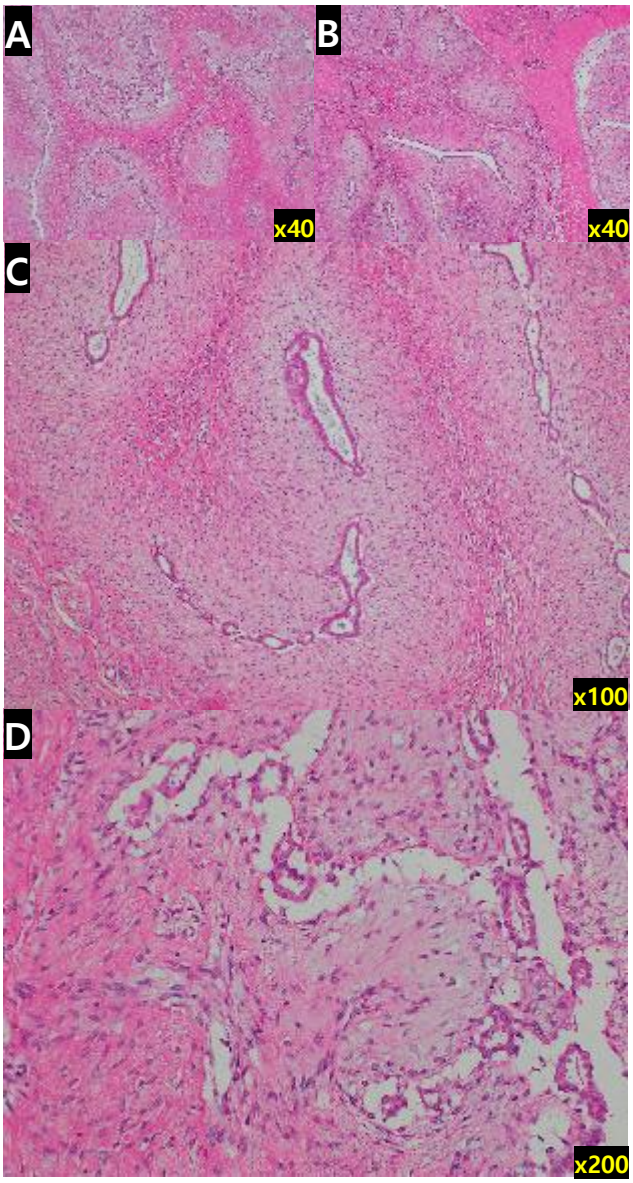

Fig. 4. Histopathologic findings of the tumor.
(A, B) Low-power views (H & E stain, ×40) demonstrate a biphasic fibroepithelial lesion with characteristic leaf-like architecture.
(C) At intermediate magnification (×100), mildly increased stromal cellularity surrounding epithelial-lined clefts is observed.
(D) High-power view (×200) reveals spindle-shaped stromal cells with mild cytologic atypia and low mitotic activity (<5 per 10 high-power fields), consistent with a benign phyllodes tumor.

EP-165

대흉근 전방 유방 재건술에서 포켓형 무세포 동종진피를 이용한 유방상부 표면 주름의 예방

(Prevention of upper pole rippling in prepectoral breast reconstruction using pocket-type ADM)

국민건강보험공단 일산병원

송준호, 전여름*

Purpose: Although prepectoral direct-to-implant (DTI) reconstruction offers several advantages, it carries a risk of implant rippling due to soft tissue deficiency, particularly in the upper pole. This study evaluated whether the use of a pocket-type acellular dermal matrix (ADM) could effectively reduce upper pole rippling by providing additional implant coverage and a smoother implant–flap transition.

Methods: Prepectoral DTI reconstruction was performed using a pocket-type ADM. As shown in **Figure 1**, the pocket-type ADM was first prepared on the sterile field, then opened to allow implant placement, and finally used to fully wrap the implant. The lower pole of the ADM was trimmed to fit the inframammary fold, while the superior portion was preserved to reinforce the upper pole as a mechanical barrier over the implant edge. The ADM construct was then secured with 3-0 PDS and prepared for final insertion, as shown in **Figure 2**. For comparison, a case using a square-type ADM wrapped in a round configuration was also reviewed. Postoperative clinical evaluation focused on visible or palpable rippling, especially in the upper pole.

Results: In the case reconstructed with the square-type ADM wrapped in a round configuration, visible rippling was observed postoperatively in the reconstructed breast (**Figure 3**). In contrast, in the case reconstructed using the pocket-type ADM, no visible upper pole rippling was noted (**Figure 4**). The preserved superior portion of the pocket-type ADM appeared to effectively mask the transition between the implant and the overlying skin flap, resulting in a smoother upper pole contour.

Conclusion: The use of pocket-type ADM in prepectoral breast reconstruction may serve as an effective mechanical buffer that compensates for soft tissue deficiency and helps prevent upper pole rippling. Preservation of the superior ADM portion may be particularly useful in reinforcing the upper pole and improving contour smoothness.

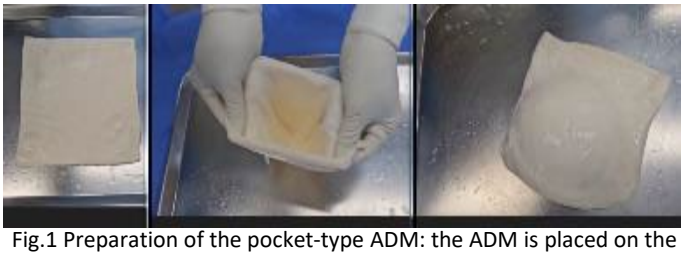

Fig.1 Preparation of the pocket-type ADM: the ADM is placed on the sterile field, opened to allow implant placement, and used to fully wrap the implant.

Fig.2 Final ADM construct: the lower pole was trimmed to fit the inframammary fold, while the superior portion was preserved and secured with 3-0 PDS for final insertion.

Fig.3 Postoperative result after implantation of a square-type ADM-wrapped implant in a round configuration, showing visible rippling

Fig.4 Postoperative result after implantation with a pocket-type ADM, showing no visible rippling.

EP-166

원발성 혈관육종에서의 유방 재건

Immediate Breast Reconstruction After Resection of Primary Breast Angiosarcoma: A Case Report

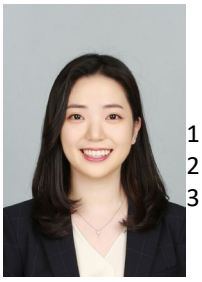

1 서울대학교병원 성형외과
2 서울특별시 보라매병원 성형외과
3 서울대학교 의과대학 성형외과학교실

김소연[1], 김재우*[2,3]

Purpose : Primary breast angiosarcoma is a rare and aggressive vascular malignancy, and there is no established consensus regarding optimal reconstructive strategies. This study aims to present the clinical feasibility of immediate breast reconstruction using a prepectoral implant following oncologic resection.

Methods : A 52-year-old female presented with an abnormal finding in the right breast detected during a health screening. Ultrasonography revealed a 2.1 cm irregular hypoechoic lesion (BI-RADS 4). Excisional biopsy confirmed angiosarcoma. Breast-conserving surgery with sentinel lymph node biopsy was initially performed; however, due to positive margins, nipple-sparing mastectomy was subsequently carried out. Immediate breast reconstruction was performed using a prepectoral implant with an acellular dermal matrix (MegaDerm).

(A) (B)

Fig. 1. Preoperative clinical photographs.
(A) Frontal view with arms at the sides.
(B) Frontal view with arms akimbo.

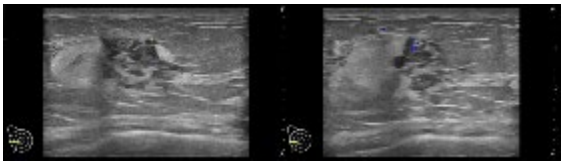

Fig. 2. Preoperative ultrasonography demonstrating an irregular hypoechoic lesion with increased vascularity.

Results : No lymph node metastasis was identified. Final pathology after mastectomy revealed no residual tumor with negative margins. Reconstruction was performed using the anterior tenting technique to create a prepectoral pocket, followed by insertion of a 360-cc silicone implant. The postoperative course was uneventful. At 6 months follow-up, the patient showed no evidence of recurrence and maintained satisfactory aesthetic outcomes.

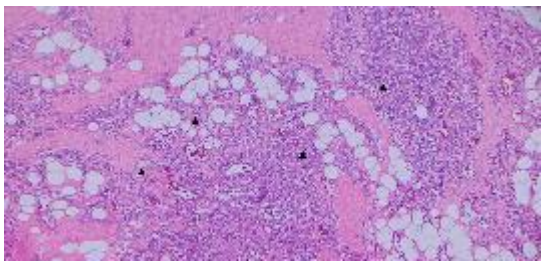

Fig. 3. Histopathologic findings (H&E, ×10). Anastomosing vascular channels, atypical endothelial proliferation, and red blood cell extravasation (arrows).

(A) (B)

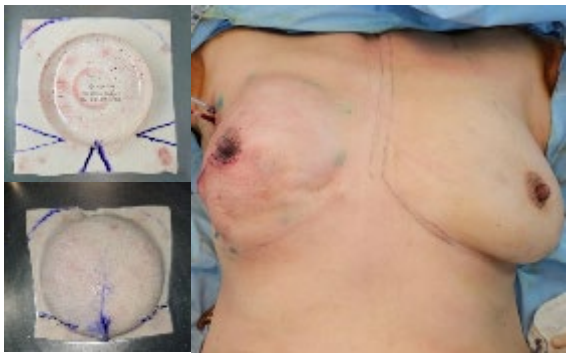

Fig. 4. Intraoperative findings.
(A) Acellular dermal matrix prepared using anterior tenting technique.
(B) Immediate postoperative view after prepectoral implant reconstruction.

Conclusion : When complete oncologic resection is achieved, immediate breast reconstruction using a prepectoral implant may be a safe and effective option in selected patients with primary breast angiosarcoma. Further studies are required to evaluate long-term oncologic outcomes.

Fig. 5. Postoperative clinical photographs at 6 months showing maintained breast contour.
(A) Frontal view with arms at the sides.
(B) Frontal view with arms akimbo.

EP-167

VRAM 중심 재건 전략을 넘어: 골반 장기 적출술 후 골반부 재건을 위한 단계적 알고리즘

(Beyond the VRAM-First Paradigm: A stepwise Algorithm for Pelvic Area Reconstruction After Pelvic Exenteration)

가톨릭중앙의료원
성빈센트병원

김지연, 김동연*

Purpose: Pelvic exenteration is a radical oncologic procedure involving en bloc resection of pelvic organs, frequently resulting in complex pelvic floor and perineal defects. Although the vertical rectus abdominis myocutaneous (VRAM) flap remains the standard reconstructive option, its use is often limited in patients requiring abdominal stomas or urostomy. In addition, coccygectomy performed during rectal cancer surgery creates sacral defects that further increase reconstructive complexity. This study proposes a VRAM-sparing reconstructive algorithm for pelvic floor and perineal defects following pelvic exenteration.

Methods: A stepwise algorithm was applied according to pelvic floor defect size, presence of sacral defects after coccygectomy, and extent of perineal skin loss. Unilateral or bilateral gracilis muscle flaps were used for small to moderate defects. When gracilis flaps were insufficient, particularly in sacral defects, gluteus maximus–based reconstruction, including adipofascial turnover flaps, was employed. Cutaneous defects were reconstructed using IGAP- or SGAP-based skin paddles, while pedicled profunda artery perforator fasciocutaneous flaps were used for ischial defects.

Results: The algorithm achieved stable reconstruction with effective dead space obliteration. Gracilis muscle flaps provided adequate coverage for selected defects but demonstrated vulnerability to postoperative compression and reduced distal skin paddle reliability in sacral reconstructions. In such cases, adjunctive gluteal muscle–based flaps improved durability and resistance to pressure-related complications. Donor site complications were minor and managed conservatively.

Conclusion: When VRAM reconstruction is contraindicated, a tailored algorithm using gracilis and gluteal muscle–based flaps provides a practical alternative for pelvic floor and perineal reconstruction after pelvic exenteration, expanding reconstructive options beyond the traditional VRAM-first paradigm.

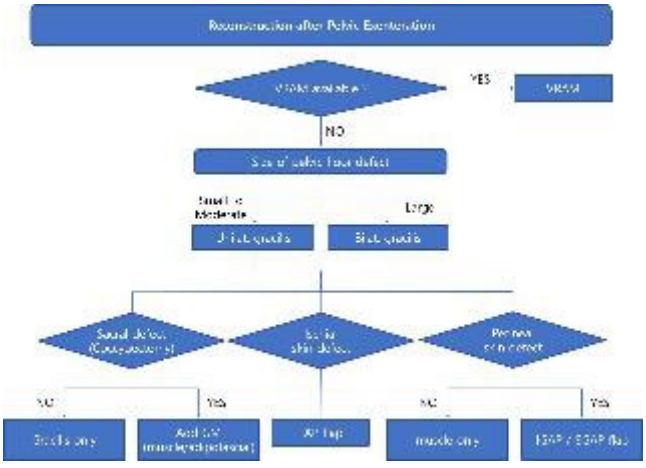

Figure. 1
VRAM-sparing reconstructive algorithm for pelvic floor and perineal defects following pelvic exenteration.

EP-167

VRAM 중심 재건 전략을 넘어: 골반 장기 적출술 후 골반부 재건을 위한 단계적 알고리즘

(Beyond the VRAM-First Paradigm: A stepwise Algorithm for Pelvic Area Reconstruction After Pelvic Exenteration)

가톨릭중앙의료원
성빈센트병원

김지연

Figure. 2
Case: small to moderage pelvic floor defect
(A) Intraoperative pelvic defect after pelvic exenteration
(B) Reconstruction using unilateral gracilis muscle flap, immediate postoperative appearance

Figure. 3
Case: large pelvic floor defect
(A) Intraoperative pelvic defect after pelvic exenteration
(B) Reconstruction using bilateral gracilis muscle flap, immediate postoperative appearance

Figure. 4
Case: small to moderage pelvic floor defect with ischial skin defect
(A) Intraoperative pelvic defect after pelvic exenteration
(B) Reconstruction using unilateral gracilis muscle flap and transpositional pedicled PAP FC flap coverage, immediate postoperative appearance

EP-168

욕창 환자에서 치유 결과 및 예측 인자에 대한 후향적 연구

Retrospective Analysis of Healing Outcomes and Associated Factors in Patients with Pressure Ulcers

서울대학교[1]

김진우[1], 김종호*[1]

Purpose: Pressure ulcers are serious complications among immobilized or chronically ill patients, often resulting in prolonged hospitalization, morbidity, and increased healthcare costs. Despite therapeutic advances, predictors of long-term healing remain unclear. This study aimed to identify factors associated with one-year healing outcomes in patients with advanced pressure ulcers.

Methods: This retrospective cohort study included adult patients diagnosed with pressure ulcers of grade 2 or higher between January 2020 and January 2025. Clinical, laboratory, and wound-related variables were obtained from electronic records, including demographic data, comorbidities, nutritional indicators, ulcer features (stage, location, size, infection, and bone exposure), and treatment modalities such as negative pressure wound therapy and surgical debridement. The primary outcome measure was complete wound healing within 12 months. Univariate and multivariate logistic regression analyses identified independent predictors of healing.

Results: A total of 240 patients (mean age, 61.5 ± 10.6 years; 69.6% male) were included in the final analysis. Complete healing at 12 months was achieved in 48.8% of the patients. In the multivariate logistic regression model, negative pressure wound therapy (NPWT), hospital-based treatment, lower initial ulcer stage, and absence of paralysis were independently associated with complete healing, with all predictors reaching statistical significance (all $p < 0.01$).

Conclusion: NPWT, hospital-based management, lower initial ulcer stage, and absence of paralysis were strongly associated with improved one-year healing outcomes in patients with advanced pressure ulcers. These findings highlight the importance of early, structured wound care and suggest that both the treatment setting and patient mobility status play critical roles in long-term recovery.

Variable/Category	Complete Healing (n=117)	Incomplete Healing (n=123)	OR/ Mean Diff	*p*-value	Test
Continuous Variables					
Age (years)	61.16±10.79	62.91±10.39	-	0.20	t-test
BMI (kg/m²)	23.92±3.82	24.39±3.27	-	0.30	t-test
Hemoglobin (g/dL)	11.58±1.53	11.37±1.65	-	0.31	t-test
Albumin (g/dL)	3.12±0.59	3.17±0.57	-	0.50	t-test
CRP (mg/L)	3.51±2.89	3.70±2.92	-	0.64	Mann-Whitney U
ESR (mm/h)	44.40±14.58	44.89±14.96	-	0.80	t-test
Initial Ulcer Size (cm²)	53.08±20.76	60.62±35.84	-	0.44	Mann-Whitney U
Initial Stage	2.94±0.81	3.39±0.75	-	<0.01***	t-test
Categorical Variables					
Dressing Type				<0.01***	Chi-square
NPWT	40/50 (80.0%)	10/50 (20.0%)	5.87		
Conventional	77/190 (40.5%)	113/190 (59.5%)	Ref		
Treatment Location				<0.01***	Chi-square
Hospital	86/139 (61.9%)	53/139 (38.1%)	3.66		
Home	31/101 (30.7%)	70/101 (69.3%)	Ref		
Paralysis Status				0.025*	Chi-square
No Paralysis	73/131 (55.7%)	58/131 (44.3%)	Ref		
Paralysis	44/109 (40.4%)	65/109 (59.6%)	0.54		
Sex (Female)	34/73 (46.6%)	39/73 (53.4%)	0.88	0.76	Chi-square
Diabetes Mellitus	29/66 (43.9%)	37/66 (56.1%)	0.77	0.44	Chi-square
Chronic Kidney Disease	31/67 (46.3%)	36/67 (53.7%)	0.87	0.74	Chi-square
Cardiovascular Disease	21/49 (42.9%)	28/49 (57.1%)	0.74	0.44	Chi-square
Infection Status	42/78 (53.8%)	36/78 (46.2%)	1.35	0.34	Chi-square

Ref, reference category. *** p<0.001, * p<0.05

Data presented as mean ± standard deviation for continuous variables and n/N (%) for categorical variables.

NPWT, negative pressure wound therapy.

Table 1. Univariate Analysis of Variables Associated with One-Year Complete Healing

Variable	Coefficient	Odds Ratio	95% CI	Std Error	Z-Value	*P-value*
NPWT (vs. Conventional)	2.080	8.005	3.321-19.298	0.449	4.633	<0.01 ***
Hospital (vs. Home)	1.494	4.457	2.367-8.392	0.323	4.629	<0.01***
Initial Stage (per unit)	-0.973	0.378	0.252-0.567	0.207	-4.708	<0.01***
No Paralysis (vs. Paralysis)	0.987	2.684	1.442-4.997	0.317	3.114	<0.01***

Model Performance: ROC-AUC=0.8124, Accuracy=75.00%, Sensitivity=65.81%, Specificity=83.74%, PPV=79.38%, NPV=72.03%,

NPWT, negative pressure wound therapy.

Table 2. Multivariate Logistic Regression Analysis – Independent Predictors of Complete Healing

EP-169

음문질 재건을 위한 새로운 서혜부 천공지 피판: 표재외음부동맥 천공지(SEPP) 피판

A Novel Inguinal Perforator Flap for Vaginal Reconstruction: The Superficial External Pudendal Artery Perforator (SEPP) Flap

아주대학교 성형외과[1]
홍순호 [1], 한형민*[1], 임효섭 [1], 이일재 [1]

Purpose: Vulvovaginal reconstruction following oncologic resection remains challenging because of the region's complex three-dimensional anatomy and the need for thin, pliable, and sensate tissue coverage. Conventional reconstructive options, including local advancement flaps and distal-based perforator flaps, are often limited by bulkiness, contracture, or donor-site morbidity. Here, we present our institutional experience with a novel inguinal fasciocutaneous flap based on the superficial external pudendal artery perforator (SEPP flap) for vulvovaginal reconstruction, and evaluate its surgical reliability, tissue qualities, and versatility according to defect size and location.

Methods: We retrospectively reviewed 29 patients who underwent vulvovaginal reconstruction with pedicled SEPP flaps at our institution from March 2010 to May 2025. Patients requiring concurrent inguinal lymph node dissection or complex reconstruction involving urethral or anal sphincter preservation were excluded to minimize confounding factors. We analyzed patient demographics, tumor pathology, operative details, and postoperative outcomes. A total of 45 flaps were elevated.

Results: Mean patient age was 64.1 years (range 42-82). Primary pathologies included extramammary Paget's disease (51.7%, n=15), squamous cell carcinoma (31.0%, n=9), and vulvar melanoma (17.2%, n=5). Bilateral reconstruction was performed in 16 patients (55.2%). All 45 flaps survived completely without total necrosis or vascular compromise. Minor complications occurred in 4 patients (13.8%): one surgical site infection and three partial marginal necrosis cases, all successfully managed conservatively or with bedside debridement. All donor sites achieved primary closure with well-concealed inguinal crease scars.

Conclusion: The SEPP inguinal flap offers dependable vascularity, thin and pliable tissue, and low donor-site morbidity, making it well suited for superficial vulvovaginal resurfacing with favorable aesthetic and functional outcomes.

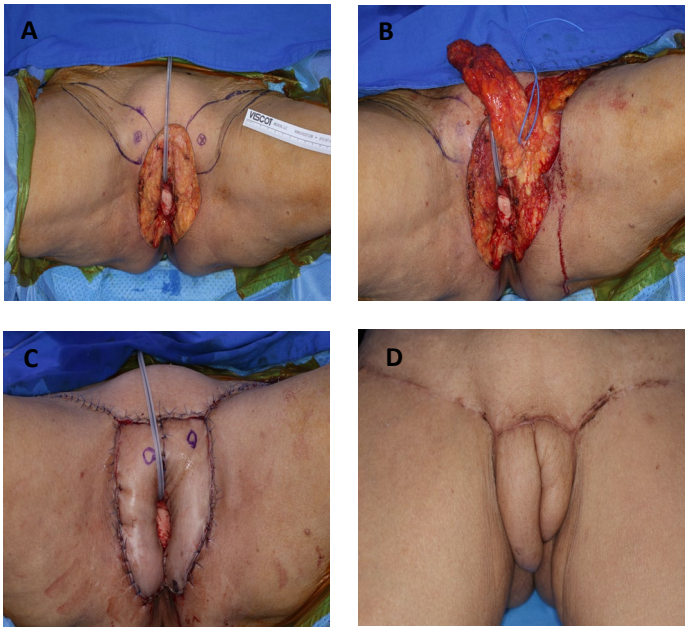

Figure 1. **Primary donor-site closure following adequate subcutaneous undermining; (A) Preoperative view, (B) flap elevation, (C) immediate postoperative view, and (D) follow-up view.**

Table 1. Patient Characteristics, Flap Dimensions, and Surgical Outcomes

Case no.	Age	BMI	Preop RTx.	Pathology	Vaginal involve	Flap	Width 1st flap (cm)	Length 1st flap (cm)	Width 2nd flap (cm)	Length 2nd flap (cm)	Complication
1	69	22.3	no	EMPD	Vulva	Left	4.5	11			No
2	19	19.2	no	Hemangioma	Vulva	Left	5	12			No
3	47	19.9	no	BCC	Vulva	Left	4.5	12			No
4	68	21.9	no	SCC	vulvovaginal	Bilateral	5	11	6	10	No
5	69	31.5	no	EMPD	Vulva	Left	6.5	13			No
6	64	23.3	no	Melanoma	Vulva	Left	6	10.5			No
7	54	25.4	no	VIN	vulvovaginal	Bilateral	7	12	5	11	No
8	72	22.2	no	EMPD	Vulva	Right	5.5	12.5			No
9	49	16.8	no	SCC	Vulva	Right	6	11.5			No
10	76	22.7	no	EMPD	vulvovaginal	Bilateral	5	12	6	11	No
11	34	26.4	no	SCC	vulvovaginal	Bilateral	4.5	12	5	12	Wound dehiscence
12	67	18.9	yes	SCC	Vulva	Left	6	9.5			No
13	72	19.1	no	BCC	Vulva	Right	4.5	9			No
14	76	25.1	yes	SCC	Vulva	Left	5.5	10			No
15	63	27	no	SCC	vulvovaginal	Bilateral	6	11	5.5	12	Debulking
16	80	24.8	no	EMPD	vulvovaginal	Bilateral	6	10	6	11	No
17	74	25	no	EMPD	vulvovaginal	Bilateral	4.5	10	5.5	11	No
18	78	25.6	no	EMPD	Vulva	Bilateral	7	13	6	10	Infection
19	86	26.3	no	EMPD	vulvovaginal	Bilateral	4	11	6	12	Flap necrosis
20	52	24	no	EMPD	vulvovaginal	Bilateral	5	12	5.5	12	No
21	78	21.3	no	SCC	Vulva	Bilateral	5	12	6	11	Debulking, Flap necrosis
22	46	22.6	no	EMPD	Vulva	Left	5	11			No
23	62	26.8	no	EMPD	vulvovaginal	Right	4.5	13			No
24	83	19	no	EMPD	vulvovaginal	Bilateral	7	12	5	11	No
25	67	24.6	no	SCC	vulvovaginal	Bilateral	5	10.5	4	10	No
26	60	22.9	no	EMPD	Vulva	Bilateral	5	4	5	3	No
27	65	27.6	no	EMPD	Vulva	Bilateral	4	15	4	15	No
28	64	22.8	no	SCC	Vulva	Left	8	14			No
29	76	21.1	no	EMPD	Vulva	Bilateral	5	12	6	12	No

BMI, Body Mass Index; Preop RTx, Preoperative Radiotherapy; EMPD, Extramammary Paget's Disease; SCC, Squamous Cell Carcinoma; BCC, Basal Cell Carcinoma; VIN, Vulvar Intraepithelial Neoplasia

EP-170

요도 협착 교정을 위한 맞춤형 구강점막 이식법

(Tailored Methods of Buccal Mucosal Grafting: Autologous material for Urethral Stricture Repair)

고려대학교 안암병원

김지현, 이재민, 정재호*, 윤을식

Purpose: In cases of short urethral stricture and mild cavernosal fibrosis, a buccal mucosa graft may be performed. However, clear standards and methods for how to harvest the buccal mucosa and the appropriate amount to harvest remain unclear. This presentation aims to provide a more detailed explanation of the senior author's buccal mucosa graft harvesting technique.

Methods: To harvest buccal mucosa, we mark the area anteriorly 1 cm behind the corner of the mouth, superiorly 5 mm from Stensen's duct, and posteriorly along the pterygomandibular raphe. (Fig. 1)
After injection of local anesthesia, harvesting oral mucosal tissue was performed in an anterior-to-posterior direction within the supra-muscle plane. To enhance engraftment rates, defat the muscle and fat components.

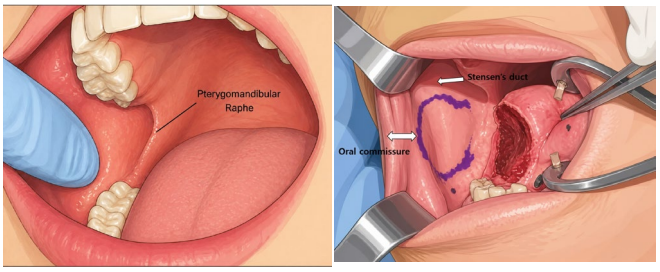

Fig 1. Preoperative design

The harvested buccal mucosa (Fig. 2) was sutured over the urethral stricture site using a vertical incision and dorsal onlay technique. The donor site was sutured watertightly using Vicryl 3-0.

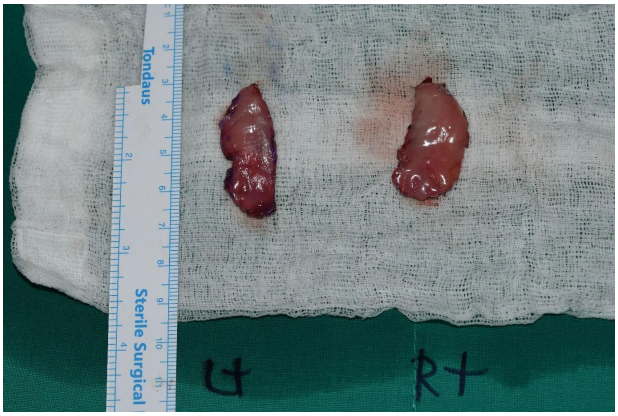

Fig 2. Harvested buccal mucosa graft

Results: A total of 16 buccal mucosa grafts were performed in 12 patients. The average graft size was 5.64 cm². (Tabld 1)
In all patients, buccal mucosa grafts were successfully placed at the stricture site without complications. There were no cases requiring reoperation due to graft failure. Patients may experience initial temporary trismus and pain, which improved over time.

No.	Sex	Age	Diagnosis	Operation	Size	Site
1	M	71	Rectovaginal fistula	Fistulectomy, BMG	2.5×4cm, 2 pieces	Bilateral
2	M	65	Urethra stricture	Urethroplasty, BMG	1.5×2.5cm, 2 pieces	Bilateral
3	M	21	Urethrostricture	Urethroplasty, BMG	1.5×4cm	Unilateral
4	M	73	Urethra stricture	Urethroplasty, BMG	1.5×3cm, 2 pieces	Bilateral
5	F	54	Urethra stricture	Urethroplasty, BMG	2.0×4cm	Unilateral
6	M	75	Urethra stricture	Urethroplasty, BMG	1.5×4cm	Unilateral
7	F	56	Urethra stricture	Urethroplasty, BMG	2×2.5cm	Unilateral
8	F	56	Urethra stricture	Urethroplasty	2×2.5cm, 1×3cm	Bilateral
9	F	64	Urethra stricture	Urethroplasty	1.5×3cm	Unilateral
10	F	70	Urethra stricture	Urethroplasty	2×2.5cm	Unilateral
11	F	55	Urethra stricture	Urethroplasty	1.5×3cm	Unilateral
12	F	60	Urethra stricture	Urethroplasty	1.5×4.5cm	Unilateral
					avg. 5.64cm²	16 pieces

※ BMG; buccal mucosa graft

Table 1. Patient demographics

Conclusion: The buccal mucosa offers advantages such as ease of harvesting, low donor site complication rates, and abundant vascular supply. It is anticipated to be a useful option for urethral reconstruction following careful patient selection.

EP-171

근육보존 광배근 유리피판을 이용한 광범위 둔부 화상의 미용적 보존 재건

Aesthetic-Preserving Reconstruction for Extensive Gluteal Burn Using a Muscle-Sparing Latissimus Dorsi Free Flap

충남대학교병원 성형외과[1]
충남대학교 의과대학 성형외과학교실[2]

박주영[1,2], 권혁재[1], 김순제[1], 송승한[1,2], 오상하[1,2], **하유석*[1,2]**

Purpose : Extensive coccygeal and gluteal burn defects with bone exposure require not only durable coverage but also restoration of three-dimensional contour. In young female patients, preservation of buttock projection, symmetry, and weight-bearing function is particularly important. We present a case reconstructed using a muscle-sparing latissimus dorsi (msLD) free flap, emphasizing aesthetic-based decision-making and functional improvement.

Methods : A 30-year-old woman sustained a full-thickness coccygeal burn after prolonged contact with an electric heating pad following collapse due to pulmonary thromboembolism. Despite two split-thickness skin grafts at another hospital, central necrosis with bone exposure persisted. Serial debridement and negative pressure wound therapy were performed, leaving a 12×12 cm defect with deep dead space. Given the need to preserve gluteal contour and avoid distortion of the weight-bearing surface, an msLD free flap was performed. End-to-end microvascular anastomoses were completed between the thoracodorsal descending branch and branches of the superior gluteal vessels. The flap was contoured and inset to provide stable coverage and effectively obliterate the dead space.

Results : The flap survived completely without vascular complications. Stable coverage of exposed bone and effective dead space obliteration were achieved. Buttock projection and contour symmetry were maintained, resulting in a satisfactory aesthetic outcome. Notably, the patient's preoperative lower-extremity pain associated with myelopathy improved postoperatively. No major complications occurred.

Conclusion : Reconstruction of extensive gluteal burn defects should address both aesthetic contour and functional recovery. The msLD free flap provides reliable vascularity, adequate bulk, preservation of buttock symmetry, and potential functional benefit, making it a valuable option in young patients.

Fig. 1. Preoperative view of the coccygeal defect demonstrating a full-thickness soft tissue defect with central necrosis and exposed bone. The rectangular erythematous area superior to the defect represents a split-thickness skin graft (STSG) donor site performed at a previous hospital.

Fig. 2. Intraoperative photograph of the harvested muscle-sparing latissimus dorsi (msLD) free flap. The flap measured 12 × 12 cm, including well-vascularized skin and subcutaneous tissue.

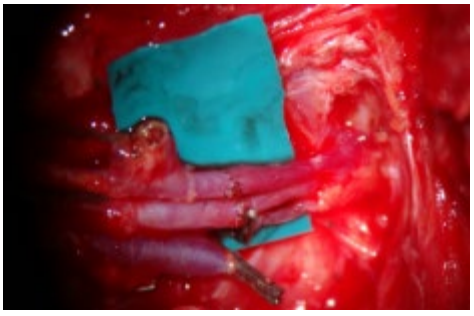

Fig. 3. Intraoperative view of microvascular anastomosis between the thoracodorsal vessels and the superior gluteal vessels (TDV–SGV).

Fig. 4. Postoperative outcomes following reconstruction with a muscle-sparing latissimus dorsi free flap (POD 43).

EP-172

이물질 육아종에 대한 단일 단계 음경 피부 재건술: 피부 대체재를 사용한 간소화된 음압 상처 치료 보조 프로토콜

(Single-Stage Penile Resurfacing for Foreign Body Granuloma: A Simplified NPWTAssisted Protocol with Dermal Substitute)

한양대학교 의과대학
성형외과학교실
한양대학교병원 성형외과

박상현, **김연환***

Purpose: To present a simplified single-stage protocol using negative pressure wound therapy (NPWT) combined with dermal substitute and split-thickness skin graft (STSG) for penile foreign body granuloma resulting from subcutaneous injection of various substances.

Methods: A retrospective review was conducted on 11 consecutive patients who underwent penile resurfacing for foreign body granuloma between March 2018 and June 2025. All patients received complete excision of granulomatous tissue, Matriderm Flex application, STSG, and NPWT (−125 mmHg). Primary outcomes included graft take rate, complications, hospital stay, and patient satisfaction assessed by a 9-item questionnaire.

Results: Mean patient age was 55.3 years. Foreign body types included Vaseline alone (n = 6), Vaseline with hyaluronic acid (n = 1), hyaluronic acid alone (n = 1), and unknown fillers (n = 3). The first dressing change was performed on postoperative day 5 with near-complete graft take achieved in 10 of 11 cases (90.9%). Complications included partial graft loss with hematoma requiring evacuation (n = 1) and chronic discharge from remnant filler material (n = 1). Mean satisfaction score was 37.5/45. Mean follow-up was 18.9 months.

Conclusion: NPWT-assisted single-stage reconstruction using dermal substitute and STSG provides a simple, reliable, and reproducible option for penile foreign body granuloma, avoiding complex flap surgery while achieving excellent graft take and high patient satisfaction.

Fig. 1. Representative case of penile resurfacing for foreign body granuloma. (A, B) Preoperative appearance demonstrating diffuse penile swelling with characteristic footballshaped deformity. (C, D) Postoperative day 5 showing successful graft take with wellvascularized appearance.

Fig. 2. Long-term outcome of a representative case. (A) Preoperative appearance showing penile foreign body granuloma. (B) Postoperative day 5 demonstrating successful graft take. (C) Eighteen months postoperatively showing durable skin coverage with natural appearance and excellent elasticity.

Variable	Value
No. of patients	11
Sex, male, n (%)	11 (100)
Age (years), mean ± SD	55.3 ± 4.6
Age (years), range	49-63
Foreign body type, n (%)	
Vaseline	6 (54.5)
Vaseline + hyaluronic acid	1 (9.1)
Hyaluronic acid	1 (9.1)
Unknown filler	3 (27.3)
Defect location, n (%)	
Penis only	8 (72.7)
Penis and scrotum	3 (27.3)
Penile defect size (cm^2), mean ± SD	17.4 ± 16.4
Penile defect size (cm^2), range	6-56
Reconstruction method, n (%)	
Matriderm Flex + STSG	8 (72.7)
Matriderm Flex + STSG + advancement flap	3 (27.3)
Operation time (min), mean ± SD	63.6 ± 10.3
Operation time (min), range	50-80
Hospital stay (days), mean ± SD	5.2 ± 0.6
Hospital stay (days), range	5-7
Follow-up (months), mean ± SD	18.9 ± 7.6
Follow-up (months), range	12-36

SD, standard deviation; STSG, split-thickness skin graft.

Table 1. Patient Demographics and Clinical Characteristics

Technique	Stage	Advantages	Disadvantages
Scrotal flap	Single	Reliable vascularity, single procedure	Hair-bearing, bulky, donor morbidity
STSG alone	Single	Technical simplicity	Poor elasticity, contracture, tethering
Integra + STSG	Two	Good dermal regeneration, elasticity	2-3 week interval, multiple procedures
Perforator flap	Single	Thin, pliable, hidden donor scar	Doppler required, complex positioning, specialized skills
Present protocol	**Single**	**Good elasticity, simple, reproducible, early discharge (POD 5)**	**Not for extensive defects or poor wound beds**

STSG, split-thickness skin graft; POD, postoperative day.

Table 2. Comparison with Existing Reconstructive Techniques

EP-173

난치성 켈로이드 치료에서 선행 5-플루오로우라실/트리암시놀론 병변내 주사 후 절제술 및 수술 후 방사선치료를 병합한 상승적 다중모달 치료 전략

Synergistic Multimodal Therapy for Refractory Keloids: Neoadjuvant 5- Fluorouracil/Triamcinolone Injections Followed by Excision and Postoperative Radiotherapy

충남대학교병원 성형외과[1]
충남대학교 의과대학 성형외과학교실[2]

김정희[1,2], 권혁재[1], 하유석[1,2], 김순제[1], 오상하[1,2], **송승한*[1,2]**

Purpose : Keloids are associated with high recurrence rates, particularly when treated with surgical excision alone. Large or refractory lesions are characterized by increased mechanical tension, a key factor contributing to recurrence. Although intralesional 5-fluorouracil (5-FU) and triamcinolone acetonide (TAC) are effective in reducing scar volume, their role as neoadjuvant therapy before surgery has not been standardized. This study evaluates a multimodal protocol incorporating neoadjuvant 5-FU/TAC injections, surgical excision, and postoperative radiotherapy (RT).

Methods : Patients with large or refractory keloids underwent three sessions of intralesional 5-FU/TAC injections at four-week intervals. Surgical excision was performed four weeks after the final injection to enable tension-free primary closure. Postoperative electron-beam RT was initiated within 24 hours, followed by a total of three sessions. Clinical outcomes were assessed using the Vancouver Scar Scale (VSS), Patient and Observer Scar Assessment Scale (POSAS), and recurrence rates during a 12-month follow-up.

Results : Neoadjuvant treatment reduced mean keloid volume by 30–50%, facilitating surgical excision and minimizing reconstructive complexity. At 12 months, recurrence was less than 10%, lower than historical controls treated with surgery and RT alone. Significant improvements were observed in scar height, erythema, and density, with corresponding VSS and POSAS score reductions. The combined use of 5-FU with reduced-dose TAC minimized corticosteroid-related adverse effects.

Conclusion : Neoadjuvant 5-FU/TAC combined with excision and RT is a safe and effective strategy for refractory keloids. Preoperative volume reduction and tension modulation appear to enhance surgical outcomes and reduce recurrence, supporting this multimodal protocol as a practical clinical framework.

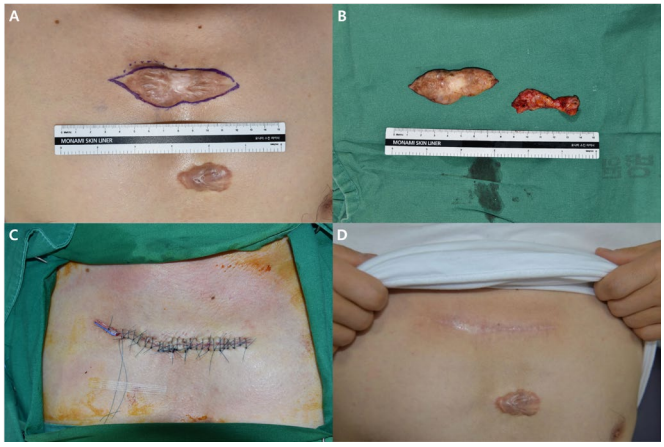

Fig. 1. Clinical photographs of multimodal treatment for the keloid on anterior chest.
(A) Preoperative surgical design outlining a 7 × 3 cm keloid on the anterior chest.
(B) Excised keloid specimen following complete removal.
(C) Immediate postoperative appearance after primary closure.
(D) Five-month postoperative photograph showing a stable scar without recurrence.

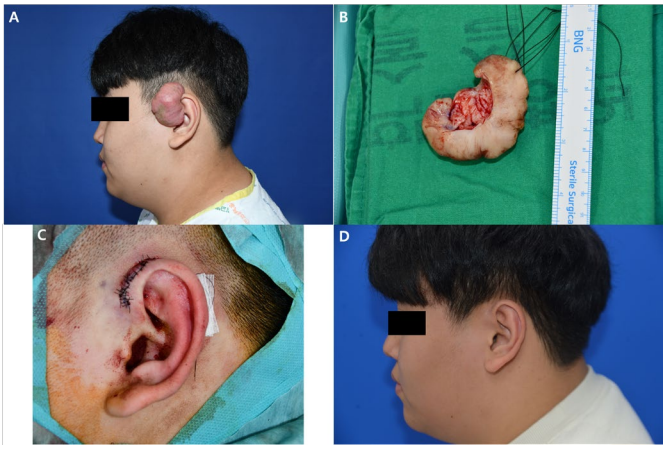

Fig. 2. Clinical photographs of multimodal treatment for left auricular keloid.
(A) Preoperative photograph demonstrating a large keloid involving the left auricular helix.
(B) Excised keloid specimen measuring 6.5 × 4.5 cm.
(C) Immediate postoperative appearance after primary closure.
(D) Nine-month postoperative follow-up showing satisfactory contour restoration without recurrence.

EP-174

림버그 피판을 이용한 배꼽하부 재발성 켈로이드의 장력 재배치 치료

(Management of Recurrent Infraumbilical Keloid by Tension Redirection Using a Limberg Flap)

가톨릭대학교 의과대학
성형외과학교실

이창준, 김라윤, 백상운, 유결, 이준용*

Purpose: Keloids represent a pathologic form of wound healing characterized by excessive collagen deposition and progressive scar enlargement beyond the original wound margin. Mechanical tension has been recognized as a critical factor in scar widening and keloid formation, particularly when repetitive forces act perpendicular to the scar axis. Therefore, careful mechanical tension redistribution should be considered in keloid management. We report a case of recurrent infraumbilical keloid successfully managed through biomechanical correction using tension redistribution with a Limberg flap.

Methods: A 63-year-old man presented with an infraumbilical mass that had developed 8 months earlier and underwent surgical excision with satisfactory healing (Fig. 1). Three years later, the lesion recurred and was treated with repeat excision. Progressive scar widening with subsequent keloid formation was observed at 1-year follow-up (Fig. 2A). Conservative management including intralesional triamcinolone injections and silicone gel sheet application failed to control progression. Considering persistent mechanical stretching perpendicular to transverse scar caused by involuntary rectus abdominis contraction and gravitational forces, surgical revision was planned to modify the tension environment (Fig. 2B). The keloid was excised, and a Limberg flap was designed as a geometric solution to redirect perpendicular force vectors and redistribute mechanical tension through Z-limb extension (Fig. 3).

Results: At 3-month follow-up, the wound healed well without recurrence under a more favorable tension vector (Fig. 4). After one year, patient reported no recurrence of the keloid.

Conclusion: Tension redistribution using a Limberg flap may offer an effective geometric solution for managing keloids caused by unfavorable tension vector and preventing recurrent scar widening.

Fig. 1. Clinical photograph at initial presentation showing an infraumbilical mass.

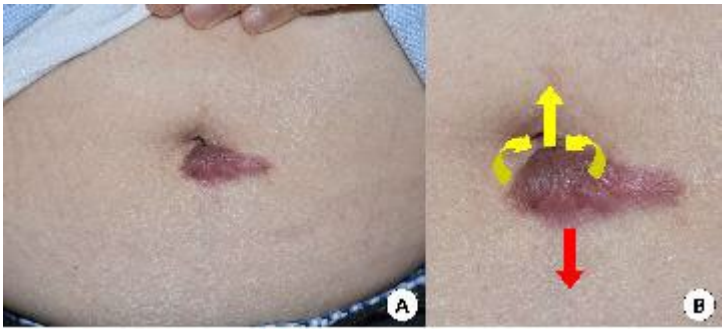

Fig. 2. Postoperative scar changes following repeated excisions. (A) Scar widening with keloid formation along the transverse incision. (B) Illustration showing perpendicular tension vectors acting on the scar caused by involuntary rectus abdominis contraction (yellow arrows) and gravitational force (red arrow).

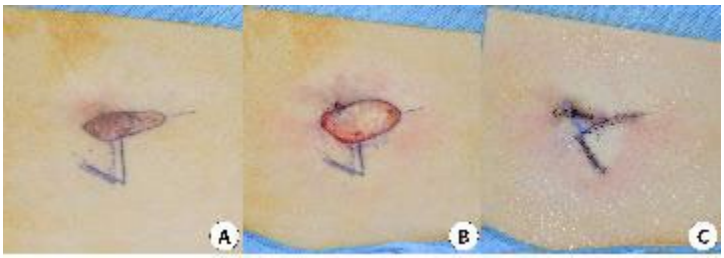

Fig. 3. Intraoperative photographs demonstrating Limberg flap reconstruction. (A) Flap design. (B) Defect after keloid excision. (C) Flap inset and immediate postoperative appearance. Suture lines are aligned along the tension vectors.

Fig. 4. Clinical photograph at 3-month follow-up showing stable scar healing with improved alignment following tension redistribution.

EP-175

아시아 환자에서 로봇 복막 질성형술 후 기능적 및 심리사회적 결과 분석

(Beyond Feasibility: Functional and Psychosocial Outcomes after Robotic Peritoneal Vaginoplasty in Asia)

강동성심병원 성형외과[1]
강동성심병원 외과[2]
강동성심병원 비뇨의학과[3]

정지원 [1], 김결희* [1], 장용준 [1], 박준호 [2], 정현철[3], 채한규[3]

Purpose: Robotic peritoneal vaginoplasty (RPV) has recently gained attention as an advanced gender-affirming technique offering enhanced precision and visualization. However, data from Asian centers remain limited, and little is known about patients' functional and social outcomes following surgery.

Methods: A descriptive analysis was performed of 61 transfeminine or non-binary patients who underwent RPV between 2023 and 2025. Baseline demographics, preoperative laboratory findings, operative parameters, concurrent procedures, complications, and six-month postoperative outcomes were reviewed.

Results: Mean age was 27.4 ± 6.9 years and mean BMI 21.8 ± 3.9 kg/m². Average hormone therapy duration was 40 months; 34 % had partners and 54 % identified as heterosexual. (Table 1) Mean operative time was 427.9 ± 71.4 minutes and blood loss 300 ± 244 mL. Concurrent procedures were performed in 36 %, most commonly breast augmentation (21 %) and voice feminization (18 %). Minor in-hospital complications occurred in 8 patients (13 %); 1 (2 %) underwent hematoma evacuation under general anesthesia. Mean hospital stay was 11.7 ± 2.4 days. At 6 months, 97 % reported sensory recovery, 57 % attempted intercourse, 52 % achieved successful intercourse, and 87 % completed legal gender recognition. (Table 3)

Conclusion: Among the earliest Asian experiences of robotic peritoneal vaginoplasty, this series demonstrates that RPV provides safe and reproducible results with excellent sensory and functional recovery. In addition to favorable surgical outcomes, most patients achieved meaningful sexual activity and social affirmation within 6 months, supporting the value of robotic approaches in gender-affirming care.

Table 1. Baseline characteristics of patients undergoing robotic peritoneal vaginoplasty (n = 61)

Variable	Value
Age at operation (years)	27.4 ± 6.9 (16.3–39.9)
Height (cm)	170.7 ± 6.3 (154.1–185.8)
Weight (kg)	63.7 ± 12.3 (40.2–103.5)
BMI (kg/m²)	21.8 ± 3.9 (14.4–32.6)
	14 (23%)
18.5–24.9	36 (59%)
25–29.9	10 (16%)
≥30	1 (2%)
Smoking status	
Never	43 (74%)
Ex-smoker†	5 (8%)
Current	11 (18%)
Gender identity (assigned male at birth)	
Trans women	59 (97%)
Non-binary	2 (3%)
Hormone therapy duration (months)	40.4 ± 29.1 (3.7–128.5)
Physical comorbidity‡	13 (21%)
Psychiatric comorbidity§	19 (31%)
History of suicide attempt	8 (13%)
Prior circumcision	22 (36%)
Prior orchiectomy	5 (8%)
Prior abdominal surgery	7 (11%)
Partner status	
Alone	36 (59%)
Has partner	21 (34%)
Not reported	4 (7%)
Sexual orientation	
Heterosexual	33 (54%)
Bisexual	14 (23%)
Pansexual	8 (13%)
Homosexual	3 (5%)
Questioning	1 (2%)
Not reported	2 (3%)

Values are presented as mean ± standard deviation (range) or number (percentage).

† Ex-smoker = stopped smoking ≥ 6 months before surgery.

‡ Physical comorbidities included diabetes mellitus (type 1), asthma, hyperthyroidism, Glanzmann's syndrome, Cushing disease, ankylosing spondylitis, gastroesophageal reflux disease, gallbladder stone, atrophic gastritis, and hypertension.

§ Psychiatric comorbidities were confirmed diagnoses by board-certified psychiatrists, including major depressive disorder, mild depressive episode, bipolar affective disorder, anxiety disorder, and attention-deficit/hyperactivity disorder.

Table 2. Preoperative clinical and operative characteristics (n = 61)

Variable	Value
Preoperative systolic BP (mmHg)	115.5 ± 10.3 (100–140)
Preoperative diastolic BP (mmHg)	76.6 ± 8.1 (60–93)
Preoperative hemoglobin (g/dL)	13.9 ± 1.4 (10–19)
Preoperative platelet (×10³/μL)	265.2 ± 74.5 (83–510)
Preoperative glucose (mg/dL)	107.3 ± 45.6 (70–341)
Concurrent procedures	
Any concurrent surgery	22 (36%)
Breast augmentation	13 (21%)
Voice feminization surgery	11 (18%)
Thyroid notch saving	12 (20%)

Values are presented as mean ± standard deviation (range) or number (percentage).

Table 3. Operative outcomes and postoperative course (n = 61)

Variable	Value
Total operative time (min)	427.9 ± 71.4 (305–700)
Estimated blood loss (mL)	300.0 ± 244.0 (50–1300)
Transfusion (intra- or postoperative)	6 (10%)
Hemoglobin POD#1 (g/dL)	11.6 ± 1.2 (8–15)
Hemoglobin POD#3 (g/dL)	10.9 ± 1.6 (7–14)
Hemoglobin POD#7 (g/dL)	10.6 ± 1.5 (7–14)
In-hospital complication (any)	8 (13%)
Port site infection	1 (2%)
Neovaginal hematoma	5 (8%)
Suprapubic hematoma	2 (3%)
Voiding difficulty	1 (2%)
Foley catheter removal (POD#)	6.9 ± 1.3 (5–12)
Length of hospital stay (days)	11.7 ± 2.4 (8–17)
Return to OR (hematoma evacuation)	1 (2%)
Aesthetic revision performed	7 (11%)
Able to have intercourse (6-month follow-up)	
Yes (successful intercourse)	32 (52%)
No (attempted but not possible)	3 (5%)
Not attempted / unknown	26 (43%)
Legal sex change completed (6-month follow-up)	53 (87%)
Sensation recovered (6-month follow-up)	59 (97%)

Values are presented as mean ± standard deviation (range) or number (percentage).

POD, postoperative day.

EP-176

국소 산소 치료와 음압 상처 치료 병합의 임상적 유용성

(The Clinical Usefulness of Combining Topical Oxygen Therapy and Negative Pressure Wound Therapy)

인제대학교 해운대백병원

김동규, 윤성호, 선욱, 이경아*

Purpose: Negative pressure wound therapy (NPWT) is a standard for advanced wound care; however, its efficacy can be limited by tissue hypoxia in pressure injuries. This study evaluated the clinical usefulness of combining topical oxygen therapy (TOT) with NPWT compared to NPWT monotherapy.

Methods: We retrospectively reviewed 16 patients with stage 3 or 4 pressure injuries. Patients were divided into two groups: combining TOT-NPWT (n=8) and NPWT alone (n=8). In the combination group, TOT was initiated when granulation was delayed under NPWT (Fig. 1). Clinical outcomes, including wound area, granulation tissue percentage, and exudate levels, were assessed at baseline and after 4 weeks of bi-weekly treatment (Table 1).

Results: The combination group showed a superior reduction in mean wound area (42.5%; 35.2 cm^2 to 20.2 cm^2) compared to the NPWT group (36.0%; 39.4 cm^2 to 25.2 cm^2). Granulation tissue formation significantly increased in the combination group (20% to 80%) compared to NPWT alone (15% to 50%). Furthermore, exudate levels in the combination group decreased from heavy to low, whereas the NPWT group only achieved a reduction to moderate levels (Table 2).

Conclusion: Combining TOT and NPWT significantly improved wound contraction, granulation, and exudate management compared to NPWT monotherapy. These findings suggest that TOT is a highly effective adjunct to NPWT in optimizing the healing environment for hypoxic chronic wounds.

Fig. 1. (A) Pressure injury before treatment with combining TOT and NPWT. (B) Application of TOT to the pressure injury. (C) Decreased wound size and formation of healthy granulation tissue after combining TOT and NPWT.

	TOT & NPWT	NPWT
Patients, n	8	8
Age, mean	72	70
Stage (3 / 4), n	2 / 6	2 / 6
Baseline wound area (cm^2), mean	35.2 cm^2	39.4 cm^2
Mean TOT-treatment time	3 weeks	-

Table 1. Baseline patient and wound characteristics.

Outcome	TOT & NPWT		NPWT	
	Baseline	4-week follow-up	Baseline	4-week follow-up
Wound area (cm^2), mean	35.2 cm^2	20.2 cm^2	39.4 cm^2	25.2 cm^2
Granulation tissue (%), mean	20%	80%	15%	50%
Exudate level	heavy	low	Heavy	Moderate
TOT-related complications	-	none	-	-

Table 2. Clinical outcomes at baseline and 4 weeks.

EP-177

림프부종에서 보조적 지방흡입술의 수술적 치료 효과(압박 치료 이탈 및 장기적 상하지 부피 감소) 개선

Adjunctive Liposuction Improves Garment Weaning and Long-Term Volume Reduction After Surgical Treatment of Lymphedema

이화여자대학교 의과대학[1],
성균관대학교 의과대학[2]

김수민[1], **조정목***[1], **박진우**[1], **우경제**[2]

Purpose : Lymphedema is a chronic progressive disease characterized by lymphatic dysfunction and subcutaneous fibrosis. Liposuction has recently been combined with physiologic procedures such as lymphaticovenous anastomosis (LVA), lymph node–venous anastomosis (LNVA), and vascularized lymph node transfer (VLNT) to improve surgical outcomes. This study evaluated the impact of adjunctive liposuction on postoperative outcomes in patients with lymphedema.

Methods : A retrospective analysis was conducted on patients who underwent surgical treatment for lymphedema between August 2024 and January 2026. Limb circumferences were measured preoperatively and at 1, 3, 6, and 12 months postoperatively to estimate limb volume. Garment weaning was categorized as no change, partial weaning, or complete weaning. Postoperative outcomes were compared between patients who underwent liposuction and those who did not.

Results : The garment-free rate was significantly higher in the liposuction group than in the non-liposuction group (31.0% vs. 8.8%). Ordinal logistic regression showed a significantly higher likelihood of garment weaning in the liposuction group (odds ratio 3.12, 95% CI 1.12–8.66; p=0.029). At postoperative 1 year, limb volume reduction was greater in the liposuction group than in the non-liposuction group (18.2% vs. 8.3%). After adjustment for baseline limb volume, the liposuction group demonstrated significantly lower limb volume at 1 year (p=0.011).

Conclusion : Adjunctive liposuction significantly improved garment weaning and was associated with greater long-term limb volume reduction compared with physiologic surgery alone.

Figure 1. Garment weaning status according to surgical treatment.
Stacked bar chart demonstrating the distribution of garment weaning outcomes in the liposuction and non-liposuction groups.

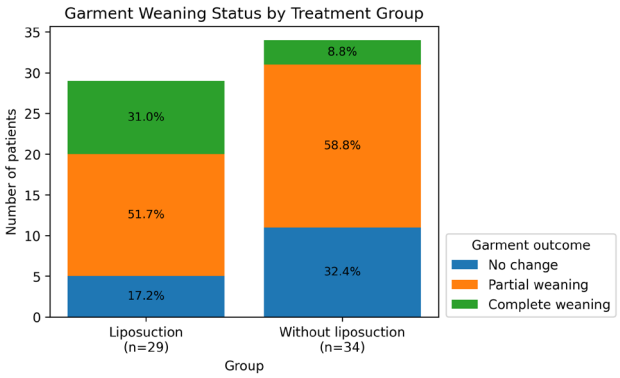

Figure 2. Percent volume reduction over time after surgery.
(a) Mean percent change in limb volume relative to baseline at postoperative 1 month, 3 months, 6 months, and 1 year in the liposuction and non-liposuction groups.
(b) One-year volume reduction between groups.
Volume change at postoperative 1 year in the liposuction and non-liposuction groups.

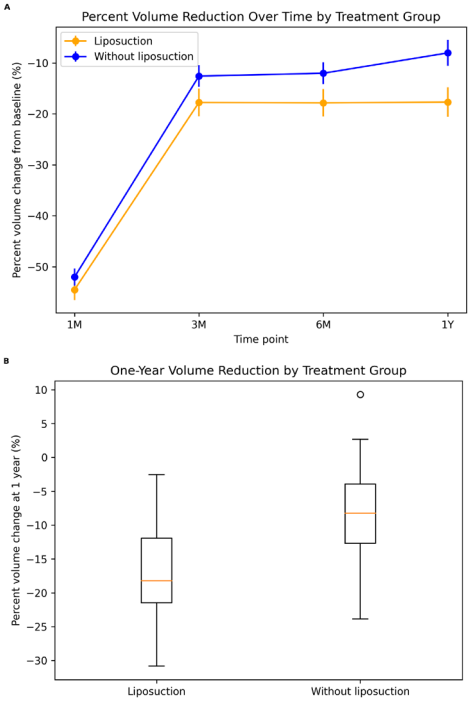

EP-178

새열 기원을 시사하는 조직병리학적 소견을 보인 드문 선천성 흉골 중앙부 피부동에 대한 증례보고

(A Report of an Unusual Congenital Midline Sternal Sinus with Histopathologic Features Consistent with a Branchial Cleft Origin)

경희대학교병원

김영진, 강상윤, 범진식, 박준*

Purpose : Congenital sinus lesions in the anterior chest region are rare, and their embryologic origin remains unclear. Most reported cases are located laterally near the sternoclavicular joint and are considered part of the dermoid spectrum. However, some cases have shown features overlapping with branchial cleft anomalies, questioning their true embryologic origin. We report a case of a midline sternal sinus in an adult, in which intraoperative findings were consistent with a dermoid origin, yet histopathologic examination revealed features more characteristic of a branchial cleft origin.

Methods : A 25 years old man was referred from the department of dermatology for anterior chest complicated cyst with dermal sinus. The mass gets bigger during winter and had a mucinous discharge occasionally. Ultrasonography revealed a well-defined heterogeneous echoic soft tissue lesion in deep subcutaneous layer. Complete excision and biopsy were performed under local anesthesia.

Results : Intraoperatively, the sinus tract was firmly attached to the manubrium and surrounded by dense fibrosis, likely due to chronic inflammation. Multiple secondary branching tracts required two additional incisions for complete en bloc excision. Adnexal structures, including hair follicles, were observed within the tract.

However, Histopathologic examination revealed ciliated respiratory-type epithelium, stratified squamous epithelium, lymphoid aggregates with reactive germinal centers, and salivary gland tissue, findings more consistent with a branchial cleft origin. No postoperative complications were observed, with the patient maintaining satisfactory recovery at 4-month follow-up.

Conclusion : This case demonstrates a rare midline anterior chest sinus with discordant features: intraoperative findings consistent with a dermoid sinus and histopathologic features suggestive of a branchial cleft anomaly. Unlike previously reported cases, which are typically lateral and dermoid in nature, this lesion supports the possibility of a spectrum or hybrid entity between dermoid and branchial cleft origins. Recognition of such atypical presentations is important for accurate diagnosis and may provide insight into the embryologic development of anterior chest congenital sinuses.

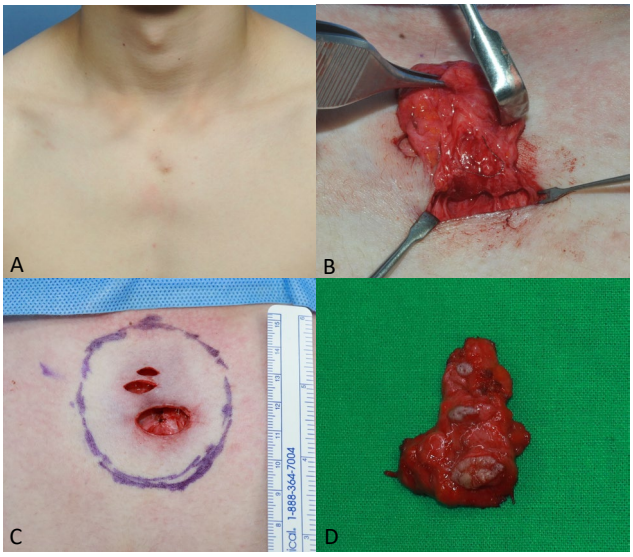

Fig. 1. Clinical and intraoperative photographs. (A)Preoperative view of the midline anterior chest sinus. (B)Intraoperative view showing hair follicles within the tract, suggesting dermoid origin. (C)Intraoperative view of multiple secondary branching tracts requiring two additional incisions. (D)Gross specimen demonstrating complex sinus tract architecture.

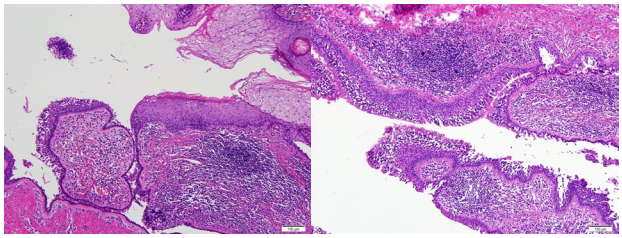

Fig. 2. Histopathologic findings (H&E stain). Left : demonstrating stratified squamous epithelium with adjacent lymphoid aggregates, Right : ciliated respiratory-type epithelium

EP-179

괴사성 근막염 후 발생한 광범위 골반부 연부조직 결손을 위한 맞춤형 재건 전략: 기능 보존을 위한 선택적 접근법

(Tailored Reconstructive Strategy for Extensive Pelvic Soft Tissue Loss After Necrotizing Fasciitis: Selective Approach for Functional Preservation)

분당서울대학교병원
이창건, **김종호***

Purpose: Necrotizing fasciitis of the pelvic region often results in extensive soft tissue loss, posing significant reconstructive challenges. Specifically, defects involving joint-related areas such as the inguinal region and hip joint require careful consideration to prevent postoperative contracture and long-term functional impairment.

Methods: We report two cases of pelvic necrotizing fasciitis resulting in massive soft tissue defects following aggressive surgical debridement. Given the extensive wound dimensions, complete flap coverage was impractical. Reconstruction was therefore planned using a selective approach: Flap coverage was prioritized for functionally critical regions involving inguinal area and hip joint, while the remaining defects were managed with split-thickness skin grafting.

Results:
Both patients achieved stable wound coverage without major complications. Flap reconstruction over joint-related regions successfully preserved range of motion and prevented contracture. Skin-grafted areas also healed without significant morbidity. Both patients demonstrated satisfactory reconstructive outcomes with no significant functional limitations during follow-ups.

Conclusion:
In extensive pelvic soft tissue defects caused by necrotizing fasciitis, a tailored reconstructive strategy is essential. Prioritizing flap coverage for joint-related regions while selectively applying skin grafts to non-critical areas can optimize both functional and reconstructive outcomes.

Fig. 1. Preoperative photographs of a 74-year-old female with extensive soft tissue defect at bilateral pelvic region (40 x 40cm) and Rt. inner thigh (20 x 11cm) due to necrotizing fasciitis (A, C).
Postoperative (4 months) photographs of the patient with pedicled VRAM flap, bilateral pelvic region and STSG, Rt. inner thigh (B, D).

Fig. 2. Preoperative photographs of a 65-year-old male with extensive soft tissue defect at Lt. pelvic region and Lt. thigh (30 x 20cm) due to necrotizing fasciitis.

Fig. 3. Postoperative (15 months) photographs of the 65-year-old male with free LD flap and STSG, Lt. pelvic region and Lt. thigh

EP-180

미골부 척추 통증주사 부위에서 발생하여 모소낭종으로 오인된 편평세포암

(Squamous Cell Carcinoma Arising at a Spinal Injection Site in the Coccygeal Region Mimicking Pilonidal Disease)

전남대학교

나희로, 최준호*

Purpose: Chronic wounds in the coccygeal region are often difficult to heal due to the deep intergluteal cleft, which creates a warm, moist environment with poor aeration and repeated mechanical irritation. The occurrence of skin cancer arising from a chronic wound after spinal injection in this region is extremely rare, and deep-seated masses located near the coccygeal bone may be misdiagnosed as pilonidal disease. We report a case of squamous cell carcinoma that developed in a chronic wound following spinal injection.

Methods: A 72-year-old woman presented with a non-healing lesion measuring 4 × 2 cm in the coccygeal area, accompanied by pus-like discharge and skin defect. Two years prior, the patient had undergone a spinal injection for pain associated with a herniated nucleus pulposus. Thereafter, she developed persistent pain and recurrent discharge at the injection site, which did not improve despite ongoing conservative treatment. Magnetic resonance imaging suggested a pilonidal cyst located above the periosteum of the coccyx. En bloc excision was performed, and histopathological examination revealed squamous cell carcinoma with a positive surgical margin. Positron emission tomography–computed tomography showed no distant metastasis but confirmed residual tumor at the surgical site. A wide excision with a 1-cm safety margin was subsequently performed.

Results: Adjuvant radiotherapy was administered to the surgical site. Radiation dermatitis developed but improved with conservative management. No evience of recurrence was observed during the 6-month follow-up period.

Conclusion: Squamous cell carcinoma should be included in the differential diagnosis of non-healing skin lesions in the coccygeal area following spinal injection.

Fig. 1. A 72-year-old woman presented with a 4 × 2 cm chronic wound in the coccygeal area following a spinal injection. (A) Preoperative photograph. (B) Magnetic resonance imaging showing a lesion in the coccygeal region initially diagnosed as a pilonidal cyst (red arrow). (C) Postoperative positron emission tomography–computed tomography demonstrating residual tumor at the surgical site (red arrow).

Fig. 2. Intraoperative photographs. (A) Preoperative design with a 1-cm safety margin. (B) The coccygeal region exposed after wide excision. (C) Immediate postoperative photograph.

Fig. 3. Postoperative photograph obtained 6 months after surgery. Radiation dermatitis developed but healed satisfactorily.

EP-181

등 상부의 방치된 표피낭종에서 기인한 광범위 피부 결손 및 괴사성 근막염의 치료 증례

한림대학교성심병원

김준일, 김재현, 정찬민*

Purpose: While epidermal cysts are typically easily treatable, complications may occur when these cysts are overlooked, potentially resulting in severe outcomes. This case report presents a 37-year-old male with an extensive skin and soft tissue defect with necrotizing fasciitis resulting from the neglected epidermal cyst on the upper back.

Methods: A 37-year-old male presented to our clinic with a 12 x 10 cm epidermal cyst on his back. Seven days before, the patient had been diagnosed with two 2 x 3 cm epidermal cysts at a local clinic but did not seek treatment. Upon admission, the cyst had ruptured, necessitating incision and drainage (I & D) (Fig. 1). Magnetic Resonance Imaging (MRI) revealed a wide soft tissue defect with necrotizing fasciitis in the back muscles (Fig. 2). Further debridement was performed and intraoperative findings showed extensive necrotic tissue and involvement of muscles (Fig. 3). After debridement, a soft tissue defect measuring 35 x 30 cm was identified. The defect was covered with negative pressure wound therapy (NPWT) followed by split-thickness skin grafting (STSG).

Results: Surgical debridement eliminated inflammatory tissue, and the resulting soft tissue defect was managed with NPWT. Following the alignment of wound margins, STSG was performed. At 6 weeks postoperatively, the patient fully recovered without complications (Fig. 4).

Conclusion: This case report emphasizes the potential consequences of neglecting an epidermal cyst, leading to life-threatening conditions such as necrotizing fasciitis. It also presents a significant skin defect that requires surgical coverage when an epidermal cyst is left untreated.

Fig 1. Preoperative gross photography after incision and drainage (I & D)

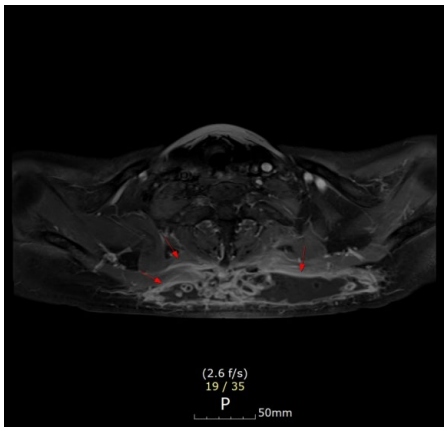

Fig 2. Preoperative Magnetic Resonance Imaging (MRI)

Fig 3. Intraoperative gross photography

Fig 4. Postoperative gross photography (after 6 weeks)

EP-182

폐쇄동맥 천공지 피판을 이용한 방사선 관련 직장질루 재건술

(Reconstruction of Radiation-Associated Rectovaginal Fistula Using Obturator Artery Perforator Island Flap)

전북대학교 의과대학
성형외과학교실

이상훈, 이내호, 신진용, 정윤규, 노시균*

Purpose: Radiation-associated rectovaginal fistula following multimodal treatment for rectal cancer represents complex reconstructive challenges. Fibrosis, impaired vascularity, and repeated surgical intervention causes high recurrence rates after primary repair. We report salvage reconstruction using pedicled obturator artery perforator (OAP) island flap to achieve durability in heavily irradiated field.

Methods: A 59-year-old woman with rectal adenocarcinoma with liver metastases underwent chemoradiotherapy and laparoscopic ultra-low anterior resection. Due to tumor proximity, intraoperative vaginal tearing occurred. A rectovaginal fistula subsequently developed during postoperative chemotherapy, and recurred despite primary repair.

Definitive reconstruction was performed with colorectal surgery. After rectal re-repair, the radiated scar tissue was excised and pedicled OAP island flap was elevated from proximal medial thigh. The perforator from obturator artery was identified using Doppler guidance and dissected proximally to secure sufficient pedicle. A portion of obturator muscle was included to provide vascularity and bulk. Part of subcutaneous fat of the flap was debrided to match the thickness of vaginal defect. The flap was transferred through subcutaneous tunnel lateral to labia majora and covered the fistula and defect area.

Results: Complete flap survival was achieved without vascular compromise. The flap provided adequate bulk to obliterate dead space and cover the fistula. Early follow-up demonstrated stable vaginal reconstruction and absence of recurrent fistula without complication.

Conclusion: Recurrent rectovaginal fistula after chemoradiotherapy and rectal surgery requires robust vascularized interposition. The pedicled obturator artery perforator island flap offers sufficient perfusion with tissue bulk, and tension-free transfer without microsurgical burden. This technique provides practical and durable options for complex radiation-associated rectovaginal fistula.

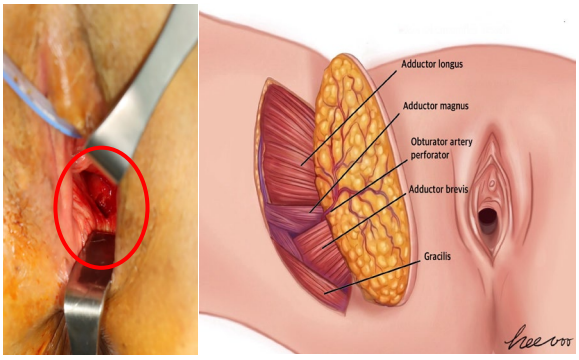

Fig. 1. Rectovaginal fistula and schematic illustration of the pedicled obturator artery perforator (OAP)–based island flap. The perforator arising from the obturator artery is centered within a proximal medial thigh skin paddle, with inclusion of a portion of the obturator muscle to provide vascularized bulk for interposition.

Fig. 2. Intraoperative view demonstrating elevation of the pedicled OAP island flap from the proximal medial thigh, centered over the Doppler-identified perforator. Tension-free inset of the OAP island flap into the vaginal defect was done, providing well-vascularized interposition after radical debridement and rectal repair.

EP-183

자가지방이식 후 발생한 골반부 피부괴사의 단계적 재건 치료

(Pelvic Skin Necrosis Following Autologous Fat Grafting: Successful Management with Staged Reconstruction)

순천향대학교 부속 서울병원

김경빈, **송우진***

Purpose: Autologous fat grafting is widely used for body contour augmentation and is generally considered safe; however, complications such as fat necrosis, cellulitis, and skin necrosis may occur. We report a case of pelvic skin necrosis following autologous fat grafting, successfully managed with staged surgical treatment.

Methods: A 41-year-old woman with no significant past medical history underwent autologous fat grafting to the gluteal and pelvic regions at another hospital one month before presentation. One week after the procedure, she developed bilateral pelvic soft tissue inflammation and received antibiotic injections. The left side improved, but the right progressively worsened. On presentation, a 3 × 4 cm area of skin necrosis was observed in the right pelvic region (Fig. 1). Laboratory evaluation showed mildly elevated C-reactive protein. Intravenous antibiotics were initiated. Magnetic resonance imaging revealed cellulitis and fat necrosis (Fig. 2). Debridement under local anesthesia exposed necrotic fat with inflammatory discharge and underlying soft tissue, and negative pressure wound therapy was applied.

Results: After one week of negative pressure therapy, healthy granulation tissue had formed (Fig. 3). Definitive reconstruction was performed using a local rotation flap under local anesthesia. The postoperative course was uneventful, without flap-related complications, fluid collections, or recurrent infection. The wound healed without complications (Fig. 4).

Conclusion: Skin necrosis after autologous fat grafting can cause cosmetically significant defects distressing to patients. Staged surgical management, including initial debridement with negative pressure wound therapy followed by local flap reconstruction, can achieve favorable functional and aesthetic outcomes.

Figure 1. Initial presentation at outpatient clinic. A necrotic skin defect in the right pelvic region is observed with inflammatory discharge and exposure of underlying soft tissue.

Figure 2. Coronal T1-weighted magnetic resonance image obtained after admission, demonstrating a low-signal lesion in the right pelvic region consistent with fat necrosis.

Figure 3. Wound condition after negative pressure wound therapy, showing well-formed granulation tissue and design of the planned local rotation flap.

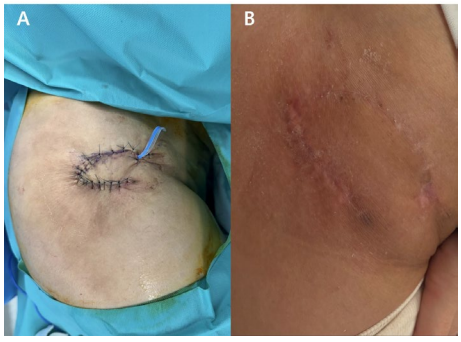

Figure 4.

(A) Immediate postoperative photograph following local rotation flap reconstruction.
(B) One-month postoperative photograph obtained at outpatient follow-up.

EP-184

화상 반흔에서 발생한 편평세포암 절제와 반흔 구축 동시 교정 : 증례보고

(Removal of squamous cell carcinoma caused by burn scars and concurrent scar revision surgery - Case report)

경상국립대학교병원
성형외과

신재봉, 이경석*

Purpose : Burn scars can lead to chronic skin complications, including malignant transformation such as squamous cell carcinoma (SCC). Managing both oncologic safety and functional limitations from scar contracture remains challenging. This study reports a case in which SCC arising from a long-standing burn scar was excised while simultaneously correcting scar contracture.

Methods : A 73-year-old female presented with a chronic abdominal burn scar sustained 50 years earlier. A progressive ulcerative lesion developed within the scar and biopsy confirmed squamous cell carcinoma. Surgical treatment consisted of wide excision of the tumor with intraoperative frozen biopsy to confirm clear margins. Reconstruction of the defect was performed using a bilobed local flap. In addition, a long-standing scar contracture measuring approximately 30×5 cm was released using zig-zag scar revision (Z-plasty).

Results : Complete excision of the carcinoma with negative margins was achieved. The bilobed flap provided stable coverage of the abdominal defect. Simultaneous scar contracture release improved abdominal tension and relieved associated discomfort. Postoperatively, the patient experienced resolution of pain and discharge, improved abdominal mobility, and satisfactory aesthetic outcomes. No complications were observed during the recovery period.

Conclusion : Simultaneous tumor excision and scar contracture release can effectively address both oncologic and functional problems in burn scar–associated SCC. Combined reconstruction using local flap coverage and scar revision may provide favorable functional and aesthetic outcomes.

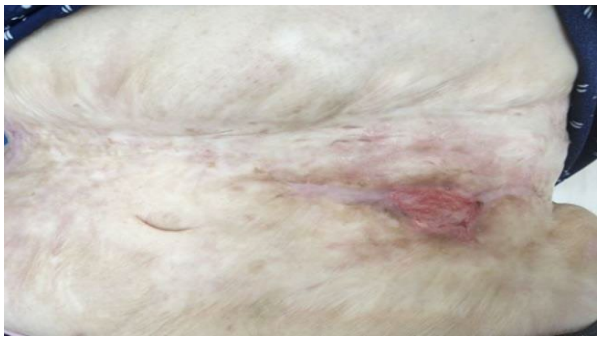

Fig. 1. Photograph of the patient's abdominal area before surgery. A 30x5cm burn scar is observed horizontally, and squamous cell carcinoma is observed in the lower left abdomen.

Fig. 2. Photograph of the squamous cell carcinoma that was removed during surgery

Fig. 3. Photograph of the patient's abdomen one month after the surgery

EP-185

광배근 근피 피판을 이용한 인공심박동기 삽입 후 발생한 피부 결손의 재건

(Reconstruction of Skin Defect Following Pacemaker Insertion Using a Pedicled Latissimus Dorsi Muscle Flap)

인제대학교 일산백병원
지정민, 이수향*

Purpose: The incidence of cardiac implantable electronic device (CIED) infections and pocket erosions is reported to range from 1% to 7%. Compromised tissue integrity often leads to high recurrence and systemic infection, making conservative management challenging. When such approaches fail, well-vascularized soft tissue coverage is essential. We report two cases successfully treated with pedicled latissimus dorsi (LD) muscle flaps

Methods: Two patients presented with localized infections and skin defects 1 year and 8 years post-pacemaker implantation. Despite initial conservative management with intensive dressing, the skin continued to thin, and the defect size remained unchanged, posing a high risk of permanent device failure. To provide durable coverage, a pedicled LD muscle flap was utilized. The surgical procedure involved Harvesting the LD muscle through a lateral thoracic incision and transposing it via a subcutaneous tunnel to the anterior chest. The flap was meticulously positioned to cover the hardware and obliterate the dead space.

Results: In both cases, the LD flaps survived completely without congestion or necrosis. The robust vascularity of the muscle flap facilitated the resolution of the localized infection and provided sufficient bulk to prevent further device exposure. The pacemakers remained fully functional throughout the follow-up period, with no recurrence of skin thinning or defects.

Conclusion: The pedicled LD flap is a versatile and reliable option for reconstructing chest wall defects involving pacemaker exposure. It provides superior vascularized tissue compared to conservative approaches, effectively preventing recurrent infection and hardware complications.

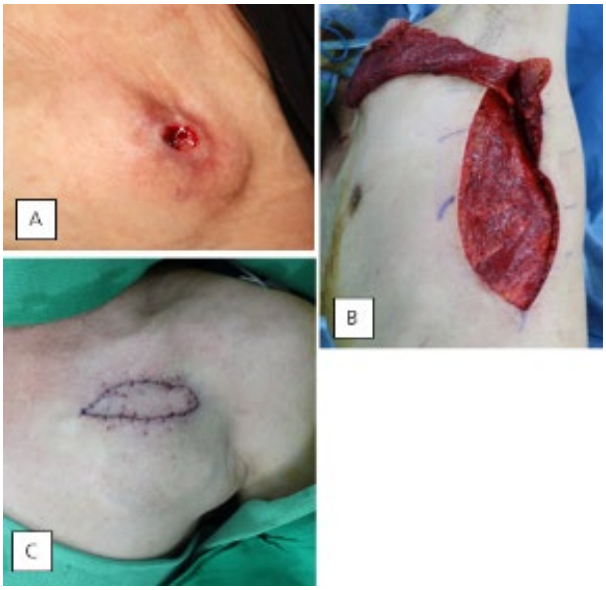

Fig. 1. Photographs of a patient who underwent surgery for inflammation and a skin defect that developed 8 years after pacemaker implantation.
(A) Preoperative photograph
(B) Intraoperative photograph
(C) Postoperative photograph

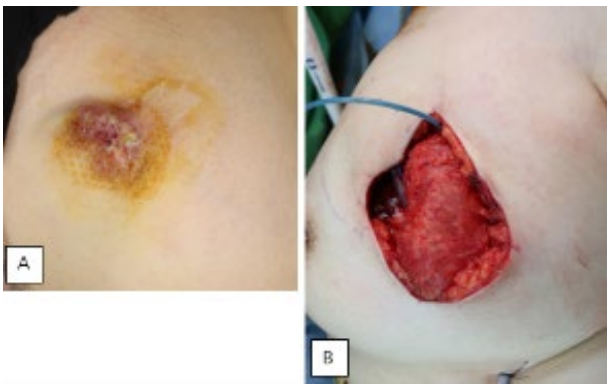

Fig. 2. Photographs of a patient who underwent surgery for inflammation and a skin defect that developed 1 years after pacemaker implantation.
(A) Preoperative photograph
(B) Intraoperative photograph

EP-186

융기성 피부섬유육종 광범위 절제 후 어깨 결손의 재건에 있어 흉견봉동맥 천공지 기반 프로펠러 피판의 임상적 의의

(Thoracoacromial Artery Perforator Propeller Flap for Shoulder Reconstruction After Wide Excision of Dermatofibrosarcoma Protuberans)

순천향대학교 부속
부천병원 성형외과

안동혁, 최창용, 신호성, 박은수*

Purpose: Dermatofibrosarcoma protuberans (DFSP) is a rare, locally aggressive cutaneous soft tissue sarcoma with a high propensity for local recurrence. Wide local excision with adequate margins is the standard treatment; however, reconstruction after tumor resection in the shoulder and upper anterior chest wall region remains challenging due to functional and aesthetic considerations

Methods: Immediate reconstruction was achieved using a thoracoacromial artery perforator–based fasciocutaneous propeller flap. The flap was elevated in the subfascial plane and rotated 120 degrees to achieve tension-free coverage.

Results: A 43-year-old male presented with a slowly growing mass in the right shoulder region. An initial excisional biopsy confirmed the diagnosis of DFSP. Subsequently, wide local excision with a 3-cm safety margin, including the deep fascia, was performed, resulting in a 6 × 6 cm soft tissue defect. Immediate reconstruction was achieved using a thoracoacromial artery perforator–based fasciocutaneous propeller flap. The flap was elevated in the subfascial plane and rotated 120 degrees to achieve tension-free coverage. Postoperatively, the flap survived completely without complications. Final histopathological examination confirmed negative peripheral and deep resection margins.

Conclusion: This case demonstrates that a thoracoacromial artery perforator–based fasciocutaneous propeller flap is a reliable and effective reconstructive option following wide excision of DFSP in the shoulder and upper anterior chest wall region. The technique provides durable soft tissue coverage while preserving shoulder function and minimizing donor-site morbidity, making it a valuable option for oncologic reconstruction in this anatomically demanding area.

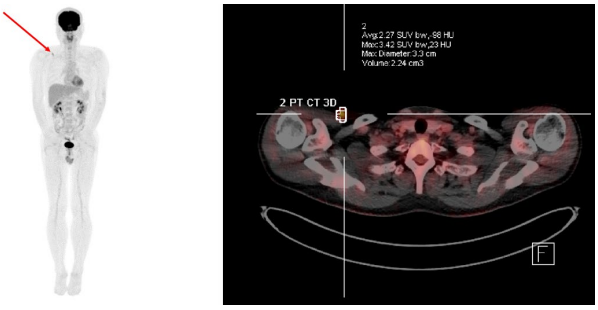

Figure 1 PET–CT demonstrated increased residual uptake at the site of cancer excision.

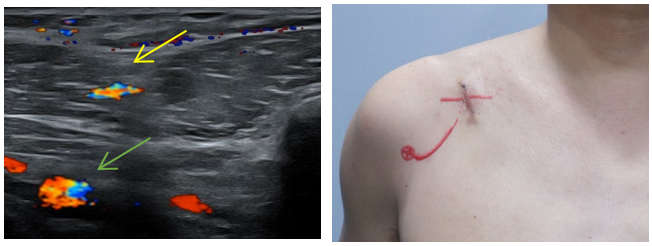

Figure 2a USG image shows tracing of the deltoid branch of the thoracoacromial artery (Yellow arrow) & axillary artery (Green arrow)

Figure 2b Marking of the traced thoracoacromial artery.

Figure 3a Design of a thoracoacromial artery perforator–based propeller flap (6 × 11 cm).

Figure 3b Subfascial thoracoacromial artery perforator–based propeller flap with preservation of the dominant perforator

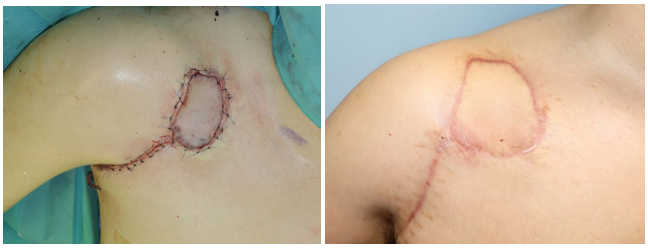

Figure 4 Thoracoacromial artery perforator–based fasciocutaneous propeller flap after 120-degree rotation, achieving tension-free coverage of the defect.

Figure 5 Postoperative photograph (March 10, 2026; POD 36) showing a stable thoracoacromial artery perforator–based propeller flap with well-maintained defect coverage.

EP-187

성인 피부근염 환자에서 다발성 석회침착증에 대한 단계적 수술적 절제를 통한 기능 회복: 증례보고

(Stepwise Surgical Excision of Multifocal Calcinosis Cutis Restores Function in Adult Dermatomyositis: A case report)

부산대학교 의과대학
영상의학교실[1] ,성형외과학교실[2]

황민희[1], 강동협[2], 이치현[2], 이창렬*[2]

Purpose: Calcinosis cutis associated with dermatomyositis can cause significant pain, neurologic symptoms, and joint restriction. Surgical excision is considered for refractory symptomatic lesions; however, experience with staged procedures in multifocal adult disease is limited. This study aimed to evaluate the clinical effectiveness of staged selective excision in a patient with multifocal calcinosis cutis causing neurologic compromise and functional limitation.

Methods: A woman in her sixties with dermatomyositis presented with painful calcified masses in the left buttock, both axillae, and left upper arm. Imaging confirmed multifocal dystrophic calcifications. Surgical excision was performed in stages according to symptom severity: first the buttock lesion due to sciatic-type radiating pain, followed by the right axillary lesion for shoulder motion restriction, and subsequently the left axillary and upper-arm lesions. Clinical outcomes, functional improvement, and recurrence were evaluated during follow-up.

Results: Excision of the buttock lesion resulted in immediate resolution of radiating pain. Subsequent axillary excisions led to improvement in shoulder abduction and functional mobility. Histopathology confirmed dystrophic calcification in all specimens. No recurrence or major complications were observed during 30 months of follow-up.

Conclusion: Conclusion: Staged, selective excision provided substantial symptomatic relief and functional improvement in a patient with multifocal calcinosis cutis associated with dermatomyositis. An individualized, symptom-based surgical approach may represent an effective treatment strategy, particularly in cases where lesions result in neurologic compromise or mechanical restriction of movement.

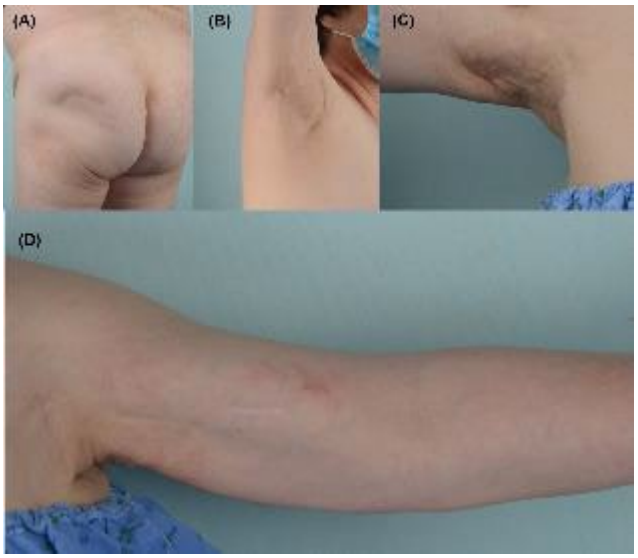

Fig. 1. Examination revealed an 8-cm firm, irregular mass in the left buttock producing sciatic-type radiating pain (Fig. 1A). Large palpable calcifications were present in both axillae (Fig. 1B, C), and a smaller lesion was noted in the left upper arm (Fig. 1D)

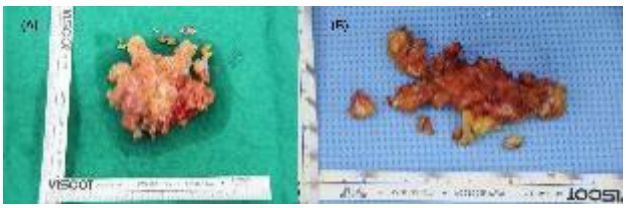

Fig. 2. Multiple firm, lobulated calcified nodules were removed en bloc (Fig. 2A), and radiating pain resolved immediately. Persistent restriction of right shoulder motion prompted excision of the right axillary lesion four months later (Fig. 2B).

EP-188

장관 봉합 없이 노출된 장의 복부 재건을 위한 전외측 대퇴 피판 교차 맞물림 기법

Interdigitation of an Anterolateral Thigh Flap for Abdominal Coverage of Exposed Bowel Without Enteric Repair

한양대학교 의과대학
성형외과학교실

이수인, 장란숙, 김효성, 김지영, 김연환*

Purpose: Abdominal wall reconstruction is generally deferred until bowel continuity is restored because persistent enterocutaneous fistula increases the risk of infection and flap failure. We report a salvage case of abdominal wall reconstruction performed despite unrepaired bowel rupture when further enteric repair was not feasible.

Methods: A 59-year-old woman (BMI 37.2) underwent a Hartmann procedure for panperitonitis due to sigmoid colon perforation. Primary abdominal closure was impossible because of severe inflammation. Repeated debridement was performed, and an initial free latissimus dorsi musculocutaneous flap (33 × 20 cm) failed due to vascular complications. Subsequent dermal substitute application with split-thickness skin grafting revealed two bowel rupture sites (2 cm and 5 cm) with persistent leakage. As re-exploration was considered high risk and conservative management failed after prolonged fasting, definitive reconstruction was undertaken using a 25 × 17 cm pedicled anterolateral thigh flap. The distal flap was divided into three finger-like projections and inset in a watertight interdigitated fashion around the exposed bowel.

Results: The flap survived completely without necrosis or dehiscence. At 2-month follow-up, the abdominal wall remained stable without new fistula formation. The pre-existing fistulas were managed conservatively, and controlled oral feeding was initiated without exacerbation of leakage.

Conclusions: In carefully selected high-risk patients where definitive bowel repair is not feasible, strategically designed pedicled ALT flap reconstruction may serve as a viable salvage option for complex abdominal wall defects with persistent enteric exposure.

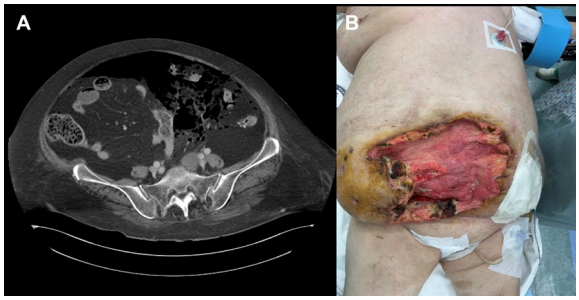

Fig. 1. Initial presentation. (A) Abdominal computed tomography demonstrating sigmoid colon perforation with diffuse panperitonitis. (B) Intraoperative view after Hartmann procedure showing an open abdominal wall defect due to severe edema and inflammation.

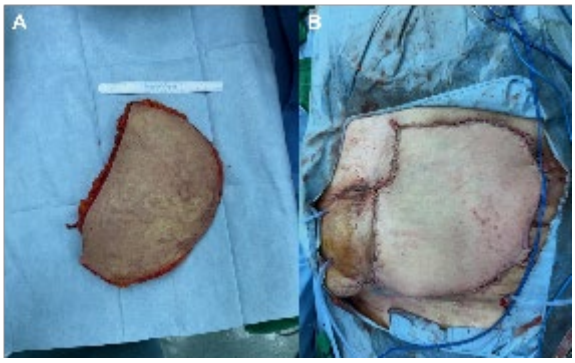

Fig. 2. (A) Free latissimus dorsi musculocutaneous flap inset (33 × 20 cm). (B) Initial abdominal wall reconstruction attempt.

Fig. 3 Development of enterocutaneous fistula. Two exposed bowel defects measuring approximately 2 cm and 5 cm with persistent enteric leakage.

Fig. 4 Salvage reconstruction using pedicled anterolateral thigh (ALT) flap. (A) Harvested 25 × 17 cm pedicled ALT flap. Distal portion divided into three finger-like projections. Interdigitated and watertight inset around exposed bowel segments. (B) Postoperative outcome at 2 months. Stable abdominal wall coverage without new fistula formation. The pre-existing fistulas were conservatively managed with controlled oral feeding.

EP-189

비전형적 양상으로 나타난 탄력섬유종: 전형적 2예와 한 가지 진단적 함정

Elastofibroma in Atypical Settings: Two Typical Cases and One Diagnostic Pitfall

순천향대학교부속
천안병원 성형외과
김민욱, 김준혁, 이다운, 변제연, 최환준*

Purpose : Elastofibroma dorsi is a benign fibroelastic lesion that often presents as an infrascapular mass but may be confused with other soft-tissue tumors. We describe two typical cases and one atypical case to highlight practical imaging clues.

Methods : We reviewed three representative patients evaluated for posterior shoulder or back masses. Imaging included contrast-enhanced computed tomography (CT) and/or magnetic resonance imaging (MRI) in the typical cases, and ultrasonography with Doppler in the pitfall case. Diagnosis was supported by image-guided biopsy or excision, as clinically indicated.

Results : In two typical cases, MRI and CT demonstrated a poorly marginated, heterogeneous laminated or striated mass with interspersed fat at the scapulothoracic interface, deep to the serratus anterior (Figure 1), leading to radiologic suspicion of elastofibroma. In the pitfall case, a young patient was referred after minor trauma with suspected hematoma. However, ultrasonography showed a well-defined hypoechoic lesion in the deep subcutaneous layer without Doppler flow and was interpreted as lipoma (Figure 2). Given persistent concern and diagnostic uncertainty, excision was performed and ultimately confirmed elastofibroma (Figure 3).

Conclusions : A fat-streaked, striated mass deep to the serratus anterior on CT or MRI is strongly suggestive of elastofibroma. Pitfalls include presentation in younger patients and in non-infrascapular locations, and ultrasonography may mimic lipoma. Familiarity with the typical imaging pattern can help streamline evaluation, while elastofibroma should still be considered in atypical presentations to guide appropriate follow-up and tissue diagnosis when needed.

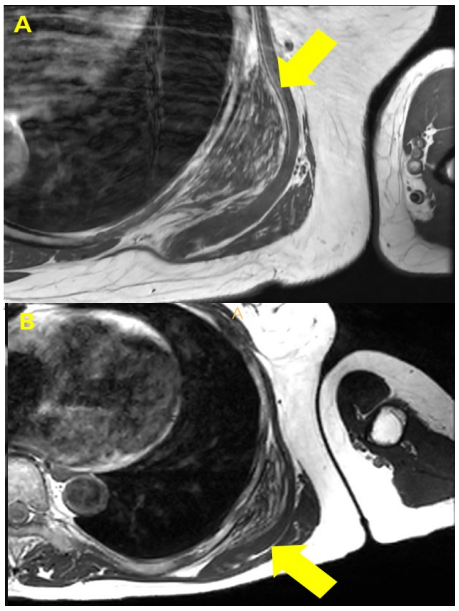

Figure 1. Representative imaging findings from two typical cases of elastofibroma. (A, B) Axial MR images show a poorly marginated, heterogeneous lesion with interspersed fat at the scapulothoracic interface, deep to the serratus anterior.

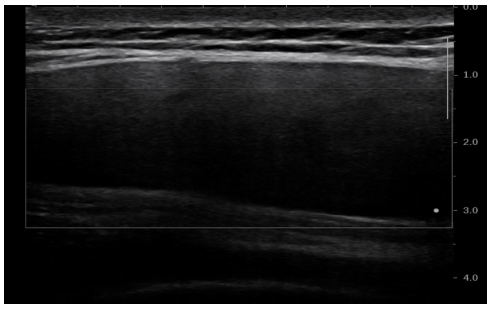

Figure 2. Ultrasonography of the pitfall case showing a well-defined hypoechoic lesion in the deep subcutaneous layer without Doppler flow, initially interpreted as lipoma.

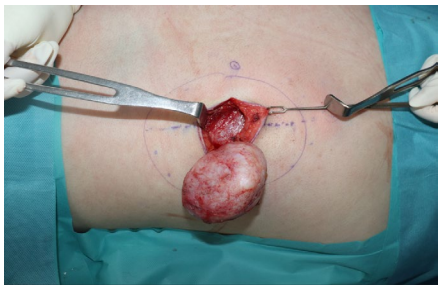

Figure 3. Intraoperative photograph of the pitfall case showing excision of a well-defined mass from the deep subcutaneous layer, which was subsequently confirmed as elastofibroma.

EP-190

등부위 괴사성 근막염에 대한 유경 광배근 피판술을 이용한 치험례

(Treatment of necrotizing fasciitis on back using a pedicled latissimus dorsi flap : A case report)

한양대학교 의과대학
성형외과학교실
한양대학교구리병원
성형외과

이보현, 장정우*

Purpose: Necrotizing fasciitis suddenly emerges on immunosuppressed patient with life-threatening condition. Immediate fasciectomy with debridement is inevitable, but it often leaves large defect with dead space. For this reason, appropriate reconstruction is essential for complete treatment. We present a case of necrotizing fasciitis on back, treated successfully using a pedicled latissimus dorsi flap.

Methods: A 46-year-old female with necrotizing fasciitis on back was referred to plastic surgery department. The patient had uncontrolled diabetes mellitus and showed a 12 x 10cm sized skin necrosis with extensive fasciitis on upper back. The necrosis progressed with forming large amount of abscess, and immediate debridement including fasciectomy was performed. After four weeks, reconstruction was planned with a pedicled latissimus dorsi musculocutaneous flap.

Results: A pedicled latissimus dorsi flap was elevated from right side under lateral position. After doppler tracing, a skin flap was designed on lower lateral region, and an island type latissimus dorsi musculocutaneous flap was elevated. The flap was rotated to the wound with 25cm length of pedicle. The muscular portion occupied dead space with enough volume, and the fasciocutaneous portion resurfaced skin defect adequately. The flap survived without major complication.

Conclusion: Treating necrotizing fasciitis is always difficult especially when it emerges on back. Since it is dependent portion, complete obliteration of dead space is necessary to reduce seroma formation. Protecting the lesion from friction by resurfacing with durable skin flap is essential as well.

Fig. 1. A 46-year-old female with necrotizing fasciitis on back. (Left) A 12 x 10cm sized skin necrosis with extensive fasciitis on upper back. (Right) Reconstruction using a pedicled latissimus dorsi musculocutaneous flap after 4 weeks.

Fig. 2. 6 months after the reconstruction. (Left) Successful reconstruction without recurrence. (Right) No donor site morbidity including contracture.

EP-191

피부암 절제 후 두 개의 초승달형 피판을 이용한 재건

(Reconstruction using two crescentic flaps after wide excision of skin cancer)

건국대학교 의과대학
성형외과학 교실
육유정, 이명철*

건국대학교 의과대학
성형외과학 교실
신동혁, 최현곤, 김지남, 이명철

Purpose: Skin cancers are common cutaneous malignancies. They involve various anatomical areas, including the face, neck, trunk, and extremities. To achieve optimal outcome, wide excision of the malignant lesion should be prioritized. When adjacent tissues are confirmed to be free of malignancy, an appropriate reconstructive procedure can be performed after pathologic examination. Reconstruction should preserve the natural contour and aesthetic appearance of the involved area. We performed reconstruction of skin and soft-tissue defects after wide excision of skin cancer using two crescentic flaps and report the postoperative outcomes herein.

Methods: From June 2023 to April 2025, we used two crescentic flaps to reconstruct skin and soft-tissue defects remaining after oncologic surgery. Two crescent-shaped flaps were created from dog-ear deformities after approximation of the adjacent tissues following wide excision. The crescentic flaps were then transposed to the defect, and the wound was repaired without excessive tension. Postoperative outcomes were evaluated on the basis of the healing process, tissue contour, and wound-related complications.

Results: Thirty-four patients underwent wide excision followed by reconstruction with two crescentic flaps. Transposition of the two crescentic flaps provided adequate coverage of the defects while preserving a natural contour. Five patients developed transient congestion in one of the two flaps; however, the congestion resolved within 10 days postoperatively. Additional geometric analysis using the amount of approximation, and the length-to-width ratio of the defect, showed the estimation of dissection for successful reconstruction.

Conclusion: Substantial tissue defects after wide excision of skin cancer require appropriate reconstructive options. Two crescentic flaps created from dog-ear tissue successfully covered these defects. Various reconstructive procedures can be considered after oncologic surgery for skin cancer, and two crescentic flaps may be one option because of their tissue efficiency and minimal donor-site morbidity.

Fig. 1. Sequential procedures of two crescentic flaps. The 78-year-old male patient presented with malignant melanoma on mid-back area. After wide excision with a 2cm safety margin, a large skin and soft tissue defect was noted. The upper and lower margins were approximated; however, a sausage-shaped defect remained with dog-ear deformities on both lateral ends. The redundant dog-ear tissue was used as a flap rather than discarded. The pedicles of the flaps were located approximately two-thirds of the distance from the center to the lateral end of the longitudinal wound **(black arrow).** The two flaps were transposed to cover the defect **(yellow arrow).** Because the crescentic flaps could be stretched without excessive tension, they met at the center of the defect. The flap margins and the donor sites from which the flaps originated were then repaired layer by layer to avoid excessive tension.

Fig. 2. The 90-year-old female patient presented with squamous cell carcinoma on the left dorsum of the foot. After wide excision with a 5mm safety margin, a large skin and soft tissue defect was noted. The proximal and distal margins were approximated; however, a sausage-shaped defect remained with dog-ear deformities on both lateral ends. The redundant dog-ear tissue was used as a flap. The two flaps were transposed to cover the defect**.** The crescentic flaps met at the center of the defect without excessive tension.

EP-192

신경섬유종증 환자에서 재발성 신경섬유종으로 의심된 비대칭적 등쪽 몸통 다발성 표피낭종

(Multiple Asymmetric Epidermal Cysts of the Posterior Trunk Mimicking Recurrent Neurofibromas in a Patient with Neurofibromatosis)

조선대학교

정화순, 천지선*, 최우영, 양정열

Purpose: Multiple subcutaneous masses in patients with a history of neurofibromatosis (NF) are frequently presumed to represent recurrent neurofibromas. However, other benign lesions may clinically mimic this presentation. We report a rare case of asymmetrically distributed multiple epidermal cysts involving the posterior trunk in a patient with prior surgery for neurofibromatosis.

Methods: A 45-year-old woman presented with multiple palpable masses extending asymmetrically from the shoulder to the gluteal region along the posterior trunk. She had undergone surgical excision for neurofibromatosis 10 years earlier. Physical examination identified a total of 15 subcutaneous nodules. Computed tomography was performed to evaluate lesion distribution and depth. Based on her medical history and clinical presentation, recurrent neurofibromas were strongly suspected preoperatively. Complete surgical excision of all lesions was performed, and specimens were submitted for histopathologic analysis.

Results: Histopathologic evaluation revealed 14 epidermal cysts and 1 lipoma, with no evidence of neurofibroma or malignancy. All lesions were completely excised. The postoperative course was uneventful, with no wound complications During 3-month follow-up period, no recurrence was observed.

Conclusion: In patients with a history of neurofibromatosis, multiple posterior trunk masses may not necessarily represent recurrent neurofibromas. Extensive asymmetric multiple epidermal cysts can clinically mimic neurofibromas, highlighting the importance of radiologic evaluation and histopathologic confirmation. Accurate diagnosis is essential for appropriate surgical planning and patient counseling.

Figure 1. Preoperative clinical photograph demonstrating multiple asymmetrically distributed subcutaneous masses extending from the shoulder to the gluteal region along the posterior trunk. (Dotted line outlines indicate masses)

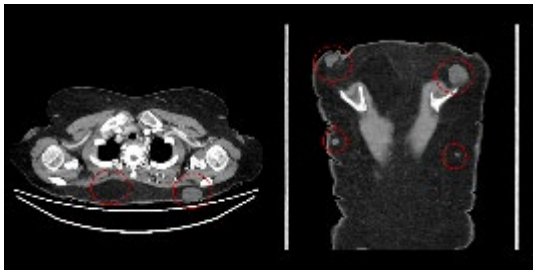

Figure 2. Preoperative computed tomography image demonstrating multiple subcutaneous masses along the posterior trunk. (Dotted line outlines indicate masses)

Figure 3. Immediate postoperative clinical image demonstrating complete excision of the multiple posterior trunk masses. (Dotted line outlines indicate masses)

Figure 4. Gross specimens of the excised posterior trunk masses, confirmed as epidermal cysts and one lipoma on histopathologic examination.

EP-193

확장 광배근 근피판을 이용한 거대 고립성 형질세포종 절제 후 전흉벽결손의 재건

Extended Latissimus Dorsi Myocutaneous Flap for Reconstruction of a Giant Sternal Plasmacytoma Defect

가톨릭대학교 의과대학 성형외과교실

권다윤, 이준호, 서보미, 권호, **정성노***

Purpose: Solitary plasmacytoma rarely presents as a massive anterior chest wall tumor requiring complex skeletal and soft tissue reconstruction. We report successful reconstruction of a giant anterior chest wall plasmacytoma defect using an extended latissimus dorsi musculocutaneous (LDMC) flap.

Methods: A 71-year-old man presented with progressive chest discomfort caused by a rapidly enlarging anterior chest wall mass. Computed tomography (CT) revealed a 13.4 × 7.0 cm enhancing tumor involving the sternum, adjacent ribs, and anterior mediastinum. Following radical tumor resection, pericardial mesh placement, and sternal bar fixation, an 8 × 16 cm chest wall defect remained. A right extended LDMC flap with a distally positioned skin paddle was elevated while preserving the thoracodorsal pedicle. The skin paddle was designed to allow primary closure of the donor site, while sufficient muscle was harvested to ensure reliable coverage of the sternal bar. A portion of the serratus anterior muscle was incorporated to augment muscular coverage over the sternal bar. The flap was tunneled through the axilla and securely fixed to the bilateral pectoralis major and rectus abdominis muscles to provide stable muscular coverage and prosthetic material protection. The donor site was closed primarily in a layer-by-layer fashion.

Results: At 6-month follow-up, the wound remained stable, and the patient was undergoing adjuvant chemotherapy without complications.

Conclusion: Extended LDMC flap reconstruction provides reliable vascularized coverage and sufficient bulk for large anterior chest wall defects after oncologic resection, ensuring durable protection of prosthetic materials and structural stability.

Fig. 1. Preoperative view showing a large anterior chest wall mass.

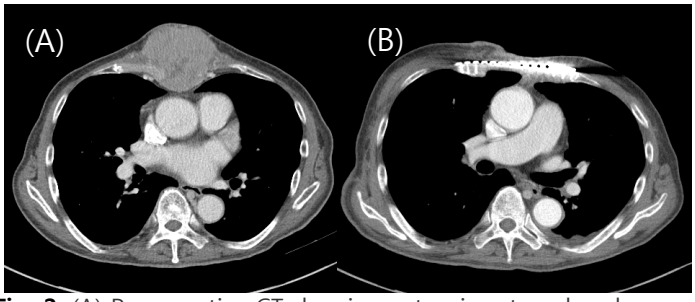

Fig. 2. (A) Preoperative CT showing extensive sternal and mediastinal involvement. (B) Postoperative follow-up CT with a sternal metallic plate covered by a LDMC flap.

Fig. 3. Intraoperative view of flap inset and muscle fixation to adjacent chest wall musculature.

Fig. 4. Postoperative 6-month follow-up showing stable reconstruction.

EP-194

단일 부위에 반복적인 인슐린 주사로 인해 발생한 복부의 광범위 괴사성 근막염 증례

한림대학교성심병원

김준일, 김재현, 정찬민*

Purpose: Injection-related complications are relatively common in patients; however, extensive necrosis of skin and soft tissue is rare. In this case, we report a severe skin and soft tissue necrosis caused by repeated insulin injections confined to a single abdominal site.

Methods: A 66-year-old female with diabetes mellitus presented with erythema and pain at the insulin injection site that had developed one day prior to admission. The patient had been administering insulin injections only to the left upper abdomen, despite knowing the importance of rotating sites. On presentation, extensive skin and soft tissue necrosis was observed, extending from the left upper abdomen to the left flank, thigh, and pubic area (Fig. 1). Surgical debridement revealed necrotizing fasciitis and was repeated until the wound bed became clear. (Fig. 2). Negative pressure wound therapy (NPWT) was then applied for approximately one month to promote granulation tissue formation. (Fig. 3). Subsequently, the defect was covered with a split-thickness skin graft (Fig. 4).

Results: Surgical debridement and NPWT resulted in granulation tissue formation. Definitive coverage with STSG achieved satisfactory wound closure.

Conclusion: This case highlights that extensive necrosis can occur even with commonly used medications when proper injection techniques are not followed. Early recognition and aggressive surgical management, including debridement and NPWT, are crucial for optimal outcomes.

Fig 1. Preoperative gross photography

Fig 2. Intraoperative gross photography (Debridement)

Fig 3. Post-vacuum assisted therapy photography

Fig 4. Postoperative gross photography (STSG)

EP-195

악성 흑색종과 유사한 양상을 보이는 하복부의 단순 한선가시세포종에서 기원한 색소성 상피내 한공암

(Pigmented Porocarcinoma In Situ Arising from Hidrocanthoma Simplex on the Lower Abdemen Mimicking Malignant Melanoma)

대전을지대학교병원

김지민[1], **정성균***[1]

Purpose : Pigmented eccrine porocarcinoma on the abdomen is an exceptionally rare adnexal tumor that is frequently misdiagnosed as malignant melanoma. We report a unique case of pigmented porocarcinoma *in situ* arising from a long-standing hidroacanthoma simplex on the lower abdomen, highlighting its significant diagnostic pitfalls.

Methods : A 72-year-old female presented with a multi-lobulated, deeply pigmented mass on her right lower abdomen. The nodule had been present for 20 years but recently enlarged. Its variegated color and irregular borders clinically mimicked malignant melanoma (Fig. 1). A wide excision with a 10-mm safety margin was performed, and the defect was reconstructed with a tension-free primary closure (Fig. 2).

Results : Histopathological examination revealed intraepidermal nests of poroid cells exhibiting marked nuclear atypia, pleomorphism, and prominent mitotic figures, confirming the malignant transformation into porocarcinoma *in situ* (Fig. 3). Immunohistochemical staining demonstrated that the tumor cells were positive for EMA and CEA, but completely negative for S-100 and Melan-A. The distinct black pigmentation was confirmed to be caused by the prominent colonization of non-neoplastic dendritic melanocytes (Fig. 4), definitively ruling out malignant melanoma.

Conclusion : When evaluating long-standing pigmented lesions on the abdomen, rare adnexal malignancies such as pigmented porocarcinoma must be considered in the differential diagnosis. Accurate histopathological and immunohistochemical evaluations are essential to differentiate these from melanocytic malignancies, thereby preventing overly aggressive surgical overtreatment.

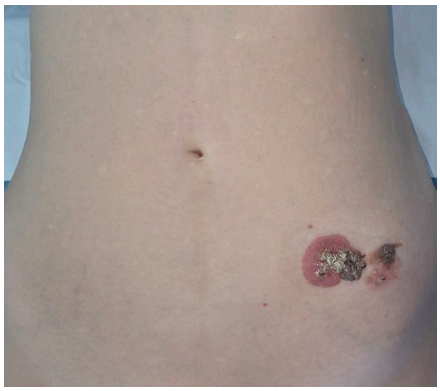

Fig 1. Preoperative clinical appearance. A multi-lobulated, deeply pigmented mass with variegated colors and irregular borders on the left lower abdomen, clinically mimicking malignant melanoma

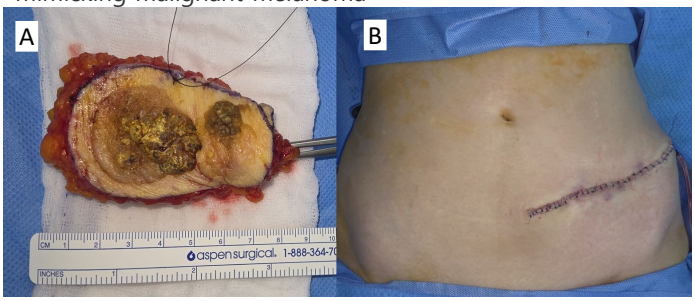

Fig 2. Surgical specimen and postoperative result. (A) Gross specimen of the excised tumor following wide excision with a 10-mm safety margin. (B)Immediate postoperative view showing the defect reconstructed with a tension-free primary closure.

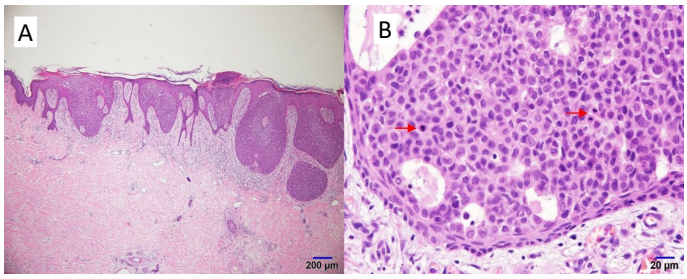

Fig 3. Histopathological findings (H&E stain). (A) Low-power view (×12.5) showing prominent intraepidermal nests of poroid cells, characteristic of porocarcinoma in situ. (B) High-power view (×400) revealing marked nuclear atypia and pleomorphism. Red arrows indicate prominent mitotic figures (daughter cells).

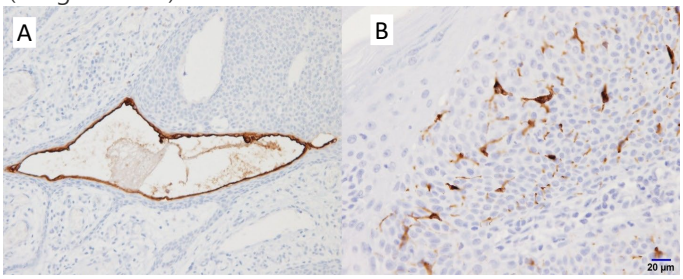

Fig 4. Immunohistochemical (IHC) analysis. (A) CEA staining (×200) highlighting the ductal structures within the tumor nests. (B) Melan-A staining (×400) showing negative results in the tumor cells, while highlighting the colonization of non-neoplastic dendritic melanocytes (brown-stained cells) responsible for the clinical pigmentation.

EP-196

이중 교차 근육 및 근막피부 피판을 이용한 광범위 수막척수류 결손의 재건

Reconstruction of an Extensive Myelomeningocele Defect Using a Double-Opposing Muscle and Fasciocutaneous Flap

가톨릭대학교

박희양, 최장연*

Purpose: To reconstruct an extensive defect following meningomyelocele repair, a double-opposing Z-plasty utilizing muscle and fasciocutaneous flaps was performed. Bilateral gluteus maximus muscles were elevated as 60-degree triangular flaps. The left muscle flap was based inferiorly and the right superiorly, crossing medially to cover the dural sac. Subsequently, bilateral fasciocutaneous flaps were elevated with opposing bases (left superiorly, right inferiorly) and crossed over the muscle layer. This double-opposing design prevents overlapping suture lines and minimizes tension.

Methods: A neonate presented with a 5x5 cm lumbosacral meningomyelocele. After neurosurgical repair, poor perfusion of the skin flaps necessitated debridement. This resulted in a massive 7x8 cm midline defect with an exposed dural sac, requiring immediate and robust multi-layered coverage to prevent cerebrospinal fluid (CSF) leakage and tissue necrosis.

Results: The defect was successfully reconstructed with minimal tension. Both the muscle and fasciocutaneous flaps survived completely without signs of ischemia. At the 5-month postoperative follow-up, the surgical site was well-healed with stable soft-tissue coverage. There were no complications such as wound dehiscence, distal necrosis, or CSF leakage despite the initial massive defect size.

Conclusion: The double-opposing gluteus maximus and fasciocutaneous flap is a highly reliable surgical technique for massive myelomeningocele defects. By crossing the muscle and skin layers in opposite directions, this method effectively disperses tension, obliterates dead space, and provides durable multi-layered coverage, significantly reducing the risk of critical postoperative complications.

Fig.1

Fig.2

Fig.3

Fig.4

EP-197

흉벽 재건을 필요로 한 재발성 고등급 액와 연부조직 육종

(Recurrent High-Grade Axillary Soft Tissue Sarcoma Requiring Chest Wall Reconstruction)

순천향대학교 부속 서울병원

김경빈, 강상규*

Purpose: High-grade soft tissue sarcomas have a high risk of recurrence when adequate margins cannot be achieved. Resection in the axilla is challenging because of complex anatomy and proximity to critical neurovascular structures and the chest wall. We report a multiply recurrent high-grade axillary soft tissue sarcoma successfully treated with chest wall resection and reconstruction.

Methods: A 51-year-old woman with a history of thyroid and left breast cancer underwent wide excision of a high-grade sarcoma of the left axilla in March 2024, followed by adjuvant radiotherapy and chemotherapy. Two sequential local recurrences occurred within the following year, resulting in repeat excisions due to persistent positive margins. After the third recurrence (Fig. 1), radical resection including the pectoralis minor muscle was performed. Frozen biopsy revealed positive deep margins, necessitating resection of the anterior chest wall. A 7 × 8 cm segment, including the third and fourth ribs, was excised (Fig. 2). The chest wall defect was reconstructed using polypropylene mesh (Fig. 3), and the overlying soft tissue defect was reconstructed with a pedicled latissimus dorsi myocutaneous transposition flap (Fig. 4).

Results: Postoperative course was uneventful, without flap-related complications, flail chest, or pneumothorax. The patient recovered well and, following adjuvant chemotherapy, has remained free of recurrence during one year of follow-up

Conclusion: In this multiply recurrent axillary sarcoma, achieving negative margins required chest wall resection. Reconstruction was performed using polypropylene mesh and a pedicled latissimus dorsi flap. This case demonstrates that complete resection and durable soft tissue reconstruction can be achieved even in complex recurrent sarcomas.

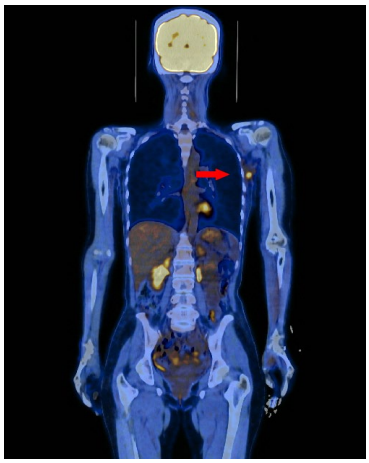

Figure 1. Positron emission tomography–computed tomography (PET-CT) obtained during follow-up demonstrating a hypermetabolic lesion in the left axilla suspicious for the third recurrence

Figure 2. Photograph of the resected specimen including rib segments and intercostal muscles following en bloc chest wall resection

Figure 3. Intraoperative photograph demonstrating chest wall reconstruction using polypropylene mesh after full-thickness resection.

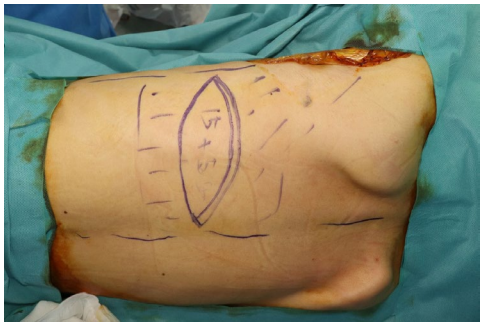

Figure 4. Intraoperative photograph showing design of a 15 x 5 cm skin paddle for pedicled latissimus dorsi flap reconstruction to cover the soft tissue defect.

EP-198

음낭 외유방 파제트병 절제 후 원격 전이를 의심하게 했던 흉벽 림프종과 후복막 종괴에 대한 증례 보고

A Case Report of Chest Wall Lymphoma and Retroperitoneal Mass Mimicking Distant Metastasis After Excision of Scrotal Extramammary Paget's Disease

연세대학교 원주의과대학
원주세브란스기독병원
성형외과학 교실

전우상, 오창훈, 김석원*, 김지예

Purpose: Extramammary Paget's disease (EMPD) is usually indolent, but invasive cases may metastasize. Newly detected deep lesions during follow-up may therefore raise suspicion for distant metastasis, although tissue confirmation remains essential. We report a case in which a deep hypermetabolic lesion initially suspected as metastatic EMPD was later diagnosed as lymphoma.

Methods: An 80-year-old man underwent wide excision and split-thickness skin grafting for scrotal EMPD in 2023. About 2 years later, abdominal computed tomography performed for dyspepsia revealed a retroperitoneal mass. Because biopsy was not feasible due to its deep location, positron emission tomography/computed tomography demonstrated a hypermetabolic lesion extending from the posterior mediastinum to the retroperitoneum. The lesion was clinically considered either distant metastasis from EMPD or lymphoma, and radiotherapy was administered. In January 2026, follow-up chest computed tomography identified a new right chest-wall lesion, and biopsy of the accessible rib lesion confirmed plasmablastic lymphoma.

Results: The retroperitoneal lesion showed marked regression on follow-up imaging after radiotherapy. Subsequent imaging revealed a new right chest-wall mass with hypermetabolism, encasing the right 8th, 9th, and 10th ribs and extending from the subcutaneous fat layer to the pleural space. For the plasmablastic lymphoma diagnosed from the accessible rib lesion biopsy, additional radiotherapy and chemotherapy were performed.

Conclusion: This case highlights that newly detected deep lesions in patients with EMPD may raise suspicion for distant metastasis while posing a diagnostic challenge. In such situations, biopsy-based tissue confirmation is important whenever feasible to distinguish metastatic disease from other malignancies and to guide appropriate management.

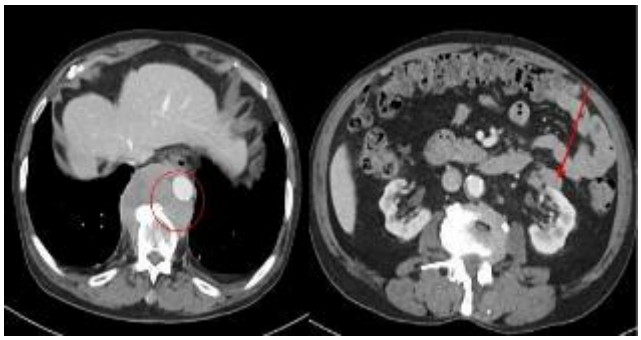

Fig. 1. Contrast-enhanced CT showing a retroperitoneal mass (arrow) with posterior mediastinal extension (circle).

Fig. 2. Clinical photographs of scrotal extramammary Paget's disease:
(A) preoperative photograph and (B) 2-year postoperative photograph after wide excision and split-thickness skin grafting.

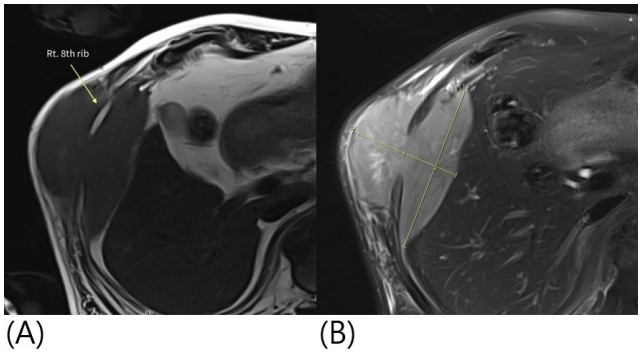

Fig. 3. Magnetic resonance imaging of the right chest wall lesion.
(A) The lesion encasing the right 8th rib. (B) Axial MRI demonstrating a soft tissue mass in the right anterolateral chest wall measuring approximately 9.5 × 6.4 × 11.9 cm.

EP-199

육종 절제 후 발생한 측복부 흉벽 결손에 대한 광배근 근육 수복 및 회전 피판을 이용한 재건: 증례 보고

(Reconstruction of a Flank Chest Wall Defect After Sarcoma Resection Using Latissimus Dorsi Muscle Repair and Rotation Flap: A Case Report)

가천대학교

김재훈, 김유진*

Purpose: Wide resection of chest wall sarcomas frequently results in composite defects involving skin, muscle, and thoracic structures. Reconstruction must restore structural stability while providing reliable soft-tissue coverage. We report a case of flank sarcoma reconstructed using latissimus dorsi muscle repair combined with a rotation flap for soft-tissue coverage.

Methods: A 75-year-old male presented with a palpable right flank mass. Imaging demonstrated a heterogeneously enhancing soft-tissue tumor involving the external abdominal oblique and intercostal muscles. Core needle biopsy suggested spindle cell sarcoma. The patient underwent wide oncologic resection including the 11th and 12th ribs with diaphragmatic and peritoneal repair and mesh reinforcement by thoracic and anorectal surgeons. Following tumor removal, a 15×5 cm defect remained in the right flank. For reconstruction, the latissimus dorsi muscle was dissected and mobilized, then repaired to the residual chest wall external oblique muscle stump to reinforce the thoracoabdominal wall. Subsequently, a rotation flap measuring 17×15 cm was designed and transposed to achieve soft-tissue coverage.

Results: Final pathology confirmed undifferentiated pleomorphic sarcoma (FNCLCC grade 3) measuring 5.5×5×3 cm with rib invasion with negative surgical margins . The rotation flap survived completely without vascular compromise, and stable soft-tissue coverage with adequate chest wall support was achieved.

Conclusion: Reconstruction combining latissimus dorsi muscle repair with a rotation flap provides both structural reinforcement and reliable soft-tissue coverage. This approach can be an effective reconstructive option for flank and lower chest wall defects following oncologic resection.

Fig1. Preoperative design of a 17 × 15 cm rotation flap on the right flank for reconstruction following wide excision of the chest wall sarcoma.
Fig 2. Intraoperative view after skin and soft tissue dissection showing the latissimus dorsi muscle and the external oblique muscle stump at the defect site.

Fig3. Latissimus dorsi muscle repair to the external oblique muscle stump for reinforcement of the chest wall defect.
Fig 4. Closure of the defect with a rotation flap.

EP-200

재생형 티슈덤 스페이서를 이용한 대형 복합 결손 재건 : 근막근피판 재건술의 대안

(Spacer-based reconstruction as an alternative to bulky flap reconstruction for large sacral composite defects)

연세대학교 의과대학 성형외과학교실

정진선, 이원재, 노태석, 백우열 *

Purpose: Wide excision of sacral chordoma often results in large composite defects involving bone, muscle, and subcutaneous tissue. Even when skin coverage is preserved, restoration of deep structural volume is essential to prevent contour deformity and maintain pelvic stability. Conventional reconstruction frequently requires bulky musculofascial flaps, such as gluteus maximus muscle flaps, which are associated with donor-site morbidity, muscle weakness, prolonged operative time, and delayed ambulation. This study presents the use of a customized TissueDerm® spacer as a potential alternative to bulky flap reconstruction in deep composite defects.

Methods: A 65-year-old female underwent sacral chordoma excision at the S2–3 level. The defect measured 7 × 9.5 × 5 cm and involved bone, muscle, and subcutaneous layers based on preoperative MRI evaluation with the neurosurgical team. A customized spacer composed of collagen to promote tissue ingrowth and a biodegradable polycaprolactone mesh was designed preoperatively. Regulatory approval and reporting to the Korean Ministry of Food and Drug Safety (MFDS) were completed. The TissueDerm spacer was fabricated intraoperatively to restore deep volume and structural support.

Results: Structural volume was restored without bulky musculofascial flap reconstruction. Reconstruction required one hour, and ambulation began on postoperative day 7. The patient was discharged on postoperative day 26 without major complications. One-month CT demonstrated minimal seroma (<50 cc) and stable defect maintenance.

Conclusion: In large composite defects excluding skin loss, a customized TissueDerm spacer may serve as a less invasive alternative to bulky musculofascial flap reconstruction.

Fig. 1. Intraoperative fabrication

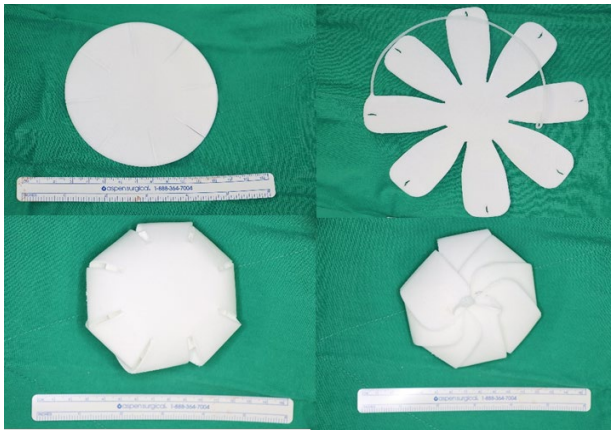

Fig. 2. Specimen & installation

Fig. 3. One-month postoperative CT

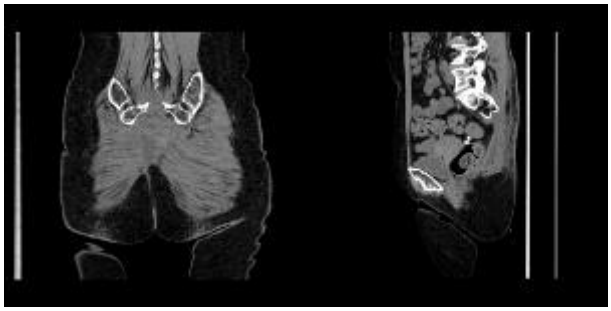

Fig. 4. An alternative to bulky musculofascial flap reconstruction

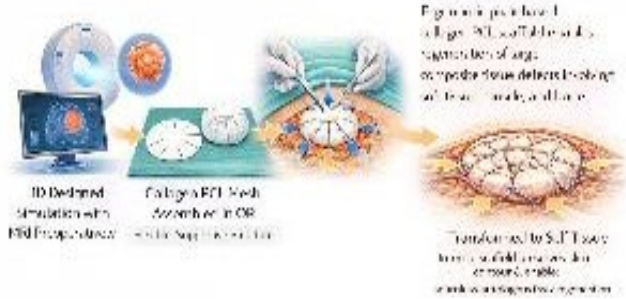

EP-201

악성 연부조직 종양으로 오인된 피하 비후성 흉터: 진단적 함정 및 증례 보고

(Subcutaneous Hypertrophic Scar Mimicking a Malignant Soft Tissue Tumor: A Diagnostic Pitfall and Case Report)

연세대학교

김태호, 김지민*

Background: Subcutaneous masses with rapid recurrence and aggressive radiological features typically raise the high suspicion of malignant soft tissue sarcomas or borderline tumors like nodular fasciitis. However, exaggerated internal scarring can present identically. We report a massive subcutaneous pseudotumor likely triggered by deep venous injury and organizing fibrosis.

Case presentation: A 25-year-old male presented with a rapidly recurring hard mass on the right popliteal area, one month post-excision. **(Fig. 1.)** Preoperative magnetic resonance imaging (MRI) revealed a 2.6 cm-sized soft tissue mass with a lobulated margin and suspected diffuse attachment to the superficial fascia. **(Fig. 2.)** Ultrasonography demonstrated a hypoechoic mass with internal vascularity and high stiffness on elastography, strongly suggesting a malignant soft tissue tumor. **(Fig. 3.)** During re-excision, the mass exhibited vague margins, a ruptured fluid collection, and densely enveloped the small saphenous vein, requiring careful ligation.

Pathological Findings and Outcome: Histopathology confirmed a hypertrophic scar with extensive myxoid degeneration and fat necrosis. We hypothesize that unrecognized popliteal venous injury caused localized fluid collection, triggering an exaggerated cascade of organizing fibrosis. When internal scar tissue began regrowing one month postoperatively, we initiated intralesional triamcinolone injections. Due to its aggressive fibrotic nature, we plan to incorporate 5-fluorouracil (5-FU) therapy to suppress fibroblast proliferation.

Conclusion: Deep subcutaneous hypertrophic scars driven by organizing fibrosis can clinically and radiologically mimic soft tissue sarcomas. Surgeons should suspect pseudotumors in rapidly recurring post-surgical masses and consider multimodal conservative management, including steroid and 5-FU injections, to prevent unnecessary surgical morbidity.

Fig. 1.
Preoperative clinical photograph of the right posterior thigh. A distinctly protruding subcutaneous mass is observed adjacent to the previous excision scar. The prominent nodular bulging and palpable firmness of the lesion clinically mimicked a soft tissue tumor, raising a high index of suspicion for malignancy prior to the re-excision.

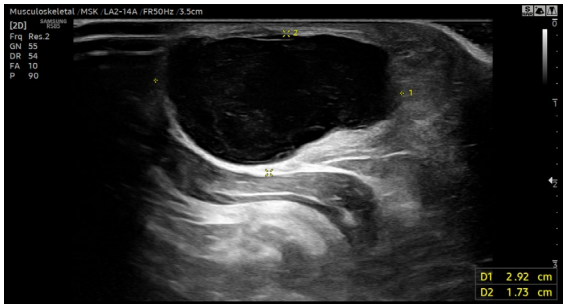

Fig. 2.
Ultrasonography presents hypoechoic mass with lobulated margin, measuring 2.9x1.7x3.6 cm, with suspicious internal vascularity and perilesional inflammatory change.
Impression : Malignant soft tissue is possible, DDx: nodular fasciitis, neurogenic tumor.

Fig. 3.
Knee MRI study showed soft tissue mass with lobulated margin at the subcutaneous layer. Suspected diffuse attachment with superficial fascia was noted.
Impression : Malignant soft tissue is possible, DDx: nodular fasciitis, neurogenic tumor.

EP-202

장기간 지속된 화상 반흔에서 발생한 천골부 Marjolin 궤양: 증례 보고

Marjolin's Ulcer of the Sacral Region Arising from a Longstanding Burn Scar: A Case Report

한양대학교 의과대학
성형외과학교실
한양대학교 구리병원
성형외과

이보현, 이장현*

Purpose: Marjolin's ulcer refers to malignant transformation arising from chronic scars or non-healing wounds, most commonly presenting as squamous cell carcinoma (SCC) in burn scars. It typically occurs after a long latency period and may demonstrate aggressive clinical behavior. We report a case of SCC arising from a longstanding burn scar in the sacral region treated with wide excision and split-thickness skin graft (STSG).

Methods: A 64-year-old male with diabetes mellitus and dyslipidemia had extensive burn scars on the buttock region from a burn injury sustained at five years of age. Several years prior to presentation, a chronic ulcer developed within the scar and gradually enlarged. Physical examination revealed a large ulcerative mass in the sacral area. Biopsy confirmed SCC. Magnetic resonance imaging (MRI) demonstrated a protruding soft tissue tumor with dermal infiltration without definite invasion into muscle or fascia. Wide excision with a 5-mm safety margin was performed, resulting in a 14 × 8 cm defect with partial muscle exposure. The defect was reconstructed with STSG harvested from the right posterior thigh.

Results: Histopathology revealed well-differentiated SCC (11 × 6.5 cm) arising from a burn scar with a depth of invasion of 17.7 mm. No lymphovascular or perineural invasion was identified, and all margins were tumor-free. The postoperative course was uneventful, and minor graft loss healed with conservative wound care.

Conclusion: Malignant transformation can occur in chronic burn scars even decades after injury. Early diagnosis and appropriate surgical management with adequate excision and reconstruction are essential for optimal outcomes.

Fig. 1. Preoperative clinical photograph showing an ulcerative, exophytic mass arising from a chronic burn scar in the sacral region.

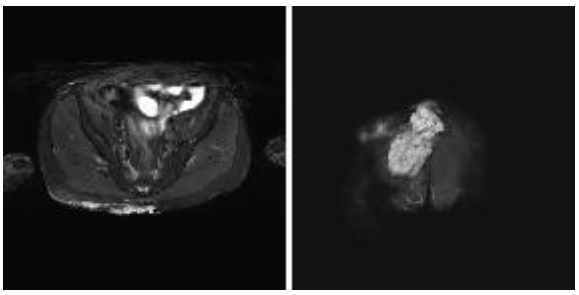

Fig. 2. Magnetic resonance imaging (MRI) of the sacral region demonstrating a protruding soft tissue tumor arising from a chronic burn scar. The axial view (left) and coronal view (right) show a mass with dermal infiltration and strong contrast enhancement without definite extension into the underlying muscle or fascia.

Fig. 3. Intraoperative gross specimen after wide excision showing an ulcerative tumor arising from a chronic burn scar in the sacral region.

Fig. 4. Postoperative clinical photograph at 6 months after wide excision and split-thickness skin graft (STSG) for squamous cell carcinoma arising from a chronic burn scar in the sacral region, demonstrating stable graft take without evidence of local recurrence.

EP-203

지방종으로 오진된 탄성섬유종 : 증례 보고

(Elastofibroma in a Relatively Young Woman Initially Misdiagnosed as Lipoma; A Case Report)

원광대학교

조규제, 나영천*

Purpose: Elastofibroma dorsi(EFD) is a benign soft-tissue pseudotumor typically presenting in elderly individuals and located deep to the scapula. We report a 47-year-old woman with prior left breast cancer surgery and implant reconstruction, who developed progressive left subscapular discomfort.

Methods: A 47-year-old woman with a history of left breast cancer treated with mastectomy and implant reconstruction visited our outpatient clinic complaining of progressive left subscapular discomfort, described as pressure sensation, stiffness, and intermittent axillary pain. Initial ultrasonography suggested fibrolipoma, but preoperative computed tomography(CT)/ magnetic resonance imaging(MRI) performed for breast cancer follow-up revealed findings consistent with elastofibroma. Fortunately, no contralateral lesion was detected.

Results: Surgical exploration identified a poorly circumscribed, fibrous mass measuring 9.8 × 3.5 × 1.2 cm deep to the scapula. The lesion was resected en bloc using marginal excision, followed by layered closure and placement of a hemovac drain. At follow-up, the patient reported complete resolution of discomfort.

Conclusion: This case highlights the need for heightened clinical suspicion for EFD even in younger patients or those with prior thoracic or breast surgery, particularly when imaging reveals characteristic features. Emerging literature indicates that EFD is underdiagnosed, more prevalent than previously believed, and can present with variable anatomical patterns.

Figure 1. Preoperative image showing protruding without shoulder flexion.

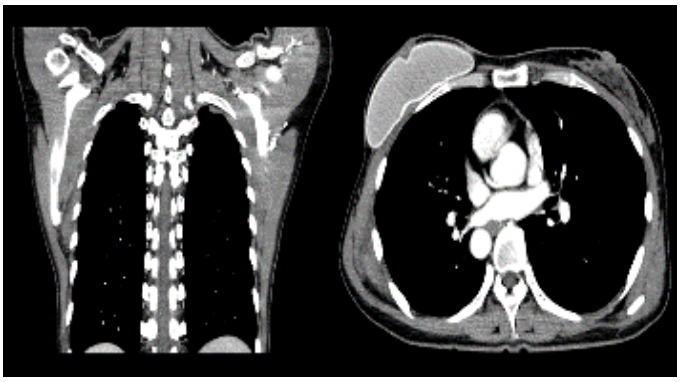

Figure 2. Axial and coronal image of CT.

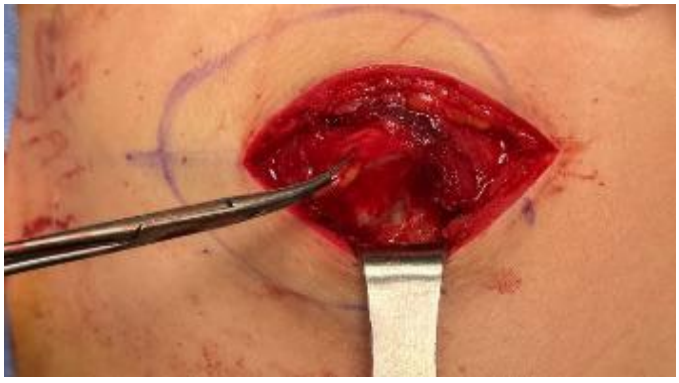

Figure 3. Intraoperative image.

Figure 4. Resected mass.

EP-204

상피양 혈관내피종: 증례 보고

(Epithelioid Hemangioendothelioma: Case Report)

가톨릭대학교
정승원, 최장연*

Purpose: Epithelioid hemangioendothelioma (EHE) is an ultrarare vascular sarcoma with highly variable clinical behavior and no standardized treatment guidelines. We present a case of recurrent soft tissue EHE in the buttock, focusing on diagnostic challenges and management strategies.

Methods: A 46-year-old woman presented with a recurrent mass in the left buttock. Initial excisional biopsy suggested a benign spindle cell tumor, delaying the diagnosis. Upon recurrence, computed tomography revealed a 4.5-cm-sized dense soft tissue lesion in the subcutaneous layer of the left buttock with diffuse contact with the left gluteal muscle (Figure 1). The patient underwent complete en bloc resection with a 1.5 cm safety margin.

Results: Gross pathology demonstrated a 5.5 × 5.5 × 4.4 cm tumor (Figure 2). R0 resection was achieved. Histopathology and immunohistochemistry for vascular markers (CD31, ERG, FLI-1) confirmed EHE. No adjuvant therapy was administered. Postoperative staging showed no metastasis. Follow-up with clinical examinations and imaging over 24 months, including an 18-month CT scan, revealed no recurrence or complications (Figure 3).

Conclusion: Accurate diagnosis of EHE requires thorough histopathological and immunohistochemical assessment, as benign-appearing features may obscure the condition. Complete surgical excision with negative margins remains the primary treatment for localized disease. Long-term surveillance is essential due to the unpredictable metastatic potential

Figure 1. Initial CT imaging showing a 4.5-cm ovoid, dense soft tissue mass at the posterior aspect of the left gluteus maximus muscle, with indistinct borders.

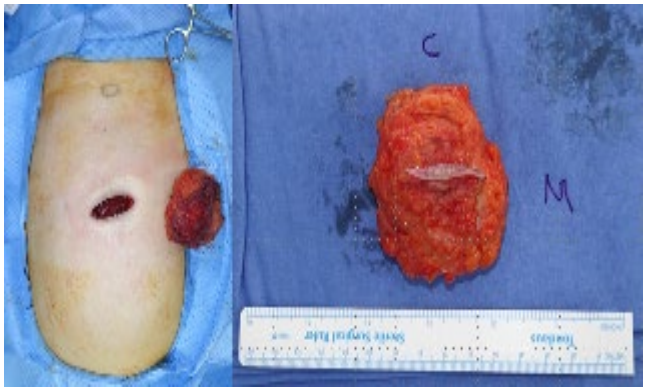

Figure 2. Gross specimen of the tumor after en bloc resection with safety margins.

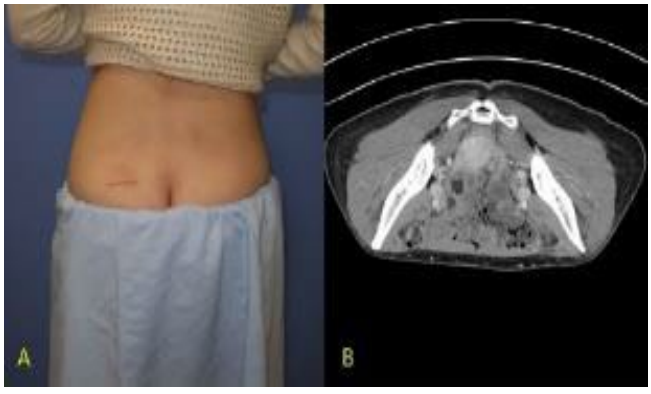

Figure 3. Clinical photograph and CT scan at the 18-month follow-up, demonstrating no evidence of recurrence or complications.

EP-205

불응성 둔부 지방육종의 재발 극복: R1 절제 및 시스플라틴 기반 동시 항암화학방사선요법을 통한 기능적 구제와 장기적 제어

Overcoming Recurrence in Refractory Gluteal Liposarcoma: Functional Salvage and Long-term Control via R1 Resection and Cisplatin-based CCRT

중앙대학교 의과대학
성형외과학교실 [1]
중앙대학교 광명병원 성형외과 [2]
정인호[1], 김우섭[2], 김한구[1], 배태희[2], 우수현[1], 김우주[2], 강신혁*[1]

Purpose: Achieving R0 resection in high-grade gluteal liposarcoma is challenging in multiply recurrent cases. We report an 81-year-old female with her sixth recurrence of Grade 3, Stage II gluteal liposarcoma. After five prior resections at external institutions and a radiotherapy course self-terminated due to bowel dysfunction, the bulky tumor rendered sitting impossible, necessitating surgery for functional restoration and breaking the cycle of rapid recurrence.

Methods: A multidisciplinary team planned debulking resection (marginal excision) to prioritize functional salvage. Orthopedic and general surgery teams collaborated to ensure preservation of the sciatic nerve and rectal integrity despite anatomical distortion. The 13x8 cm^2 defect was reconstructed using a unilateral fasciocutaneous advancement flap, achieving stable wound coverage in a gluteal bed previously exhausted by multiple prior operations.

Results: Final pathology revealed microscopic involvement despite negative intraoperative frozen sections, as post-radiation fibrosis masked tumor infiltration. Consequently, the confirmed R1 resection was followed by cisplatin-based concurrent chemoradiotherapy (CCRT) as an aggressive radiosensitizer to treat the microscopic field and preclude any potential radioresistance. The patient regained ability to sit and has remained disease-free for over two years, breaking the cycle of recurrence.

Conclusion: This case demonstrates a dual triumph in reconstructive and oncologic salvage for refractory liposarcoma. Strategically, planned R1 resection with cisplatin-based CCRT offers an effective multidisciplinary alternative when R0 resection is unfeasible. This approach ensures durable local control and critical functional restoration, such as the ability to sit, while proving viable local flap reconstruction is achievable even in a hostile, multi-operated surgical field through multidisciplinary management.

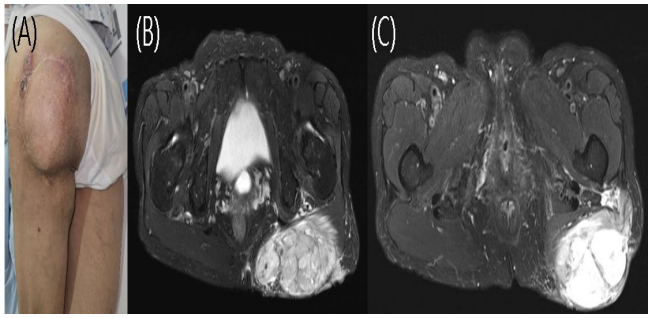

Fig. 1. (A) Gross image of the liposarcoma on left buttock before surgery and (B, C) magnetic resonance images of the lesion in axial view. Peri-tumor invasion on rectum and sciatic nerve was checked.

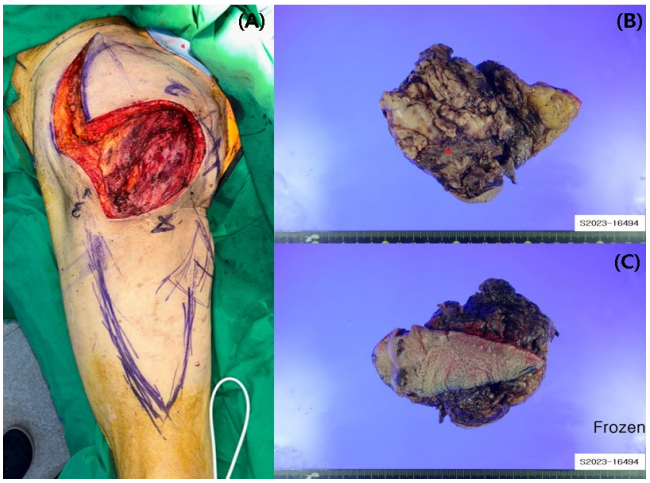

Fig. 2. (A) Intra-operative images after debulking resection on the lesion. A local flap was designed considering the size of the skin resected during the operation. (B, C) Gross images of the resected liposarcoma for the frozen section analysis.

Fig. 3. Gross image of the operation site on post-operative day 1. The patient was permitted to sit starting from postoperative day (POD) 14, and active ambulation was encouraged.

EP-206

유리피판 재건술 후 모니터링 체계의 변화: 전공의 기반 감시와 간호사 주도 감시의 비교 분석

(From Resident to Nurse Surveillance in Free Flap Reconstruction: A Comparative Analysis of Monitoring Efficiency and Flap Outcomes)

이화여자대학교 성형외과학교실(이대목동병원)

박진우, 신동렬, 박보영*

Purpose: Early detection and timely re-exploration are critical for successful free flap salvage. With increasing workforce constraints, nurse-led monitoring systems have been introduced, but direct comparisons with resident-based monitoring remain limited. This study aimed to evaluate the impact of monitoring system on workflow efficiency and flap outcomes.

Methods: A retrospective cohort analysis was conducted on patients who underwent free flap reconstruction by a single surgeon between 2014 and 2025. From February 2019, a structured nursing-led monitoring protocol replaced resident-based surveillance(Fig. 1).Monitoring characteristics, timing of detection and re-exploration, and flap outcomes were compared between the two groups.

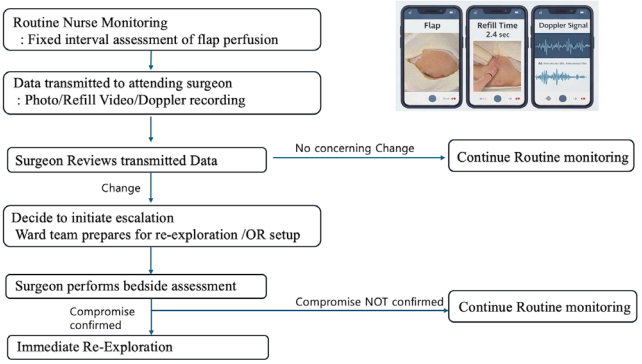

Fig. 1. Monitoring and escalation workflow. Nurses perform structured assessments and transmit data to the attending surgeon. Clinical decisions are made by the surgeon. When vascular compromise is suspected, bedside reassessment and operative preparation proceed simultaneously, enabling timely re-exploration.

Results: A total of 499 free flap reconstructions were performed, of which 40 (8.0%) required re-exploration. After excluding incomplete records, 36 cases were analyzed (resident 15, nurse 21). The time from flap operation to detection of vascular compromise was similar between groups. However, the interval from detection to re-exploration was significantly shorter in the nurse group (4.2 ± 3.6 vs 7.4 ± 5.1 hours, p = 0.041) .Early revision within 24 hours occurred more frequently in the nurse group (71.4% vs 40.0%, p = 0.048) . The flap salvage rate was higher in the nurse group (71.4% vs 46.7%), although this did not reach statistical significance (p = 0.18)(Table. 1.).

Table. 1. Monitoring and Revision Outcomes

Variable	Resident(n=15)	Nurse(n=21)	*p*-value
Time from flap operation to compromise detection (h)	28.6 ± 16.8	25.9 ± 12.4	0.54
Time from detection to re-exploration (h)	7.4 ± 5.1	4.2 ± 3.6	0.041 *
Total time (flap operation to re-exploration(h))	36.0 ± 17.9	30.1 ± 13.4	0.27
Cause of re-exploration, n (%)			0.61
Arterial	10 (66.7 %)	12 (57.1 %)	
Venous	2 (13.3 %)	2 (9.5 %)	
Mixed	3 (20.0 %)	7 (33.3 %)	
Revision within 24 h, n (%)	6 (40.0%)	15 (71.4 %)	0.048*
Flap salvaged after re-exploration, n (%)	7 (46.7 %)	15 (71.4 %)	0.18
Partial necrosis or total loss, n (%)	8 (53.3%)	6 (28.6 %)	-

Continuous data = mean ± SD; **categorical data** = number (%) using Fisher's exact or *t*-test as appropriate.
* $p < 0.05$ considered statistically significant.

In univariable analysis, early revision (<24 hours) was significantly associated with flap salvage (OR 3.45, p = 0.036). In multivariable analysis, both nurse-led monitoring (OR 3.24, p = 0.046) and early revision (<24 hours) (OR 3.01, p = 0.047) were independently associated with improved flap salvage (Table 2).

Table. 2. Univariate and Multivariable analysis for predictors of flap salvage

	Univariable analysis		*Multivariable analysis*	
Variable	OR	*p*-value	OR	*p*-value
Revision <24 hrs	3.45 (1.02 – 11.65)	0.036 *	3.01 (0.96 – 9.43)	0.047*
Group(Nurse vs Resident)	2.89 (0.82 – 10.15)	0.097	3.24 (1.02 – 10.27)	0.046*
Cause(Mixed vs Arterial)	1.64 (0.41 – 6.50)	0.49	1.38 (0.32 – 5.89)	0.66
Cause(Venous vs Arterial)	0.92 (0.12 – 6.70)	0.94		
PAOD	0.61 (0.13 – 2.94)	0.54	0.69 (0.12 – 3.78)	0.67
Diabetes mellitus	0.89 (0.21 – 3.75)	0.87		
Hypertension	0.74 (0.18 – 3.10)	0.68		
Age	0.91 (0.63 – 1.31)	0.60		
Flap size	0.98 (0.93 – 1.03)	0.43		-

(PAOD = Peripheral Arterial Occlusive Disease)

Mediation analysis demonstrated that earlier revision partially mediated the effect of nurse-led monitoring on flap salvage, accounting for approximately 52% of the total effect.

Conclusion: Structured nurse-led monitoring was associated with efficient detection and earlier re-exploration following vascular compromise. The results show that optimization of monitoring workflow may contribute to improved clinical outcomes and support a protocol-driven, team-based approach to postoperative flap surveillance.

EP-207

화상 재건에서의 흉배동맥 기반 유리피판술의 역할: 1차와 2차 화상 비교를 중심으로

Thoracodorsal Vessel-Based Free Flap Reconstruction for Burn Injuries: A Comparison of Primary and Secondary Cases

한양대학교 의과대학
성형외과학교실

왕형우, 장란숙, 김효성, 김지영, 김연환*

Purpose: Free tissue transfer plays an important role in burn management, both for acute wound coverage when simpler methods are inadequate and for subsequent scar contracture release. Thoracodorsal vessel-based flaps offer distinct advantages for burn reconstruction, including a reliable pedicle and versatility for complex defects. This study compared patient characteristics, operative parameters, and outcomes between primary reconstruction for acute burn wounds and secondary reconstruction for scar contracture release.

Methods: A retrospective review was conducted of 65 consecutive patients who underwent free flap reconstruction for burn-related defects at a single institution between 2012 and 2024. Patients were categorized into primary reconstruction (acute burn or early wound coverage) and secondary reconstruction (scar contracture release) groups.

Results: The secondary reconstruction group was significantly younger (39.4 vs 55.4 years, $p < 0.001$) and had a higher proportion of female patients (68% vs 32%, $p = 0.01$) compared to the primary group. Operative time was significantly longer in secondary reconstruction (237 vs 174 minutes, $p < 0.001$), attributable to technical challenges of dissection in scarred tissue rather than flap complexity. Overall flap survival was 98.5% with no significant difference between groups.

Conclusion: Secondary burn reconstruction patients differ demographically from primary reconstruction patients and require longer operative times due to scarred tissue dissection. Thoracodorsal vessel-based flaps demonstrated versatility across the spectrum of burn reconstruction, from perforator flaps to complex chimeric designs, with high success rates in both clinical scenarios.

Fig. 1. Primary burn reconstruction. (A-C) A 50-year-old woman with a contact burn to the hand reconstructed with a thoracodorsal artery perforator (TDAP) flap, shown 3 years and 6 months postoperatively after debulking and web space release. (D-F) A 27-year-old woman with a severe flame burn reconstructed with a TDAP-ALT linked flap to create a mitten hand, shown 3 months postoperatively

Fig. 2. Secondary burn reconstruction. (A-C) A 20-year-old woman with lower extremity contractures following friction burn, resurfaced with a TDAP flap, shown 2 years postoperatively. (D-F) A 28-year-old woman with scarring after previous latissimus dorsi flap reconstruction, revised with a latissimus dorsi muscle-sparing flap and DIEP flap, shown 2 years postoperatively

Table 1. Comparison of Primary and Secondary Reconstruction Groups

Variable	Primary (n = 37)	Secondary (n = 28)	*p*-value	Effect Size
Age (years)	55.4 ± 16.5	39.4 ± 17.6	< 0.001	$d = 0.94$
Sex (Female), n (%)	12 (32%)	19 (68%)	0.01	OR = 4.40
Operative time (min)	173.5 ± 51.0	237.3 ± 90.6	< 0.001	$d = 0.90$
Defect size (cm²)	247.9 ± 215.5	316.3 ± 225.1	0.22	$d = 0.31$
Complications, n (%)	1 (2.7%)	2 (7.1%)	0.57	-

Values are presented as mean ± SD or n (%). Effect sizes: Cohen's *d* for continuous variables, odds ratio (OR) for categorical variables.

EP-208

HPV 연관 음낭 Bowen 병: HPV 관련 편평상피암종 발생을 시사하는 증례

(HPV-Related Bowen's Disease of the Scrotum: A Case Highlighting HPV-Associated Squamous Carcinogenesis)

동국대학교 의과대학 성형외과학교실[1]

한승민[1], **이준호***[1]

Purpose: To report a rare case of HPV-related Bowen's disease of the scrotum and to highlight the potential etiologic role of human papillomavirus (HPV) infection in scrotal squamous carcinoma in situ.

Methods: A 74-year-old man presented with a scrotal lesion that was initially diagnosed as favor Bowen's disease on punch biopsy. Wide excision with intraoperative frozen section control and dartos fascia–based advancement flap coverage was performed under local anesthesia. p16 immunohistochemistry was carried out to evaluate high-risk HPV association, based on emerging evidence that HPV can contribute to genital and scrotal squamous carcinogenesis.

Results: Final histopathology confirmed HPV-related squamous carcinoma in situ (Bowen's disease) with strong p16 expression. The tumor measured 1.0 × 0.9 × 0.2 cm, and all margins were free of tumor, including a 3 mm deep margin. The postoperative course was uneventful, with complete wound healing and no local recurrence during short-term follow-up.

Conclusion: HPV-related Bowen's disease of the scrotum is extremely rare but supports the growing concept that HPV may play a causal role in a subset of scrotal squamous cell neoplasms. Routine consideration of HPV testing, including p16 immunostaining, may be useful in scrotal in situ or invasive squamous lesions for etiologic assessment, patient counseling, and surveillance planning.

Fig 1. Clinical course
A. Preoperative photograph : A solitary black nodule with erosion on the scrotal skin.
B. Intraoperative photograph : Completed wide excision with dartos fascia-based advancement flap reconstruction.

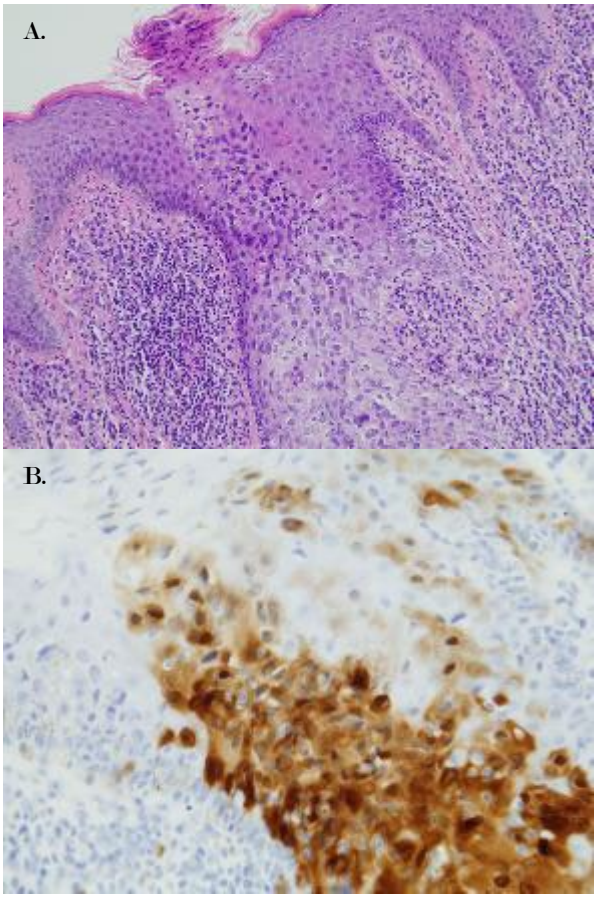

Fig. 2. Histopathology
A. H&E stain (×200) : Full-thickness atypical keratinocytes consistent with HPV-related Bowen's disease
B. p16 IHC (×400) : Strong diffuse p16 positivity supporting high-risk HPV–related squamous carcinoma in situ.

EP-209

건 및 골 노출을 동반한 만성 난치성 창상에 대한 유리피판 재건술

(Free Flap Reconstruction for Longstanding Non-Healing Wounds with Exposed Tendon and Bone)

인하대학교

기세휘*, 정도혁

Purpose: Wound healing may be delayed despite conservative care or negative pressure wound therapy (NPWT). For longstanding wounds with exposed tendon and bone, free flap reconstruction can provide a definitive option. This study evaluated outcomes and complications of free flap reconstruction.

Methods: A retrospective review from 2012 to 2023 included 15 patients who underwent 16 free flap reconstructions for chronic tendon and bone exposure. Data on demographics, wound causes, flap success, healing time, and complications were analyzed.

Results: Of 16 reconstructions, 8 used anterolateral thigh (ALT) free flaps, 5 lateral arm (LAFF), 2 latissimus dorsi musculocutaneous (LDMC), and 1 fibular osteocutaneous flap. The mean flap size was 12 × 7 cm², with an average wound exposure of 9 months. Causes included vehicle accidents (n=5), thermal burns (n=4), falls (n=3), postoperative complications (n=2), chemical burns (n=1), and industrial accidents (n=1). Nine complications occurred: partial flap necrosis (n=3), tendinitis (n=2), osteomyelitis (n=2), and wound dehiscence (n=1). All were managed successfully with local flaps, grafting, NPWT, or conservative treatment.

Conclusion: Chronic tendon and bone exposure is often associated with biofilm and subclinical infection, contributing to delayed healing. Free flap reconstruction provided stable coverage without major complications, though minor problems such as infection or partial flap loss were relatively frequent.

Fig. 1. (A) Tendon exposure (B) Coverage with lateral arm free flap (C) Postsoperative photograph, fistula formation (D) Closure with secondary closure

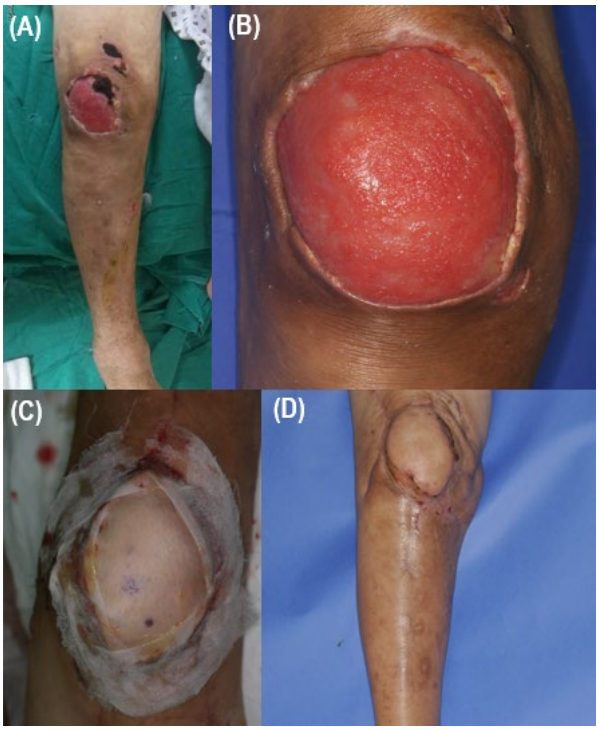

Fig. 2. (A) Patella exposure (B) Capsulated wound bed with biofilm formation
(C) Postsoperative photograph, Coverage with ALT free flap (D) Postoperative 6 months

EP-210

경피적 혈관 성형술 이후 천층회선장골동맥 천공지 유리피판 (SCIP)의 혈관경 손상에 대한 사례군 연구

(Vascular Pedicle Injury of the Superficial Circumflex Iliac Artery Perforator (SCIP) Free Flap Following Percutaneous Transluminal Angioplasty: A Case Series)

순천향대학교

이서구, 차한규,박은수,정형화*

Purpose: To retrospectively analyze four cases of flap failure due to vascular pedicle injury during reconstruction with a Superficial Circumflex Iliac Artery Perforator (SCIP) free flap in patients with a history of percutaneous transluminal angioplasty (PTA), and to evaluate the impact of prior endovascular intervention on donor vessel reliability.

Methods: We reviewed four patients who had previously undergone angioplasty or angiography of the lower extremities or major vessels and subsequently underwent reconstruction using a SCIP free flap. Preoperative ultrasonography assessed the course and patency of the superficial branch of the superficial circumflex iliac artery (SCIA). Intraoperative findings regarding the vascular pedicle and surrounding tissues were analyzed retrospectively.

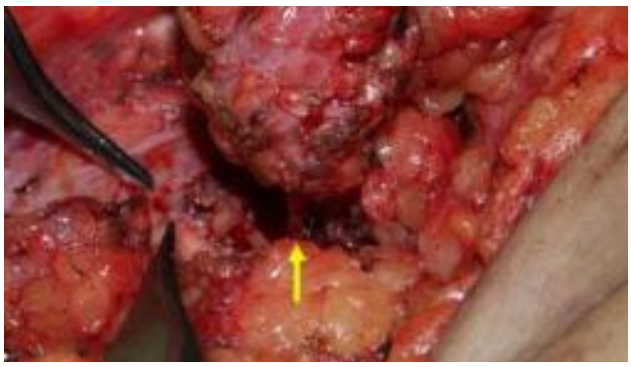

Fig. 1 Intraoperative view of SCIP flap elevation. The perforator (yellow arrow) was identified during dissection.

Results: Although preoperative ultrasonography suggested that the superficial branch of the SCIA was preserved, severe fibrosis and adhesions were observed around the origin of the vascular pedicle during flap dissection in all four cases. The main branch of the superficial SCIA was occluded, and distal perfusion was maintained through collateral flow from adjacent branches or the deep branch of the SCIA. These findings led to vascular pedicle compromise and flap failure.

Conclusion: Prior percutaneous transluminal angioplasty may reduce donor vessel stability due to perivascular injury and fibrosis. Even with preoperative ultrasonography, false-positive assessments of vessel patency may occur. Therefore, meticulous preoperative evaluation with ultrasonography and/or CT angiography is essential in patients with a history of endovascular intervention, and alternative donor site selection or modification of surgical strategy should be considered. These findings underscore the importance of careful risk stratification in microsurgical planning.

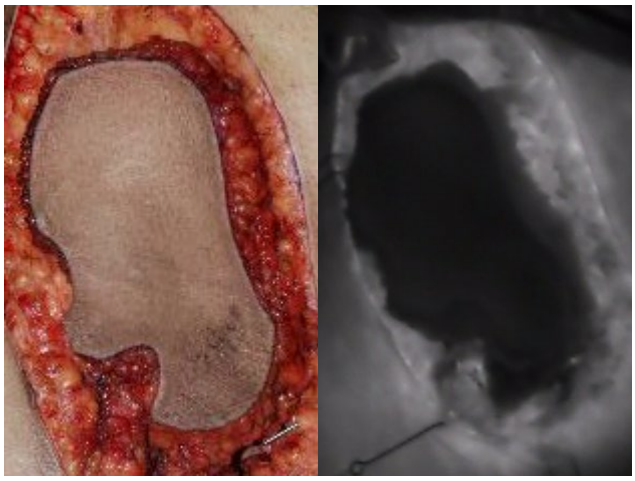

Fig. 2 Intraoperative gross view of the elevated SCIP flap before pedicle division (left) and indocyanine green angiography demonstrating absent perfusion to the flap (right).

Case	Age/Sex	Defect etiology	Preoperative vascular intervention (Approach)	Defect	Flap Side	Flap size	Definitive reconstruction
1	F/21	Postoperative wound necrosis after triple arthrodesis for congenital clubfoot	DPA angioplasty + posterior tibial artery –lateral plantar bypass (bilateral femoral)	Lt. foot dorsum & ankle	Rt.	18 × 7 cm	ALT free flap
2	M/66	Diabetic foot ulcer	Peripheral PTA (Lt. femoral)	Lt. foot, 4th–5th metatarsal area	Lt.	15 × 8 cm	Fillet flap
3	F/60	Diabetic hand ulcer	CAG + peripheral PTA (Lt. femoral)	Lt. hand, 3rd–5th metacarpal area	Lt.	15 × 8 cm	Fillet flap

Table 1. Clinical characteristics and reconstructive details of three cases.
Abbreviations: **ALT**, anterolateral thigh; **CAG**, coronary angiography; **PTA**, percutaneous transluminal angioplasty.

EP-211

전신경화증 환자에서 족배동맥 압박에 의한 Blue Toe Syndrome의 수술적 치료: 증례 보고

(Surgical Treatment of Blue Toe Syndrome due to Dorsalis Pedis Artery Compression in A Patient with Systemic Sclerosis: A Case Report)

부산대학교 의과대학
영상의학교실[1], 성형외과학교실[2]

황민희[1], 강동협[2], 이치현[2], 이창렬*[2]

Purpose: Blue toe syndrome (BTS) is characterized by painful cyanotic discoloration of the toes and is commonly associated with embolic or hematologic disorders. Compressive angiopathy is a rare cause, and its association with systemic sclerosis has seldom been reported. We present a case of BTS caused by dorsalis pedis artery compression in a patient with systemic sclerosis and describe successful surgical management.

Methods: A 26-year-old woman with systemic sclerosis presented with chronic ulcers and cold intolerance of both great toes. Physical examination revealed weak dorsalis pedis pulses and delayed capillary refill. Digital subtraction angiography demonstrated short segmental luminal narrowing of the dorsalis pedis artery and lateral tarsal branches with delayed distal runoff. Minimal improvement after intraarterial nitroglycerin injection suggested extrinsic compression. Based on multidisciplinary evaluation, surgical decompression with partial resection of the extensor hallucis brevis muscle and tendon, combined with periarterial sympathectomy, was performed in two stages.

Results: Intraoperatively, the extensor hallucis brevis was found to directly compress the artery. Arterial flow improved immediately after decompression. Postoperatively, toe ulcers healed without further intervention, and cold intolerance and discoloration resolved. At 9 months, arterial pulses and capillary refill were normal, with no recurrence.

Conclusion: BTS may result from compressive angiopathy of the dorsalis pedis artery, particularly in patients with systemic sclerosis. Advanced vascular imaging and multidisciplinary assessment are essential for diagnosis. Surgical decompression can be an effective treatment option in selected patients.

Fig. 1. Preoperative clinical photos. (a) Plantar view of the right foot. (b) Dorsal view of the right foot. (c) Chronic ulcer on the right great toe. (d) Plantar view of the left foot. (e) Dorsal view of the left foot. (f) Chronic ulcer on the left great toe.

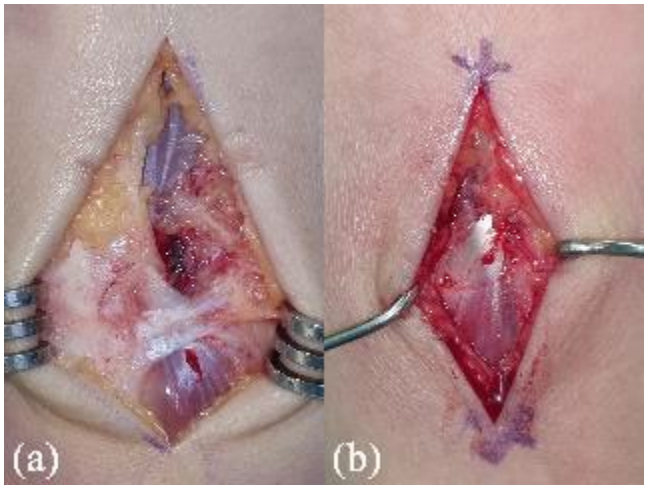

Fig. 2. Intraoperative findings of both dorsalis pedis vessels. The extensor hallucis brevis muscles and tendons were pressing across the dorsalis pedis vessels. (a) Right. (b) Left.

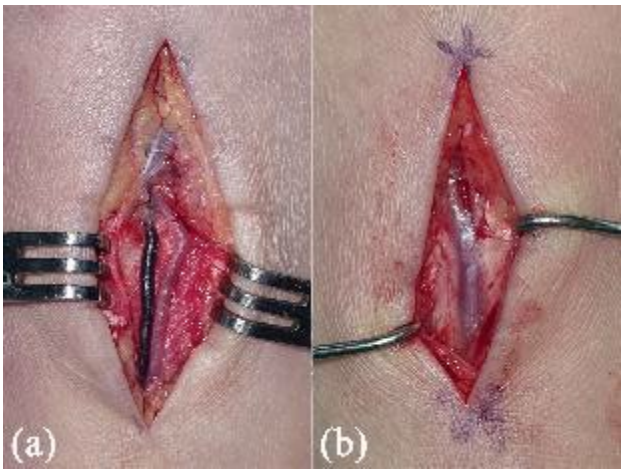

Fig. 3. Immediate postoperative findings of both dorsalis pedis vessels. The extensor hallucis brevis muscles and tendons were resected to completely relieve compression, and periarterial sympathectomies were additionally performed to promote smoother blood flow. (a) Right. (b) Left.

Fig. 4. 9- month postoperative clinical photos. (a) Plantar view of the right foot. (b) Dorsal view of the right foot. (c) Previous ulcer site on the right great toe. (d) Plantar view of the left foot. (e) Dorsal view of the left foot. (f) Previous ulcer site on the left great toe.

EP-212

Ray 절단 후 일차 봉합을 위한 항생제 함유 골 시멘트 비드 지지체 사용: 증례 보고

Antibiotics-Loaded Bone Cement Bead Scaffolding for Primary Closure After Ray Amputation: A Case Report

순천향대학교 구미병원

김정환, 김세영*

Background : Ray amputation is frequently performed in diabetic foot patients with osteomyelitis. Flap-based reconstruction, such as plantar fillet flaps, is commonly used to achieve durable coverage. However, diabetic patients are predisposed to wound healing complications due to impaired circulation, including marginal ischemia, wound dehiscence, and deep tissue infection. Persistent dead space may further compromise healing. We report a case in which antibiotic-loaded bone cement beads were used as internal scaffolding to facilitate primary closure without flap mobilization.

Methods : A 70-year-old male with diabetes mellitus presented with gangrene of the fourth toe. Imaging demonstrated osteomyelitis involving the fourth metatarsal. (Figure. 1) A fourth ray amputation with radical debridement was performed. Negative pressure wound therapy was applied to promote granulation and optimize the wound bed. After stabilization, residual medial forefoot dead space remained. Small antibiotic-loaded bone cement beads were fabricated intraoperatively and inserted to fill the space, providing structural support and localized antimicrobial effect. (Figure. 2)

Results: The wound was subsequently closed primarily with reduced tension. (Figure. 3) No wound dehiscence or recurrent infection occurred during follow-up. The wound healed without additional surgical intervention maintaining stable soft tissue coverage of the medial forefoot without the need for additional flap reconstruction.

Conclusion: Antibiotic-loaded bone cement bead scaffolding after ray amputation may facilitate primary closure while addressing dead space and providing local antimicrobial support. The bead construct effectively obliterated dead space and functioned as an internal scaffold, preventing medial soft tissue collapse. This strategy may represent a simple and reproducible adjunct in selected diabetic foot patients.

Figure 1. A 70-year-old male with diabetes mellitus presented with gangrene of the fourth toe. Imaging demonstrated osteomyelitis involving the fourth metatarsal.

Figure 3. Primary wound closure without flap coverage after filling the residual dead space with antibiotic-loaded bone cement beads acting as internal scaffolding.

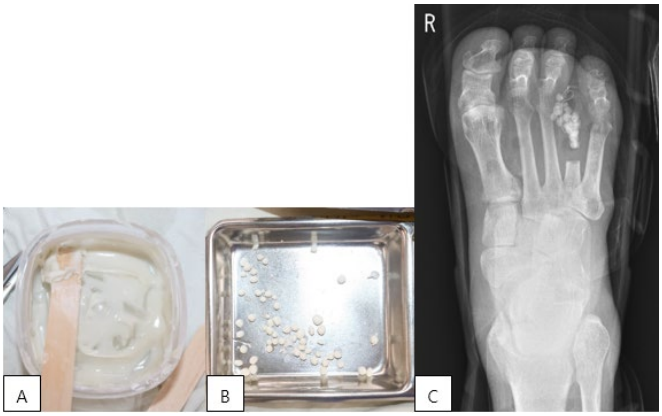

Figure 2. (A) Mixing of antibiotic-loaded bone cement. (B) Fabrication of small bone cement beads. (C) Postoperative radiograph demonstrating bead placement within the residual dead space.

EP-213

전위한 심하복벽혈관과 외측대퇴회선동맥 하행분지를 이용한 수여혈관 선택 전략

Recipient Vessel Selection Using Turnover Deep Inferior Epigastric and Lateral Circumflex Femoral Vessels in Complex Perineal Reconstruction

한양대학교 의과대학
성형외과학교실

왕형우, 장란숙, 김효성, 김지영, 김연환*

Purpose: Reconstruction of extensive perineal defects is technically demanding due to limited availability of reliable recipient vessels. We evaluated a recipient vessel selection strategy utilizing turnover deep inferior epigastric vessels (DIEV) and the descending branch of the lateral circumflex femoral artery (LCFA) for microsurgical reconstruction.

Methods: A retrospective review of 19 patients who underwent microsurgical reconstruction of perineal defects between 2006 and 2025 was performed. The collected data include: age, sex, etiology, body mass index (BMI), location, flap size, pedicle length, recipient vessels, and postoperative complications.

Results: Recipient vessels were selected according to defect location and accessibility. 8 infection cases, 8 cancer cases, a burn scar contracture deformity, a venous malformation and a lymphatic malformation cases were included. 7 cases were reconstructed with thoracodorsal artery perforator free flap (TDAP), 10 cases were reconstructed with muscle-sparing Latissimus dorsi free flap (LDms) and 2 cases were reconstructed with dual flap reconstruction of LDms flap and anterolateral thigh flap. Among the 19 cases, turnover DIEV was used as a recipient in 13 cases, and turnover descending branch of LCFA was used in 6 cases. The mean flap dimension was about 206cm2. All flaps survived without flap loss, with one patient requiring emergent hematoma evacuation due to postoperative bleeding, with successful flap salvage.

Conclusion: Turnover DIEV and LCFA descending vessels represent reliable recipient choices for complex perineal reconstruction. This strategy enables flexible flap design and facilitates sequential or combined free flap reconstruction while avoiding vein grafting and extensive recipient vessel dissection.

Fig. 1. A) About 20x20cm sized skin and soft tissue defect was identified on left perineal region after wide excision of liposarcoma. B) About 21x15cm sized TDAP free flap was harvested, the pedicle length was about 8cm. C) Immediate postoperative photo. D) 3-week postoperative photo.

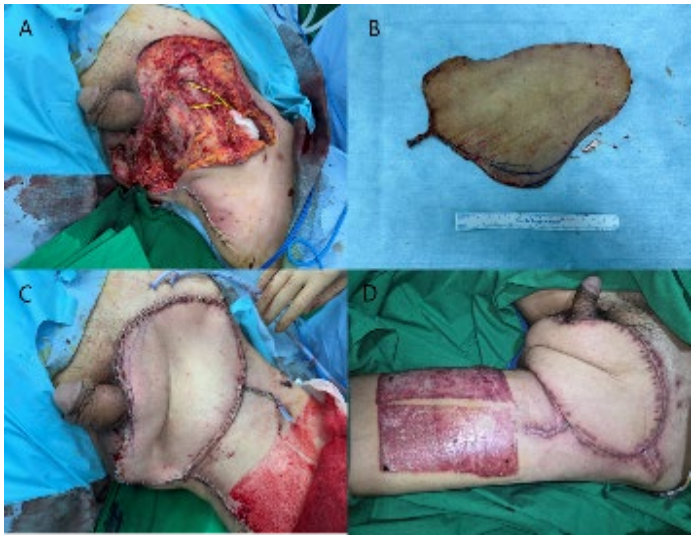

Fig. 2. A) About 20x20cm sized skin and soft tissue defect was identified on left perineal region after wide excision of liposarcoma. B) About 21x15cm sized TDAP free flap was harvested, the pedicle length was about 8cm. C) Immediate postoperative photo. D) 3-week postoperative photo.

EP-214

당뇨발 환자에서 혈관성형술 후 혈관 재협착에 대한 유리피판 재건술의 보호 효과

Protective Effect of Free Flap Reconstruction on Vascular Restenosis After Angioplasty in Diabetic Foot Patients

아주대학교 의과대학 성형외과학교실

배충현, 김민지*, 조훈길, 한형민, 이일재

PURPOSE : • PAOD in diabetic foot: one of the most refractory wound conditions
• Angioplasty: minimally invasive, high technical success rates → but restenosis remains a critical limitation
• "Nutrient flap" concept: free flap introduces well-vascularized donor tissue to ischemic recipient site
• Aim: evaluate protective effect of free flap reconstruction against vascular restenosis after angioplasty

METHODS : • Retrospective cohort study | Jan 2015 – Mar 2023
• Inclusion: DM foot ulcer + confirmed PAOD + technically successful primary angioplasty (n=60)
• Free flap group (n=30) vs. Conservative group (n=30)
• Free flap performed within 2–4 weeks after angioplasty
• Primary outcome: occurrence of re-angioplasty
• Secondary outcome: limb salvage / partial amputation / amputation

RESULTS :
• Re-angioplasty: Free flap 10.0% vs. Conservative 63.3% (p<0.001)
• Limb salvage: Free flap 66.7% vs. Conservative 20.0% (p<0.001)
• Among re-angioplasty patients → limb salvage only 4.5%
• Only ESRD on HD associated with higher re-angioplasty risk (68.2% vs. 36.8%, p=0.019)
• Demographic factors (sex, smoking, HbA1c, osteomyelitis): Not significant
• Multivariate analysis:
→ Free flap = only independent protective factor
→ aOR=0.059, ~94% risk reduction (p<0.001)
• TASC C/D more prevalent in conservative group (93.3% vs. 36.7%)
• Vessel involvement & patent infra-popliteal vessels: no sig. difference

Table 1. Univariate and multivariate analysis of factors

	Univariate Analysis		Multivariate Analysis	
Variables	OR (95% CI)	p-value	aOR (95% CI)	p-value
Age	1.003 (0.948–1.062)	0.915	0.983 (0.910–1.060)	0.651
Female sex	0.716 (0.192–2.671)	0.619		
Smoking	0.824 (0.240–2.821)	0.757		
HbA1c	0.898 (0.688–1.172)	0.427	1.028 (0.734–1.439)	0.872
ESRD on HD	3.673 (1.207–11.183)	0.022*		
Osteo-myelitis	1.169 (0.404–3.387)	0.773	0.975 (0.265–3.586)	0.970
Free flap treatment	0.064 (0.016–0.262)	<0.001*	0.059 (0.013–0.261)	<0.001*

Table 2. Comparison of angiographic characteristics and lesion distribution

		Conservative (n=30)	Free flap (n=30)	p-value
TASC Classification	A	2 (6.7)	12 (40.0)	<0.001*
	B	0 (0.0)	7 (23.3)	
	C	19 (63.3)	9 (30.0)	
	D	9 (30.0)	2 (6.7)	
Occlusive Lesion Location	Anterior tibial artery	23 (76.7)	21 (70.0)	0.559
	Posterior tibial artery	18 (60.0)	17 (56.7)	0.793
	Peroneal artery	14 (46.7)	12 (40.0)	0.602
	Superficial femoral artery	16 (53.3)	7 (23.3)	0.017*
	Popliteal artery	13 (43.3)	4 (13.3)	0.010*

Table 3. Comparison of vascular complexity and distal

Variables	Conservative (n=30)	Free flap (n=30)	p-value
Vessel involvement			0.617
Single vessel, n (%)	5 (16.7)	9 (30.0)	
Multiple vessels (≥2), n (%)	17 (56.7)	18 (60.0)	
TASC Classification			0.001*
TASC A or B, n (%)	2 (6.7)	19 (63.3)	
TASC C or D, n (%)	28 (93.3)	11 (36.7)	
Mean patent Infra-popliteal vessels	1.05 ± 0.95	1.22 ± 0.85	0.495

CONCLUSION : • Free flap reconstruction significantly reduces re-angioplasty risk after primary angioplasty in diabetic foot patients
• Free tissue transfer → maintains vascular patency beyond simple wound coverage
• Combined endovascular revascularization + free flap: effective strategy for improving limb salvage outcomes

EP-215

양측 하퇴 및 족부 3도 화염 화상 후 사지 보존: 다학제적 재건 접근

(Limb Salvage After Bilateral Lower Leg and Foot Third-Degree Flame Burns: A Multidisciplinary Reconstructive Approach)

강동성심병원 성형외과

정지원, 김결희*, 정철훈, 장용준, 황나현

Purpose: Extensive third-degree burns of the lower extremities involving deep muscle and joint structures present a significant reconstructive challenge and high risk of limb loss. Successful management requires staged debridement, infection control, skeletal stabilization, and durable soft tissue coverage. We report a case of bilateral lower leg and foot flame burns managed with a multidisciplinary limb salvage strategy.

Methods: A patient sustained bilateral lower leg and foot flame burns in a house fire, resulting in third-degree injuries with eschar formation and muscle involvement (Figure 1). Escharectomy was performed, followed by negative pressure wound therapy (Figure 2). Definitive reconstruction was performed 34 days after injury. After thorough debridement, left ankle arthrodesis with intramedullary nailing was performed by the orthopedic team. Soft tissue coverage was achieved using a free latissimus dorsi muscle flap. A full-thickness skin graft was applied to the posterior ankle and heel, and meshed split-thickness skin grafts were used to cover the remaining defects. An external fixator was applied for additional stabilization (Figure 3). Hardware removal was performed 63 days after surgery.

Results: The flap survived completely, and the skin grafts demonstrated successful engraftment. No major complications occurred (Figure 4). At the 3-month follow-up, durable soft tissue coverage was maintained with successful limb salvage. The patient was able to bear weight and ambulate on the reconstructed limb.

Conclusion: Bilateral lower extremity third-degree burns with joint involvement can be successfully treated with a staged, multidisciplinary approach. Aggressive limb salvage efforts may prevent amputation and restore structural integrity even in complex burn injuries.

Fig 1. Preoperative photographs and computed tomography demonstrating nasal deformity with anterior nasal spine defect secondary to neonatal nasal tube–related infection

Fig 2. A photograph of wound after escharectomy and application of negative pressure wound therapy

Fig 3. Intra-operative photographs demonstrating successful coverage of extensive soft tissue defects with free muscle flap after skeletal fusion

Fig 4. 3-month follow up photographs showing stable soft tissue coverage and limb preservation

EP-216

절단이 고려되었던 골수염 동반 당뇨발에서 보존적 변연절제술과 유리피판 재건을 통한 장기 사지 보존: 증례 보고

(Successful long-term limb salvage of diabetic foot with osteomyelitis by conservative debridement and free flap coverage: A Chronological Case Report)

울산대학교

박상천, 권진근, 박창식, 홍준표, 서현석*

We present a long-term limb salvage outcome in a 40-year-old woman with poorly controlled diabetes mellitus, severe systolic heart failure (left ventricular ejection fraction 26%), and chronic tarsal osteomyelitis with extensive soft tissue defect. Under conventional treatment principles, she had been considered a candidate for major amputation. However, after conservative debridement without radical bone resection, stabilization of the midfoot fractures and free flap coverage was performed to the dorsum of the foot, combined with prolonged culture-directed antibiotic therapy. The patient developed cardiac arrest owing to ventricular fibrillation but was successfully resuscitated. During long-term follow-up approaching 10 years, the flap remained viable and infection was ultimately controlled without progression to major amputation. The patient achieved and maintained full weight-bearing ambulation without episode of plantar ulceration or aggravation of deep infection. This case demonstrates that even in highly comorbid patients, individualized limb salvage incorporating conservative bone debridement, durable soft tissue reconstruction with free flap, and structured infection control can achieve sustained ambulation and long-term limb preservation.

Figure 1. Preoperative status after removal of the external fixation and multiple conservative debridements
(Left) Devitalization of the navicular, as well as the medial and middle cuneiform bones, was noted.
(Right) Fractures of the 2nd to 5th metatarsal bones, the lateral cuneiform bone, and the cuboid bone were noted.

Figure 2. 4 days after the free flap operation
Discoloration was observed at the distal flap margin. Plain radiographic images reveal navicular-talus pinning and longitudinal fixation using Kirschner wires extending from each of the five toes to the calcaneus, stabilizing the midfoot with multiple fractures.

Figure 3. Full weight-bearing ambulating status
The clinical photographs were taken 395 days after the free flap operation.

EP-217

이식편 없는 합지증 재건을 위한 변형 삼엽 피판술

(Modified trilobed flap for Graft-Free Syndactyly Reconstruction)

서울대학교 의과대학[1]
보라매병원 성형외과[2]

성효재[1,2], **박준호***[1,2]

Purpose: Surgical release of syndactyly aims to restore independent digital motion while preventing web creep and scar contracture. Conventional techniques frequently rely on full-thickness skin grafts to compensate for predictable soft-tissue deficiency at the interdigital commissure and digit bases, inevitably introducing donor-site morbidity, color mismatch, and secondary contracture risk.

Methods: We present a graftless correction of simple soft-tissue syndactyly using a modified trilobed flap design in a 16-month-old boy with right 2nd web-space involvement. The trilobed flap was planned to reconstruct the commissure and adjacent digital defects without skin grafting. The distal lobe was anchored deeply to recreate a stable web corner, the central lobe was advanced to resurface the primary defect, and the lateral lobes were inset precisely into interdigitating digital defects to achieve tension-free closure. Key technical principles included wide flap mobilization, secure distal anchoring for commissural definition, meticulous tension distribution across lobes, and application of a space-maintaining non-adherent dressing to preserve interdigital separation during early healing.

Results: The flap survived completely, and wounds healed without major complications. At 1-month follow-up, the reconstructed webspace demonstrated stable contour, preserved depth, and no evidence of early web creep or contracture. Importantly, the absence of skin graft harvest eliminated donor morbidity and contributed to uniform scar quality across the reconstructed area.

Conclusion: This case highlights that a modified trilobed flap can provide reliable graftless syndactyly correction in selected simple cases, achieving early web stability and favorable scar behavior while avoiding the disadvantages inherent to skin grafting.

Fig. 1. Preoperative photo of the right foot demonstrating soft-tissue syndactyly of the 2nd webspace

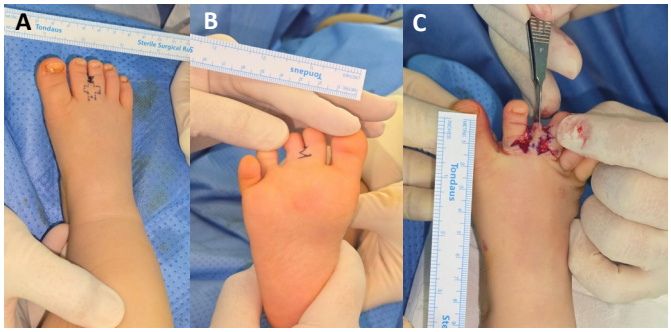

Fig. 2. Surgical design and application of the modified trilobed flap. (A, B) Design of the modified trilobed flap for web reconstruction and adjacent digital resurfacing. (C) Flap elevation and inset to recreate the interdigital webspace.

Fig. 3. Postoperative photographic finding 1 month after operation

EP-218

절단 위기 수준의 괴사성 근막염에서 수술실 중심의 고빈도 처치 및 단계적 재건을 통한 구제 전략: 3례 증례 분석과 치료 알고리즘 제안

Structured High-Frequency Operating Room–Based Salvage Strategy for Limb-Threatening Necrotizing Fasciitis: A Three-Case Series and Treatment Algorithm

중앙대학교 의과대학 성형외과학교실 [1]
중앙대학교 광명병원 성형외과 [2]

정인호[1], 김우섭[2], 김한구[1], 배태희[2], 강신혁[1], 김우주[2], 우수현*[1]

Purpose: Necrotizing fasciitis (NF) in high-risk patients often necessitates proximal amputation. Current clinical standards lack structured guidance on the precise intensity and frequency of surgical interventions required for limb salvage. We propose a "Structured High-Frequency Operating Room (OR)-based Salvage Strategy" to prevent premature or excessive amputation.

Methods: We report three high-risk diabetic patients (one upper extremity, two lower extremities) with limb-threatening NF who were initially advised to undergo amputation. Our protocol involved: 1) Proactive OR-based debridement every 48–72 hours; 2) Serial culture-driven antimicrobial adaptation; and 3) Staged decision-tree-based reconstruction timing. Patients underwent 19–23 OR-based interventions for radical irrigation, debridement, and wound control. Definitive reconstruction was performed using acellular dermal matrix (DM) and split-thickness skin grafting once objective infection control criteria were met.

Results: Despite extensive tissue loss and impaired healing capacity, stable granulation beds were achieved in all cases. Complete limb salvage was achieved in Cases 1 and 2, including the anatomically vulnerable Achilles' area. In Case 3, where an above-knee amputation was pre-determined prior to plastic surgery intervention, the protocol effectively halted proximal infection spread toward the high-femur level, successfully salvaging a functional stump for rehabilitation. All cases achieved stable epithelialization within 4–6 months without recurrence.

Conclusion: In selected diabetic patients with severe NF, a structured, high-frequency OR-based salvage algorithm may prevent premature amputation. Persistent but criteria-driven operative management combined with adaptive antimicrobial therapy can enable limb preservation even in cases initially deemed unsalvageable.

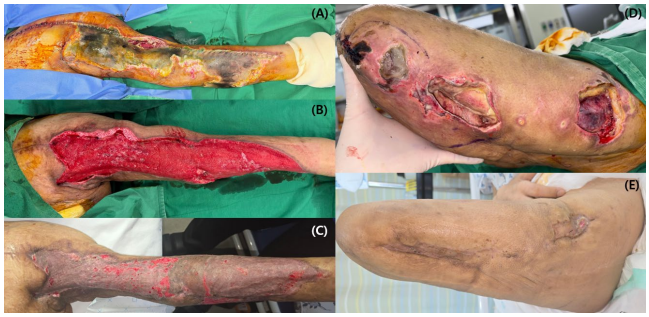

Fig. 1. (A) Initial radical debridement performed upon transfer of case 1. Despite 10 days of prior antibiotic therapy at a secondary hospital, deep tissue necrosis was evident. (B) Pre-reconstructive state just before skin graft. (C) Follow-up image 1 day after the final operating room (OR) visit, demonstrating successful wound epithelization. (D) Initial presentation of case 2 to the Department of Plastic Surgery following an above-knee (AK) amputation by Orthopedic Surgery. All wounds were found to be communicating with each other. (E) One-month follow-up showing complete epithelialization and a functional stump.

Fig. 2. (A) Initial radical debridement of figure 3, involving the entire lower leg and the lateral aspect of the thigh. (B) Appearance one month after the initial OR visit. (C) Final follow-up one month after reconstruction, showing complete epithelialization and successful prevention of proximal extension.

Category	Parameter	Case 1 (Shoulder)	Case 2 (Lower Leg)	Case 3 (Thigh/Stump)
Demographics	Age / Sex	39 / M	58 / M	54 / M
Comorbidities	Key Conditions	Humerus Fx, DM	T-SAH, Multiple Trauma, DM	HFrEF, ESRD on HD, DM, HTN
Severity at Admission	Peak CRP (mg/L)	66.3 (Pre-treated)	280.6 (PTD5)	310.0 (HD3)
	Septic Shock	No	Yes (Inotropes (+))	Yes (Inotropes (+))
	ICU Admission	No	Yes	Yes
	Osteomyelitis	Yes (humerus)	No	Yes (lower leg)
Microbiology	Primary Pathogen	Mixed / MRSA	Aeromonas hydrophilia	ESBL E. coli
Initial Proposal	Reason for Amputation	Refractory to 10d+ Abt, Multi-level joint involvement	Circumferential involvement, Achilles exposure	Life-threatening shock
Surgical Intensity	Total OR-based I&D	23 sessions	20 sessions	19 sessions
Outcome	Final Status	Limb Salvage Functional-free on elbow, wrist and hand	Limb Salvage Functional-free on whole levels of Lt. Lower extremity	Functional Stump Salvage

Fig. 3. Overall view of the whole cases.
*Fx : Fracture, *DM : Diabetes Mellitus, *T-SAH : Traumatic subarachnoid hemorrhage, *HFrEF : Heart failure with reduced ejection fraction, *ESRD : End stage renal disease, *HTN : Hypertension, *PTD : Post-trauma day, *HD : Hospital day, *Abt : Antibiotics

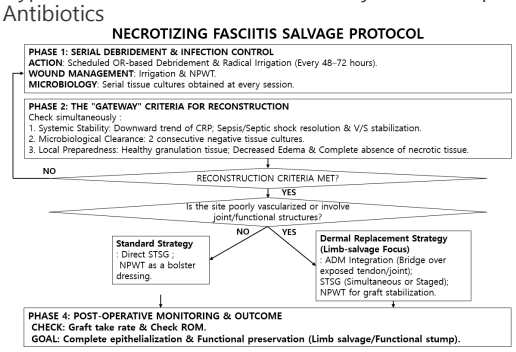

Fig. 4. Algorithm tree of necrotizing fasciitis treatment.
*OR : Operation room, *NPWT : Negative pressure wound therapy, *STSG : Split thickness skin graft, *ADM : Acellular dermal matrix, *ROM : Range of motion

EP-219

좌골 부위 욕창으로 인해 발생한 치골결합부 골수염의 치료 증례: 대퇴이두근 전위 피판을 이용한 치료

한림대학교성심병원

김준일, 김재현, 정찬민*

Purpose: A neglected or untreated pressure sore in the ischial area can lead to osteomyelitis. This case report aims to describe the successful management of a skin and soft tissue defect accompanying osteomyelitis of the symphysis pubis, resulting from a pressure sore on the ischial area. The chosen intervention involves the use of a biceps femoris turnover flap for reconstruction.

Methods: A 64-year-old male presented with a pressure sore on the right ischial area, featuring a 3 x 3 cm opening and a 7 x 10 cm area of undermined area (Fig. 1). The surgical procedure involved the elevation and detachment of the biceps femoris muscle, followed by the application of a biceps femoris turnover flap for coverage and reconstruction (Fig. 2).

Results: Two months postoperatively, MRI demonstrated marked improvement of osteomyelitis of the symphysis pubis (Fig. 3), along with successful coverage of the skin and soft tissue defect. Ultimately, the patient's skin and soft tissue defect healed completely without sequelae (Fig. 4)

Conclusion: This case report highlights the successful surgical intervention using a biceps femoris turnover flap for the reconstruction of a soft tissue defect relieving osteomyelitis of the symphysis pubis. The positive outcome observed on follow-up MRI supports the efficacy of this approach in managing complex cases of pelvic osteomyelitis.

Fig 1. Preoperative gross photography

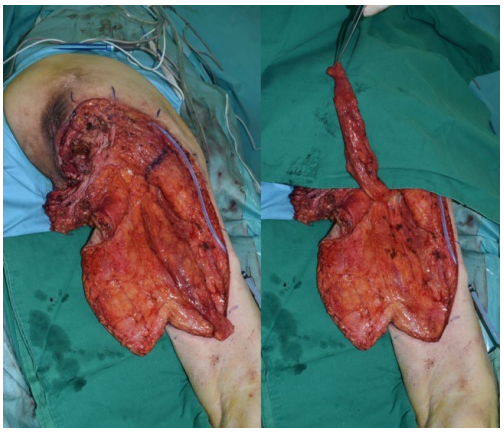

Fig 2. Intraoperative gross photography

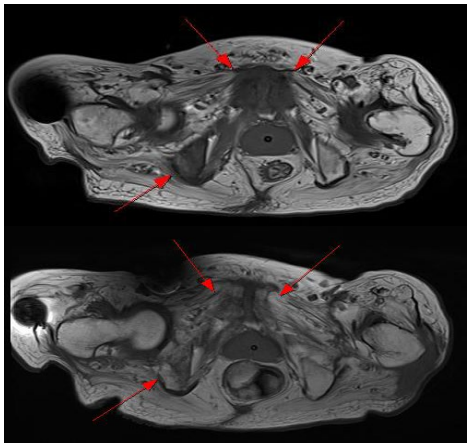

Fig 3. Pre, Postoperative MRI (Top: preoperative MRI, Bottom: postoperative MRI)

Fig 4. Post operative gross photography

EP-220

흡인 배액관과 음압창상치료를 병합한 모렐-라발레 병변의 치료

(Treatment of morel lavallee lesions using a combination of suction drain and negative pressure wound therapy)

가톨릭대학교 의과대학
성형외과학교실
서해진, 신종원*

Purpose: Morel Lavallee lesions (MLL) are closed degloving injuries in which fluid accumulates between the hypodermis and deep fascia. Although the incidence is reported to be rare, once it occurs, it often progresses chronically and is prone to recurrence. Although various treatments have been introduced, there is still no standard. The authors report successful treatment of MLL using a combination of suction drain and negative pressure wound therapy (NPWT).

Methods: A total of two patients were treated with this combination. All cases were caused by blunt trauma, and the average duration was 2.3 months. Necrotic skin was excised, and the inside of the pocket was meticulously debrided. A suction drain was inserted inside the pocket, the skin wound was closed, and then NPWT was applied widely to the area. NPWT was removed after being maintained for a week, and the suction drain was removed within 2 weeks.

Results: All cases were treated well without any specific complications. There were no signs of recurrence during the follow-up period of more than 6 months. In the case of young female patient, satisfactory cosmetic results were obtained. This combination is thought to have shown good results based on the principle of maintaining negative pressure within the pocket using suction drain and maintaining positive external pressure using NPWT.

Conclusion: MLL are difficult to treat because they tend to become chronic and recur easily. Combination of suction drain and NPWT can be a relatively simple treatment method that can reduce the recurrence rate.

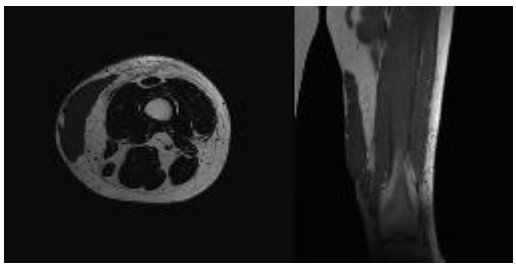

Fig. 1. MRI image of the first patient. In the T1 MRI image, a well-defined fluid signal lesion measuring approximately 11x20 cm was observed in the subcutaneous layer of the left medial thigh.

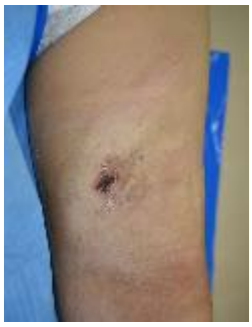

Figure 2. Clinical photograph of the first patient. Skin necrosis about 3cm in diameter was observed, and fluctuations were observed in the surrounding area.

Fig. 3. Immediat post operation clinical photograph of the first patient, showing NPWT system applied on the surface.

Fig. 4. Clinical photograph of the first patient at 6-month follow-up visit showing preserved symmetrical contour of thighs.

EP-221

Pathergy 반응 및 이차 감염을 동반한 난치성 외측 복사부 궤양에서 의심된 괴저성 농피증

(Pyoderma Gangrenosum Suspected in a Refractory Lateral Malleolar Ulcer with Pathergy and Secondary Infection)

인제대학교

윤태권, 윤지영*

Purpose: Pyoderma gangrenosum (PG) is a rare neutrophilic dermatosis that mimics infected or vasculitic ulcers and may worsen after surgical manipulation. We report a clinically suspected case of PG on the lateral malleolus complicated by secondary wound infection and a prior history of vasculitis.

Methods: A patient presented with a chronic, painful ulcer on the right lateral malleolus. The patient had been diagnosed with leukocytoclastic vasculitis 6 years earlier and had received systemic steroids and regular dressings without improvement. Two years ago, surgical debridement performed at another hospital led to rapid aggravation requiring one month of hospitalization. After discontinuing follow-up and performing self-care, the patient revisited our hospital due to worsening of the lesion. On admission, the ulcer demonstrated progressive tissue loss, a violaceous border, foul-smelling discharge, and severe pain. Wound cultures identified Klebsiella pneumoniae and Pseudomonas aeruginosa, and intravenous antibiotics were administered. Additional evaluations included skin biopsy, vascular ultrasonography, CT angiography, and ankle-brachial index measurement.

Results: Histopathology showed nonspecific ulcerative inflammation, and vascular studies were unremarkable. Despite inconclusive histology and confounding infection and vasculitic history, the clinical presentation suggested PG, supported by severe pain, violaceous margins, pathergy following debridement, and a favorable response to immunosuppressive therapy. Oral prednisolone and cyclosporine, combined with hyperbaric oxygen therapy and wound care, achieved complete healing within 3 months.

Conclusion: PG should be considered in chronic ulcers that worsen after debridement. Clinicians should be aware of this clinically suspicious case as surgical manipulation such as debridement may trigger further deterioration through pathergy.

Figure 1. Serial clinical photographs of the right lateral malleolar ulcer clinically suspected as pyoderma gangrenosum.(A) Initial presentation showing a painful ulcer with progressive tissue loss, violaceous border, and purulent exudate.(B) Persistent ulcer after infection control with intravenous antibiotics and conservative wound care.(C) Complete healing after oral prednisolone and cyclosporine combined with hyperbaric oxygen therapy and dressing care.

EP-222

유리피판 재건술 후 이차 윤곽 교정을 위한 Subunit 기반 피판 내 Debulking 기법

(Subunit-Based Intraflap Debulking Technique for Secondary Contouring After Free Flap Reconstruction)

성균관대학교
<u>류경은</u>, 이경태*

INTRODUCTION :

- Despite advances in surgical technique for flap thinning, secondary debulking is often needed in areas with thin soft tissue coverage.
- Flaps spanning multiple anatomical subunits present a unique challenge, as central bulkiness—often near subunit junctions—is difficult to address with conventional margin-based approaches and may obscure natural contours.
- We introduced a subunit-based intraflap debulking technique, placing incisions across the flap along anatomical subunit borders, and evaluated its safety and effectiveness.

METHODS :

- Patients who underwent free flap reconstruction (2021–2025) and subsequent secondary debulking using this technique were retrospectively reviewed.
- The technique consists of intraflap incisions along subunit borders, cone-shaped excision of central redundancy, and flap re-approximation to restore natural contours.
- Postoperative outcomes (wound dehiscence, seroma, delayed wound healing, hematoma, infection, etc.) were assessed.

RESULTS :

- A total of 22 cases were treated, most commonly involving lower extremity reconstruction, particularly of the foot, with the superficial circumflex iliac artery perforator flap most frequently used.
- Debulking was performed at a median of 10 months after the initial reconstruction. No postoperative complications were observed.
- The median time to complete healing was 14 days, and all patients reported satisfaction with the aesthetic outcomes.

Fig. 1. Subunit-based intraflap debulking technique. An incision was placed along the dorsum–ankle junction, followed by cone-shaped excision of central bulkiness and flap reapproximation to restore natural contour. Uneventful healing with improved contour and function was achieved.

Fig. 2. A 72-year-old man underwent ALT free flap reconstruction for melanoma of the forefoot. At 12 months, secondary debulking was performed using a midline intraflap incision between the fourth and fifth toes. Uneventful healing with resolution of bulkiness and no need for further procedures was observed at 7 months.

CONCLUSION :

- The subunit-based intraflap debulking technique appears to be a safe approach for secondary contouring after free flap reconstruction in selected cases, allowing effective central debulking and restoration of natural subunit borders.

EP-223

복합 전족부 발바닥 결손의 재건: ALT 유리피판 및 중족골 간 혈관 터널링 기법

(Salvage of Complex Plantar Forefoot Defects: ALT Free Flap with Trans-metatarsal Pedicle Tunneling)

건국대학교병원

유정환, 신동혁*

Purpose: Reconstructing plantar forefoot defects in diabetic patients is challenging due to the limited availability of recipient vessels. This case reports a successful microvascular reconstruction of a plantar forefoot defect using an Anterolateral Thigh (ALT) free flap and a trans-metatarsal pedicle route to access the dorsalis pedis artery.

Methods: A 29-year-old male with a history of a previous ALT free flap presented with a soft tissue defect on the left plantar forefoot and progressed osteolysis in the 3rd proximal phalanx and metatarsal head. The patient's HbA1c was 10.1% and glucose 301 mg/dL. To cover the plantar defect, an ALT free flap was harvested, and the dorsalis pedis artery was selected as the recipient vessel. After vessel dissection, a tunnel was created through the first intermetatarsal space. A Hemovac tube and Penrose drain were utilized as guides to safely pull the pedicle from the dorsum to the plantar region.

Results: The microvascular anastomosis was performed successfully on the dorsal side. The pedicle remained stable within the intermetatarsal tunnel without any kinking or vascular compromise. The flap survived completely without complications. During the 4-month follow-up period, the patient recovered well and is currently capable of independent ambulation.

Conclusion: The intermetatarsal tunneling technique with an ALT free flap is an effective strategy for plantar forefoot reconstruction, especially when local recipient vessels are compromised. Using a surgical guide (Hemovac/Penrose) ensures the safe passage of the pedicle, providing a reliable alternative for complex diabetic foot salvage.

Fig.1
Complex defect on the right plantar forefoot of a poorly controlled diabetic patient. A deep, extensive ulcer with exposed bone and tendon is present over the second metatarsal head.

Fig.2
An intraoperative photograph demonstrates the creation of a tunnel through the intermetatarsal. The retrieved pedicle was anastomosed to the dorsalis pedis artery and its venae comitantes.

Fig.3
A clinical photograph taken 14 days postoperatively shows the Anterolateral Thigh (ALT) free flap well-settled over the forefoot defect. This demonstrates that the trans-metatarsal pedicle tunneling provided a stable and sufficient blood supply to the flap.

EP-224

근육 내 거대 고분화 지방육종 절제 후 사지 보존에 성공한 증례

(Successful Limb Salvage After Resection of a Giant Intramuscular Well-Differentiated Liposarcoma)

순천향대학교 부속 서울병원

최현범, 김철한*

Purpose: Well-differentiated liposarcoma (WDLPS) occurring within intramuscular compartments may extend to adjacent osseous structures, posing challenges in achieving oncologic clearance while preserving limb function. We report a case of intramuscular WDLPS of the medial thigh adherent to the femur, successfully managed with limb-salvage resection.

Methods: A 63-year-old woman presented with a progressively enlarging mass in the right medial thigh for 5 years. Magnetic resonance imaging demonstrated a lipomatous lesion within the vastus medialis muscle (Fig. 1). Intraoperatively, an intramuscular mass measuring approximately 20 cm in greatest dimension was identified within the vastus medialis, with the base of the mass adherent to the femur (Fig. 2). Marginal excision of the mass was achieved, with preservation of the femur except for partial excision of the periosteum (Fig. 3).

Results: Histopathological examination revealed a well-differentiated liposarcoma with negative surgical margins. Follow-up imaging has demonstrated no evidence of local recurrence, and postoperatively, limb function was fully preserved without any deficits.

Conclusion: Wide excision of giant intramuscular WDLPS provides maximal oncologic safety. Nevertheless, careful marginal excision, with selective resection of the periosteum when the tumor is adherent to the femoral surface, can achieve complete oncologic clearance while preserving limb function.

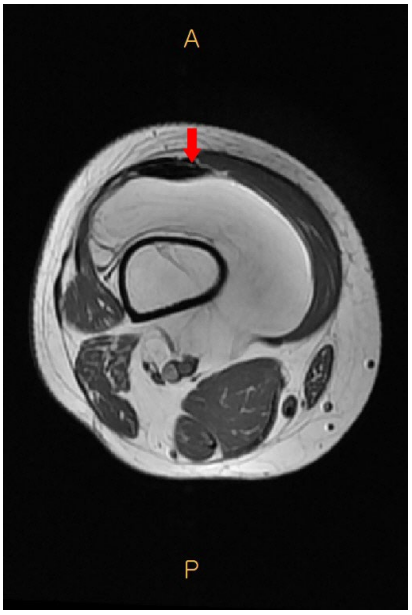

Fig. 1. Preoperative contrast-enhanced magnetic resonance imaging (axial view) demonstrating a large lipomatous mass within the medial thigh surrounding the femur.

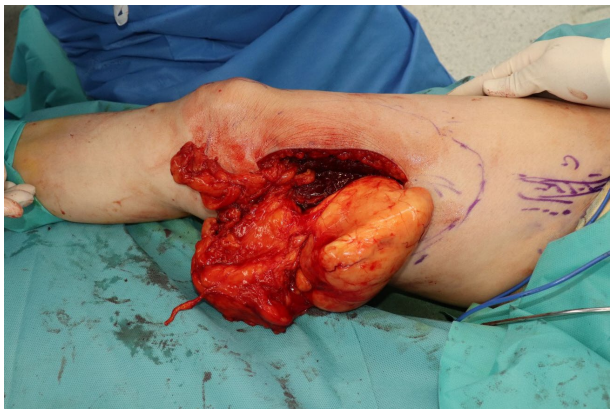

Fig. 2. Intraoperative photograph showing the giant intramuscular mass in the right medial thigh, measuring approximately 20 cm in greatest dimension.

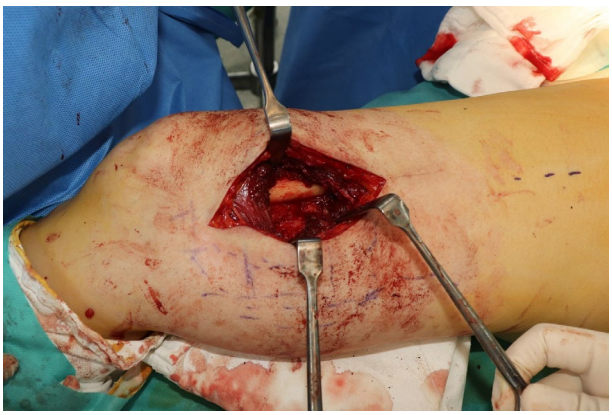

Fig. 3. Intraoperative photograph obtained after complete tumor resection, showing exposure of the distal femur following removal of the adherent mass.

EP-225

당뇨병성 족부 궤양으로 오인된 발의 악성 흑색종

(Malignant Melanoma of the Foot Misdiagnosed as Diabetic Foot Ulcers)

분당서울대학교병원
강명진, 김종호*

Purpose: Foot melanoma is a rare but aggressive malignancy that may clinically resemble diabetic foot ulcers, leading to diagnostic delay. In patients with diabetes mellitus, chronic foot lesions are frequently attributed to diabetic pathology, even when the clinical presentation is atypical. This study aims to raise awareness of the diagnostic pitfalls in patients with diabetes, highlighting the importance of considering melanoma in cases of atypical foot lesions.

Methods: We conducted a retrospective review of six patients who were initially referred with a diagnosis of diabetic foot ulcer but were ultimately diagnosed with malignant melanoma of the foot. Clinical presentation, presence of ulceration, diabetic status, time to diagnosis, Breslow depth, and nodal involvement were analyzed.

Results: Among the six cases, ulceration was present in four patients at initial presentation. Notably, all ulcerated cases demonstrated disease progression to the inguinal lymph nodes at the time of melanoma diagnosis. Despite having a history of diabetes mellitus, these patients did not exhibit severe diabetic complications that would typically account for refractory diabetic foot ulcers.

Conclusion: Non-healing foot ulcers in patients with diabetes should not be automatically attributed to diabetic foot disease, particularly when clinical features are inconsistent with typical diabetic ulcers. The presence of persistent or atypical ulceration should prompt early biopsy to exclude malignant melanoma.

Fig. 1. **Fig. 2.**

Fig. 1. Preoperative photograph of 68-year-old female with malignant melanoma of the right forefoot, initially appearing as a corn-like lesion that gradually enlarged and ulcerated. An approximately 3 × 5 cm ulcer with exposed hemorrhagic/necrotic tissue is seen at the plantar aspect of the right 2nd MTP area.

Fig. 2. Preoperative photograph of 69-year-old female with malignant melanoma of the right heel arising from a long-standing (>20 years) pigmented nevus that progressively enlarged and ulcerated. A large, darkly pigmented plaque with a protruding fungating nodular component is visible at the posterolateral heel.

Fig. 3.

Fig. 3. Preoperative photograph of 76-year-old male with a >20-year history of diabetes mellitus, initially referred as a diabetic foot ulcer. A round, ulcerated lesion with central pink–violaceous fungating tissue is shown.

EP-226

대퇴부에 발생한 재발성 이소성 피부 선낭암: 양성 낭종성 병변과의 임상적 유사성으로 인한 진단 및 치료의 지연

(Recurrent Extrasalivary Cutaneous Adenoid Cystic Carcinoma of the Thigh: Clinical Mimicry of a Benign Cystic Lesion Leading to Delayed Diagnosis and Management)

중앙대학교 의과대학 성형외과학교실 [1]

최주헌[1], 강신혁[1,*]

Purpose: Adenoid cystic carcinoma (ACC) is an exceptionally rare malignancy in extra-salivary sites, frequently presenting a diagnostic trap. Due to its indolent progression and unremarkable appearance, cutaneous ACC often disguises as common benign lesions, such as sebaceous cysts. This clinical mimicry leads to low index of suspicion, resulting in repeated incomplete excisions and significant delays in definitive diagnosis. We report a recurrent cutaneous ACC of the thigh, emphasizing the necessity of high clinical suspicion in such pitfalls.

Methods: A 49-year-old female presented with a recurrent right posterior thigh mass, previously misinterpreted as a benign cyst and excised twice without histopathological confirmation. A third recurrence finally revealed ACC with positive margins. Preoperative MRI for remnant tumor mapping showed focal T2 high signal intensity with enhancement. [Figure 1] Based on these findings, we performed a definitive wide radical excision with 1.5 cm safety margin, ensuring tumor-free boundaries via intraoperative frozen sections, followed by adjuvant radiotherapy. [Figure 2]

Results: Final pathology confirmed ACC with clear margins. Although lymphovascular and perineural invasions were absent, the history of multiple recurrences necessitated aggressive multimodal therapy. The patient has remained disease-free for 24 months. [Figure 3] However, due to the tumor's propensity for late-onset systemic spread, rigorous long-term surveillance remains mandatory.

Conclusion: The primary challenge of extra-salivary ACC lies in its benign clinical appearance, which delays early oncologic intervention. Recurrent or atypical cutaneous masses must be approached with a high degree of suspicion and mandatory biopsy. Radical surgical clearance combined with adjuvant therapy is essential to manage this persistent malignancy.

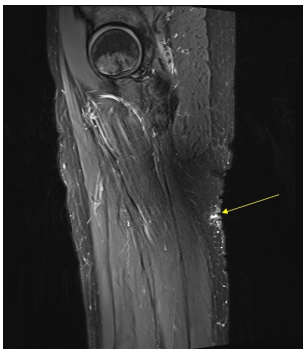

Fig. 1. Preoperative MRI findings. Contrast-enhanced MRI reveals ill-defined enhancement in the subcutaneous and skin layers of the right proximal thigh. Although suspicious for postoperative changes, the focal T2 high signal intensity indicates potential remnant tumor.

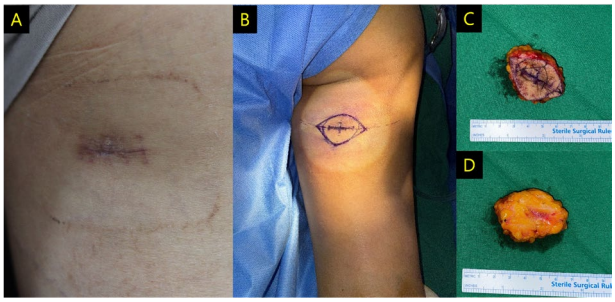

Fig. 2.
(A) Preoperative photograph of the patient's right posterior thigh shows the old scar from a previous excision, which was subsequently diagnosed as adenoid cystic carcinoma with positive resection margins on the third excision.
(B) Intraoperative photograph showing the planned incision lines designed to achieve a wide excision with a sufficient safety margin around the previous scar.
(C, D) Photographs of the resected specimen. The images show the excised skin and soft tissue, confirming the planned safety margins of 1.0 cm laterally and 1.2 cm deep. The gross appearance of the specimen indicates a successful wide excision for the recurrent tumor.

Fig. 3. A photograph of the well-sutured surgical site on post-operative day 3, on which the patient was discharged. Prophylactic radiation therapy was initiated 1.5 months later in consultation with the Department of Radiation Oncology. The patient has remained tumor-free for 2 years since, with no signs of local recurrence or distant metastasis.

EP-227

광범위한 감염성 근막절개창의 수압 기반 변연절제와 음압치료를 이용한 수복의 성공적 치료: 증례보고

(Successful Management of Extensive Infected Fasciotomy Wounds by Hydrosurgery and Negative Pressure Wound Therapy: A case report)

동국대학교 일산병원
성형외과

임수아*, 추교빈, 김경현, 조상헌, 어수락

Purpose: Acute compartment syndrome (ACS) is a surgical emergency characterized by increased pressure within a closed fascial compartment, leading to impaired tissue perfusion and requiring emergent decompressive fasciotomy. However, no standardized guidelines exist for managing wounds after extensive fasciotomy, and treatment becomes challenging when infection or poor systemic conditions are present. Split-thickness skin grafting (STSG) is commonly used for fasciotomy wound closure; however, in patients with unstable vital signs or severe anemia, skin harvest may be limited due to additional bleeding and donor-site complications.

Methods: A 67-year-old male presented with infected, extensive fasciotomy wounds (thigh 23 cm, lower leg 20 cm) following ACS and reperfusion syndrome (Fig. 1). His condition was complicated by Stevens-Johnson syndrome and severe anemia (Hb 6.5 g/dL), posing a risk of further anemia with skin graft harvest. Hydrosurgical debridement using Versajet™ system was performed to selectively remove biofilm and necrotic tissue with minimal bleeding. After repeated debridement, proximal wound was closed primarily, while a partial opening was intentionally left to facilitate drainage of purulent discharge (Fig. 2). Negative pressure wound therapy (NPWT) was applied to this window to facilitate continuous exudate evacuation.

Results: After approximately three weeks of NPWT, exudate markedly decreased and the infection was effectively controlled, enabling complete delayed primary closure (Fig. 3). At 9 months, patient showed excellent functional and cosmetic outcomes (Fig. 4).

Conclusion: In high-risk patients with extensive infected fasciotomy wounds, hydrosurgical debridement combined with strategically applied NPWT with a partial drainage window may provide an effective approach for successful wound management.

Fig. 1. Initial presentation of extensive infected fasciotomy wounds of the thigh and lower leg.

Fig. 2. Partial drainage window left after repeated debridement.

Fig. 3. Delayed primary closure after NPWT.

Fig. 4. Excellent functional and cosmetic outcomes at 9 months.

EP-228

후천성 손발톱주위 섬유각화종의 비전형적 증례: 돔형 및 분지형 혼합형

(An Unusual Presentation of Acquired Periungual Fibrokeratoma: A Mixed Dome-Shaped and Branching Type)

강원대학교병원
성형외과

박희정, 이상열*

Purpose: Acquired periungual fibrokeratoma is a rare benign fibrous tumor that typically arises from the proximal nail fold. Although it usually presents as a solitary lesion with a single morphological type—such as dome-shaped, rod-shaped/branching, or flat—its morphological variability may pose diagnostic challenges. We report a case with mixed features of dome-shaped and branching types to facilitate recognition of this unusual variant.

Methods: A 67-year-old man presented with a recurrent, asymptomatic mass on the proximal nail fold of the left second toe, previously excised 1 year earlier. Physical examination revealed a garlic-shaped, pedunculated mass with multiple elongated projections at its base measuring 1.3 × 0.9 × 0.7 cm (Figure 1). Shave excision was performed, and the specimen was subjected to histopathologic evaluation.

Results: Histopathologic examination demonstrated hyperkeratosis, parakeratosis, and acanthosis of the epidermis. The dermis showed thick collagen bundles arranged along the vertical axis with fibroblast proliferation and focal vascular dilation (Figure 2). Focal dermal necrosis and hemorrhage were also observed. The lesion was diagnosed as acquired periungual fibrokeratoma. No recurrence was observed during 6 months of follow-up.

Conclusion: This case highlights the morphological diversity of acquired periungual fibrokeratoma and its potential to present with mixed features. Accurate diagnosis is important because atypical variants can mimic verruca vulgaris, digital mucous cysts, or other periungual tumors. Complete surgical excision is recommended to minimize recurrence.

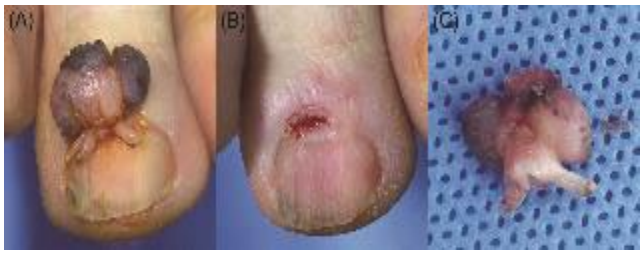

Fig. 1. A, Preoperative photograph showing the unique features of acquired periungual fibrokeratoma: the garlic-shaped mass and multiple elongated projections at its base. B, Postoperative photograph showing a tiny open wound at the proximal nail fold. C, The undersurface of the resected tumor specimen shows a narrow tumor base.

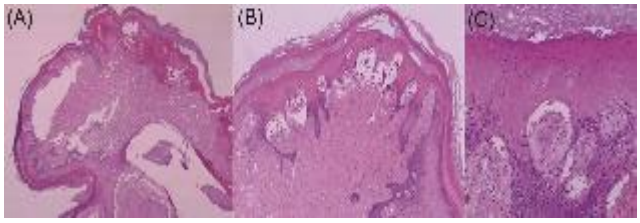

Fig. 2. Histological examination of the resected tumor. A, A papillary lesion is shown (hematoxylin and eosin [H&E], ×15). B, The dermis comprises vertically oriented collagen bundles and focal dilated blood vessels along with epidermal hyperkeratosis and acanthosis (H&E, ×40). C, Dermal papillary necrosis and hemorrhage are shown (H&E, ×200).

EP-229

피하 지방종이 동반된 화상 후 반흔 구축 1예

(A case of post-burn scar contracture associated with subcutaneous lipoma)

가톨릭대학교
정승원, 최종윤*

Purpose: Post burn scar on large joint can make joint contracture and ROM restriction, also not completely healed burn wound can be cancerous like majorlin's ulcer. We present a case of scar contracture after flame burn and release with Z-plasty, accidentally the scar tissue was confirmed lipoma with pathology.

Methods: A 50-year-old male patient presented at the outpatient clinic with scar contracture with ulceration on the right lateral knee area after flame burn 40 years ago. First, the punch biopsy of the lesion was erosion with acute suppurative inflammation and fibrosis. Then, the total excision with scar release was planned to confirm the pathology on ulceration. Under general anesthesia, the ulcerative wound was totally excised including subcutaneous layer with direct closure. Because the contracture was aggravated with closure, Z-plasty for scar release was done. Finally, the post burn ulcerative scar was confirmed lipoma with pathology.

Results: Until post operative three-months follow-up, partial necrosis was observed on the margins. After 5-months follow-up at the outpatient office showed an overall improvement of wound.

Conclusion: This is the first report of post-burn scar related lipoma. Considering the pathogenesis of the lipoma, there was lipoma subcilinically in the subcutaneous layer before the burn accident. But the lipoma may aggravating the ulceration, which looks like majorlin's ulcer, precancerous lesion. There should be timely management for burn wound to reduce scar contracture. If there is ulcerative lesion on burn scar but not pathology confirmed with cancerous lesion, consider total excision for any other previous subcutaneous lesion.

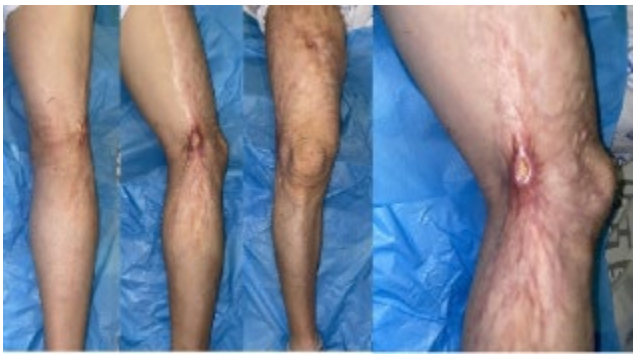

Figure 1.

Figure 2.

Figure 3.

EP-230

원인 불명의 양측성 피하 점액증

(Subcutaneous bilateral mucinosis without unknown cause)

가톨릭대학교
정승원, 최장연*

Purpose: Subcutaneous mucinosis is a disease entity of which accumulation of mucin in the subcutaneous connective tissue is the prominent feature. Subcutaneous mucinosis, in particular, bilaterally occuring mucinosis should be worked up whether there are no systemic disease coexists. We introduce a case of which bilateral subcutaneous mucinosis on both legs without any systemic disease.

Methods: We present a 26-year-old male patient who originally presented with a bulge in the both lower leg area. (Fig1) Which showed 2.2cm & 2.5cm sized non-specific soft tissue mass in CT scan. Punch biopsy was firstly performed and afterwards, excisional biopsy was proven.

Results: Punch biopsy result showed dermal mucinosis. We completely removed the remnant tissue through excisional biopsy. (Fig 2) On the pathologic findings, mucinous granules were found in subcutaneous layer and diffuse interstitial myxoid deposit was the final pathologic result. (Fig 3)

Conclusion: Subcutaneous, bilateral mucinosis can be found with systemic disease. Therefore, clinician should consider performing further work-up. Fortunately, there was no systemic disease found with the patient in this case and treatment could be completed with removal of mass on bilateral legs.

Figure 1. Preoperative findings. A 2.2x2.2cm & 2.5x2.5cm sized, soft, non-tender mass was palpated on the both lower leg area

Figure 2. Gross finding

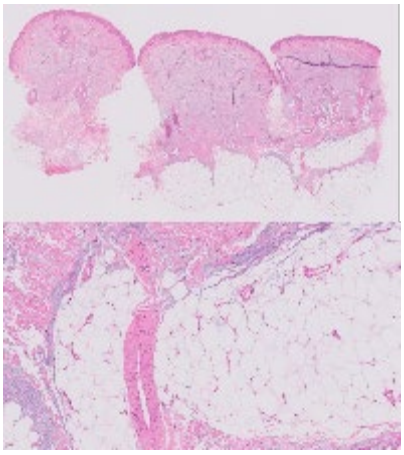

Figure 3. Hematoxylin & eosin staining. Mucinous granules are seen in subcutaneous layer

EP-231

짧은 혈관경의 부분 족지 pulp 유리피판을 이용한 수지 pulp 재건: 증례 보고

(Short-pedicle partial great toe pulp free flap for finger pulp reconstruction: a case series)

순천향대학교

황용선, 김준혁*

Purpose: Pulp defects of the fingers can lead to significant functional impairment and sensory loss, requiring durable and sensate soft-tissue reconstruction. The partial great toe pulp free flap is widely used for reconstruction because it provides glabrous skin with good sensory potential. Conventional techniques typically require proximal dissection of the pedicle to the first plantar metatarsal artery to obtain sufficient pedicle length, which may increase donor-site morbidity. We present a case series of finger pulp reconstruction using a short-pedicle partial great toe pulp free flap.

Methods: Five patients with finger pulp defects underwent reconstruction using a partial great toe pulp free flap between 2006 and 2026. The flap was harvested based on the plantar digital artery of the great toe with minimal proximal dissection. The pedicle was divided at the digital artery level rather than extending proximally to the metatarsal artery. Flap survival, donor-site morbidity, and aesthetic outcomes were evaluated.

Results: All flaps survived completely without vascular complications. The reconstructed finger pulp showed stable soft-tissue coverage with satisfactory contour. Donor-site morbidity was minimal, and the great toe maintained acceptable cosmetic appearance without significant deformity.

Conclusion: The short-pedicle partial great toe pulp free flap is a reliable option for reconstruction of finger pulp defects. This technique reduces donor-site morbidity while providing satisfactory functional and aesthetic outcomes.

Figure1. A patient with traumatic pulp defects of the thumb, second, and third fingers. (A) Preoperative image showing pulp defects. (B) Reconstruction planned using bilateral partial great toe pulp free flaps to cover the pulp defects of the thumb and second fingers. (C) Flap elevation. (D) Harvested short-pedicle partial great toe pulp flap.

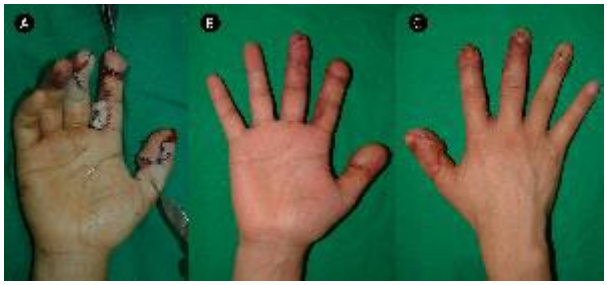

Figure2. Clinical photographs of the same patient shown in Figure 1. (A) Immediate postoperative image. (B, C) Postoperative images at 1 month.

Figure3. A patient with traumatic pulp defects involving the thumb, second, third, and fourth fingers. (A) Preoperative image. (B) Flap design. (C) Flap elevation. (D) Harvest of a short-pedicle partial great toe pulp free flap.

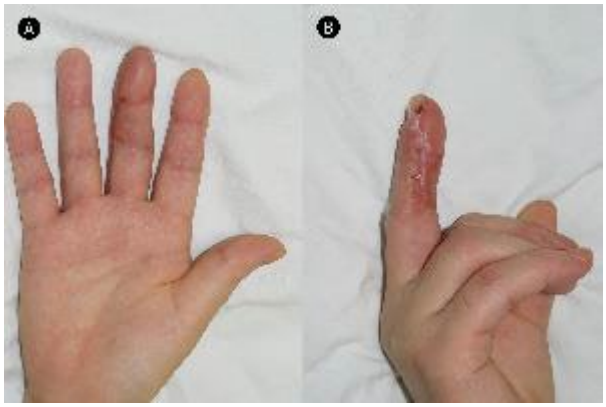

Figure4. Postoperative clinical photograph of a patient with a traumatic pulp defect of the third finger. Image obtained at 1 month after surgery.

EP-232

손가락 신경을 침범한 정맥 기형: 증례 보고

(Venous malformation involving the digital nerve of the hand: A case report)

전남대학교

김동완, 김준성, 김성순, 김승현, 최준호, 황재하, 김광석*

Purpose: Venous malformations are characterized by slow-flow hemodynamics and frequent intralesional thrombosis. Although venous malformations commonly occur in the hand, involvement of a digital nerve is rare. We report a case of venous malformation involving epineurium of a digital nerve of the hand that was successfully treated.

Methods: A 15-year-old man presented with a painless mass involving the left thumb and index finger that had been present since birth (Fig. 1). Magnetic resonance imaging revealed a lobulated vascular malformation (Fig. 2). Surgical exposure was achieved using an H-shaped incision over the thumb and a Bruner incision over the index finger. Intraoperatively, the mass extended from the volar aspect of the proximal phalanx of the thumb to the first web space and the radial aspect of the index finger. Notably, the lesion in the index finger was identified along the radial digital nerve, showing intimate epineurial involvement. The digital nerve and digital artery were carefully preserved through meticulous microsurgical dissection (Fig. 3).

Results: Histopathologic examination revealed irregularly clustered, thickened vessels with a laminated intraluminal thrombus, consistent with venous malformation (Fig. 4). Postoperatively, the patient initially experienced mild numbness on the ulnar side of the thumb and the radial side of the index finger. However, the numbness gradually improved during the 2-month follow-up period. The surgical wounds healed without complications.

Conclusion: In patients with venous malformations of the finger, possible involvement of the digital nerve should be carefully considered during evaluation and surgical planning. Meticulous microsurgical dissection can allow preservation of the nerve and safe excision of the lesion.

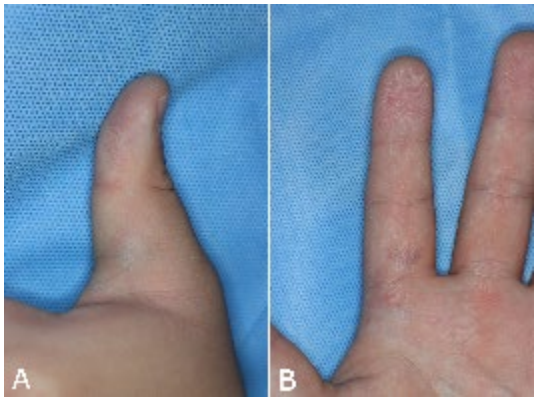

Fig. 1. Clinical photographs of the thumb and index finger. The thumb lesion shows bluish discoloration (A), whereas the index finger lesion demonstrates purple skin discoloration.

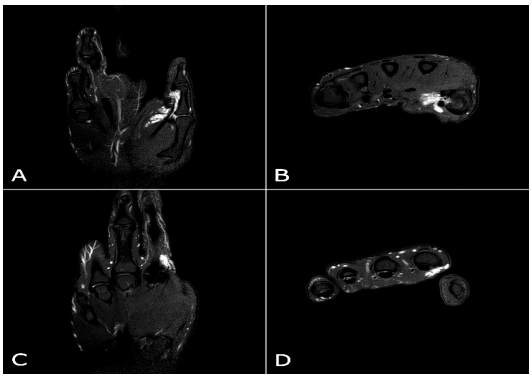

Fig. 2. T2-weighted magnetic resonance images demonstrating a lobulated vascular malformation involving the volar aspect of the proximal phalanx of the thumb (A, B) and the radial side of the index finger (C, D).

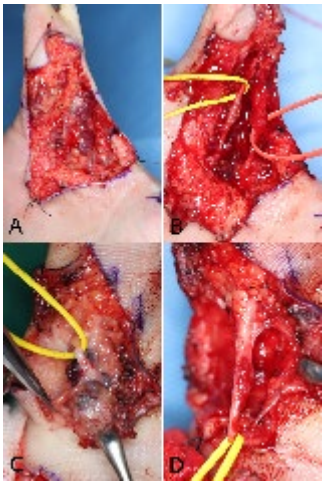

Fig. 3. Intraoperative photographs showing (A) initial exposure of the thumb mass, (B) surgical field after excision of the mass with preservation of the adjacent artery and nerve, (C) intraoperative identification of the mass along the radial digital nerve of the index finger, and (D) radial digital nerve showing intimate epineurial involvement.

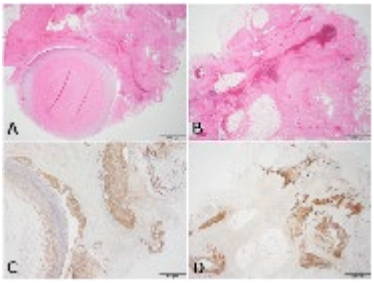

Fig. 4. Histopathologic findings of the lesions showing irregularly clustered, thickened vessels with a laminated intraluminal thrombus, consistent with venous malformation. (A, C) Hematoxylin and eosin staining and immunohistochemical staining for smooth muscle actin of the thumb lesion. (B, D) Hematoxylin and eosin staining and immunohistochemical staining for smooth muscle actin of the index finger lesion.

EP-233

활막 거대세포종으로 오인된 수장부 결핵성 건초염 (수근관 감압술 후 발생): 증례 보고

(Tuberculous Tenosynovitis of the Palm Mimicking Synovial Giant Cell Tumor After Carpal Tunnel Release: A Case Report)

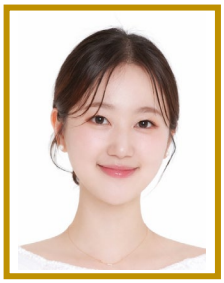

가톨릭대학교 의과대학 성형외과교실

김정현, 이준호, 서보미, 권호, **정성노***

Purpose: Tuberculous infection of the hand is rare and may mimic benign soft tissue tumors, leading to diagnostic delay. We report a case of a tuberculous granulomatous lesion of the palm that was initially suspected to be a synovial giant cell tumor in a patient with persistent neuropathic symptoms following carpal tunnel release.

Methods: A patient with a more than two-year history of numbness and pain in the left hand underwent carpal tunnel release at another institution, but postoperative symptoms persisted. Physical examination revealed a poorly circumscribed palmar mass measuring approximately 4 × 8 cm (Figure 1). MRI demonstrated a diffuse infiltrative lesion along the flexor tendon sheaths extending into the carpal tunnel, raising suspicion of synovial giant cell tumor (Figure 2). Surgical excision and biopsy were performed under general anesthesia with careful preservation of the median nerve and flexor tendons.

Results: Intraoperatively, the lesion was diffusely infiltrative and poorly encapsulated, involving multiple flexor tendon sheaths. Careful dissection was performed to preserve the flexor tendons, median nerve, and digital neurovascular structures during excision (Figure 3A). Gross examination revealed multiple pale gray–yellow soft tissue fragments measuring up to approximately 7.4 × 6.2 × 0.8 cm (Figure 3B). Histopathological examination demonstrated chronic granulomatous inflammation with necrosis. High-power microscopy revealed epithelioid histiocytes and multinucleated giant cells forming granulomatous structures suggestive of tuberculous infection (Figure 4). Acid-fast bacilli staining and polymerase chain reaction tests for Mycobacterium tuberculosis and nontuberculous mycobacteria were negative. Postoperatively, the patient's neuropathic symptoms improved without complications.

Conclusion: Tuberculous tenosynovitis should be considered in the differential diagnosis of diffuse palmar masses, particularly in patients with persistent neuropathic symptoms after carpal tunnel release. Histopathological evaluation plays a crucial role in diagnosis even when microbiological tests are negative.

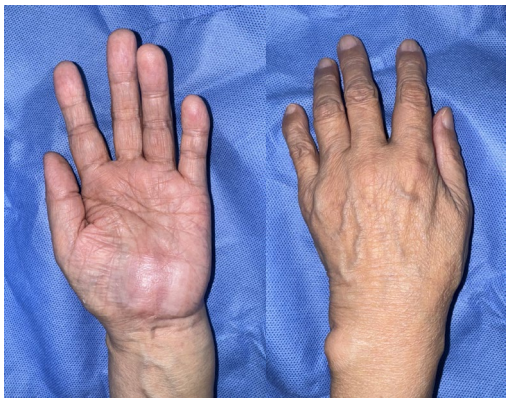

Fig. 1. Preoperative clinical photographs of the left hand. Clinical photographs demonstrate a poorly circumscribed palmar mass associated with swelling of the palm and persistent neuropathic symptoms despite previous carpal tunnel release.

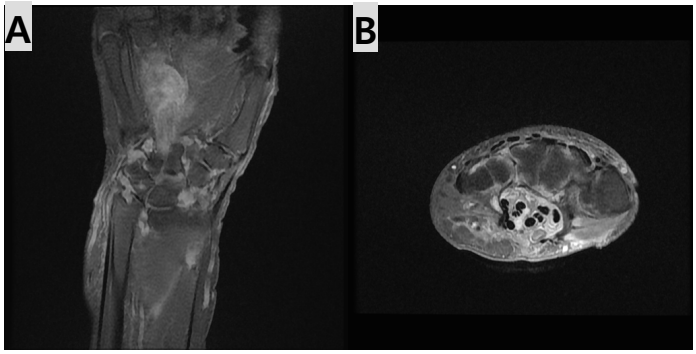

Fig. 2. Preoperative magnetic resonance imaging of the left hand.
(A) Coronal image demonstrating a diffusely infiltrative soft tissue lesion extending along the flexor tendon sheaths from the wrist to the palm and proximal digits. **(B) Axial image** showing encasement of multiple flexor tendons with extension into the carpal tunnel, resulting in crowding of the surrounding neurovascular structures.

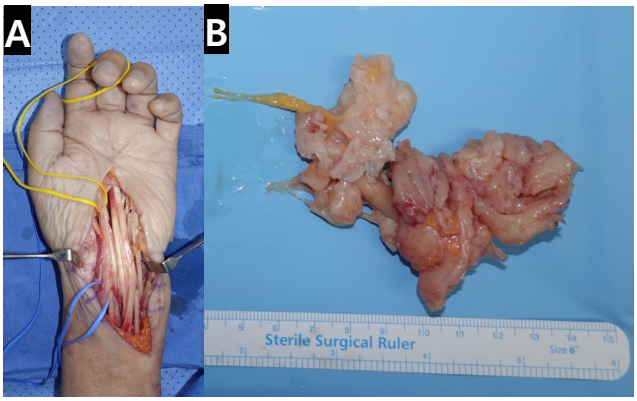

Fig. 3. Intra-operative findings of the palmar lesion.
(A) Intraoperative photograph demonstrating diffuse infiltrative tissue involving the flexor tendon sheaths with preservation of the flexor tendons and median nerve.
(B) Gross photograph of the excised specimen showing multiple irregular pale gray–yellow soft tissue fragments.

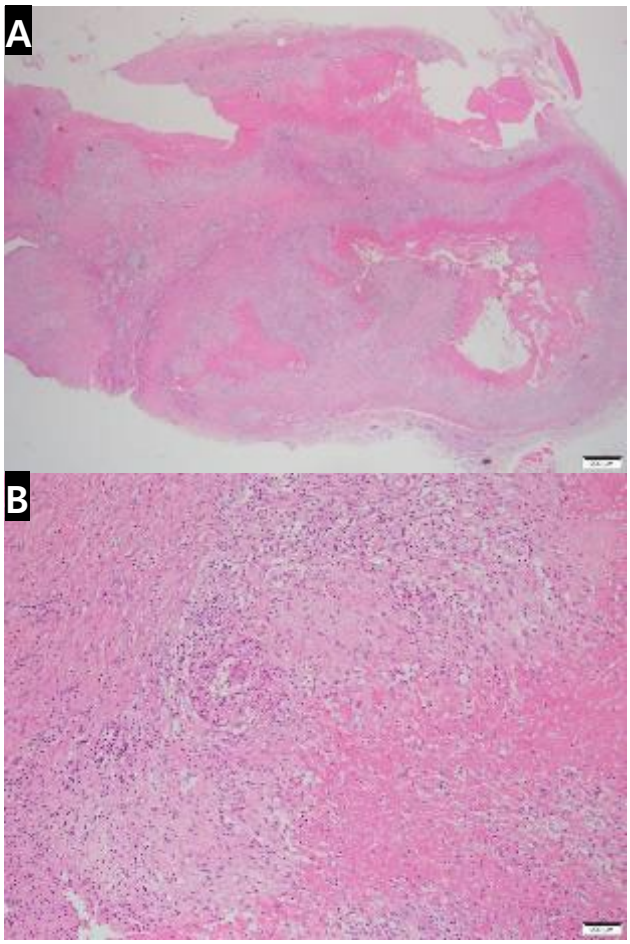

Fig. 4. Histopathological findings of the excised lesion.
(A) Low-power view (H&E stain, ×10) demonstrating extensive granulomatous inflammation with central areas of necrosis involving the soft tissue.
(B) High-power view (H&E stain, ×100) showing epithelioid histiocytes and multinucleated giant cells forming granulomatous structures, consistent with chronic granulomatous inflammation suggestive of mycobacterial infection.

EP-234

무통성 엄지 손톱밑 종괴로 발현한 후천성 손발톱 섬유각화종: 드문 증례 보고

(A Rare Case of Acquired Ungual Fibrokeratoma of the Thumb Presenting as a Painless Subungual Mass)

광명성애병원 성형외과

윤지송, 김진수*, 고성훈, 이동철, 노시영, 이경진

Purpose: Acquired ungual fibrokeratoma (ungual fibroma) is a rare/uncommon benign fibrous tumor of the nail unit, reported predominantly as case reports and small case series. We present a histopathology-confirmed case of thumb acquired ungual fibrokeratoma presenting as a painless subungual/nail-bed mass and describe surgical management and early postoperative outcome.

Methods: A 62-year-old woman presented with a 3-year history of a painless right thumb nail-unit lesion and requested excision for cosmetic reasons. Thumb range of motion was normal. Radiography and CT were obtained to evaluate osseous involvement. Under local anesthesia (Jan 19, 2026), an elliptical incision was designed. After partial nail-plate elevation, a well-demarcated proximolateral subungual/nail-bed mass was carefully dissected from surrounding nail-unit structures and excised en bloc. Hemostasis was achieved with bipolar cautery; the wound was closed with 5-0 nylon and dressed with mild compression. The patient was observed overnight due to long travel distance and discharged the next day.

Results: The mass measured approximately 1.0 × 1.0 cm intraoperatively; gross pathology measured 1.3 × 1.0 × 0.8 cm. Histopathology confirmed ungual fibroma (acquired ungual fibrokeratoma). At progressive nail-bed epithelialization with expected crusting was noted, without obvious purulent discharge. The patient reported no postoperative pain and no functional limitation.

Conclusion: Thumb acquired ungual fibrokeratoma may present as a long-standing, painless subungual/nail-bed mass. Complete excision with histopathological examination provides definitive diagnosis and satisfactory early functional and cosmetic course.

Fig. 1. Preoperative photograph of right thumb demonstrating nail-plate dystrophy.

Fig. 2. Intraoperative photographs. (A) Intraoperative exposure after partial nail-plate elevation demonstrating a well-circumscribed proximolateral subungual/nail-bed mass. (B) After excision showing the nail-bed defect and surgical bed following mass removal.

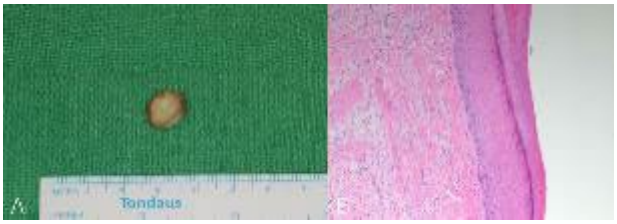

Fig. 3. (A) Intraoperative view of the subungual thumb mass. (B) Histopathology (H&E, ×100) showing hyperkeratosis and fibrocollagenous proliferation, consistent with acquired ungual fibrokeratoma.

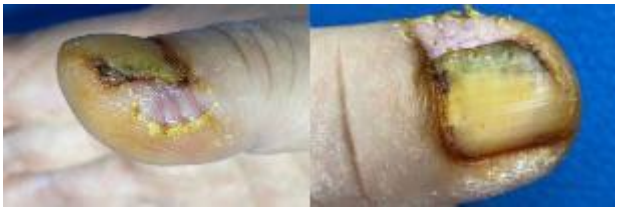

Fig. 4. Postoperative day 17 photographs. No postoperative complications were noted.

EP-235

양측 역행성 볼근 피판과 단측 비순구 피판을 이용한 광범위 하순 재건술

Reconstruction of a near-total lower lip defect using bilateral buccinator musculomucosal flaps combined with a unilateral reverse nasolabial fold flap

순천향대학교부속
천안병원 성형외과
김민욱, 김준혁, 이다운, 변제연, 최환준*

Purpose: Near-total reconstruction of the lower lip is traditionally addressed with microvascular free tissue transfer, such as the radial forearm flap. However, donor-site morbidity and discrepancies in mucosal texture remain important drawbacks. We report a successful alternative using a composite regional flap approach for a large lower lip defect, with favorable functional and aesthetic outcomes.

Methods: A 69-year-old man presented with a lower lip mass initially diagnosed as squamous cell carcinoma after biopsy at an outside institution. Following wide excision at our hospital, a near-total full-thickness lower lip defect was created (Figure 1). Reconstruction was performed using bilateral buccinator musculomucosal flaps for the vermilion and oral lining, combined with a unilateral reverse nasolabial fold flap for external skin coverage (Figure 2). To improve intraoperative precision and flap safety, endoscopy and indocyanine green fluorescence angiography were used for real-time assessment of internal alignment and perfusion (Figure 3).

Results: Final histopathology confirmed verrucous carcinoma. The reconstructed lower lip showed excellent viability without marginal necrosis or venous congestion. Intraoperative fluorescence angiography provided objective evidence of adequate retrograde flow in the transposed flap. The patient achieved satisfactory oral competence, speech, and mouth opening, with preserved lower lip contour and good color and texture match at follow-up (Figure 4).

Conclusion: Near-total lower lip reconstruction using bilateral buccinator musculomucosal flaps combined with a unilateral reverse nasolabial fold flap is an effective alternative to free flaps. Advanced intraoperative monitoring may further enhance the safety and functional outcome of this regional composite reconstruction.

Figure 1. Preoperative and intraoperative photographs showing the lower lip lesion (A), the design for wide excision (B), and the near-total full-thickness defect after tumor resection (C).

Figure 2. Intraoperative photographs showing elevation of the bilateral buccinator musculomucosal flaps (A), elevation of the unilateral reverse nasolabial fold flap (B), transposition of the flap through a tunnel for outer lower-lip coverage (C), and the immediate postoperative appearance after flap inset and closure (D).

EP-235

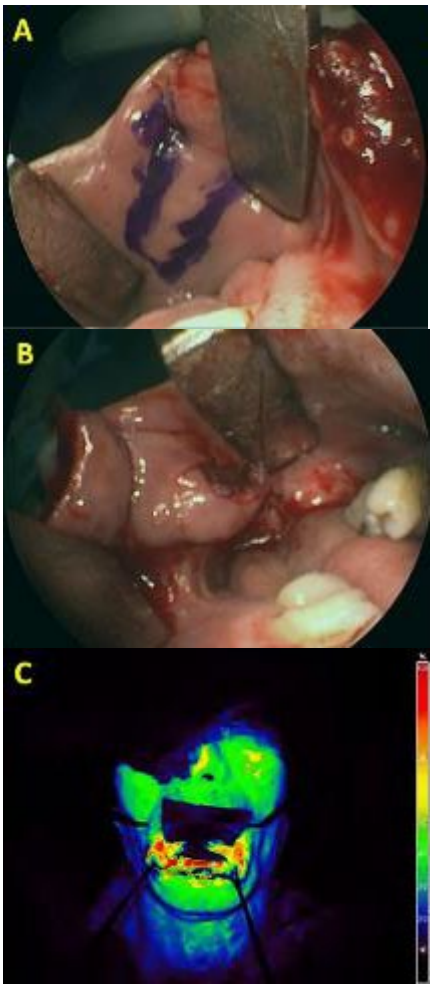

Figure 3. Intraoperative endoscopic and fluorescence images showing the design of the buccal mucosal flap (A), inset of the flap for restoration of the intraoral lining (B), and Fluobeam confirmation of flap perfusion and viability after transposition (C).

Figure 4. Postoperative follow-up photographs showing preserved lip contour at rest (A) and adequate mouth opening with maintained oral function (B).

EP-236

괴사성 근막염 후 유경 측상완 피판을 이용한 주관절 결손부 재건

(Reconstruction of an elbow defect after necrotizing fasciitis using a pedicled lateral arm flap)

가톨릭대학교 성형외과학교실

서희성, 최종윤*

Purpose: Necrotizing fasciitis of the upper extremity often requires extensive debridement, resulting in complex elbow defects that demand reliable soft tissue coverage. This case report describes the successful use of a pedicled lateral arm flap for reconstruction of an elbow defect after infection control in necrotizing fasciitis secondary to a rose thorn injury in a florist, highlighting its usefulness as a reconstructive option in this setting.

Methods: A 53-year-old female florist developed necrotizing fasciitis of the elbow after being pricked by a rose thorn and undergoing initial observation. Emergency fasciotomy was performed, followed by one week of intensive intravenous antibiotic therapy and continuous wound irrigation until infection was controlled. (Figure 1.) After stabilization, soft tissue coverage of a 10 × 5 cm defect around the elbow was performed with a pedicled lateral arm flap. (Figure 2. & 3.)

Results: The pedicled lateral arm flap provided stable coverage of the exposed structures with good flap perfusion and no evidence of partial or total flap loss. Wound healing progressed without major complications, and elbow joint motion was preserved sufficiently to allow the patient to return to her flower arrangement work. No recurrence of infection or significant donor site morbidity was observed during follow-up. (Figure 4.)

Conclusion: This case suggests that a pedicled lateral arm flap is a reliable option for elbow reconstruction after necrotizing fasciitis, providing durable soft tissue coverage and acceptable functional outcomes once infection has been adequately controlled.

Fig 1. Initial clinical photograph showing necrotizing fasciitis of the elbow after a rose thorn injury.

Fig 2. & 3. Intraoperative photographs showing a 10 x 5 cm defect around the elbow after infection control and debridement, followed by reconstruction using a pedicled lateral arm flap.

Fig 4. Postoperative follow-up photograph demonstrating stable flap coverage and satisfactory wound healing

EP-237

고위험군 고령 환자의 광범위 수배부 결손에 대한 서혜부 피판 및 부분층 피부 이식을 이용한 단계적 재건술: 증례 보고

(A Staged Approach Using a Combined Groin Flap and Split-Thickness Skin Graft for a Massive Dorsal Hand Defect in a High-Risk Elderly Patient : A Case Report)

경상국립대학교

김지승, 김태호, 김민형, 신재봉, 김남균*, 이경석, 김준식

Purpose: Extravasation is a serious clinical complication that can lead to irreversible skin defects. In areas with minimal soft tissue, such as the hand dorsum, extensive necrosis frequently results in tendon exposure, necessitating robust coverage. While skin grafting is a conventional option, it often fails in patients with impaired peripheral circulation. This report presents the successful reconstruction of a massive dorsal hand defect in an 82-year-old patient with multiple cardiovascular comorbidities using a staged groin flap combined with a split-thickness skin graft (STSG).

Methods: To ensure adequate blood supply for a 13X 8cm doxorubicin-induced defect in a high-risk patient with a history of DVT and PTE, a three-stage hybrid reconstruction was performed(Fig. 1) . In Stage 1, a groin flap was transferred to the central defect, while peripheral margins were left as raw surfaces with wet dressings to prevent excessive tension(Fig. 2). In Stage 2, an STSG was applied to these peripheral margins once the wound bed stabilized(Fig. 3). Finally, in Stage 3, pedicle division and definitive wound remodeling were completed(Fig. 4). This staged approach ensured total coverage while minimizing tension-related ischemia.

Results: A five-month follow-up revealed complete engraftment without any complications. This strategy effectively reconstructed a defect larger than what a standard groin flap could safely cover, despite the patient's significant surgical risks.

Conclusion: For elderly patients with extensive hand defects and compromised circulation, combining a groin flap with an STSG provides a reliable reconstructive solution. This method enhances flap survival by effectively relieving tension through supplemental grafting.

Fig. 1. Preoperative view of a 13X 8cm extensive soft tissue defect on the dorsal hand and wrist, resulting from doxorubicin-induced extravasation injury.

Fig. 2. Insetting of a pedicled groin flap to the central portion of the defect. Note the peripheral margins left as raw surfaces with wet dressings to minimize tension and preserve flap perfusion.

Fig. 3. Application of a Split-Thickness Skin Graft (STSG) to the stabilized peripheral wound beds surrounding the pedicled groin flap

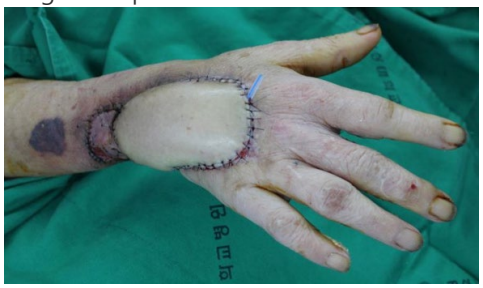

Fig. 4. Definitive view following pedicle division and final wound remodeling, showing successful coverage of the initial defect.

EP-238

광범위 복합 결손을 동반한 중증 수지 압착 손상의 수지 재건술: 역행성 지방근막 피판술과 관절유합술을 이용한 길이 보존 재건

(Digit Salvage in Severe Crush Injury with Extensive Composite Defects: Length-Preserving Reconstruction Using a Reverse Adipofascial Flap and Arthrodesis)

동국대학교 경주병원
성형외과학 교실

안유진, 이준호*

Purpose: To report a successful length-preserving reconstruction using bone shortening arthrodesis and a reverse adipofascial flap in a severely crushed digit initially recommended for terminal amputation.

Methods: A 42-year-old male presented with a severe crush injury to the left hand from a woodworking machine. The ring finger sustained a severely comminuted fracture, an extensive composite tissue defect, and 75% destruction of the distal interphalangeal (DIP) joint. Despite indications for stump revision, length-preserving surgery was performed at the patient's strong request. Following debridement, bone shortening and DIP joint arthrodesis were performed using K-wire fixation. To reconstruct the remaining 2-cm composite defect over exposed bone lacking viable periosteum, a reverse adipofascial flap, pedicled on a digital proper artery perforator near the proximal interphalangeal (PIP) joint, was elevated and combined with a full-thickness skin graft (FTSG).

Results: At the 1-year follow-up, the reverse adipofascial flap and FTSG had survived completely without any marginal necrosis or infection. Radiographs confirmed stable bone union at the arthrodesis site. The severely crushed digit was successfully salvaged, fulfilling the patient's demand for functional length preservation without requiring secondary amputation

Conclusion: Bone shortening arthrodesis paired with a reverse adipofascial flap is a reliable salvage option for complex digital defects, providing stable coverage while maximizing length preservation.

Fig. 1. Preoperative findings. (A) Severe crush injury with a composite tissue defect on the left ring finger. (B) Radiograph showing comminuted phalangeal fractures and extensive DIP joint destruction.

Fig. 2. Defect evaluation and surgical design. (A) A 2-cm composite defect with exposed bone following debridement. (B) Marking of the reverse adipofascial flap with a 1-cm pedicle base near the PIP joint to incorporate the digital artery perforator.

Figure 3. Surgical procedure. (A) Flap elevation and K-wire fixation for bone shortening and DIP arthrodesis. (B) Reverse flap coverage and FTSG application from the groin.

Fig. 4. Postoperative outcomes at 1 year. (A) Complete flap and graft survival with preserved functional digital length. (B) Radiograph confirming stable bone union at the arthrodesis site.

EP-239

골수염을 동반한 폐외 결핵에서 광배근 근피판을 이용한 흉벽 재건

(Chest Wall Reconstruction Using a Latissimus Dorsi Musculocutaneous Flap in Extrapulmonary Tuberculosis with Osteomyelitis)

강동성심병원 성형외과

정지원, 김결희*, 정철훈, 장용준, 황나현

Purpose: Extrapulmonary tuberculosis of the chest wall can cause progressive soft tissue necrosis and rib osteomyelitis, leading to complex defects that are difficult to manage with conservative treatment. Radical debridement and well-vascularized soft tissue coverage are essential for infection control and durable reconstruction.

Methods: A patient was referred after excision of an enlarging left chest wall mass. Despite prior antibiotic therapy, and negative pressure wound therapy, the wound deteriorated with persistent drainage and exposure of the sternum and anterior ribs (Figure 1). Tissue biopsy confirmed extrapulmonary tuberculosis, and antituberculous medication was initiated. Repeated debridement was performed; however, the defect progressed with osteomyelitis of both third anterior ribs and the left fourth anterior rib (Figure 2). Radical debridement including resection of a 6-cm segment of the left third rib encompassing the osteomyelitic portion was performed. The pleura was not exposed, and skeletal reconstruction with plate or mesh was not required due to the limited extent of rib resection. The defect was reconstructed using a 6 × 12 cm latissimus dorsi musculocutaneous flap (Figure 3).

Results: The flap survived without vascular compromise. No recurrent infection, wound breakdown, or evidence of postoperative flail chest was observed. The patient was discharged two weeks after surgery. At the 6-month follow-up, the reconstructed chest wall remained stable, with no wound-related complications except for minor inferior scarring (Figure 4).

Conclusion: In chest wall tuberculosis complicated by osteomyelitis, infection control requires radical debridement, and durable reconstruction depends on vascularized muscle flap coverage rather than prolonged wound care alone.

Fig 1. Initial clinical photograph of the patient referred from the Department of Cardiothoracic Surgery, demonstrating chest wall necrosis

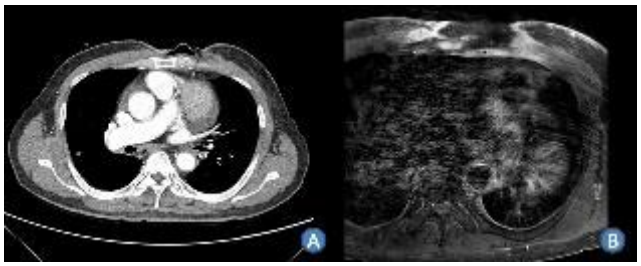

Fig 2. Intraoperative views showing V-Y advancement flap and fixation of autologous iliac bone graft to the anterior nasal spine and alar base

Fig 3. Six-month follow-up photographs demonstrating improved nasal contour, alar base, and restored structural support

Fig 4. 6-month follow up photograph demonstrating stable wound healing without recurrence of infection

EP-240

봉와직염으로 발현한 손목의 원발성 연부조직 결핵: 증례 보고

(Primary Soft-Tissue Tuberculosis of the Wrist Presenting as Cellulitis: A Case Report)

순천향대학교부속
천안병원 성형외과
김민욱, 김준혁, 이다운, 변제연, 최환준*

Purpose: Chronic cellulitis-like lesions of the wrist and hand may represent atypical infections. We present a case of soft-tissue tuberculosis involving the hand and forearm, confirmed by tissue-based testing.

Methods: A 70-year-old patient developed progressive swelling, erythema, and pain over the dorsal wrist and hand beginning in August 2024 (Figure 1), with poor response to repeated antibiotics. On January 23, 2025, excisional biopsy and debridement were performed under general anesthesia. Specimens from the hand and forearm underwent histopathologic examination, acid-fast bacilli (AFB), Grocott methenamine silver (GMS), and periodic acid-Schiff (PAS) staining, and real-time polymerase chain reaction (PCR) for Mycobacterium tuberculosis (MTB) and nontuberculous mycobacteria (NTM). Systemic evaluation included contrast-enhanced chest CT and sputum AFB studies.

Results: Exploration revealed diffuse inflammatory and granulomatous tissue in the deep soft tissues of the dorsal wrist and hand, extending into the forearm, without a drainable abscess (Figures 2–3). Histopathology showed chronic non-caseating granulomatous inflammation suspicious for tuberculosis; AFB, GMS, and PAS stains were negative. PCR was positive for MTB and negative for NTM. Chest CT showed pulmonary nodules and lymphadenopathy interpreted as inflammatory or nonspecific, and sputum AFB smears and cultures were negative. Anti-tuberculous therapy was started after surgery. The wound healed uneventfully, with no recurrence at 8 months of follow-up (Figure 4).

Conclusion: Soft-tissue tuberculosis of the wrist and hand may mimic chronic cellulitis, and negative AFB staining or sputum studies do not exclude the diagnosis. In persistent cases, early deep-tissue biopsy with MTB/NTM PCR should be considered to avoid diagnostic delay and progressive soft-tissue damage.

Figure 1. Preoperative photograph showing diffuse swelling and erythema over the dorsal wrist and hand.

Figure 2. Intraoperative photograph demonstrating inflammatory and granulomatous soft-tissue involvement of the dorsal wrist and hand..

Figure 3. Intraoperative photograph showing proximal extension of the inflammatory lesion into the forearm with excised tissue submitted for biopsy.

Figure 4. Postoperative photograph at 8 months showing complete wound healing without recurrence.

EP-241

노출된 지골 골결손에서 인공진피를 이용한 피복

(Artificial Dermis Coverage of Exposed Phalangeal Bone Defects)

광명성애병원 성형외과

윤지송, 이경진*, 김진수, 고성훈, 이동철, 노시영

Purpose: Traumatic phalangeal bone defects with soft-tissue loss often necessitate complex reconstruction including bone grafting. We present a case series in which artificial dermis (MegaDerm®) was applied over exposed phalangeal bone defects to report our observation of secondary bone remodeling.

Methods: Four male patients (age range, 16–64 years) treated between 2021 and 2025 were retrospectively reviewed. Injury mechanisms included industrial saw, crush, sports-related, and cutting-machine injuries involving the thumb to the ring finger at the proximal phalanx, middle phalanx, and proximal interphalangeal (PIP) joint levels. Following thorough debridement and indicated repairs—open reduction and internal fixation, extensor or extensor pollicis longus tenorrhaphy, and volar plate and collateral ligament repair as needed—MegaDerm was tailored to defect size, placed over the exposed bone or joint capsule, and secured with absorbable sutures. Serial radiographs were obtained preoperatively and during follow-up (mean, 8.1 months; range, 2.8–17.7 months).

Results: All four cases demonstrated progressive defect fill-in and improved cortical contour on follow-up radiographs. No radiographic evidence of osteomyelitis was observed. Stable soft-tissue coverage was achieved without additional bone grafting.

Conclusion: Artificial dermis coverage of exposed phalangeal bone defects was associated with secondary radiographic bone remodeling in all cases. The material may serve as a biological barrier limiting soft-tissue interposition and supporting organized hematoma formation, thereby creating a favorable environment for bone regeneration. Prospective comparative studies are warranted to clarify the mechanism and define optimal indications.

Fig. 1. Case 1 (64-year-old man). Preoperative radiograph (A, Nov 8, 2025) shows middle-phalangeal bone defects of the left 3rd and 4th fingers. Follow-up radiograph (B, Feb 2, 2026) shows interval defect fill-in and improved cortical continuity after MegaDerm coverage.

EP-242

조갑 섬유각화종으로 인한 손톱판 종축 고랑 및 변형

Longitudinal Grooving and Nail Plate Deformity Induced by an Ungual Fibrokeratoma

가톨릭대학교 의과대학 성형외과교실

진기환, 서보미, 권호, 정성노, 이준호*

Purpose: Acquired ungual fibrokeratoma (AUFK) is an uncommon benign fibrous tumor of the nail unit that may induce nail deformities and clinically mimic malignant lesions. Nail unit tumors presenting with longitudinal grooving and nail plate deformity pose diagnostic challenges. This study reports a case of AUFK causing nail plate deformity and highlights the importance of histologic confirmation and surgical management

Methods: A 70-year-old woman presented with nail plate deformity of the right third finger characterized by longitudinal grooving and a solitary subungual mass. Under local anesthesia, the nail plate was removed to expose the lesion, and complete surgical excision of the subcutaneous mass was performed with preservation of the surrounding nail structures. The nail bed defect was covered with an acellular dermal matrix, and the excised specimen was submitted for histopathologic evaluation.

Results: Histopathologic examination confirmed acquired ungual fibrokeratoma. The postoperative course was uneventful, with no complications such as infection, wound dehiscence, or nail dystrophy. At follow-up, resolution of longitudinal grooving and restoration of normal nail plate contour were observed, with satisfactory functional and cosmetic outcomes. Although full evaluation of the nail plate typically requires at least 6 months, the current follow-up period of 2 months is relatively short; however, nail growth appears intact, and the patient remains under close follow-up for further assessment.

Conclusion: Ungual fibrokeratoma should be considered in patients presenting with nail plate deformity and longitudinal grooving. Complete surgical excision with histologic confirmation not only establishes a definitive diagnosis but also restores nail morphology and function.

Fig. 1. Initial clinical photograph. Preoperative photograph of the right hand showing nail plate deformity of the third finger associated with longitudinal grooving caused by a subungual lesion.

Fig. 2. Intraoperative view of the lesion. After removal of the nail plate, a subungual mass located beneath the nail plate was exposed. The lesion was carefully dissected from the nail bed and excised using surgical instruments while preserving the surrounding nail structures.

Fig. 3. Excised specimen obtained after surgical removal of the nail unit lesion from the right third finger. The keratinized mass is shown alongside a surgical ruler for size reference.

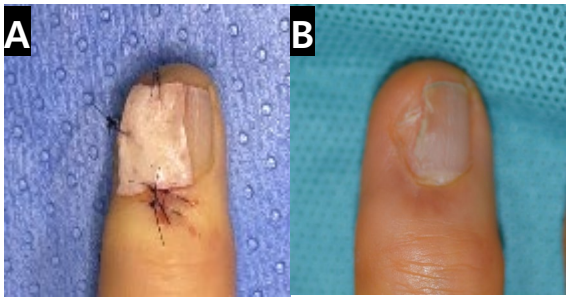

Fig. 4. (A) Postoperative view after excision of the nail unit lesion. The nail bed defect was covered with an acellular dermal matrix (ADM) to facilitate healing. (B) At postoperative month 2 (POD 2 months), the wound demonstrated satisfactory healing without complications.

EP-243

다발성 기저 질환을 동반한 초고령 환자의 상완 육종 절제술 후 전층 피부 이식(FTSG) 재건: 보조 방사선 치료 환경에서의 성공적 생존 사례

(Full-Thickness Skin Graft Reconstruction After Upper Arm Sarcoma Resection in a Multimorbid Super-Elderly Patient: Successful Graft Survival Following Adjuvant Radiotherapy)

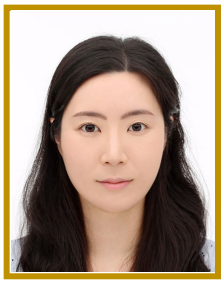

경상국립대학교

김지승, 김태호, 김민형, 신재봉, 김남균, 김준식, 이경석*

Purpose: Defects following wide excision of soft-tissue pleomorphic sarcoma around a joint are typically reconstructed using local or free flaps. However, in the joint area, there is often insufficient skin tissue to perform a local flap. Additionally, considering the patient's age and comorbidities, a free flap may pose a significant burden. This case demonstrates that a full-thickness skin graft (FTSG) can serve as an effective, low-burden alternative, providing reliable coverage and helping to preserve joint mobility even after adjuvant radiotherapy.

Methods: An 89-year-old man presented with a progressively enlarging mass in the right upper arm and underwent wide excision, including the muscle fascia (Fig. 1). A full-thickness skin graft (FTSG), harvested from the right inguinal region, was applied to the defect and secured with simple nylon sutures, followed by a tie-over dressing (Fig. 2).

Results: A One month after surgery, the graft remained stable without complications. As the sarcoma was close to the resection margin, adjuvant radiotherapy was recommended. Starting three months postoperatively, the patient received adjuvant radiotherapy to the right upper arm, including the surgical bed. At seven months postoperatively (three months after completion of radiotherapy), the graft demonstrated stable integration without complications. The range of motion of the elbow was preserved. MRI of the right upper arm showed no evidence of local recurrence. (Fig.3)

Conclusion: Although flap reconstruction is preferred for extremity defects, particularly when adjuvant radiotherapy is anticipated, if there are concerns regarding surgical burden, FTSG, which is simpler and quicker, may provide comparable functional and aesthetic outcomes in the upper arm.

Fig. 1. Photograph of 8-cm mass in upper arm

Fig. 2. Photograph of performed FTSG

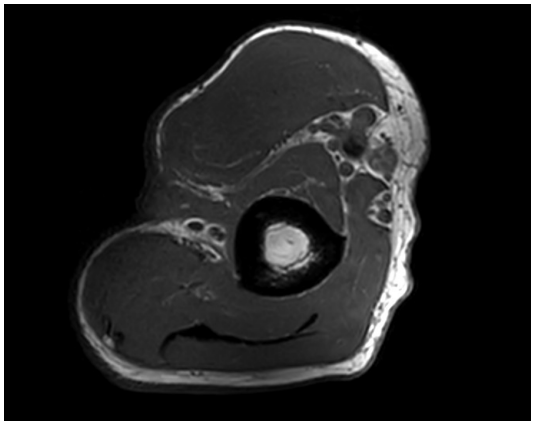

Fig. 3. MRI after 7 months after FTSG

EP-244

견갑골 종괴에 의해 발생한 익상견갑: 수술적 절제를 통한 기능 회복 증례

Winged scapula caused by a scapular mass: Restoration of function through surgical excision

가톨릭대학교
신은채, 최종윤*

Purpose: Winged scapula is typically caused by neuromuscular conditions, particularly long thoracic nerve palsy. However, cases resulting from localized scapular mass effects are exceedingly rare and often misdiagnosed. This case report presents a 38-year-old athletic male with winged scapula secondary to a scapular mass and demonstrates the effectiveness of surgical excision in restoring normal scapulothoracic motion.

Methods: A 38-year-old male engaged in regular high-intensity exercise presented with progressive scapular prominence and discomfort during shoulder motion. (Figure 1.) Clinical evaluation revealed scapular winging without neurological deficit. Imaging studies identified a mass lesion on the ventral surface of the scapula exerting mechanical pressure on scapulothoracic movement. Surgical excision was performed via a posterior approach, preserving adjacent musculature and neurovascular structures.

Figure 1. Preoperative posterior view of the patient showing prominent medial border winging of the right scapula.

Results: The scapular mass was successfully excised without intraoperative complications. (Figure 2.) Postoperatively, scapular winging was markedly corrected, with near-normal scapulothoracic motion restored. The patient resumed full physical activity without limitation and reported high satisfaction with both functional and cosmetic outcomes at 6 months follow-up. (Figure 3.)

Conclusion: This case presents that scapular winging may occur from purely mechanical causes such as localized mass effect. Surgical excision can effectively correct the deformity and restore function in appropriately selected patients. Thorough evaluation of atypical winged scapula is crucial to identify surgically correctable etiologies beyond nerve palsy.

Figure 2. Gross appearance of the completely excised mass measuring 3.5cm.

Figure 3. Postoperative clinical outcomes at 6 months. Significant resolution of scapular winging and restoration of smooth, full range of scapulothoracic motion

EP-245

사지 및 체간에 발생한 다발성 혈관지방종의 임상적 분석: 3례의 증례 보고

(Clinical Analysis of Multiple Angiolipomas in the Extremities and Trunk: A Case Series of Three Patients)

노원을지대학교 성형외과

김건휘, 민경희*

Purpose: Angiolipomas are a rare variant of lipomas comprising mature adipocytes and proliferating vessels. While they typically present as solitary, painful nodules, multiple or painless presentations can occur. We report a rare clinical series of three patients presenting with multiple angiolipomas predominantly involving the upper extremities and trunk.

Methods: A retrospective review was conducted on three male patients (ages 43, 48, and 63) presenting with multiple subcutaneous masses on their upper extremities, flanks, and anterior chest. Symptom duration ranged from 1 to 5 years. Two patients had a history of prior excisions at other clinics. Surgical excision was performed for lesions that were either clinically symptomatic or posed cosmetic concerns. A total of 13, 9, and 13 masses were completely removed from the three patients, respectively.

Results: All excised masses were well-encapsulated, soft, and yellowish, ranging from 1 cm to 4 cm in size. Histopathological examinations of the specimens uniformly confirmed the diagnosis of angiolipoma. The clinical presentation showed notable variation among the cases. While some lesions were completely painless, others exhibited distinct pressure-induced tenderness. Postoperative recovery was uneventful for all patients.

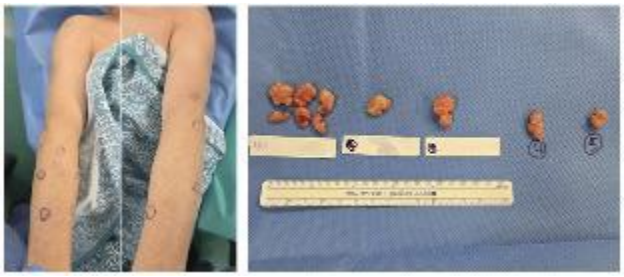

Fig.1 Case 1.

Fig.2 Case 2.

Fig.3 Case 3.

Conclusion: Multiple angiolipomas should be strongly considered in the differential diagnosis of multiple subcutaneous masses, even without the classic symptom of pain. Complete surgical excision remains the definitive treatment of choice. This approach provides symptomatic relief, prevents local recurrence, and allows for accurate histopathological confirmation to rule out malignancies.

EP-246

반려 단안코브라에 의한 독상 후 발생한 전완부 중증 연부조직 괴사를 변연절제술과 부분층 피부이식으로 치료한 증례

한림대학교성심병원

심승용*, 김재현, 정찬민

Purpose: Monocled cobra envenomation can cause severe cytotoxic injury leading to progressive soft tissue necrosis. With the increasing ownership of exotic reptiles, snakebite injuries from pet venomous snakes are emerging as a clinical concern. This report presents a case of severe forearm necrosis caused by a pet monocled cobra and its surgical management.

Methods: A 17-year-old male presented with a 1.7 × 0.5 × 3 cm necrotic wound on the left forearm following monocled cobra envenomation, for which antivenom had been administered. A central eschar with surrounding soft tissue necrosis was noted (Figure 1). MRI demonstrated intramuscular involvement with a localized necrotic cavity (Figure 2). Extensive debridement under general anesthesia revealed subcutaneous fat necrosis with partial muscle involvement extending beyond clinically visible margins (Figure 3). After removal of all nonviable tissue, incision and drainage were performed, followed by split-thickness skin grafting (STSG) for definitive coverage.

Results: Complete removal of necrotic tissue was achieved, and the defect was reconstructed with STSG. The graft showed satisfactory take without recurrent infection. During follow-up through July 11, 2025, the wound healed progressively with preserved forearm contour and no major complications (Figure 4)

Conclusion: Monocled cobra envenomation may cause deep tissue and muscle necrosis requiring aggressive surgical management. Early debridement and appropriate reconstruction can result in favorable outcomes, highlighting the need for vigilance in injuries related to exotic pet ownership.

Fig 1. Preoperative gross photography

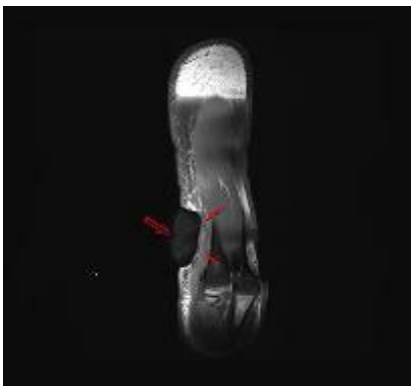

Fig 2. Preoperative Magnetic Resonance Imaging (MRI)

Fig 3. Intraoperative gross photography

Fig 4. Post operative gross photography

EP-247

하악골에 발생한 골막주위 지방종: 수술적 시사점을 고찰한 증례 보고

(Parosteal Lipoma of the Mandible: A Case Report Highlighting Surgical Implications)

대전을지대학교병원

김지민[1], 정성균[1], 황영중*

Purpose: Parosteal lipoma is a rare benign neoplasm arising from the periosteum, accounting for only 0.3% of all lipomas. Mandibular involvement is exceptionally rare, with fewer than 20 reported cases. Its clinical fixity often mimics malignancy, posing a diagnostic challenge. We report a rare case of a mandibular parosteal lipoma and discuss its surgical implications.

Methods: A 75-year-old male presented with a 1-year history of a painless, fixed mass on the left chin (Fig. 1). Physical examination revealed a firm, immobile mass measuring 3.0 cm on the buccal mandible. Computed tomography (CT) showed a well-demarcated, homogeneous, low-density mass originating from the cortex. Notably, there was no evidence of internal ossification or bony erosion (Fig. 2).visibility, surgical convenience, and operative time.

Results: The tumor was excised via an extraoral submandibular approach. Intraoperatively, the mass was firmly adherent to the periosteum, lacking a capsule at the bone-tumor interface (Fig 3). Meticulous subperiosteal dissection was performed for en bloc removal. The specimen was a yellowish, lobulated mass, and histopathology confirmed a mature simple lipoma without atypia (Fig 4). The patient remained recurrence-free at 6 months.

Conclusion: Mandibular parosteal lipoma is an extremely rare entity. This case is clinically significant as it presented asymptomatically without intrinsic ossification. CT imaging is crucial for accurate preoperative planning. Complete subperiosteal excision via an external approach is the treatment of choice to ensure removal of the periosteal attachment and minimize the risk of recurrence.

Fig 1. Preoperative clinical photograph of the 75-year-old male, showing a visible, firm swelling in the left mandible/chin region (red arrow).

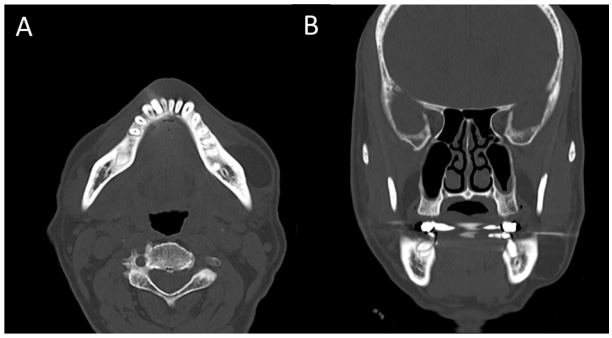

Fig 2. Preoperative computed tomography (CT) scans. (A) Axial view shows a well-demarcated, fat-density mass abutting the buccal cortex. (B) Coronal view confirms the parosteal location of the lesion, showing close contact with the underlying bone without cortical invasion or internal ossification.

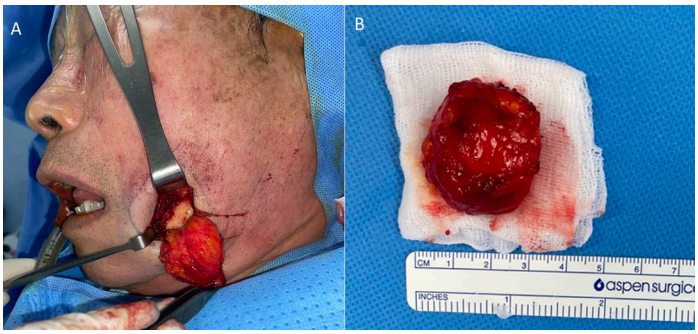

Fig 3. (A)Intraoperative photograph showing the dissection of the encapsulated, yellowish lipomatous mass from its firm attachment to the mandibular periosteum through the skin incision.(B)The en bloc resected gross specimen, measuring approximately 3.5 x 3.0 cm, showing its lobulated, encapsulated, and yellowish appearance consistent with a lipoma.

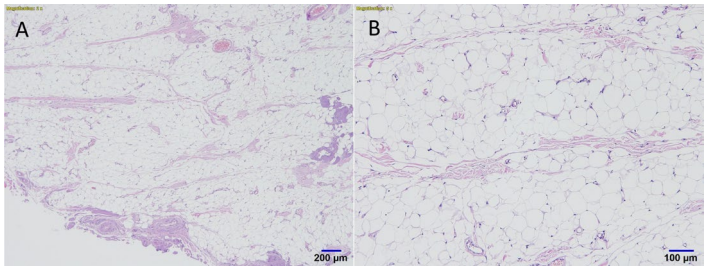

Fig 4. Histopathological examination. (A) Low-power view showing mature adipocytes arranged in lobules (H&E, ×40). (B) High-power view confirming uniform adipocytes with clear cytoplasm and eccentric nuclei, with no evidence of atypia or malignancy (H&E, ×100).

EP-248

유방보존수술 후 무세포동종진피를 이용한 유방종양성형술의 유용성

(Usefulness of ADM Assisted Oncoplastic Breast Reconstruction Following Breast Conserving Surgery)

경북대학교 의과대학
성형외과학교실

김석기, 장용준, 조현근, 류정엽, 이준석, 서만수, 최강영, 정호윤, 양정덕*

Purpose: After breast-conserving surgery (BCS), localized defects can be challenging to reconstruct with volume displacement techniques alone. Acellular dermal matrix (ADM) has been proposed as an oncoplastic material to supplement volume and reduce contour deformity. This study evaluated the safety and clinical usefulness of ADM assisted oncoplastic breast reconstruction following BCS.

Methods: Between October 2020 and September 2023, 43 patients who underwent partial mastectomy followed by volume displacement with ADM assistance were retrospectively analyzed. The number of ADM sheets (1-2), insertion techniques (sheet/stacked/rolling), and placement planes (below the skin flap/below glandular tissue/within the defect) were tailored to defect characteristics (Fig. 1). Patients were assessed preoperatively and at 1, 3, 6, and 12 months post-operatively (Fig. 2 & 3). Breast shape and symmetry were evaluated clinically, complications were recorded, and structural integrity of the ADM were evaluated radiologically.

Results: Mean age was 49.3 years, and median follow-up was 32 months. ADM insertion techniques included sheet (n=32), stacked (n=2), and rolling (n=9). Planes were below the skin flap (n=21), below glandular tissue (n=13), and within the defect (n=9), with mean ADM size of 31.2 cm^2. Within 1 year, five patients (11.6%) experienced eight complications, including seroma, hematoma, wound-related complica-tions, and red breast syndrome. No major complications, such as flap loss or fat necrosis, were observed. Radiotherapy was administered postoperatively by standard oncologic protocols.

Conclusion: ADM-assisted breast reconstruction after BCS provides effective volume supplementation and contour preservation with a relatively simple techn-ique. This approach demonstrated low complication rates and stable outcomes, even in patients receiving postoperative radiotherapy.

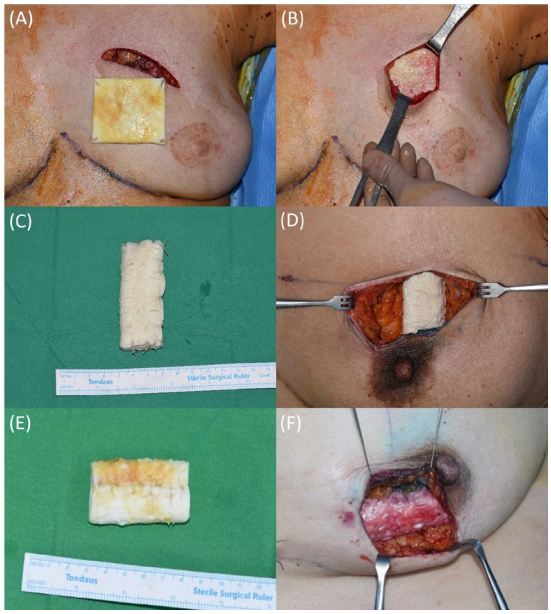

Fig. 1. (A), (B) Intraoperative images. ADM (Megaderm 5x6cm, 3-5mm) insertion using sheet method within the defect. (C), (D) ADM (Megaderm 6x12cm, 3-5mm) insertion using stacked method within the defect. (E), (F) ADM (Megaderm 5x6cm, 3-5mm) insertion using rolling method within the defect.

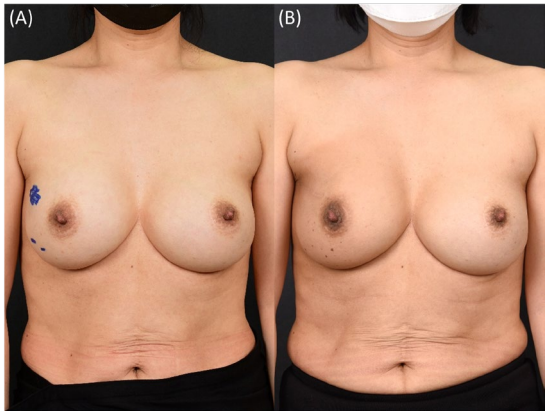

Fig. 2. Sheet-method ADM assisted oncoplastic breast reconstruction after BCS. (A) Preoperative photograph. (B) 6.9 months after operation.

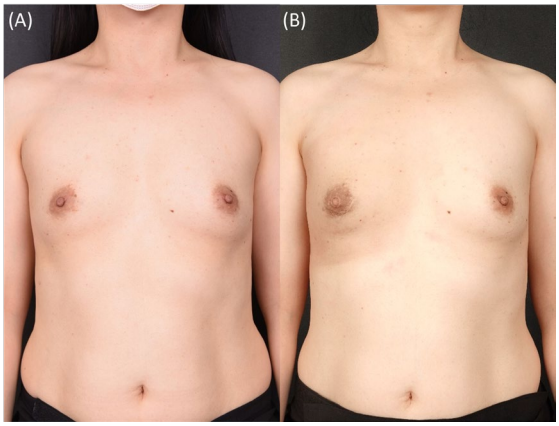

Fig. 3. Rolling-method ADM assisted oncoplastic breast reconstruction after BCS. (A) Preoperative photograph. (B) 2 years after operation.